



Australian Government  
Geoscience Australia

# Geological and energy implications of the Pine Creek region airborne electromagnetic (AEM) survey, Northern Territory, Australia

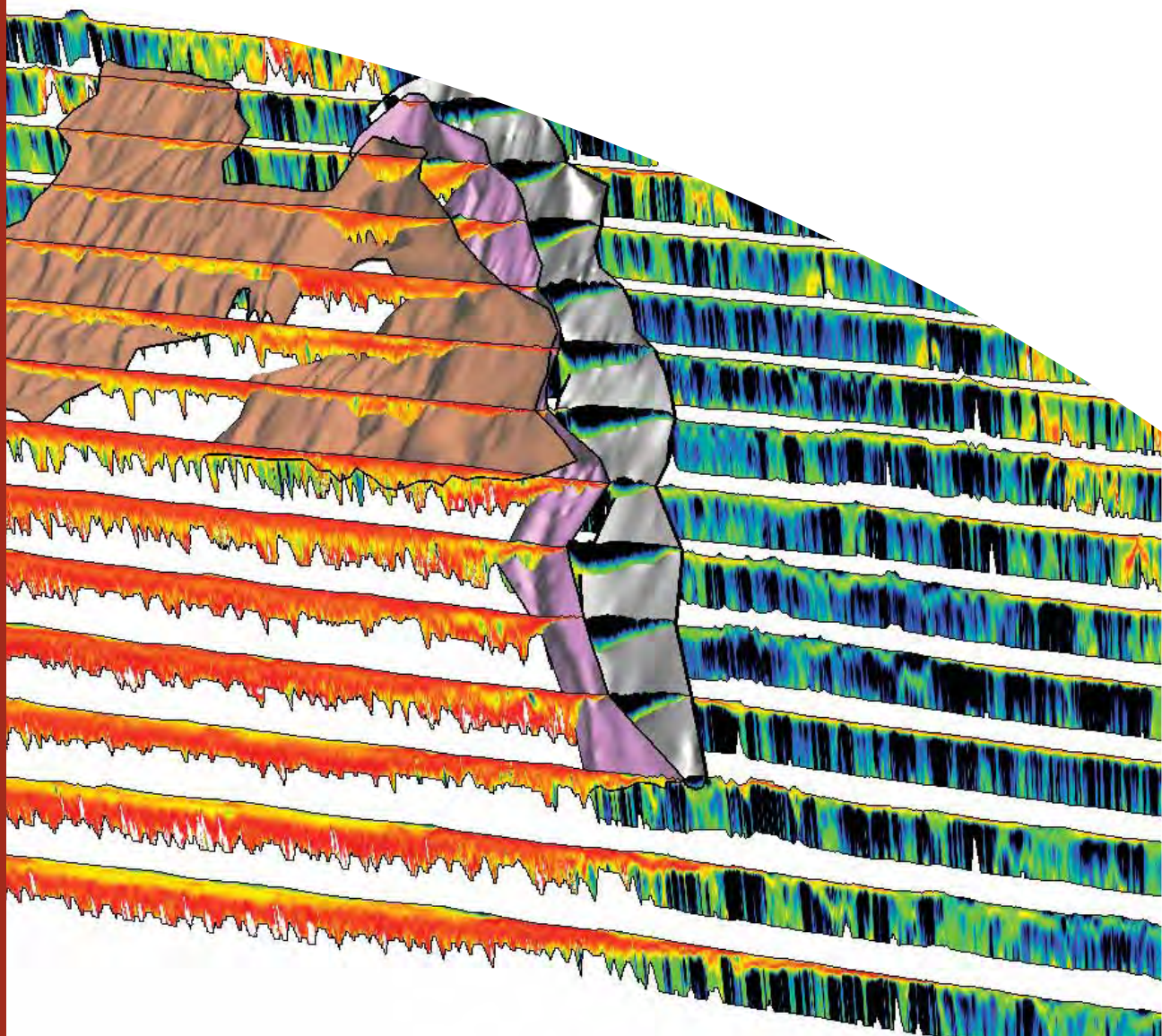
M.A. Craig (editor)

*With contributions from: R.C. Brodie, M.T. Costelloe, M.A. Craig,  
D.K. Hutchinson, S. Jaireth, S.F. Liu, and N.C. Williams.*

Record

2011/18

GeoCat #  
71854



# Geological and energy implications of the Pine Creek region airborne electromagnetic (AEM) survey, Northern Territory, Australia

GEOSCIENCE AUSTRALIA  
RECORD 2011/18

By

M.A. Craig (editor)

With contributions from:

R.C. Brodie<sup>1</sup>, M.T. Costelloe<sup>1</sup>, M.A. Craig<sup>1</sup>, D.K. Hutchinson<sup>2,4</sup>, S. Jaireth<sup>1</sup>, S.F. Liu<sup>1</sup>,  
and N.C. Williams<sup>2,3</sup>.



**Australian Government**  
**Geoscience Australia**

- 
1. Airborne EM Project, Onshore Energy and Minerals Division, Geoscience Australia, GPO Box 387 Canberra ACT 2601 Australia.
  2. Formerly Airborne EM Project, Onshore Energy and Minerals Division, Geoscience Australia, GPO Box 387 Canberra ACT 2601 Australia.
  3. Present address: Ivanhoe Australia Ltd, Level 13, 484 St Kilda Road Melbourne VIC 3004 Australia.
  4. Present address: Climate Change Research Centre, Level 4, Matthews Building, University of New South Wales, Sydney NSW 2052.

**Department of Resources, Energy and Tourism**

Minister for Resources and Energy: The Hon. Martin Ferguson, AM MP  
Secretary: Mr Drew Clarke

**Geoscience Australia**

Chief Executive Officer: Dr Chris Pigram



© Commonwealth of Australia (Geoscience Australia) 2011

With the exception of the Commonwealth Coat of Arms and where otherwise noted, all material in this publication is provided under a Creative Commons Attribution 3.0 Australia Licence (<http://creativecommons.org/licenses/by/3.0/au/>)

Geoscience Australia has tried to make the information in this product as accurate as possible. However, it does not guarantee that the information is totally accurate or complete. Therefore, you should not solely rely on this information when making a commercial decision.

**ISSN 1448-2177**

**ISBN 978-1-921954-06-1 print**

**ISBN 978-1-921954-05-4 web**

**GeoCat # 71854**

**Bibliographic reference:** Craig, M.A. ed. 2011. Geological and energy implications of the Pine Creek region airborne electromagnetic (AEM) survey, Northern Territory, Australia. **Record 2011/18**, 292 pp.

Example chapter reference: Liu S.F. and Craig, M.A. Geology. In: Craig, M.A. ed . *Geological and energy implications of the Pine Creek region airborne electromagnetic (AEM) survey, Northern Territory, Australia*. Geoscience Australia Record 2011/18, pp. 35-54

# CONTENTS

<b>1 INTRODUCTION .....</b>	<b>1</b>
1.1 SURVEY DESIGN CHARACTERISTICS.....	2
1.2 SURVEY LOCATION.....	3
1.3 SURVEY PURPOSE .....	4
1.4 UNCONFORMITY-RELATED URANIUM DEPOSITS.....	7
1.4.1 <i>Sandstone uranium deposits</i> .....	7
1.5 OTHER MINERAL SYSTEMS.....	7
1.6 GROUNDWATER SYSTEMS.....	8
1.7 SURVEY ECONOMIC FRAMEWORK.....	9
1.8 SURVEY DESIGN CONSIDERATIONS .....	9
1.9 CLIMATE.....	10
1.10 NATIONAL PARKS.....	10
1.11 TERRAIN (DRAPE).....	11
1.12 LAND ACCESS AND NATIVE TITLE ISSUES.....	12
1.13 OTHER NO FLY ZONES .....	13
1.14 AIRCRAFT ACCESS .....	14
1.15 FORWARD MODELLING .....	14
1.16 COMMUNICATION STRATEGY.....	14
1.17 FINAL SURVEY DESIGN .....	15
1.18 SURVEY PARTNERS, CONTRIBUTORS AND COST .....	17
1.19 CLIMATE.....	18
1.20 VEGETATION .....	19
1.21 TOPOGRAPHY .....	19
1.22 REFERENCES.....	22
<b>2 PREVIOUS AND CONCURRENT WORK.....</b>	<b>23</b>
2.1 GEOLOGICAL MAPPING .....	23
2.2 GEOPHYSICS .....	29
2.3 BOREHOLE DATA COMPILATION .....	30
2.4 REFERENCES.....	34
<b>3 GEOLOGY .....</b>	<b>35</b>
3.1 GEOLOGICAL FRAMEWORK.....	35
3.1.1 <i>Archean complexes</i> .....	37
3.1.2 <i>Pine Creek Orogen</i> .....	38
3.1.2.1 Stratigraphy.....	39
3.1.2.2 Structural and tectonic history .....	39
3.1.3 <i>McArthur Basin and correlates</i> .....	44
3.1.4 <i>Fitzmaurice Basin</i> .....	44
3.1.5 <i>Victoria Basin</i> .....	44
3.1.6 <i>Daly Basin</i> .....	44
3.1.7 <i>Bonaparte Basin</i> .....	44
3.1.8 <i>Money Shoal Basin</i> .....	45
3.1.9 <i>Cretaceous sediments</i> .....	45
3.2 REGOLITH GEOLOGY.....	46
3.2.1 <i>Introduction</i> .....	46
3.2.2 <i>What is regolith</i> .....	46
3.2.3 <i>Palaeoweathering and palaeoregolith</i> .....	50
3.3 REFERENCES.....	51
<b>4 MINERAL SYSTEMS OVERVIEW .....</b>	<b>55</b>
4.1 INTRODUCTION .....	55
4.2 ARCHEAN MINERAL SYSTEMS .....	55

4.2.1	<i>Paleoproterozoic (2500 Ma to 2020 Ma)</i> .....	64
4.2.2	<i>Stratabound Pb-Zn-Ag</i> .....	64
4.2.3	<i>Iron ore</i> .....	66
4.2.4	<i>Stratabound Pb, Zn, Cu</i> .....	67
4.2.5	<i>Uranium</i> .....	68
4.2.6	<i>Magnesite</i> .....	68
4.3	PALEOPROTEROZOIC (1900 Ma TO 1860 Ma) .....	69
4.3.1	<i>Copper and Lead-Zinc</i> .....	70
4.3.2	<i>Iron ore</i> .....	70
4.4	NIMBUWAH EVENT (1860 Ma TO 1847 Ma) .....	71
4.5	FELSIC MAGMATISM (CULLEN SUPERSUITE AND JIM JIM/DAVID SUITE; 1835 Ma TO 1818 Ma) 72	
4.5.1	<i>Lode gold deposits</i> .....	74
4.5.1.1	Host rocks .....	74
4.5.1.2	Structural control .....	74
4.5.1.3	Proximity to felsic intrusions.....	75
4.5.1.4	Metamorphic grade of host rocks .....	75
4.5.1.5	Wall rock alteration .....	75
4.5.1.6	Composition of ore fluid and temperature of formation.....	76
4.5.1.7	Timing of mineralisation .....	76
4.5.2	<i>Polymetallic deposits (Pb-Zn-Ag)</i> .....	80
4.5.3	<i>Skarn and/or vein (Fe, Cu and Pb-Zn-Ag) deposit</i> .....	81
4.5.4	<i>Tin-Tantalum-Tungsten veins, greisens and pegmatites</i> .....	83
4.6	EL SHERANA AND EDITH RIVER GROUP (1830 Ma TO 1825 Ma) .....	84
4.6.1	<i>Mineral systems associated with El Sherana and Edith River Groups</i> .....	85
4.7	SHOOBRIDGE EVENT (ca. 1780 Ma) .....	85
4.7.1	<i>Mineral systems associated with the Shoobridge Event</i> .....	85
4.8	KATHERINE RIVER GROUP/TOLMER GROUP (1800 – 1710 Ma) .....	86
4.9	MID-TAWALLAH INVERSION (CA. 1750 Ma – 1730 Ma) .....	87
4.10	DEPOSITION OF UPPER PART OF KATHERINE RIVER GROUP (Ca. 1730 Ma – 1710 Ma).....	88
4.11	EXTENSION AND DEPOSITION OF MOUNT RIGG GROUP (ca. 1610 Ma - 1590 Ma).....	88
4.12	BASIN-RELATED MINERAL SYSTEMS ASSOCIATED WITH POST-SHOOBIDGE EVENTS.....	88
4.13	UNCONFORMITY-RELATED URANIUM DEPOSITS .....	88
4.13.1	<i>Geological Architecture</i> .....	90
4.13.2	<i>Setting with respect to unconformity</i> .....	93
4.13.3	<i>Source of uranium</i> .....	94
4.13.4	<i>Source of fluids</i> .....	95
4.13.5	<i>Wall-rock alteration</i> .....	95
4.13.6	<i>Type of reductant</i> .....	96
4.13.7	<i>Timing of uranium mineralisation</i> .....	96
4.13.8	<i>Timing of uranium mineralisation relative to deformation events</i> .....	97
4.13.9	<i>Relation between uranium and base metal deposits (Rum Jungle Mineral Field)</i> .....	99
4.13.10	<i>Iron ore deposits</i> .....	101
4.14	SUMMARY .....	103
4.15	REFERENCES .....	104
5	AEM GEOPHYSICS .....	110
5.1	INTRODUCTION .....	110
5.2	GEO-ELECTRICAL MODELS .....	110
5.3	AEM SYSTEMS .....	111
5.3.1	<i>TEMPEST™</i> .....	111
5.3.2	<i>VTEM™</i> .....	112
5.4	PREVIOUSLY RELEASED AEM DATA.....	113
5.5	PHASE-2 - TEMPEST™ GA–LEI INVERSIONS .....	115
5.5.1	<i>Background on the GA–LEI algorithm</i> .....	115
5.5.2	<i>GA–LEI Inversions</i> .....	116
5.5.2.1	Algorithm outline.....	116
5.5.2.2	Conductivity model parameterization.....	116
5.5.2.3	Reference model .....	118

5.5.2.4	Data misfit .....	119
5.5.3	<i>Depth of Investigation</i> .....	119
5.5.4	<i>Derived products</i> .....	120
5.5.4.1	Point located data.....	121
5.5.4.2	Layer conductivity grids.....	121
5.5.4.3	Depth slice grids .....	121
5.5.4.4	Elevation slice grids.....	122
5.5.4.5	AEM DOI Go map.....	123
5.5.4.6	Gridding procedures .....	125
5.5.4.7	Sections.....	125
5.5.4.7.1	Georeferenced JPEGs.....	125
5.5.4.7.2	Multiplots .....	126
5.6	PHASE-2 – VTEM™ EM FLOW™ CONDUCTIVITY DEPTH IMAGING.....	128
5.6.1	<i>Background</i> .....	128
5.6.2	<i>Penetration depth</i> .....	128
5.6.3	<i>Derived products</i> .....	128
5.6.3.1	Point located data.....	129
5.6.3.2	Grids .....	129
5.6.3.3	Sections.....	130
5.6.3.3.1	Georeferenced JPEGs.....	130
5.6.3.3.2	Multiplots .....	131
5.7	DISCRETE CONDUCTORS .....	132
5.8	COMPARISON OF AEM INVERSIONS WITH CONDUCTIVITY LOGS .....	133
5.9	REFERENCES.....	137
<b>6</b>	<b>GEOLOGICAL INTERPRETATION OF AEM DATA .....</b>	<b>139</b>
6.1	INTRODUCTION .....	139
6.2	DATASETS, INTERPRETATION METHODS AND ARTEFACTS .....	140
6.2.1	<i>EM Flow™ and GA's Layered Earth Inversion (GA–LEI) data</i> .....	140
6.2.2	<i>TEMPEST™ vs VTEM™ data for geological interpretation</i> .....	141
6.2.3	<i>The influence of man-made features on conductivity</i> .....	141
6.3	GEOLOGICAL INTERPRETATION OF THE TEMPEST™ DATA IN THE WESTERN PINE CREEK REGION .....	146
6.3.1	<i>AEM signatures of geological provinces</i> .....	146
6.3.2	<i>Correlation of AEM conductivity data with geological features</i> .....	146
6.3.2.1	Coastal areas .....	147
6.3.2.2	Regolith and related features .....	147
6.3.2.2.1	Regolith Character and distribution .....	147
6.3.2.2.2	General observations .....	147
6.3.2.2.2.1	Transported regolith.....	147
6.3.2.2.2.2	Pedolith .....	149
6.3.2.2.2.3	Saprolith.....	149
6.3.2.2.3	Assessments of gridded data (depth slices) .....	150
6.3.2.2.3.1	Transported regolith.....	150
6.3.2.2.3.2	Pedolith .....	152
6.3.2.2.3.3	Saprolith.....	155
6.3.2.2.3.4	Assessments of GA–LEI conductivity sections and EM Flow™ CDI sections .....	157
6.3.2.2.3.5	Palaeochannel environments – possible indicators and AEM evidence .....	160
6.3.2.2.3.6	Image assessments .....	160
6.3.2.2.3.7	Geomorphic and geological indicators and AEM data .....	160
6.3.2.3	Interpreted Palaeovalleys in the Pine Creek Survey area .....	172
6.3.2.4	Granite plutons.....	174
6.3.2.5	Faults.....	174
6.3.2.6	Folds .....	175
6.3.2.7	Unconformities and geological provinces in the TEMPEST™ data .....	177
6.3.2.8	Cretaceous sediments.....	177
6.3.2.9	Bonaparte Basin.....	177
6.3.2.10	Daly Basin and Birrindudu Basin .....	178
6.3.2.10.1	Correlation with Daly Basin boundary and sedimentary units.....	178
6.3.2.10.2	The Depot Creek unconformity.....	181
6.3.2.10.3	3D-modelling of the eastern Daly and Birrindudu basins .....	185

6.3.2.11	Victoria Basin .....	188
6.3.2.12	Fitzmaurice Basin .....	191
6.3.2.13	Pine Creek Orogen.....	191
6.3.2.13.1	Strong conductors in the Central Domain.....	191
6.3.2.13.2	Apparent shallow conductivity anomalies in GA–LEI conductivity sections.....	192
6.3.2.13.3	Zamu Dolerite.....	196
6.3.2.14	Archean.....	197
6.3.2.14.1	Rum Jungle Complex .....	197
6.3.2.14.2	Woolner Granite .....	197
6.4	GEOLOGICAL INTERPRETATION OF THE VTEM™ DATA IN THE EASTERN PINE CREEK REGION .....	199
6.4.1	<i>Geological units and conductivity</i> .....	199
6.4.2	<i>Geological interpretations</i> .....	202
6.4.3	<i>Kombolgie unconformity</i> .....	204
6.4.4	<i>Nungbalgarri Volcanics and Gilruth Volcanic Member</i> .....	204
6.4.5	<i>Oenpelli Dolerite</i> .....	204
6.4.6	<i>Sub-McArthur Basin conductors</i> .....	204
6.4.7	<i>Interpretation of GA–LEI data of the Kombolgie area</i> .....	205
6.5	CONCLUSIONS .....	206
6.6	REFERENCES.....	208
<b>7</b>	<b>IMPLICATIONS FOR URANIUM MINERAL SYSTEMS.....</b>	<b>210</b>
7.1	UNCONFORMITY–RELATED URANIUM MINERAL SYSTEMS .....	210
7.1.1	<i>Nabarlek area</i> .....	216
7.1.2	<i>Birrindudu Basin in the Pine Creek–Fergusson area</i> .....	217
7.1.3	<i>Westmoreland-style</i> .....	217
7.1.4	<i>Other areas</i> .....	218
7.2	SANDSTONE-HOSTED URANIUM MINERAL SYSTEMS.....	218
7.3	CONCLUSIONS .....	218
7.4	REFERENCES.....	220
<b>8</b>	<b>SUMMARY AND CONCLUSIONS .....</b>	<b>221</b>
8.1	AEM DATA ACQUISITION .....	221
8.2	ADDITIONAL DATASETS .....	222
8.3	MINERAL DEPOSITS .....	224
8.4	AEM DATA PROCESSING .....	224
8.5	AEM DATA INTERPRETATION.....	226
8.6	RUM JUNGLE AEM INTERPRETATION .....	227
8.7	KOMBOLGIE AEM INTERPRETATION.....	231
8.8	URANIUM EXPLORATION IMPACT .....	232
<b>9</b>	<b>ACKNOWLEDGEMENTS .....</b>	<b>234</b>
<b>10</b>	<b>APPENDICES.....</b>	<b>235</b>
10.1	INVERSION DATA .....	235
10.2	GA–LEI INVERSION OF TEMPEST™ DATA .....	236
10.2.1	<i>Introduction</i> .....	236
10.2.2	<i>Formulation</i> .....	236
10.3	REFERENCES .....	247
10.4	CLIMATIC DATA .....	248
10.5	GA–LEI INVERSION OUTPUT ASCII HEADER INFORMATION.....	249
10.6	TECHNICAL SPECIFICATIONS OF MAP PROJECTIONS .....	251
10.7	KOMBOLGIE EM FLOW™ SETTINGS .....	252
10.8	QUALIFYING REMARKS ON KOMBOLGIE CONDUCTIVITY ESTIMATES.....	280
10.8.1	<i>Conductive Areas of the Kombolgie Dataset</i> .....	280
10.8.2	<i>Resistive Areas of the Kombolgie Dataset</i> .....	282
10.9	REFERENCES .....	287
10.10	REGOLITH AND LANDFORM: THEIR CLASSES, PATTERNS, MAP SYMBOLS AND MEANINGS .....	288

# LIST OF FIGURES

Figure 1-1:	Pine Creek AEM survey area names, boundaries, mineral deposits, settlements, access roads and National Parks. ....	2
Figure 1-2:	Location of National Parkes, existing mining tenements, major uranium deposits in relation to the AEM survey boundaries. ....	4
Figure 1-3:	Pine Creek Regional survey line spacing. Woolner Granite survey area, the regional flight line spacing was 5 km with two Geoscience Australia (GA) infill blocks conducted at 1.67 km. Two National Water Commission (NWC) blocks were infilled at 555 m and an additional four company infill blocks were also within this survey area. The Rum Jungle survey area was flown with 5 km line spacing. Internal to the regional block three GA infill blocks were flown at 1.67 km line spacing. One small NWC block was flown at 250 m line spacing. The Kombolgie survey area was flown with 5 km line spacing. Internal to the regional block, one GA infill block was flown at 1.67 km line spacing.....	5
Figure 1-4:	Major commodity (Cu, Co, Ni, Gold and Uranium) deposits and prospects occurring within the Pine Creek survey area. Commodity data are from the GA MINLOC database .....	8
Figure 1-5:	Major current drainage networks and lowland drainage tracts within the Pine Creek AEM survey area.....	9
Figure 1-6:	Flight path flying, trimming and delivery.....	11
Figure 1-7:	Drape analysis results for the Pine Creek AEM survey area. White dots indicate areas where the contracted flight parameters were altered to provide adequate terrain clearance for the aircraft and towed receiver bird. ....	12
Figure 1-8:	Native Title Application and Determination Areas recognised by the Federal Court (30 June 2007) for the Pine Creek survey areas. ....	13
Figure 1-9:	Major physiographic elements within and surrounding the Pine Creek AEM Survey .....	20
Figure 1-10:	Simplified physiographic areas within the AEM Survey areas as shown by an SRTM DEM image. Blue areas are general lowland regions and green areas are higher parts of the landscape.....	21
Figure 2-1:	Pine Creek Survey Area 250k and 100k map sheet names and numbers. ....	23
Figure 2-2:	Regional geophysical data sets available for the Pine Creek AEM survey area. A: Bouger anomaly gravity; B: Reduced-to-pole total magnetic intensity (RTP TMI) image; C: Ternary radiometric (gamma-ray spectrometric) image with KThU as RGB; D: Space Shuttle Radar Topographic Mission Digital Elevation Model (SRTM DEM) with 30 m ground pixel resolution.....	30
Figure 2-3:	Boreholes (and their depths) within and adjacent to the Pine Creek survey area which were consulted during AEM interpretations .....	32
Figure 2-4:	Unfiltered borehole population associated with Pine Creek survey area including publicly available mineral and water boreholes.....	32
Figure 2-5:	Locations of boreholes associated with the Pine Creek survey area for which conductivity-logs have been acquired.....	33
Figure 3-1:	Geological regions in the northern part of the Northern Territory with AEM survey boundaries (geological regions after NTGS (2010)).....	36
Figure 3-2:	Geological domains of the Pine Creek Orogen (geological regions after NTGS (2010))......	37

Figure 3-3:	A generalized terminology for in situ regolith (from Craig et al., 2008 and Craig 2006,) .....	47
Figure 3-4:	Regolith-Landform legend symbols constructed according to Geoscience Australia's RTMAP conventions. Possible combinations can be seen in Tables 10–4 and 10–5 in Appendix10.10. ....	48
Figure 3-5:	Regolith-Landform units are represented at a compilation scale of 1: 250 000 for the Woolner and Rum Jungle section of the Pine Creek AEM survey areas. A more detailed regolith map of the NT including the AEM Survey area is available for download from the NTGS website ( <a href="http://www.nt.gov.au/d/Minerals_Energy/Geoscience/index.cfm?header=Territory-wide%20and%20regional%20maps">http://www.nt.gov.au/d/Minerals_Energy/Geoscience/index.cfm?header=Territory-wide%20and%20regional%20maps</a> ). Regolith map symbols used on this map are explained by referring to Tables 10–4 and 10–5 in Appendix10.10. ....	49
Figure 4-1:	Nimbuwah Domain. Time-event plots of three domains in the Pine Creek Orogen. The age data and relevant references are summarised in Table 4–1.....	57
Figure 4-2:	Central Domain. Time-event plots of three domains in the Pine Creek Orogen. The age data and relevant references are summarised in Table 4–1.....	58
Figure 4-3:	Litchfield Domain. Time-event plots of three domains in the Pine Creek Orogen. The age data and relevant references are summarised in Table 4–1.....	59
Figure 4-4:	Map of the Pine Creek Orogen showing the known ages of deposits and prospects.. The map is based on an NTGS dataset, i.e., Pine Creek interpreted geology (2005). Deposits, prospects and occurrences are from GA's OZMIN and MINLOC datasets. The age data for deposits and references are summarised in Table 4–1.....	63
Figure 4-5:	Map of the Pine Creek Orogen showing basemetal (Cu, Pb-Zn) deposits and occurrences. The map is based on an NTGS dataset, i.e., Pine Creek interpreted geology (2005). Deposits, prospects and occurrences are from GA's OZMIN and MINLOC datasets. ....	65
Figure 4-6:	New Pb-Pb model for Pine Creek deposits showing Pb-Pb model ages for selected deposits. Model ages calculated by David Huston.....	66
Figure 4-7:	Map of the Pine Creek Orogen showing Iron ore deposits and occurrences. The map is based on an NTGS dataset, i.e., Pine Creek interpreted geology (2005). Deposits, prospects and occurrences are from GA's OZMIN and MINLOC datasets. ....	67
Figure 4-8:	Map of the Pine Creek Orogen showing gold deposits and occurrences. The map is based on an NTGS dataset, i.e., Pine Creek interpreted geology (2005). Deposits, prospects and occurrences are from GA's OZMIN and MINLOC datasets. ....	75
Figure 4-9:	Map of the Pine Creek Orogen showing tin-tantalum and tungsten deposits, and occurrences. The map is based on an NTGS dataset, i.e., Pine Creek interpreted geology (2005). Deposits, prospects and occurrences are from GA's OZMIN and MINLOC datasets. ....	83
Figure 4-10:	Map showing possible pre-erosion extent of Katherine River and Tolmer Group sediments. The map is based on an NTGS dataset, i.e., Pine Creek interpreted geology (2005). ....	87
Figure 4-11:	Map of the Pine Creek Orogen showing uranium deposits and occurrences. The map is based on an NTGS dataset, i.e., Pine Creek interpreted geology (2005). Deposits, prospects and occurrences are from GA's OZMIN and MINLOC datasets. ....	90

Figure 4-12:	Schematic cross-section of the Pine Creek Orogen showing position of major uranium deposits. Modified after Mckay and Miezitis (2001). ....	90
Figure 4-13:	Schematic cross-sections showing four types of setting of unconformity-related uranium deposits. Modified after Lally and Bajwah (2006). ....	93
Figure 4-14:	Map showing basemetal and uranium deposits in the Rum Jungle Mineral Field. The map is based on an NTGS dataset, i.e., Pine Creek interpreted geology (2005). Deposits, prospects and occurrences are from GA's OZMIN and MINLOC datasets. ....	101
Figure 5 1:	An example of a geo-electric model (1.1) from the Kombolgie AEM Survey area. Forward modelling of this scenario was used to predict if the presence of the unconformity, under 0 – 1000 m of 0.1 mS/m cover sediments, could be detected within the AEM system noise levels .....	111
Figure 5-2:	Schematic diagram of 1D vertically smooth layered earth model used in the GA–LEI. The thickness of each layer ( $t_n$ ) is fixed, but the conductivity ( $\sigma_n$ ) is not fixed and can vary between layers. From Brodie and Fisher (2008) ....	117
Figure 5-3:	Sample conductivity depth sections comparing the results of inversions using reference models of (a) 0.04 S/m and (b) 0.004 S/m. the black line marks the depth of investigation (DOI) in each case. Above the DOI the results are similar for both inversions, whereas below the DOI the conductivity differs according to the reference model value. From: Hutchinson et al. (2010b).....	120
Figure 5-4:	A selection of depth slices showing a) 0-5 m, b) 30-40 m, c) 100-150 m and d) 200-250 m. Data falling below the DOI have been masked out, and appear white..	122
Figure 5-5:	Selection of elevation slices, showing a) 0-10 m above sea level (a.s.l.), (b) 100-110 m a.s.l., (c) 200-210 m a.s.l. and (d) 300-310 m a.s.l .....	123
Figure 5-6:	The DOI grid (AEM go map) for the Pine Creek TEMPEST™ Survey areas. ....	124
Figure 5-7:	GA–LEI Multiplot for line 1000801 .....	127
Figure 5-8:	Kombolgie Survey total conductance to 2 000 m .....	130
Figure 5-9:	Georeferenced JPEG for a 20 km subsection of line 20360. ....	131
Figure 5-10:	A section of multiplot 1001501 expanded to highlight the discrete anomaly that is present at fiducial 2980 .....	133
Figure 5-11:	The location of the boreholes plotted over conductance from 0-200 m .....	136
Figure 6-1:	(a) Apparent conductivity anomalies in the vicinity of the Pine Creek shear Zone. (b) Correlation between the apparent conductivity anomalies and the location of powerlines and pipelines. Conductivity sections displayed at three times vertical exaggeration. ....	143
Figure 6-2:	Solid geology of the Woolner Granite – Rum Jungle AEM survey area in the Pine Creek Orogen (simplified from NTGS, 2005).....	144
Figure 6-3:	Conductance image (0-400 m) of Woolner Granite – Rum Jungle AEM survey area by TEMPEST™. Note resistive granite plutons rimmed by more conductive metasedimentary rocks.....	145
Figure 6-4:	The distribution of saprolith throughout the Woolner-Rum Jungle AEM survey area, represented by white polygons. Non-saprolith materials are shown in grey... 147	
Figure 6-5:	Regolith-landform polygons (in white) indicate the mapped distribution of residual regolith (pedolith) materials throughout the Woolner and Rum Jungle AEM survey areas. Grey areas represent non-residual materials both inside and outside the survey areas. In subsequent figures, white polygons, when made transparent, serve as windows through which the underlying AEM responses at various depths below the regolith may be examined and assessed.....	148

Figure 6-6:	The distribution of alluvial and coastal regolith materials within the survey area is shown in white. All other regolith polygons are masked by grey. In subsequent figures, white polygons, when made transparent, serve as windows through which the underlying AEM responses at various depths below the regolith may be examined and assessed.....	148
Figure 6-7:	The GA-LEI conductivity image from 0-5 m highlighting high conductivity areas associated with the position of alluvial and coastal materials along the coastal plain, especially to the north and to the east, nearer the coastal fringes.....	150
Figure 6-8:	GA-LEI conductivity responses at the 15-20 m depth interval. These are slightly lower than those responses occurring at similar locations in the 0-5 m interval. Reduced conductivity responses are more obvious along the northern coastal plain and are present but to a lesser extent elsewhere across the survey area. ....	151
Figure 6-9:	GA-LEI conductivity responses in the 40-60 m depth slice. This image shows the greatest decline in conductivity in areas previously most conductive at shallower intervals. ....	151
Figure 6-10:	GA-LEI conductivity depth slice 80-100 m viewed through windows through transparent coastal and alluvial regolith polygons. Conductivity continues to decline significantly possibly due to reduced pore spaces in weathered rocks and reduced influence of seawater. No other significant anomalies are observed in this image. ....	152
Figure 6-11:	GA-LEI conductivity depth slice 0-5 m. The location of pedolith provides windows through to the conductivity depth slice images. The conductivity slice in this image represents the very resistive pedolith exposed at the surface and persisting at least to a depth of 5 m.....	153
Figure 6-12:	GA-LEI conductivity depth slice 20-30 m. Windows show that beneath the pedolith there are significant areas of moderate to highly conductive materials present within the 20-30 m depth slice. ....	153
Figure 6-13:	GA-LEI conductivity responses in the 40-60 m depth slice. Conductivity in this interval has continued to decline and is interpreted to correspond with the decline of saline saturated regolith. Elsewhere, away from the coast, there is a marked increase in non-conductive saprock .....	154
Figure 6-14:	GA-LEI conductivity responses in the 80-100 m depth slice. At greater depths (80-100 m) below the mapped pedolith, conductivity values appear to have peaked with some parts declining significantly especially around the coast.....	154
Figure 6-15:	GA-LEI conductivity depth slice 0-5 m. The bright blue responses involve shallow saprolith and show mostly low to very low conductivity and are located in higher parts of the landscape.....	155
Figure 6-16:	GA-LEI conductivity depth slice 20-30 m. The responses show an increase in the relative proportion of moderate conductivity responses in the central NW-SE trending area which is more likely related to an increased proximity to the saprolite in the lower parts of the landscape. The relatively higher areas tend to be less weathered and are therefore likely to be more resistive.....	156
Figure 6-17:	GA-LEI conductivity depth slice 40-60 m. Responses in the central NW-SE trending region show that conductivity may well have peaked and that signal penetration is approaching the saprock zone where the degree of weathering is expected to be less compared with that of the saprolite zone and accordingly shows a decline in conductivity. ....	156
Figure 6-18:	GA-LEI conductivity depth slice 80-100 m. The declining conductivity patterns in this windowed view appear to follow the same general trend towards the increasing influence of bedrock geology which is highlighted in the previous example, except for the new red highly conductive patches.....	157

- Figure 6-19: Block diagram indicating an AEM CDI section generated along line 12460 and related 1: 250 000 scale surface regolith landform units superimposed (with 30% transparency) onto an extract from the 9 second SRTM DEM. The southern half of the block diagram has been artificially lowered to the base of the CDI section to enable easier visual correlation with the conductivity features..... 159
- Figure 6-20: Block diagram illustrating an AEM CDI section generated along line 12460 and related 1:1 million scale surficial geology units superimposed (with 30% transparency) onto an extract from the 9 second SRTM DEM. The southern half of the block diagram has been artificially lowered to the base of the CDI section to enable easier visual correlation with the conductivity features..... 159
- Figure 6-21: A MRVBF Image derived from the 9 second DEM of Australia showing current drainage (digitised from 1:250 000 scale topographic mapping) in blue. White to light grey areas indicate the high variability of valley floor lowlands across the region. The darker areas indicate the higher elevation uplands, ridges and tablelands... 162
- Figure 6-22: A MRVBF Image derived from the 3 second DEM of Australia showing current drainage (digitised from 1:250 000 scale topographic mapping) in blue. White to light grey areas indicate simplified, broader valley-floor lowland expanses and major plains including extensive coastal plains. The darker areas indicate major higher-elevation uplands, ridges and tablelands (for example, the highly dissected Kombolgie plateau to the NE and in contrast, to the SW the relatively lower expanse of the Daley Basin here shown as a NW-SE trend grey trough). Roads are in yellow. Major town names are indicated..... 163
- Figure 6-23: A 9 second colour-shaded SRTM DEM (extracted from an SRTM DEM image prepared by R. Clifton, NTGS) showing current drainage lines in white connecting over the mid north-western end of the Daly Basin (mostly shown in shades of blue). The feint dashed lines represent major access roads in the area. Town names are shown in white text..... 164
- Figure 6-24: A 9 second colour-shaded SRTM DEM (extracted from an SRTM DEM image prepared by R. Clifton, NTGS) showing a large upland area of Cretaceous cover immediately west of the area in Figure 6-23. Older, major trunk drainage patterns progressively superimposed onto underlying older bedrock structures..... 165
- Figure 6-25: GA LEI conductivity section of line 1101901 in the Pine Creek area. An alluvial plain marked at the far eastern end of the line corresponds to an area of moderate conductivity..... 166
- Figure 6-26: An EM-Flow<sup>TM</sup> CDI section of line 12080 in the Kombolgie survey area. An alluvial plain on the western end of the line is interpreted to represent a wedge of saline water saturating alluvium, and is mapped by very high conductivities. .... 166
- Figure 6-27: GA-LEI conductivity section of line 10280 across part of the Daly Basin overlain on a DEM image. The section shows a major area of pedolith marked A, and minor unmapped pedolith residual rises marked B..... 168
- Figure 6-28: Area marked A from Figure 6-27 showing an upper-most resistive layer correlates with the surface expression of pedolith developed on weathered Cretaceous rocks. .... 169
- Figure 6-29: Areas marked B from Figure 6-27 showing an upper-most thin blue resistive layer correlated with the surface expression of residual rises (pedolith) also developed on weathered Cretaceous rocks. .... 169
- Figure 6-30: GA-LEI conductivity sections of lines 10050 & 10060 from the Rum Jungle survey displayed over a DEM image with interpreted regolith units. . Pedolith is revealed at locations A and B, south of the triple junction of the Pine Creek Orogen, Birrindudu and Daly Basins regolith. .... 170

Figure 6-31:	Areas marked A on line 10050 from Figure 6-30 shows an upper-most resistive layer correlated with the surface expression of pedolith developed on weathered Cretaceous rocks. ....	171
Figure 6-32:	Areas marked B on line 10060 from Figure 6-30 shows an upper-most resistive layer correlated with the surface expression of residual rises (pedolith) developed on weathered Cretaceous rocks. ....	171
Figure 6-33:	Current surface drainage channels and palaeochannels at depth in the Mt Boulder area (a) AEM conductance image (0-400 m) from the Rum Jungle Survey (b) Digital elevation model (c) Current drainages mapped in the Pine Creek 1:250 000 surface geology map (Malone, 1962) (d) Palaeovalleys palaeodrainage at depth interpreted from the AEM conductance image (a).....	173
Figure 6-34:	Faults depicted in GA-LEI conductivity sections (lines 1004401 and 1004601). Solid geology after NTGS (2005). Conductivity sections displayed at three times vertical exaggeration. ....	175
Figure 6-35:	GA-LEI conductivity section 1001501 from the Rum Jungle Survey. Solid geology from NTGS (2005). Conductivity sections displayed at three times vertical exaggeration. Folds are defined by the strong conductor present within the South Alligator Group.....	176
Figure 6-36:	GA-LEI conductivity section (line 1004601) overlies the surface geology map in the Bonaparte Basin. Conductivity sections displayed at three times vertical exaggeration. Conductors A and B are interpreted to be within the Permian Kulshill Formation. Surface geology from Raymond and Retter (2010). ....	178
Figure 6-37:	GA-LEI conductivity sections 10140-10150 over surface geology in the Limestone Hill area. Surface geology from Raymond and Retter (2010). AEM conductivity sections displayed at three times vertical exaggeration. ....	180
Figure 6-38:	GA-LEI conductivity sections 10140-10160 over surface geology in the Mt Briggs area. Surface geology from Raymond and Retter (2010). AEM conductivity sections displayed at three times vertical exaggeration. ....	181
Figure 6-39:	GA-LEI conductivity sections 10090-10100 over surface geology southeast of the Douglas township. Surface geology from Raymond and Retter (2010). Conductivity sections displayed at 40% transparency to show geology underlying, and at three times vertical exaggeration. ....	183
Figure 6-40:	GA-LEI conductivity sections 1004001 – 1004401 over surface geology in the Mt Boulder area. Surface geology from Raymond and Retter (2010). AEM conductivity sections displayed at three times vertical exaggeration. ....	184
Figure 6-41:	GA-LEI conductivity sections used in 3D modelling of the eastern Daly and Birrindudu basins .....	186
Figure 6-42:	GOCAD® images illustrate the construction of the 3D model for the Daly and Birrindudu basins. AEM sections displayed at five times vertical exaggeration.....	187
Figure 6-43:	GA-LEI conductivity sections in 3D of the Pine Creek area and a 3D model of part of the Daly and Birrindudu basins. Five times vertical exaggerations. The conductivity sections are 600 m deep. ....	188
Figure 6-44:	GA-LEI conductivity and EM Flow™ CDI sections over surface geology in the northern part of the Victoria Basin. Surface geology from Raymond and Retter (2010). ....	190
Figure 6-45:	GA-LEI conductivity sections in the Rum Jungle area. Solid geology: after NTGS (2005). Conductivity sections displayed at three times vertical exaggeration. Strong conductors are attributed to carbonaceous and pyritic sediments within the South Alligator and Mount Partridge Groups. ....	194

Figure 6-46:	Interpretation of faults and folds SSE of Rum Jungle Complex. Conductivity sections displayed at three times vertical exaggeration. (a) AEM conductivity sections over solid geology (NTGS, 2005), (b) & (c) Interpretation on AEM sections Strong conductors are attributed to carbonaceous and pyritic sediments within the South Alligator and Mount Partridge Groups.....	195
Figure 6-47:	GA–LEI conductivity section of line 1001401 east of the Rum Jungle complex. (a) Solid geology with AEM survey line marked (solid geology after Lally, 2003). (b) Interpretation of the AEM section over semi-transparent solid geology map.....	196
Figure 6-48:	GA–LEI conductivity sections over solid geology in the Woolner Granite area. Solid geology after NTGS (2005). Conductivity sections displayed at three times vertical exaggeration.....	198
Figure 6-49:	GA–LEI conductivity sections over solid geology in the Kombolgie area. Solid geology after NTGS (2005). Conductivity sections displayed at two and half times vertical exaggeration.....	200
Figure 6-50:	Geological cross-section interpretations along selected EM Flow™ sections in the Kombolgie AEM Survey. Solid geology after NTGS (2005). Conductivity sections are displayed at a vertical exaggeration of 2.5.....	203
Figure 7-1:	Pre-Kombolgie solid geology map of the Nabarlek area.....	214
Figure 7-2:	Pre-Daly Basin solid geology map of the Pine Creek – Fergusson River area.....	215
Figure 7-3:	Pre-Depot Creek solid geology map of the Pine Creek – Fergusson River area .....	216
Figure 10-1:	Schematic representation of the framework for GA–LEI inversion of TEMPEST™ AEM data. Red elements are the unknowns to be solved .....	238
Figure 10-2:	Average annual thunder days for Australia, From BOM (2009) .....	248
Figure 10-3:	Average annual total lightning flash density for Australia. From BOM (2009).....	248
Figure 10-4:	GA–LEI and EM Flow™ conductivity sections from a conductive part (Line 10010) of the Kombolgie survey area.....	280
Figure 10-5:	VTEM data (left) at the sample located at ‘A’ on Figure 10–4 and the corresponding GA–LEI and EM Flow™ CDI conductivity models (right). .....	281
Figure 10-6:	GA–LEI and EM Flow™ conductivity sections from a resistive part (Line 20390) of the Kombolgie survey area. ....	282
Figure 10-7:	VTEM data (left) at the sample located at ‘B’ on Figure 10–6 and the corresponding GA–LEI and EM Flow™ CDI conductivity models (right). .....	283
Figure 10-8:	GA–LEI and EM Flow™ conductivity sections from a resistive part (Line 12100) of the Kombolgie survey area. ....	284
Figure 10-9:	VTEM data (left) at the sample located at ‘C’ on Figure 10–6 and the corresponding GA–LEI and EM Flow™ CDI conductivity models (right). .....	285
Figure 10-10:	Similar to Figure 10-6, except in this case conductivity sections were generated from the drift corrected data (i.e., green transients on Figure 10–7) instead of the final levelled data (black transients). .....	286
Figure 10-11:	VTEM data (left) at the sample located at ‘B’ on Figure 10–6 and the corresponding GA–LEI and EM Flow™ CDI conductivity models, and two alternative models that also fit the data (right). .....	287

# LIST OF TABLES

Table 1-1:	Potential Uranium interest in the proposed survey areas .....	6
Table 1-2:	Priority Assessment .....	6
Table 1-3:	Mining development summary (NT Gov: Orestruck, 2010).....	7
Table 1-4:	Pine Creek AEM survey infill subscribers.....	18
Table 2-1:	Available geological maps in the Pine Creek AEM survey area.....	24
Table 3-1:	Archean to Proterozoic stratigraphy of the Pine Creek Orogen.....	40
Table 3-2:	Structural correlation in the Pine Creek Geosyncline (after Johnston 1984) .....	42
Table 3-3:	Deformation history in the Pine Creek region .....	43
Table 4-1:	Ages of deposits/prospects.....	60
Table 4-2:	Paleoproterozoic felsic intrusive magmatism in Pine Creek Orogen.....	73
Table 4-3:	Major gold deposits and prospects in the Pine Creek Orogen .....	78
Table 4-4:	Tin, Tantalum, and Tungsten deposits in the Pine Creek Orogen.....	82
Table 4-5:	Principal features of main uranium fields in the Pine Creek Orogen.....	89
Table 4-6:	Summary of important mineral system in the Pine Creek Orogen and related events .....	102
Table 5-1:	Conductivities used in the forward modelling .....	110
Table 5-2:	Summary of AEM system specifications.....	112
Table 5-3:	GA–LEI Model layer thicknesses and depths from surface for Woolner Granite and Rum Jungle survey areas.....	118
Table 5-4:	Contents of the JPEG world file line 1000201.....	125
Table 5-5:	Description of each panel of the GA–LEI multiplots .....	126
Table 5-6:	Description of each panel of the multiplots .....	131
Table 5-7:	Coordinates (MGA94 Zone 52 and Zone 53) and depths of 16 boreholes .....	134
Table 6-1:	AEM datasets for geological interpretation in the Pine Creek area .....	139
Table 6-2:	Other datasets used in geological interpretation in the Pine Creek area .....	139
Table 6-3:	Characteristics of TEMPEST™ and VTEM™ data for geological interpretation.....	141
Table 6-4:	Major AEM signatures of geological provinces in the Pine Creek area .....	146
Table 6-5:	Stratigraphy of the Daly River Group on the Pine Creek 1:250 000 map sheet .....	179
Table 6-6:	Stratigraphy of the Tolmer Group.....	179
Table 6-7:	The three marker horizons used to build the 3D model of part of the Birrindudu Basin south of Hayes Creek .....	185
Table 6-8:	Stratigraphy of the Auvergne Group on the Fergusson River 1:250 000 map sheet .....	189
Table 6-9:	Stratigraphy of the Fitzmaurice Group on the Port Keats 1:250 000 sheet.....	191
Table 6-10:	Paleoproterozoic metasedimentary rocks in the Pine Creek Orogen .....	193
Table 6-11:	Stratigraphy of the Katherine River Group in the Pine Creek region .....	199
Table 6-12:	Stratigraphy of the pre-Kombolgie basement geological units in the Kombolgie AEM survey area .....	201
Table 7-1:	Critical mineral system features for unconformity-related uranium deposits .....	212

Table 10-1:	GA–LEI inversion products for the Woolner Granite and Rum Jungle survey areas .....	235
Table 10-2:	The EM Flow™ settings .....	252
Table 10-3:	The EM Flow™ descriptor file .....	253
Table 10-4:	Regolith classes, unit codes, descriptions and map symbols. ....	288
Table 10-5:	Landform classes, unit codes, descriptions and map symbols. ....	290

**Geological and energy implications of the Pine Creek airborne electromagnetic (AEM) survey,  
Northern Territory, Australia**

# Executive Summary

## **THE PINE CREEK REGION AIRBORNE ELECTROMAGNETIC (AEM) SURVEY, NORTHERN TERRITORY**

Funded by the Australian Government's Onshore Energy Security Program (OESP) the Pine Creek airborne electromagnetic (AEM) survey was flown over the Pine Creek Orogen and parts of the McArthur, Victoria River and Daly Basins in the Northern Territory between August 2008 and 24th May 2009. The survey comprises three survey areas: Kombolgie, east of Kakadu National Park; Woolner Granite, near Darwin; and, Rum Jungle, west of Kakadu National Park. The Pine Creek survey was the second regional AEM survey flown in Australia as part of the OESP managed by Geoscience Australia (GA).

The survey cost approximately \$3 745 000 and collected 29 900 line-kilometres of new data at various line spacings (555 m, 1666 m and 5000 m) and covered approximately 74 000 km<sup>2</sup>. The Woolner Granite and Rum Jungle survey areas were flown by Fugro Airborne Surveys Pty. Ltd. (FAS) using the TEMPEST™ time-domain AEM system. The Kombolgie survey area was flown by Geotech Airborne Pty. Ltd using the VTEM™ time-domain AEM system.

The Pine Creek AEM survey was designed to deliver reliable, pre-competitive AEM data to promote exploration for uranium, copper-gold, base metals, tin and nickel in both brownfield and greenfield areas. The survey area hosts several uranium deposits, including the Ranger Uranium Mine, Rum Jungle and Nabarlek.

Airborne electromagnetic data were subjected to quality assurance and quality control procedures before being inverted using sample-by-sample GA layered earth inversion (GA–LEI) software. Data products released to the public include the contractor-supplied data, ASCII format GA–LEI data, PDF-format multiplots of GA–LEI line data and georeferenced raster images of the GA–LEI conductivity sections, GA–LEI conductance grids, GA–LEI conductivity depth slices and GA–LEI conductivity elevation slices. The GA–LEI data were validated using both confidential and public-domain drill hole conductivity data collected during field trips to the region by GA staff and from public-domain drill hole lithological data compiled during the data processing phase of the survey. AEM provides a unique dataset which gives depth information about geological features in the shallow crust at a regional scale. The Pine Creek regional AEM data are very useful in assisting mineral exploration (including uranium) in the top few hundred metres below surface. The surveys also indicate where more detailed airborne and ground surveys would add maximum value for exploration.

Interpretation of AEM data in the Pine Creek region has shown that AEM can successfully map critical elements of prospective unconformity-related uranium systems. Those critical elements include: the unconformity at the base of the Katherine River and Tolmer groups; the thickness of the Katherine River and Tolmer groups above the unconformity, the metasedimentary rocks below the unconformity (especially rocks containing reductants); and, faults in the metasedimentary rocks. The interpretation of these data has demonstrated that a regional-scale AEM survey in combination with drill-hole data can help to create a 3D model of basin architecture. The example given in this report is the McArthur River and Birrindudu basins in the Pine Creek region. This architecture can provide information on the direction of fluid flow during diagenesis of basin sediments and thereby outline areas prospective for unconformity-related uranium systems.

The Pine Creek Province is prospective for unconformity related uranium deposits, particularly where the Kombolgie Sandstone (latest Palaeoproterozoic) of the McArthur Basin unconformably overlies early Palaeoproterozoic metasediments of the Pine Creek Orogen. There is also potential for sandstone-hosted and Westmoreland-type deposits associated with mafic rocks (such as Oenpelli Dolerite) within the sandstone south of Rum Jungle, and further to the southeast lies an area with potential for buried Cenozoic palaeochannel-hosted uranium deposits.



# 1 Introduction

*M.T. Costelloe and M.A. Craig*

Airborne Electromagnetic (AEM) geophysical systems commonly sense 150 m to 250 m into the earth's crust but up to 500 m in areas of resistive surface materials. Of Geoscience Australia's Onshore Energy Security Initiative commodities (Uranium, Thorium, hydrocarbons and geothermal), hydrocarbons and geothermal systems require information from deeper in the crust than AEM senses. Thorium resources are largely associated with mineral sands and can be explored for by more cost effective methods than AEM. Uranium is suitable for sensing by AEM systems.

Of the uranium mineral systems, AEM is best suited to providing geological context to unconformity style (depth to unconformity, distribution of graphitic units in basement, location of fluid pathways) and palaeochannel sandstone style (delimiting channel position and vertical form) deposits. Multiple moderate to large tonnage examples of these deposit types occur in fertile regions.

The Northern Territory and South Australia allow uranium mining and have active mines. Uranium exploration/mining is not allowed in Victoria and New South Wales. In Western Australia, the ban on mining in place since 2002 was removed in November 2008. However, there are no currently active uranium mines in Western Australia. National Parks and other areas excluded from the pegging of exploration tenements should not be over-flown except on operational/logistics grounds.

The Pine Creek Province in the Northern Territory is prospective for unconformity related uranium deposits, particularly where the Kombolgie Sandstone (latest Palaeoproterozoic) of the McArthur Basin unconformably overlies early Palaeoproterozoic metasediments of the Pine Creek Orogen. There is also potential for sandstone-hosted and Westmoreland-type deposits associated with mafic rocks (such as Oenpelli Dolerite) within the sandstone south of Rum Jungle, and east of the Southern Area is an area that has a potential for buried Cenozoic palaeochannel-hosted uranium.

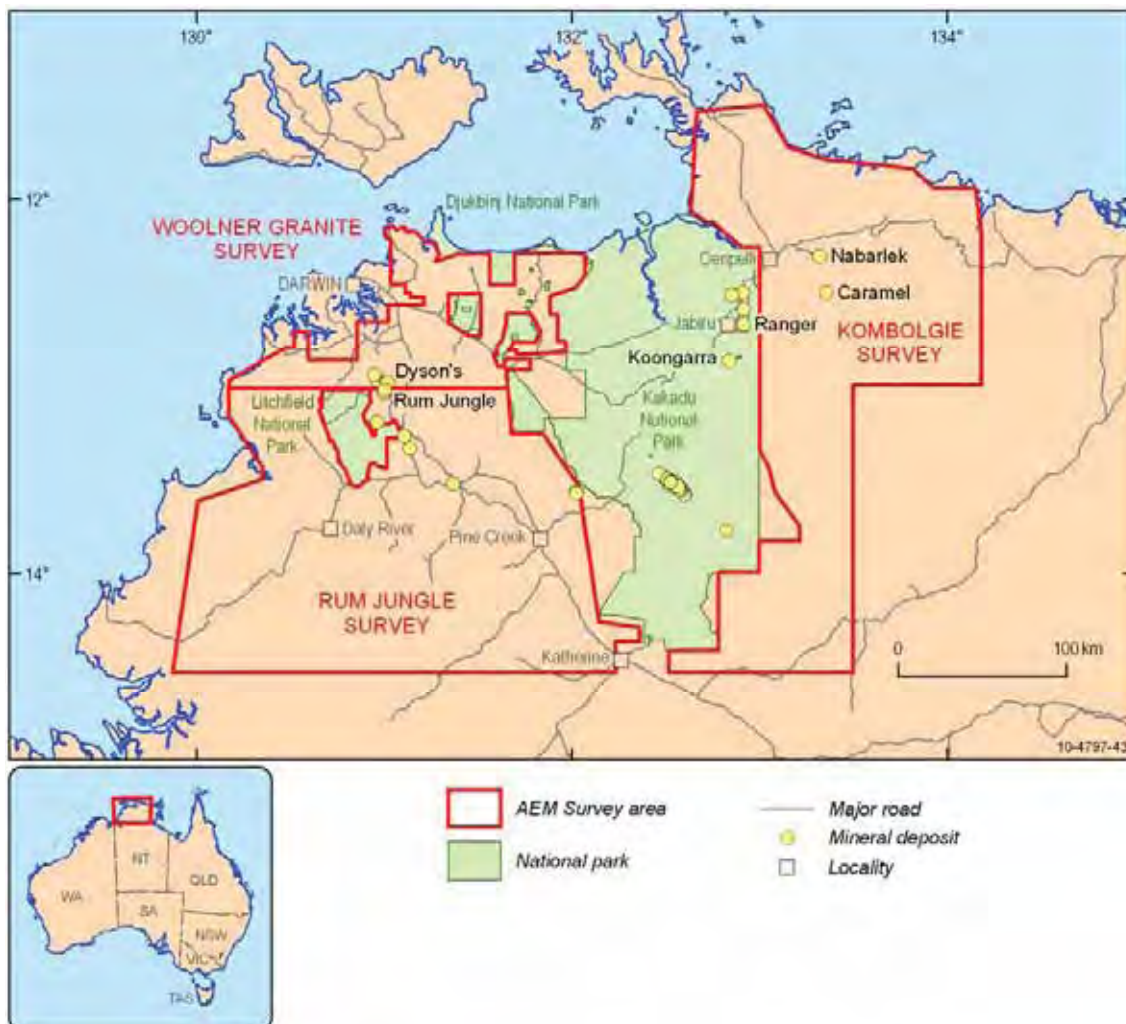


**Figure 1-1:** Pine Creek AEM survey area names, boundaries, mineral deposits, settlements, access roads and National Parks.

## 1.1 SURVEY DESIGN CHARACTERISTICS

The Pine Creek AEM survey was designed to deliver reliable, pre-competitive AEM data and scientific analysis of the energy resource potential of the Pine Creek region of the Northern Territory (Figure 1-1). This survey was the second regional AEM survey conducted within the Onshore Energy Security Program (OESP) and Geoscience Australia (GA). The Pine Creek AEM survey is the largest AEM survey to be undertaken in the Northern Territory.

The Pine Creek AEM survey comprises three areas: Kombolgie to the east of Kakadu National Park; Woolner Granite near Darwin; and, Rum Jungle to the west of Kakadu National Park. Data in the Woolner Granite and Rum Jungle survey areas were acquired using the TEMPEST™ fixed wing AEM system. The acquisition and processing were carried out by Fugro Airborne Surveys Pty. Ltd. (FAS), under contract to GA. In the Kombolgie survey area, the data were acquired by Geotech Airborne Pty. Ltd. (Geotech) using the VTEM helicopter AEM system.

The survey was conducted with the aims of reducing exploration risk, stimulating exploration investment and enhancing prospectivity for various energy commodities, particularly uranium, in the Pine Creek area. The survey area covers parts of the Alligator River, Cape Scott, Cobourg Peninsula,

Darwin, Fergusson River, Fog Bay, Junction Bay, Katherine, Milingimbi, Mount Evelyn, Pine Creek and Port Keats 1:250 000 map sheets (Costelloe et al., 2009).

The Pine Creek AEM survey was designed as a regional mapping program, primarily for the mapping of subsurface geological features that may be associated with uranium mineralisation. Potential uranium systems within the Pine Creek survey area include sandstone-hosted, roll-front or palaeochannel styles; Proterozoic unconformity sedimentary-related; Westmoreland-type; and Vein-type. The data are also useful for the interpretation for other commodities including metals and potable water as well as for landscape evolution studies.

## **1.2 SURVEY LOCATION**

The Pine Creek AEM survey area ([Figure 1–2](#)) is bounded by the approximate latitudes 11.5° S to 15° S. and approximate longitudes 129° E to 135° E. The total survey area is approximately 74 000 km<sup>2</sup>. The Pine Creek survey area is bounded by the Kakadu National Park, Litchfield National Park, Mary River National Park, Djukbinj National Park and Nitmiluk (Katherine) National Park, the coast, the area directly to the east of Darwin – which is within restricted air-space, the Mount Bundy Training Area, Tindal and Kangaroo Flats Training Area.

The survey area includes the large prospects of Ranger Uranium Mine, Rum Jungle, Ranger and Nabarlek. Many smaller uranium prospects occur in the Pine Creek Orogen. The region is also prospective for metals including copper, lead, zinc, gold, tin, rare earths, tantalum, tungsten, molybdenum and nickel. The following figure shows the extent of mining tenements in relation to the Pine Creek AEM survey area.

Road access to the region is limited. The Stuart Highway, connecting Darwin to Katherine, runs through the Woolner Granite and Rum Jungle survey areas and is an all-weather road. The Arnhem Highway is another all-weather road connecting Darwin to Jabiru. Secondary roads are *dry-weather only* and include access roads to Arnhem Land. Travel permits for Arnhem Land were obtained by contractors (Geotech) and GA staff for the logging program and field verification visits.

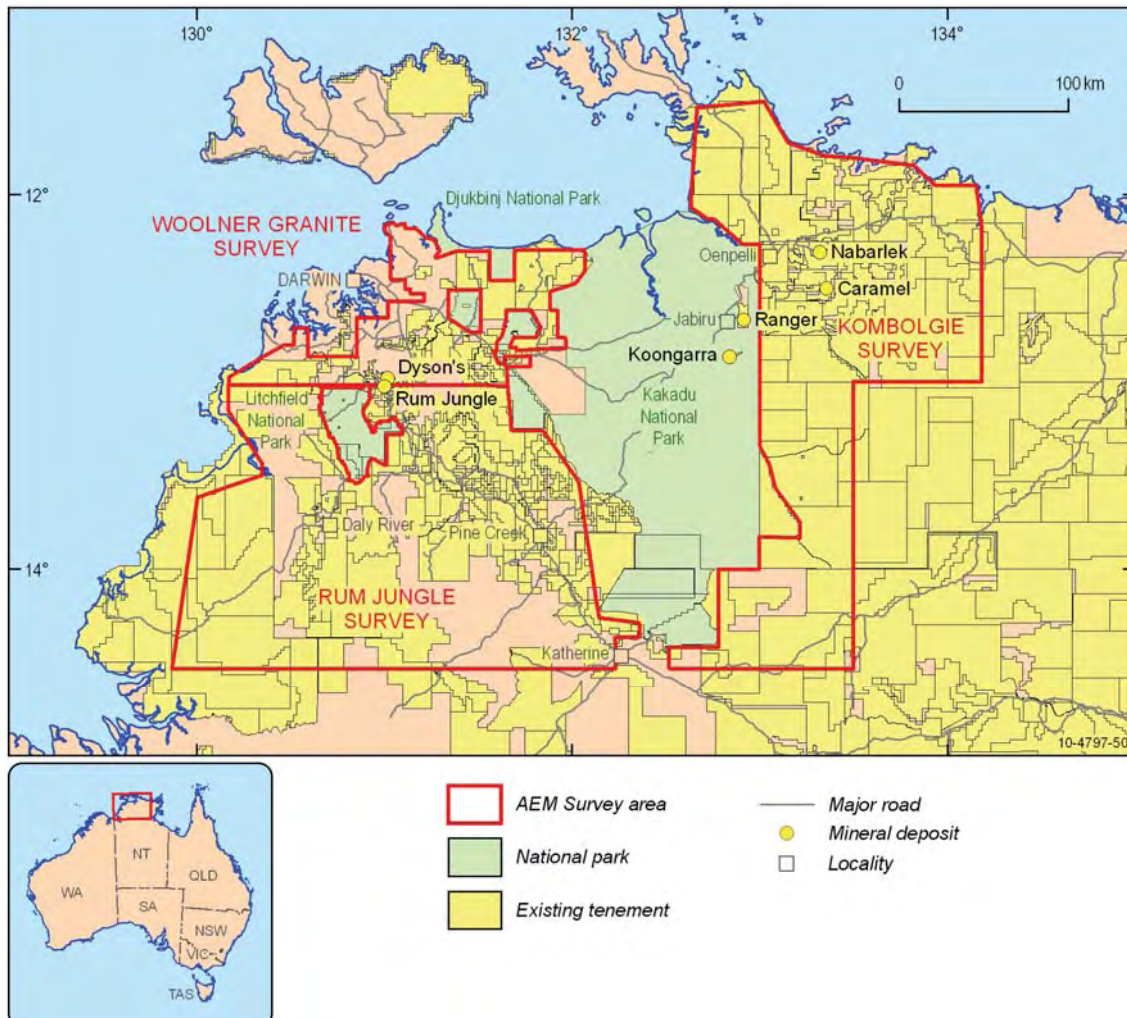


**Figure 1-2:** Location of National Parks, existing mining tenements, major uranium deposits in relation to the AEM survey boundaries.

### 1.3 SURVEY PURPOSE

The Pine Creek AEM survey was designed primarily to map regional geology and to uncover geological settings with uranium mineralisation potential. The region is well known for its uranium potential hosting many of Australia's uranium deposits including Jabiluka (204 000 t U<sub>3</sub>O<sub>8</sub>) and Ranger (143 000 t U<sub>3</sub>O<sub>8</sub>) (McKay and Miezitis, 2001; Beckitt, 2003; Ahmad, 1998; Lane et al., 2007). Through its Geological Reference Group, GA assessed the Pine Creek area as having high prospectivity for uranium mineral systems detectable using AEM. Assessment of the potential interest in uranium is shown in [Table 1-1](#) and a priority assessment is provided in [Table 1-2](#).

**Geological and energy implications of the Pine Creek airborne electromagnetic (AEM) survey,  
Northern Territory, Australia**

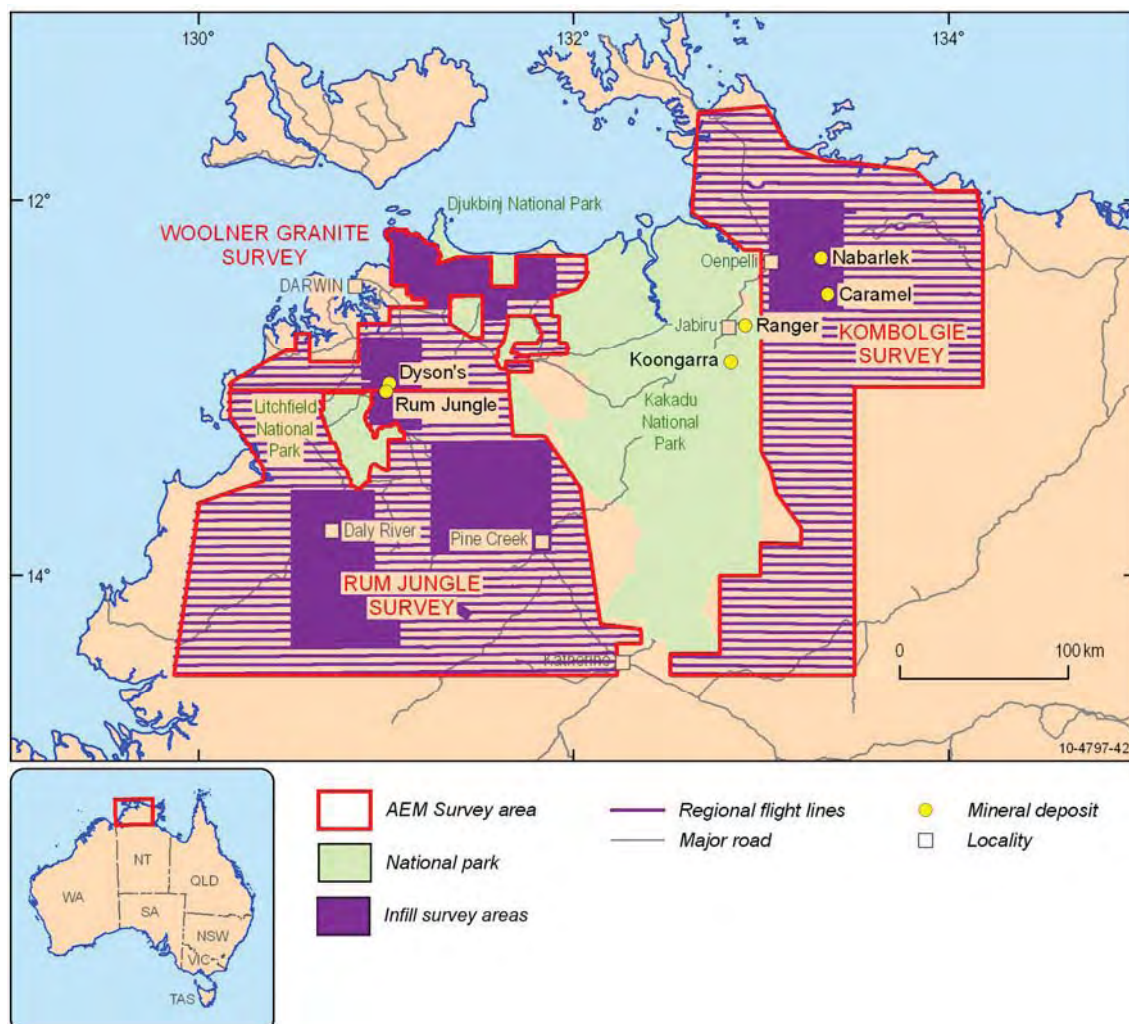


**Figure 1-3:** Pine Creek Regional survey line spacing. Woolner Granite survey area, the regional flight line spacing was 5 km with two Geoscience Australia (GA) infill blocks conducted at 1.67 km. Two National Water Commission (NWC) blocks were infilled at 555 m and an additional four company infill blocks were also within this survey area. The Rum Jungle survey area was flown with 5 km line spacing. Internal to the regional block three GA infill blocks were flown at 1.67 km line spacing. One small NWC block was flown at 250 m line spacing. The Kombolgie survey area was flown with 5 km line spacing. Internal to the regional block, one GA infill block was flown at 1.67 km line spacing.

**Table 1-1:** Potential Uranium interest in the proposed survey areas.

URANIUM POTENTIAL	HIGH
Uranium system	The Pine Creek Province is prospective for unconformity related uranium deposits, particularly where the Kombolgie Sandstone (latest Palaeoproterozoic) of the McArthur Basin unconformably overlies early Palaeoproterozoic metasediments of the Pine Creek Orogen. There is also potential for sandstone hosted and Westmoreland-type deposits associated with mafic rocks (such as Oenpelli Dolerite) within the sandstone. The area south of Rum Jungle and east of the Southern Area, have a potential for buried Cenozoic palaeochannel-hosted uranium.
Uranium deposits	There are many uranium deposits and occurrences in the Pine Creek region, with the main deposits being: Ranger, Jabiluka, Koongarra and Narbarlek in the Alligator Rivers area; Dysons and Whites in the Rum Jungle area; and, Coronation Hill in the South Alligator Valley area. All known deposits are located below the unconformity within Palaeoproterozoic metasediments.
Current exploration	A number of companies are exploring in the Pine Creek region including Energy Resources of Australia Ltd, Cameco Australia Ltd, Uranium Equities Limited and Compass Resources NL.
AEM targets	<ul style="list-style-type: none"> <li>• AEM acquisition will provide a 3D model of the basin architecture</li> <li>• (thickness of the Kombolgie Sandstone; palaeo-topography of the unconformity surface; major structures cutting the basement and the Kombolgie Sandstone; and the thickness of the palaeo-regolith)</li> <li>• Map graphitic conductors in the basement;</li> <li>• Locate major structures and possible mineralising fluid pathways;</li> <li>• Locate or negate existence of palaeochannels</li> <li>• Map regolith and Mesozoic-Cenozoic sediment thickness.</li> </ul>

**Table 1-2:** Priority Assessment

PINE CREEK – HIGH PRIORITY	
POSITIVES:	NEGATIVES:
Full NTGS support	Areas of intermittent basement outcrop have undergone a long period of exploration but of unknown effectiveness.
High potential for large uranium deposits above (Egress - type) and below (Ingress - type) the unconformity in areas of the Kombolgie Sandstone. This is a Greenfields area with little prior drilling.	
The western survey areas are extensively covered with regolith. Basement rocks are poorly magnetised and poorly discriminated in aeromagnetic data. Limited AEM surveys in the Pine Creek region have successfully mapped graphitic schists and the thickness of Kombolgie Sandstone to >600 m.	

## **1.4 UNCONFORMITY-RELATED URANIUM DEPOSITS.**

Unconformity-related uranium deposits occur at or are associated with major geological contact surfaces and are likely to be associated with basin structures involving very old (Proterozoic) rocks although some are associated with comparatively younger (Phanerozoic) rocks. These deposits tend to involve higher grades of uranium than many other deposits. The Athabasca Basin deposit of Canada is a typical example of such deposits and potential areas within the Pine Creek survey have been likened to this type of environment.

### **1.4.1 Sandstone uranium deposits**

Sandstone uranium deposits involve the highly soluble heavy metal uranium which has been transported from an original source located elsewhere and then precipitated in a host environment involving medium to coarse grained sandstone sediments. These sandstone sediments are generally marginal marine or continental fluvial in origin and may include minor shales and mudstones. Under favourable weathering conditions, involving oxidising environments uranium can be relocated commonly by groundwater circulation and then, under reducing conditions, it may be precipitated within the sandstones. Tabular bodies, roll-front or palaeochannel deposits may be the final deposit style recognised but commonly their uranium grade is low to medium.

## **1.5 OTHER MINERAL SYSTEMS**

The Pine Creek Orogen is highly prospective for a range of other minerals including gold, base metals, iron ore and water ([Figure 1-4](#)). Mines currently operating within the survey area extract gold, copper, cobalt, and nickel. Many prospects for other commodities occur widely throughout the area.

**Table 1-3:** Mining development summary (NT Gov: Orestruck, 2010)

COMPANY	PROJECT	LOCATION	PRODUCT
<b>MINES CURRENTLY OPERATING</b>			
Compass / HNC	Browns Oxide	Batchelor	Cu, Co, Ni
Crocodile Gold	Brocks Creek	Pine Creek	Gold
Crocodile Gold	Toms Gully	Mt Bundy	Gold
Crocodile Gold	Union Reefs	Pine Creek	Gold
Crocodile Gold	Howley	Pine Creek	Gold
<b>MINES PENDING</b>			
Crocodile Gold	Princess Louise	Pine Creek	Gold
Crocodile Gold	Cosmo Deep	Pine Creek	Gold
HAR (HNC)	Browns Oxide	Batchelor	Cu, Co, Ni
HAR (HNC)	Area 55	Batchelor	Cu, Co, Ni

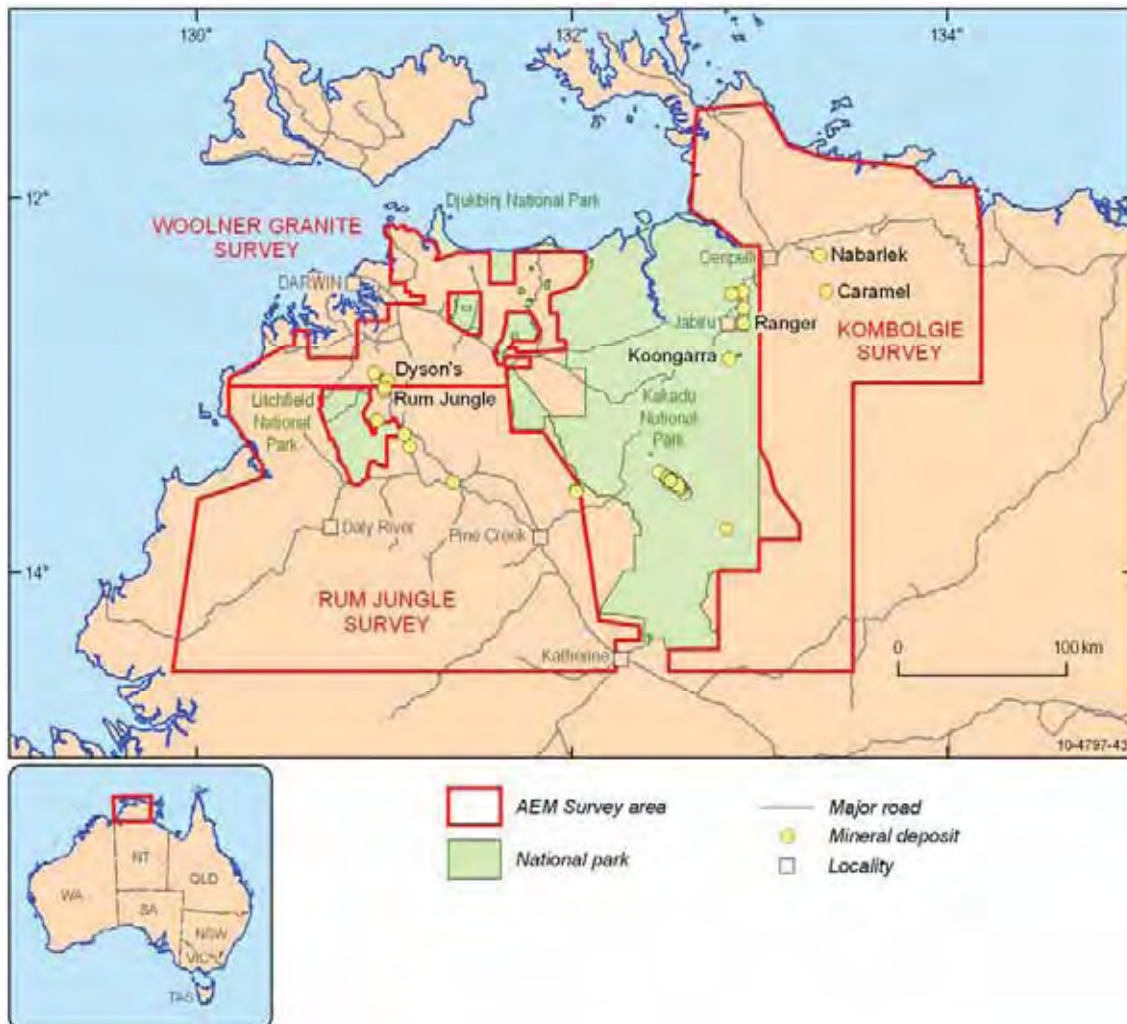


**Figure 1-4:** Major commodity (*Cu, Co, Ni, Gold and Uranium*) deposits and prospects occurring within the Pine Creek survey area. Commodity data are from the GA MINLOC database.

## 1.6 GROUNDWATER SYSTEMS

The Pine Creek region hosts groundwater systems associated with fractured rock aquifers, palaeovalleys and sedimentary units of various ages. These systems are exploited by Darwin residents, indigenous communities, farmers (agriculture) as well as mining and exploration operations. A successful joint project (the Northern Territory Coastal Plain project) involving the National Water Commission and Geoscience Australia was established to map seawater intrusion in coastal plain aquifers using airborne electromagnetic data. The AEM data collection was undertaken as a part of the Pine Creek survey. This hydrogeologically-focussed project utilised the Pine Creek AEM survey data in combination with additional geophysical, geological and hydrogeological datasets to assess the occurrence and potential risk of seawater intrusion into coastal aquifers in the Darwin peri-urban area as well as surface water – groundwater connectivity within the Daly Basin (English, 2007).

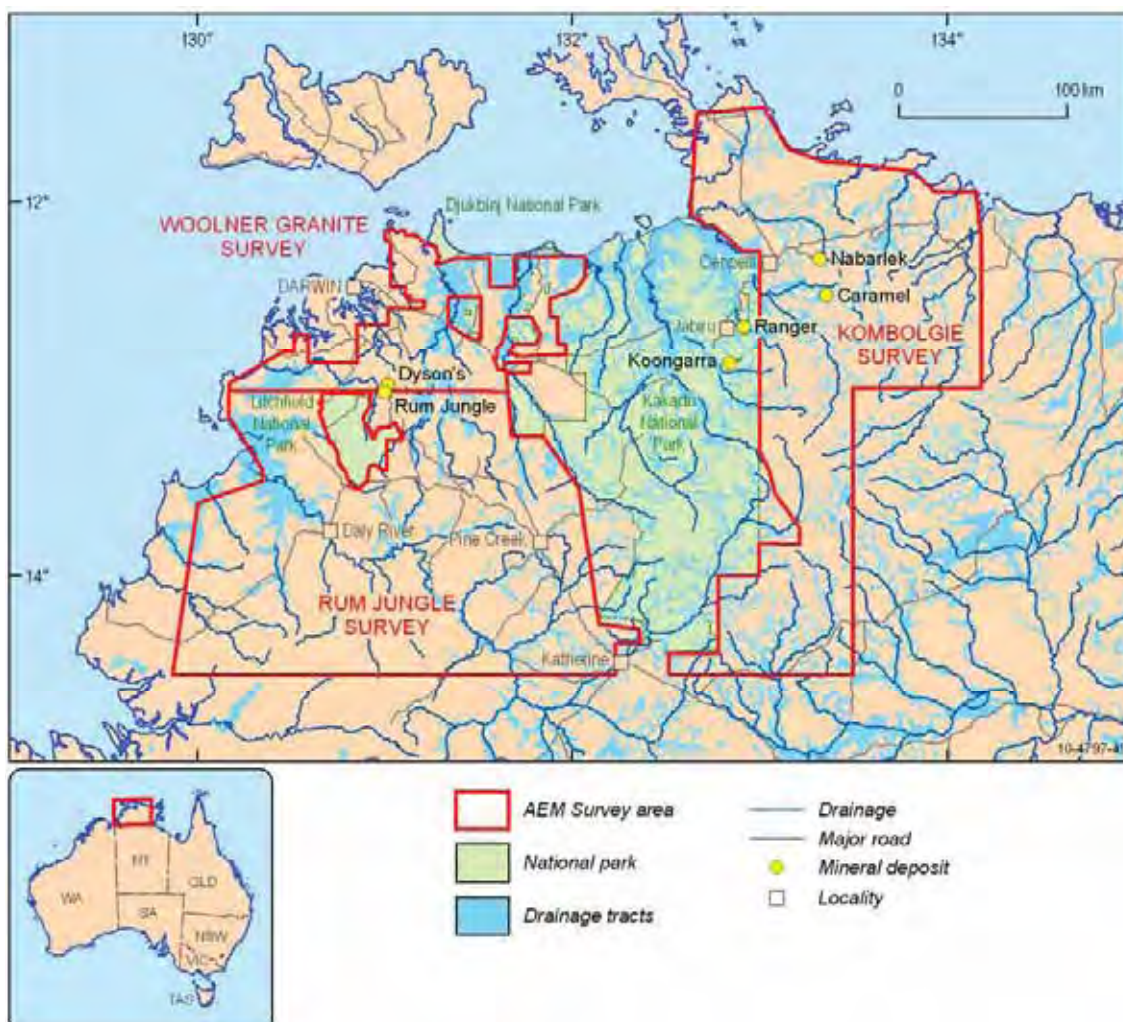


**Figure 1-5:** Major current drainage networks and lowland drainage tracts within the Pine Creek AEM survey area

## 1.7 SURVEY ECONOMIC FRAMEWORK

Funding of this work was by the Australian Government and was provided under the OESP to secure energy resources for Australia's future including uranium, petroleum and geothermal energy in areas that are under-explored for these commodities. The OESP funds for the Pine Creek survey were directed towards acquiring and providing pre-competitive data to the minerals and energy exploration industry for locating unconformity, palaeovalley and calcrete-hosted uranium and associated mineral systems, the results of which are the subject of this report.

## 1.8 SURVEY DESIGN CONSIDERATIONS

Flight planning exceeded 75 000 km<sup>2</sup>, which is larger than the state of Tasmania. The survey at its most northerly is flown along the coast and extends down to the township of Katherine. Survey flying was not undertaken close to Darwin as it is the largest and most populated city in the Northern Territory.

## **1.9 CLIMATE**

Climatic conditions (see [Appendix 10.4](#)) are an important consideration when planning any flight operations, but particularly so when planning airborne geophysical operations which must be flown much closer to ground level than normal aircraft operations. In the case of the Pine Creek AEM survey acquisition the aircraft was contracted by GA to maintain an average ground clearance of 121 m and the towed receiver (the “bird”) only 81 m. Therefore, accurate knowledge of atmospheric conditions is crucial to maintain both flight safety and data reproducibility.

Air temperature plays an important role in maximum take-off weight (MTOW) and aircraft endurance in aerial surveys. For some models of aircraft, particularly the Fugro CASA, as air temperature increases the flight duration decreases rapidly, up to 30 minutes duration decrease per 5°C increase in temperature. Details of survey aircraft flight considerations and other parameter affecting flight operations are detailed in a memorandum provided by Fugro Airborne Services.

Atmospheric turbulence increases as daytime temperatures increase, making successful data acquisition difficult. Severe turbulence results in “coil knock events” that introduce noise into the processed data (Lawrence and Stenning, 2008).

Pine Creek region also experiences a high degree of spheric activity. A spheric is the electromagnetic signal associated with lightning activity. These signals travel large distances around the Earth. Background levels of spherics are present at all times from lightning activity in tropical areas of the world. Additional higher amplitude signals are produced by “local” lightning activity, at distances of kilometres to hundreds of kilometres (Lawrence and Stenning, 2008). Darwin has the highest recorded number of average annual thunder days in Australia. Most of this storm activity occurs during the build-up to the summer monsoon and during it; flight planning needs to ensure operations are scheduled away from this time. The survey logistics report confirms a high number of no-fly days due to high spherics activity.

## **1.10 NATIONAL PARKS**

National Parks in the Pine Creek survey area include: Kakadu National Park, Litchfield National Park, Mary River National Park, Djukbinj National Park and Nitmiluk National Park. Information packs were sent to all National Park boards. Consensus was reached for a 1 km overfly ([Figure 1–6](#)) at the edges of Litchfield National Park, Mary River National Park and Djukbinj National Park for the fixed wing aircrafts (Fugro – TEMPEST™ system). A small amount of overflying is necessary at the start and end of each flight line ([Figure 1–6](#)) to reduce geophysical data processing artefacts at the ends of lines.

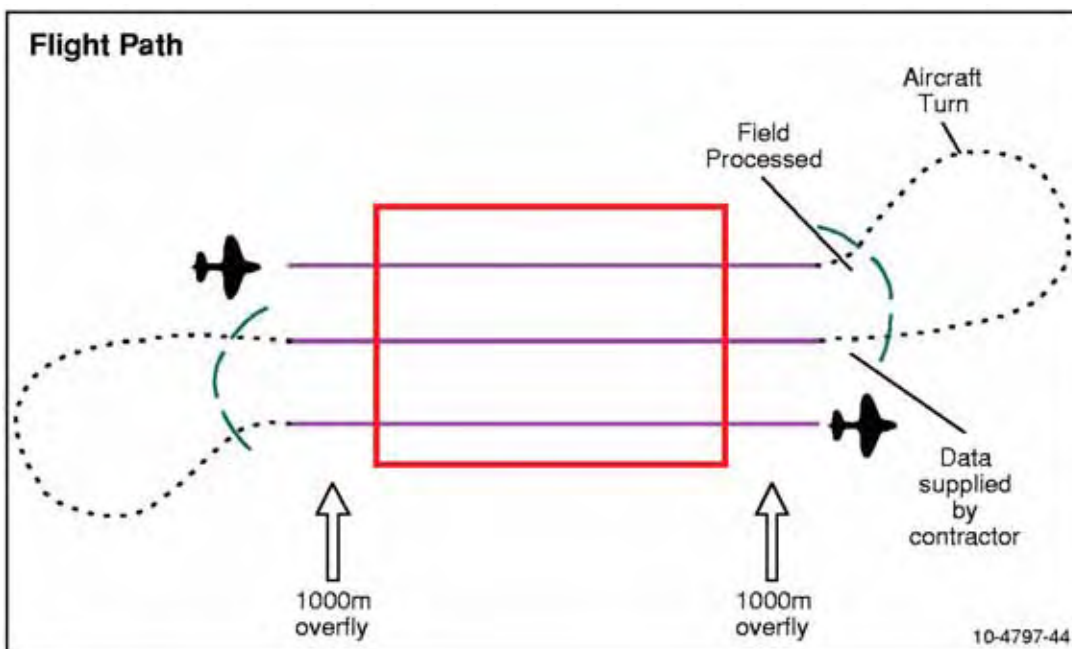


**Figure 1-6:** Flight path flying, trimming and delivery.

### 1.11 TERRAIN (DRAPE)

Prior to requesting tenders for AEM flight operations a “drape” check is performed. The drape check tests whether the proposed survey can be performed by a nominated aircraft, within its safety specifications over the survey area, or whether the proposed flight plan or aircraft type needs to be modified. The aircraft specifications are set out in a deed of standing offer between GA and survey contracting companies. The drape check is a necessary part of flight planning that ensures that it is legally possible to fly the survey with the nominated aircraft within the Federal legislation governing aerial survey operations.

The drape check is performed by entering a digital elevation model of the survey area, together with the proposed flight lines, into specialist GA-proprietary software to highlight areas where the flight lines cross terrain that would cause the aircraft to exceed its maximum rate of climb. For instance, the Fugro CASA aircraft fitted with the TEMPEST™ TEM system has an average rate of climb of only 100 m/km. [Figure 1-7](#) illustrates the results of the drape analysis, indicating that the bulk of the Pine Creek survey area would allow the Fugro CASA aircraft to operate within its specifications at the contracted flying height of 121 m above ground. In areas where the drape check indicated that the aircraft would exceed its specifications, permission was given to allow the aircraft to fly at slightly higher altitude to provide adequate ground clearance.

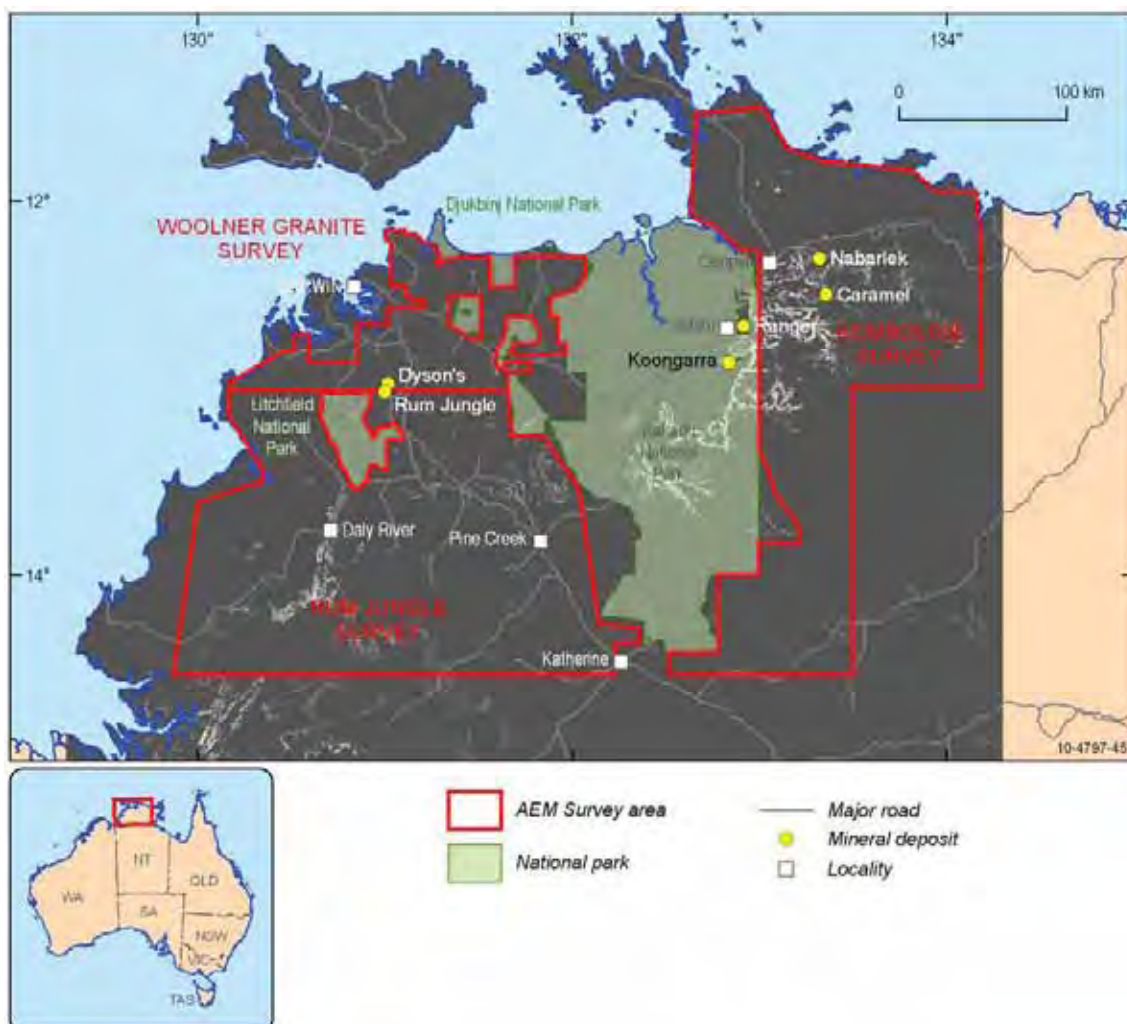


**Figure 1-7:** Drape analysis results for the Pine Creek AEM survey area. White dots indicate areas where the contracted flight parameters were altered to provide adequate terrain clearance for the aircraft and towed receiver bird.

## 1.12 LAND ACCESS AND NATIVE TITLE ISSUES

The traditional owners of land within the survey boundaries were identified via the National Native Title Tribunal. The principal traditional owners were recognised as members of the Northern Land Council, who have Native Title Determinations, and Native Title Claims (Figure 1-8). Communications with the Northern Land Council (NLC) commenced in November 2007 with a letter outlining the survey. Communications included letters, emails and personal meetings with traditional owners outlining the survey boundaries for the purpose of identifying the potential social and cultural impacts of the project, giving an outline of how the survey would be implemented and showing maps that outlined the areas where the survey would be focused.

Stuart Huys from the Australian Archaeological Association Inc. (AASC) and Centre for Historic and Military Archaeology (CHMA) was contracted by GA to undertake a desk top cultural sensitivity assessment for the Woolner – Rum Jungle survey areas. Stuart Huys submitted a desktop cultural sensitivity report to GA.

Rachel Wedd from Radion was contracted by Geoscience Australia (GA) to undertake consultation with Indigenous communities within the West Arnhem region of the Northern Territory in relation to the Pine Creek survey proposed for the Kombolgie Region. Rachel Wedd submitted a desktop cultural sensitivity report which included a communications summary to GA.

As a result of the discussion the Pine Creek survey boundary was modified to exclude sensitive areas. Instruction was provided to the pilots to fly at considerable height and at least 1 000 m around outposts and sites nominated by traditional owners during the course of survey.

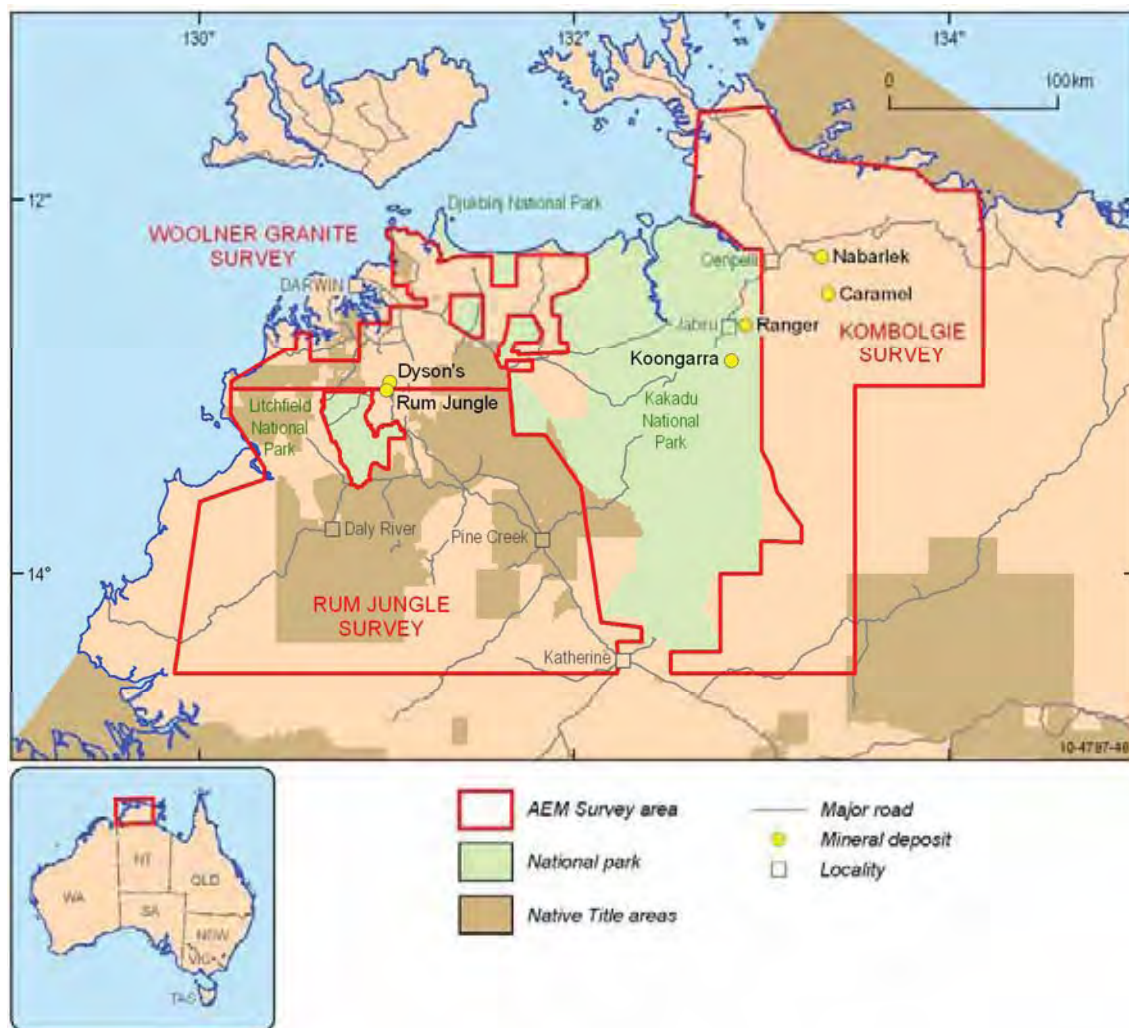


**Figure 1-8:** Native Title Application and Determination Areas recognised by the Federal Court (30 June 2007) for the Pine Creek survey areas.

### 1.13 OTHER NO FLY ZONES

Other no fly zones included the area directly to the east of Darwin – which is within restricted Darwin International Airport airspace, the Mount Bundy Training Area, RAAF Base Tindal, Kangaroo Flats Training Area and the Nina Keener wildlife sanctuary. During December survey flights were also limited by RAAF operations.

## **1.14 AIRCRAFT ACCESS**

Aircraft access in the region is limited, with private all-weather airstrips utilised at Katherine, Bachelor and Daly River and Jabiru. Airstrips in King River, Oenpelli, Murgeonella, Noni, South Alligator and Nabarlek were used with permission from traditional owners. Adequate road access to these airstrips for fuel pre-placement was also another important consideration for aerial survey operations for both fixed wing aircraft and helicopters.

## **1.15 FORWARD MODELLING**

The Pine Creek AEM survey was advertised to aerial geophysics contractors on the GA deed of standing offer and four contractors with five different AEM systems responded with an expression of interest. Before the survey could proceed, the different AEM systems needed to be assessed by forward modelling to test each system's expected performance in the survey area. This was achieved by creating a series of synthetic geological settings which approximated the known target conditions for the Pine Creek region. These scenarios were transferred into electrical models and entered into GA-proprietary software which tests for probability of detection with a false alarm rate of 1%. When all models were deemed of equal relevance in this assessment the Fugro TEMPEST™ TEM was awarded the Woolner Granite and Rum Jungle survey areas and the Geotech Airborne VTEM™ system was awarded the Kombolgie survey. Details of the geological models, electrical models and forward model results are discussed further in [Section 5](#) of this report.

## **1.16 COMMUNICATION STRATEGY**

Geoscience Australia was aware of the high visual impact of this type of survey and the amount of scientific interest it might generate within local, state and federal government agencies, exploration companies, title holders and the general public. Together with the contractors, GA developed a communication strategy including:

- Letters to the relevant national park board;
- Meetings with relevant indigenous communities and councils;
- Notices and advertisements in local papers;
- Posters and pamphlets to relevant national park boards;
- Letters to all landholders, schools and government agencies in the area; and,
- E-mails to all tenement holders in the area.

The Pine Creek hotline was set up, this was a free call 24 hour phone line to GA (1800 091 964) and was printed on all communication material.

Communication also included presentations to relevant parties and the industry in general including:

- Oral and poster presentations at the Australian Society of Exploration Geophysicists' conference in 2009;
- Poster presentations at the Geological Survey of Western Australia's open day in Perth, WA, in 2009;

- Oral presentations at the Australian Institute of Mining and Metallurgy's International Uranium Conference in Darwin, NT, in 2009;
- An oral presentation at the Australian Regolith Geoscientists Association conference in Arkaroola, SA, February 2010;
- Oral presentations at the Australasian Institute for mining and Metallurgy International uranium Conference in Adelaide, SA, in June 2010;
- Oral and poster presentations at the Australian Earth Science Convention in Canberra, ACT, in July 2010; and,
- Oral and poster presentations at the Australian Society for Exploration Geophysics conference in Sydney, NSW, in August 2010.
- A one-day workshop for state government and industry representatives in Alice Springs March 2011;
- A one-day workshop for Western Australian state government and industry representatives in Perth June 2011;
- A presentation for Northern Territory government, industry representatives, and a Chinese Economic Delegation at the NT Annual Geoscience Exploration Conference (AGES) in Alice Springs March 2011;
- A presentation for Western Australia government, industry representatives, and international delegates of the AusIMM Conference International Uranium Conference in Perth, June 2011; and,
- Regular articles about the AEM project design and results in Preview: The Magazine of the Australian Society of Exploration Geophysicists, 2011;

### **1.17 FINAL SURVEY DESIGN**

The final survey design was set after careful consideration by the Geological Reference Group, the Geophysical Reference Group, traditional owner, subscribing companies and the contractors. A wide range of cultural, geological, geophysical, remote sensing and topographical data were compiled covering the Pine Creek survey area over a period of several months to aid the final survey design process. These data included:

- Cultural data including mines, roads, tracks, pipelines;
- Cadastral data including place names;
- Topographic data;
- Hydrological data including water courses and lakes;
- Tenement boundaries from the NTGS Data and Software Centre;

- Mineral occurrences from the NTGS Data and Software Centre;
- Mineral exploration drill hole locations;
- Geoscience Australia 1:1 000 000 Surface Geology of Australia (Stewart, 2008 );
- Geoscience Australia Radiometric Map of Australia (Minty et al., 2009);
- Magnetic Anomaly Map of the Australian Region;
- Gravity Anomaly of the Australian Region Map;
- Reduced-to-pole (RTP) total magnetics;
- RTP 1st vertical derivative magnetics;
- Shuttle Radar Topography Mission (SRTM) 3 second (90 m) digital elevation model;
- Shuttle Radar Topography Mission (SRTM) 1 second (30 m) digital elevation model;
- Landsat Thematic Mapper mosaic;
- Advanced Spaceborne Thermal Emission and Reflection radiometer (ASTER) mosaic; and,
- Existing ground electromagnetic and AEM surveys.

Survey boundaries were determined by integrating the above data with consideration for the geological targets. Flight line spacing was determined by assessing the extents of known geological units and structures and predicted uranium potential. The data interpretation process used magnetics, gravity, radiometrics and geology associated with sandstone-hosted: roll-front or palaeochannel styles; Proterozoic Unconformity Sedimentary-related style; Westmoreland-type; and Vein-type uranium mineralisation to identify subsurface geological features. The process indicated that regional geological features could be mapped with 5 km flight lines. This criterion helped define the final line spacing in the survey area.

The final survey design included the following generalisations which influence the line spacing and survey boundaries.

High uranium prospectivity and low risk areas:

- Unconformity related uranium deposits, where the Mesoproterozoic Kombolgie Sandstone of the McArthur Basin unconformably overlies Archaean to Palaeoproterozoic granites and metasediments of the Pine Creek Orogen.
- Sandstone hosted uranium (Westmoreland style) where the Kombolgie Sandstone is intruded by Oenpelli Dolerite.

Lower uranium prospectivity, higher risk areas:

- Regolith and Mesozoic-Cenozoic sediment thickness
- The thickness of the Kombolgie Sandstone
- Locate conductors within the basement
- Locate major structures.
- Sandstone-hosted: roll-front or palaeochannel styles within Permian, Mesozoic or Cenozoic sediments in palaeovalleys or sediment sheets adjacent to U-rich granitoids, for example the Waterhouse granites; and,
- Vein-type: Within the Palaeoproterozoic rocks of the Pine Creek Orogen.

In the Woolner Granite survey area, the regional flight line spacing was 5 km with two GA infill blocks conducted at 1.67 km. Two NWC blocks were infilled at 555 m and an additional four company infill blocks were also within this survey area.

The Rum Jungle survey area was flown with 5 km line spacing. Internal to the regional block three GA infill blocks were flown at 1.67 km line spacing. One small NWC block was flown at 250 m line spacing and an additional twenty infill blocks, funded by subscriber companies, were flown at various line spacings.

The Kombolgie survey area was flown with 5 km line spacing. Internal to the regional block, one GA infill block was flown at 1.67 km line spacing. Two internal blocks and one external block were flown and were funded by subscriber companies.

#### **1.18 SURVEY PARTNERS, CONTRIBUTORS AND COST**

The Pine Creek AEM survey was opened to public subscription in the interests of stimulating further exploration in the region. The intention to fly the survey was advertised in GA's Minerals Alert email notification service and via GA's magazine publication, AusGEO News, email and phone calls directly to tenement holders and through various conferences, inviting partners to purchase infill flight lines. Contributors were also sought for drill-hole data, land access and field assistance.

A total of twelve companies expressed an interest to the initial subscription request. Further negotiations with these interested parties resulted in nine that decided to purchase infill flight lines within the survey area ([Table 1–2](#)). The companies paid the same line kilometre amount as GA when purchasing the infill lines.

**Table 1-4:** Pine Creek AEM survey infill subscribers.

SUBSCRIBER NAME	NUMBER OF INFILL AREAS	SURVEY AREA
Crossland Uranium Mines Ltd.	3	Rum Jungle
Hapsburg Exploration Pty. Ltd.	1	Rum Jungle
National Water Commission	3	Woolner and Rum Jungle
Rio Tinto Exploration Pty. Ltd.	2	Kombolgie
Rum Jungle Uranium*	7	Woolner and Rum Jungle
Southern Uranium Ltd.	1	Woolner
Thundelarra Exploration	6	Rum Jungle
United Uranium Ltd.	2	Rum Jungle and Kombolgie
Uranex NL.	5	Rum Jungle

\*now known as Rum Jungle Resources Ltd

A number of non-subscribers also contributed in-kind support: Northern Territory Geological Survey, Natural Resources, Environment, The Arts and Sport (NRETAS), Cameco Australia, Uranium Equities Ltd and Energy Resources of Australia Ltd for field support as well as land access, access to open borehole and lithological logs supporting the conductivity logging phase of the program

In all, infill companies contributed \$1.14 million to the survey budget and GA, through the OESP contributed \$2.6 million for a total survey cost of \$3.74 million, a survey area of approximately 74 000 km<sup>2</sup> and length 29 900 line km. Infill areas to the main survey are shown in [Figure 1-3](#). All infill companies expected to spend an amount equal or greater than their contribution to the AEM survey in follow-up exploration programs after the AEM data were delivered. This is conservatively estimated to be worth an additional \$2 million in industry exploration investment in the region.

## 1.19 CLIMATE

The survey area is part of Australia's wet-dry tropical climatic zone. It is essentially a monsoonal climate with a short summer wet season lasting between 3 to 5 months with moderate to intense rainfall (1.5 m, annually), which declines by as much as 50% away from the coastal region. This decline is especially noticeable at Katherine, some 200 km inland to the south-east, where annual rainfall is approximately 90 cm. The region has a contrasting longer dry winter period lasting between 7 to 9 months. The period in which most rainfall occurs is generally between the months of November through to April.

The temperatures in the survey region are generally quite high and are around 34°C at Darwin and other nearby coastal regions. Such high temperatures are usual in the approach to the wet season and are accompanied by high relative humidity with values around 70%. The humidity is considerably lower in inland regions, but in contrast, temperatures are more likely to be very much higher with values in excess of 95°C being frequent especially well away from the coastal regions. In the dry period, the humidity nearer the coast may be more often around 60% and sometimes even a little lower. Temperatures may be more commonly around 28°C in coastal and near-coastal locations but noticeably higher inland. Flooding in the wet season is not uncommon but rare in the dry period.

The climate of the survey region and its daily weather variability during the AEM survey has a significant impact on the AEM acquisition. Contractor operations were affected and consequently data delivery timetables required adjustment.

## **1.20 VEGETATION**

The uplands parts of the survey area are characterised by mixed open forest and woodland communities, and palm scrub. However, in wetter lowlands areas, grasslands or even swampy grasslands are dominant. Eucalypts, Banksias, Grevilleas are easily recognised in the forest communities whereas Pandanus and Melaleucas feature strongly in fringe communities adjacent to wetter areas. Tableland regions have some scattered, stunted forest community members present but more frequently consist of large areas of spinifex grasslands dotted with stunted trees.

Most notable in the region is extensive growth of sorghum grass, especially on the wetter plains in the region. Sorghum is often 3 m or more high and subject to extensive burning during the months prior to the dry season. Fires often result from lightning strikes but sometimes are lit deliberately in the course of extensive fuel reduction programs in and around major National and Territory parklands.

## **1.21 TOPOGRAPHY**

The survey region contains a variety of landscape units and this diversity is best portrayed by using simple physiographic subdivisions. An entirely adequate subdivision of a major part of the survey area was produced by Walpole et al, (1968) in the course of their previous geological investigations. [Figure 1–9](#) shows current physiographic subdivisions of the survey area whereas [Figure 1–10](#) gives a much-simplified physiographic division of the area as shown by the SRTM DEM image.

**Geological and energy implications of the Pine Creek airborne electromagnetic (AEM) survey,  
Northern Territory, Australia**

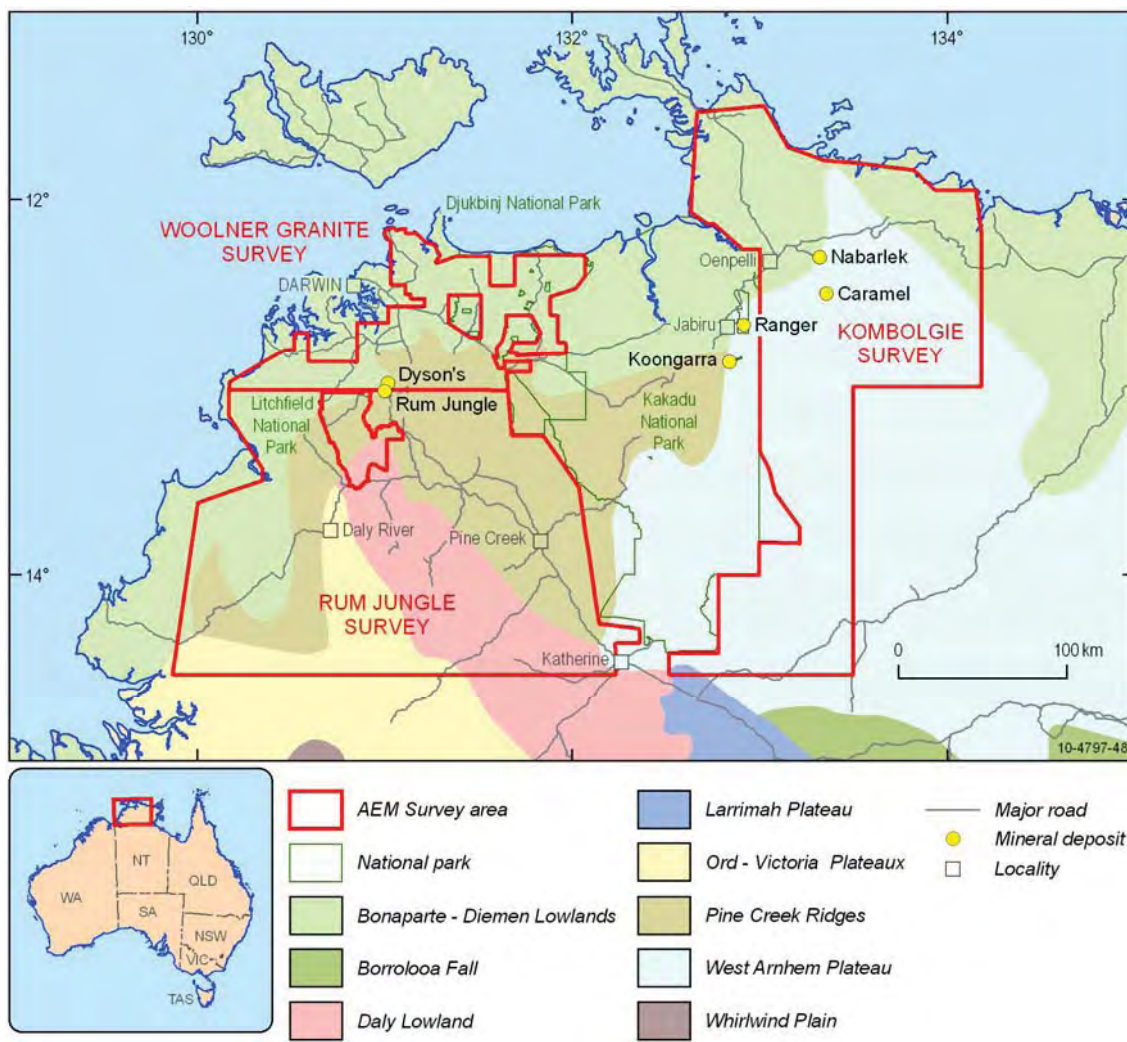


**Figure 1-9:** Major physiographic elements within and surrounding the Pine Creek AEM Survey

**Geological and energy implications of the Pine Creek airborne electromagnetic (AEM) survey,  
Northern Territory, Australia**

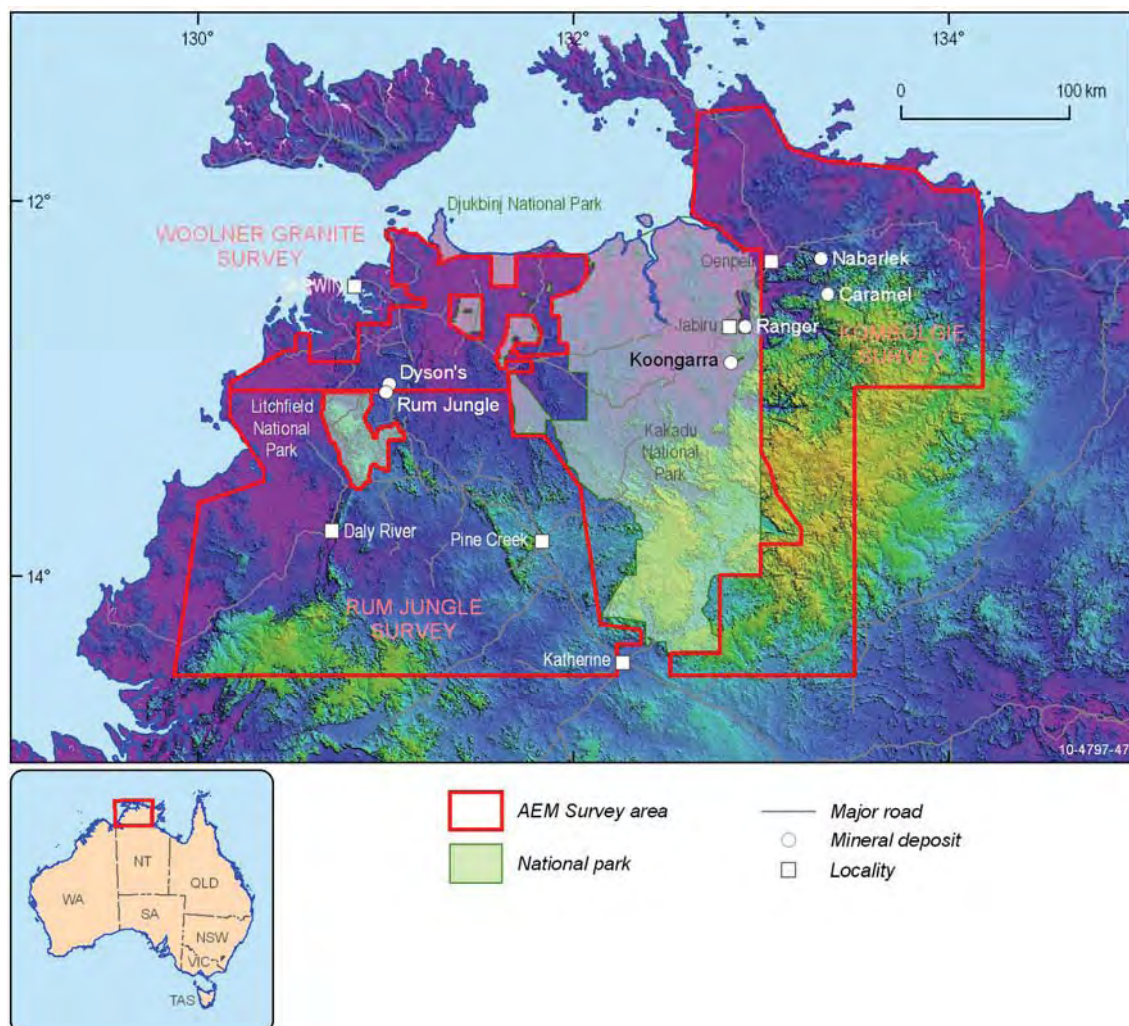


**Figure 1-10:** Simplified physiographic areas within the AEM Survey areas as shown by an SRTM DEM image. Blue areas are general lowland regions and green areas are higher parts of the landscape

## **1.22 REFERENCES**

- Ahmad, M. 1998. Geology and mineral deposits of the Pine Creek Inlier and McArthur basin, Northern Territory. AGSO Journal of Australian Geology and Geophysics 17(3) p1-17
- Beckitt, G., 2003. Exploration for unconformity uranium in Arnhem Land (NT): Exploration Geophysics, **34**, 137-142.
- Costelloe, M., Sorensen, C. & English, P. 2009. Pine Creek Airborne Electromagnetic Survey, Onshore Energy and Minerals, Geoscience Australia. *ASEG 2009, Extended Abstracts*.
- English, P., 2007. Memorandum of understanding in relation to funding from the Australian Government water fund for the following groundwater assessment initiative project: northern territory coastal plain: mapping seawater intrusion in coastal plain aquifers using airborne electromagnetic data. Geoscience Australia, Canberra.
- Lane, R., Beckitt, G., & Duffett, M., 2007. 3D geological mapping and potential field modelling of West Arnhem Land, Northern Territory. *ASEG Extended Abstracts 2007*.
- Lawrence, M. and Stenning, L., 2008. Paterson North Airborne Electromagnetic (AEM) Mapping Survey - Acquisition and Processing Report for Geoscience Australia. Fugro Airborne Surveys. **Unpublished report**, 108 p.
- McKay, A. D. and Miezitis, Y., 2001, Australia's uranium resources, geology and development of deposits. *Mineral Resource Report*, AGSO - Geoscience Australia, Canberra. **Mineral Resource Report 1**, 200 p.
- Minty, B.R.S., Franklin, R., Milligan, P.R., Richardson, L.M., and Wilford, J., 2008. Radiometric Map of Australia (First Edition), scale 1:5 000 000, Geoscience Australia, Canberra.
- Northern Territory Government, 2010. Mining development summary (accessed 2010)  
(<http://www.nt.gov.au/d/orestruck/>)
- Stewart, A. J., 2008. Surface Geology of Australia 1:1 000 000 scale, Western Australia. Geoscience Australia, Canberra. (First viewed at web address:  
[http://www.ga.gov.au/minerals/research/national/nat\\_maps/nat\\_geol\\_maps.jsp](http://www.ga.gov.au/minerals/research/national/nat_maps/nat_geol_maps.jsp).)
- Walpole B.P., Crohn P.W., Dunn P.R. & Randal, M.A., 1968. Geology of the Katherine-Darwin region, Northern Territory. Bureau of Mineral Resources, Geology and Geophysics, Bulletin 82, 304 pp.

## 2 Previous and concurrent work

*M.A. Craig and M.T. Costelloe*

### 2.1 GEOLOGICAL MAPPING

The Pine Creek AEM survey area includes a number of 1:2 500 000, 1:1 000 000, 1:250 000 and 1:100 000 scale and special edition geological maps. The entire area is mapped at 1:2 500 000 scale by the Northern Territory Geological Survey (NTGS) 1:1 000 000 by the Geoscience Australia Surface Geology of Australia (released in 2009), which was compiled from 1:250 000 maps of the area. NTGS 1:250 000 map series dates from 1987 to the most recent published in 2010. Mapping of the 1:100 000 series commenced in 1980 and is ongoing. The available map sheet names and numbers associated with the AEM survey area are provided in [Figure 2–1](#). A comprehensive list is given in [Table 2–1](#).

Geological interpretations for the Pine Creek AEM survey rely principally on the NT portion of the GA 1:1 000 000 Surface Geology Map of Australia together with airborne geophysical datasets (see [p 35](#)), drill hole information (described below) and NTGS's Pine Creek Interpreted Solid Geology. The project generated three solid geology maps respectively covering the Narbalek, Woolner and Birrindudu areas. The solid geology interpretation was based on magnetic data, gravity data inversions, GA LEI and EMFlow™ AEM data and limited borehole data as well as the NTGS solid geology mapping

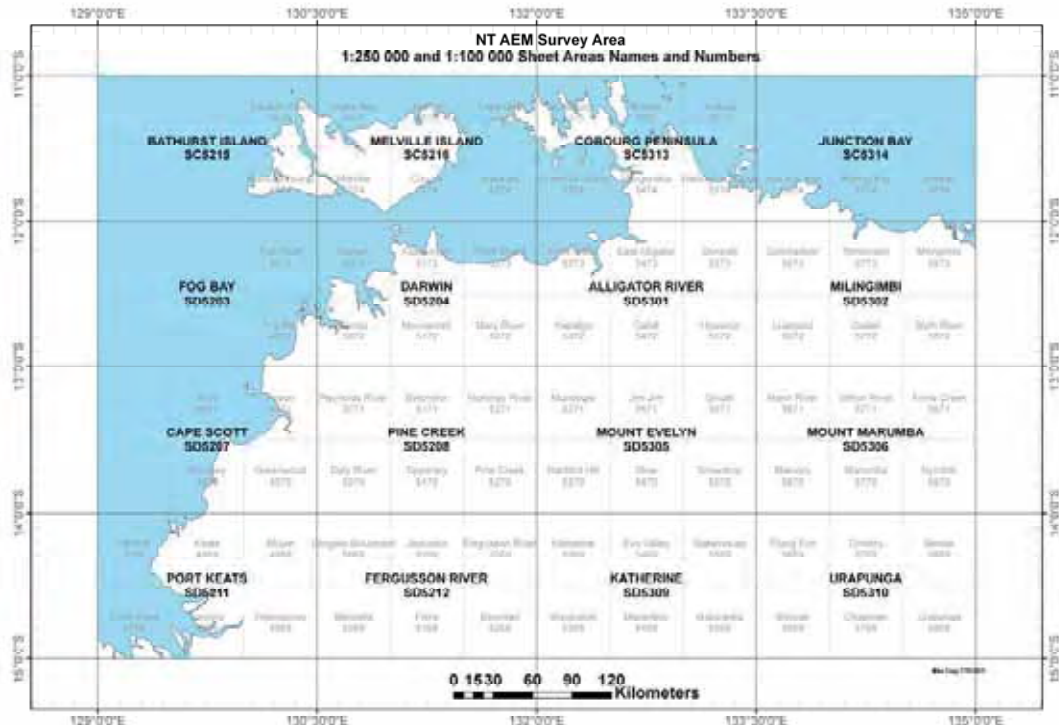


**Figure 2–1:** Pine Creek Survey Area 250k and 100k map sheet names and numbers.

**Table 2-1:** Available geological maps in the Pine creek AEM survey area.

SCALE	NAME	AUTHOR(S) REFERENCE
<b>NORTHERN TERRITORY GEOLOGICAL SURVEY (NTGS)</b>		
1:2 500 000	Geological Map of the Northern Territory (2006)	M. Ahmad and I.R. Scrimgeour.
	Geological Regions of the Northern Territory (2010)	NTGS
	Regolith Map of the Northern Territory (2006)	M.A. Craig
	Magnetic Map of the Northern Territory (2008)	R Clifton
	Elevation Map of the Northern Territory (2007)	R Clifton
	Radiometric Map of the Northern Territory (2009)	R Clifton
	Gravity Map of the Northern Territory (2010)	R Clifton
	Relief Map of the Northern Territory (2005)	R Clifton
	Magnetic Depths of the Northern Territory (2008)	R Clifton
	Metallogenic Map of the Northern Territory (2010)	M Khan, M Ahmad and AS Wygralak
1:1 000 000	Regolith GIS of the Northern Territory	Compilers: May, T.A., Edgoose, C.J., Craig, M.A., Robertson, I.D.M. and Anand, R.R.
<b>GEOSCIENCE AUSTRALIA</b>		
1:1 000 000	Surface Geology of Australia (Northern Territory)	A.J., Liu, S.F., Phillips, D., Retter, A.J., Connolly, D.P., and Stewart, G., 2009. Surface geology of Australia 1:1,000,000 scale, Northern Territory. Online: <a href="http://www.ga.gov.au/minerals/research/national/nat_maps/nat_geol_maps.jsp">http://www.ga.gov.au/minerals/research/national/nat_maps/nat_geol_maps.jsp</a>
1:250 000	Cobourg Peninsula	Senior, B.R., and Smart, P.G., 1976. Cobourg Peninsula – Melville Island, Northern Territory 1:250 000 geological series explanatory notes. Sheets SC/53-13 -16, Bureau of Mineral Resources, Australia, 10pp
	Junction Bay	Rix, P., 1964, Junction Bay Northern Territory 1:250 000 geological series explanatory notes. Sheet SC/53-14., Bureau of Mineral Resources, Australia, 10pp
	Milingimbi	Carson, L.J., Haines, P.W., Brakel, A., T., Pietsch, B.A. and Ferenczi, P.A., 1999—Milingimbi, Northern Territory. 1:250 000 Geological map series. Northern Territory Geological Survey, Explanatory Notes Sheet SD53-2

**Geological and energy implications of the Pine Creek airborne electromagnetic (AEM) survey,  
Northern Territory, Australia**

SCALE	NAME	AUTHOR(S) REFERENCE
	Alligator River	Needham, R.S., O'Donnell, I.C., 1983, Alligator River, Northern Territory, 1:250 000 geological map series. Sheet SD/53-01
	Darwin	Malone, E.J., 1961, Darwin Northern Territory 1:250 000 geological series map. Sheet SD52-4, Bureau of Mineral Resources, Australia, First Edition, Map Legend
	Fog Bay	Senior, B.R., Green, D., 1975, Fog Bay, Northern Territory, 1:250 000 geological map series. Sheet SD/52-03, 1st edition., Bureau of Mineral Resources, Australia, 1v, Map
	Cape Scott	Morgan, C.M., 1971, Cape Scott NT 1:250 000 geological map series. Sheet SD/52-07, 1st edition
	Pine Creek	Malone E.J., 1967, Pine Creek, N.T. Sheet D/52-8. 1:250,000 Geological map series - Explanatory Notes.
	Mount Evelyn	Walpole, B.P., 1962, Mount Evelyn, NT 1:250 000 Geological map series, Sheet SD/53 5, BMR [AGSO], Canberra
	Mount Marumba	Roberts & Plumb, K., 1965, Mount Marumba, NT 1:250 000 Geological Series, SD/53 6, BMR [AGSO], Canberra
	Mount Marumba	Sweet, I.P., Brakel, A.T., Rawlings, D.J., Haines, P.W., Pietsch, B.A., 1999: Mount Marumba SD53 6, 1:250 000 Geological Map Series explanatory notes, NTGS AGSO.
	Port Keats	Morgan, C.M., Sweet, I.P., Johnston, I.D., 1971, Port Keats, Northern Territory, 1:250 000 Geological map series. Sheet SD/52-11, 1st edition., Bureau of Mineral Resources, Australia, 1v
	Fergusson River	Mendum, J.R., 1972, Fergusson River, Northern Territory, 1:250 000 Geological map series. Sheet SD/52-12, 2nd edition., Bureau of Mineral Resources, Australia, 1v
	Katherine	Randal, M.A., 1962, Katherine, Northern Territory, 1:250 000 geological series map. Sheet SD53-9., Bureau of Mineral Resources, Australia, 1v, map Randal, M.A., 1963, Katherine, NT 1:250 000 Geological map series, Explanatory notes, Sheet SD/53 9, BMR, Canberra
	Katherine	Kruse, P.D., Pillinger, D.M., Sweet, I.P., Pieters, P.E., Crick, I.H., 1994, Katherine 1:250 000 geological map. Second Edition, Australian Geological Survey Organisation, 1v, map
	Urapunga	Dunn, P.R. 1963 Urapunga Northern Territory 1:250 000 geological series explanatory notes. Sheet SD/53-10. Bureau of Mineral Resources, Australia 1v 17pp

**Geological and energy implications of the Pine Creek airborne electromagnetic (AEM) survey,  
Northern Territory, Australia**

SCALE	NAME	AUTHOR(S) REFERENCE
<b>NTGS</b>		
1:250 000	Mount Evelyn	Ferenczi, P.A., Sweet, I.P., 2004, Mount Evelyn, Northern Territory, 1:250 000 geological map series, Sheet SD 53-05 - Second Edition, Northern Territory Geological Survey, 1v, Map
	Darwin	Pietsch, B.A. 1987 - Darwin NT 1:250 000 map and notes SD52-04
	Pine Creek -Metallogenic	Ahmad, M., Wygralak, A.S., Ferenczi, P.A., Bajwah, Z.U., 1993, Pine Creek Sheet SD52-8, Northern Territory Geological Survey. 1:250 000 Metallogenic map series, 1v, Map
<b>NTGS</b>		
1:100 000	Darwin	Pietsch, B. A. 1983. Darwin 5073 – 1:100 000 Geological map series Explanatory Notes. Northern Territory Department of Mines and Energy, Darwin, 28 pp.
	Koolpinyah	Pietsch, B.A., 1984, Koolpinyah, Northern Territory, 1:100 000 geological map series. Sheet 5173, 1st edition., Northern Territory Geological Survey, 1v, Map
	Fog Bay	Hickey, S.H., 1984, Fog Bay, Northern Territory, 1:100 000 geological map series. Sheet 4972, 1st edition., Northern Territory Geological Survey, 1v, Map
	Bynoe	Pietsch, B.A., 1986, Bynoe, Northern Territory, 1:100 000 geological map series. Sheet 5072, 1st edition., Northern Territory Geological Survey, 1v, Map
	Noonamah	Doyle, N., Lally, J.H., 2004, Noonamah, Northern Territory, 1:100 000 geological map series. Sheet 5172 - First edition, Northern Territory Geological Survey, 1v, Map
	Anson	Fahey, J.E. and Edgoose, C.J. (1986) 1:100,000 Geological map series – Explanatory Notes, Anson 4971. Northern Territory Geological Survey, Department of Mines and Energy, Darwin.
	Reynolds River	Pietsch, B.A. 1989, Reynolds River 1:100 000 Geological map series
	Batchelor	Crick, I.H., 1985, Geology of the Batchelor-Hayes Creek region. 1:100 000 geological special map. First edition., Bureau of Mineral Resources, Australia, 1v
	Greenwood	Dundas, D.L., Edgoose, C.J., Fahey, G.M. and Fahey J.E., 1987a, 1:100,000 Geological map series – Explanatory Notes, Greenwood 4970. Northern Territory Geological Survey, Department of Mines and Energy, Darwin.

**Geological and energy implications of the Pine Creek airborne electromagnetic (AEM) survey,  
Northern Territory, Australia**

SCALE	NAME	AUTHOR(S) REFERENCE
	Daly River	Dundas, D.L., Edgoose, C.J., Fahey, G.M., Fahey, J.E., 1987, Daly River, Northern Territory, 1:100 000 Geological map series, Sheet 5070 - First Edition, Department of Mines and Energy, Darwin, 1v, Map
	Tipperary	Whitehead, B.R., Mulder, C.A., 1990, Tipperary, Northern Territory, 1:100 000 Geological map series. Sheet 5170., Northern Territory Geological Survey, 1v, Map
	Moyle	Edgoose, C.J., 1988, Moyle, Northern Territory, 1:100 000 Geological map series. Sheet 4969. First edition. Northern Territory. Department of Mines and Energy, 1v, Map
	Wingate Mountains	Edgoose, C.J., 1988, Wingate Mountains, Northern Territory, 1:100 000 geological map series. Sheet 5069. First Edition., Northern Territory. Department of Mines and Energy, 1v, Map
Special Digital	Pine Creek Orogen Interpreted Geology	Lally, J. and Doyle, N., 2005. Pine Creek Orogen 1:500,000 Solid Geology Interpretation, preliminary release. Northern Territory Geological Survey, Darwin.
Special Series	Atlas of regolith materials of the Northern Territory (2006)	Robertson IDM, Craig MA, Anand RR
	Rum Jungle Mineral Field: integrated interpretation of geophysics and geology	Lally, J.H., 2003, Rum Jungle Mineral Field: integrated interpretation of geophysics and geology, Part Sheets 5071, 5072, 5171 and 5172 - First edition, Northern Territory Geological Survey, 1v, Map
<b>GEOSCIENCE AUSTRALIA</b>		
1:100 000	East Alligator	Smart, P.G., Needham, R.S., Fuchs, P., Callaghan, D.J., Hughes, R.J., 1980, East Alligator, Northern Territory, 1:100 000 Geological map series. Sheet 5473, 1st edition., Bureau of Mineral Resources, Australia, 1v, Map
	Cahill	Needham, R.S., Smart, P.G., Fuchs, P.H., 1981, Cahill, Northern Territory, 1:100 000 Geological map series. Sheet 5472, 1st edition., Bureau of Mineral Resources, Australia, 1v, Map
	McKinlay River	Wallace, D.A., Stuart-Smith, P.G., Needham, R.S., Brown, T.W., O'Donnell, I.C., Roarty, M.J., 1985, McKinlay River, Northern Territory, 1:100 000 Geological map series. Sheet 5271, 1st edition., Bureau of Mineral Resources, Australia & Geological Survey of NT, 1v, Map

**Geological and energy implications of the Pine Creek airborne electromagnetic (AEM) survey,  
Northern Territory, Australia**

SCALE	NAME	AUTHOR(S) REFERENCE
	Pine Creek	Stuart-Smith, P.G., Needham, R.S., Wallace, D.A., O'Donnell, I.C., Bagas, L., 1985, Pine Creek, Northern Territory, 1:100 000 Geological map series. Sheet 5270, 1st edition., Bureau of Mineral Resources, Australia & Geological Survey of NT, 1v
	Mundogie	Brown, T.W., Roarty, M.J., Stuart-Smith, P.G., Crick, I.H., Needham, R.S., 1982, Mundogie, Northern Territory, 1:100 000 Geological map series. Sheet 5371, 1st edition., Bureau of Mineral Resources, Australia, 1v, Map
	Ranford Hill	Bagas, L., Stuart-Smith, P.G., Needham, R.S., Gallagher, J.A., 1986, Ranford Hill, Northern Territory, 1:100 000 Geological map series. Sheet 5370, 1st edition., Bureau of Mineral Resources, Australia & Department of Mines & Energy, NT, 1v
	Howship	Needham, R.S., Lachlan, P.R., 1979, Howship, Northern Territory, 1:100 000 Sheet 5572 - Preliminary edition, Bulletin of the Bureau of Mineral Resources, Geology and Geophysics, 1v, Map
	Kapalga	Stuart-Smith, P.G., Needham, R.S., Lachlan, P.R., Blythe, P., 1978, Kapalga, Northern Territory 1:100 000 Geological map series, Sheet 5372 - Preliminary Edition, Bureau of Mineral Resources, Geology and Geophysics, 1v, Map
	Noonamah	Crick, I.H., Johnson, K., Needham, S., Rhodes, M., 1983, Noonamah, Northern Territory, 1:100 000 Sheet 5172 - Preliminary edition, Bureau of Mineral Resources, Geology and Geophysics, 1v, Map
Geoscience Australia	Stow Region	Stuart-Smith, P.G., Needham, R.S., Bagas, L., Dodson, R.G., 1988, Geology of the Stow Region, Northern Territory, 1:100 000 Geological special map. Sheets 5470, 5570 (part) 1st edition., Bureau of Mineral Resources, Australia & Geological Survey of NT, 1v
Special Maps	Mary River-Point Stuart	Stuart-Smith, P.G., Wallace, D.A., Brown, T.W., Roarty, M.J., 1983, Mary River-Point Stuart Region, Northern Territory, 1:100 000 Geological special map, Sheets 5272 and 5273 (part). 1st edition., Bureau of Mineral Resources, Australia & Geological Survey of NT, 1v
	Edith River Region	Needham, R.S., Stuart-Smith, P.G., Bagas, L., 1989, Geology of the Edith River Region, Northern Territory, 1:100 000 Geological special map. Sheets 5269 & 5369, 1st edition., Bureau of Mineral Resources, Australia & Geological Survey of NT, 1v

SCALE	NAME	AUTHOR(S) REFERENCE
	Nabarlek Region	Needham, R.S., Fuchs, P.H., Lachlan, P.R., 1982, Geology of the Nabarlek region, 1:100 000 Geological series special map. Sheet 5573 and part 5572, 1st edition., Bureau of Mineral Resources, Australia, 1v
	Batchelor-Hayes Creek Region	Crick, I.H., 1985, Geology of the Batchelor-Hayes Creek region. 1:100 000 Geological special map. First edition., Bureau of Mineral Resources, Australia, 1v
	Rum Jungle Uranium Field	Crick, I.H., 1984, Geology of the Rum Jungle Uranium Field. 1:100 000 Geological special map, 1st edition., Bureau of Mineral Resources, Australia, 1v, Map
	Yeuralba Region	Needham, R.S., Gallagher, J., 1990, Geology of the Yeuralba Region, Northern Territory 1:100 000 Special - First Edition, Bureau of Mineral Resources, Geology and Geophysics, 1v, Map
	Mt Gilruth Region	Needham, R.S., Lachlan, P.R., 1983, Geology of the Mount Gilruth Region - Preliminary Edition, Bureau of Mineral Resources, Geology and Geophysics
	Cullen Mineral Field	Stuart-Smith, P.G., 1987, Geology and Metallogeny of the Cullen Mineral Field, Northern Territory, 1:250 000 scale map. Sheet SD/52-08, SD/53-05, SD/53-09, 1st edition., Bureau of Mineral Resources, Australia, 1v, map

Geological maps are available for download at the NTGS website. A comprehensive product catalogue is available at the same location.

## 2.2 GEOPHYSICS

There are a range of publicly-available airborne geophysical data covering the Pine Creek AEM survey area including detailed and regional magnetics, radiometrics, gravity, AEM and Digital Elevation Models (DEMs). These surveys may have been commissioned by minerals exploration companies, or by State, Commonwealth or other government agencies. The Space Shuttle Radar Topographic Mission Digital Elevation Model (SRTM DEM) is also included in this compilation for completeness, although it is a satellite-borne data acquisition platform. Most public-domain data are held within the Geophysical Archive Data Delivery System (GADDS) at GA and are available for free download through the Australian Geoscience Portal (<http://www.geoscience.gov.au/>). The SRTM DEM is available for free download from the United States Geological Survey (USGS) at the National Map Seamless Server (<http://seamless.usgs.gov/>).

Figure 2–2 illustrates the fundamental regional ground gravity, airborne magnetic and radiometric geophysical data and the SRTM DEM data sets covering the Pine Creek AEM survey area. A number of other products are derived from each data set, including First and Second Vertical Derivative (1VD, 2VD) gravity and magnetics (or variations thereof, including 0.5 and 1.5 VD magnetics) to depict the rate of change of the potential fields, and various filters to enhance or subdue different wavelengths and directional trends. Radiometric data can also be displayed as

single channel (potassium, thorium, uranium), total counts (dose rate), channel ratio (potassium/thorium, thorium/uranium, potassium/uranium) or variants thereon including uranium<sup>2</sup>/thorium ( $U^2/Th$ ), which can be used to highlight surface uranium concentrations for uranium prospecting (Mernagh et al., 1998; Wilford et al., 2009). The SRTM DEM can be processed further to provide slope, aspect and surface drainage vector maps as well as having more advanced calculations such as the MRVBF algorithm (Gallant and Dowling, 2003) applied, to partition the landscape into areas with low, moderate and high slope to aid landscape and surface hydrology studies.

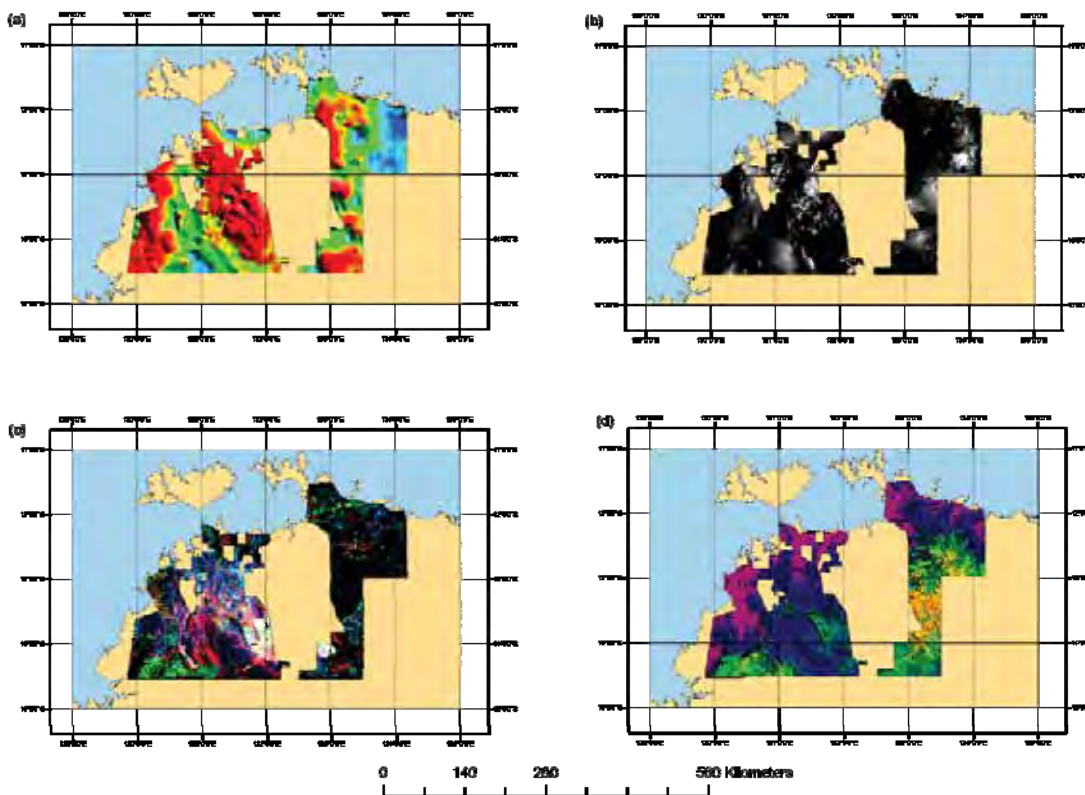


**Figure 2-2:** Regional geophysical data sets available for the Pine Creek AEM survey area. A: Bouger anomaly gravity; B: Reduced-to-pole total magnetic intensity (RTP TMI) image; C: Ternary radiometric (gamma-ray spectrometric) image with KThU as RGB; D: Space Shuttle Radar Topographic Mission Digital Elevation Model (SRTM DEM) with 30 m ground pixel resolution

### 2.3 BOREHOLE DATA COMPILATION

Borehole data were gathered from the Northern Territory Geological Survey's borehole collar database. Collar location information for those boreholes located within the AEM survey area was subsampled from the bulk data provided. A separate dataset was also compiled consisting of Open File reports relevant to the AEM survey area. From those many reports, only those Open File reports that pertained to boreholes within, or outside but proximal to, the survey boundaries were separated for further consideration.

Collar and orientation data were added to the project GIS database and reports that contain pertinent and interpretable stratigraphic logs (mostly scanned pages of original driller's logs) were matched with collar and orientation data and then to borehole ID. Some boreholes with logs within Open File reports were not part of the collars file available from NTGS. Where it was possible and desirable these data were added to the projects Collars and orientation database. In many cases this was not possible because the location information was obscured or appeared to be inaccurate or did not have any datum information at all. Some location data for boreholes were recalculated from data extracted from information recorded elsewhere within reports. This process proved time-consuming and carried varying degrees of uncertainty in many cases. Only those locations of which we were confident were transferred to the project's GIS borehole database.

In addition to the minerals-related borehole information held by NTGS, the Northern Territory Department of Natural Resources Arts and Environment (NRETAS) holds information for water boreholes within the Northern Territory. The NRETAS Department is responsible for a wide range of water resource information. The Pine Creek AEM Survey boundary file was provided to the Department so that waterbore collars and linked report files in the on-line database could be extracted and provided to the AEM project for subsequent examination. No filters were applied to the data extraction and this resulted in about 2,000 water bore collars being returned to the project (see [Figure 2–3](#)). Many proved to be of limited or no use to the projects requirement of boreholes suitable for AEM section and grid calibration requirements. Some however were of sufficient depth and had suitable and interpretable logs and are located near AEM CDI sections so were included in the projects GIS borehole database.

Overall, the process of gathering, locating and selecting of boreholes suitable for interpreting conductivity contrasts visible in CDI sections was not very productive and less than 100 boreholes proved helpful for these purposes ([Figure 2–4](#)). It took considerable time and effort to assess and compile this number of reliable useful records. Conductivity logging was undertaken by Geoscience Australia project geophysics staff to provide conductivity measurements for selected areas. The locations of conductivity-logged boreholes are shown in [Figure 2–5](#).

The borehole database has been useful in showing the thickness of regolith and Cenozoic cover materials, rock types and depth to major bedrock rock groups e.g., depth to the Kombolgie subgroup and Tolmer Group sediments, granites and depth to Paleoproterozoic metamorphic rocks. Due to drilling methodologies used, dominated by percussion, reverse circulation percussion and rotary drilling, accurate assignment of intersections to formations, either by the logging geologist or interpreted as part of the present project, has been difficult.

**Geological and energy implications of the Pine Creek airborne electromagnetic (AEM) survey, Northern Territory, Australia**

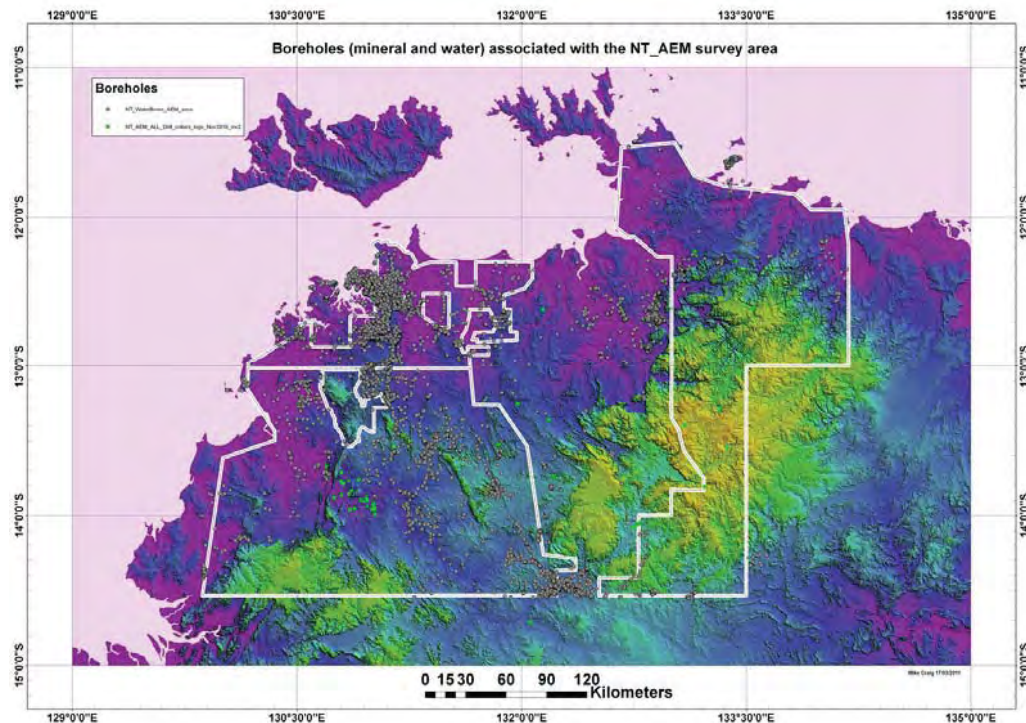


**Figure 2-3:** Unfiltered borehole population associated with Pine Creek survey area including publicly available mineral and water boreholes.

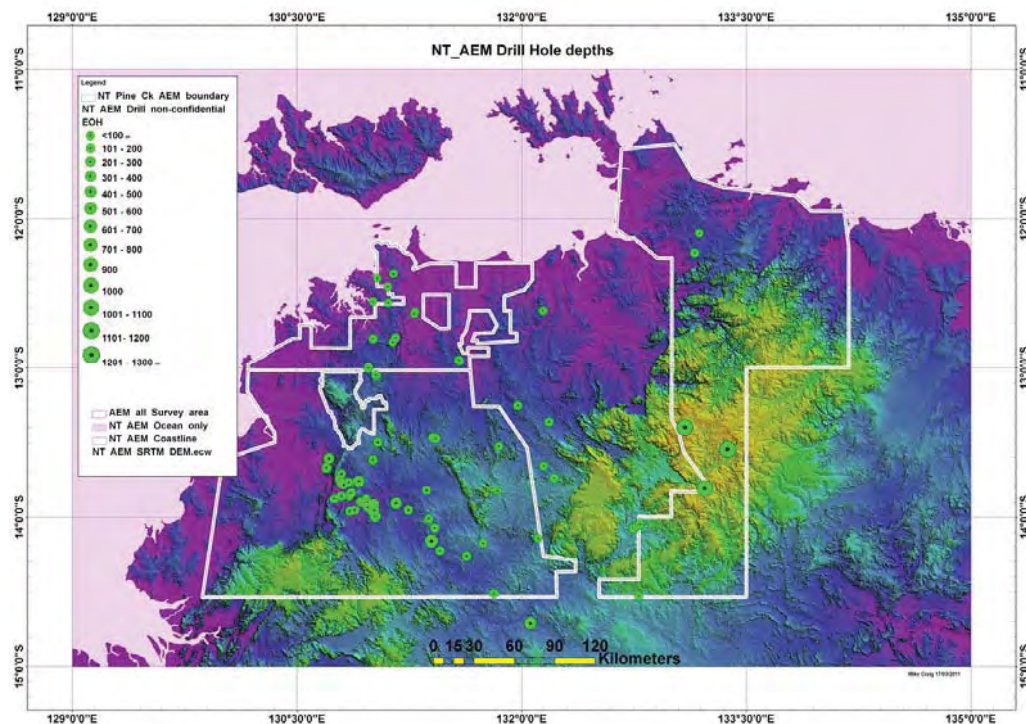


**Figure 2-4:** Boreholes (and their depths) within and adjacent to the Pine Creek survey area which were consulted during AEM interpretations

**Geological and energy implications of the Pine Creek airborne electromagnetic (AEM) survey, Northern Territory, Australia**

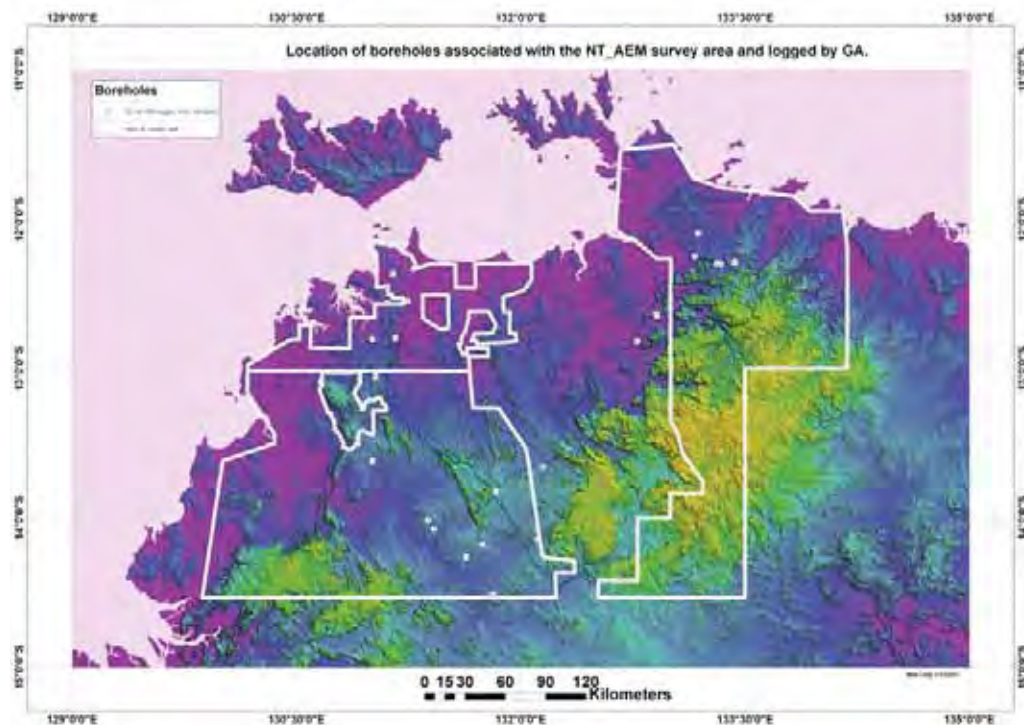


**Figure 2-5:** Locations of boreholes associated with the Pine Creek survey area for which conductivity-logs have been acquired.

Most public domain data are held within the Geophysical Archive Data Delivery System (GADDS) at GA and are available for free download through the Australian Geoscience Portal (<http://www.geoscience.gov.au/>). The SRTM DEM is available for free download from the United States Geological Survey (USGS) at the National Map Seamless Server (<http://seamless.usgs.gov/>)

## **2.4 REFERENCES**

- Gallant, J.C., and Dowling, T.I., 2003. A multi-resolution index of valley bottom flatness for mapping depositional areas. *Water Resources Research* 39 (1), 1347
- Mernagh, T.P., Wyborn L.A.I., & Jagodzinski, E.A., 1998. ‘Unconformity-related’ U ± Au ± platinum-group-element deposits. *AGSO Journal of Australian Geology and Geophysics*. **17** (4), 197-205.
- Minty, B.R.S., Franklin, R., Milligan, P.R., Richardson, L.M., and Wilford, J., 2008. Radiometric Map of Australia (First Edition), scale 1:5 000 000, Geoscience Australia, Canberra.

## 3 Geology

*S.F. Liu and M.A. Craig*

### 3.1 GEOLOGICAL FRAMEWORK

Geoscience Australia's AEM survey areas in the Pine Creek region of Northern Territory cover much of the Darwin-Moyle-Katherine-Jabiru area. Geological regions from younger to older geological ages in the AEM survey areas include ([Figure 3–1](#)):

- Money Shoal Basin
- Bonaparte Basin
- Daly Basin
- Victoria Basin
- Fitzmaurice Basin
- Birrindudu Basin
- McArthur Basin
- Pine Creek Orogen (Geosyncline), and
- Archean complexes in the Rum Jungle and Jabiru areas

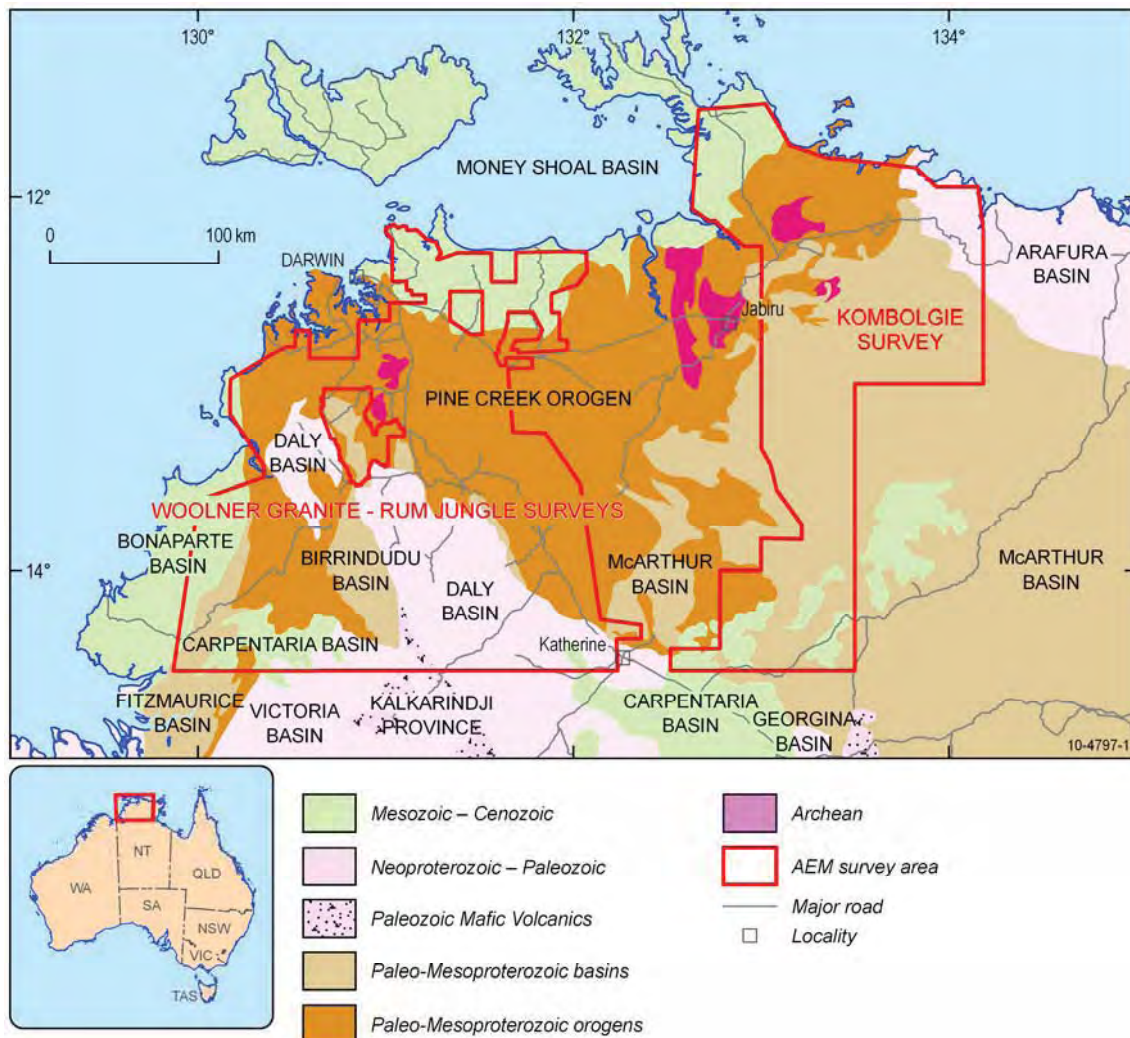


**Figure 3-1:** Geological regions in the northern part of the Northern Territory with AEM survey boundaries (geological regions after NTGS (2010))

The geology and mineral resources in the Northern Territory are described in detail in a special NTGS publication (Ahmad and Munson, in prep.). Summaries of geological regions in the Northern Territory are available on the NTGS website. This section presents a brief summary of the geology of the above-listed geological regions with respect to the geological interpretations of GA's AEM surveys in the Pine Creek region. This summary discusses the rocks in the region in the order of oldest rocks to youngest including surface materials, i.e., regolith. It provides background information to support interpretations of AEM data and includes discussion on the implications of observations for uranium exploration and for uranium mineral systems.

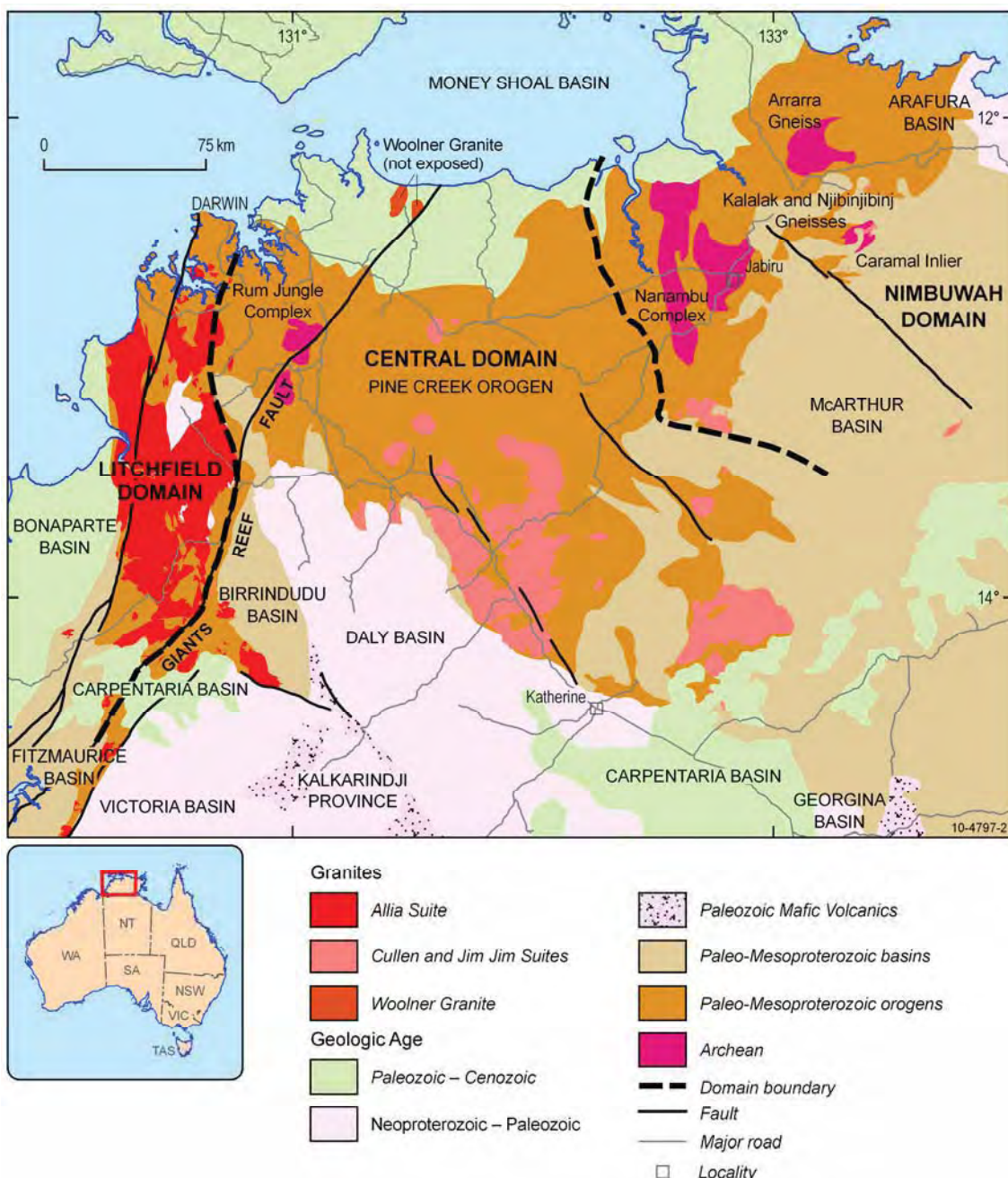


**Figure 3-2:** Geological domains of the Pine Creek Orogen (geological regions after NTGS (2010).

### 3.1.1 Archean complexes

Archean complexes in the Pine Creek region include:

- Nanambu Complex (2470+47/-40, Page et al. 1980);
- Kukalak Gneiss (2530-2510 Ma, Hollis et al. 2009a, Carson et al. 2010, Hollis et al. 2011) ;
- Rum Jungle Complex (ca. 2545-2520, Cross et al. 2005);

- Arrarra Gneiss (2670-2640 Ma, Hollis et al. 2009a Carson et al. 2010, Hollis et al. 2011);
- Njibinjibinj Gneiss (2671 Ma, Hollis et al. 2009a Carson et al. 2010, Hollis et al. 2011); and,
- Woolner Granite (2675±15 Ma, McAndrew *et al.* 1985)

The Woolner Granite, representing the oldest rock in the Pine Creek region, is a subsurface granite complex close to the coast of Chambers Bay. The eastern granite body is interpreted to be faulted along the northern extension of the Giants Reef Fault ([Figure 3–2](#)).

The Kukalak, Arrarra and Njibinjibinj gneisses were recently discovered Neoarchean basement rocks in the Nabarlek area of western Arnhem Land, (Hollis et al. 2009), Carson et al. 2010, Hollis et al. 2011). According to these authors, Kukalak Gneiss represents the layered biotite quartz-feldspathic gneisses in the Caramal and Myra Falls inliers. Arrarra Gneiss represents the quartz-feldspathic gneiss in a broad area northeast of Oenpelli. The Njibinjibinj Gneiss refers to an isolated outcrop of heavily altered gneiss in the northeast of Myra Falls Inlier.

The Rum Jungle Complex includes granitic rocks, schist, gneiss and banded ironstone in the Rum Jungle Dome and Waterhouse Dome (Ahmad et al. 2006). The elliptical shapes of these complexes and the doming of surrounding sedimentary rocks have been the subject of several interpretations, including “mantled gneiss dome” (Rhodes 1965), diapiric intrusion (Stephansson and Johnson 1974), and non-cylindrical folding modified by fold interference and late faulting (Johnson 1984).

The Nanambu Complex comprises granite and granitic gneiss with minor amphibolite and mica schist in three oval-shaped domes known as the Magela, Jim Jim and Munmarlary masses in the Nimbuwah Domain (Needham 1988; Needham et al. 1988). A fourth subcropping area was confirmed by drilling west of Jabiluka (Hollis et al. 2009).

### **3.1.2 Pine Creek Orogen**

The Pine Creek Orogen is located to the east and south of Darwin ([Figure 3–1](#)). The Orogen refers to the folded and faulted Paleo- to Mesoproterozoic sedimentary sequence, commonly referred to as the Pine Creek Geosyncline sequence, the deformation of which was terminated by the Top-End Orogeny (Needham et al. 1988).

The regional geology of the Pine Creek Orogen has been documented in detail by Walpole et al. (1968), Needham et al. (1980), Needham et al. (1988), and Needham and De Ross (1990). The structural geology of the Orogen was studied in detail by Johnston (1984) for the Central Domain to Nimbuwah Domain, and, by Hammond et al. (1984) for Litchfield Province. The geochronology of the region was updated by Worden et al. (2008) and Carson et al. (2008). Evidence for the existence of new Archean basement in western Arnhem Land was reported by Hollis et al. (2009).

The Litchfield Domain (or Province) ([Figure 3–2](#)) consists of low- to high-grade metamorphics and granitic rocks at the west margin of the Pine Creek Orogen and at the northern extremity of a major fault zone that extends from the Hall Creek Mobile Zone (Pietsch and Edgoose 1988). The tectonic affinity of the Litchfield Domain has been the subject of discussion. It is has long been considered a north-eastern extension of the Halls Creek Orogen (Pietsch and Edgoose 1988). Recent geochronological work by Carson et al. (2008) correlates high-grade metamorphism at about 1855 Ma in the Litchfield Province and Halls Creek Orogen. The lack of pervasive deformation during the mid- to high-grade metamorphism at ca. 1855 Ma in both the Hermit Creek and Fog Bay Metamorphics led Carson et al. (2008) to suggest an intra-crustal extension model for the tectonic evolution of the Litchfield Domain (Province) at this time, not a plate tectonic model as postulated

for the evolution of the Halls Creek Orogen. Their intra-crustal extensional model implies that the Litchfield Domain and the Pine Creek Orogen were contiguous and coeval with the Kimberley Craton.

The lack of evidence for deformation at 1845–1835 Ma in the Litchfield Domain led those authors to consider the observation that, if a continental suture of this age does exist in the Halls Creek Orogen, it does not extend to the Litchfield Domain.

### **3.1.2.1 Stratigraphy**

The tectonic evolution of the Pine Creek Geosyncline Sequence was summarised in Needham et al. (1988) and involved two crustal extension periods which were separated by a sagging phase. In brief, the Pine Creek Geosyncline Sequence was deposited in an intra-cratonic basin in alternating continental and shallow marine environments. The basin was formed on c. 2500 Ma largely granitic Archean basement. The Pine Creek Geosyncline sequence includes Paleoproterozoic sediments and volcanic rocks to a thickness of about 10 km. The Archean to Proterozoic stratigraphy in the Pine Creek region is summarised in [Table 3–1](#).

The lower part of the geosynclinal sequence is quartz-rich with bimodal volcanics (Kakadu Group, Namoona Group and Mt Partridge Group). This part of the sequence consisted mainly of fluvialite deposits that accumulated during the initial phase of crustal extension.

The middle part of the geosyncline sequence includes the South Alligator Group and Finnis Group. Early deposits of the South Alligator Group marked a transition from mainly distal pelitic sediments to mainly proximal carbonate deposits in a shallow marine environment, probably representing widespread sagging of the basin which might be related to post-extensional subsidence. The upper South Alligator Group and Finnis Group are turbiditic, and may represent provenance and intrabasinal uplift associated with the onset of the Top End Orogeny.

The Katherine Volcanic Sequence (El Sherana and Edith River Groups) were deposited in a rift valley environment and appear to indicate a second period of crustal extension.

### **3.1.2.2 Structural and tectonic history**

Based on structural style and metamorphic grade, Johnston (1984) divided the Pine Creek Inlier into five domains:

1. Nimbuwah Complex: gneisses with shallowing dipping foliations of amphibolite to granulite metamorphic grade;
2. East Alligator River Domain: amphibolite facies metamorphism and dominated by east facing recumbent to shallowing inclined folds;
3. South Alligator River Domain: greenschist metamorphism with westerly verging thrusting and upright folding;
4. Central Marrakai Domain: similar in structural style and metamorphic grade to the South Alligator River Domain, but lacks thrusts; and,
5. Rum Jungle Domain: upper greenschist metamorphism and early decollement zones refolded by upright folds.

Johnston (1984) presented a regional structural correlation as summarised in [Table 3–2](#) here.

**Table 3-1:** Archean to Proterozoic stratigraphy of the Pine Creek Orogen

ERA	UNIT	LITHOLOGY	THICKNESS (M)	AGE (MA)
Paleo- to Mesoproterozoic 1780-1200 Ma	Minor Dolerite	Quartz dolerite dykes and small plug-like bodies		
	Mudginberri Phonolite	Phonolite dykes	1	1200±35
	Munmarlary phonolite	Phonolite dykes	1	1316±50
	Tolmer Group (shallow shelf)	Sandstone, dolostone, siltstone	1000	
	Katherine River Group (braided alluvial fan)	Sandstone, conglomerate, minor greywacke, siltstone, interbedded basalt-andesite volcanics and pyroclastics	3000-4500	1780-1700
Late Paleoproterozoic metamorphism and igneous activity 1870-1800 Ma	Oenpelli Dolerite	Layered tholeiitic dolerite lopoliths	<250	1720
	Edith River Group (felsic volcanism in terrestrial rifts)	Ignimbrite, microgranite, rhyolite, minor basalt and cherty sediments; basal sandstone, arkose	1200	1820
	Post-tectonic granite emplacement	Biotite granite, quartz monzonite, syenite, granodiorite (numerous plutons)		1840-1820
	El Sherana Group (felsic volcanism in terrestrial rifts)	Rhyolite, greywacke, siltstone, sandstone, basalt		1835
	Nimbuwah Complex	Granitoid migmatite, granite, gneiss, schist (anatexis of Early Proterozoic granite)		1865
Early Paleoproterozoic 2100-1870 Ma	Zamu Dolerite	Layered tholeiitic dolerite, siltstones and minor dykes	<2500	1890
	Finniss River Group (flysch)	Siltstone, shale, greywacke, arkose, quartzite, schist; minor interbedded volcanics	1500-5000	
	South Alligator Group (shallow marine chemical, volcanics)	Carbonaceous and pyritic black shale and siltstone, chert-banded and nodular hematitic siltstone and black shale, algal carbonate, banded iron formation, jaspilite, tuff, greywacke near top	<5000	1885±3 (tuff)
	Nourlangie Schist	Layered schist, gneiss		
	Cahill Formation (supratidal, fluviatile)	Quartz schist, pelitic and partly carbonaceous near base, with magnesite lenses	<3500	
	Mt Partridge Group (fluviatile, near-shore chemical, supratidal, fluviatile)	Sandstone, siltstone, arkose, shale, conglomerate, quartzite, carbonaceous siltstone and shale, dolostone, magnesite; minor interbedded volcanics	<5000	
	Namona Group	Pyritic carbonaceous shale and	3000	

ERA	UNIT	LITHOLOGY	THICKNESS (M)	AGE (MA)
	(shallow marine, chemical, detrital, supratidal)	siltstone, calcareous in places, calcareous sandstone, tuff, conglomerate; arkose, sandstone and massive dolostone/magnesite in west		
	Kakadu Group (fluvialite)	Sandstone, arkose, siltstone, conglomerate, quartzite, schist, gneiss	<1000	
Archean Basement	Nanambu Complex	Granite, augen gneiss, leucogneiss, minor quartzite and schist (includes accreted Early Proterozoic metamorphics)		>2470
	Rum Jungle Complex	Coarse, medium, and porphyritic adamellite, biotite-muscovite granite, migmatite, gneiss, schist, pegmatite, metadiorite, banded iron formation		>2525

*After Needham and De Ross 1990 and, Ahmad and Lally 2003*

Johnston (1984) reached this regional structural correlation on the assumption that the shallowly dipping fabrics with an east-trending stretching lineation which occur in the South Alligator River, East Alligator River and Nimbuwah Complex, described above, all formed during the same deformation event, D2. He subsequently correlated all upright N-S to NW-SE trending folds from Rum Jungle to East Alligator River, and reclined NW-trending folds as D3 structures.

Hammond et al. (1984) proposed a similar five-event deformational history for the Litchfield Province but interpreted D1 and D2 as earlier events, possibly Archean. Their model includes overthrusting and overfolding both eastwards and westwards. This also raises the questions, (a) whether the early deformations (D1 and D2) in the Rum Jungle area and Nimbuwah Complex were Archean and (b) whether they correlate with the early deformations (D1 and D2) in the South Alligator and Eastern Alligator areas.

The structural geology and deformation history of the Pine Creek region was the subject of several studies (Needham et al. 1988; Stuart-Smith et al. 1988a & b; Valenta 1991; Ferenczi & Sweet 2005; Hollis et al. 2009a) Johnston (1984). Correlation of deformation history by these studies and Johnston (1984) is summarised in [Table 3–3](#).

For simplicity of discussions in this record, our observations are focussed on the Litchfield Province, Central Domain and Nimbuwah Domain of the Pine Creek Orogen, unless the context makes it clear that a specific area or structural domain like Johnston's (1984) is referred to.

**Table 3-2:** Structural correlation in the Pine Creek Geosyncline (after Johnston 1984)

REGIONAL DEFORMATION	RUM JUNGLE	CENTRAL MARRAKAI	SOUTH ALLIGATOR	EAST ALLIGATOR	NIMBUWAH
D5	F5 kinks related to basement block movement				
D4	F4 E-W open folds	F4 E-W open folds	F4 E-W open to close folds	F4 E-W folding	?
D3	F3 upright, N-S folds	F3 upright, N-S folds	F3 upright, N-S to NW-SE folds	F3 upright, NW folds	F3 reclined NW folds
D2	-	-	S1 bedding parallel foliation, low angle faulting; recumbent isoclinal fold, mylonites or brecciation in the fault zones	F2 recumbent folds, S2 schistosity and tectonic sliding with low angle high strain thrust zones	F2 recumbent folding and thrusting
D1	? local D1 not regionally correlated	-	Local S1 in the South Alligator Hinge region	S1 bedding parallel foliation	S1 bedding parallel foliation F1 isocline?

**Table 3-3:** Deformation history in the Pine Creek region

TECTONIC EVENT	CULLEN MINERAL FIELD (STUART-SMITH ET AL., 1993)	RANFORD HILL AND STOW (STUART-SMITH ET AL., 1988A,B)	PINE CREEK OROGEN (NEEDHAM ET AL., 1988)	PINE CREEK OROGEN (JOHNSTON 1984)	MT EVENLYN (FERENCZI & SWEET, 2005)	NIMBUWAH (HOLLIS ET AL., 2009)
Post-Aptian		Reactivation of NW faults			Local fault reactivation	
Roper inversion					Late N to NW faults (Bulman trend)	
Post-Roper extension		E-NE faults			E to ENE faults (Deaf Adder trend)	
Post-Nathan compression		Post-Kombolgie faulting	Post-Kombolgie faulting		NE reverse faults (Koongarra trend)	
1700-1600 Ma		D5: Open to tight folds in El Sherana, Edith River and Katherine River groups	D5: Fault-related drag folds in Mamadawerre Sandstone	D5?: kinks related to basement block movement	D5: Reactivation of NW and E faults to produce drag folds and basins in Edith River and Katherine River groups	
1780-1830 Ma Shoobridge & Maud Creek events	Development or reactivation of linear shear zones during Shoobridge Event (1780 Ma); D3 folding associated with emplacement of Cullen Batholith (1835-1820 Ma); D2 during Maud Creek event (1830 Ma): open to tight and N to NE-trending folds of S1, confined to south of Wolfram Hill	D4: Local development of S to SSW, near vertical kink cleavage and minor small-scale open folds; modification of regional fold axes adjacent to granitoid contacts	D4: Minor small-scale kink folds	D4: Easterly, open to closed folds	D4: Reactivation of NW faults in SAVMF produce folds in Namoona Group, and local kink cleavages; regional E to NE open (interference type) folds related to granite intrusion	D4: N-NW-trending, upright open
1865 Ma Nimbuwah event	D1: upright NW-trending folds, vertical N to NW-trending faults	D3: NW to WNW, tight to isoclinal folds with penetrative slaty to phyllitic cleavage	D3: Upright, open to tight folds with development of a crenulation cleavage (S3)	D3: Upright, NW, closed to tight macroscopic folds	D3: Upright NW, open to tight folds and penetrative phyllitic cleavage developed; bedding-parallel shearing and thrust faulting; crenulation cleavage in northeast	D3 N- to NW-trending upright open to tight folds; D2 Meso- to macroscale shallow E- to W-plunging isoclinal folds, with heterogeneous development of S2
pre-Nimbuwah event		D2: Small isoclinal folds associated with thrust faults	D2: Recumbent isoclinal folding (F2) with dominant regional schistosity (S2)	D2: Stratigraphically confined zones of low angle faulting, recumbent isoclinal folding and transposition	D2: Thrusting of Koolpin Formation and recumbent isoclinal folding in NE; bedding-parallel penetrative cleavage developed	D1 Isoclinal folds
pre-Nimbuwah event		D1: Local development of S to SSW, near vertical kink cleavage and minor small-scale open folds; modification of regional fold axes adjacent to granitoid contacts	D1: Upright isoclinal folding with penetrative axial plane foliation	D1: Early warping represented by horizontal east-facing solution cleavage (S1)	D1: Local early warping in Mundogie Sandstone as solution cleavage (S1)	

\* expanded and revised after Ferenczi & Sweet (2005) with geochronological data from Worden et al. (2008)

### **3.1.3 McArthur Basin and correlates**

Palaeoproterozoic to Mesoproterozoic McArthur Basin (1430-1800 Ma) consists of sedimentary and minor volcanic rocks, including dolostone, sandstone, shale, felsic and mafic volcanic rocks (Rawlings 1999). The basin extends from Jabiru in the Northern Territory to Mt Isa in Queensland.

A major constituent of the basin in the NT is the Katherine River Group to the south and east of Jabiru. The Kombolgie Subgroup, or the commonly called “Kombolgie Sandstone”, occupies the lower part of the Group.

To the west, north and east of the Daly Basin, three units of the Tolmer Group are exposed, namely Depot Creek Sandstone, Stray Creek Sandstone and Hindrance Dolostone. These rocks are understood to extend below the Daly Basin. The Tolmer Group correlates with the Katherine River Group of the McArthur Basin (Ahmad and Lally 2003).

### **3.1.4 Fitzmaurice Basin**

The Fitzmaurice Basin consists of a Palaeo- to Mesoproterozoic deformed package of sedimentary and volcanic rocks, including sandstone, siltstone, shale, conglomerate, minor dolostone and minor volcanic rocks that occur west of the Giants Reef Fault (Dunster et al. 2000). It overlies the Pine Creek Orogen and is unconformably overlain by the Bonaparte Basin ([Figure 3–1](#)).

### **3.1.5 Victoria Basin**

The Victoria Basin consists of a Neoproterozoic sedimentary sequence up to 950 m thick of dolostone, sandstone, limestone and shale (Dunster et al. 2000). It unconformably overlies the Pine Creek Orogen and Birrindudu Basin and, in turn, it is overlain by the Daly Basin, and the Kalkarindji Igneous Province ([Figure 3–1](#)).

### **3.1.6 Daly Basin**

The Cambrian-Ordovician Daly Basin is a large, gently dipping intracratonic basin that extends from the northwest to southeast. It consists of a sedimentary and volcanic sequence dominated by limestone, dolostone, sandstone and siltstone. The basin unconformably overlies the Pine Creek Orogen and Birrindudu Basin to the north and east and Victoria Basin to the west. In turn, it is overlain by the Carpentaria Basin to the south ([Figure 3–1](#)); Kruse et al. 1990 & 1994).

### **3.1.7 Bonaparte Basin**

The Bonaparte Basin is a composite basin, outcropping near the Joseph Bonaparte Gulf and extending offshore. It consists of Cenozoic to Cambrian limestone, sandstone, siltstone, basalt and coal plus coarse clastic sediments of glacial origin. The basin overlies the Paleoproterozoic Pine Creek Orogen and Proterozoic Fitzmaurice Basin ([Figure 3–1](#); Dunster et al. 2000; Ellis et al. 2004; NTGS 1990).

Sediments of the Bonaparte Basin are at least 5 km thick onshore, deepening to 17 km off shore. The AEM surveys cover part of the Bonaparte Basin on Cape Scott and Port Keats maps where the Permian Kulshill Formation and undivided Cretaceous sediments are mapped on the 1:1 000 000 surface geology map of Australia.

### **3.1.8 Money Shoal Basin**

The Money Shoal Basin is a pericratonic basin and extends from the Arnhem Land coastline to West Irian. It consists of a Jurassic to Eocene sedimentary sequence up to 4 km thick of sandstone, coal, shale, claystone and marls overlain by a Cenozoic carbonate sequence ([Figure 3–1](#); NTGS 1989; Ellis et al. 2004).

### **3.1.9 Cretaceous sediments**

The Cretaceous stratigraphy and palaeontology of the NT were studied in detail by Skwarko (1966), who described the Cretaceous rocks in NT as flat-lying or gently dipping, mainly unfolded and unfaulted. Most of the Cretaceous rocks form mesas and are silicified and ferruginised to various degrees. Skwarko (1966) mapped the Cretaceous in three depositional areas in the NT, namely, the Coastal Belt (60 m thick), the Inland Belt (40 m thick), and the Darwin area (900 m thick). The Cretaceous sediments are, almost invariably, capped by ferruginous-duricrust materials (Morgan 1972).

Cretaceous sediments were largely mapped as Mullaman Beds by Skwarko (1966) and in the first edition of 1:250 000 surface geology maps and consist of shale, claystone, siltstone, sandstone, conglomerate, and grit, deposited in marine, lacustrine, and fluvial environments. In later studies, including the second edition of 1:250 000 surface geology mapping, the Mullaman Beds, in some areas, have been remapped as Bathurst Island Formation and/or as Petrel Formation (e.g., Pietsch & Stuart-Smith 1988b; Ahmad et al. 1993).

## **3.2 REGOLITH GEOLOGY**

### **3.2.1 Introduction**

Craig (2006) mapped the distribution of regolith and landforms of the entire NT. The initial map compilation was at a scale of 1:250 000 but was first published as hardcopy at 1:2.5 M scale. A new regolith–landform GIS, based on the compilation scale but generalised to 1:1 M scale is now available from the NTGS and covers the Pine Creek AEM survey area.

An Atlas of regolith materials of the Northern Territory (Robertson, Craig & Anand, 2006) [CRC LEME Open File Report 196; 25.78MB, in pdf format] compliments the 1:2.5 million scale map. It describes in detail, specimens of regolith, including weathered rocks, sands and soils and their secondary cemented products (silcrete, ferricrete, calcrete) that were collected along approximately 20 000 km of traverses. Regolith terminology, weathering processes, regolith modification, associated fabric changes, weathering mineral reactions and mineral stability are explained briefly as an introduction to assist those new to regolith concepts and terms.

These data extend beyond the Pine Creek AEM survey area and therefore, in selected conductivity depth inversion sections as well as some depth and elevation slices, parts of the AEM imagery can be correlated with known regolith materials. Examples of these correlations are discussed later in this section.

### **3.2.2 What is regolith**

In simple terms, “regolith” is everything between fresh air and fresh rock. Eggleton (2001) provides a concise definition of regolith in the Regolith Glossary published by the Cooperative Research Centre for Landscape Evolution and Mineral Exploration (CRC LEME).

Some regolith is not in place, and may have been moved by a geomorphic agent such as water, wind or gravity (or any combination thereof) and, when identified, is commonly referred to as transported regolith. Conversely, some regolith appears to be relatively undisturbed and is referred to as *in-situ*. Transported regolith is relatively straightforward but *in-situ* regolith may need some clarification to ensure a common understanding of the terminology. [Figure 3–3](#) (from Craig 2006 and Craig et al., 2008) shows the combined variation of *in-situ* regolith materials commonly found in regolith profiles. A naming hierarchy is used to group regolith types where the individual materials are not clearly identifiable. The term pedolith serves to include a range of *residual materials* that may occur above the *saprolite* (weathered bedrock). Where it is useful or necessary to group both the weathered bedrock (*saprolite*) and the slightly weathered bedrock together, the term *saprolith* is preferred. In the field, such terms may be convenient until such times as the saprolite boundary can be more clearly distinguished from the adjacent saprock. In other cases, the gross terms may be sufficient for most applications or conceptualisations.

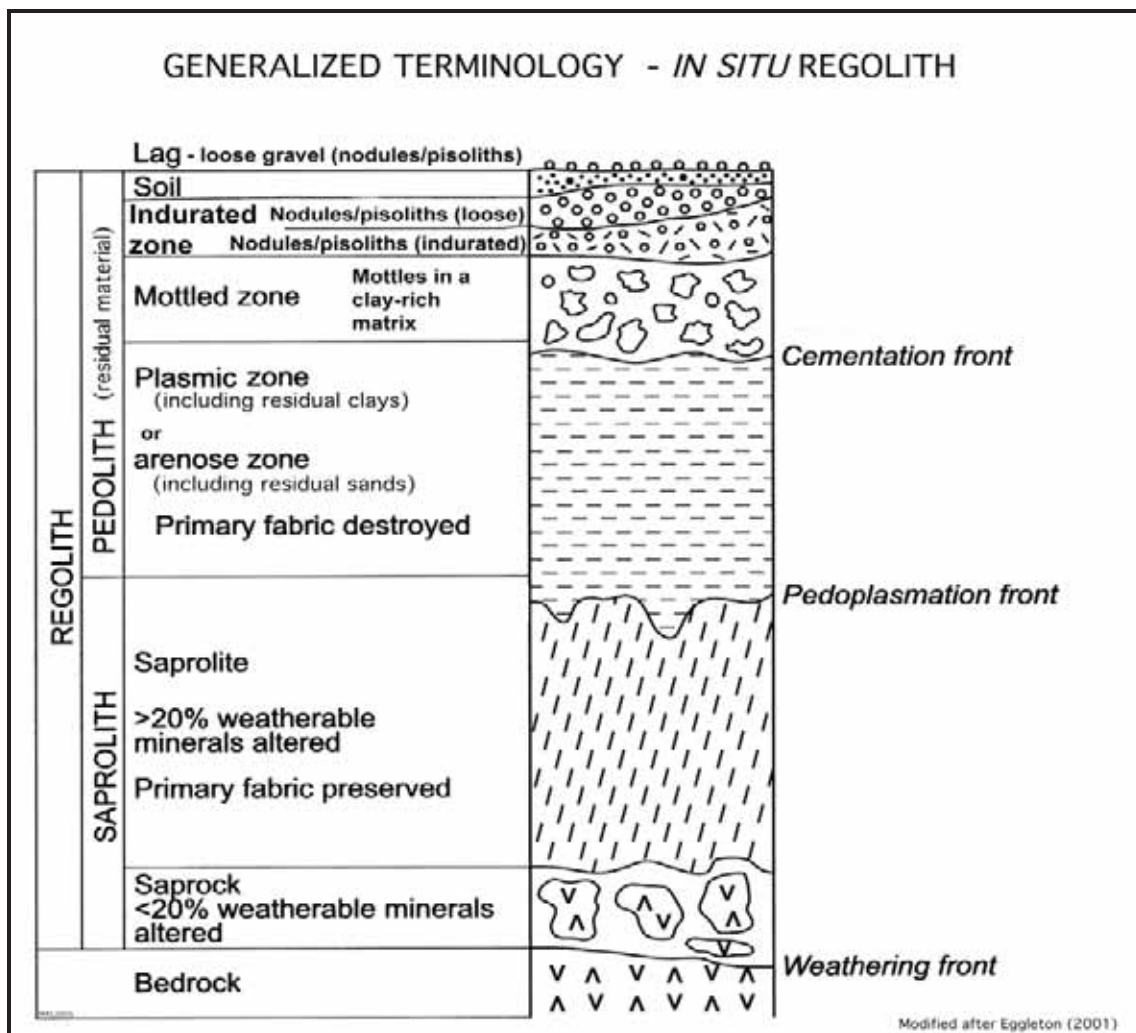


Figure 3-3: A generalized terminology for *in situ* regolith (from Craig et al., 2008 and Craig 2006.)

It is important to appreciate that regolith consists of not only the lag, but also includes any duricrust or ferricrete indicated on local geologic maps. In addition, the regolith consists of much more than the residual materials exposed at the surface and equally includes all those weathered and partly weathered rocks extending below the surface. In highly weathered materials, the parent rock type might be unknown.

The map symbol conventions used in the regolith-landform maps referred to in this report, follows a standard regolith materials and regolith-landform map-unit naming convention (Craig, et al., 1999; Craig et al., 2008) and is shown in Figure 3-4. Figure 3-5 is based on a compilation scale of 1:250 000 and shows the distribution of regolith materials that occur throughout the Woolner-Rum Jungle NT AEM survey areas.

There are a number of interfaces in the *in-situ* regolith section shown in Figure 3-3. Depending on the depth of weathering that may have developed across the Pine Creek survey area some of these interfaces may be visible in AEM inversion sections. One likely interface is the weathering front. Weathering fronts are often interfaces of increased groundwater or soil moisture flow. They may be clay rich and could thereby provide a significant conductivity contrast. Moderate to extensive weathering of bedrock material leads to the development of saprolites. They are also clay rich. These

changes in the once fresh bedrock are thereby likely to lead changes in the original bedrock electrical responses. In examining AEM imagery for possible regolith influence a clear understanding of the nature of the regolith is required and its likely position within the weathering profile. At the surface, depending on the style and extent of erosion, regolith exposures may be representative of any of the regolith horizon elements shown in [Figure 3–3](#).

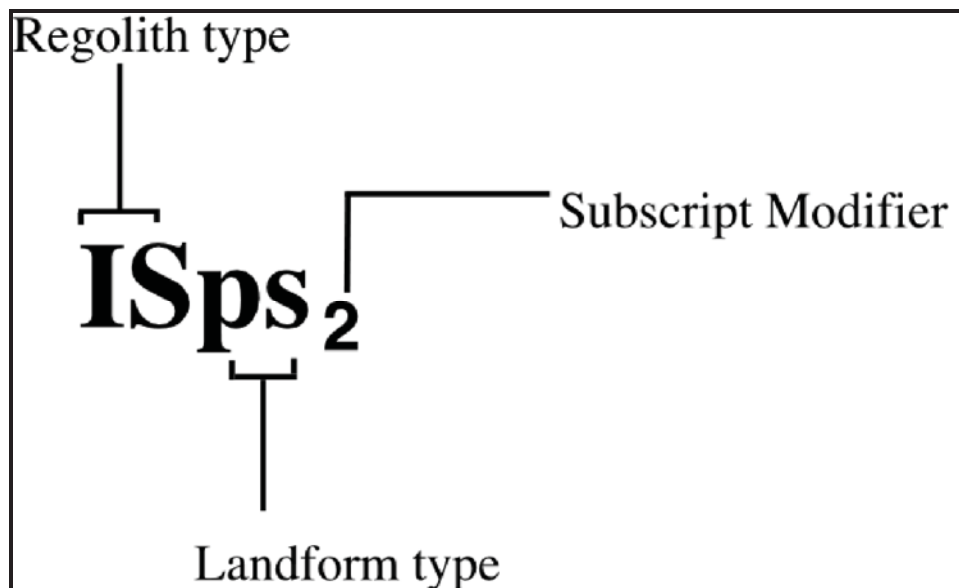
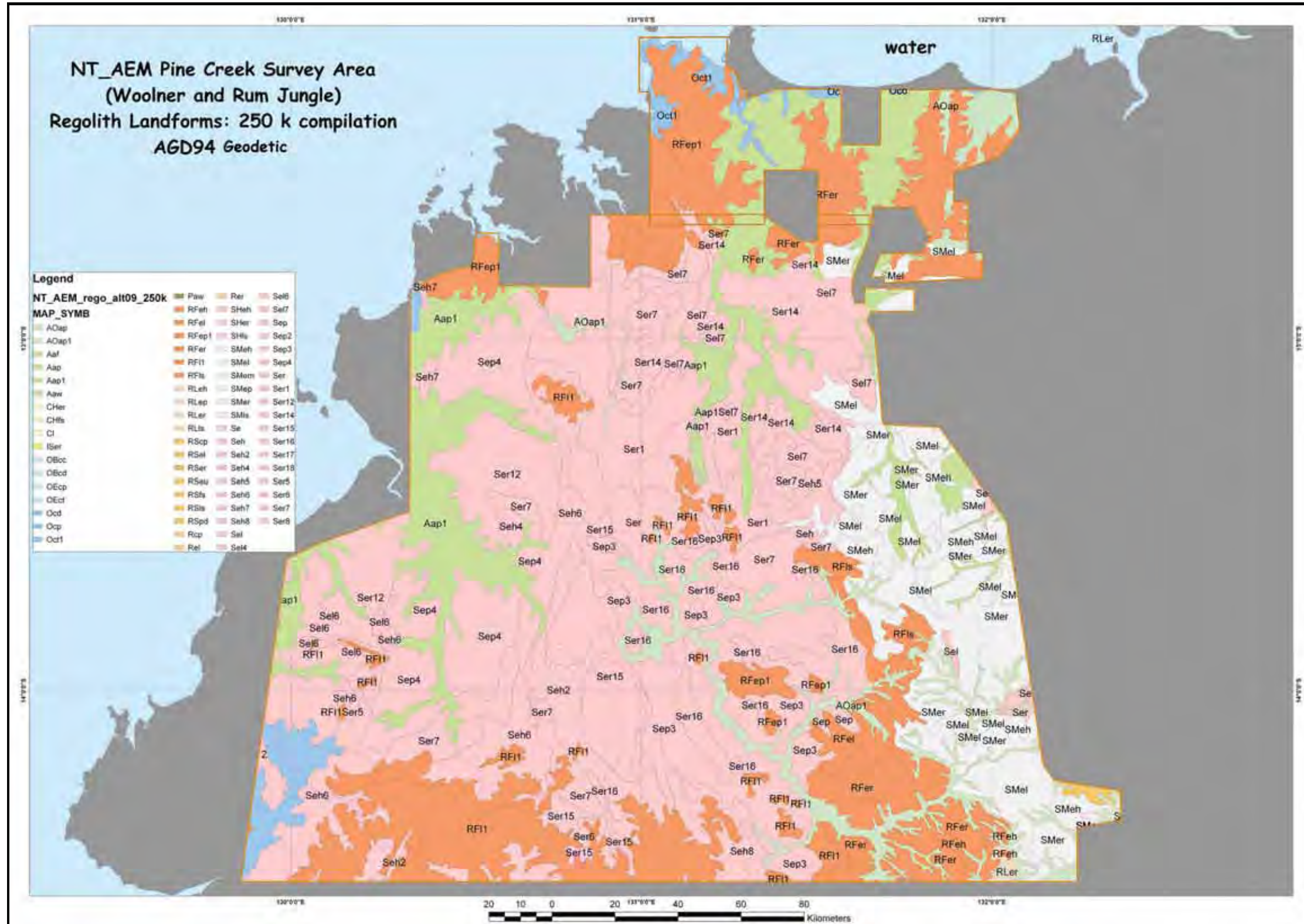


**Figure 3-4:** Regolith-Landform legend symbols constructed according to Geoscience Australia's RTMAP conventions. Possible combinations can be seen in [Tables 10–4](#) and [10–5](#) in [Appendix 10.10](#).



### **3.2.3 Palaeoweathering and palaeoregolith**

A systematic study of palaeoweathering or the possible occurrence of palaeoregolith either at surface or at depth from exposures or information contained in borehole records was outside the scope of this AEM survey. Land surfaces reported by Hays (1965, 1967 and 1968) have been used extensively to explain the observed planar features of the NT landscapes. Commonly extensive weathering profiles (up to 60 m thick) are reportedly superimposed on the respective surfaces. Palaeoweathering is reported to occur below the Kombolgie Subgroup and below the Cretaceous by Needham et al., (1988) in widespread locations and observations also noted in some borehole records.

The palaeotopographic surface at the base of the Kombolgie Subgroup is thought to be similar to that of the undulating sand plains, which cover much of the Pine Creek Inlier today. The unconformity undulates gently with amplitudes of ~20 m, though some scattered hills and ridges they approach a height of approximately 250 m. Development of this surface appears to have involved the prior removal by erosion of some 1-2 km of crustal materials. Chemical weathering produced a saprolitic weathering profile greater than 50 m deep over a period of c.40 Ma before deposition of the overlying Kombolgie Subgroup.

This information about the NT regolith and ancient weathering profiles and their distribution and subsequent erosion is pertinent to conductivity patterns and the sensible interpretation of regolith influences in the AEM survey data.

### **3.3 REFERENCES**

- Ahmad, M. and Lally, J. H., 2003. Pine Creek Orogen: field excursion guide. Chief Government Geologists Conference, 28 April - 2 May 2003. Northern Territory Geological Survey, Record 2003-003.
- Ahmad, M., Lally J. H. and McCready, A. J., 2006. Economic geology of the Rum Jungle Mineral Field., Northern Territory. Northern Territory Geological Survey, **Report 19**.
- Ahmad, M. and Munson, T. J., in prep. Geology and mineral resources of the Northern Territory Northern Territory Geological Survey, **Special Publication 5**.
- Ahmad, M., Wygralak A. S., Ferenczi, P. A. and Bajwah, Z. U., 1993. Pine Creek SD 52-8, explanatory notes and mineral deposit data sheets. 1:250 000 metallogenic map series. Northern Territory Geological Survey, Darwin.
- Carson, C. J., Hollis, J. A., Glass, L. M., Close, D. F., Whelan, J. A. and Wygralak, A. S., 2010. Summary of results. Joint NTGS-GA geochronology project: East Arunta Region, Pine Creek Orogen and Murphy Inlier, July 2007 - June 2009. Northern Territory Geological Survey, **Record 2010-004**, Darwin.
- Carson, C. J., Worden, K. E., Scrimgeour, I. R. and Stern, R. A., 2008. The Palaeoproterozoic evolution of the Litchfield Province, western Pine Creek Orogen, northern Australia: Insight from SHRIMP U-Pb zircon and in situ monazite geochronology. *Precambrian Research* **166**, 145-167.
- Craig, M.A., 2006. Regolith map of the Northern Territory, 1:2 500 000 scale. Northern Territory Geological Survey, Darwin.
- Craig, M.A., Anand, R.R., Churchward, M.C., Gozzard, R.J., Smith, R.E., and Smith, K., 1999. Regolith-landform mapping in the Yilgarn Craton, Western Australia: Towards a standardized approach CRC LEME Open File Report 72.
- Craig, M.A., Robertson, I.D.M., Thomas, M., Chamberlain, T., Jones, M.R. and Pillans, B.J., 2008. Atlas of regolith materials of Queensland - Companion to the 1:2 500 000 Queensland regolith-landform map and GIS. CRC LEME Open File Report 242.
- Cross, A., Claoué-Long, J. C., Scrimgeour, I. R., Ahmad, M. and Kruse, P. D., 2005. Summary of results. Joint NTGS-GA geochronology project: Rum Jungle, basement to southern Georgina Basin and eastern Arunta Region 2001–2003. Northern Territory Geological Survey, **Record**, Darwin.
- Dunster, J. N., Beier, P. R., Burgess, J. M. and Cutovinos, A., 2000. Auvergne, Northern Territory (second edition), 1:250 000 geological map series explanatory notes, SD 52-15. Northern Territory Geological Survey, Darwin.
- Eggleton, Richard, A., (editor), 2001. The Regolith Glossary: surficial geology, soils and landscapes. CRC LEME, Canberra.
- Ellis, G. K., Baillie, P. W. and Munson, T. J. E., 2004. Timor Sea Petroleum Geoscience. Proceedings of the Timor Sea Symposium, Darwin, Northern Territory, 19-20 June, 2003. Northern Territory Geological Survey, Special Publication 1 (CD-ROM), Darwin.
- Ferenczi, P. A. and Sweet, I. P., 2005. Mount Evelyn, Northern Territory. 1:250 000 geological map series explanatory notes, SD 53-05. Northern Territory Geological Survey Darwin & Alice Springs.

- Ferguson, J. and Needham, R.S. 1978. The Zamu Dolerite. A Lower Proterozoic preorogenic continental tholeiitic suites from the Northern Territory, Australia. *J. Geol. Soc. Aust.*, **25**: 309-322.
- Hammond, R. L., Nisbet, B. W., Etheridge, M. A. and Wall, V. J., 1984. The Litchfield Complex, North-West Northern Territory; Archaean basement or Proterozoic cover? *Australian Journal of Earth Sciences* **31**, 485-496.
- Hays, J., 1965. The relations between laterite and land surfaces in the northern part of the Northern Territory of Australia. Part XIV. Laterite. 22nd International Geological Congress, Dehhi, pp.14-28.
- Hays, J., 1967. Land surfaces and laterites in the north of the Northern territory. In: J.N. Jennings and J.A. Mabbutt (Editors). Landform studies from Australia and New Guinea. ANU Press, Canberra pp 182-210.
- Hays, J., 1968. Notes on geomorphology. In: B.P. Walpole, P.R. Dunn and M.A. Randal (Editors). Geology of the Katherine-Darwin region, Northern Territory. *Bureau of Mineral Resources, Geology and Geophysics. Bulletin* **82**. 304pp.
- Hollis, J. A., Carson, C. J. and Glass, L. M., 2009. SHRIMP U-Pb zircon geochronological evidence for Neoarchean basement in western Arnhem Land, northern Australia. *Precambrian Research* **174**, 364-380.
- Hollis, J. A., Glass, L. M., Carson, C., J., Armstrong, R., Yaxley, G. M., Kemp, A. I. S., Scherstén, A. and Phillips, D., 2011. The geological evolution of the Pine Creek Orogen: new pieces in the puzzle on orogen and craton scale. Paper presented at Annual Geoscience Exploration Seminar (AGES) 2011, Alice Springs (unpubl.).
- Johnston, J. D., 1984. Structural evolution of the Pine Creek Inlier and mineralization therein, N.T. Ph.D thesis, Monash University, Melbourne (unpubl.).
- Kruse, P. D., Sweet, I. P., Stuart-Smith, P. G., Wygralak, A. S., Pieters, P. E. and Crick, I. H., 1994. Katherine, Northern Territory. 1:250 000 geological map series explanatory notes, SD 53-9 (second edition). Northern Territory Geological Survey, Darwin.
- Kruse, P. D., Whitehead, B. R. and Mulder, C. A., 1990. Tipperary, Northern Territory. 1:100 000 geological series explanatory notes, sheet 5170. Northern Territory Geological Survey, Darwin.
- McAndrew, J., Williams, I. S. and Compston, W., 1985. A concealed Archaean complex in the Pine Creek Geosyncline. In: N.T. CSIRO Division of Mineralogy and Geochemistry Research Review 1985, pp. 56-57. CSIRO, Melbourne.
- Morgan, C. M., 1972. Port Keats (1st edition), N.T. 1:250 000 geological series explanatory notes, Sheet SD52-11. Northern Territory Geologic Survey, Darwin.
- Needham, R. S., 1988. Geology of the Alligator Rivers uranium field, Northern Territory. *Bureau of Mineral Resources, Geology and Geophysics, Bulletin No. 224*. Australian Geological Survey Organization, Canberra.
- Needham, R. S., Crick, I. H. and Stuart-Smith, P. G., 1980. Regional geology of the Pine Creek Geosyncline. In: Ferguson J. a. G., A.B. ed. Uranium in the Pine Creek Geosyncline, pp. 1-22. International Atomic Energy Agency, Vienna.
- Needham, R. S. and De Ross, G. J., 1990. Pine Creek Inlier - Regional geology and mineralisation. In: Hughes F. E. ed. Geology of the mineral deposits of Australia and Papua New Guinea, pp. 727-737. The Australasian Institute of Mining and Metallurgy, Monograph 14.

- Needham, R. S., Stuart-Smith, P. G. and Page, R. W., 1988. Tectonic evolution of the Pine Creek Inlier, Northern Territory. *Precambrian Research* **40-41**, 543-564.
- NTGS, 1989. Petroleum Basin Study-Arafura Basin. Prepared by Petroconsultants Australasia Pty Ltd. Northern Territory Government Printer, Darwin.
- NTGS, 1990. Petroleum Basin Study-Arafura Basin. Prepared by Petroconsultants Australasia Pty Ltd. Northern Territory Government Printer.
- NTGS, 2010. Geological regions of the Northern Territory (1:40 million scale map). Northern Territory Geological Survey, Darwin.
- Page, R. W., Compston, W. and Needham, R. S., 1980. Geochronology and evolution of the late-Archaean basement and Proterozoic rocks in the Alligator Rivers uranium field, Northern Territory, Australia. Proceedings Series - International Atomic Energy Agency = Collection Comptes Rendus - Agence Internationale de l'Energie Atomique, 39-68.
- Pietsch, B. A. and Edgoose, C. J., 1988a. The stratigraphy, metamorphism and tectonics of the Early Proterozoic Litchfield Province and western Pine Creek Geosyncline, Northern Territory. *Precambrian Research* **40-41**, 565-588.
- Pietsch, B. A. and Stuart-Smith, P. G., 1988b. Darwin, Northern Territory. 1:250 000 geological series explanatory notes SD 52-04. Northern Territory Geological Survey, Darwin.
- Rawlings, D. J. and Page, R. W., 1999. Geology, geochronology and emplacement structures associated with the Jimbu Microgranite, McArthur Basin, Northern Territory. *Precambrian Research* **94**, 225-250.
- Rhodes, J. M., 1965. The geological relationships of the Rum Jungle Complex, Northern Territory. Bureau of Mineral Resources, **Report 89**, Canberra.
- Robertson, I.D.M., Craig, M.A. and Anand, R.R., 2006. Atlas of regolith materials of the Northern Territory. CRC LEME Open File Report 196.
- Skwarko, S. K., 1966. Cretaceous stratigraphy and palaeontology of the Northern Territory. Australia, Bureau of Mineral Resources, Geology and Geophysics, **Bulletin 73**; 136 pp, Canberra.
- Stephansson, O. and Johnson, K., 1976. Granite diapirism in the Rum Jungle area, northern Australia. *Precambrian Research* **3**, 159-185.
- Stuart-Smith, P. G., Bagas, L. and Needham, R. S., 1988a. Ranford Hill, Northern Territory. 1:10 000 map commentary. Australia, Bureau of Mineral Resource, Geology and Geophysics, Canberra.
- Stuart-Smith, P. G., Needham, R. S. and Bagas, L., 1988b. Stow Region, Northern Territory, 1:100 000 map commentary. Australia, Bureau of Mineral Resources, Geology & Geophysics, Canberra.
- Stuart-Smith, P. G., Needham, R. S., Page, R. W. and Wyborn, L. A. I., 1993. Geology and mineral deposits of the Cullen mineral field, Northern Territory.. *Australia, Bureau of Mineral Resources, Geology and Geophysics, Bulletin 229*, Canberra.
- Valenta, R. K., 1991. Structural controls on mineralisation of the Coronation Hill deposit and surrounding area. Australia, Bureau of Mineral Resources, Geology and Geophysics, **Record**, Canberra.

- Walpole, B. P., Crohn, P. W., Dunn, P. R. and Randal, M.A. R., 1968. Geology of the Katherine-Darwin region, Northern Territory. *Mineral Resources, Geology and Geophysics, Bulletin No. 82*, Canberra.
- Worden, K., Carson, C., Scrimgeour, I., Lally, J. and Doyle, N., 2008. A revised Palaeoproterozoic chronostratigraphy for the Pine Creek Orogen, northern Australia: Evidence from SHRIMP U-Pb zircon geochronology. *Precambrian Research* **166**, 122-144.

## 4 Mineral systems overview

*S. Jaireth*

### 4.1 INTRODUCTION

The Pine Creek Orogen (PCO) hosts world-class, unconformity-related uranium deposits. It is one of Australia's most metal-endowed Proterozoic provinces hosting several mineral occurrences, prospects, and mineral deposits of uranium, gold, tin-tantalum, tungsten, copper and lead-zinc deposits. A brief overview of mineral deposits in the PCO is presented by (Ahmad, 1998). A more detailed description of deposits and mineral systems in the Rum Jungle Mineral Field is available in a review by Ahmad *et al.* (2006). More recent reviews of uranium and gold deposits have been published by Lally and Bajwah (2006) and Ahmad *et al.* (2009). Significant pegmatite-associated tin-tantalum mineralisation in the PCO is reviewed by Frater (2005). A brief review of mineral systems in the PCO presented in this chapter draws largely on these publications.

Recent geochronological studies provide constraints on the timing of important mineralising events ([Table 4–1](#); [Figure 4–1](#); [Figure 4–2](#); [Figure 4–3](#)) in the PCO. The deposit ages are also shown on [Figure 4–4](#). These data assist to understand mineral systems in relation to sedimentary, diagenetic, deformation, metamorphic, magmatic, uplift and erosional events in the Orogen.

### 4.2 ARCHEAN MINERAL SYSTEMS

Archean (2700-2500 Ma) granite gneisses, granite and minor metasedimentary (schist and banded iron formation) rocks (Rum Jungle Complex and Woolner Granite in the Central Domain and Njibinjibinj, Arrarra and Kukalak Gneisses and Nanambu Complex in the Nimbuwah Domain) are exposed locally in the PCO (Hollis *et al.*, 2011).

Recent geochronological studies have revealed additional exposures of Neoarchean in the Nimbuwah Domain. These studies identify three distinct episodes of felsic magmatism across the PCO (Hollis *et al.*, 2009a; Hollis *et al.*, 2011): ca. 2670 Ma (Woolner Granite and Njibinjibinj Gneiss), ca. 2640 Ma (Arrarra Gneiss), and ca 2530-2510 Ma (Rum Jungle Complex, Nanambu Complex, and Kukalak Gneiss). The dominance of ca. 2550-2500 Ma zircon ages related to older Archean components (2670-2640 Ma) in detrital spectra from Paleoproterozoic rocks and the prevalence of granitic basement rocks (ca. 2530-2500 Ma) suggests that the late Neoarchean felsic magmatism volumetrically dominated within the Archean basement (Hollis *et al.*, 2009; 2009a; Hollis *et al.*, 2009b).

Strongly fractionated Neoarchean granites show pronounced depletion in heavy rare-earth elements indicative of garnet in the source (Glass *et al.*, 2009). There are some differences in the  $\epsilon_{\text{Nd}}$  and  $\epsilon_{\text{Hf}}$  isotope compositions of these rocks, but overall the correlation of the geochemistry and Nd and Hf isotope composition of the magmatic rocks indicate that the Central and Nimbuwah domains formed a coherent Neoarchean crustal block (Hollis *et al.*, 2011).

Narrow homogenous rims on zircons from the gneisses in the Nimbuwah Domain suggest that metamorphic crystallisation occurred at ca. 2500 Ma. This metamorphic event was broadly coeval with the Kukalak felsic magmatism (ca. 2530-2510 Ma) in the Nimbuwah Domain (Hollis *et al.*, 2009a).

The metasediments (Stanley Metamorphics) have been metamorphosed to almandine-amphibolite facies. Ahmad *et al.* (2006) infer at least two episodes of Pre-Paleoproterozoic deformations affecting Archean rocks. According to them several shear zones mapped within the Archean

basement do not appear to correspond to faults or folds in the overlying Proterozoic rocks. Some of these structures mark boundaries between geophysical subdivisions of the Archean complexes.

The Archean granites in the Rum Jungle Complex have anomalously high uranium (2.9 – 39.9 ppm; average 12.5 ppm; McCready *et al.*, 2003) and could be important as first-stage source rock of uranium to form uranium deposits in the PCO (see discussion below).

No known deposits or occurrence of Neoarchean age are reported in PCO.

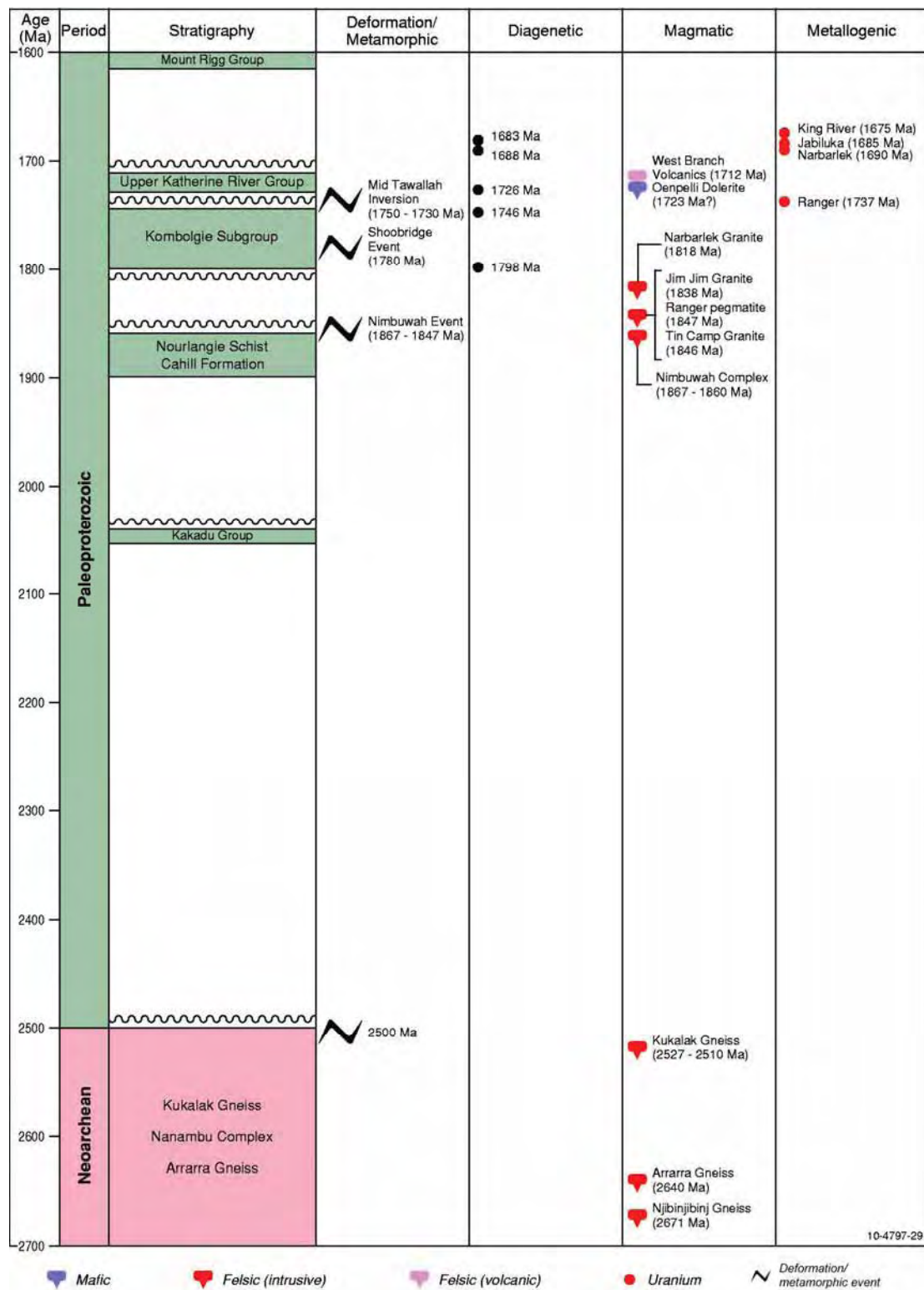


**Figure 4-1:** Nimbuwah Domain. Time-event plots of three domains in the Pine Creek Orogen. The age data and relevant references are summarised in Table 4-1.

Geological and energy implications of the Pine Creek airborne electromagnetic (AEM) survey,  
Northern Territory, Australia

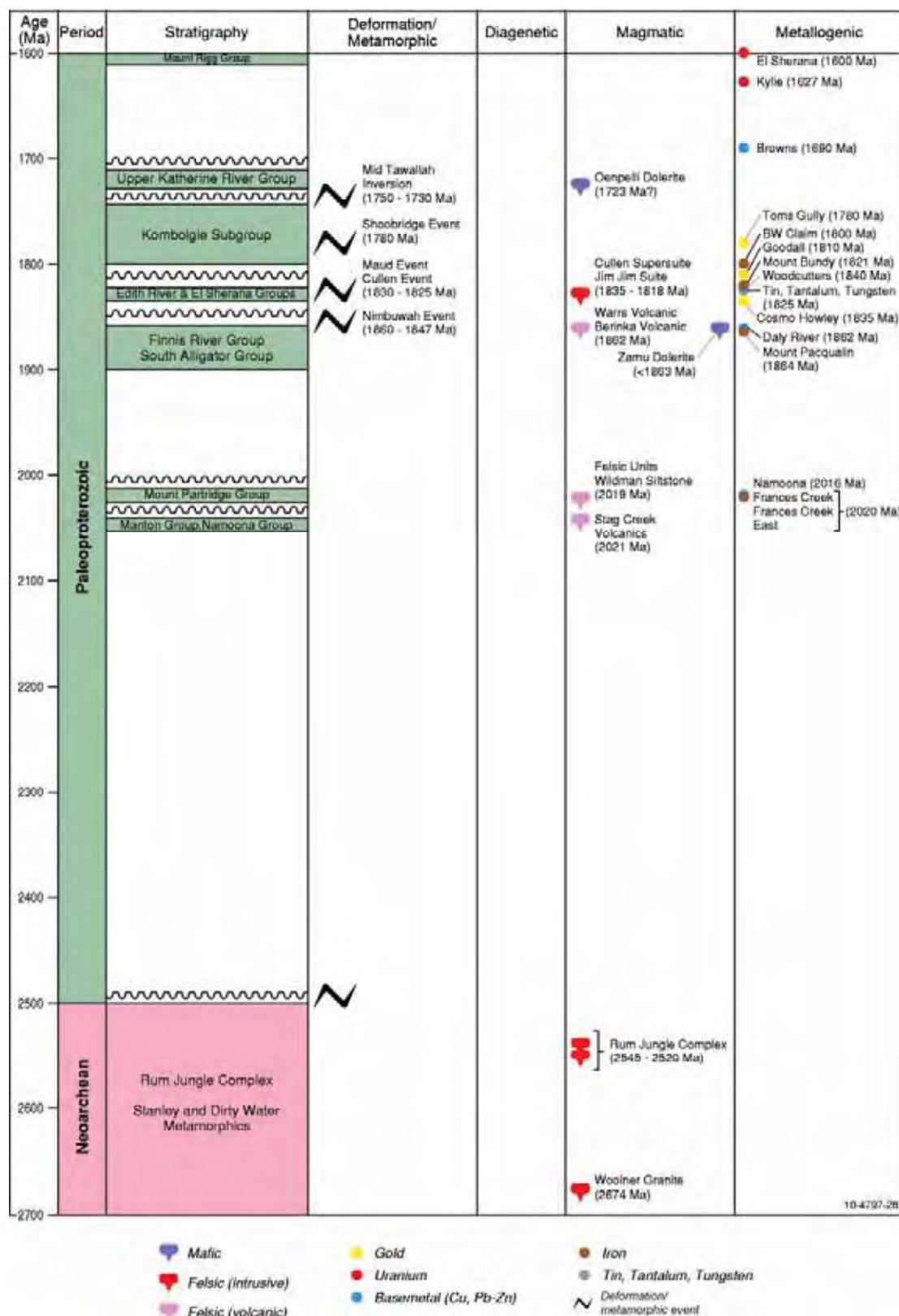
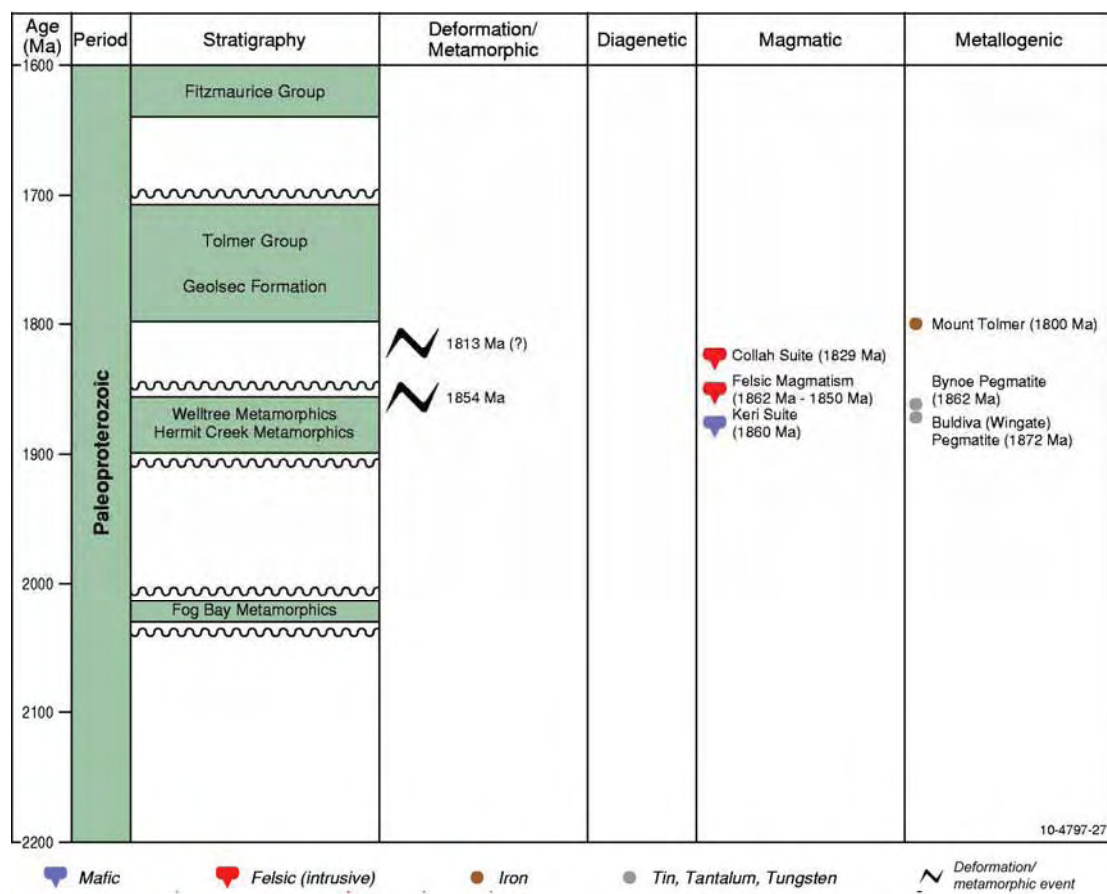


Figure 4-2: Central Domain. Time-event plots of three domains in the Pine Creek Orogen. The age data and relevant references are summarised in Table 4-1.



**Figure 4-3:** Litchfield Domain. Time-event plots of three domains in the Pine Creek Orogen. The age data and relevant references are summarised in [Table 4-1](#).

**Table 4-1:** Ages of deposits/prospects

DEPOSIT	DOMAIN	COMMODITY	TYPE	AGE (MA)	ERROR (MA)	COMMENT	REFERENCE
Adelaide River	Central	U	Unconformity-related uranium	701	190	LA-HR-ICPMS age of uraninite. Upper intercept of concordia	1
Palette	Central	U	Unconformity-related uranium	841	94	LA-HR-ICPMS age of uraninite. Upper intercept of concordia	1
Koongarra	Central	U	Unconformity-related uranium	870		Whole rock U-Pb age of uraninite from upper intercept of concordia	2
El Sherana	Central	U	Unconformity-related uranium	1600		Whole rock U-Pb age of uraninite. Upper intercept of concordia; La-HR-ICPMS of uraninite gives $1573 \pm 160$ Ma	3; 1
Kylie	Central	U	Unconformity-related uranium	1627	45	Whole rock U-Pb age of uraninite from upper intercept of concordia	4
Nabarlek	Nimbuwah	U	Unconformity-related uranium	1642 (or ca.1690)	33	LA-HR-ICPMS age of uraninite. Ar/Ar age of sericite in the alteration zone gives $1696 \pm 7$ to $1715 \pm 7$ Ma. Resetting at ca. 1360 Ma, ca. 1100 Ma, and ca. 900 Ma	5
King River	Nimbuwah	U	Unconformity-related uranium	1675		Interpreted age. Method unknown.	6
Jabiluka	Nimbuwah	U	Unconformity-related uranium	1685	17	LA-HR-ICPMS age of uraninite. Ar/Ar age of illite in the sandstone gives $1683 \pm 11$ Ma. Resetting at $1302 \pm 37$ Ma, $1191 \pm 27$ Ma and $802 \pm 57$ Ma	7
Browns	Central	Cu, Pb, Zn, Ni	Sediment hosted base metal	1690		Average Pb-Pb model age of galena, reinterpreted	18

DEPOSIT	DOMAIN	COMMODITY	TYPE	AGE (MA)	ERROR (MA)	COMMENT	REFERENCE
Ranger	Nimbuwah	U	Unconformity-related uranium	1737	20	Whole rock U-Pb date of ore. Upper intercept of concordia	7
Toms Gully	Central	Au	Lode gold	1780	10	SHRIMP U-Pb analysis of monazite from gold vein	8
B.W Iron Claim	Central	Fe	Banded iron formation	1800 (?)		Interpreted age of the host Geolsec Formation	9; 10
Goodall	Central	Au	Lode gold	1810	10	SHRIMP U-Pb analysis of xenotime and monazite from gold vein	11
Woodcutters	Central	Zn, Pb	Sediment hosted lead-zinc	1840		Pb-Pb model age of galena, reinterpreted	18
Evelyn Mine	Central	Pb, Zn, Ag	Skarn	1822	6	Interpreted from the age of the Allamber Springs Granite	13
Mount Diamond	Central	Cu, Pb, Ag, Au	Felsic-intrusive related vein	1825		Average age of Cullen Supersuite (Mount Davies Granite)	14
Mount Wells	Central	Sn, Ta	Vein	1825		Average age of Cullen Supersuite (Price Springs Granite )	14
Barretts (Tipperary)	Central	Sn, Ta	Pegmatite	1825		Interpreted age of the Shoobridge Granite	14
Wolfram Hill	Central	W, Cu, Sn	Vein	1825		Average age of Cullen Supersuite (Wolfram Hill Granite)	14
Yederalba	Central	W, Sn	Vein	1825		Average age of Cullen Supersuite (Yederalba Granite)	14
Mount Bunney	Central	Fe	Skarn	1821	5	Interpreted from the age of the Mount Bunney Granite	8

DEPOSIT	DOMAIN	COMMODITY	TYPE	AGE (MA)	ERROR (MA)	COMMENT	REFERENCE
Cosmo Howley	Central	Au	Lode gold	1835	6	Interpreted from the age of felsic rocks, emplaced during mineralisation	16; 14
Hayes Creek	Central	Sn, Ta	Vein	1835	6	Age of the McMinn's Bluff Granite	14
Bynoe Area	Litchfield	Sn, Ta	Pegmatite	1862		Interpreted age of the Two Sisters Granite	17; 14
Daly River	Central	Zn, Pb, Cu	Volcanic associated massive sulphide	1862	3	Interpreted from the age of the host Warrs Volcanic Member	10
Mount Pacqualin	Central	Fe	Banded iron formation	1864		Interpreted age of the host Koolpin Formation	9; 10
Buldiva (Wingate)	Litchfield	Sn, Ta	Pegmatite	1872 (max. age)		Age of the Allia Creek Granite, Soldiers Creek Granite	17; 14
Frances Creek	Central	Fe	Volcanogenic hydrothermal iron	2019	4	Age of the host Wildman Siltstone	9; 10
Winchester	Central	Mg	Sedimentary Diagenetic, remobilised	2019	4	Interpreted from the geological age of the Coomalie Dolostone	12; 10
Frances Creek East	Central	Fe	Volcanogenic hydrothermal iron	2021	10	Interpreted from the age of the host Mason Formation	12; 10
Namoona	Central	Zn, Pb	Sediment hosted lead-zinc	2016		Pb-Pb model age of galena, reinterpreted	12; 10

References: 1-Chipley *et al.* (2007); 2-Hills and Richards (1976); 3-Greenhalg and Jeffery (1959); 4-von Pechmann (1992); 5-Polito *et al.* (2004); 6-Polito *et al.* (2005); 7-Ludwig *et al.* (1987); 8-Rasmussen *et al.* (2006); 9-Ahmad *et al.* (1993); 10-Worden *et al.* (2008); 11-Compston and Matthai (1994); 12-Ahmed *et al.* (2006); 13-Ferenczi and Sweet (2005); 14-Budd *et al.* (2001); 15-Ferenczi (2002); 16-Matthai *et al.* (1995); 17-Frater (2005); 18-This publication.

**Geological and energy implications of the Pine Creek airborne electromagnetic (AEM) survey, Northern Territory, Australia**

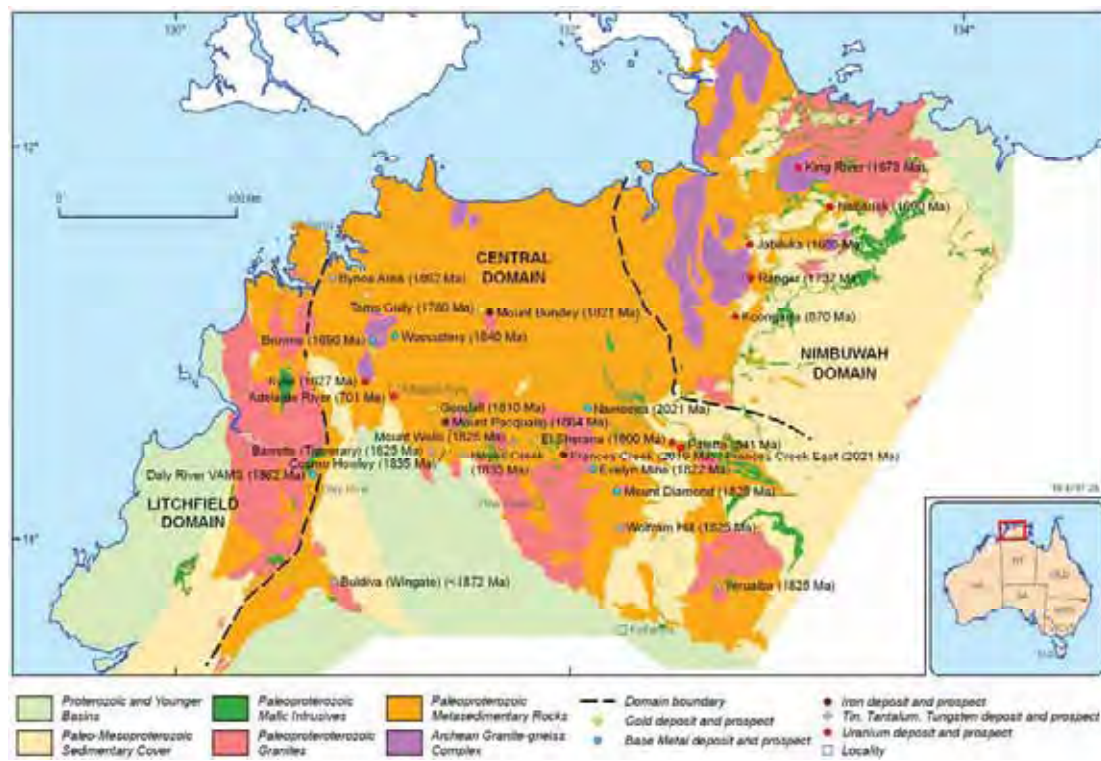


**Figure 4-4:** Map of the Pine Creek Orogen showing known ages of deposits and prospects. The map is based on an NTGS dataset, i.e., Pine Creek interpreted geology (2005). Deposits, prospects and occurrences are from GA's OZMIN and MINLOC datasets. The age data for deposits and references are summarised in [Table 4-1](#).

#### **4.2.1 Paleoproterozoic (2500 Ma to 2020 Ma)**

The earliest Paleoproterozoic succession is interpreted to have been deposited as a response to continental rifting and subsidence of the Neoarchean basement. The rifting and extension is thought to be part of a major extensional event in the North Australian Craton during which Archean continental crust underwent ENE-WSW extension (de Vries *et al.*, 2008). In the PCO the extension led to the formation of a series of tilted blocks progressively deepening to the east, resulting in an increase in sediment thickness from 2 km to 18 km (Ahmad *et al.*, 1993).

This event saw deposition of two packages. The first, represented by the Manton and Namoona Groups in the Central Domain and the Kakadu Group in the Nimbuwah Domain, comprises immature fluvial arkoses and conglomerate (e.g. Beestons Formation) and supra- to inter-tidal conglomerates. The sedimentation of relatively fine-grained sediments occurred in probably low-energy environment (Masson Formation in the eastern part of the Central Domain) and was accompanied by localised basaltic-andesitic volcanism (Stag Creek Volcanics).

The second package, which unconformably overlies the first package (Mount Partridge Group in the Central Domain), comprises fluvial immature clastic carbonate, and carbonaceous sediments. The sediments were deposited in shallow marine-intertidal conditions. The upper part of the package contains subtidal to shallow marine terrigenous sandstones, mudstones interbedded with volcanics and volcanogenic sedimentary rocks (Wildman Siltstone). This package is absent in the eastern region of the Central Domain and in the Nimbuwah Domain. The tentative correlation between the Wildman Siltstone with the Nourlangie Schist proposed by (Needham, 1988) has been questioned by recent studies (Hollis *et al.*, 2009b).

SHRIMP U-Pb zircon geochronological studies indicate that sediments of the two packages have restricted provenance and were derived predominantly from Neoarchean sources (Hollis *et al.*, 2011; Worden *et al.*, 2008a; Cross *et al.*, 2005). However detrital zircons in the Crater Formation (the lowermost unit of the Mount Partridge Group) indicate that some sedimentary rocks were probably derived from the Eoarchean crust (Hollis *et al.*, 2011).

The Fog Bay Metamorphics in the Litchfield Domain comprises quartz-feldspar-biotite gneiss interlayered with para-amphibolite and very minor calc-silicate and marble (Pietsch and Edgoose, 1988). Hickey (1985) reported an Nd-Sm model age of  $2280 \pm 40$  Ma and a whole rock Rb-Sr isochron age of  $2002 \pm 42$  Ma for the gneiss. A SHRIMP U-Pb analysis of the detrital component of a zircon yielded a maximum age of deposition of  $2028 \pm 8$  Ma for the metasediments (Carson *et al.*, 2008). These ages are interpreted to correlate the Fog Bay Metamorphics with the Mount Partridge Group in the Central Domain. A metamorphic event at ca. 2000 Ma is interpreted from the SHRIMP U-Pb analysis of zircon cores. This metamorphic event either affected the sediments directly or the source region from which the zircons were derived (Carson *et al.*, 2009).

A variety of mineral systems are associated with this event. They are syngenetic, diagenetic and epigenetic in relation to the host rocks.

#### **4.2.2 Stratabound Pb-Zn-Ag**

Eight stratabound occurrences of Pb-Zn-Ag are reported in the dolomitic, pyritic, graphitic shales of the Masson Formation (Ferenczi and Sweet, 2005). Poorly bedded, massive sulphide mineralisation at the Namoona and Namoona South Pb-Zn prospects is intersected in a succession, which contains rhyolitic tuff and tuffaceous shale (Figure 4–5). The main ore minerals comprise fine- to medium-grained galena, sphalerite and pyrite. Some drill intersections located high-grade Pb-Zn-bearing quartz and carbonate veins in breccia zones. This mineralisation may be the result of remobilisation

of stratiform ore bodies. Some rhyolitic tuffaceous beds also contain poddy mineralisation of variable grade (Ferenczi and Sweet, 2005).

The SHRIMP U-Pb analysis of zircons in the Stag Creek Volcanics (a constituent of the Masson Formation) yields an age of  $2021 \pm 10$  Ma (Worden *et al.*, 2008a). If the stratabound mineralisation is broadly syngenetic with the host sediments, the age of the Stag Creek Volcanics can provide a good constraint on the age of mineralisation. Galena from the deposit gives a Pb-Pb model age ca. 2016 Ma (Figure 4–6). Figure 4–6 shows the isotopic composition of a number of other lead-bearing mineral deposits from the Pine Creek Orogen. The data are plotted on a isotopic evolution grid determined by modifying a Cumming and Richards (1975) lead isotope evolution model to fit the least radiogenic analyses of galena from the ~1862 Ma Daly River VHMS district ( $\varepsilon = 0.098835 \times 10^{-9}$ ). This model, informally called the Pine Creek model, gives ages significantly older (50-70 million years) than the North Australia model of Sun *et al.* (1996). This new Pine Creek model also yields geologically realistic ages of other base metal deposits (Woodcutters and Browns) in the Pine Creek Orogen, which are discussed in the following sections.

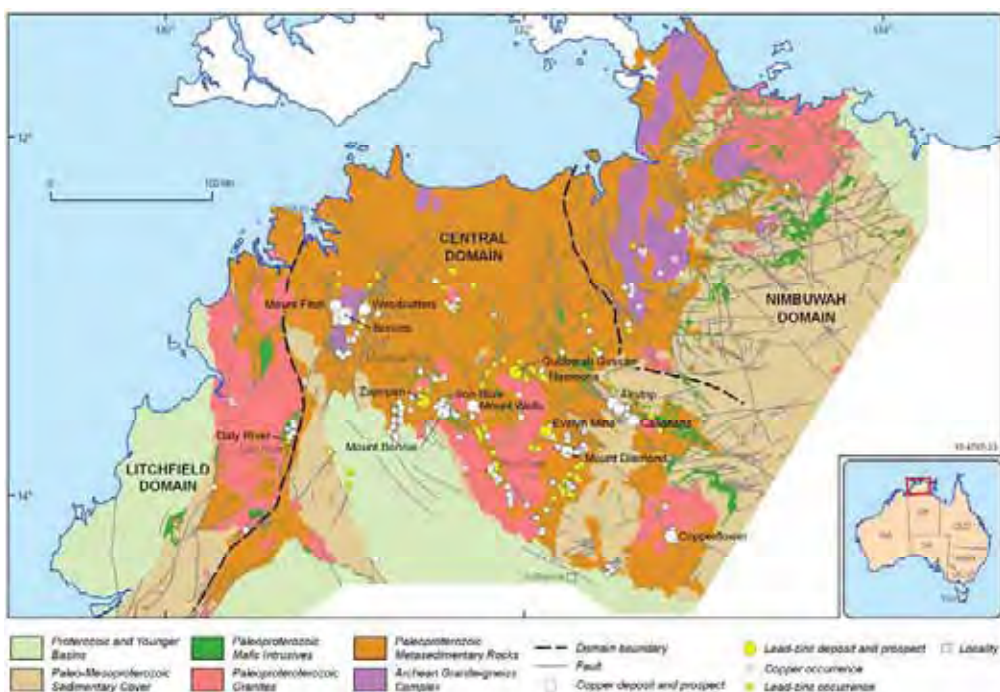


**Figure 4-5:** Map of the Pine Creek Orogen showing basemetals (Cu, Pb-Zn) deposits and occurrences. The map is based on an NTGS dataset, i.e., Pine Creek interpreted geology (2005). Deposits, prospects and occurrences are from GA's OZMIN and MINLOC datasets.

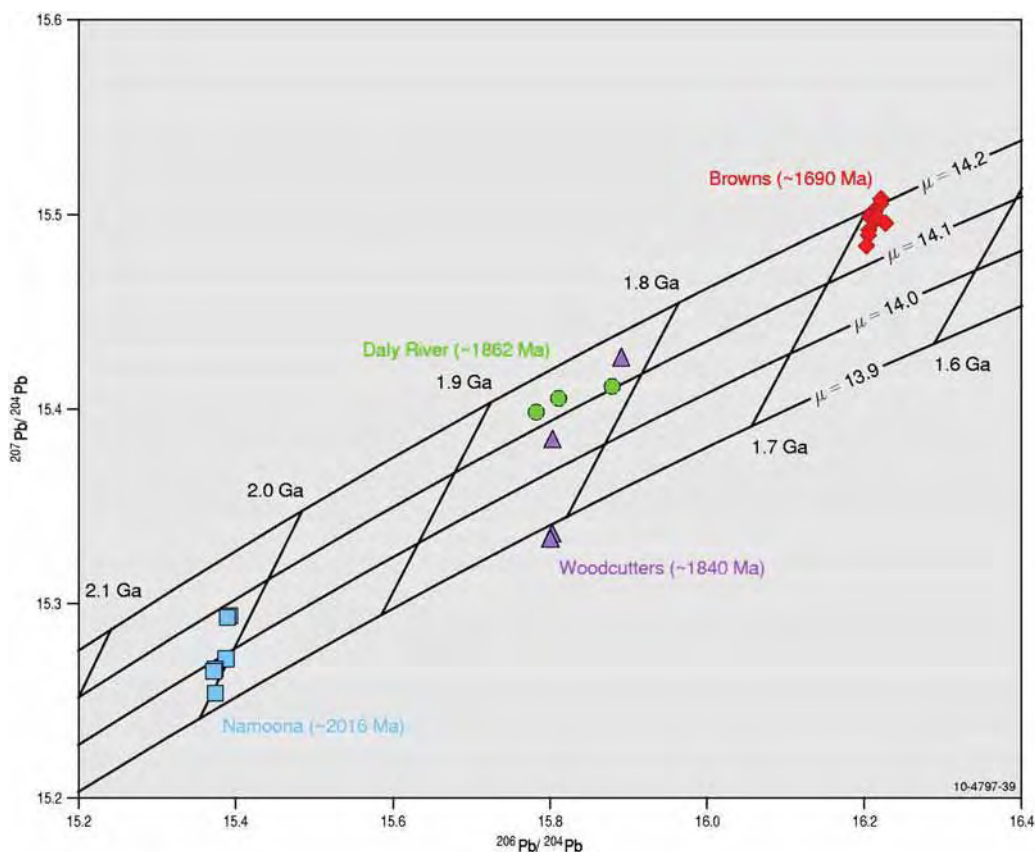


**Figure 4-6:** New Pb-Pb model for Pine Creek deposits showing Pb-Pb model ages for selected deposits.  
Model ages calculated by David Huston.

#### 4.2.3 Iron ore

Several iron ore deposits and prospects in the Frances Creek Ironfield (Figure 4-7) are hosted by, the Wildman Siltstone (Frances Creek) and the Masson Formation (Frances Creek East). At Frances Creek massive hematitic conformable bodies are located in carbonaceous, pyritic shale at the base of the Wildman Siltstone. The ore bodies and the host rock are deformed into open folds. Locally in proximity to faults ore is brecciated and overprinted by weathering. At the Frances Creek East the comfortable ore bodies are within tightly folded carbonaceous, pyritic shales and phyllites of the Masson Formation (Ahmad *et al.*, 1993).

The origin of these deposits is unknown. The presence of rhyolitic tuff and other volcaniclastic sediments in the Masson Formation are interpreted to be the first volcanic episode in the PCO (Ferenczi and Sweet, 2005). The amount of volcanic material increases in the Stag Creek Volcanic, which conformably overlies the Masson Formation. The Stag Creek Volcanics comprises altered amygdaloidal basalt, basaltic andesite, basaltic agglomerate and volcaniclastic shale and arenite. Rare pillow structures indicate a subaqueous depositional environment. Geochemistry of basalts points to a low-K tholeiite basaltic composition. Rocks in both Masson Formation and Stag Creek Volcanics are variably altered and contain alteration chlorite, clinozoisite, hematite, sericite and calcite. The mineralisation may be either volcanogenic hydrothermal or sedimentary and broadly syngenetic with the host sequence.

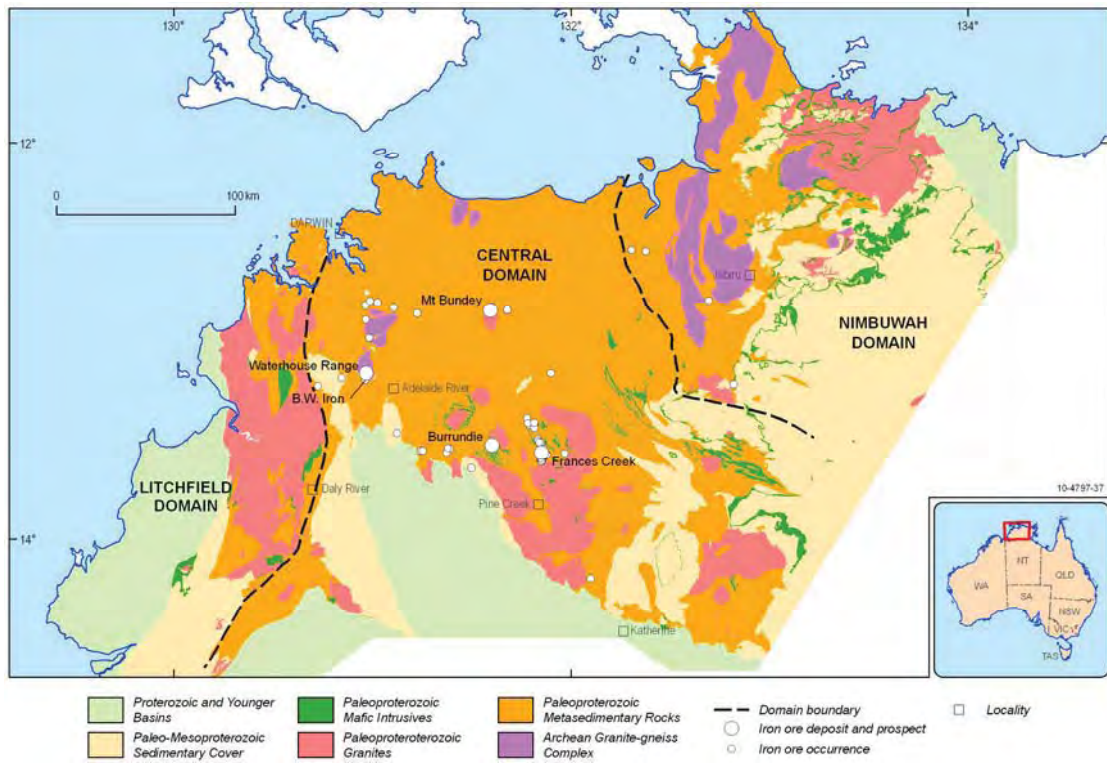


**Figure 4-7:** Map of the Pine Creek Orogen showing Iron ore deposits and occurrences. The map is based on an NTGS dataset, i.e., Pine Creek interpreted geology (2005). Deposits, prospects and occurrences are from GA's OZMIN and MINLOC datasets.

#### 4.2.4 Stratabound Pb, Zn, Cu

The polymetallic (Pb, Zn, Cu, Ni, Co) Browns deposit is hosted predominantly in the carbonaceous Whites Formation (Figure 4-4). The deposit is located on the northern limb of a regional syncline that plunges gently to south-west. The ore body is cross cut by north-trending splay of the Giants Reef Fault. The mineralisation is localised in the basal part of the Whites Formation close to its contact with the Coomalie Dolostone (Ahmad *et al.*, 2006). The host rock has been deformed, metamorphosed (green-schist facies) and intruded by locally transgressive mafic sills thought to be part of the Zamu Dolerite.

Two types of base metal mineralisation are present at the Browns deposit. In one of them sulphides are generally distributed along the dominant bedding parallel foliation. This type of mineralisation is fine-grained (< 50µm). Galena and sphalerite whisps occur in microfolds and are crosscut and deformed by crenulation cleavage. The second type of mineralisation is coarse grained and locally forms clots and veins which crosscut bedding, bedding-parallel foliation and the crenulation cleavage (McCready *et al.*, 2004).

McCready *et al.* (2004) interpret the first type of mineralisation syndiagenetic in relation to the host Whites Formation and the second type epigenetic most probably linked to metamorphism. As the age of deposition of the Whites Formation is constrained to be ca. 2020 Ma the ‘syndiagenetic’ mineralisation could have occurred at ca. 2020 Ma. At this stage the presence of syndiagenetic mineralising event is inferred solely on the basis of textural evidence (see above). The above conclusion is inconsistent with the Pb-Pb model ages of galena. The new Pine Creek lead model

yields a Pb-Pb model age of ca. 1690 Ma for galena (both fine- and coarse-grained) from the Brown deposit ([Figure 4–6](#)), which is much younger than the age of the host Whites Formation ( $2019 \pm 4$  Ma). The significance of this age and the relationship between uranium and base metal deposits in the Rum Jungle Mineral Field is discussed in more detail in the later section of this chapter.

#### **4.2.5 Uranium**

Several base metal and uranium prospects and deposits are located in close proximity in the Rum Jungle Mineral Field. The timing and relation between uranium and base metal mineralisation will be discussed in more detail in later sections. For uranium systems this period is important because the atmosphere during this period was anoxic with oxygenation beginning only at ca. 2200 Ma and reaching its present-day level at ca. 1900 Ma. It is possible that during reduced atmospheric conditions some detrital uraninite was deposited with sediments particularly within conglomerates. The Beestons Formation, which unconformably overlies the Rum Jungle Complex, contains conglomerates which also include vein quartz pebble conglomerate (Ahmad *et al.*, 2006). Similarly the Crater Formation, which unconformably overlies the Namoona Group, also comprises poorly sorted, pebble to boulder-size, subrounded clasts of hematitic, banded ironstone and vein quartz within a quartz-hematite sandstone matrix.

On the airborne radiometric data, Beestons Formation does not show strong and consistent uranium response. Relatively higher uranium response is observed on the southeastern side of the Rum Jungle Complex. The Crater Formation, on the other hand, shows higher uranium response particularly at the margins of the Rum Jungle Complex.

Most uranium prospects and deposits in the Rum Jungle Mineral Field are interpreted to be part of unconformity-related uranium systems hosted in the reduced rocks below the unconformity between the Depot Creek Sandstone and the Whites Formation (Ahmad *et al.*, 2006). However whole-rock U-Pb analysis of uraninite-bearing ore samples from the Whites East deposit gives a significantly older age. Three samples yielded a Discordia; its upper intercept indicates an age of slightly over 2200 Ma (von Pechmann, 1992). Von Pechmann (1992) regards the age geologically without meaning however it is possible the age reflects the age of detrital uraninite, which was remobilised later. It is also likely that the age is a mixture of the age of the host rock and uraninite.

Intensive exploration in the area has failed to find paleoplacer-hosted uranium mineralisation (Blind River-Elliot Lake style) in the Rum Jungle Mineral Field. It is possible that if this style of mineralisation was formed in the area, it was either eroded or recycled by interaction with oxidised fluids in more oxygenated atmospheric conditions.

#### **4.2.6 Magnesite**

Stratabound occurrences and deposits of magnesite (such as Winchester) in the Rum Jungle Mineral Field are hosted in the Celia and Coomalie Dolostones. Dolomite, magnesite, and talc are some of the major minerals. Some prospects contain traces of pyrite. Other minor minerals include quartz, chlorite, iron oxides (hematite), apatite, and minor tourmaline. Both the Celia and Coomalie Dolostones show extensive styolitisation. Brecciated sulphide ore at the boundary between Coomalie Dolostone and Whites Formation is interpreted to be caused by styolitisation (Muir, 1980; cited in Ahmad *et al.*, 2006).

The origin of magnesite mineralisation is unknown. The deposits are classified as Vietsch-type and their formation is explained through the following sequence of events (Ahmad *et al.*, 2006): deposition of carbonate-rich sediments and subsequent dolomitisation along an island shoreline at ca. 2000 Ma; deformation and metamorphism of PCO rocks during the Nimbuwah Event at ca. 1865 Ma; thermal metamorphism of PCO rocks during the Cullen Event at ca. 1825 Ma ([Table 4–1](#)); widespread sericitic alteration of rocks during the thermal event at ca. 1780 Ma releasing Mg-rich fluids that reacted with dolomite to produce magnesite.

#### **4.3 PALEOPROTEROZOIC (1900 Ma TO 1860 Ma)**

In the Nimbuwah Domain the Kakadu Group is overlain by a package of middle to upper amphibolite facies metasedimentary rocks (Cahill Formation and Nourlangie Schist). This package was formerly correlated with the Mount Partridge Group (Needham, 1988), but recent studies show that it was formed in a distinct depocentre at ca. 1870 Ma. The deposition age of this package which hosts world-class uranium deposits is constrained by a youngest detrital population of  $1866 \pm 11$  Ma (Hollis *et al.*, 2011).

The sedimentation of the South Alligator and Finniss River Groups occurred after period of uplift, erosion and deformation (Worden *et al.*, 2008a; Stuart-Smith *et al.*, 1980). The difference in the determined ages of the Wildman Siltstone (ca. 2019 Ma) and the Gerowie Tuff (ca. 1863 Ma) suggests a gap in sedimentation of more than 160 million years. However no structural evidence of deformation of the Pre-South Alligator Group has as yet been reported in the Rum Jungle area (Ahmad *et al.*, 2006). The mature character of sediments (e.g. Koolpin Formation) is interpreted to be indicative of deposition during a thermal subsidence following cessation of major extension and faulting (Needham *et al.*, 1988).

The sedimentation of the South Alligator River and Finniss River Groups took place at ca. 1860 Ma. The age of deposition is constrained by the age of felsic volcanism (between 1863 Ma and 1861 Ma) and the maximum age of the Burrell Creek Formation between 1868 Ma and 1860 Ma (Worden *et al.*, 2008a; Worden *et al.*, 2008b; Hollis *et al.*, 2011).

The South Alligator Group comprises carbonaceous and pyritic shales and cherts (Koolpin Formation) and sub-areal to sub-aqueous felsic tuffs and volcanogenic sedimentary sediments of the Gerowie Tuff and Mount Bonnie Formation. The basal unit (Ella Creek Member) of the Koolpin Formation is inferred to be similar to a paleoregolith formed during weathering of the underlying strata (Crick, 1987; cited in Ahmad *et al.*, 2006). It comprises ironstone, chert breccia siltstone with chert nodules and rare ferruginous grit, pebble and boulder conglomerate. However, Pietsch and Stuart-Smith (1988) dispute the paleoregolith nature of the unit and consider some features to be the products of recent weathering.

The sediments of the South Alligator Group were formed in conditions, which varied from shallow marine supratidal to subtidal (Koolpin Formation) to shallow marine inner shelf to deeper mid-shelf (turbidites in the Mount Bonnie Formation) environment (Ferenczi and Sweet, 2005).

The sedimentation in shallow-marine conditions was followed by deposition of the Finniss River Group in proximal mid-submarine fan environment (Ferenczi and Sweet, 2005). These sediments are dominated by greywackes and siltstones. Along the western margin of the Central Domain a number of felsic units occur in the basal part of the package (Worden *et al.*, 2008a).

The detritus in the Burrell Creek Formation is dominated by 1865-1860 Ma material with a small contribution from the Neoarchean source which indicates that sedimentation occurred in an active margin setting (Hollis *et al.*, 2011).

The Hermit Creek Metamorphics in the Litchfield Domain comprising a composite package of undeformed granulite facies migmatitic metasediments and highly deformed amphibolite facies metasediments are interpreted as higher-grade equivalents of the Finniss River Group in the Central Domain. However, Pietsch and Edgoose (1998) suggest that they are older and are unconformably overlain by the Finniss River Group. The upper-amphibolite facies graphite-bearing gneiss, schists and quartzites of the Welltree Metamorphics in the Litchfield Domain are reported to be in an apparent metamorphic gradational contact with the low-grade metasedimentary rocks of the Burrell Creek Formation in the Central Domain and the two units are considered to be stratigraphic equivalents (Carson *et al.*, 2008).

The sediments are intruded by a number of mafic sills and dykes, the most prominent of which is the Zamu Dolerite at ca.  $1870 \pm 6$  Ma (Page, 1996; cited in Worden *et al.*, 2008a).

The deposition of the South Alligator and Finniss River Groups was followed by an intensive deformation and metamorphism (Nimbuwah Event).

Sedimentary sequence of the two groups hosts several gold, base metal, uranium, iron, tin, tantalum, and tungsten deposits of which only base metal and iron ore deposits are temporally associated with the sedimentary package.

#### **4.3.1 Copper and Lead-Zinc**

Several copper and lead-zinc prospects and deposits are located in the Daly River Mineral Field ([Figure 4-4](#)). Anomaly A prospect (Zinc) is hosted within sub-vertical, tightly-folded, predominantly volcanic sequence assigned to the Warrs Volcanic Member (Ahmad *et al.*, 1993). The volcanic pile is rhyolitic at the base and becomes progressively more mafic upwards. Some pillow-lava-like structures have been identified in the basaltic rocks. The volcanic sequence comprises mafic and felsic volcanics, minor tuffaceous phyllite, schist and agglomerate. Ore zones form conformable to semi-conformable stacked lenses of banded massive sulphide. Chlorite is the main alteration mineral. Other alterations include sericitisation, silicification and carbonatisation. The main ore minerals are pyrite, pyrrhotite, and iron-rich sphalerite with minor amount of chalcopyrite, galena, tetrahedrite-tennantite and silver. The ores have been deformed and metamorphosed.

Other lead-zinc prospects in the mineral field include Anomaly B and Warrs Prospect.

The Warrs Volcanic Member and the adjacent schist and phyllites of the Burrell Creek Formation host several copper prospects, the most significant of which is the Daly River Copper Mine. The mine was discovered around 1884 and produced ~ 6000 tonnes of ore grading about 20% copper (Ahmad *et al.*, 1993). The deposit is located in a tongue of Burrell Creek Formation between the Warrs Volcanics to the east and the Mulluk Mulluk Volcanics to the west. The mineralisation occurs close to the contact with the overlying Warrs Volcanic Member. The host rock comprises volcanioclastic greywacke and minor siltstone, metamorphosed to quartz-chlorite and quartz-sericite schist. The mineralisation contains at least three zones associated with bedding-parallel, near vertical shears. No massive sulphide lenses have been intersected, but Maddocks (1979; cited in Ahmad *et al.*, 1993) notes similarities with the stringer zone mineralisation in volcanic-associated massive sulphide deposits. Similar to many volcanic-associated massive sulphide deposits the ores contain gold-rich zones with some samples reporting up to 9 ppm gold.

Other copper deposits in the mineral field include Empire Cooper Mine and Wheal Danks Mines.

As volcanic-associated massive sulphide mineralisation is thought to be syngenetic (with possible partial remobilisation during metamorphism) the age of the Warrs Volcanic Member ( $1862 \pm 3$  Ma; Worden *et al.*, 2008a) provides a reliable constraint on the age of the volcanogenic hydrothermal system.

#### **4.3.2 Iron ore**

The Koolpin Formation hosts several conformable iron-ore bodies ([Figure 4-7](#)). They are located in proximity to the Burnside Granite. These comprise gossans of hematite and limonite with minor chert, slated and brecciated quartz. The origin of these ore bodies is unknown although it has been suggested that they are in origin similar to the Frances Creek iron ore deposits discussed in the preceding section (Ahmad *et al.*, 1993). If the mineralisation is volcanogenic it could be related to the volcanism that also formed volcanic units in the Gerowie Tuff ( $1863 \pm 2$  Ma, Worden *et al.*, 2008a).

#### **4.4 NIMBUWAH EVENT (1860 Ma TO 1847 Ma)**

Regional deformation and metamorphism took place across the PCO during Nimbuwah event. The event is considered part of the Barramundi Orogeny, interpreted to be a large basement-stabilising event for the Proterozoic basin in North Australian Craton (Etheridge *et al.*, 1987, cited in de Vries *et al.*, 2008). The Craton-wide event, which appeared to have affected different orogens and regions at slightly different time intervals, was associated with a sequence of continent-continent collisions (de Vries *et al.*, 2008).

Out of five regional deformational events in the PCO described by Johnston (1984) and Ahmad *et al.* (1993) and summarised in [Table 3–2](#), the first two ( $D_1$  and  $D_2$ ) are interpreted to be pre-Nimbuwah (Ahmad *et al.*, 1993) in age. The  $D_3$  event, which is more widespread in the Central Domain, resulted in the development of major folds (upright, N-S-trending in the Rum Jungle field; upright N-S to NW-SE-trending in the Central Domain; and reclined NW-trending in the Nimbuwah Domain) (Worden *et al.*, 2008a). These folds are cross-cut by granites which induced formation of open, low amplitude, E-W trending folds, which become tighter in the Nimbuwah Event. The deformation also produced faults, the most important of which are associated with the  $D_3$  event. These faults trend NW and they have vertical to steep dips and crosscut Early Proterozoic sediments. Some faults terminate against granitoid-sediment contact whereas others continue through the granites suggesting either a post-granitoid age or post-granitoid reactivation (Ahmad *et al.*, 1993).

During the Nimbuwah Event the three domains underwent different style of metamorphism. The Litchfield Domain experienced high-T, low-P metamorphism to upper amphibolite to granulite grade at ca. 1855 Ma (Carson *et al.*, 2008). The younger whole-rock Rb-Sr ages ( $1768 \pm 16$  Ma) of foliated Mount Litchfield and Two Sisters Granites are interpreted to represent the age of greenschist to amphibolite facies metamorphism (Carson *et al.*, 2008).

The Central Domain underwent low-P (locally andalusite-bearing), lower greenschist facies metamorphism with local contact-metamorphism at the margins with syn- to post-orogenic granitoids. The Nimbuwah Domain experienced high-P, amphibolite to granulite grade metamorphism. The metamorphism in the Nimbuwah Domain is dated between  $1871 \pm 4$  Ma and  $1867 \pm 4$  Ma (Hollis *et al.*, 2009b; Hollis *et al.*, 2011).

The  $1861 \pm 3$  Ma age of Berinka Volcanics of the Finniss River Group and the  $1847 \pm 1$  Ma age of a undeformed pegmatite at the Ranger deposit constrain the Nimbuwah Event to between ca. 1861 and 1847 Ma (Worden *et al.*, 2008a).

#### **4.5 FELSIC MAGMATISM (CULLEN SUPERSUITE AND JIM JIM/DAVID SUITE; 1835 Ma TO 1818 Ma)**

The period between 1835 ma and 1818 Ma saw major igneous activity in the PCO, although some felsic rocks in the Litchfield and Nimbuwah domains are slightly older ([Table 4-2](#)). Geochronological studies constrain felsic magmatism in the Litchfield Domain to be at ca. 1850 Ma. In the Nimbuwah Domain felsic rocks of the Nimbuwah Complex were emplaced at between 1867 Ma and 1860 Ma (Worden *et al.*, 2008a; Hollis *et al.*, 2011). Although available age data show a large spread in the age of emplacement of the Cullen Supersuite and Jim Jim/David Suite, the SHRIMP U-Pb analysis of zircons provides a much tighter range varying between 1835 Ma and 1818 Ma for the Cullen Supersuite and between 1846 Ma and 1818 Ma for the Jim Jim/David Suite.

The 1835 – 1818 Ma granitoids of the Central Domain (mainly Cullen Supersuite) are considered to be part of the Cullen Event during which felsic igneous activity was accompanied by minor deformation and rift-related sedimentation (El Sherana and Edith River Groups) comprising clastic rocks and felsic volcanics (Ahmad *et al.*, 2009).

Allia Suite granites are fractionated S-type and contain abundant pegmatites and greisens (Budd *et al.*, 2001). In contrast the Cullen Supersuite and Jim Jim/David Suite granites in the Central Domain are predominantly fractionated, I-type.

**Table 4-2:** Paleoproterozoic felsic intrusive magmatism in the Pine Creek Orogen

LITCHFIELD DOMAIN	CENTRAL DOMAIN	NIMBUWAH DOMAIN
Allia Suite ca. 1850 Ma <sup>1</sup> S-type, fractionated	Cullen Supersuite ca. 1835 Ma to 1818 Ma <sup>2</sup> I-type, fractionated	Nimbuwah Complex ca. 1867 Ma to 1860 Ma I-type, fractionated
Wagait Granite ca. 1863 Ma <sup>3</sup>	Jim Jim Suite or David Suite ca. 1838 Ma to 1820 Ma <sup>4</sup> I-type, fractionated, oxidised	Jim Jim Suite or David Suite ca. 1846 Ma to 1818 Ma I-type, fractionated, oxidised
Collah Suite ca. 1829 Ma		

1 – The oldest maximum age of intrusion in the Litchfield Domain is obtained for the Soldiers Creek Granite ( $1872 \pm 12$  Ma) and the youngest maximum age for the Allia Creek Granite ( $1806 \pm 7$  Ma; Worden *et al.*, 2008). The age in the table is based on the SHRIMP U-Pb monazite age of Murra-Kamangee Granodiorite (Worden *et al.*, 2008b) and SHRIMP U-Pb age of zircon of the Fish Billabong Adamellite (Worden *et al.*, 2008); 2 - The oldest published age for Cullen Supersuite granite is an ID-TIMS age of  $1860 \pm 45$  Ma. 3 - SHRIMP U-Pb zircon age of Wagait Suite (Worden *et al.*, 2008b); In this table only available SHRIMP U-Pb age are used; 4 – the oldest published age for the Jim Jim/David Suite is for the Grace Creek Granite ( $1863 \pm 5$  Ma). The result is considered unreliable as it contains a significant amount of inherited zircons (Neumann and Fraser, 2007). For a detailed discussion see Neumann and Fraser (2007).

The majority of Cullen Batholith granites are late-orogenic. The granites have produced zones of contact metamorphism up to several kilometres wide. Geochemically the granite have elevated levels of K, Ba, Rb, Sr, U and particularly light rare-earth elements, and are low in Ni and Mg (Bajwah, 1994). Budd *et al.* (2001) classify the granites as reduced, metaluminous to weakly peraluminous. On regional aeromagnetic and gravity data all plutons are magnetic and gravity lows (Budd *et al.*, 2001). Uranium and thorium concentration of granites varies between 1 ppm to 28 ppm and 1 ppm to 78 ppm respectively (OZCHEM database).

Most granites of the Cullen Supersuite show an overprint of greenschist facies metamorphism and have been affected by shearing associated along the north-northwest trending Pine Creek Shear Zone. The shear zone is believed to be active during the emplacement of granites (Budd *et al.*, 2001).

Compared with other felsic suites in the PCO, the Jim Jim/David Suite is predominantly oxidised. The granites vary from metaluminous to strongly peraluminous. On the regional gravity data these granites are gravity lows whereas on the regional magnetic data there is a weak correlation between magnetic response and abundance of mafic units in the suite (Budd *et al.*, 2001). Uranium and thorium concentration of granites varies between 4 ppm to 30 ppm and 24 ppm to 88 ppm respectively (OZCHEM database).

The emplacement of granites is associated with D<sub>4</sub> deformation (Table 3; Ahmad *et al.*, 1993). Hein (2003) interprets a more complicated relationship between emplacement of granites and deformation events at the Mount Todd gold deposit. According to Hein (2003) the emplacement of the Yenberrie Leucogranite (Cullen Supersuite) preceded D<sub>1</sub> (D<sub>3</sub> of Ahmad *et al.*, 1993) deformation and regional greenschist facies metamorphism, whereas the Tennysons Leucogranite (Cullen Supersuite) was emplaced either synchronous with D<sub>2</sub> (D<sub>4</sub> of Ahmad *et al.*, 1993) or predated it.

Several important minerals systems are interpreted to be associates with the Nimbuwah Event. These systems formed deposits which include lode gold, tin-tantalum and tungsten deposits.

#### **4.5.1 Lode gold deposits**

Ahmad *et al.* (2009) describe gold deposits in the PCO in detail. The largest gold deposit in the orogen is Mount Todd with a global resource (production + remaining resources) of ca. 211 tonnes ([Fig 4–8](#) and [Table 4–3](#)). These deposits have features similar to those described either for orogenic gold deposits (Goldfarb *et al.*, 2001; Groves *et al.*, 1998) and/or intrusion-related gold deposits (Lang and Baker, 2001).

##### **4.5.1.1 Host rocks**

The most favourable host of gold deposits is the turbiditic sediments of the Mount Bonnie Formation. The underlying Gerowie Tuff and Koolpin Formation are also good hosts. A few deposits are located in the Burrell Creek Formation of the Finniss River Group. A characteristic feature of the host lithologies is the abundance of carbonaceous and ferruginous material (Koolpin and Mount Bonnie Formations). However the host rock of the largest gold deposit (Mount Todd; Burrell Creek Formation) does not contain carbonaceous material, although part of the mineralisation is associated with massive brecciated iron oxides (Ahmad *et al.*, 2009).

##### **4.5.1.2 Structural control**

All gold deposits are structurally controlled. On a regional scale a large number of deposits and goldfields seem to be controlled by northwest-trending faults such as the Pine Creek Shear Zone ([Fig 4–8](#)). This shear zone lies within the Noonamah-Katherine Lineament Zone that has a coincident TM signature, magnetic and gravity anomaly. The shear zone traverses several plutons of the Cullen Batholith and splay into a series of parallel to anastomosing northwest-trending faults. The faults are associated with sinistral reverse displacement (Hein, 2003).

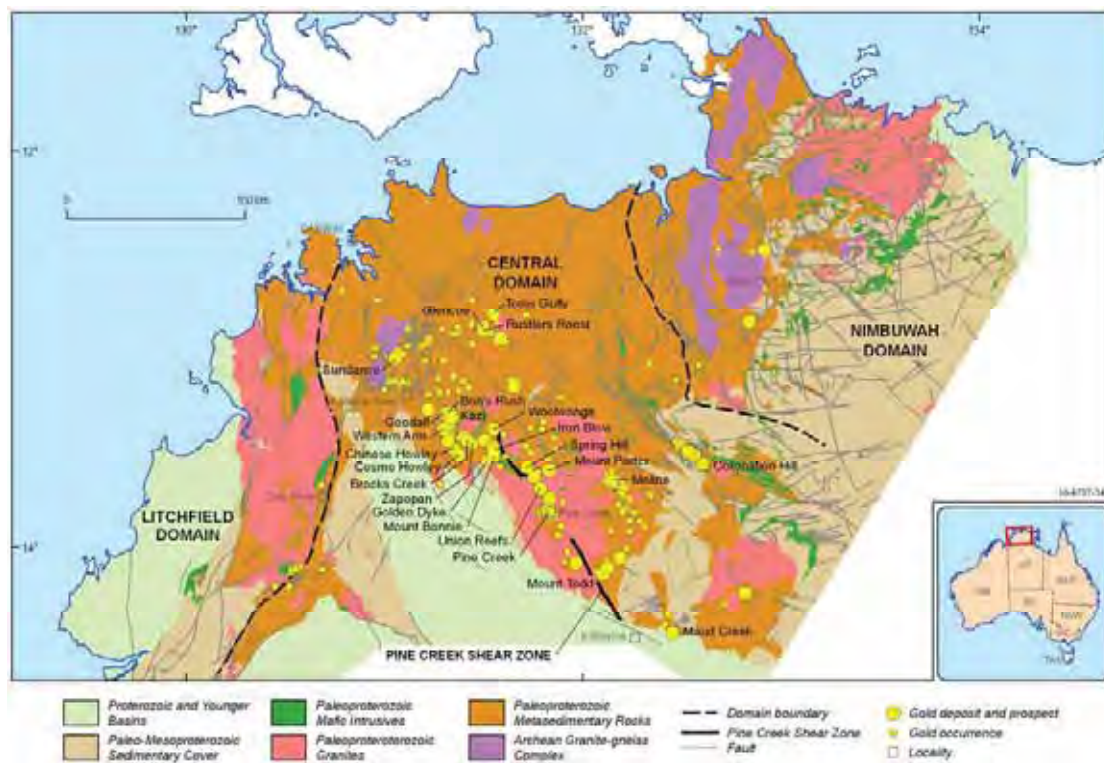


**Figure 4-8:** Map of the Pine Creek Orogen showing gold deposits and occurrences. The map is based on an NTGS dataset, i.e., Pine Creek interpreted geology (2005). Deposits, prospects and occurrences are from GA's OZMIN and MINLOC datasets.

At a more local scale the mineralisation is controlled by folds and faults occurring along the axial planes. Mineralised quartz veins comprise saddle reefs, subvertical veins, stockworks associated with shear zones and veins parallel of axial plane cleavage (Ahmad *et al.*, 2009).

#### 4.5.1.3 Proximity to felsic intrusions

Most gold deposits and goldfields are in close proximity to granites of the Cullen Supersuite. In many deposits such as Mount Todd and Cosmo Howley mineralisation is located within contact metamorphic zones of hornfels around granitoids (Hein, 2003; Matthai *et al.*, 1995a). The role of granitoids and magmatic fluids is not clear (see discussion below).

#### 4.5.1.4 Metamorphic grade of host rocks

All known gold deposits are located in the Central Domain of PCO where host rocks reached greenschist facies metamorphism. These deposits do not occur in the Litchfield and Nimbuwah domains where metamorphic grades are relatively higher (amphibolite to granulite facies).

#### 4.5.1.5 Wall rock alteration

Wall-rock alteration near veins and zones of mineralisation is generally minor. The main alteration minerals are sericite, quartz, chlorite and minor carbonate, pyrite and arsenopyrite. In deposits

hosted by iron-rich host rocks, chlorite is the main alteration mineral. It is often replaced by darker green chlorite and sericite. At the Maud Creek deposit the mineralisation is associated with chlorite-carbonate-sericite and silica-sericite-carbonate-fuchssite-graphite alteration assemblage (Morrison and Treacy, 1998). In many deposits (Mount Todd, Cosmo Howley, Brocks Creek goldfield) alteration zones are superimposed on contact metamorphic hornfels containing chiastolite and cordierite (Ahmad *et al.*, 2009; Hein, 2003; Miller *et al.*, 1998). At the Cosmo Howley deposits, prograde contact metamorphism produced an assemblage containing Mn-poor almandine garnet with inclusion of carbon and clots of biotite (Matthai *et al.*, 1995b). At the Mount Todd deposit contact metamorphism generated a quartz-cordierite-muscovite-biotite-chlorite assemblage (Hein, 2003).

#### **4.5.1.6 Composition of ore fluid and temperature of formation**

Fluid inclusion studies indicate involvement of fluids very similar to that reported from other mesothermal deposits (Ahmad *et al.*, 2009). The studies reveal presence of two fluids:  $\text{CO}_2 + \text{CH}_4$  – bearing low salinity (3 to 5 wt% eq. NaCl) fluid and high salinity (average salinity of about 10 wt% eq. NaCl) with temperatures of entrapment varying between 250°C and 350°C (Ahmad *et al.*, 2009). These fluid inclusions are interpreted to represent mixing of a dominantly magmatic fluid with a dominantly metamorphic fluid (Ahmad *et al.*, 2009). The involvement of magmatic fluid is also interpreted from the chloride content of alteration biotite in the alteration zone of Cosmo Howley deposit (Matthai *et al.*, 1995b).

#### **4.5.1.7 Timing of mineralisation**

Direct dating of gold mineralisation has been undertaken only for two gold deposits ([Table 6–3](#)). At the Goodall deposit (Compston and Matthai, 1994) reported an age of  $1810 \pm 10$  Ma from SHRIMP U-Pb analyses of xenotime and monazite from a gold-bearing quartz vein. Sener *et al.* (2005) reported a much younger age of  $1727 \pm 17$  Ma from the SHRIMP analysis of monazite from gold veins. However, Rasmussen *et al.* (2006) reinterpreted the data of Sener *et al.* (2005) to suggest an older age of  $1776 \pm 13$  Ma. Cross (2009), reinterpreted the data of Sener *et al.* (2005) again to come up with an age of  $1822 \pm 37$  Ma. The reinterpreted age proposed by Rasmussen *et al.* (2006) for Goodall is very close to  $1780 \pm 10$  Ma age they reported for the Toms Gully gold deposits from SHRIMP U-Pb analysis of ore-related monazite.

At the Cosmo Howley deposits Matthai *et al.* (1995a) document mutual crosscutting relations of gold quartz veins with aplite dikes. The mineralisation is spatially close (less than 1 km) to the McMinns Bluff Granite and if aplite dikes are related to the granite, the age of the granite ( $1835 \pm 6$  Ma; Budd *et al.*, 2001) can be interpreted to be close to the age of gold mineralisation. The close spatial and temporal relation between gold mineralisation and magmatism is also suggested at the Mount Todd deposit. The gold mineralisation postdates emplacement of the Yenberrie Leucogranite but is contemporaneous with D<sub>2</sub>-deformation event that is synchronous with, or immediately after the emplacement of the Tennysons Granite (Hein, 2003). The two felsic intrusions belong to the I-type Cullen Batholith and although they have not been directly dated their emplacement age can be interpreted to be between 1835 Ma and 1818 Ma (ca. 1825 Ma; Budd *et al.*, 2002). A close spatial and temporal relation between gold mineralisation and hornfelsic rocks also suggests that gold mineralisation could have immediately followed the emplacement of felsic rocks.

A general feature of most mesothermal orogenic (or slate-belt hosted) deposits is that gold mineralisation is closely related to deformation, metamorphism and felsic magmatism (Foster *et al.*, 1998; Goldfarb *et al.*, 2001; Stüwe, 1998). A similar relationship is observed for gold deposits in the PCO. The turbiditic package of host sediments (South Alligator and Finniss River groups) was deposited at ca. 1860 Ma. The package underwent deformation and greenschist metamorphism

during the Nimbuwah Event, which occurred later than ca. 1860 Ma and earlier than ca 1847 Ma (based on the age of the undeformed Ranger pegmatite). Dewatering during metamorphism of these sediments is capable of producing gold-bearing metamorphic fluids. Felsic magmatism in the Central Domain of PCO took place between 1830 Ma and 1810 Ma. The interpretation of age data for the Goodall and Cosmo Howley deposits suggests that the main gold mineralisation was formed at between ca. 1830 Ma and 1810 Ma. Although these deposits are often discussed as intrusion-related gold deposit the genetic model proposed for these deposits invokes a close relation between metamorphic and magmatic events. Ahmad *et al.* (2009) and Matthai *et al.* (1995a) suggest a close interplay and mixing of metamorphic and magmatic fluids.

The relatively younger age (ca. 1770 Ma) for the Toms Gully deposit is interpreted to suggest that gold mineralisation could be related to an younger tectonic metamorphic event, the Shoobridge Event. The definition and nature of this event in the PCO is not clear. Needham *et al.* (1988) described it as the last regional metamorphic event of the Top End Orogeny, which caused reactivation of shear zones within granitoids and Early Proterozoic metasedimentary rocks. The event was accompanied by widespread retrogressive metamorphism in granitoids and low-grade metamorphism adjacent to some of the major shear zones. It is doubtful if this event produced large quantities of gold-bearing fluid to form gold deposits, however it is possible that it caused local-scale remobilisation of gold and also created a thermal overprint on gold deposits.

Table 4-3: Major gold deposits and prospects in the Pine Creek Orogen

NAME	HOST ROCK	GRANITE (SPATIALLY ASSOCIATED)	METAMORPHISM	ORE (TONNES)	GRADE (G/T)	GOLD (T)	AGE OF SPATIALLY ASSOCIATED GRANITE	AGE OF MINERALISATION	REFERENCE
Bons Rush	Mount Bonnie Formation, Gerowie Tuff	Burnside Granite	Lower greenschist	540000	2.51	1.4	1800 ± 5	Unknown	1
Bridge Creek	Koolpin Formation, Gerowie Tuff	Burnside Granite	Lower greenschist	1037500	1.59	1.6	1800 ± 5	Unknown	1
Brocks Creek	Gerowie Tuff	Burnside Granite	Lower greenschist	6587571	2.241	14.8	1800 ± 5	Unknown	1
Chinese Howley	Koolpin Formation	McMinns Bluff Granite	Lower greenschist	4043800	1.76	7.1	1835 ± 6; 1818 ± 3	Unknown	2; 1
Cosmo Howley	Koolpin Formation	McMinns Bluff Granite	Lower greenschist	11831827	3.243	38.4	1835 ± 6; 1818 ± 3	1835 ± 6	2; 1
Glencoe	Mount Bonnie Formation	Burnside Granite	Lower greenschist	1549000	1.912	3.0	1800 ± 5	Unknown	2; 1
Golden Dyke Dome	Koolpin Formation	McMinns Bluff Granite	Lower greenschist	100000	7.5	0.8	1835 ± 6; 1818 ± 3	1835 ± 6	2; 1
Goodall	Burrell Creek Formation	Burnside Granite	Lower greenschist	4095000	1.99	8.1	1800 ± 5	1810 ± 10	3; 4
Iron Blow	Mount Bonnie Formation	Princes Spring Granite	Lower greenschist	No data	No data	No data	1804 ± 50	Unknown	2
Kazi	Mount Bonnie Formation, Gerowie Tuff	Burnside Granite	Lower greenschist	676000	2.91	2.0	1800 ± 5	Unknown	2
Maud Creek	Tollis Formation	Unknown	Lower greenschist	13580000	2.28	31.0	Unknown	Unknown	5
Moline	Mount Bonnie Formation	Allamber Springs Granite, McCarthy's Granite	Lower greenschist	2953840	1.16	3.4	1822 ± 6	Unknown	1

**Geological and energy implications of the Pine Creek airborne electromagnetic (AEM) survey, Northern Territory, Australia**

NAME	HOST ROCK	GRANITE (SPATIALLY ASSOCIATED)	METAMORPHISM	ORE (TONNES)	GRADE (G/T)	GOLD (T)	AGE OF SPATIALLY ASSOCIATED GRANITE	AGE OF MINERALISATION	REFERENCE
Mount Bonnie	Mount Bonnie Formation	Prices Springs Granite	Lower greenschist	760000	2.467	1.9	1804±50	Unknown	1
Mount Porter	Gerowie Tuff	Allamber Springs Granite, McCarthy's Granite	Lower greenschist	355000	3	1.1	Unknown	Unknown	5
Mount Todd	Burrell Creek Formation	Yenberrie Granite, Tennyson Leucogranite	Lower greenschist	234703000	0.899	211.1	1825; 1760 ± 20	Unknown	1
Pine Creek	Contact of Burrell Creek and Mount Bonnie Formations	Tabletop Granite	Lower greenschist	17248000	2.36	40.7	1825	Unknown	1
Rustlers Roost	Mount Bonnie Formation	Mount Bunney Granite	Lower greenschist	26908000	1.129	30.4	1821± 5	Unknown	6
Spring Hill	Burrell Creek Formation	McKinlay Granite	Lower greenschist	12750000	0.8	10.2	1804 ± 50	Unknown	1
Sundance	Coomalie Dolomite, Whites Formation	Not related to granite (palaeokarst?)	Lower greenschist	200000	5	1.0	Unknown	Unknown	5
Toms Gully	Wildman Sandstone	Mount Bunney Granite	Lower greenschist	2149243	8.291	17.8	1831 ± 6	1780 ± 10	6
Union Reef	Burrell Creek Formation	McMinns Bluff Granite	Lower greenschist	20932000	1.556	32.6	1835 ± 6; 1818 ± 3	Unknown	1
Western Arm	Mount Bonnie Formation, Gerowie Tuff	Burnside Granite	Lower greenschist	1790000	1.4	2.5	1800 ± 5	Unknown	1
Woolwonga	Mount Bonnie Formation	Burnside Granite	Lower greenschist	2821057	2.566	7.2	1800 ± 5	Unknown	1
Zapopan	Gerowie Tuff	Burnside Granite	Lower greenschist	463708	10.341	4.8	1800 ± 5	Unknown	1

**References:** 1 – Budd *et al.* (2001); 2 – Matthai *et al.* (1995); 3 - Compston and Matthai (1995); 4 - Cross (2009); 5 – Ahmad *et al.* (2009); 6 – Rasmussen *et al.* (2006). Resources for gold deposits represent mined resources + remaining resources. Resource data from OZMIN.

#### **4.5.2 Polymetallic deposits (Pb-Zn-Ag)**

As mentioned previously, the Rum Jungle Mineral Field hosts several polymetallic deposits with variable amount of uranium, lead, zinc, copper, silver and nickel ([Figure 4-8](#)). The two largest polymetallic deposits, (Woodcutters and Browns), are structurally controlled by D<sub>2</sub> folds related to the Nimbuwah Event and by faults related to the Late Nimbuwah-Cullen Event (Lally, 2002).

At the Woodcutters deposit, mineralisation (essentially discordant) is hosted within the Whites Formation. This is different from other polymetallic deposits in the areas such as Browns where the mineralisation is located close to the contact between the Whites Formation and the Coomalie Dolostone. The mineralisation at the Woodcutters deposit starts at the contact and extends 700 m up-section (Ahmad *et al.*, 2006). The orebodies are located along the apical part of a north-trending, upright, doubly-plunging anticline and follow subparallel, near-vertical transpressional fault. Northward, dextral movement along the Giants Reef Fault offsets the anticline and the fault zone. The lenticular ore zones transgress the anticline and swell in the dolomudstone and pinch in the black shale. Two main types of mineralisation have been identified: thicker bodies replacing dolomudstone near the fault and thinner sheeted veins associated with faults. Locally a third type of stratiform mineralisation is also reported. The main sulphide minerals are pyrite, pyrrhotite, chalcopyrite, sphalerite and galena. The ores contain anomalous concentrations of gold, nickel, cobalt, indium and tin. The main gangue minerals comprise dolomite, quartz, tourmaline, calcite and apatite. Fluid inclusion studies reveal that sphalerite (and hence the ore) was formed from high-temperature (temperature of homogenisation varies between 220°C and 290°C) saline, CO<sub>2</sub>-rich fluids. These studies in sphalerite indicate that formation of sulphides occurred at minimum lithostatic pressures of 700 to 1000 bars which is equivalent of a depth between 2.6 to 3.8 kms (Smolnogov, 1988; cited in Ahmad *et al.*, 2006). The later quartz veins in comparison were formed at much lower pressure indicating significant erosion of overlying strata.

The sulphur isotopes values of sulphides show enrichment in heavier (<sup>34</sup>S) isotope (up to 22 per mil) indicating that sulphur for the sulphides may have been sourced by inorganic reduction of seawater sulphate. The sulphur isotope geothermometer using coexisting galena and sphalerite yield a temperature of equilibrium (and hence formation) of around 320°C, which is in accordance with the temperatures obtained from fluid inclusions (Ahmad *et al.*, 2006).

The lead isotope ratios of galena from the Woodcutters deposit are homogeneous but differ from those at the Browns deposits indicating that the lead for these deposits may have been derived from different sources (McCready *et al.*, 2004) or the deposits were formed at different times. The oldest galena gives a lead-lead model age of 1775 Ma. However the new Pine Creek lead model ([Figure 4-6](#)) gives a least radiogenic Pb-Pb model age of ca. 1840 Ma indicating that mineralisation may be related to the Cullen Event (ca. 1850 to 1820 Ma as defined by Lally, 2002). This is supported by, a close association of mineralisation with structures (folds and faults) interpreted to be generated during the Nimbuwah and/or Cullen events (Lally, 2002).

Ahmad *et al.* (2006) discuss syngenetic and epigenetic models for the genesis of mineralisation. The model preferred by them is epigenetic and the mineralisation is thought to be formed from ore fluids generated by shortening of the basin during and after the Barramundi Orogeny. The orogeny caused migration of ore fluids towards the margin of the basin where they were tapped by major fracture system. However it is also possible that the mineralisation is related to fluids generated during greenschist facies metamorphism of sedimentary package (Mount Partridge Group) that occurred during Nimbuwah and/or Cullen events.

#### **4.5.3 Skarn and/or vein (Fe, Cu and Pb-Zn-Ag) deposit**

There are several skarn occurrences in MOUNT EVELYN, all of which are hosted by marble and calc-silicate hornfels of the Koolpin Formation adjacent to the Allamber Springs Granite. SHRIMP U-Pb analysis of zircon from the granite gives an emplacement age of  $1818 \pm 5$  Ma (Budd *et al.*, 2001), which can also be interpreted as the age of skarn mineralisation. The mineralisation at the Evelyn lead-zinc-silver mine is described in some detail by Ferenczi and Sweet (2005).

The largest of these deposits is the Mount Diamond copper deposit ([Figure 4-5](#)). It is located along the southern edge of the Mount Davis Granite, in tightly folded and hornfelsed rocks of the Burrell Creek Formation (Ferenczi and Sweet, 2005). The wall rocks in proximity to the mineralised quartz vein are brecciated and altered (sericitisation, silicification and chloritisation).

One of the largest iron ore deposits in the PCO is the Mount Bundey skarn deposit ([Figure 4-7](#)) where concordant, tabular ironstone bodies are hosted in the metasediments of the Wildman Siltstone and the Mount Goyder Syenite (Ferenczi, 2001). The tabular lenses are composed of magnetite with minor sulphides below the zone of oxidation. The mineralisation is probably associated with the Mount Bundey Granite (emplacement age of  $1821 \pm 6$  Ma; Rasmussen *et al.*, 2006) which comprises a pluton of shoshonitic Mount Goyder Syenite and calc-alkaline Mount Bundey Granite, and lamprophyre dykes and later felsic and aplitic dykes (Ferenczi, 2001).

Table 4-4: Tin, Tantalum, and Tungsten deposits in the Pine Creek Orogen

FILED/DISTRICT/DEPOSIT/PROSPECT	DOMAIN	COMMODITY	TYPE	GRANITE	AGE (MA) <sup>A</sup>	REFERENCE
Bynoe Pegmatite Field	Litchfield	Sn, Ta	Pegmatite	Two Sisters Granite	1862 (max. age)	1; 2
Mount Wells	Central	Sn, Ta	Tin quartz vein	Prices Springs Granite	1825	3; 6
Wolfram Hill	Central	W, Cu, Sn	Vein	Wolfram Hill Granite	1825	4; 6
Yeuralba Mineral Field	Central	W, Sn	Greisen	Yeuralba Granite	1825	5; 6
Hayes Creek	Central	Sn, Ta	Tin quartz vein	McMinns Bluff Granite	1835	6
Mount Shoobridge	Central	Ta, Sn	Pegmatite	Allia Suite?	1850	3; 6
Maranboy Tin Field	Central	Sn	Tin quartz vein	Maranboy Porphyry, Yeuralba Granite	1825	5; 6
Grace Creek	Central	Sn	Tin quartz vein	Grace Creek Granite (Jim Jim Suite)	1825	7; 6
Myra Falls	Nimbuwah	Sn	Tin quartz vein	Tin Camp Granite	1846	7; 2
Wingate Mountains (Muldiva, Buldiva, Collia)	Central/Litchfield	Sn, Ta	Pegmatite	Allia Creek Granite, Soldiers Creek Granite	1872 (max. age)	1; 2
Big Mouth, Grants Au	Central	Sn, Au	Tin quartz vein	Allia Creek Granite (Allia Suite)	1806 (max. age)	1; 2
Tipperary (Shoobridge Pegmatite Group)	Central	Sn	Pegmatite	Shoobridge Granite	1825	1; 6
Tipperary (Plateau Point Pegmatite Group)	Central	Sn	Pegmatite	Fenton Granite	1825	1
Horseshoe and Morris Tin Fields	Central	Sn, Cu	Tin sulphide vein	Cullen Suite?	1825	5; 6
Emerald Creek Tin Field	Central	Sn	Tin sulphide vein	Cullen Suite?	1825	5; 6
Yenberrie Mineral Field	Central	W, Mo, Bi	Greisen	Yenberrie Leucogranite	1825	5; 6
Hidden Valley Tin	Central	Sn	Tin quartz vein	Wolfram Hill Granite	1825	4; 6
Crest of the Wave Mine	Central	Sn	Tin sulphide vein	Unknown	1825	4; 6
Mary River Camp, Ross	Central	Sn	Tin quartz vein	Mount Davis Granite	1825	4; 6
Jimmy Knobs Mine	Central	Sn	Tin quartz vein	Prices Springs Granite	1825	3; 6

**References:** 1 – Frater (2002); 2 – Worden *et al.* (2008b); 3 – Ahmad *et al.* (1996); 4 – Ferenczi and Sweet (2005); 5 – Kruse *et al.* (1994); 6 – Budd *et al.* (2001); 7 – MINLOC database. a – For granites which have not been dated, an average age of suite and/or Supersuite is assigned using Budd *et al.* (2001).

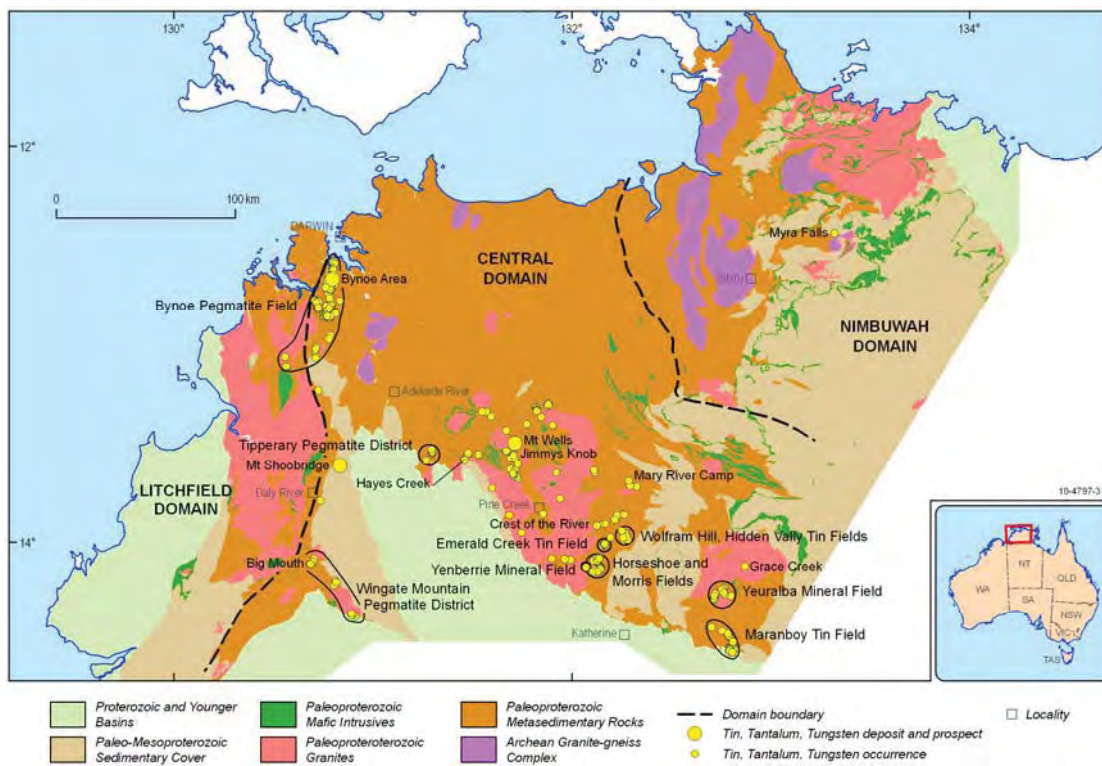


**Figure 4-9:** Map of the Pine Creek Orogen showing tin-tantalum and tungsten deposits, and occurrences. The map is based on an NTGS dataset, i.e., Pine Creek interpreted geology (2005). Deposits, prospects and occurrences are from GA's OZMIN and MINLOC datasets.

#### 4.5.4 Tin-Tantalum-Tungsten veins, greisens and pegmatites

Felsic magmatism (Cullen, Allia and Jim Jim/David suites) produced several deposits and prospects containing tin, tantalum and tungsten in the PCO (Figure 4-9). They are predominantly located in the Central and Litchfield domains (Frater, 2005). These deposits are of three types: veins (tin sulphide and tin quartz), greisens; and pegmatites (Table 4-4).

The deposits in the Litchfield Domain are predominantly pegmatite-related and are interpreted to be associated with granites of the Allia Suite. The Allia Suite is fractionated S-type and contains peraluminous minerals such as andalusite, cordierite and muscovite. Geochemical data suggest that the granites are reduced but some samples show that they become increasingly oxidised with decreasing iron content (Budd *et al.*, 2001). The granites of the Allia Suite have emplacement ages of ca. 1860 Ma to 1854 Ma and are thus older than the granites of the Cullen Suite (Table 4-2). These ages also provide constraints on the age of mineralisation as pegmatites are spatially and temporally related to the granites (Frater, 2005).

The Bynoe pegmatite field comprises pegmatite dykes hosted in the Burrell Creek Formation and the Welltree Metamorphics. They are located at the margins of the Two Sisters Granite (Ahmad *et al.*, 2006; Frater, 2005). The pegmatites are strongly zoned and also contain massive quartz veins. The main ore minerals are cassiterite and tantalite, which are irregularly distributed in the pegmatite (Frater, 2005).

In the Wingate Mountain pegmatite district, the pegmatites are related to the Allia Creek Granite (Fletchers Gully Group) and the Soldiers Creek Granite (Soldiers Creek field containing mineralised

pegmatites at Muldiva and Buldiva; Frater, 2005). In the Tipperary pegmatite district (Shoobridge and Plateau Point fields), the pegmatite bodies occur within the Burrell Creek and Mount Bonnie formations and in the Wildman Siltstone (Frater, 2005). The Shoobridge and Fenton Granites are considered to be the parent granites to the pegmatites. The main ore minerals are cassiterite, tantalite and tapiolite (Frater, 2005).

The Cullen and Jim Jim/David Suites in the Central domain produced several vein, greisen and pegmatite deposits of tin, tantalum and tungsten. The most prominent of these is the Mount Wells Mine, which has been described in detail by Ahmad *et al.* (1993). The tin-quartz veins at the Mount Wells Mine are hosted in the siltstone and greywacke of the Burrell Creek Formation. These steep-dipping tension-fill quartz veins follow a north-trending anticline. Cassiterite is the main ore mineral and is accompanied by wolframite and sulphides (pyrite, pyrrhotite, chalcopyrite and molybdenite). The main gangue minerals are quartz, muscovite, tourmaline, feldspar and chlorite. The immediate parent granitoids have not been mapped but the closest granite to the mine is the Prices Sprigs Granite. Granite intersected in the drill holes is greisenised.

The Horseshoe, Morris and Emerald Creek tin fields contain tin-sulphide veins (Kruse *et al.*, 1994). In the Horseshoe and Morris fields the veins are hosted by greywacke and siltstone of the Tolls Formation.

Tungsten deposits and prospects (Yeuralba and Yenberrie fields and the Wolfram Hill deposit) are hosted by greisenised granites (Yeuralba and Yenberrie leucogranites, and the Wolfram Hill Granite). In addition to tungsten, the ore zones contain anomalous concentrations of molybdenum and bismuth (Ferenczi and Sweet, 2005; Kruse *et al.*, 1994).

#### **4.6 EL SHERANA AND EDITH RIVER GROUP (1830 Ma TO 1825 Ma)**

The deformation and metamorphism of the Nimbuwah Event was followed by localised extension in the South Alligator Valley region of the Central Domain, which produced a shallow elongate basin. This extension partly overlapped with emplacement of felsic intrusions in the Central Domain. This period of minor deformation, rift-related sedimentation and igneous activity is described as the Cullen Event (Ahmad *et al.*, 2009). The deposition in the graben followed planation and deep weathering of the older rocks. The graben resulted from the reactivation of major northwest-trending faults and produced the Jawoyn Sub-basin centred over Mount Stow (Ferenczi and Sweet, 2005).

The first package (El Sherana Group) comprises coarse fluvial clastics, felsic to mafic lavas, minor rhyolitic intrusions and thick ignimbritic sheets. The age of the package is constrained by a SHRIMP U-Pb date of zircon from the Pul Pul Rhyolite of  $1829 \pm 5$  Ma (Jagodzinski, 1998; cited in Ferenczi and Sweet, 2005).

An interesting feature of the package is the presence of a hematite-apatite-rich breccia (Scinto Breccia) at the base of the El Sherana Group. The Scinto Breccia appears to unconformably overlie the Koolpin Formation. The origin of the breccia is uncertain. One interpretation describes the breccia as an *in situ* regolith developed over carbonate-bearing rocks at the unconformity surface whereas the other suggests it to be local talus deposit located at within and adjacent to synsedimentary faults that had acted as conduits for hydrothermal fluids (Ferenczi and Sweet, 2005).

The El Sherana Group sequence is unconformably overlain by a package (Edith River Group) of fluvial clastics, arenite, rudite and extensive bimodal volcanic rocks. A SHRIMP U-Pb analysis of zircon from rhyolite porphyry within the Plum Tree Creek Volcanics gives an age of  $1825 \pm 4$  Ma for the volcanic unit (Worden *et al.*, 2008a).

Prior to the deposition of the Edith River Group, the El Sherana Group rocks were folded, faulted and eroded (Maud Creek Event). The deformation produced tight, mainly horizontal folds with vertical axial surfaces (Needham *et al.*, 1988). The dating of El Sherana and Edith River Group constrains the event to be between 1829 Ma and 1825 Ma.

#### **4.6.1 Mineral systems associated with El Sherana and Edith River Groups**

Although uranium ( $\pm$  Au, PGE) mineralisation in many prospects and deposits in the South Alligator Valley Mineral Field is hosted by the Coronation Sandstone (e.g., Rockhole, El Sherana, Palette), the available age data suggest that uranium mineralisation was related to much younger events (see discussion in the following sections).

At the Saddle Ridge South uranium prospect a hematite-apatite-rich breccia (Scinto Breccia) contains angular fragments of euhedral apatite and hematite in a finer matrix of the same composition. At the Coronation Hill quartz-hematite alteration is described within and proximal to faults (Ferenczi and Sweet, 2005). The Scinto Breccia commonly contains elevated concentrations of Th, U, Cu, Ni, As and, locally, Au (Ferenczi and Sweet, 2005).

The Coronation Sandstone, which comprises coarse to very coarse, cross-bedded sandstone, pebble to cobble conglomerate, amygdaloidal basalt and minor intrusive rhyolitic porphyry, is interpreted to have formed in juvenile braided fluvial conditions. In this respect it is similar to the sandstones in the Kombolgie Subgroup. The Coronation Sandstone unconformably overlies metasediments of the Finniss River and South Alligator Group, which include carbonaceous Koolpin Formation. It is likely that diagenesis of the Coronation Sandstone could have released uranium-rich fluids. A reaction between these fluids and carbonaceous Koolpin Formation could have formed unconformity-related uranium deposits. However, The Koolpin Formation is also unconformably overlain by the Katherine River Group. Diagenesis of the Katherine River Group is interpreted to have formed world-class uranium deposits in the Nimbuwah Domain. Hence it is more likely that uranium deposits in the South Alligator River Mineral Field were also formed from fluids generated in the Katherine River Group sediments. However it is also possible that diagenetic fluids from the Katherine River Group could have remobilised uranium from uranium-rich zones formed from the diagenesis of the Coronation Sandstone.

The presence of bimodal volcanics in the El Sherana and Edith River Groups formed along with sediments deposited in a syn-rift setting suggests that this extensional basin may be favourable for volcanic-associated massive sulphide deposits of lead, zinc and copper. Similarly, the presence of rhyodacitic ignimbrites, glassy rhyolite and andesites in the Plum Tree Creek Volcanics, formed in subaerial conditions suggests that this felsic magmatism could have generated epithermal vein deposits of gold and silver.

#### **4.7 SHOOBRIDGE EVENT (ca. 1780 Ma)**

The Shoobridge Event is defined as the last regional metamorphic and deformational event of the Top End Orogeny (Needham *et al.*, 1988). The event is thought to have caused reactivation of linear shear zones parallel to the regional north-south to northwest-southeast trends within granitoids and Early Proterozoic sediments. It also caused widespread retrogressive metamorphism and localised prograde, low-grade regional metamorphism adjacent to some major shear zones.

The age of the event is defined by Rb-Sr total rock ages of the granitoids and by the K-Ar and Rb-Sr systematics of the metasediments. This age needs to be redefined in view of new geochronological data on the ages of granites in the Central Domain.

#### **4.7.1 Mineral systems associated with the Shoobridge Event**

As the event and its age are poorly defined it is difficult to link known mineral systems with the event. However SHRIMP U-Pb analysis of monazite from gold veins at the Toms Gully Deposit gives an age of  $1780 \pm 10$  Ma. Rasmussen *et al.* (2006) use this age to suggest that the gold mineralisation may be related to the Shoobridge Event.

#### **4.8 KATHERINE RIVER GROUP/TOLMER GROUP (1800 Ma – 1710 Ma)**

The deformation and metamorphism of the Shoobridge Event was followed by a brief period of planation and weathering replaced by deposition of the Katherine River Group in the Central and Nimbuwah domains. The Tolmer Group, which was deposited in the Central and Litchfield domains, is thought to be correlative of the Katherine River Group (Needham *et al.*, 1988).

The Katherine River Group is the basal unit of the McArthur Basin. It is part of the large intracontinental Leichhardt Superbasin, which resulted from NNE-SSW directed extension (Leichhardt Extension) in the northern part of Australia (de Vries *et al.*, 2008). Sedimentation of the Tolmer Group occurred in the Birrindudu Basin resulting from N-S directed extension (Calvert Extension; de Vries *et al.*, 2008). However, recent SHRIMP U-Pb data on detrital zircon from the Depot Creek Sandstone (Tolmer Group) provide a maximum age of deposition of  $1837 \pm 15$  Ma, which is quite similar to the maximum deposition ages obtained from the Kombolgie Sandstone (Carson, 2010; unpublished report in OZCHRON), suggesting that the Tolmer Group may also be related to the Leichhardt Extension.

The Katherine River Group unconformably overlies the Nabarlek Granite ( $1818 \pm 8$  Ma; Worden *et al.*, 2008a) providing a maximum age of deposition of the sediments. An Ar/Ar analysis of diagenetic illite in the sandstone of the Kombolgie Subgroup at the Jabiluka uranium deposit yielded an age of  $1798 \pm 18$  Ma (Polito *et al.*, 2005), suggesting that sedimentation of the basal part of the Katherine River Group could have started between ca. 1810 Ma and 1800 Ma. The age of the top part of the Katherine River Group is constrained by the depositional age for the West Branch Volcanics. A porphyritic rhyolite from the units yields a SHRIMP U-Pb age of  $1712 \pm 6$  Ma (Kruse *et al.*, 1994). Hence deposition of the Katherine River Group could have begun at ca. 1810 Ma and continued till around 1710 Ma during which at least 3000 metres of sediments were deposited.

The Mamadawerre Sandstone, the lowermost unit of the Kombolgie Subgroup, was formed in braided fluvial to shallow marine (minor upper portion) conditions. The rest of the Kombolgie Subgroup was also deposited in fluvial and shallow marine conditions (Ferenczi and Sweet, 2005). The sediments, which unconformably overlie the Kombolgie Subgroup (upper part of the Katherine River Group), were formed in conditions that changed from the shallow marine and fluvial at the base to shallow marine and marine shelf conditions at the top (Ferenczi and Sweet, 2005). A more detailed analysis of sedimentary facies is available in Hiatt *et al.* (2007).

The Katherine River Group sediments are interlayered with two mafic units (Nungbalgarri Volcanics and Gilruth Volcanics) the thickest of which is the Nungbalgarri Volcanics (~ 200 m) and comprises altered massive and amygdaloidal basalt flows, minor tuffs and siltstone. The thinner Gilruth Volcanics (~ 14 m) is represented by highly ferruginised and weathered basalt (Ferenczi and Sweet, 2005). The Oenpelli Dolerite (~ 175 m thick) intrudes the Kombolgie Subgroup. The felsic units in the West Branch Volcanic Member contain up to 11 ppm uranium (Kruse *et al.*, 1994) indicating their potential to be a good source of uranium for fluids.

Limited SHRIMP U-Pb studies of detrital zircon show that the sediments of both the Kombolgie Subgroup in the Nimbuwah Domain and the Depot Creek Sandstone in the Litchfield Domain may have been derived from local Archean and Paleoproterozoic rocks (Carson, 2010; unpublished report in OZCHRON).

Ojakangas (1979) demonstrated a strong trend in the paleocurrent measurements in the Kombolgie Subgroup (Figure 4–10). In the Nimbuwah Domain the pattern suggests transport of sediments from the west and northwest towards the east and southeast, although measurements at Jabiluka show considerable spread and divergence. The transport direction supports the idea that the sediments were possibly derived from Archean and Paleoproterozoic rocks in the west (Nanambu Shelf, Ahmad *et al.*, 2006). The paleocurrent measurements near the Slesbeck and El Sherana deposits (Central Domain) indicate either the effects of local highs (sources) within the depositional basin or

the lateral accretion on edges of sandbars. In the Katherine Gorge area (KATHERINE) a northwesterly provenance is suggested by Kruse *et al.* (1994) for the Kombolgie Subgroup sediments, however in the Waterhouse Syncline area the paleocurrent measurements suggest a strong northerly to northeasterly provenance. On MOUNT MARUMBA the transport direction was to the west-southwest (Sweet *et al.*, 1999). On MILINGIMBI measurements in the Mamadawerre Sandstone suggest that transport was directed to west and south-southwest in the northernmost outcrop and southerly in the vicinity of the headwaters of the Goomadeer River (Carson *et al.*, 1999). This indicates that some of the sediments could have been derived from the topographically high areas of the Nanambu Complex. The map in Figure 4-10 represents possible pre-erosional extent of the Katherine River and Tolmer Groups. The interpretation of the extent is based on available paleocurrent measurements discussed above and assumes that the regions occupied by Archean rocks and by the Cullen-event granitoids constituted topographic highs during sedimentation in the McArthur River and Birrindudu Basins. This interpretation is highly speculative and needs more work to confirm the nature and extent of depositional centres within these basins. The assessment of the pre-erosional extent of these sediments is critical for evaluating prospectivity of unconformity-related uranium deposits in the PCO (see following discussion).

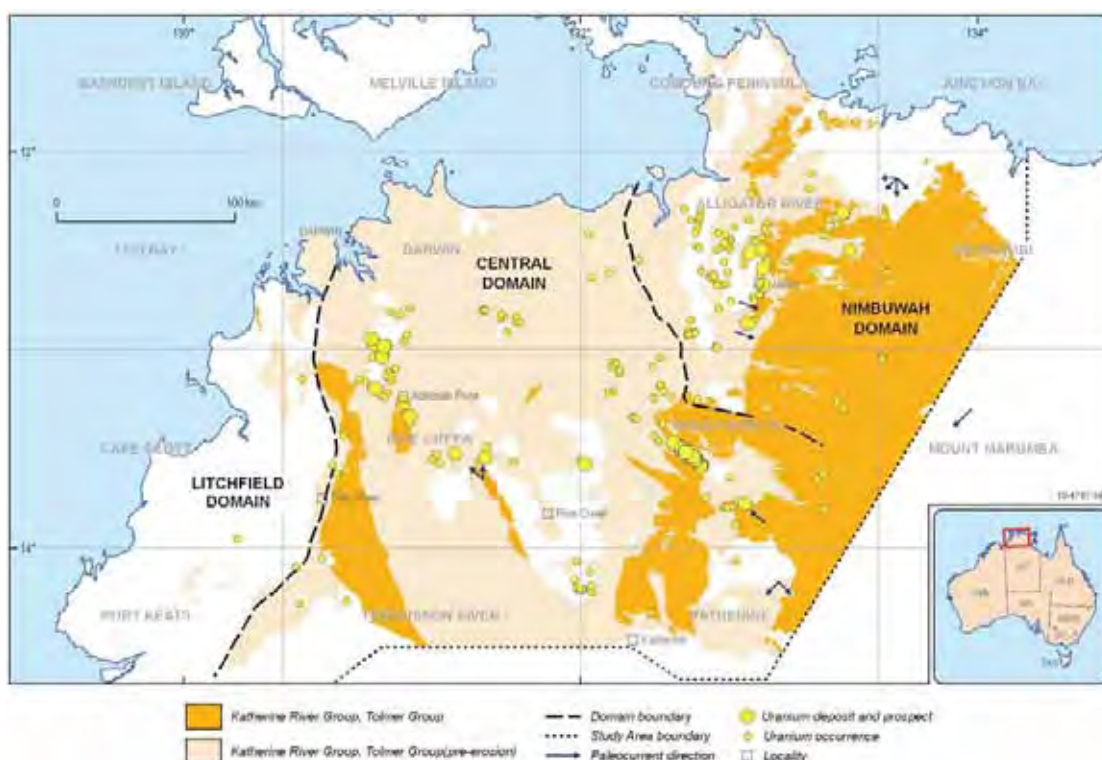


**Figure 4-10:** Map showing possible pre-erosion extent of Katherine River and Tolmer Group sediments. The map is based on an NTGS dataset, i.e., Pine Creek interpreted geology (2005).

#### 4.9 MID-TAWALLAH INVERSION (ca. 1750 Ma – 1730 Ma)

Deposition of the Katherine River Group was affected by a regional compressive event, the mid-Tawallah inversion. This east-west compression/inversion produced a contemporaneous, ~20 million years gap in the stratigraphic record and caused tilting, folding (broad open folds) and faulting in the Lower Katherine Group sediments (Ferenczi and Sweet, 2005).

#### **4.10 DEPOSITION OF UPPER PART OF KATHERINE RIVER GROUP (ca. 1730 Ma – 1710 Ma)**

The Mid-Tawallah inversion was followed by a period of subsidence and deposition of fluvial and shallow-marine sands. The sedimentation was accompanied by mafic volcanism (McCaw Formation) and comagmatic felsic intrusive and volcanism (West Branch Volcanics). SHRIMP U-Pb analysis of quartz-feldspar porphyry gives ages of  $1712 \pm 6$  Ma and  $1705 \pm 16$  Ma (Kruse *et al.*, 1994) for the West Branch Volcanics. Similarly a SHRIMP U-Pb analysis of Tanumbirini Rhyolite from the upper part of the Tawallah Group, interpreted to be a correlative of the Katherine River Group also gives an age of  $1713 \pm 6$  Ma (Rawlings *et al.*, 2004). These ages provide a constraint on the age of deposition of the upper Katherine River Group.

Synchronous with deposition of sediments (upper Katherine River Group), the lower part of the group was intruded by a lopolithic olivine dolerite (Oenpelli Dolerite). A drillhole (DAD006) intersected 175 m of Oenpelli Dolerite intruding the upper Mamadawerre Sandstone at about 1014 m depth (Ferenczi and Sweet, 2005). The intrusion produced contact metamorphism (pyroxene hornfels) in the metasedimentary rocks and granites. In the Mamadawerre Sandstone it shows a sharp upper contact and minor brecciation along the sheared lower contact (Ferenczi and Sweet, 2005). The dolerite is subalkaline in composition and shows geochemical trends similar to intraplate tholeiites and was emplaced at relatively shallow levels (1 – 2 km depth) as sheet-like bodies.

Conventional U-Pb analysis of baddleleyite grains from a sample of a mafic dyke near the Nabarlek deposit gave a crystallisation age of  $1723 \pm 6$  Ma for the dyke (Worden *et al.*, 2008a). This dyke has been described in literature as Oenpelli Dolerite. However, recent studies show that the sample is geochemically quite distinct from the mafic suite mapped as the Oenpelli Dolerite (Hollis *et al.* 2011). Thus the age of emplacement of the Oenpelli Dolerite remains open and is constrained to < 1820 Ma by the maximum depositional age of the Kombolgie Subgroup (Hollis *et al.* 2011).

#### **4.11 EXTENSION AND DEPOSITION OF MOUNT RIGG GROUP (ca. 1610 Ma - 1590 Ma)**

A mixed siliciclastic-dolomitic sequence comprising Mount Rigg Group overlies unconformably the Katherine Group. The Mount Rigg Group sequence is considered to be a correlative of the Nathan Group in the Southern McArthur Basin and is interpreted to be part of Isa Superbasin (Ferenczi and Sweet, 2005; de Vries *et al.*, 2008). This correlation suggests a prolonged unconformity and hiatus in sedimentation in the PCO. Geochronological studies constrain sedimentation of the Nathan and Mount Rigg Groups to between 1613 Ma and 1590 Ma (Ferenczi and Sweet, 2005).

#### **4.12 BASIN-RELATED MINERAL SYSTEMS ASSOCIATED WITH POST-SHOORBRIDGE EVENTS**

Available age data on unconformity-related uranium deposits suggests that although uranium mineralisation is remobilised and the age reset, bulk of the uranium mineralisation is related to Post-Shoobridge events which involved deposition of the Katherine River Group, diagenesis of the sediments and deformation associated with basin inversion.

#### **4.13 UNCONFORMITY-RELATED URANIUM DEPOSITS**

Uranium deposits in PCO are grouped in three fields ([Figure 4–11](#); [Table 4–5](#): Lally and Bajwah, 2006): Alligator Rivers Uranium Field (ARUF); South Alligator Valley Mineral Field (SAVMF), and Rum Jungle Mineral Field (RJMF). In recent years new uranium prospects (e.g., Thunderball, Bella Rose, Corkscrew) have been reported in a zone between Adelaide River and Emerald Springs. This new Hayes Creek Mineral Field (HCMF) also contains the Fleur De Lys deposit. Uranium deposits in the PCO have been described in detail in many publications (Ahmad *et al.*, 2006; Lally and Bajwah, 2006; McKay and Miezitis, 2001). The summary presented in this section draws on these publications. Significant features of the four uranium fields are summarised in [Table 4–5](#).

**Table 4-5:** Principal features of main uranium fields in the Pine Creek Orogen

ATTRIBUTE\URANIUM FIELD	ALLIGATOR RIVERS	SOUTH ALLIGATOR VALLEY	RUM JUNGLE	HAYES CREEK
<b>DOMAIN</b>	<b>NIMBUWAH</b>	<b>CENTRAL</b>	<b>CENTRAL</b>	<b>CENTRAL</b>
Resource (tonnes U <sub>3</sub> O <sub>8</sub> )	408055	2649	6354	0.1
Number of deposits	7	11	5	2
Metal association	U, Au	U, Au, PGEs	U, Cu, Pb, Zn, Co, Ni	U, PGE
Host rocks	Cahill Formation	Koolpin Formation, Coronation Sandstone	Whites Formation	Mount Bonnie Formation, Gerowie Tuff
Age of host rock (Ma)	ca. 1870	ca. 1860, ca. 1829	ca. 2019	ca. 1860
Sandstone above unconformity	Mamadawerre Sandstone	Mamadawerre Sandstone	Depot Creek Sandstone, Geolsec Formation	Depot Creek Sandstone
Metamorphic grade of the host (facies)	Amphibolite	Greenschist	Greenschist	Greenschist
Nearby Archean complex	Nanambu, Arrarra Gneiss, Kukalak Gneiss	Unknown	Rum Jungle	Unknown
Age of Archean complex (Ma)	2670, 2640, 2520		2545, 2520	Unknown
Associated mafic rocks (< 1800 Ma)	Oenpelli Dolerite (?), mafic volcanics in the Katherine River Group	Oenpelli Dolerite (?)	None	None
Mafic rocks (> 1800 Ma)	Zamu Dolerite present near Caramel	Zamu Dolerite, Goodparla Dolerite	Zamu Dolerite	Zamu Dolerite
Alteration in the metasedimentary rocks	Chloritic, sericitic, hematitic, desilicification	Chloritic, sericitic, hematitic, desilicification	High-Mg chloritic, Fe-Mg Chloritic, sericitic, hematitic. In some deposits magnesite, dolomite and tourmaline present	Sericitic
Alteration in the sandstone	Chloritic, sericitic hematitic, desilicification	Hematitic	Hematitic	Unknown

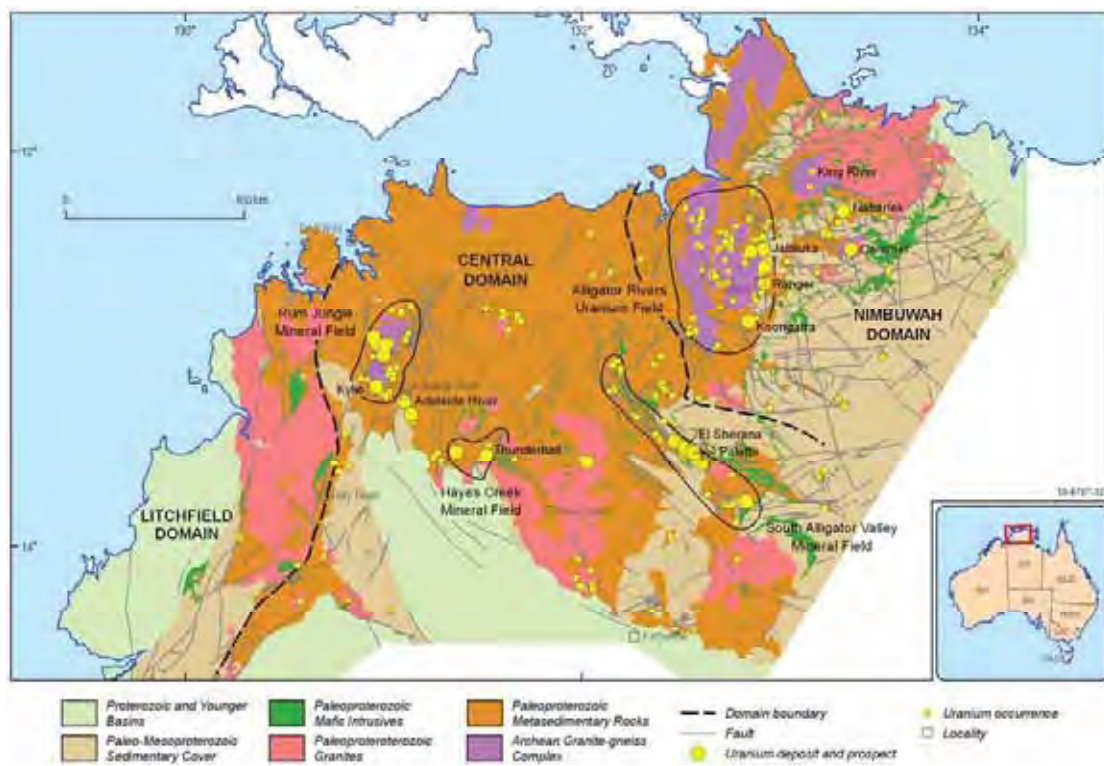


**Figure 4-11:** Map of the Pine Creek Orogen showing uranium deposits and occurrences. The map is based on an NTGS dataset, i.e., Pine Creek interpreted geology (2005). Deposits, prospects and occurrences are from GA's OZMIN and MINLOC datasets.

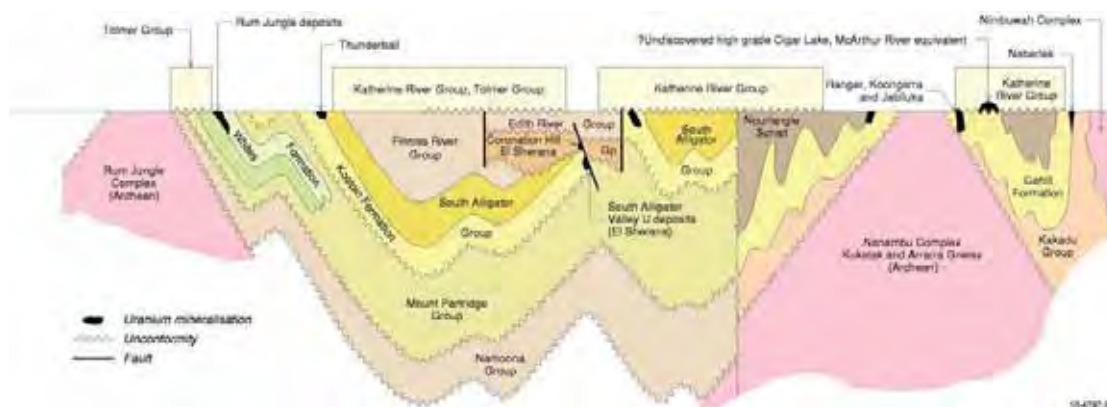


**Figure 4-12:** Schematic cross-section of the Pine Creek Orogen showing position of major uranium deposits. Modified after Mckay and Miezitis (2001).

#### 4.13.1 Geological Architecture

Geological architecture of unconformity-related uranium systems in the PCO can be defined by four important components which include: 1) major unconformity; 2) reduced Paleoproterozoic metasedimentary rocks below the unconformity; 3) a relatively thick (> 4 to 5 km) package of Paleoproterozoic coarse-grained, dominantly fluvial sedimentary rocks overlying the unconformity; and 4) ore-localising faults.

- Major unconformity.

In the Nimbuwah Domain the major unconformity is between reduced metasediments of the Paleoproterozoic Cahill Formation and Nourlangie Schist (both broadly equivalent of the South Alligator River Group) and relatively oxidised sediments of the Katherine River Group ([Figure 4–12](#)). In the Central Domain the unconformity is between the reduced metasediment of the South Alligator River Group and the Katherine River Group in the eastern part of the domain. In the South Alligator Valley Mineral Field, the unconformity between the El Sherana Group, which contains a package of oxidised sediments (Coronation Sandstone), and the reduced metasediments of the South Alligator River Group could have played an important role. In the Rum Jungle Mineral Field the important unconformity is between the reduced metasediments of the Mount Partridge Group (Whites Formation) and the oxidised sediments of the Depot Creek Sandstone, most of which has been eroded. Similarly in the Hayes Creek Uranium Field a large portion of the original package of oxidised sediments (Depot Creek Sandstone) has most probably been eroded. Where present, they overlie reduced metasediments of the South Alligator River Group (Koolpin Formation). Remnants of the Depot Creek Sandstone outline the margins of the Palaeozoic Daly Basin and continue under the basin. The AEM data reveals the presence of unconformity between the Depot Creek Sandstone and reduced metasediments of the South Alligator River Group. Drilling records support the presence of the unconformity (see [chapter 6 – AEM interpretation](#)). In the northern Litchfield Domain, it is possible that Depot Creek Sandstone overlies unconformably graphite-bearing metasediments of the Welltree Metamorphics.

In the Arnhem Land Plateau, the unconformity commonly has a local relief of up to 20 m (Needham, 1988). Pebble-filled paleovalleys up to 20 m across have been observed along the unconformity. Locally steep paleovalleys are filled with massive breccia-conglomerate which grades into coarse conglomerate, and coarse quartz sandstone (Needham, 1988). A truncated regionally extensive palaeo-saprolitic profile (commonly over 50 m thick) developed in rocks of the Nanambu Complex has been described by Needham (1988). The profile shows mineralogical and geochemical zoning from the chlorite zone just above the protolith to a hematite zone at the top. The profile was most probably modified following burial under the Kombolgie Subgroup sediments. A hematite-apatite-rich breccia (Scinto Breccia) in the South Alligator Valley is interpreted by Stuart-Smith *et al.* (1988) as an *in situ* regolith developed over carbonate-bearing rocks (mainly Koolpin Formation) at the unconformity surface, however it has also been interpreted to be of hydrothermal origin (Ferenczi and Sweet, 2005). Hematite-quartz breccia within the Geolsec Formation in the Rum Jungle Mineral Field has some similarities with the Scinto Breccia. It is considered to be either the product of *in situ* weathering and collapse of Coomalie Dolostone or as reworked talus slope breccia (Ahmad *et al.*, 2006).

- Reduced Paleoproterozoic metasedimentary rocks below the unconformity.

The metasediment enriched in carbonaceous material (graphite) and/or Fe<sup>+2</sup>-bearing silicates (such as chlorite) include the Whites Formation (Rum Jungle Mineral Field – RJMF), Koolpin Formation (Hayes Creek Mineral–HCMF and South Alligator Valley Mineral Fields– SAVMF) and Cahill Formation (Alligator River Uranium Field – ARUF) and Welltree Metamorphics (Litchfield Domain). The metasediments were metamorphosed to greenschist and amphibolite to granulite facies metamorphism which produced Fe<sup>+2</sup>-bearing silicates (amphibole and chlorite). A characteristic feature of the metasedimentary package is the presence of calcareous sediments (dolomudstone in the Koolpin Formation; dolostones of the Coomalie Dolomite interfingering with the Whites Formation and dolomitic rocks in the Cahill Formation). The significance of calcareous

sediments in the favourable host rocks is not clear although it may indicate that the favourable package was deposited in low-energy supra-tidal to subtidal conditions rather than in deeper-marine turbiditic environment.

- A relatively thick (> 4 to 5 km) package of Paleoproterozoic coarse-grained, dominantly fluvial sediments overlying the unconformity.

In both the Nimbuwah and Central Domains, the bulk of the Katherine River Group sediments (> 3 km in thickness) represent alluvial fan to braided fluvial facies. Although sediments of the Tolmer Group (> 4 to 5 km) have not been studied in as much detail as the Katherine River Group, the available information suggests that a bulk of them were also deposited in similar conditions (Malone, 1962). The Depot Creek Sandstone (the basal unit of the Tolmer Group) occupies a similar stratigraphic position to that of the Mamadawerre Sandstone (basal unit of the Katherine River Group) and is interpreted to have formed in fluvial conditions (Carson, 2010 unpublished report in OZCHRON). Matrix minerals in the sandstones contain iron-oxide and some units in the Katherine River Group are distinctly ferruginous (e.g., Marlgowa Sandstone, McKay Sandstone; Needham, 1988; Carson *et al.*, 1999). Similarly the sandstone in the Tolmer Group contains lenses of hematite-rich calcarenite (Malone, 1962). The presence of ferruginous minerals in the sandstone can be an important indicator of the oxidation state of fluids formed from the diagenesis of these sediments.

- Ore-localising faults

All known deposits in the PCO are structurally controlled. At the Nabarlek deposit mineralisation is located along a northwest trending reverse fault/shear zone (Wilde and Wall, 1987). At the Jabiluka deposit, mineralisation is structurally controlled within semi-brittle shears that are sub-conformable to the basement stratigraphy, and breccias that are developed within the hinge zone of fault-related folds adjacent to shears (Polito *et al.*, 2005). The Ranger 1 deposits occur along the sheared contact (north-south trending low-angle reverse fault) between the Cahill Formation and the underlying Nanambu Complex (Lally and Bajwah, 2006). At the Koongarra deposit the mineralisation is located at the faulted and brecciated contact (northwest trending, steeply dipping reverse fault) between the Cahill Formation and the Mamadawerre Sandstone (Lally and Bajwah, 2006).

In the South Alligator Valley Mineral Field all major deposits are within the northwest-trending Rockhole-El Sherana-Palette Fault system and were formed in dilational zones at fault bends or intersections (Valenta, 1991).

A similar structural control is described for uranium deposits in the Rum Jungle Mineral Field. The four uranium deposits and Browns basemetal deposit lie along a northeast-trending shear zone located on the northern limb of a northeast-trending asymmetric syncline (Ahmad *et al.*, 2006). At the Rum Jungle Creek South deposit uranium ore body is located within the hinge zone of a northwest-trending doubly plunging syncline in proximity to a northwest-trending steep fault (Ahmad *et al.*, 2006). There is limited information on uranium prospects in the Hayes Creek Uranium Field, but main uranium prospects appear to be located within a structural zone defined by northeast-trending Hayes Creek and Bella Rose faults (Thundelarra Exploration, 2010).

#### 4.13.2 Setting with respect to unconformity

The unconformity-related deposits in the PCO are described as Proterozoic subunconformity deposits because mineralisation is located within reduced metasedimentary rocks below the unconformity (Dahlkmap, 2009). In Canada similar deposits are classified as Ingress-style in contrast to the Egress-style deposits in which the mineralisation is located in the sandstone package overlying the unconformity (Jefferson *et al.*, 2007). The Katherine River and Tolmer Group sediments overlying the unconformity have been preserved only in and near a few deposits. The known deposits and prospects in the PCO can be grouped into four types (Figure 4–13):

- Deposits in which the Proterozoic sandstone package is preserved (such as Jabiluka);
- Deposits in which the Proterozoic sandstone package is partially preserved (such as Koongarra where the Mamadawerre Sandstone is present in the footwall of a shear zone);
- Deposits in which the Proterozoic sandstone package is located within a few kilometres of the mineralised zone (such as Nabarlek, Caramal); and,
- Deposits in which the mineralised zone is covered by Phanerozoic sediments (such as Ranger 68 and Austatom). At these deposits, the mineralised zones are unconformably overlain by Cretaceous sediments. The uranium mineralisation however is interpreted to be related to Proterozoic rather than Cretaceous uranium system.

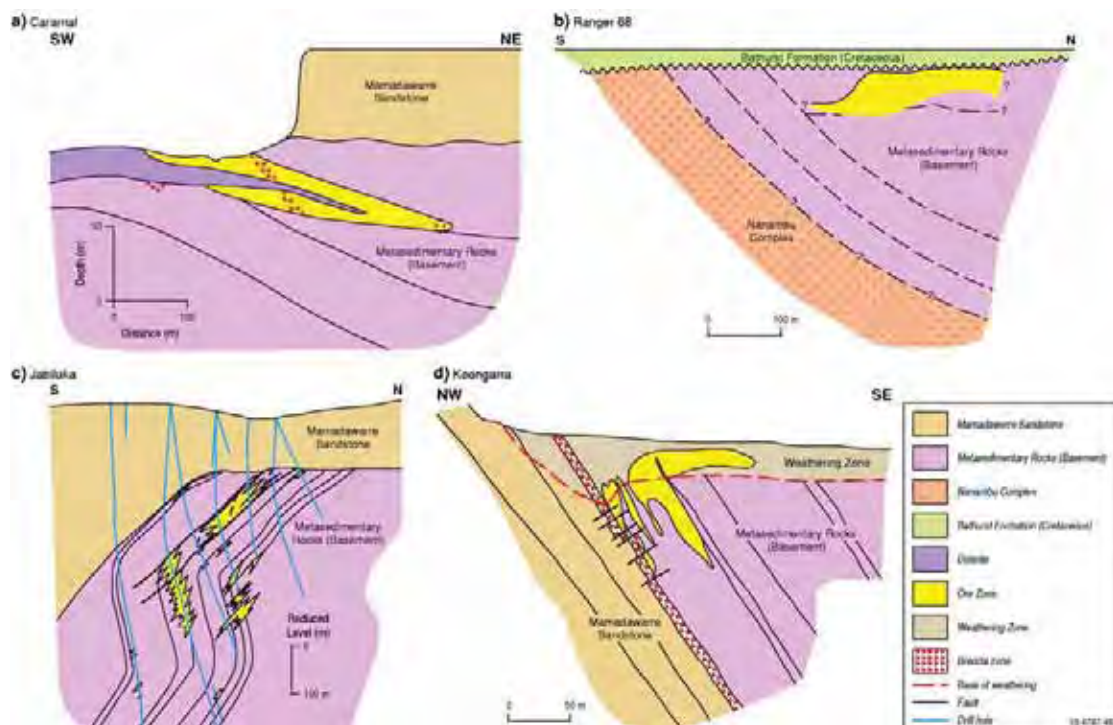


**Figure 4-13:** Schematic cross-sections showing four types of setting of unconformity-related uranium deposits. Modified after Lally and Bajwah (2006).

#### **4.13.3 Source of uranium**

Although Archean and Paleoproterozoic metasediments in the PCO contain abundant uranium and could have been the first-stage source of uranium for the deposits the immediate source of uranium remains uncertain. Two types of immediate sources of uranium have been postulated for unconformity-related uranium deposits: primary detrital heavy minerals in the sandstones overlying the unconformity or uranium-bearing minerals in the metasedimentary rocks below the unconformity (Kyser and Cuney, 2009). It has been suggested that diagenesis of the Athabasca Group in Canada caused extensive mobility of rare-earth elements and that rare-earth elements and uranium were most likely derived from detrital fluorapatite and zircon in the sandstone (Fayek and Kyser, 1997). In the Athabasca Group primary detrital heavy minerals are essentially absent except for rare zircon and tourmaline, but fluorapatite and zircon are abundant as inclusions in detrital quartz. Detrital zircon in the matrix of sandstones is commonly corroded and shows evidence of increase in uranium relative to zirconium hence detrital zircon could not have been the source of uranium. However, in situ alteration of monazite results in the formation of uranium-poor phosphate minerals, releasing excess uranium into diagenetic fluids. The former presence of detrital monazite in sandstones is indicated by high thorium contents of 18 ppm in the lower Manitou Formation of the eastern Athabasca Basin (Quirt *et al.*, 1991). Although no detailed studies have been carried out in the Katherine River and Tolmer groups, a scenario similar the one in the Athabasca Basin has also been suggested in the PCO (Kyser and Cuney, 2009).

As the uranium content of metasedimentary rocks, granites, and pegmatites below the unconformity is an order of magnitude higher than the sandstones overlying the unconformity, they can be another possible source of uranium (Kyser and Cuney, 2009). The Archean granites in the Rum Jungle Complex have anomalously high uranium (2.9 – 39.9 ppm; average 12.5 ppm; McCready *et al.*, 2003). The Archean and Paleoproterozoic rocks generally contain abundant zircon and monazite, alteration of which can provide a good source of uranium. Altered zircons from these rocks in the Athabasca Basin, however, are depleted in Zr, Si and enriched in P, Y, Fe, Ca and U. Hence zircon grains may not be a good source of uranium unless they are completely altered (Hecht and Cuney, 2000). Monazite, on the other hand, is the dominant uranium-bearing mineral in the basement rocks below the unconformity and has undergone intensive alteration in proximity to uranium deposits suggesting that around 75% of its uranium has been leached. Thus monazite in the basement rocks interacting with fluids can be a good potential source of uranium in unconformity-related uranium deposits (Kyser and Cuney, 2009).

In the PCO the sandstones in the Katherine River Group are not anomalous in uranium. In the drill hole DAD0006, the concentration of uranium in the sandstone units of the Kombolgie Subgroup varies between 0.29 ppm and 17.4 ppm. The uranium concentration increases to ~ 20 ppm at the upper and lower contact with mafic units with the Kombolgie Subgroup (Jaireth *et al.*, 2007). A similar variation is observed in the drill holes DAD0002 and DAD007. Saproitic paleoweathered zones such as those described at Granite Hill (Needham, 1988) can also be a good source of uranium. At the Granite Hill, the paleoweathered zone has lost up to 5 ppm uranium compared to the Nanambu Complex protolith. Although the origin of the Geolsec Formation in the Rum Jungle Field and the Scinto Breccia in the South Alligator Valley Mineral Field is not clear, such paleoweathering zones overprinted and altered by later fluid influx can also be effective sources of uranium. Similar zones of paleoweathering have been described in the Athabasca Basin (Kyser and Cuney, 2009).

#### **4.13.4 Source of fluids**

Numerous fluid inclusion studies in the PCO and in the Athabasca Basin suggest that uranium deposits formed during peak diagenesis of the sandstone units overlying the unconformity at temperatures between 180°C and 250°C (Kyser and Cuney, 2009 and references therein). Derome *et al.* (2003) studied fluid inclusion in quartz-breccia veins in the basal sandstone units of the Kombolgie Subgroup and showed presence of three distinct fluids: 1) a sodium-rich brine corresponding to a diagenetic fluid at a temperature close to  $150 \pm 5^\circ\text{C}$ ; 2) a calcium-rich brine, probably corresponding to a residual basinal evaporitic brine that had reacted with the rocks below the unconformity; and 3) a low-salinity fluid heated in the basement. Wilde *et al.* (1989) documented similar hypersaline fluids (ca. 23 eq. wt% CaCl<sub>2</sub>) in secondary halite-saturated inclusions in altered host rock quartz and in early hydrothermal quartz veins. A detailed reconstruction of fluid evolution based on fluid inclusion studies in the sandstone-hosted unconformity deposit at McArthur River (Athabasca Basin) reveals similar types of fluids: 1) an NaCl-rich brine (25 wt% NaCl, up to 14 wt% CaCl<sub>2</sub>, and up to 1 wt% MgCl<sub>2</sub>) interpreted to be basinal fluid expelled from evaporites; and 2) a CaCl<sub>2</sub>-rich brine (5 to 8 wt% NaCl, 20 wt% CaCl<sub>2</sub>, and up to 11 wt% MgCl<sub>2</sub>) interpreted to be formed during the interaction of the basinal fluid with Ca-rich minerals in the rocks below the unconformity (Derome *et al.*, 2005). Thus at least two fluids are interpreted to be involved in the formation of these deposits: a basinal fluid derived from the diagenesis of sandstone overlying the unconformity, and a fluid resulting from the interaction of the basinal fluid with rocks below the unconformity.

At the Coronation Hill deposit in the South Alligator Valley Miner Field the syn-ore fluid is likewise highly saline (20 to 25 wt% CaCl<sub>2</sub>) with median homogenisation temperatures of 140°C (Mernagh *et al.*, 1994). The interpreted temperatures of formation of 180 to 250°C suggest that the sandstone package overlying unconformity was at least 5 km thick (assuming a geothermal gradient of 35°C/km).

#### **4.13.5 Wall-rock alteration**

Uranium deposits are associated with extensive alterations zones. At the Nabarlek deposit the outer alteration halo extends as far as 1 km from the Nabarlek Fault and is dominated by chlorite and sericite. In this zone biotite, muscovite and hornblende in the schists are partially, to completely, replaced by Fe-chlorite and minor fine-grained sericite, which also replaces plagioclase. An extensive zone of silicification occurs in the schists at the footwall side of the Oenpelli Dolerite. The inner alteration halo comprises illite, hematite, and Fe-chlorite but complete lacks quartz. A finely disseminated hematite making up to 20% of the assemblage is the distinguishing feature of this zone. The abundance of illite continues to increase toward the ore zone. Within the ore zone illite locally forms a massive monomineralic rock. The deposit also contains post-ore chloritic alteration which crosscuts uraninite-illite-hematite assemblage (Polito *et al.*, 2004). Similar alteration assemblages are observed at the Jabiluka deposit where the alteration halos extends at least 200 m beyond known uranium ore in the basement rocks. At the Jabiluka deposit the outer and inner alteration halos are mineralogically similar but the content of chlorite and illite increases in the inner halo. Within the mineralised areas multiple generations of chlorite and sericite occur with and/or without quartz, uraninite and hematite (Polito *et al.*, 2005). At the Jabiluka deposit alteration related to mineralisation is observed in the sandstone overlying the unconformity. In the sandstones, illite formed during peak diagenesis is overprinted by chlorite. Chlorite replacement of illite varies from limited amounts usually well above the unconformity to massive zones adjacent to the unconformity (Polito *et al.*, 2005). At the Ranger deposit, a faulted outlier of brecciated Mamadawerre Sandstone is chloritised and hematitised (Ahmad *et al.*, 2006). In the metasediments below the unconformity, the alteration zone is similar to those described at Jabiluka and Nabarlek deposits, and likewise contains zones of chlorite, hematite and silica (Hein, 2002; McCoy *et al.*, 2009).

#### **4.13.6 Type of reductant**

All major host rocks of uranium deposits in PCO are enriched in carbonaceous material (graphite), which is interpreted as the main reducing agent for uranium-bearing hydrothermal fluids. However, a genetic link between basement graphite and uranium deposits is not clear and has been questioned by many researchers (Cuney, 2005). Graphite has not been reported in the host sequence at the Nabarlek deposit (Polito *et al.*, 2004). In the Athabasca Basin significant uranium deposits are hosted by units, which do not contain graphite (Jefferson *et al.*, 2007). An additional problem with graphite functioning as a reductant is a relatively low reactivity of graphite at temperatures below 300°C (French, 1966; Frost, 1979).

In the absence of graphite in the host rock (as at the Nabarlek deposit), Fe<sup>+2</sup>-bearing silicates, especially Fe-chlorite, can be good reductants. A reaction between relatively oxidised uranium-bearing fluids with Fe-chlorites can liberate Fe<sup>+2</sup> to reduce the fluid. The evidence of such a reaction can be seen in the presence of illite in inner alteration halo proximal to ore zones. These zones also contain abundant hematite, which could have been formed due to the oxidation of Fe<sup>+2</sup> liberated during replacement of Fe-chlorite by illite.

Radioelement-rich bitumen occurring in both Archean granites and the Paleoproterozoic metasediments has been reported in the Rum Jungle Mineral Field (McCready *et al.*, 2003). Landais (1996) reported similar carbon isotope compositions between barren bitumens ( $U < 500$  ppm) and graphite in metasediments below the unconformity in the Athabasca Basin and suggested that these bitumens could have formed due to hydrogenation of carbon. A similar model is proposed for the bitumens in the Rum Jungle Mineral Field where hydrogenation is thought to be related to the fluids, which caused sericitic alteration of organic-rich metasediments of the Whites Formation (McCready *et al.*, 2003). It is not clear if bitumens generated by hydrogenation of organic material had played a role in reducing uranium-bearing diagenetic fluids, but such a possibility cannot be ruled out.

#### **4.13.7 Timing of uranium mineralisation**

Results of geochronological studies of major uranium deposits have been summarised by Lally and Bajwah (2006). Some of the more cited ages for uranium deposits in the PCO are shown in [Table 4–1](#). The oldest age of ca. 2000 Ma for the Whites East deposit in the Rum Jungle Mineral Field is probably not correct as discussed by von Pechmann (1992). The other ages lying between ca. 1740 Ma and ca. 1630 Ma ([Table 4–1](#)) are interpreted to show that unconformity-related uranium deposits in PCO were formed close in time with the peak diagenesis of the sandstone package overlying the unconformity.  $^{40}\text{Ar}/^{39}\text{Ar}$  dating of diagenetic illite in the Kombolgie Subgroups aquitards and aquifers yields ages of  $1798 \pm 13$  Ma,  $1747 \pm 11$  Ma,  $1726 \pm 5$  Ma, and  $1688 \pm 7$  Ma (Polito *et al.*, 2005).

The  $1798 \pm 13$  Ma age of diagenetic illite provides a good minimum constraint on the age of sedimentation in the basal sediment of the Katherine River Group. The  $1747 \pm 11$  Ma age of diagenetic illite is very close to the  $1737 \pm 20$  Ma U-Pb age obtained from uraninite at the Ranger deposit ([Table 4–1](#)). The third diagenetic age of  $1726 \pm 5$  Ma is very close to  $1723 \pm 6$  Ma age of emplacement of the dolerite dyke at the Nabarlek deposit. The  $1688 \pm 7$  Ma age obtained from diagenetic illite is similar to  $1685 \pm 17$  Ma age of uraninite at the Jabiluka deposit. If the dating of uraninite at the Ranger and Jabiluka deposits is correct it can be argued that the bulk of uranium mineralisation at these deposits is associated with different but sequential episodes of diagenesis of sediments in the Kombolgie Subgroup.

The U-Pb chemical age of  $1642 \pm 33$  Ma obtained from uraninite at the Nabarlek deposit is younger than the  $^{40}\text{Ar}/^{39}\text{Ar}$  ages of sericite from the alteration zone and vary between  $1715 \pm 7$  Ma and  $1696$

$\pm 7$  Ma (Polito *et al.*, 2004). Polito *et al.* (2004) prefer ca. 1640 Ma as the age at which massive uraninite was formed at the Nabarlek deposit with wall-rock alteration occurring at ca. 1700 Ma. This interpretation does not fit the post-peak diagenetic model of uranium mineralisation as no diagenetic event around 1640 Ma has as yet been detected. However it is possible that the 1696  $\pm 7$  Ma age of alteration sericite also represents the age of uranium mineralisation or is very close to it. This age is very similar to the age of fourth diagenetic event (1688  $\pm 7$  Ma) in the Kombolgie Subgroup. Hence it is possible that uranium mineralisation at the Nabarlek deposit occurred at ca. 1690 Ma instead of ca. 1640 Ma and thereby close in time to the age of mineralisation at the Jabiluka deposit.

A U-Pb analysis of uraninite at the Kylie deposit in the Rum Jungle Mineral Field yields an age of 1627  $\pm 45$  Ma (upper intercept of Concordia; [Table 4–1](#)). This age is close to the 1642  $\pm 33$  Ma chemical age of uraninite at the Nabarlek deposit. The diagenetic history of the Depot Creek Sandstone in the Rum Jungle Mineral Field is unknown and hence at this stage it cannot be directly linked to its diagenesis. The lead-lead model age of galena at the Browns deposit (Rum Jungle Mineral Field) constrains the age of basemetal mineralisation at ca. 1690 Ma ([Figure 4–6](#)). If basemetal mineralisation at the Browns deposit and unconformity-related uranium mineralisation at the Kylie deposit were formed from the same diagenetic fluid expelled during the diagenesis of Depot Creek Sandstone, the age of uranium mineralisation in the Rum Jungle Mineral Field could be close to ca. 1690 Ma, similar to ages of uranium mineralisation at the Jabiluka and Nabarlek deposits.

Geochronological studies at uranium deposits in the South Alligator Valley Mineral Field yield a much wider spectrum of ages. The oldest ages have been interpreted for the El Sherana deposits ([Table 4–1](#)). The upper intercept of U-Pb concordia of uraninite gives ages of 1600 Ma (Greenhalgh and Jeffery, 1959) and 1573  $\pm 160$  Ma (Chipley *et al.*, 2007). However the laser ablation-HR-ICP-MS analysis of uraninite at the nearby Palette deposits gives an upper intercept age of 841  $\pm 94$  Ma (Chipley *et al.*, 2007). At this stage it is not clear if uranium deposits in the South Alligator Valley Mineral Field represent two different episodes of mineralisation (Paleoproterozoic and Neoproterozoic) or if the Neoproterozoic ages (between ca. 850 Ma and 700 Ma) so often reported from uranium deposits in PCO represent remobilisation of older uranium and/or isotopic resetting of ages.

Both  $^{40}\text{Ar}/^{39}\text{Ar}$  analysis of alteration and diagenetic minerals and U-Pb analysis of uraninite at various deposits in the PCO consistently show resetting of ages of at ca. 1300 Ma, ca. 1190 Ma, and ca. 800 Ma, which can be related to several proximal and distal thermal events such as the intrusion of Maningkorir/Mudginberri phonolitic dykes and the Derim Derim Dolerite between 1370 Ma and 1316 Ma, the Grenville Orogeny at ca. 1140 Ma and the break up of Rodinia between 1000 Ma and 750 Ma (Polito *et al.*, 2005).

#### **4.13.8 Timing of uranium mineralisation relative to deformation events**

At Jabiluka and Nabarlek deposits, the mineralisation crosscuts dolerite dykes, which provides the maximum age constraint for uranium mineralisation of 1723  $\pm 6$  Ma. At the Ranger deposit the mineralisation also crosscuts mafic dykes but it is not clear if the dykes are similar to the one mapped at the Nabarlek deposit.

In all deposits uranium mineralisation is structurally controlled. At the Nabarlek deposits, the Nabarlek Fault which controls mineralisation, is a reverse fault formed during a regional compressional event. The fault offsets the dolerite dyke suggesting that faulting and compressional event post-date emplacement of the dyke. Uranium mineralisation is interpreted to be broadly synchronous with the compressional event (Wilde and Wall, 1987). However, according to Polito *et*

*al.* (2004) the reverse faults were older and were reactivated during emplacement of mafic dykes and uranium mineralisation followed reactivation of the faults at ca. 1640 Ma.

Polito *et al.* (2005) propose a similar event-chronology for the Jabiluka deposit. At this deposit reverse faulting and fluid flow into the breccia zones and uranium mineralisation occurred a number of times between 1680 Ma and 1616 Ma. The major north-south trending normal faults (Rowntree and Hedge Faults) are younger and post-ore in age.

Two slightly different interpretations have been proposed for the Ranger deposit. Hein (2002) infers uranium mineralisation to be related to an east-west extension, which caused normal faulting and brecciation. The extension was broadly synchronous with the deposition of the Kombolgie Subgroup and followed emplacement of the Oenpelli Dolerite. Hein (2002) notes that uranium mineralisation could be related to a northeast-southwest compressional event which caused folding and reactivation of shear zones but rejects this interpretation based on the ca. 1690 Ma age (Page *et al.*, 1980) of the Oenpelli Dolerite. McCoy *et al.* (2009) relate uranium mineralisation at the Ranger deposit with an ENE-WSW compression and reverse faulting. The compression and faulting post dated deposition of the Kombolgie Subgroup.

Based on available information, following general sequence of events can be inferred for unconformity-related uranium deposits in PCO:

1. Post-Shoobridge event extension (at ca. 1800 Ma). A regional NNE-SSW directed extension (Leichhardt Extension) causing deposition of the Katherine River Group sediments;
2. Mid-Tawallah basin inversion (ca. 1750 to ca. 1730 Ma). A regional east-west compression event, which caused tilting, folding (broad open folds) and faulting in the Lower Katherine River Group sediments. This event either formed ore-controlling shears or reactivated older shear zones. The  $1747 \pm 11$  Ma  $^{40}\text{Ar}/^{39}\text{Ar}$  age of diagenetic illite in the Kombolgie Subgroup may reflect this event. The event corresponds to the 1755 Ma to 1730 Ma Wonga Event in the Mount Isa Basin (Polito *et al.*, 2005). Uranium mineralisation at the Ranger deposit also occurred at ca. 1737 Ma.
3. Intrusion of Oenpelli Dolerite at ca. 1720 Ma. Recent studies, however, show that the mafic dyke dated at the Nabarlek deposit is geochemically different from the Oenpelli Dolerite (Hollis *et al.*, 2011)
4. Reactivation of shears and uranium mineralisation at the Jabiluka and possibly Nabarlek deposit (between ca. 1700 Ma and ca. 1680 Ma). Mineralisation is probably associated with compressional deformation. The apparent polar wonder path curve for the McArthur Basin records a tight bend at ca. 1700 Ma (Idnurm and Wyborn, 1998) suggesting a major restructuring event in the basin.
5. Post-ore extension and normal faulting; and,
6. Post-ore remobilisation of uranium mineralisation.

Critical features of unconformity-related uranium mineral system are summarised in [Table 7-1](#).

#### **4.13.9 Relation between uranium and base metal deposits (Rum Jungle Mineral Field)**

The Rum Jungle Mineral Field features several uranium and base metal deposits and prospects hosted by the Whites Formation and located in close spatial proximity ([Figure 4–14](#)). A pre-Giants reef Fault reconstruction of the field highlights the metallogenic zoning observed in the mineral field (Ahmad *et al.*, 2006). Most uranium-rich deposits (Kylie, Waterhouse, Bachelor, Rum Jungle Creek South, and Dysons) are located on the eastern and northeastern side of the Waterhouse Dome ([Figure 4–8](#)). Moving westward these change to base metal deposit with uranium (Whites, Intermediate) and only base metal deposits with no or very minor uranium (Browns, and Area 55). The uranium, copper deposits of Mount Burton and Mount Fitch are also located on the western side of the Waterhouse and Rum Jungle domes. The Woodcutters lead-zinc and Woodcutters South uranium deposits are located to the east of the Rum Jungle Dome. Complicating this crude metallogenic zoning are several uranium and base metal occurrence interspersed in the Rum Jungle Mineral Filed. The spatial, temporal and genetic relation between uranium and base metal deposits in the Rum Jungle Mineral Filed has been discussed in detail by many researchers (see Ahmad *et al.*, 2006 for a summary). The most significant geological features of these deposits include:

1. Carbonaceous-rich host rock (Whites Formation or at the contact of the Whites Formation and Coomalie Dolostone).
2. Mineralisation is structurally controlled by the Nimbuwah- and/or Cullen-event (ca. 1870 - 1850 Ma and/or 1850 -1820 Ma) folds and faults (Lally, 2002).
3. The Rum Jungle Mineral Field has been overprinted by the Post-Shoobridge Event and the post-Tolmer Group deformation (compression as well as extension; Lally, 2002).
4. No felsic magmatism similar in age to the Cullen Supersuite has been reported in the area.
5. At the Browns deposit the mineralisation is broadly stratiform but also crosscuts bedding, whereas at the Woodcutters lead-zinc deposit it is located along a major structure crosscutting bedding.
6. Lead isotope composition of galena from the Browns and Woodcutters deposits are different and lead was most probably derived from a different source (McCready *et al.*, 2004) or was formed at different times. The new Pine Creek lead model ([Fig. 4–6](#)) yields ages of ca. 1690 Ma and ca. 1840 Ma for the Browns and Woodcutters deposits, respectively.
7. The only reliable date of uranium mineralisation comes from the Kylie deposit where a U-Pb whole-rock analysis of ores (upper intercept of the concordia) yields an age of  $1627 \pm 45$  Ma.
8. The Whites Formation sediments were deposited at ca. 2020 Ma. They underwent diagenesis, deformation and metamorphism during or before the Nimbuwah Event (ca. 1860 to 1847 Ma). The diagenetic fluids could have been derived from the younger sediments of the Burrell Creek Formation but even these sediments underwent diagenesis, metamorphism and deformation during the Nimbuwah Event. The lead-lead model ages for the Woodcutters (ca. 1840 Ma) and the Browns (ca 1690 Ma) deposits suggest that they are most probably not related to the diagenetic fluids derived from the Whites Formation or the Burrell Creek Formation.
9. The structurally controlled basemetall mineralisation at the Woodcutters deposit (ca. 1840 Ma) may be related to the Nimbuwah and/or Cullen events.

10. Paleoproterozoic sediments of the Depot Creek Sandstone (Tolmer Group) are correlated with the Katherine River Group sediments. Like the Katherine River Group sediments they had undergone basin inversion at ca. 1750 Ma -1730 Ma. The diagenetic history of the Tolmer Group is unknown but it is likely that it too underwent episodes of diagenesis starting at ca. 1700 Ma. The diagenetic xenotime in the Gardiner Sandstone (basal Birrindudu Group in the Birrindudu Basin) gives SHRIMP U-Pb age of  $1632 \pm 3$  Ma (Vallini *et al.*, 2007) similar to the age of the Kylie uraninite ( $1627 \pm 45$  Ma) and the age of uranium mineralisation at the Nabarlek deposit ( $1642 \pm 33$  Ma; Polito *et al.*, 2004). The Birrindudu Group (1735 Ma to 1640 Ma) is considered to be a correlative of the Tolmer Group (Crispe *et al.*, 2007), but could be younger as shown by recent dating of the Depot Creek Sandstone (maximum deposition age of  $1837 \pm 15$  Ma, OZCHRON database). The new Pine Creek lead-lead model yields an age of ca. 1690 Ma for the Browns deposits, which is close in age to the age of diagenetic illite in the Kombolgie Subgroup sediments (see above for details). Thus fluids expelled during diagenesis of the Depot Creek Sandstone (Tolmer Group), assuming that it underwent a similar in age diagenetic event, could have formed both uranium and some of the base metal deposits from the same diagenetic fluid. Geochemical studies shows that relatively oxidised diagenetic fluids can transport geologically realistic concentrations of uranium and base metals (copper, lead and zinc) and can deposit these metals after reacting with rocks rich in carbonaceous and/or other reductants (Jaureth *et al.*, 2009; Bastrakov *et al.*, 2010).
11. Base metal and uranium deposits in the Rum Jungle Mineral Filed have thus resulted from at least two mineralising events: The Woodcutters base metal deposit is probably related to the Nimbuwah and/or Shoobridge event deformation and metamorphism, whereas uranium and other base metal deposits, such as the Browns deposit, could have been formed from fluids expelled during diagenesis of Depot Creek Sandstone (Tolmer Group).

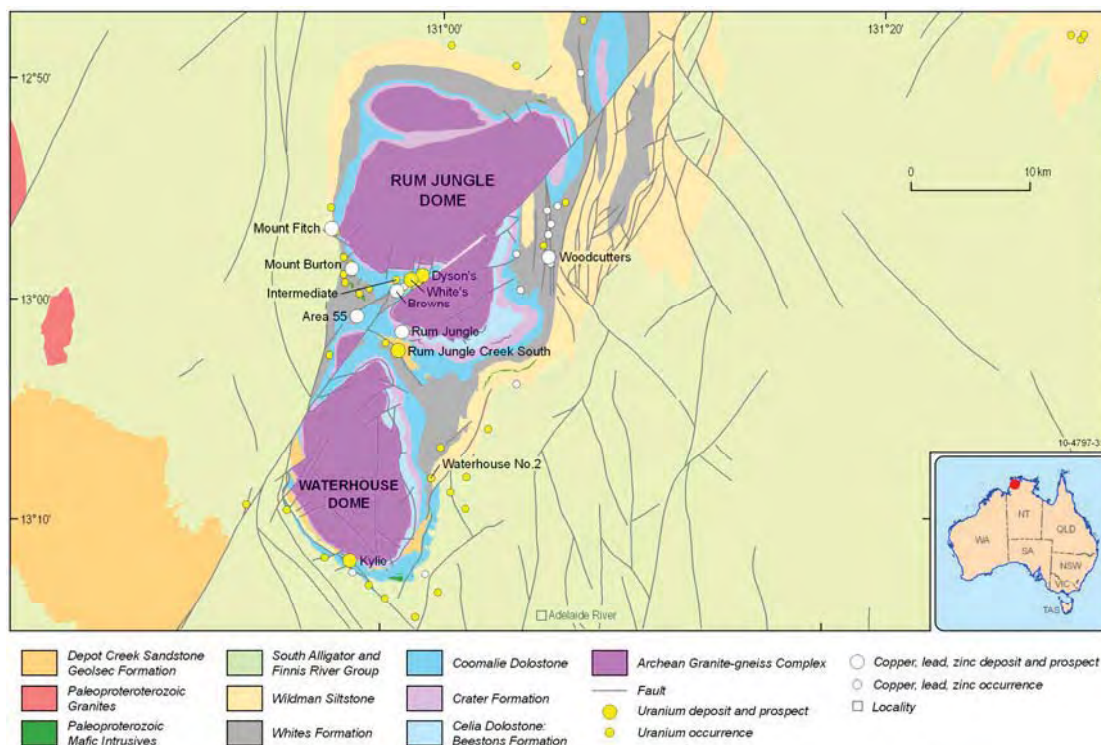


**Figure 4-14:** Map showing basmetal and uranium deposits in the Rum Jungle Mineral Field. The map is based on an NTGS dataset, i.e., Pine Creek interpreted geology (2005). Deposits, prospects and occurrences are from GA's OZMIN and MINLOC datasets.

#### 4.13.10 Iron ore deposits

The Rum Jungle Mineral Field also contains several iron ore deposits and prospects such as B.W Claim, Rum Jungle, and Beestons (Figure 4-7). In these deposits, massive hematite lenses are hosted in ferruginous metasediments, the exact stratigraphic position of which is unclear. Ferenczi (2002) describes the host sediments as purple siltstone and shales of the Whites Formation, whereas Ahmad *et al.* (2006) interpret the host sediments belonging to the much younger Geolsec Formation. The Geolsec Formation unconformably overlies the Coomalie Dolostone and, less commonly overlies the Whites Formation. It comprises hematite-quartz-breccia (HQB), hematitic sandstone, siltstone, mudstone and rare shale breccia (Ahmad *et al.*, 2006). The HQB is the dominant rock type of the Geolsec Formation and consists of several different types of breccias. The origin of the breccia is unclear and may be either the product of in situ weathering and collapse of the Coomalie Dolostone due to karst processes or may represent talus slope breccia formed in fault-bounded blocks of the Coomalie Dolostone. The presence of phosphatic siltstone in the Geolsec Formation suggests that the breccia may have deposited in shallow-marine environment. The initial breccia may have also been overprinted by hydrothermal fluids of an unknown origin (Ahmad *et al.*, 2006). It is possible that in some prospects, such as the Mount Mable Prospect, mineralisation was formed by supergene enrichment of ferruginous sediments of the Geolsec Formation (Ahmad *et al.*, 2006).

At the Mount Tolmer deposit massive ironstone body is located at the unconformity between the Depot Creek Sandstone and the Burrell Creek Formation and consists of hematite and minor limonite. The origin of iron ore bodies is not clear (Ferenczi, 2002).

**Table 4-6:** Summary of important mineral system in the Pine Creek Orogen and related events

EVENT	AGE (MA)	MINERAL DEPOSITS/SYSTEMS	DEPOSIT EXAMPLES	DISTAL TECTONIC EVENTS
Masson Formation	2020	Stratabound lead-zinc-silver	Namoona	Barramundi Extension 1
Basaltic to andesitic volcanism (Stag Creek Volcanics)	2020	Volcanogenic iron	Frances Creek East	Barramundi extension 1
Felsic volcanism (Wildman Siltstone)	2019	Volcanogenic iron	Frances Creek	Barramundi Extension 1
Felsic volcanism (Gerowie Tuff)	1863	Volcanogenic iron	Mount Pacqualin	Barramundi extension 2
Felsic and mafic volcanism (Warrs and Mulluk Mulluk Volcanic Members)	1861	Volcanic associated massive sulphide	Daly River	Barramundi Extension 2
Nimbuwah deformation and metamorphism	1860 to 1847			Barramundi Orogeny
Felsic magmatism (Allia Suite)	1870 to 1850	Pegmatite (tin, tantalum)	Bynoe	
Cullen deformation	1840 to 1820	Structurally controlled lead-zinc	Woodcutters	Halls Creek Orogeny
Felsic magmatism (Cullen Supersuite, Jim Jim/David and Allia Suites)	1835 to 1818	Lode gold; Tin-Tantalum (pegmatite, greisen, vein); Tungsten (vein); Skarn (copper, lead-zinc, iron); Polymetallic vein	Goodall; Mount Bunney; Wolfram Hill; Mount Wells	
Extension (Katherine River Group, Tolmer Group)	1800 to 1750	Sedimentary iron ore; sedimentary/diagenetic phosphate	B.W. Claim	Leichhardt Extension
Basin inversion	1750 to 1730	Unconformity-related uranium	Ranger	Mid-Tawallah Inversion, Wonga Event
Compression (?)	1720 to 1680	Unconformity-related uranium; Diagenetic hydrothermal base metal	Jabiluka, Nabarlek; Browns	Davenport Orogeny, Strangways Orogeny; Sharp bend at ca. 1700 Ma on the apparent polar wonder path curve for the McArthur Basin

#### **4.14 SUMMARY**

The preceding discussion shows that mineral systems in the PCO are intricately related to sedimentary, diagenetic, deformation/metamorphic and magmatic events in the PCO ([Table 4–6](#)). Some of these events are synchronous with events occurring within or at the margins of the North Australian Craton. The geological evolution of the three domains in the PCO also controls differences in their metallogeny. The Nimbuwah Domain is characterised by world-class unconformity-related uranium deposits, but no significant gold, basemetal and tin-tantalum-tungsten deposits have yet been found in the domain.

The Central Domain, on the other hand, hosts a diverse set of mineral systems, which include unconformity-related uranium, iron ore, basemetal, tin-tantalum-tungsten, and gold. The abundance of gold deposits in this domain is probably related to a combination of the following factors: presence of a thick package of turbiditic sediments; lower-greenschist facies of metamorphism, widespread felsic magmatism, and the presence to a major regional-scale structure (Pine Creek Shear zone).

The metallogeny of the Litchfield Domain is dominated by mineral systems associated with felsic magmatism (tin-tantalum pegmatite and veins). The absence of significant gold mineralisation is probably related to the granulite facies of metamorphism in the domain, as most lode gold regions are often associated with terranes with lower grade of metamorphism (greenschist to lower amphibolite facies).

#### **4.15 REFERENCES**

- Ahmad, M., 1998. Geology and mineral deposits of the Pine Creek Inlier and McArthur Basin, Northern Territory: AGSO Journal of Australian Geology and Geophysics, v. **17**, p. 1-17.
- Ahmad, M., Lally, J. H., and McCready, A. J., 2006. Economic geology of the Rum Jungle mineral field: Darwin, Northern Territory Geological Survey, 75 p.
- Ahmad, M., Wygralak, A. S., and Ferenczi, P. A., 2009. Gold deposits of the Northern Territory (Second edition updated by Wygralak, A. S., and Scrimgeour, I. R.): Darwin, Northern Territory Geological Survey, 131 p.
- Ahmad, M., Wygralak, A. S., Ferenczi, P. A., and Bajwah, Z. U., 1993. Pine Creek SD 52-8, explanatory notes and mineral deposit data sheets, Northern Territory Geological Survey, 178 p.
- Bajwah, Z. U., 1994. A contribution of geology, petrology, and geochemistry to the Cullen Batholith and related hydrothermal activity responsible for mineralization, Pine Creek Geosyncline, Northern Territory: Darwin, Northern Territory Geological Survey, 71 p.
- Bastrakov, E. N., Jaireth, S., and Mernagh, T. P., 2010. Solubility of uranium in hydrothermal fluids at 250°C to 300°C: implications for the formation of uranium deposits, Geoscience Australia Record 2010/29: Canberra, Geoscience Australia, p. 91.
- Budd, A. R., Wyborn, L. A. I., and Bastrakova, I. V., 2001. The metallogenetic potential of Australian Proterozoic granites, Record 2001/12: Canberra, Geoscience Australia.
- Carson, C. J., Worden, K. E., Scrimgeour, I. R., and Stern, R. A., 2008. The Palaeoproterozoic evolution of the Litchfield Province, western Pine Creek Orogen, northern Australia: Insight from SHRIMP U-Pb zircon and in situ monazite geochronology: Precambrian Research, v. **166**, p. 145-167.
- Carson, L. J., Haines, P. W., Brakel, A. T., Pietsch, B. A., and Ferenczi, P. A., 1999. Milingimbi SD; 53-2, Northern Territory Geological Survey, Darwin, Northern Territory, Australia, 46 p.
- Chipley, D., Polito, P. A., and Kyser, T. K., 2007. Measurement of U-Pb ages of uraninite and davidite by laser ablation-HR-ICP-MS: American Mineralogist, v. **92**, p. 1925-1935.
- Compston, D. M., and Matthai, S. K., 1994. Age Constraints on early Proterozoic gold deposits, Pine Creek Inlier and Tennant Creek Inlier, northern Australia: Geology, 1994.
- Crispe, A. J., Vandenberg, L. C., and Scrimgeour, I. R., 2007. Geological framework of the Archean and Paleoproterozoic Tanami Region, Northern Territory: Mineralium Deposita, v. **42**, p. 3-26.
- Cross, A., Claoué-Long, J. C., Scrimgeour, I. R., Ahmad, M., and Kruse, P. D., 2005. Summary of results. Joint NTGS-GA geochronology project: Rum Jungle, basement to southern Georgina Basin and eastern Arunta Region 2001–2003: Darwin, 42 p.
- Cross, A. J., 2009. SHRIMP U-Pb xenotime geochronology and its application to dating mineralisation, sediment deposition and metamorphism, Australian National University, 298 p.
- Cumming, G. L., and Richards, J. R., 1975. Ore lead isotope ratios in a continuously changing Earth: Earth and Planetary Science Letters, v. **28**, p. 155-171.

- Cuney, M. L., 2005. World-class unconformity-related uranium deposits; key factors for their genesis: Proceedings of the ... Biennial SGA (Society for Geology Applied to Mineral Deposits) Meeting, v. **8**, Vol. **1**, p. 245-248.
- Dahlkmap, F. J., 2009. Uranium deposits of the world: Asia: Berlin, Springer-Verlag, 493 p.
- de Vries, S. T., Poyer, L. L., and Fry, N., 2008 Evolution of Neoarchaean and Proterozoic basins of Australia: Precambrian Research, v. **166**, p. 39-53.
- Derome, D., Cathelineau, M., Cuney, M., Fabre, C., and Lhomme, T., 2005. Mixing of Sodic and Calcic Brines and Uranium Deposition at McArthur River, Saskatchewan, Canada: A Raman and Laser-Induced Breakdown Spectroscopic Study of Fluid Inclusions: Economic Geology, v. **100**, p. 1529-1545.
- Fayek, M., and Kyser, T. K., 1997. Characterization of multiple fluid-flow events and rare-earth-element mobility associated with formation of unconformity-type uranium deposits in the Athabasca Basin, Saskatchewan: The Canadian Mineralogist, v. **35**, Part 3, p. 627-658.
- Ferenczi, P. A., 2001. Iron ore, manganese and bauxite deposits of the Northern Territory: Darwin, Northern Territory Geological Survey, 113 p.
- Ferenczi, P. A., and Sweet, I. P., 2005. Mount Evelyn, Northern Territory. 1:250 000 geological map series explanatory notes, SD 53-05.: Darwin, Northern Territory Geological Survey
- Foster, D. A., Gray, D. R., Kwak, T. A. P., and Bucher, M., 1998. Chronology and tectonic framework of turbidite-hosted gold deposits in the Western Lachlan Fold Belt, Victoria: - results: Ore Geology Reviews, v. **13**, p. 229-250.
- Frater, K. M., 2005. Tin-tantalum pegmatite mineralisation of the Northern Territory: Darwin, Northern Territory Geological Survey, 184 p.
- French, B. M., 1966. Some geological implications of equilibrium between graphite and a C-H-O gas phase at high temperatures and pressures: Reviews of Geophysics, v. 4, p. 223-253.
- Frost, B. R., 1979. Mineral equilibria involving mixed-volatiles in a C-O-H fluid phase; the stabilities of graphite and siderite: American Journal of Science, v. **279**, p. 1033-1059.
- Glass, L. M., Hollis, J. A., and Carson, C. J., 2009. Geochemical and isotopic discrimination methods for neoarchaean and palaeoproterozoic rocks in western Arnhem Land, Pine Creek Orogen: applications for uranium exploration, Annual Geoscience Exploration Seminar (AGES) 2009. Record of abstracts. Northern Territory Geological Survey, Record, 2009-002: Darwin, Northern Territory Geological Survey, p. 18-21.
- Glass, L. M., Hollis, J. A., Carson, C. J., Yaxley, G. M., and Armstrong, R., 2010. Archean and Paleoproterozoic crustal evolution processes in the Pine Creek Orogen: U-Pb, Hf, O, Nd isotopic data and geochemistry, Annual Geoscience Exploration Seminar (AGES) 2010. Northern Territory Geological Survey, Record 2010-002: Darwin, Northern Territory Geological Survey, p. 39-44.
- Goldfarb, R. J., Groves, D. I., and Ragdoll, S., 2001. Orogenic gold and geologic time: a global synthesis: Ore Geology Reviews, v. **18**, p. 1-75.
- Greenhalgh, D., and Jeffery, P. M., 1959. A contribution to the pre-Cambrian chronology of Australia: Geochimica et Cosmochimica Acta, v. **16**, p. 39-57.
- Groves, D. I., Goldfarb, R. J., Gebre-Mariam, M., Hagemann, S. G., and Robert, F., 1998. Orogenic gold deposits: A proposed classification in the context of their crustal distribution and relationship to other gold deposit types: Ore Geology Reviews, v. **13**, p. 7-27.

- Hecht, L., and Cuney, M., 2000. Hydrothermal alteration of monazite in the Precambrian crystalline basement of the Athabasca Basin (Saskatchewan, Canada); implications for the formation of unconformity-related uranium deposits: *Mineralium Deposita*, v. **35**, p. 791-795.
- Hein, K. A. A., 2002. Geology of the Ranger uranium mine, Northern Territory, Australia; structural constraints on the timing of uranium emplacement: *Ore Geology Reviews*, v. 20, p. 83-108.
- Hein, K. A. A., 2003. Relative timing of deformational, metamorphic and mineralisation events at the Mt. Todd (Yimuyn Manjerr) Mine, Pine Creek Inlier, Northern Territory, Australia: *Ore Geology Reviews*, v. **22**, p. 143-175.
- Hickey, S. H., 1985. Fog Bay, Northern Territory 1:100 000 Geological Map Series. Northern Territory Geological Survey Explanatory Notes, SE 52-3 (4972). Darwin, Northern Territory Geological Survey.
- Hills, J. H., and Richards, J. R., 1976. Pitchblende and galena ages in the Alligator Rivers Region, Northern Territory, Australia: *Mineralium Deposita*, v. **11**, p. 133-154.
- Hollis, J. A., Carson, C. J., and Glass, L. M., 2009a. Extensive exposed neoarchaean crust in Arnhem Land, Pine Creek Orogen: U-Pb zircon SHRIMP geochronology, Annual Geoscience Exploration Seminar (AGES) 2009. Record of abstracts. Northern Territory Geological Survey, Record, 2009-002: Darwin, Northern Territory Geological Survey, p. 15-18.
- Hollis, J. A., Carson, C. J., and Glass, L. M., 2009b. SHRIMP U-Pb zircon geochronological evidence for Neoarchean basement in western Arnhem Land, northern Australia: *Precambrian Research*, v. **174**, p. 364-380.
- Hollis, J. A., Schersten, A., Glass, L. M., and Carson, C., 2009c. Stratigraphic and tectonic evolution of the Nimbuwah Domain: A separate terrane to the rest of the Pine Creek Orogen?, Annual Geoscience Exploration Seminar (AGES) 2009. Record of abstracts. Northern Territory Geological Survey, Record, 2009-002: Darwin, Northern Territory Geological Survey, p. 21-27.
- Idnurm, M., and Wyborn, L., 1998. Palaeomagnetism and mineral exploration related studies in Australia; a brief overview of Proterozoic applications: AGSO Journal of Australian Geology and Geophysics, v. **17**, p. 277-284.
- Jaireth, S., Bastrakov, E., Skirrow, R. G., and Mernagh, T., 2009, Geochemical modelling of uranium-copper-lead-zinc systems: can basins with stratiform copper deposits host zones enriched in uranium?: AusIMM Uranium2009, Darwin, 2009, p. 93-94.
- Jaireth, S., Meixner, T., Milligan, P., Lambert, I., and Miezitis, Y., 2007. Unconformity-related uranium systems: regional-scale constraints: AusIMM Uranium 2007, Darwin, 2007, p. 31-32.
- Jefferson, C. W., Thomas, D. J., Gandhi, S. S., Ramaekers, P., Delaney, G., Brisbin, D., Cutts, C., Portella, P., and Olson, R. A., 2007. Unconformity-associated uranium deposits of the Athabasca basin, Saskatchewan and Alberta: *Bulletin of the Geological Survey of Canada*, p. 23-67.
- Kruse, P. D., Sweet, I. P., Stuart-Smith, P. G., Wygralak, A. S., Pieters, P. E., and Crick, I. H., 1994. Katherine, N.T. - sheet SD/53-9 Australian National Grid, Australian Government Publishing Service, Canberra, A.C.T., Australia, p. 69.
- Kyser, K., and Cuney, M., 2009. Unconformity-related uranium deposits, in Cuney, M., and Kyser, K., eds., Recent and not-so-recent developments in uranium deposits and implications for exploration, **39**: Quebec, Mineralogical Association of Canada, p. 161-220.

- Lally, J. H., 2002. Stratigraphy, structure and mineralisation, Rum Jungle mineral field, Northern Territory, Northern Territory Department of Mines and Energy, Darwin, North. Territ., Australia, 21 p.
- Lally, J. H., and Bajwah, Z. U., 2006. Uranium deposits of the Northern Territory: Darwin, Northern Territory Geological, 87 p.
- Lang, J. R., and Baker, T., 2001. Intrusion-related gold systems: the present level of understanding: Mineralium Deposita, v. **36**, p. 477-489.
- Ludwig, K. R., Grauch, R. I., Nutt, C. J., Nash, J. T., Frishman, D., and Simmons, K. R., 1987. Age of uranium mineralisation at the Jabiluka and Ranger deposits, Northern Territory, Australia: new U-Pb isotope evidence: Economic Geology, v. **82**, p. 857-874.
- Malone, E. J., 1962. Darwin, N. T.; 1:250,000 geological series, sheet D/52-4, Australian national grid, explanatory notes, p. 20.
- Matthai, S. K., Henley, R. W., Bacigalupo-Rose, S., Binns, R. A., Andrew, A. S., Carr, G. R., French, D. H., McAndrew, J., and Kananagh, M. E., 1995a. Intrusion-related, high-temperature gold quartz veining in the Cosmopolitan Howley metasedimentary rock-hosted gold deposit, Northern Territory, Australia: Economic Geology, v. **90**, p. 1012-1045.
- Matthai, S. K., Henley, R. W., and Heinrich, C. A., 1995b. Gold precipitation by fluid mixing in bedding-parallel fractures near carbonaceous slates at the Cosmopolitan Howley gold deposit, northern Australia: Economic Geology, v. **90**, p. 2123-2142.
- McCoy, A., Schaubs, P., and Pope, A., 2009. Structural setting of Ranger Uranium orebodies: implications for exploration: AusIMM Uranium 2009, Darwin, 2009, p. 27.
- McCready, A. J., Stumpfl, E. F., Lally, J. H., Ahmad, M., and Gee, R. D., 2004. Polymetallic mineralization at the browns deposit, Rum Jungle mineral field, Northern Territory, Australia: Economic Geology, v. **99**, p. 257-277.
- McKay, A. D., and Miezitis, Y., 2001. Australia's uranium resources, geology and development of deposits, Mineral Resource Report, 1: Canberra, AGSO - Geoscience Australia, p. 200.
- Mernagh, T. P., Heinrich, C. A., Leckie, J. F., Carville, D. P., Gilbert, D. J., Valenta, R. K., and Wyborn, L. A. I., 1994. Chemistry of low-temperature hydrothermal gold, platinum, and palladium (+ or - uranium) mineralization at Coronation Hill, Northern Territory, Australia: Economic Geology and the Bulletin of the Society of Economic Geologists, v. **89**, p. 1053-1073.
- Miller, G. C., Kirk, C. M., Hamilton, G., and Horsburgh, J. R., 1998. Brocks Creek gold deposits, Pine Creek: Monograph Series - Australasian Institute of Mining and Metallurgy, v. **22**, p. 409-415.
- Morrison, I. J., and Treacy, J. A., 1998. Gold Creek gold deposit: Monograph Series - Australasian Institute of Mining and Metallurgy, v. **22**, p. 433-438.
- Needham, R. S., 1988. Geology of the Alligator Rivers uranium field, Northern Territory: Bulletin - Bureau of Mineral Resources, Geology & Geophysics, Australia, v. 224.
- Needham, R. S., Stuart-Smith, P. G., and Page, R. W., 1988. Tectonic evolution of the Pine Creek Inlier, Northern Territory: Precambrian Research, v. **40-41**, p. 543-564.
- Neumann, N. L., and Fraser, G. L., 2007. Geochronological synthesis and Time-Space plots for Proterozoic Australia, Geoscience Australia Record, 2007/06: Canberra, Geoscience Australia, p. 216.

- Ojakangas, R. W., 1979. Sedimentation of the basal Kombolgie Formation (Upper Precambrian-Carpentarian) Northern Territory, Australia: possible significance in the genesis of the underlying Alligator Rivers unconformity-type uranium deposits, U.S. Department of Energy report GJBX-173(79), p. 38.
- Page, R. W., Compston, W., and Needham, R. S., 1980. Geochronology and evolution of the late-Archaean basement and Proterozoic rocks in the Alligator Rivers uranium field, Northern Territory, Australia: Proceedings Series - International Atomic Energy Agency = Collection Comptes Rendus - Agence Internationale de l'Energie Atomique, p. 39-68.
- Pietsch, B. A., and Edgoose, C. J., 1988. The stratigraphy, metamorphism and tectonics of the Early Proterozoic Litchfield Province and western Pine Creek Geosyncline, Northern Territory: Precambrian Research, v. **40-41**, p. 565-588.
- Pietsch, B. A., and Stuart-Smith, P. G., 1988. Darwin, Northern Territory. 1:250 000 geological series explanatory notes SD 52-04: Darwin, Northern Territory Geological Survey.
- Polito, P., Kurt Kyser, T., Thomas, D., Marlatt, J., and Drever, G., 2005. Re-evaluation of the petrogenesis of the Proterozoic Jabiluka unconformity-related uranium deposit, Northern Territory, Australia: Mineralium Deposita, v. **40**, p. 257-288.
- Polito, P. A., Kyser, T. K., Marlatt, J., Alexandre, P., Bajwah, Z., and Drever, G., 2004. Significance of Alteration Assemblages for the Origin and Evolution of the Proterozoic Nabarlek Unconformity-Related Uranium Deposit, Northern Territory, Australia: Economic Geology, v. **99**, p. 113-139.
- Quirt, D., Kotzer, T., and Kyser, T. K., 1991. Tourmaline, phosphate minerals, zircon and pitchblende in the Athabasca group: Maw Zone and McArthur River areas, Saskatchewan: Saskatchewan Geological Survey Technical Report, v. **91-4**, p. 181-191.
- Rasmussen, B., Sheppard, S. and Fletcher, I. R., 2006. Testing ore deposit models using in situ U-Pb geochronology of hydrothermal monazite; Paleoproterozoic gold mineralization in northern Australia. Geology (Boulder) **34(2)**, 77-80.
- Rawlings, D. J., Korsch, R. J., Goleby, B. R., Gibson, G. M., Johnstone, D. W., and Barlow, M., 2004. The 2002 southern McArthur Basin seismic reflection survey: Canberra, Geoscience Australia, Canberra, Australia, 78 p.
- Sener, A. K., Young, C., Groves, D. I., Krapez, B. and Fletcher, I. R., 2005. Major orogenic gold episode associated with cordilleran-style tectonics related to the assembly of Paleoproterozoic Australia? Geology (Boulder) **33(3)**, 225-228.
- Stuart-Smith, P. G., Wills, K., Crick, I. H., and Needham, R. S., 1980. Evolution of the Pine Creek Geosyncline: Proceedings Series - International Atomic Energy Agency = Collection Comptes Rendus - Agence Internationale de l'Energie Atomique, p. 23-37.
- Stüwe, K., 1998. Tectonic constraints on the timing relationships of metamorphism, fluid production and gold-bearing quartz vein emplacement: Ore Geology Reviews, v. 13, p. 219-228.
- Sun, S. S., Carr, G. R., and Page, R. W., 1996. A continued effort to improve lead-isotope model ages: AGSO Research Newsletter, v. **24**, p. 19-20.
- Sweet, I. P., Brakel, A. T., Rawlings, D. J., Haines, P. W., Plumb, K. A., and Wygralak, A. S., 1999. Mount Marumba Northern Territory; SD 53-6, Northern Territory Geological Survey, Darwin, Australia, p. 84.

- Thundelarra, and Exploration, 2010. Sydney Uranium Conference Presentation - December, Shaw Stockbroking Uranium Conference Sydney, Thundelarra Exploration (<http://www.thundelarra.com/documents/6%20Dec%202010%20Sydney%20Uranium%20Conference%20Presentation.pdf>)
- Valenta, R. K., 1991. Structural controls on mineralisation of the Coronation Hill deposit and surrounding area, Geoscience Australia, Canberra, A.C.T., Australia, 220 p.
- Vallini, D. A., Groves, D. I., McNaughton, N. J., and Fletcher, I. R., 2007. Uraniferous diagenetic xenotime in northern Australia and its relationship to unconformity-associated uranium mineralization: Mineralium Deposita, v. **42**, p. 51-64.
- von Pechmann, E., 1992. Mineralogy and geochronology of U (-Au) deposits from the Pine Creek Geosyncline, Northern Territory, Australia, and from the Athabasca Basin, Saskatchewan and Alberta, Canada, Heidelberger Geowissenschaftliche Abhandlungen, **Band 59**, 474 p.
- Wilde, A. R., and Wall, V. J., 1987. Geology of the Nabarlek uranium deposit, Northern Territory, Australia: Economic Geology, v. **82**, p. 1152-1168.
- Worden, K., Carson, C., Scrimgeour, I., Lally, J., and Doyle, N., 2008a. A revised Palaeoproterozoic chronostratigraphy for the Pine Creek Orogen, northern Australia: Evidence from SHRIMP U-Pb zircon geochronology: Precambrian Research, v. **166**, p. 122-144.
- Worden, K. E., Carson, C. J., Close, D. F., Donnellan, N., and Scrimgeour, I. R., 2008b. Summary of results. Joint NTGS-GA geochronology project: Tanami Region, Arunta Region, Pine Creek Orogen and Halls Creek orogen correlatives, January 2005 - March 2007: Darwin, Northern Territory Geological Survey, 180 p.

## 5 AEM Geophysics

*M.T. Costelloe, R. Brodie and D.K. Hutchinson*

### 5.1 INTRODUCTION

Airborne Electromagnetic (AEM) surveys are used to map the electrical conductivity of the subsurface over extents too large to be covered on the ground. A time-domain AEM system aircraft carries a transmitter loop through which a time-varying current is passed inducing eddy (secondary) currents to flow in any electrically conductive subsurface material. The secondary eddy currents are recorded via the voltage that is induced in the receiver coils towed by the same aircraft. The current flow in the subsurface is related to its conductivity. An inversion of the received signal allows estimates of the conductivity to be made. The depth to which the signals can be used to map conductivity depends on the system configuration and the subsurface conductivity (Smith, 2001; Lane *et al.*, 2004b).

The Pine Creek survey areas were flown using two different AEM systems. The TEMPEST™ fixed wing AEM system acquired data in the Woolner Granite and Rum Jungle survey areas. The TEMPEST™ survey data were publicly released by GA in July and September 2009, respectively. The VTEM™ helicopter AEM system acquired data in the Kombolgie survey area. GA publicly released these data in December 2009.

### 5.2 GEO-ELECTRICAL MODELS

Geo-electrical models were created utilising a priori knowledge of conductivity ranges for targeted geological units. [Table 5–1](#) is a summary of the conductivity ranges used for geological targets in the forward modelling exercise (Richardson *et al.*, 2008).

**Table 5–1:** Conductivities used in the forward modelling

Mudflats (saltwater)	500 mS/m
Cretaceous	10 - 200 mS/m
Daly River Group	1 mS/m
Tolmer Group	0.1 mS/m
Finniss River Group	1 mS/m
Woolner Granite	1 mS/m
Koolpinyah Dolomite	1 - 10 mS/m
Litchfield Complex	1 mS/m
Kombolgie	0.1 mS/m
Pine Creek Orogen	0.2 mS/m

### Model 1.1

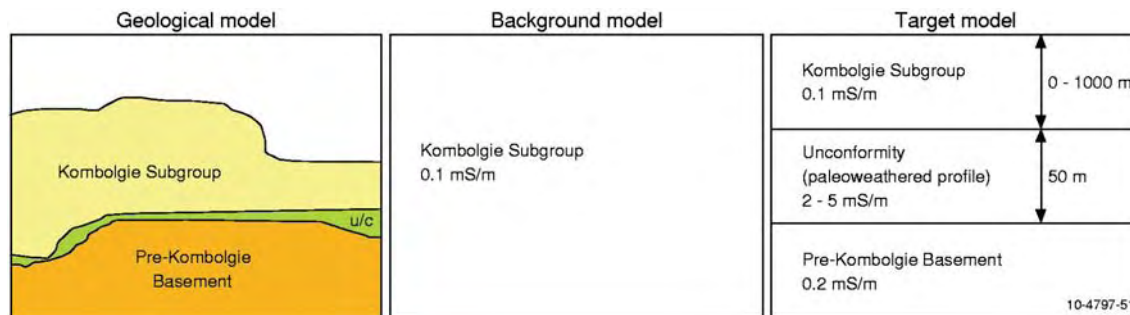


**Figure 5-1:** An example of a geo-electric model (1.1) from the Kombolgie AEM Survey area. Forward modelling of this scenario was used to predict if the presence of the unconformity, under 0 – 1000 m of 0.1 mS/m cover sediments, could be detected within the AEM system noise levels.

Forward modelling results from the geological model in Figure 5.1 indicated that, of the various AEM systems considered for the Kombolgie survey, only two would be successful in detecting the target unconformity under up to 500 m of 0.1 mS/m conductivity sediments (Kombolgie Sandstone). Further modelling predicted the VTEM™ system would be most likely to detect the target to 1000 m under a thin regolith (5 mS/m) over the Kombolgie Subgroup in this highly resistive geological environment.

Similar forward modelling was undertaken on other geological targets in the Woolner Granite and Rum Jungle survey areas to predict the likelihood of successfully detecting targets given different scenarios, for example, it is shown in the resolution of the near surface and under varying degrees of cover. Modelling for the Woolner Granite and Rum Jungle areas predicted the TEMPEST™ system would be most likely to detect target geology in these areas.

## 5.3 AEM SYSTEMS

### 5.3.1 TEMPEST™

The Woolner Granite and Rum Jungle survey areas were flown by Fugro Airborne Surveys' Pty Ltd using the TEMPEST™ AEM System (Lane *et al.*, 2000), installed on two aircraft with registrations VH-TEM and VH-WGT. A summary of the system configuration, acquisition and processing is detailed in Lawrence and Stenning (2009a) and Lawrence and Stenning (2009b) respectively. A summary of the specifications of the TEMPEST™ and VTEM™ systems is shown in Table 5–2.

TEMPEST™ is a fixed-wing, time-domain system. It employs an approximate square-wave, 50% duty cycle current waveform with a base frequency of 25 Hz. The current is transmitted through a single turn transmitter (TX) loop draped around the nose, wings and tail of the aircraft. The survey was flown with the TX loop at an average of 122.4 m above ground level. The receiver (RX) coils are housed in a ‘bird’ towed approximately 120 m behind and 35m below the aircraft. The RX consists of three orthogonal coils that sense the rate of change of the magnetic field ( $\text{dB}/\text{dt}$ ) flux threading each coil. The axes of the three coils are nominally aligned in the horizontal flight line direction (X-component), horizontal direction perpendicular to the flight line (Y-component), and vertical directions (Z-component). However, only the X and Z components are recorded and processed at full resolution and available for interpretation.

The TX height and the orientations and relative separations of the TX and RX are also known as the system geometry. The system geometry continuously varies as the aircraft moves along a flight line. The TEMPEST™ instrumentation includes a GPS unit for the aircraft’s position, radar and laser

altimeters to measure its height above ground level and gyroscopes to measure its roll, pitch and yaw angles (i.e., its orientation). The relative separations of the TX and RX and the orientation of the RX are not measured by the system because of the logistical difficulty in doing so.

Since the system geometry affects the measured response, it must be input into quantitative forward modelling of the system response, and hence estimation of subsurface conductivity from the recorded data. Therefore, in the data processing the unmeasured elements of the system geometry need to be estimated. For the TEMPEST™ system this involves separation of the measured total field response into its primary field (due to direct coupling between TX and RX) and secondary field (due to eddy currents induced in the ground) components. This requires an assumption to be made about the unknown subsurface conductivity, which typically is that the subsurface is resistive at depth. Once separated into primary and secondary components, the horizontal and vertical offsets between the TX and RX can be analytically determined from the primary field if it is assumed that the receiver bird is oriented with zero roll, pitch and yaw. It is these estimated and assumed values of system geometry that are taken to be the real values in standard algorithms for estimating subsurface conductivity from the measured data.

**Table 5-2:** Summary of AEM system specifications.

System	TEMPEST™	VTEM™
Contractor	Fugro Airborne Surveys	Geotech
Platform type	fixed-wing towed-bird	helicopter slung loop
Base frequency	25 Hz	25 Hz
Peak dipole moment	55,800 A.m <sup>2</sup> .turns	424,528 A.m <sup>2</sup> .turns
Pulse width	10 ms <sup>†</sup>	7.33 ms
Turn-off ramp width	40 µs <sup>†</sup>	1.33 ms
Off time	10 ms <sup>†</sup>	12.66 ms
Transmitter loop height above ground	122 m (nominal)	45 m (nominal)
Transmitter-receiver horizontal separation	120 m (nominal)	0 m
Transmitter-receiver vertical separation	35 m (nominal)	0 m
Receiver coil height above ground	87 m (nominal)	45 m (nominal)
Receiver components	X and Z	Z
Number of receiver windows	15	30
Window centre times	13.66 µs to 16.2 ms	62.5 µs to 9.244 ms
† Actual transmitted waveform (i.e., not the processed data equivalent waveform)		

### 5.3.2 VTEM™

The Kombolgie survey area was flown by Geotech Airborne and using the VTEM™ AEM System. The VTEM™ system was installed on an AS 350 B3 helicopter, registration VH-IPW.

The system is a concentric or central loop design, with the receiver positioned at the centre of a 26.1 metre wide dodecahedron shaped transmitter loop that is towed below the helicopter. The transmitter produces a dipole moment up to 424,528 A.m<sup>2</sup>.turns at peak current. The 25 Hz base frequency waveform is bipolar, having a 7.33 ms pulse-width, including the 1.33 ms turn-off ramp, and a 12.66 ms off-time (Table 5-2).

Measurements are made during the off-time, when the secondary field resulting from eddy currents flowing in conductors in the ground are not swamped by the primary field. VTEM™ B-Field data are obtained through real-time electronic integration of the dB/dt data, similar in concept to the process described by Smith and Annan (2000).

Details of the system configuration, survey infill areas, acquisition and processing are described in Carter *et al.*, 2009.

#### **5.4 PREVIOUSLY RELEASED AEM DATA**

Data were delivered into the public domain in two Phases. Phase-1 data are quality controlled, contractor supplied data owned by GA and the National Water Commission. Phase-2 data are quality controlled GA layered earth inversions (GA-LEI) owned by GA and the National Water Commission. Phase-1 and Phase-2 data flown for subscriber companies has also been released to the public domain as detailed below.

Phase-1 GA and National Water Commission owned data were released in three separate blocks Woolner Granite, Rum Jungle and Kombolgie. The blocks are shown on the locality map ([Figure 1–1](#)). Internal to the three main survey blocks are twenty-nine sub-areas of infill flying that were funded by subscriber exploration companies and the National Water Commission ([Figure 1–3](#)). Under the terms of the funding agreements with subscription companies, there were moratoriums on the release of infill data until: after July 2010 for Woolner Granite; after September 2010 for Rum Jungle; and after December 2010 for Kombolgie. All Phase-1 subscriber company infill data have now been released to the public domain. Geoscience Australia gratefully acknowledges the support of the subscription companies who permitted the early release of their data.

The Pine Creek Phase-1 data release contained:

- Survey operations and processing report;
- Point-located electromagnetic response data without correction to a standard geometry;
- Point-located electromagnetic response data with correction to a standard geometry;
- Point-located conductivity depth image data derived using EM Flow™ software;
- Gridded electromagnetic response and conductivity depth interval (CDI) data; and,
- Graphical multiplot profiles showing electromagnetic, CDI and ancillary data for each line.

These data are available from the GA Sales Centre and are also available by free download from the GA web site using the links below:

- Pine Creek - Woolner Granite Area Phase-1 data and processing report;  
[https://www.ga.gov.au/products/servlet/controller?event=GEOCAT\\_DETAILS&catno=69228](https://www.ga.gov.au/products/servlet/controller?event=GEOCAT_DETAILS&catno=69228)
- Pine Creek - Rum Jungle Area Phase-1 data and processing report;  
[https://www.ga.gov.au/products/servlet/controller?event=GEOCAT\\_DETAILS&catno=69230](https://www.ga.gov.au/products/servlet/controller?event=GEOCAT_DETAILS&catno=69230)
- Pine Creek Kombolgie Area Phase-1 VTEM™ data and processing report (in part);  
[https://www.ga.gov.au/products/servlet/controller?event=GEOCAT\\_DETAILS&catno=69230](https://www.ga.gov.au/products/servlet/controller?event=GEOCAT_DETAILS&catno=69230)

Due to its size the complete Kombolgie Phase-1 dataset is available from the sales centre on DVD.

- Pine Creek - Kombolgie VTEM™ AEM Survey, NT, 2010 Final Data including infill areas: K1, K2 and K3.  
[https://www.ga.gov.au/products/servlet/controller?event=GEOCAT\\_DETAILS&catno=71372](https://www.ga.gov.au/products/servlet/controller?event=GEOCAT_DETAILS&catno=71372)

Due to its size the entire Kombolgie Phase-2 dataset is available from the sales centre on DVD.

Phase-1 data included CDIs generated by FAS and Geotech using the EM Flow™ (v3.30) software package. The EM Flow™ CDI program is an industry standard method for deriving conductivity estimates from AEM surveys.

The Phase-2 Pine Creek TEMPEST™ conductivity estimates (Woolner Granite and Rum Jungle survey areas), have been produced using a layered earth inversion (GA–LEI) algorithm developed at GA. The Phase-2 data release contained the GA–LEI 1D “sample-by-sample” inversion data, including:

- Pine Creek AEM Survey Inversion Report;
- Point-located GA–LEI inversion data;
- Point-located GA–LEI inversion data (secondary) used to calculate the percent data influence (PDI);
- GA LEI georeferenced JPEG sections;
- GA LEI multiplots;
- ER Mapper™ grids of depth slices, elevation slices (10 and 50 m slices), 0-200 m conductance, 0-400 m conductance, AEM depth of investigation (DOI) Go Map;
- Shape files: flight lines, survey boundary and National Park; and,
- JPEG images of depth slices, elevation slices (10 and 50 m slices), 0-200 m conductance, 0-400 m conductance, AEM DOI Go Map.

The Pine Creek TEMPEST™ AEM Phase-2 data are available from the GA Sales Centre and also by free download from the GA website at the links below.

**Downloads are available through the links below:**

Woolner Granite and Rum Jungle TEMPEST™ Phase-2 data including all infill areas (apart from RJ7) are available from the GA Sales Centre and are also available by free download from the GA website. Downloads are available through the link below.

[https://www.ga.gov.au/products/servlet/controller?event=GEOCAT\\_DETAILS&catno=70584](https://www.ga.gov.au/products/servlet/controller?event=GEOCAT_DETAILS&catno=70584)

The Pine Creek TEMPEST™ AEM Phase-1 and Phase-2 data for the infill area RJ7 is available from the GA Sales Centre and are also available by free download from the GA website. Downloads are available through the link below:

[https://www.ga.gov.au/products/servlet/controller?event=GEOCAT\\_DETAILS&catno=71350](https://www.ga.gov.au/products/servlet/controller?event=GEOCAT_DETAILS&catno=71350)

The GA–LEI inversion products created for the Woolner Granite and Rum Jungle survey areas are documented in the Woolner Granite and Rum Jungle TEMPEST™ AEM Surveys: Inversion Report (Costelloe and Hutchinson 2010). This is summarised in [Appendix 10](#) and is accompanied by a product listing.

The Phase-2 Kombolgie VTEM™ AEM Survey comprising revised EM Flow™ conductivity estimates to 2 km depth conductivity estimates have been generated using a research version of EM Flow™ (v5.23-13 - STEMFlow\_FULL523-13.exe). The Phase-2 data release includes:

- Pine Creek Kombolgie explanatory notes;
- Point-located EM Flow™ v5.23-13 point located data;
- Point-located EM Flow™ v5.23-13 sub-sampled point located data;
- Georeferenced JPEG sections;
- GA multiplots;
- ER Mapper™ grids of estimated conductance 0 – 2000 m and estimated penetration depth; and,
- Shape files: flight lines and survey boundary;

The Pine Creek VTEM™ AEM Phase-2 data are available from the GA sales Centre and are also available by free download from the GA website. Downloads are available through the link below:

[https://www.ga.gov.au/products/servlet/controller?event=GEOCAT\\_DETAILS&catno=71371](https://www.ga.gov.au/products/servlet/controller?event=GEOCAT_DETAILS&catno=71371)

The Kombolgie VTEM™ Inversion Data Package can be accessed from

[https://www.ga.gov.au/products/servlet/controller?event=GEOCAT\\_DETAILS&catno=72582](https://www.ga.gov.au/products/servlet/controller?event=GEOCAT_DETAILS&catno=72582)

## **5.5 PHASE-2 - TEMPEST™ GA–LEI INVERSIONS**

The Phase-2 products consist of two parts; (a) the GA–LEI inversion of the TEMPEST™ data from the Rum Jungle and Woolner Granite survey areas, and the EM Flow™ conductivity-depth imaging of the VTEM™ data from the Kombolgie survey area. This section reports on the Rum Jungle and Woolner Granite products and [section 5.6](#) reports on the Kombolgie products.

### **5.5.1 Background on the GA–LEI algorithm**

Conversion of the non-linear electromagnetic response data into estimates of subsurface conductivity allows for much easier and more accurate integration with independent subsurface information and facilitates better interpretation. The conversion can use either approximate transformation methods or geophysical inversion, both of which produce model-dependent conductivity estimates.

The Phase-1 data release of Pine Creek data included conductivity predictions produced by FAS from the industry standard EM Flow™ algorithm (Macnae *et al.*, 1998; Stoltz and Macnae, 1998). EM Flow™ is a fast approximate transformation method based on the concept that the response of a quasi-layered earth can be approximately represented by a mirror image of the transmitter dipole that recedes below the surface and expands with delay-time. By determining the vertical depth distribution of the mirror image dipoles a quasi-layered estimate of the subsurface conductivity can be estimated.

Some complications arise however because not all components of the TEMPEST™ system geometry are measured, and they must be estimated by FAS during the standard data processing (cf. [Section 5.3.1](#)).

Since the EM Flow™ routine relies on these estimates, the accuracy of the resultant conductivity estimates is dependent on the accuracy of the geometry estimates. Accordingly, the estimates tend to be biased towards producing results that are consistent with the assumptions made in the FAS data processing, typically a resistive basement earth model. This bias can in turn create an overestimate of the conductivity near the surface, since the model must compensate for the lack of conductance at depth (Lane *et al.*, 2004a; Brodie and Fisher, 2008).

A further problem is caused by the assumptions made in the system geometry estimation that the receiver is orientated in its nominal position (i.e., with zero roll, pitch, and yaw). If the receiver is in fact rotated from its nominal position, which is generally the case, it may be impossible to simultaneously fit both the X- and Z-component data using the same subsurface conductivity distribution because the data are inconsistent with the system geometry information provided to the routine. For this reason it is often necessary to calculate the EM Flow™ estimates using just the X or the Z-component data. While this is possible, a different conductivity model will result from each component.

These issues led to the development of the GA–LEI algorithm (Lane *et al.*, 2004b). In the GA–LEI inversion algorithm, the idea is to not rely on the primary field separation and hence geometry estimates made in the standard FAS data processing. Instead, the total field (primary plus secondary)

data are inverted directly. The inversion solves not only for a layered earth conductivity model, but it simultaneously solves for the horizontal and vertical separations between the TX and RX and the pitch of the receiver coils. By solving for the system geometry during the final inversion the method allows the information from both the X- and Z-components to be simultaneously fitted using a single common conductivity model. It prevents the assumptions made during the standard data processing from being automatically imposed onto the inversion results. Furthermore, if prior information exists about the electrical structure of the survey area, these can be included as specific constraints on the inversion results.

Previous work at GA, in which downhole conductivity log data were compared to conductivity estimates (Lane *et al.*, 2004a; Reid and Brodie, 2006; Brodie and Fisher, 2008), has shown that improvements on the standard FAS EM Flow™ conductivity estimates can be made using the GA–LEI algorithm.

### **5.5.2 GA–LEI Inversions**

#### *5.5.2.1 Algorithm outline*

The inversion products released for the Pine Creek TEMPEST™ survey data have been derived with the GA–LEI algorithm. A complete technical description of the algorithm is provided in [Appendix 10.2](#). A brief non-technical description of its application to the Pine Creek TEMPEST™ data is provided below.

The GA–LEI is a 1D “sample-by-sample” inversion in which each of the airborne samples, acquired at approximately 12 m intervals along a flight line, are inverted independently of their neighbours. The inversion of each individual sample involves the estimation of a 1D layered earth conductivity structure ([Figure 5–2](#)), and three elements of the system geometry (TX-RX horizontal and vertical separations and RX pitch), that are all consistent with the data. A 1D layered earth conductivity structure means that the earth is considered to be a series of horizontal layers stacked in layer-cake fashion. Each layer extends to infinity in the horizontal direction and the conductivity within each layer is constant.

Since the data are non-linear with respect to the model parameters, an iterative inversion technique is used. Starting from an initial model, the layer conductivities and system geometry parameters are iteratively updated until the forward response of the model fits the measured data to within the noise levels of the data, or in other words, until a satisfactory data misfit (cf. [Section 5.5.2.4](#)) is achieved.

Because of non-uniqueness, the estimated conductivity model must be constrained. In the GA–LEI, it is constrained to be vertically smooth and to be as close as possible to a reference conductivity model (cf. [Section 5.5.2.3](#)). The aim of smoothness and reference model constraints is to ensure that the model is as simple as possible, and complex structure is only permitted where necessary, see for example Constable *et al.* (1987).

Once all individual samples are inverted they are compiled into a pseudo-3D model by ‘stitching’ the 1D models together. The inversion program control file is included in Costelloe *et al.* (2010). The inversion output ASCII header information from the inversion is presented in [Appendix 10.3](#).

#### *5.5.2.2 Conductivity model parameterization*

In the Pine Creek TEMPEST™ surveys the subsurface was parameterized with 30 layers whose thicknesses were chosen and remained fixed throughout the inversion (i.e., they were not solved for). The layer thicknesses gradually increase from 4 m in the top layer of the model up to approximately 60 m in the second deepest layer. The bottom layer was set to infinite thickness and thus represents a half-space below all other layers. The parameters of each layer used in the GA–LEI are shown in [Table 5–3](#).

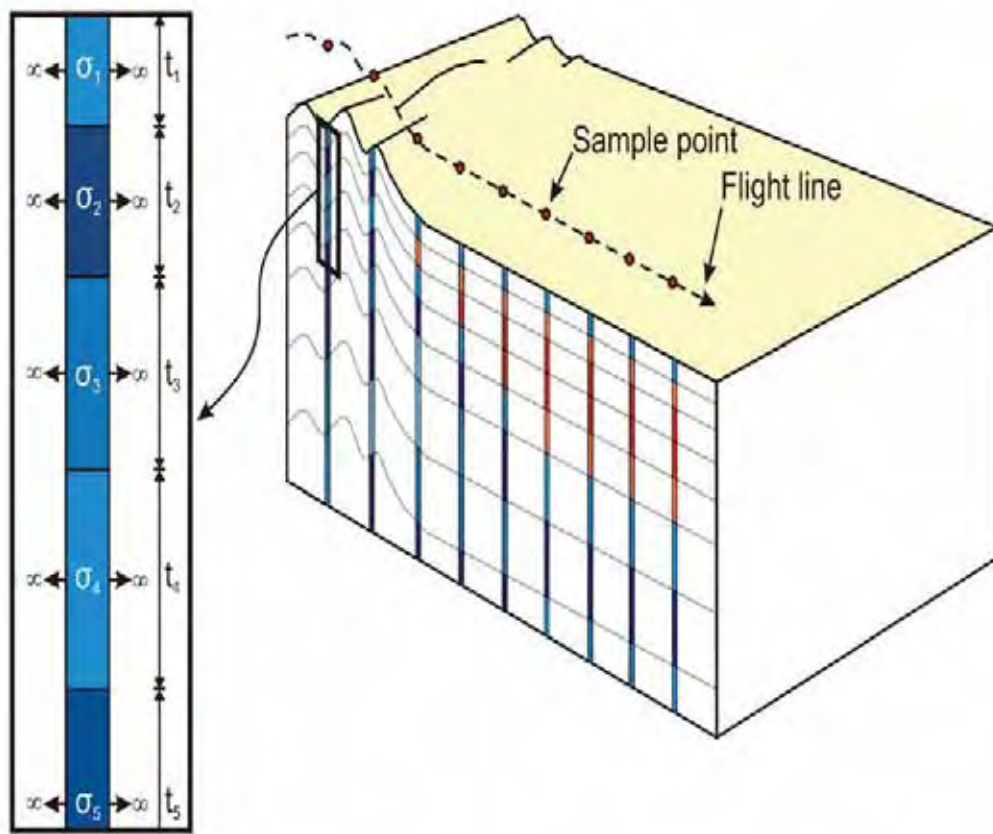


**Figure 5-2:** Schematic diagram of 1D vertically smooth layered earth model used in the GA–LEI. The thickness of each layer ( $t_n$ ) is fixed, but the conductivity ( $\sigma_n$ ) is not fixed and can vary between layers. From Brodie and Fisher (2008)

**Table 5-3:** GA–LEI model layer thicknesses and depths from surface for Woolner Granite and Rum Jungle survey areas.

LAYER NUMBER	THICKNESS (m)	DEPTH TO TOP (m)	DEPTH TO BOTTOM (m)
1	4.00	0.00	4.00
2	4.40	4.00	8.40
3	4.84	8.40	13.24
4	5.32	13.24	18.56
5	5.86	18.56	24.42
6	6.44	24.42	30.86
7	7.09	30.86	37.95
8	7.79	37.95	45.74
9	8.57	45.74	54.31
10	9.43	54.31	63.74
11	10.37	63.74	74.11
12	11.41	74.11	85.52
13	12.55	85.52	98.07
14	13.81	98.07	111.88
15	15.19	111.88	127.07
16	16.71	127.07	143.78
17	18.38	143.78	162.16
18	20.22	162.16	182.38
19	22.24	182.38	204.62
20	24.46	204.62	229.08
21	26.91	229.08	255.99
22	29.60	255.99	285.59
23	32.56	285.59	318.15
24	35.82	318.15	353.97
25	39.40	353.97	393.37
26	43.34	393.37	436.71
27	47.67	436.71	484.38
28	52.44	484.38	536.82
29	57.68	536.82	594.50
30	∞	594.50	∞

### 5.5.2.3 Reference model

In principle, conductivity logs can be used to create a detailed reference model that varies across the survey in order to constrain the inversion. In the Pine Creek survey, just 16 conductivity logs were available for use in the inversion. Since there were relatively few conductivity logs available over a large survey area, it was not feasible in this case to define a conductivity reference model that was spatially variable. Therefore the reference model used in this inversion is simply a half-space of homogeneous conductivity across the survey area. We chose to use a conductivity reference value of 0.001 S/m, based on the average value of the resistive basement. The reference model was also used as the starting model for the iterative inversion.

For the TX to RX horizontal and vertical separation inversion model parameters we used the values (i.e. different for each sample) estimated during the standard FAS data processing as the starting and reference model values. Zero was used for the starting and reference model value for the receiver coils' pitch parameter.

#### 5.5.2.4 Data misfit

The inversion would ideally converge until the data misfit ( $\Phi_d$ ) reaches a value of 1.0 (cf. Equation 9 in [Appendix 10.2](#)). The data misfit is simply a measure of fit (agreement) between the forward response of the inversion model and the observed data. It is not a measure of confidence or certainty or uniqueness in the model parameters. In a 1D geological environment it is usually possible to achieve a data misfit of 1.0 or close to 1.0. However, in geological environments with 2 or 3D geology, 1D inversions usually have a higher data misfit, reflecting the fact that a 1D model is insufficient to explain anomalies caused by the 2 or 3D geology.

The data misfit of the inversion is displayed on the GA–LEI multiplots (cf. [Section 5.5.4.7](#)) as a number between 0 and 1000. When reviewing these multiplots, it is important to understand the data misfit is not a direct reflection of the quality of the AEM data or the certainty in the inversion results.

#### 5.5.3 Depth of Investigation

The conductivity model estimated by the GA–LEI inversion of the TEMPEST™ data is determined not only by the AEM data, but it is also influenced by the reference model. It is important to ascertain how much the solution is influenced by the choice of reference model and how much it is influenced by the AEM data itself. The relative contributions of the data and the reference model can be estimated by defining a parameter called the percentage data influence (PDI); which compares two inversions created from different reference models. In this work, the PDI for the  $k$ th layer is defined as:

$$PDI_k = 100 \times \left[ 1 - \frac{\log \sigma_{k,i1} - \log \sigma_{k,i2}}{\log \sigma_{k,r1} - \log \sigma_{k,r2}} \right] \%$$

where  $\sigma_{k,i1}$  and  $\sigma_{k,i2}$  are the  $k$ th layer conductivities of the two inversion models at a given location and  $\sigma_{k,r1}$  and  $\sigma_{k,r2}$  are the corresponding reference model conductivities (Lane *et al.*, 2004a). We define the PDI using the logarithm of the conductivity, since this is the quantity used in each inversion.

If the PDI is greater than 50%, for a particular layer, then the inversion is deemed to be more influenced by the AEM data than the reference model at the depth of that layer, whereas if it is less than 50% then the reference model is deemed to be dominant.

The depth of investigation (DOI) is defined as the depth of the layer at which the PDI falls below 50%. Thus the DOI marks the depth to which the inverted layer conductivity is relatively independent of the chosen reference model. Note that the 50% PDI threshold is arbitrary and a different threshold could have been chosen.

[Figure 5–3](#) illustrates the effect of the DOI, showing conductivity sections from two different inversion models for part of a flight line. In [Figure 5–3a](#), the inversion uses a reference conductivity of 0.04 S/m, whereas in [Figure 5–3b](#) the inversion uses a reference conductivity of 0.004 S/m. It can be seen that above the DOI (black line) the results are similar for both inversions. However, below the DOI, particularly under the conductive wedge on the right hand side, the conductivity reverts to the reference model conductivity value. This indicates that AEM data were not sensitive to the conductivity of layers below the DOI, and are thus constrained by the reference model instead.

In addition to the above calculation, we also set a maximum value, or cap, of 400 m on the DOI based on the results of the detectability analysis described in [Section 5.2](#). This analysis indicated that 400 m was the theoretical maximum depth at which the targets could be detected in the Woolner Granite and Rum Jungle survey areas. It can be seen on the left hand side of the section in [Figure 5–3a](#), and [5–3b](#) how the DOI has been capped at 400 m.

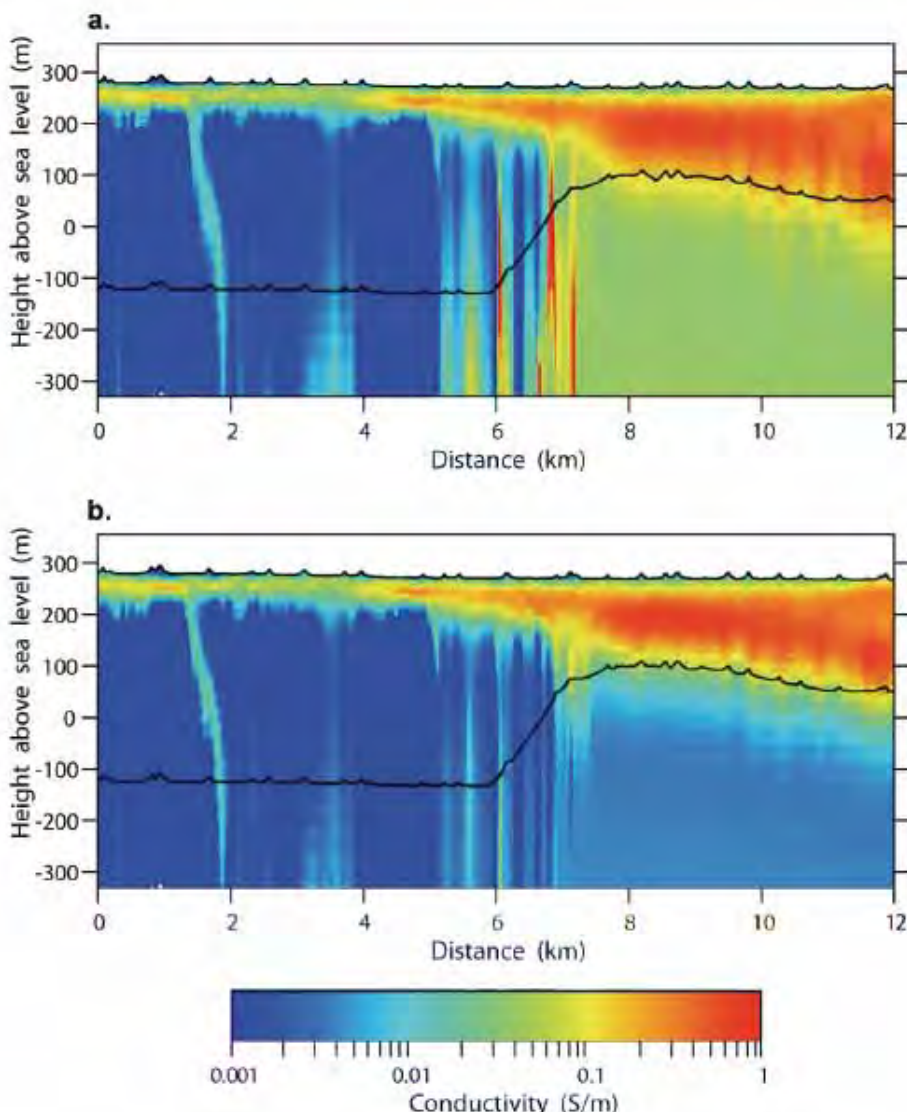


**Figure 5-3:** Sample conductivity depth sections comparing the results of inversions using reference models of (a) 0.04 S/m and (b) 0.004 S/m. The black line marks the depth of investigation (DOI) in each case. Above the DOI the results are similar for both inversions, whereas below the DOI the conductivity differs according to the reference model value. From: Hutchinson et al. (2010b).

#### 5.5.4 Derived products

The Phase-2 TEMPEST™ data releases include the following products:

- Point located GA–LEI conductivity estimates;
- Gridded layer conductivities;
- Gridded depth slices;
- Gridded elevation slices;
- Gridded depth of investigation information;
- Georeferenced JPEG conductivity-depth sections; and,
- Multiplot PDF conductivity-depth sections and auxiliary information.

#### **5.5.4.1 Point located data**

ASCII point located data including: GA–LEI conductivity estimates; number of layers, data misfit reconstructed from the inversion non-geometry-corrected X and Z-component window data; transmitter height; measured transmitter pitch and roll and other system geometry measurements.

#### **5.5.4.2 Layer conductivity grids**

The conductivity of all 30 of the layers in the inversion model is the fundamental output of the inversion program. Several other products are then derived from these layer conductivities. Layer conductivities are included in the digital data package as point located line data and as grids. Since the inversion actually solves for base ten logarithm of the layer conductivities, we grid the point located layer conductivity data in these units. We have found that this produces better quality grids than gridding in linear conductivity units.

#### **5.5.4.3 Depth slice grids**

A conductivity depth slice is the average estimated conductivity over a given constant depth interval below the topographic surface.

A series of depth slices have been created between 0 and 400 m, with the slices becoming progressively thicker with depth. The depth slices are set to 5 m thickness between 0 and 20 m depth, 10 m thickness between 20 and 40 m depth, 20 m thickness between 40 and 100 m depth, and 50 m thickness between 100 and 400 m depth. The increase in thickness with depth reflects the lower sensitivity of the inversion with depth.

A selection of two depth slices is illustrated in [Figure 5–4a-d](#), showing the (a) 0-5 m, (b) 30-40 m, (c) 100-150 m, and (d) 200-250 m depth intervals. [Figure 5–4a](#), and [Figure 5–4b](#) show a range of conductive and resistive areas and there is no DOI masking, since the depth slices are relatively shallow. However, [Figure 5–4c-d](#) shows isolated areas of DOI masking, The degree of masking reflects the different penetration of the AEM signal in resistive (deep penetration) and conductive (shallow penetration) areas.

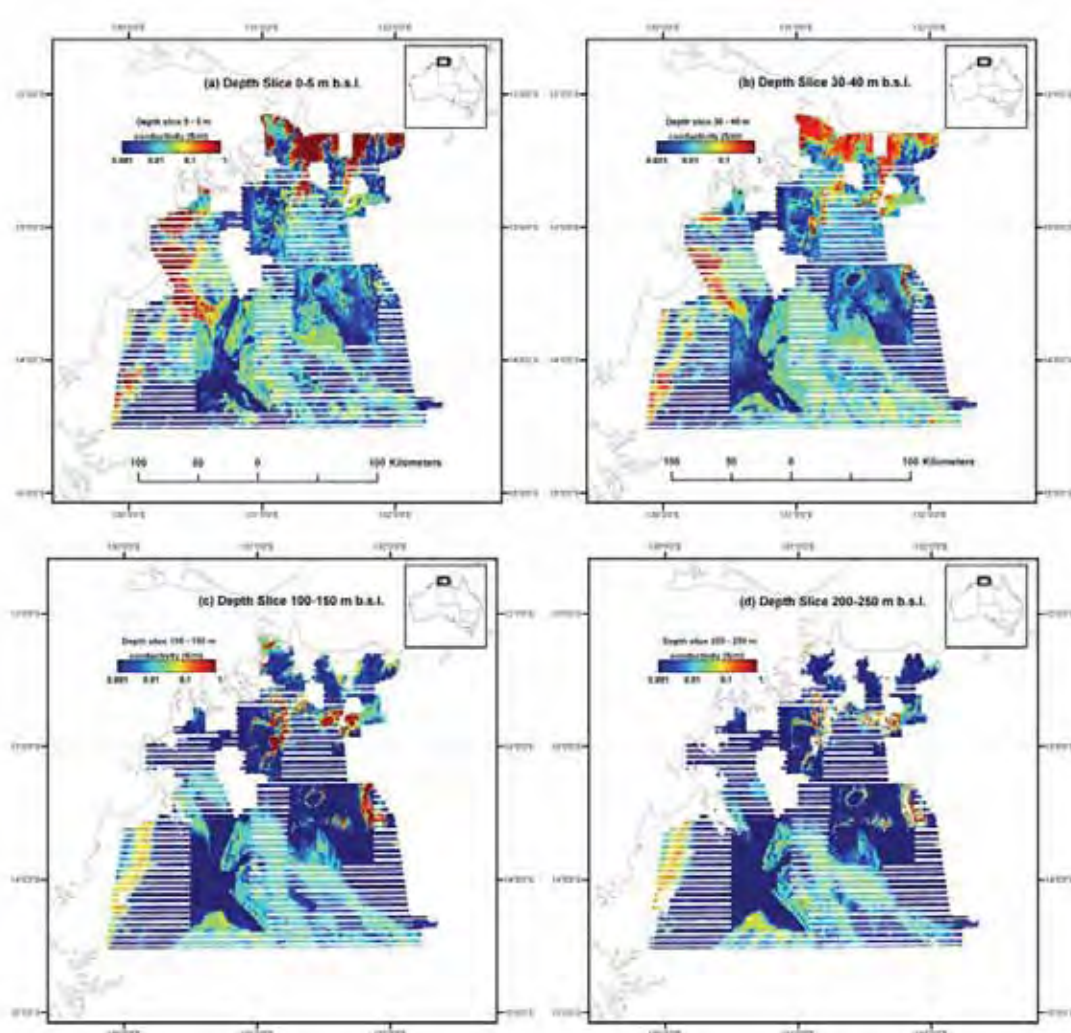


**Figure 5-4:** A selection of depth slices showing a) 0-5 m, b) 30-40 m, c) 100-150 m and d) 200-250 m. Data falling below the DOI have been masked out, and appear white.

#### 5.5.4.4 Elevation slice grids

In contrast to the depth slices, the elevation slices present the same inversion results, but the slices are relative to the height above sea level rather than depth below ground surface. This is useful because it removes the complications that a rough topography may introduce into depth slice interpretation. Furthermore, elevation slices provide a simpler means of importing the data into modelling and visualization packages. The drawback of using elevation slices over the entire survey is that there is a substantial altitude difference across the Pine Creek survey - approximately 300 m of relief between the highest and lowest points of the survey. Therefore a given elevation slice may display near-surface data from one corner of the survey area with much deeper data from other parts of the survey area.

Elevation slices were created for the Pine Creek TEMPEST™ data from 400 m below sea level to 310 m above sea level at 10 m intervals. [Figure 5-5](#) shows a selection of the elevation slices, with (a) 0-10 m, (b) 100-110 m, (c) 200-210 m and (d) 300-310 m above sea level. [Figure 5-5a](#) has no

masking by elevation or DOI due to the slice being shallow at 0 – 10 m asl. [Figure 5–5b](#) has substantial areas of masking due to the DOI as well as parts of these slices lying deep below the surface. In [Figure 5–5c](#) and [Figure 5–5d](#) there is little or no masking from the DOI, but there are still substantial areas of null data values due to the land surface being lower than the elevation slice itself. These null data values are especially prevalent in the north, where the surface elevation is significantly lower, and hence much of this area is below the 200 and 300 m elevation of the slices.

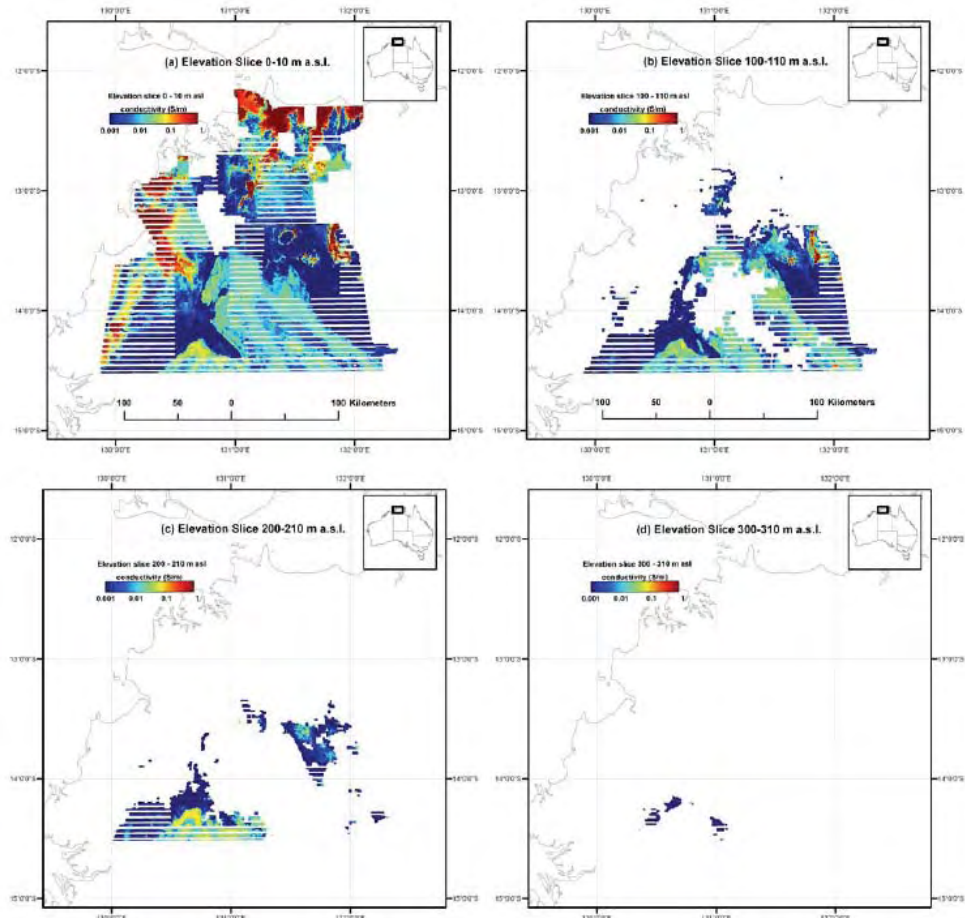


**Figure 5-5:** Selection of elevation slices, showing a) 0-10 m above sea level (a.s.l.), (b) 100-110 m a.s.l., (c) 200-210 m a.s.l. and (d) 300-310 m a.s.l

#### 5.5.4.5 AEM DOI Go map

The DOI is presented as a 2D grid in [Figure 5–6](#). The probability of detection assumption required to cap the percent data influence (PDI) threshold, was set to 400 m, based on forward modelling in resistive terrain (Richardson *et al.*, 2008). In the resistive areas of the survey the DOI reaches this maximum depth. The yellow and red colours (7 - 30 m) in [Figure 5–6](#) are areas where the DOI is much shallower, and in places near the coast is less than 10 m. These shallower areas of the DOI correspond closely to conductive saline regions of the survey area.

The DOI grid can be interpreted as an AEM “Go map”. AEM surveys are relatively costly, and carry an inherent risk since the depth of penetration is highly variable. This DOI grid can reduce the risk of exploration using AEM surveys by indicating to what depth AEM can explore in the Pine Creek

survey area, making AEM surveying a more attractive tool for mineral exploration (Hutchinson *et al.*, 2010a; 2010b).

The main gridded products of the AEM inversion are the depth slices and elevation slices. These grids present the inversion model conductivity values in 2D spanning the entire survey area. In the depth and elevation slice grids, conductivities below the DOI surface have been masked out or nulled. The purpose of this masking is to focus attention on the data-driven results of the inversion and to ensure that spurious features in the inversion model are not misinterpreted as real features.

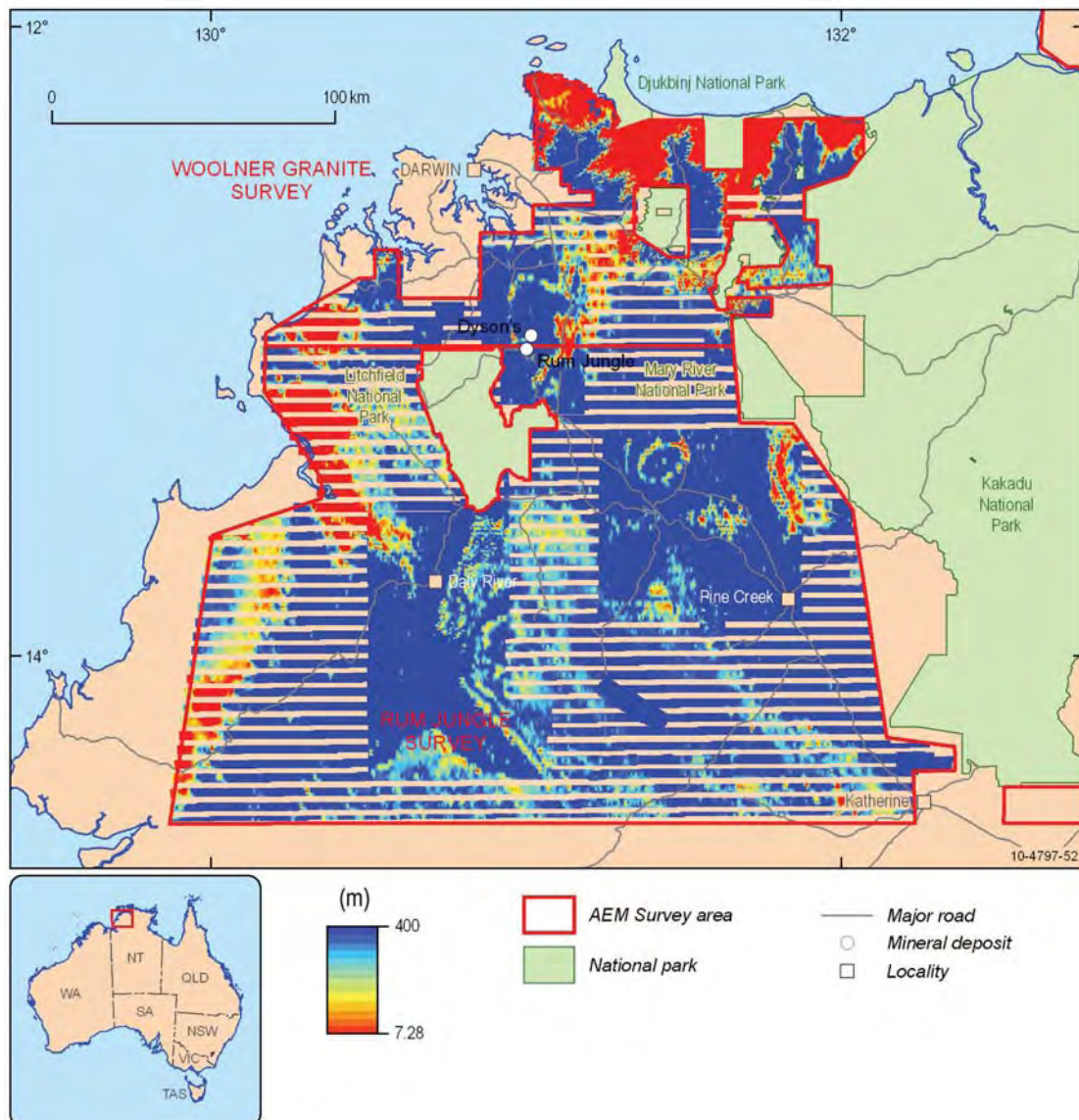


**Figure 5-6:** The DOI grid (AEM Go map) for the Pine Creek TEMPEST™ Survey areas.

#### **5.5.4.6 Gridding procedures**

All of the depth slice and elevation slice grids store the base-10 logarithm ( $\log_{10}$ ) of conductivity, since this is the value that is solved for in the inversion. For interpretation purposes we have found that geological structures are more evident in grids that use the logarithm of conductivity, rather than conductivity itself.

Users who wish to grid the data without logarithms may obtain the data from the inversion output explained in [Section 5.5.4.1](#). Alternatively the grids may also be converted to linear-conductivity units using formulas in software packages (such as ER Mapper™, Intrepid™ and Geosoft™).

The AEM inversion results were gridded using Intrepid™ software and are stored in binary files as ER Mapper™ single band IEEE 4 Byte Real data types. A comprehensive ER Mapper™ header (.ers) file is associated with each grid file, which describes the data type and the coordinate system used to geographically position the grid. Gridded data are stored in a projected coordinate system only, in this case Universal Transverse Mercator (metric) coordinates of the Map Grid of Australia Zone 52 using the Geodetic Datum of Australia 1994. Technical details of the projection used are given in [Appendix 10.6](#).

In the Pine Creek survey the line spacing is as wide as 5 km. It was deemed more appropriate to not interpolate data across 5 km to reduce artefacts that obscure the structure evident in the data in some areas. In this area the data appears as coloured stripes with null values in between. This “Venetian blind” effect can be seen in the DOI grid, the depth slices and elevation slices.

#### **5.5.4.7 Sections**

Conductivity-depth sections depicting the GA–LEI inversion results along each flight line are provided as Georeferenced JPEG images and as multiplots. The details of each presentation are explained in the following sections.

##### **5.5.4.7.1 Georeferenced JPEGs**

Georeferenced JPEGS have been included as a convenient way to overlie inversion results into GIS software. Each of the survey flight lines has a JPEG image file (.jpg) depicting the conductivity-depth section of the GA–LEI results along the flight line. Each image file has an associated JPEG world file (.jgw) that spatially locates or georeferences the image file ([Table 5–4](#)). The images are georeferenced such that the average topographic height on the section will be displayed coincident with the line-of-best-fit of the flight line when loaded into a GIS package.

**Table 5–4:** Contents of the JPEG world file for line 1000201

COLUMN	DATA
1 x scale (per pixel)	4.228194
2 rotation about y axis	0.00522
3 rotation about x axis	0.00522
4 y scale	-4.228194
5 x reference point	772907.1473
6 y reference point	8599052.851

#### 5.5.4.7.2 *Multiplots*

The multiplots show the conductivity depth section for each flight line along with a number of auxiliary panels showing information such as the system geometry. They are provided as Portable Document Format (.pdf) files. An example is shown in [Figure 5–7](#). [Table 5–5](#) details the information that is shown in each panel, from top to bottom, of the multiplot.

**Table 5–5:** Description of each panel of the GA–LEI multiplots

PhiD	Data misfit of the inversion, the optimal misfit is 1.0
TX Height	Measure transmitter height in metres
TX attitude	Measured transmitter pitch and roll in degrees
Dx	Inline horizontal separation between the transmitter loop and the receiver coils in metres. Two traces showing the processing estimate and output inversion model estimate
Dz	Vertical separation between the transmitter loop and the receiver coils in metres. Two traces showing the processing estimate and output inversion model estimate
Rp	Receiver pitch in degrees. Two traces showing the processing assumption (zero degrees) and output inversion model estimate
X component	Non-geometry corrected X-component window data profiles scaled using the arcsinh function, (i.e. in units of $\text{asinh}(fT)$ ).
Z component	Non-geometry corrected Z-component window data profiles scaled using the arcsinh function, (i.e. in units of $\text{asinh}(fT)$ ).
Conductivity section	GA–LEI conductivity-depth section image with conductivity colour bar in ( $\text{S}/\text{m}$ ).

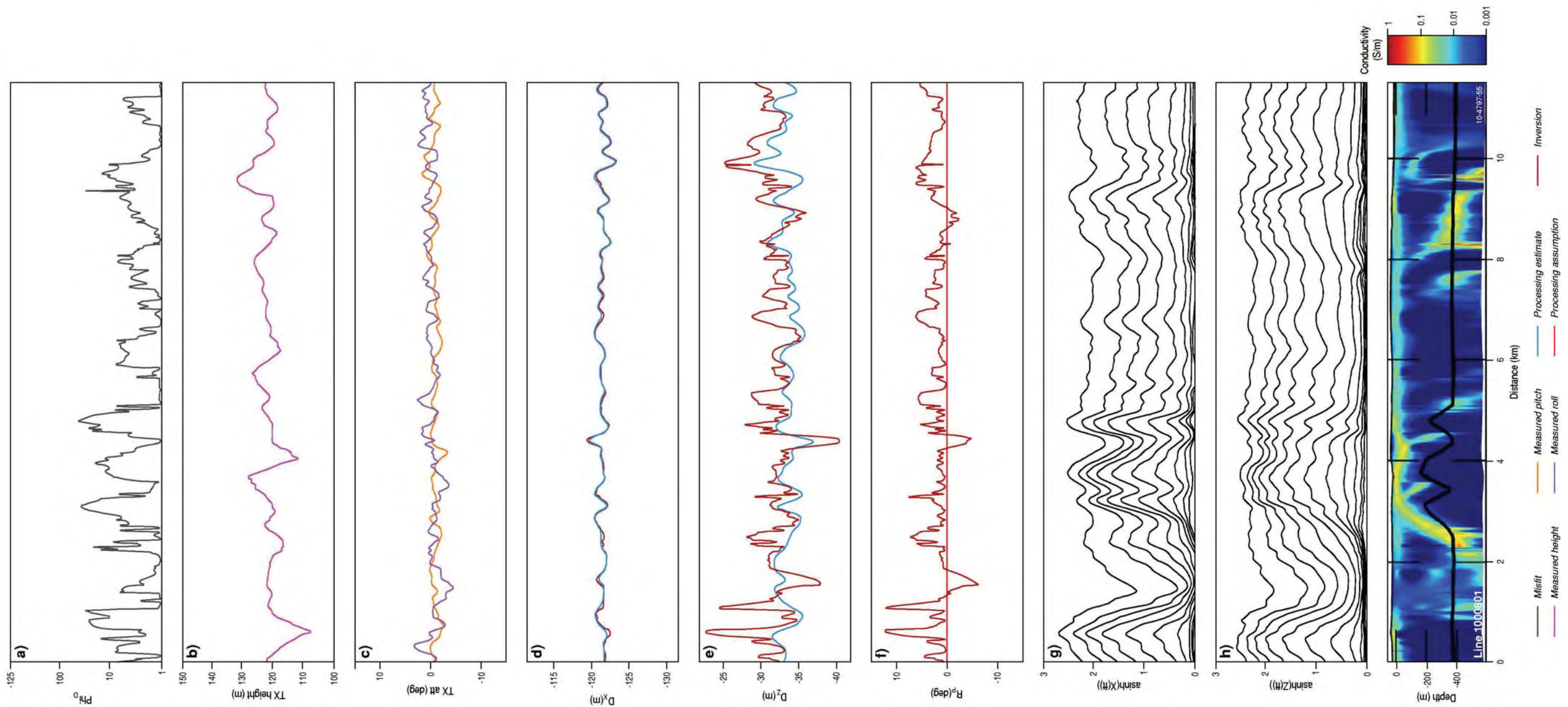


Figure 5-7: GA-LEI Multiplot for line 1000801

## **5.6 PHASE-2 – VTEM™ EM FLOW™ CONDUCTIVITY DEPTH IMAGING**

### **5.6.1 Background**

Since the release of Phase-1 Kombolgie EM Flow™ conductivity estimates generated by the contractor, Geotech Airborne, further work has been carried out by Geoscience Australia in order to extract additional value from the electromagnetic data. In this process, Richard Lane (Geoscience Australia) and Professor James Macnae (RMIT) discovered that in parts of the survey area geologically plausible conductivity estimates could be generated to depths exceeding 1500 m.

The difference between the Phase-1 and Phase-2 Kombolgie EM Flow™ datasets can be summarized as follows:

- Use of the most recent research version of EM Flow™ (v5.23-13) developed through AMIRA project P407b and more recently enhanced by RMIT;
- Extension of the maximum depth of conductivity estimates from 600 m to 2000 m;
- A different waveform definition was used;
- Corrections were made to incorrect window time definitions and amplitude scaling factors;
- A different range of Taus (time constant) were chosen for the basis functions; and,
- A different range of discrete conductivities was chosen.

Geotech Airborne used the commercial version (3.30) of EM Flow™ in the generation of the Phase-1 data. The research version (v5.23-13 - STEMflow\_FULL523-13.exe) was used to generate the Phase-2 Kombolgie results. [Appendix 10.5](#) details the settings used in the EM Flow™ for the generation of the Phase-2 results and some background on the program's development. Brodie and Costelloe (2010) also describe additional information and examples.

This enhanced EM Flow™ data presents conductivity predictions, at depths deeper than previously documented, in resistive areas across the Kombolgie survey. This technique represents a significant improvement in mapping conductivity in greater detail and identifying features such as unconformities and major structures at much greater depths than the Phase-1 data, or indeed any documented AEM data world-wide.

### **5.6.2 Penetration depth**

An estimate of the penetration depth is computed by EM Flow™ to provide an indication of the depth of investigation of the AEM survey data. This estimate is included in the released point located and gridded data and is also plotted on the conductivity depth sections presented in both multiplot and georeferenced JPEG formats. The estimated penetration depth in some areas reaches 2000m.

### **5.6.3 Derived products**

The released Phase-2 VTEM™ includes the following products:

- Point located EM Flow™ conductivity estimate line data;
- Gridded conductance;
- Gridded penetration depth;
- Georeferenced JPEG conductivity-depth sections; and,
- Multiplot PDF conductivity-depth sections and auxiliary information.

### **5.6.3.1 Point located data**

The conductivity estimates exported from EM Flow™ results are available in point located format. This includes the conductivity estimate for all 201 of the 10 metre thick layers at each AEM sample point along the flight lines. It also includes the estimated penetration depth.

### **5.6.3.2 Grids**

The total conductance to 2000 m ([Figure 5–8](#)) and the estimated penetration depth have been gridded at 1250 m (1/5 major line spacing) cell size. Grids were generated using the Intrepid™ software package and are stored in binary files as ER Mapper™ single band IEEE 4 Byte Real data types. A comprehensive ER Mapper™ header (.ers) file is associated with each grid file, which describes the data type and the coordinate system used to geographically position the grid. Gridded data are stored in a projected coordinate system only, and in this case Universal Transverse Mercator (metric) coordinates of the Map Grid of Australia Zone 53 using the Geodetic Datum of Australia 1994. Technical details of the projection used are given [Appendix 10.6](#).

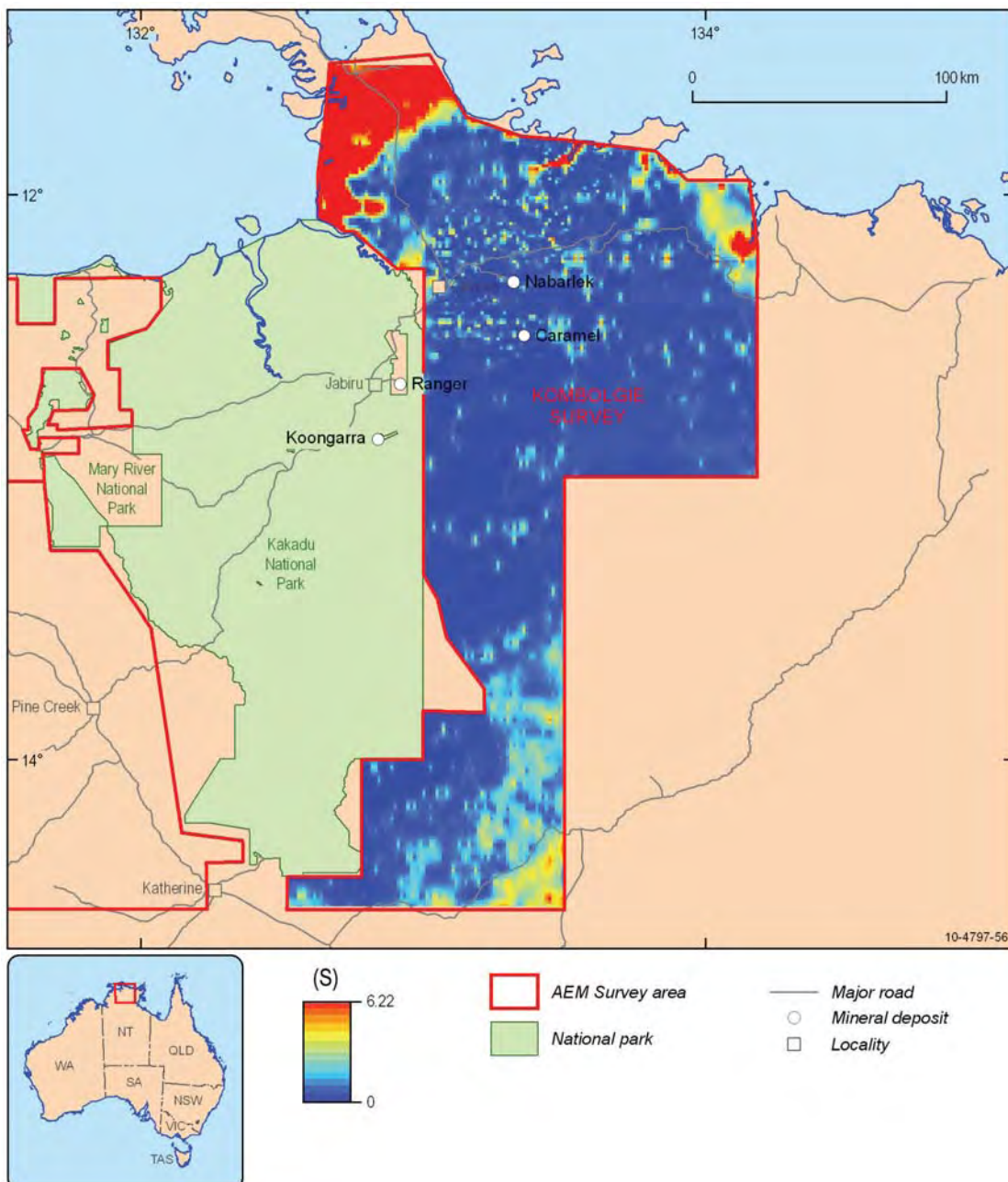


**Figure 5-8:** Kombolgie survey total conductance to 2 000 m

### 5.6.3.3 Sections

Conductivity-depth sections depicting the EM Flow™ conductivity estimates and the estimated penetration depth along each flight line are provided as Georeferenced JPEG images and as Multiplots. The details of each presentation are explained in the following sections.

#### 5.6.3.3.1 Georeferenced JPEGs

Georeferenced JPEGs have been included as a convenient way to overlie inversion results into GIS software. Each of the survey flight lines has a JPEG image file (.jpg) depicting the conductivity-depth section of the EM Flow™ results along the flight line. An example is shown in [Figure 5-9](#).

Each image file has an associated JPEG world file (.jgw) that spatially locates or georeferences the image file (see [Figure 5–9](#) for details). The images are georeferenced such that the average topographic height on the section will display coincident with the line-of-best-fit of the flight line when loaded into a GIS package.

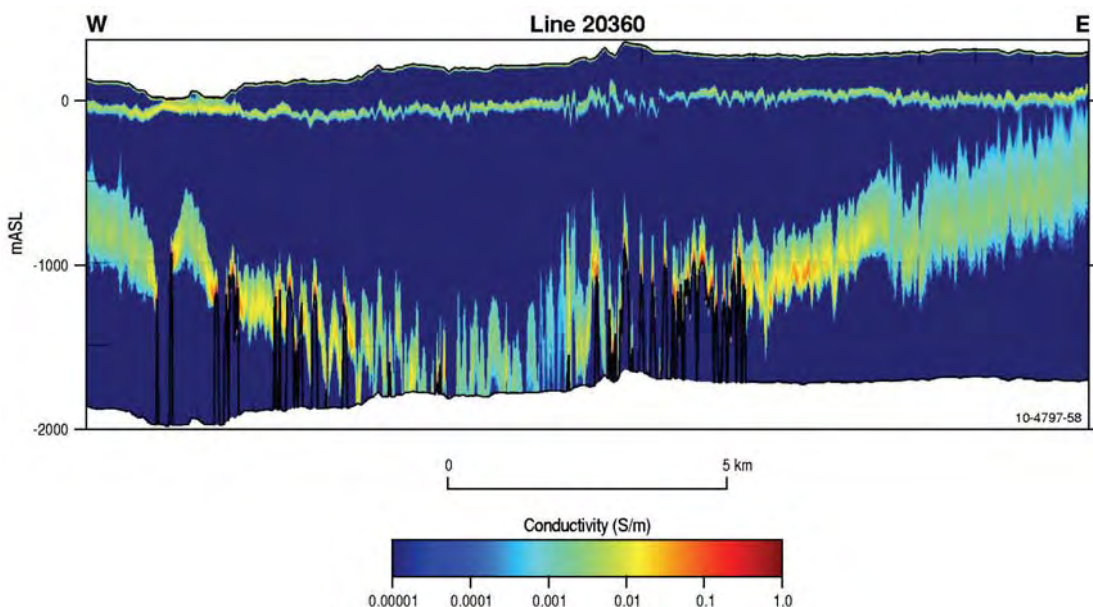


**Figure 5–9:** Georeferenced JPEG for a 20 km subsection of line 20360.

#### 5.6.3.3.2 Multiplots

The multiplots show the GA–LEI conductivity depth section for each flight line along with a number of auxiliary panels showing additional information. [Table 5–6](#) details the information that is shown in each auxiliary panel. The multiplots are provided as Portable Document Format (.pdf) graphics files.

**Table 5–6:** Description of each panel of the multiplots

<b>DATA</b>	VTEM™ window data
<b>GEOLOGY</b>	Raster strip of the 1:1 000 000 surface geology
<b>ELEVATION</b>	Raster strip of the gradient enhanced DEM image
	Raster strip of the satellite imagery
<b>CONDUCTIVITY SECTION</b>	EM Flow™ conductivity-depth section image with conductivity colour bar in (S/m). A trace above the section showing the transmitter loop height. The estimated penetration depth is also displayed on the section
<b>EASTING</b>	labelled every 2 000m
<b>NORTHING</b>	labelled every 2 000m

## **5.7 DISCRETE CONDUCTORS**

The primary reason for conducting the AEM survey in the Pine Creek area is to map regional geology, as well as potential unconformity-uranium deposit host-rocks. However, as a procedural step in the QA/QC process, the data were scanned for the presence of discrete conductors. It is very important to assess the data for noise and artefacts prior to interpretation.

Multiplots delivered by FAS and Geotech were used for interpreting the presence of discrete conductors using the process described in Lane and Worrall (2002). Discrete windowed-amplitude anomalies are observed on the multiplots when system geometry, receiver coil vibration and “sferics” occur, and can be confused by the novice as geological signal. Sferics are noise caused by lightning flashes within about 1500 km of the survey area. It is important to determine if the source of the discrete conductor anomaly is noise, poorly processed data from sferic noise or variations in the subsurface conductivity distribution. [Figure 5–10](#) shows an example of an X and Z component multiplot for line 1001501, with a discrete conductor feature at fiducial 2980, trimmed to highlight the discrete conductor.

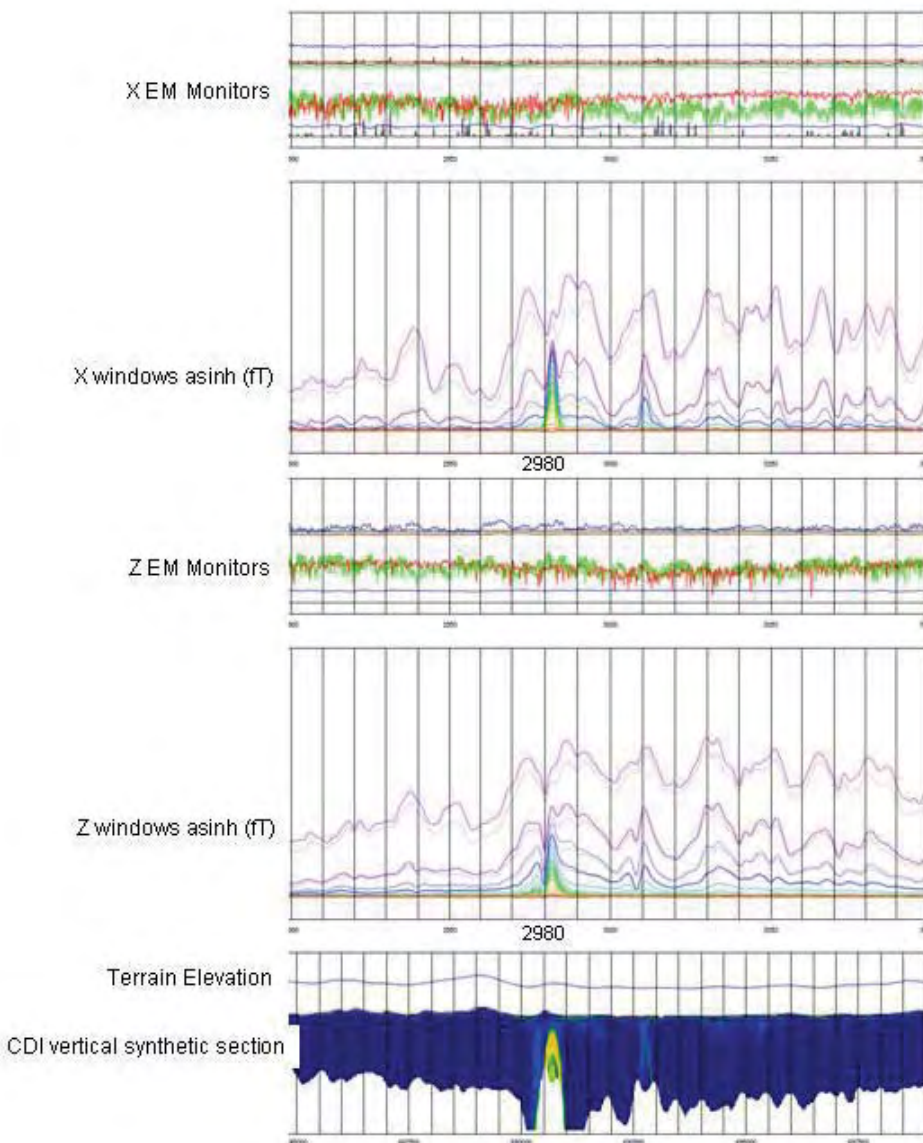


**Figure 5-10:** A section of multiplot 1001501 expanded to highlight the discrete anomaly that is present at fiducial 2980.

The analysis of these confined highly conductive features or anomalies is a valuable exploration method and can be used to interpret target conductors. Since the line spacing in the Pine Creek area was up to 5 km, interpretation of the discrete conductors is limited. Ideally interpretation of discrete conductors is made across several proximal (less than 300m spaced) flight lines and with alternating line direction to allow for detailed correlation for mineral explorers. Copper and base metal mineralisation are often associated with discrete conductors, as are graphite-bearing fault zones which may be prospective for uranium mineralisation.

## 5.8 COMPARISON OF AEM INVERSIONS WITH CONDUCTIVITY LOGS

A conductivity-logging program was conducted in the Pine Creek survey area to assist the interpretation of the survey data. Geoscience Australia would like to acknowledge Camilla Sorensen, the Northern Territory Geological Survey, National Water Commission, the Northern Territory Government Department of

Natural Resources, Environment, The Arts and Sport (in particular Jon Sumner), Cameco Australia (in particular Geoff Beckitt) and Energy Resources of Australia Ltd. for field support, land access and technical information supporting the conductivity logging program. Some of the company data remain “in-confidence” and are not expanded upon further.

Induction conductivity data (referred to as conductivity logs) were acquired in boreholes during April and October 2009 in support of the Pine Creek AEM survey. The data were acquired from 24 boreholes widely distributed across different geological formations. The logs are used to guide the construction of reference models for geophysical inversions of the AEM data, and also to provide an independent dataset for assessing the inversion results.

**Table 5–7** provides location coordinates and depths of the logged boreholes and **Figure 5–11** shows the location of the logged boreholes plotted over the conductance from 0-200 m derived from the AEM data. The conductivity logs collected in the Kombolgie survey area are “in-confidence”, and are not displayed.

The majority of the holes are water bores managed by the Water Resources Branch (WRB) at the Department of Natural Resources, Environment the Arts and Sports, Northern Territory Government. The remaining two bores were located at Moline mine and Mt Todd mine. Most of the holes were cased with PVC, but a few were open holes. The majority of the holes had steel casing in the top several metres, but one hole was steel cased from the surface to 125m, and this hole was only logged from 125-180 m depth.

Induction conductivity logging tools measure the electrical conductivity of the material surrounding the borehole and provide a detailed indication of changes in conductivity with depth. These tools permit measurements of the electrical conductivity of the ground outside PVC cased boreholes - generally without being sensitive to the presence of more conductive borehole fluid within the casing. These tools are capable of making reliable scientific measurements, however, their method of use has not been standardised. The principle of operation of inductive conductivity borehole logging tools (McNeill, 1986 and McNeill *et al*, 1990) and other conductivity logging information can be found in Costelloe *et al.* 2010.

In order to assess the performance of the inversion, we compare the results of the GA–LEI at selected points to the borehole conductivity logs collected in that part of the survey area. There are limitations to this technique (Reid and Vrbancich 2004, Ley-Cooper and Davis 2010) related to the footprint of the conductivity log vs. the AEM footprint.

**Table 5-7:** Coordinates (MGA94 Zone 52 and Zone 53) and depths of 16 boreholes

BOREHOLE	ZONE EASTING	NORTHING	DEPTH (M)
RN08262	52 L 0796125	8431145	184
RN20565	52 L 0720015	8556364	99
RN21556	52 L 0806582	8470008	41
RN21762	52 L 0729148	8622455	73
RN25288	52 L 0756988	8449802	117
RN25669	53 L 0191537	8488081	78
RN25791	52 L 0717316	8493445	300
RN29387	52 L 0718106	8583756	120
RN31324	52 L 0748330	8602179	35

**Geological and energy implications of the Pine Creek airborne electromagnetic (AEM) survey,  
Northern Territory, Australia**

RN32461	52 L 0734537	8584558	47
RN32750	52 L 0803443	8393890	60
RN33035	52 L 0761272	8442954	114
RN33308	52 L 0784191	8421633	118
RN34679	52 L 0733214	8631955	47
RN35972	52 L 0729232	8610354	51
Mt Todd	53 L 0188103	8434470	49

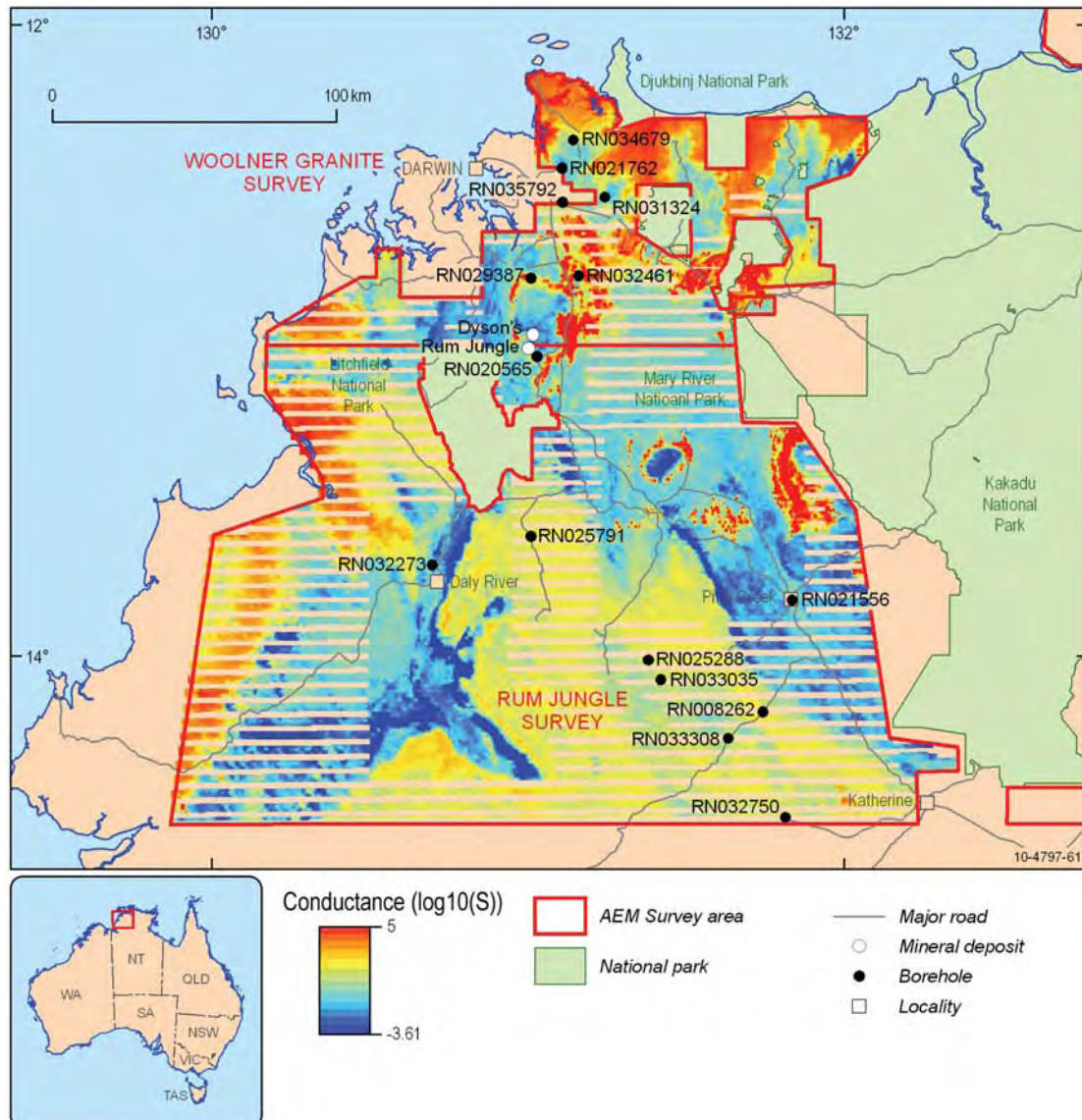


**Figure 5-11:** The location of the boreholes plotted over conductance from 0-200 m

Bore holes were sparse and in many cases not close to flight lines therefore the assessment of logs immediately adjacent to the Geoscience Australia layered earth inversion (GA–LEI) results were limited. Generally the GA–LEI results show agreement with the bore hole logs in close proximity to flight lines. For a full description of the GA–LEI inversion results see Costelloe and Hutchinson (2010). For a full description of the conductivity results see Costelloe, Hutchinson and Sorensen 2010.

## **5.9 REFERENCES**

- Brodie, R. and Fisher, A., 2008. Inversion of TEMPEST AEM survey data, Honeysuckle Creek, Victoria. Geoscience Australia for the Bureau of Rural Sciences, Canberra. Unpublished.
- Brodie, R.C. and Costelloe, M.T., 2010. Kombolgie VTEM™ AEM Survey: Revised EMFlow Conductivity Estimates to 2 km Depth. Geoscience Australia internal report.
- Carter, S., Baron-Hay., Combrinck M. and Moreton M. 2009. Survey and Logistics report on a helicopter borne versatile time domain electromagnetic (VTEM) survey for the Pine Creek (Kombolgie) Project area Northern Territory. Online:  
[https://www.ga.gov.au/products/servlet/controller?event=GEOCAT\\_DETAILS&catno=69230](https://www.ga.gov.au/products/servlet/controller?event=GEOCAT_DETAILS&catno=69230)
- Constable, S., Parker, R. and Constable, C., 1987. Occam's inversion; a practical algorithm for generating smooth models from electromagnetic sounding data. *Geophysics* **52**, 289-300.
- Costelloe, M., 2010. Pine Creek Airborne Electromagnetic Survey Results. ASEG Extended Abstracts 2010.
- Costelloe, M., Craig, M.A., Liu, S.F., Whitaker, A.J. Hutchinson, D.K., 2010. Reducing exploration risk and promoting exploration with results from the Pine Creek airborne electromagnetic survey, Northern Territory.  
[https://www.ga.gov.au/products/servlet/controller?event=GEOCAT\\_DETAILS&catno=70135](https://www.ga.gov.au/products/servlet/controller?event=GEOCAT_DETAILS&catno=70135)
- Costelloe, M and. Hutchinson, D. 2010. Woolner Granite and Rum Jungle TEMPEST™ AEM Survey: Inversion Report. Geoscience Australia internal report. Online:  
[https://www.ga.gov.au/products/servlet/controller?event=FILE\\_SELECTION&catno=70584](https://www.ga.gov.au/products/servlet/controller?event=FILE_SELECTION&catno=70584)
- Costelloe, M.T., Hutchinson, D.K. and Sorensen, C. 2010. Logistics report for down-hole conductivity logging in the Pine Creek AEM Survey area, Northern Territory, 2008.
- Hutchinson, D. K., Roach, I. C. and Costelloe, M. T., 2010a. Reducing Exploration Risk for Airborne Electromagnetic Surveys in the Paterson Region, WA and Pine Creek, NT. In: *Australian Society of Exploration Geophysicists Abstracts*, Sydney.
- Hutchinson, D. K., Roach, I. C. and Costelloe, M. T., 2010b. Depth of Investigation Grid for Regional Airborne Electromagnetic Surveys. *Preview April 2010*(**145**), 38-39.
- Lane, R., Brodie, R. and Fitzpatrick, A., 2004a. Constrained inversion of AEM data from the Lower Balonne area, Southern Queensland, Australia. Cooperative Research Centre for Landscape Environments and Mineral Exploration, Perth. **Open File Report 163**. Online:  
<http://crcleme.org.au/Pubs/OFRSindex.html>
- Lane, R., Brodie, R. and Fitzpatrick, A., 2004b. A revised inversion model parameter formulation for fixed wing transmitter loop – towed bird receiver coil time-domain airborne electromagnetic data. In: *ASEG 17th Geophysical Conference and Exhibition*, Sydney.
- Lane, R., Green, A., Golding, C., Owers, M., Pik, P., Plunkett, C., Sattel, D. and Thorn, B., 2000. An example of 3D conductivity mapping using the TEMPEST airborne electromagnetic system. *Exploration Geophysics* **31**(2), 162-172.
- Lane, R. and Worrall, L., 2002. Interpretation of Airborne Electromagnetic Data: Summary report on the Challenger Workshop. Geoscience Australia Gawler Craton Mineral Promotion Project Canberra. *Geoscience Australia Record* **2002/2**.
- Lawrence, M. and Stenning, L., 2009a. Woolner Airborne Electromagnetic (AEM) Mapping Survey Acquisition and Processing Report for Geoscience Australia. Unpublished report. Lawrence,

- M. and Stenning, L., 2009b. Rum Jungle Airborne Electromagnetic (AEM) Mapping Survey Acquisition and Processing Report for Geoscience Australia. Unpublished report.
- Ley-Cooper, Y. and Davis, A., 2010. Can a borehole conductivity log discredit a whole AEM survey? *ASEG Extended Abstracts* 2010.
- Macnae, J., King, A., Stoltz, N., Osmakoff, A. and Blaha, A., 1998. Fast AEM processing and inversion. *Exploration Geophysics* 29, 163-169.
- McNeill, J. D., 1986. Geonics EM39 borehole conductivity meter-theory of operation. Geonics Ltd, Mississauga, Ontario. Technical Note 20(11). Online: <http://www.geonics.com/pdfs/technicalnotes/tn20.pdf>.
- McNeill, J. D., Bosnar, M. and Snelgrove, F. B., 1990. Resolution of an electromagnetic borehole conductivity logger for geotechnical and ground water applications. Geonics Limited, Mississauga, Ontario. Technical Note TN-25, 29 p. Online: <http://www.geonics.com/pdfs/technicalnotes/tn25.pdf>.
- Reid, J. E. and Brodie, R. C., 2006. Preliminary inversions of Honeysuckle Creek airborne electromagnetic data: Comparison with borehole conductivity logs and previously derived conductivity models. Geoscience Australia for the Bureau of Rural Sciences. Unpublished report.
- Reid, J. E. and Vrbancich, J., 2004. A comparison of the inductive-limit footprints of airborne electromagnetic configurations. *Geophysics* 69, 1229-1239.
- Richardson, M.L., Brodie R., Costelloe M. and Sorensen, C., 2008. Assessment of AEM systems for the Pine Creek survey. Unpublished GA internal report (in-confidence).
- Smith, R. S., 2001. On removing the primary field from fixed wing time-domain airborne electromagnetic data: some consequences for quantitative modelling, estimating bird position and detecting perfect conductors. *Geophysical Prospecting* 49, 405-416.
- Smith, R.S. and Annan, P., 2000. Using an induction coil sensor to indirectly measure the B-field response in the bandwidth of the transient electromagnetic method: *Geophysics*, 65, 1489-1494.
- Survey area, Western Australia, September 2008. Geoscience Australia. Unpublished report.
- Sorensen, C. and Lane, R., 2007b. Guidelines for conductivity borehole logging procedures. Geoscience Australia. Unpublished report.
- Stoltz, E. and Macnae, J., 1998. Evaluating EM waveforms by singular-value decomposition of exponential basis function. *Geophysics* 63, 64-74.

# 6 Geological interpretation of AEM data

*S.F. Liu, M.A. Craig, and N.C. Williams*

## 6.1 INTRODUCTION

This chapter presents geological interpretations of the Pine Creek AEM data. The interpretations will focus on: (1) correlation of AEM data with major geological features such as stratigraphic units and structures including faults and folds; and (2) the AEM data's contribution to defining the architecture of the geological provinces in the area, particularly their boundaries (*e.g.*, unconformities). The limitations of the data and the care that should be exercised in interpretation in some cases will also be discussed.

This chapter describes the interpretation methods, datasets used, the correlation of AEM anomalies with selected geological features, and the geological interpretation of AEM data in major geological provinces.

**Table 6-1:** Selected AEM datasets for geological interpretation in the Pine Creek area

DATASET	COMMENTS
Conductance map	Helpful for understanding the overall conductivity of different geological regions and delineating major geological features
Conductivity sections	Graphic displays of conductivity, allows convenient correlations with geological features: Geoscience Australia – Layered Earth Inversion (GA–LEI) – derived conductivity sections for the Woolner Granite – Rum Jungle surveys; and EM Flow™ conductivity sections for Kombolgie survey.
Multiplots	Allow close examination of various aspects of the AEM data

**Table 6-2:** Other selected datasets used in geological interpretation in the Pine Creek area

DATASET	COMMENTS
Surface geology mapping	1:250 000 and 1:100 000 surface geology mapping by NTGS and BMR; and 1:1 000 000 surface geology compilation by GA
Solid geology	1:500 000 solid geology interpretation by NTGS (2005); new basement solid geology maps in this study, <i>i.e.</i> , pre-Kombolgie, pre-Depot Creek and pre-Daly Basin solid geology maps
Regolith geology	From Craig (2006) and surface geology mapping
Satellite image	For correlation with near surface features
Drill hole data	To assist validation and interpretation of AEM conductivity data, particularly discrete anomalies

## **6.2 DATASETS, INTERPRETATION METHODS AND ARTEFACTS**

For the Pine Creek region, two AEM survey systems were used i.e., TEMPEST<sup>TM</sup> for the Woolner Granite – Rum Jungle areas and VTEM<sup>TM</sup> for the Kombolgie area (see [Chapter 5](#)). A number of derivative AEM datasets are used for geological interpretations in conjunction with other spatial data including surface and solid geology and remote sensing data, which are listed in [Table 6–1](#) and [Table 6–2](#).

The primary focus of geological interpretation of AEM data is for correlation with geological features and defining the architecture of geological provinces, particularly sedimentary basins, for the top few hundred metres (in most cases). These features are often not evident in other geological or geophysical datasets.

The following sections provide a brief summary of the data used for interpretations, including the inversion methods employed.

### **6.2.1 EM Flow<sup>TM</sup> and GA's Layered Earth Inversion (GA–LEI) data**

The vertical AEM conductivity sections are most useful for geological interpretations because of their graphic presentation of conductivity that allows convenient correlation with geological features. For the Woolner Granite–Rum Jungle surveys flown using TEMPEST<sup>TM</sup>, GA has released two sets of such sections, namely, EM Flow<sup>TM</sup> (Macnae *et al.* 1998, Stoltz *et al.* 1998) and GA–LEI (Lane *et al.* 2004) conductivity sections. However, initially only EM Flow<sup>TM</sup> conductivity sections were available for interpretation of the Kombolgie survey. During the final preparation of this report GA–LEI conductivity sections became available for interpretation. Some analysis is included in this report (See [section 6.4](#)).

The EM Flow<sup>TM</sup> software package is a fast approximate transformation method that produces a quasi-layered estimate of the subsurface conductivity (see [Chapter 5](#)). For the TEMPEST<sup>TM</sup> system, this involves separation of the measured total field response into primary and secondary fields, with the primary field due to direct coupling between the transmitter (TX) and receiver (RX) and secondary field due to eddy currents induced in the ground.

The GA–LEI method does not rely on the primary field separation and the geometry estimates made in the standard FAS data processing of AEM data. Instead, the GA–LEI inverts the total field data (both primary and secondary) directly (see [Chapter 5](#)).

Those interpreting the two datasets need to be aware of the assumptions and models in both EM Flow<sup>TM</sup> and GA–LEI processing. For the TEMPEST<sup>TM</sup> system, the EM Flow<sup>TM</sup> processing assumes that the subsurface is resistive at depth, while the GA–LEI uses a layered earth model of 30 layers and the estimated conductivity model is constrained to be vertically smooth and to be as close as possible to a reference conductivity model.

In the process of inversion modelling, the GA–LEI method starts with a reference conductivity value, and then inputs different conductivity values for each layer, and attempts to best fit the measured and modelled conductivity values. How well the two sets of data fit is reflected in the Percentage Data Influence (PDI, [Chapter 5](#)). A 100% value of the PDI means the inversion is totally data-driven, while 0% means the inversion is totally model-driven.

Hutchinson *et al.* (2010) introduced a concept of Depth of Investigation (DOI). The DOI is defined as the depth at which the PDI is 50%. Above the DOI, where PDI is greater than 50%, the inversion is considered relatively robust. The DOI should be regarded as indicative depth of reliable data according to the GA LEI modelling.

In a layered earth situation, such as sedimentary basins in which the sedimentary rocks are sub-horizontal, both EM Flow<sup>TM</sup> and GA–LEI modelling provide meaningful conductivity data at depth. Geological interpretations can be reliably made. In areas of folded sequences, however, particularly in areas of tightly to upright isoclinally folded sequences like the Pine Creek Orogen, both EM Flow<sup>TM</sup> and GA–LEI modelling may fail because of their assumptions using models of a horizontally layered earth.

In such folded areas the geological units may be steeply dipping or nearly vertical, which are not modelled in the layered earth assumptions for both EM Flow™ and GA–LEI modelling. Thus, caution should be exercised when interpreting AEM data, either EM Flow™ or GA–LEI, in areas of folded geological sequences. The EM Flow™ conductive section always has a resistive basement and therefore may give a false impression that the rocks at depth are resistive. The GA–LEI method may not be able to fit the measured and modelled data, thus giving low PDI values. In highly conductive areas, the DOI may be shallow. We may not be able to “see” much below the strong conductors thus, meaningful interpretation may be difficult below the DOI. More discussions will be presented in relevant sections of interpretation.

### **6.2.2 TEMPEST™ vs VTEM™ data for geological interpretation**

The technical aspects of the TEMPEST™ and VTEM™ AEM surveys are described in detail in [Chapter 5](#) of this report.

In relation to the geological interpretations of the AEM data, the characteristics of these two AEM survey methods are summarised in [Table 6–3](#).

**Table 6–3:** Characteristics of TEMPEST™ and VTEM™ data for geological interpretation

FEATURE	TEMPEST™	VTEM™
High conductivity body	Well detected and reveal details	Well detected
Low conductivity body	Well detected and reveal details	Well detected to greater depth in resistive areas
Level of detail	Reveals fine detail	Broader feature; subtle details may not always be revealed
Depth of investigation	Down to 400-500 m	Down to 2 km in resistive areas

### **6.2.3 The influence of man-made features on conductivity**

A number of man-made features such as powerlines (Lawrence and Stenning, 2009), gas pipelines and railways, may have significant effects on AEM data because of their extremely high conductivity, or because they produce their own electromagnetic fields. This may confuse the geological interpretation of AEM data.

When interpreting AEM data it is important to pay attention to man-made structures, particularly powerlines, railways and gas pipelines, which may cause multiple anomalies. The effects of other man-made structures, such as buildings, tailings, heap leach pads, ponds and roads, or anything that may have conductivities different from the undisturbed geology, will also need to be considered.

For example, the Pine Creek Shear Zone trends north-westerly through the vicinity of Pine Creek Township. The apparent conductivity anomalies in the vicinity of the known linear Shear Zone could be interpreted to reflect enhanced conductivities along the Shear Zone. However, after closer examination, the cause of these apparent conductivity anomalies was correctly attributed to known major powerlines and a major gas pipeline.

The most spectacular display of the effects of powerlines on conductivity is depicted in the 1.67 km line spacing AEM sections northwest of Pine Creek Township ([Figure 6–1](#)). This area is largely very resistive, being Jim Jim Suite granites and Burrell Creek Formation. There are a few weak anomalies in the area. However, there is an array of conductivity anomalies right under the northwest-trending powerlines from

Pine Creek. Each AEM section shows two to three conductivity anomalies under the powerlines. The anomalies may spread up to 900 m across at the base of the AEM section, but they point to the position of the powerlines at the top of section. The cause of these conductivity anomalies cannot be mistaken for a geological effect because of the close spatial correlation between the powerlines and the gas pipeline, and the conductivity anomalies.

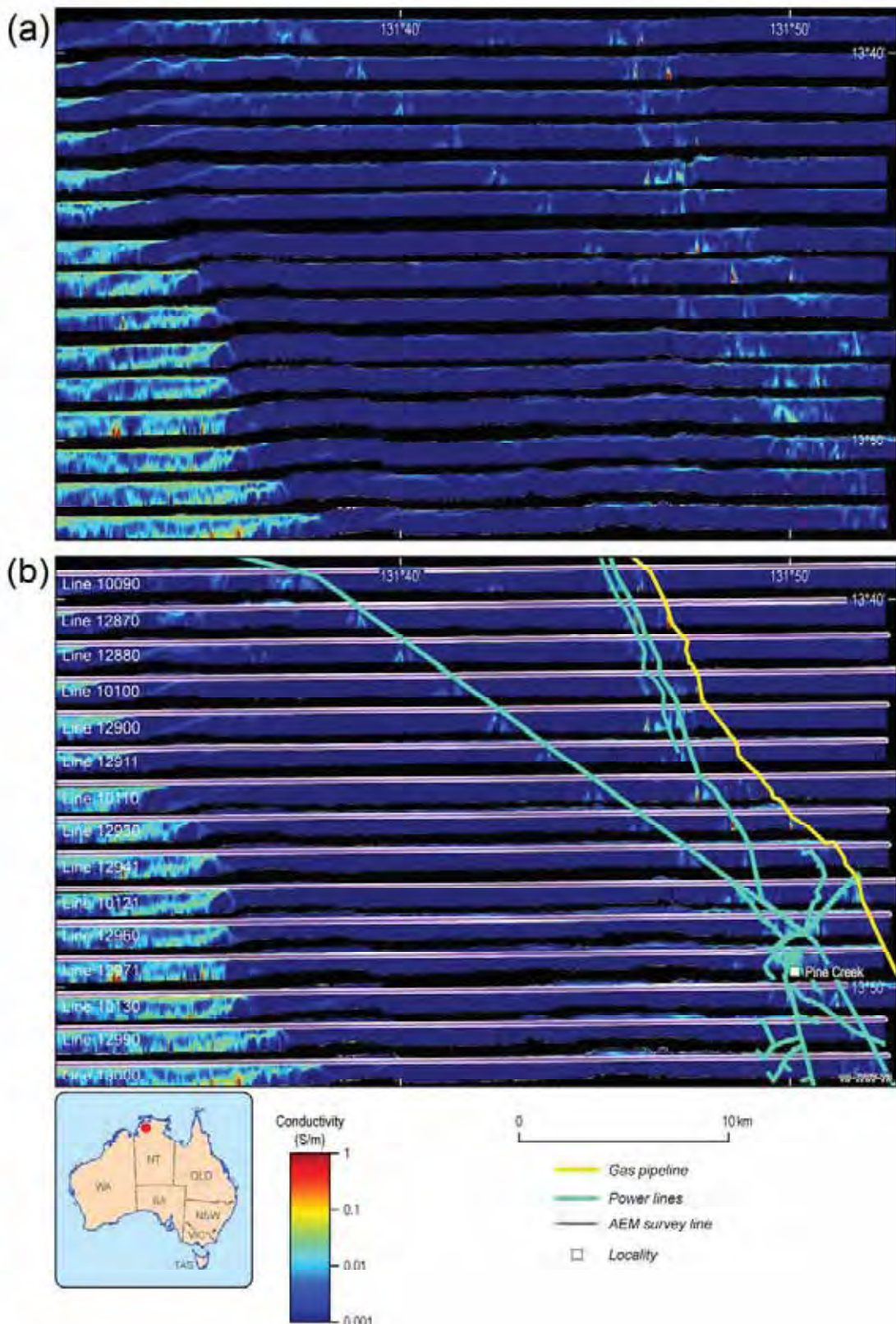


**Figure 6-1:** (a) Apparent conductivity anomalies in the vicinity of the Pine Creek shear Zone. (b) Correlation between the apparent conductivity anomalies and the location of powerlines and pipelines. Conductivity sections displayed at three times vertical exaggeration.

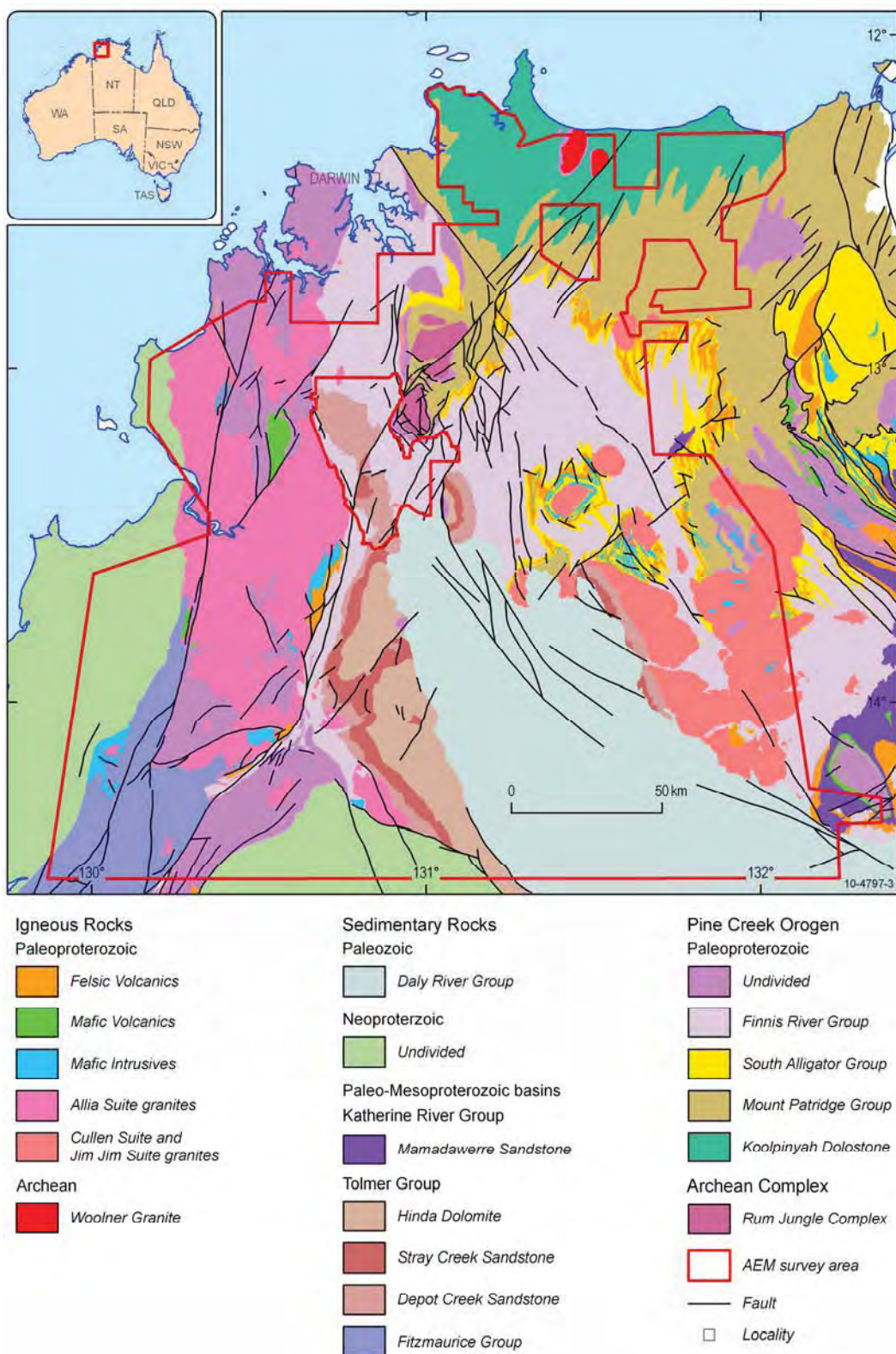


**Figure 6-2:** Solid geology of the Woolner Granite – Rum Jungle AEM survey area in the Pine Creek Orogen (simplified from NTGS, 2005)

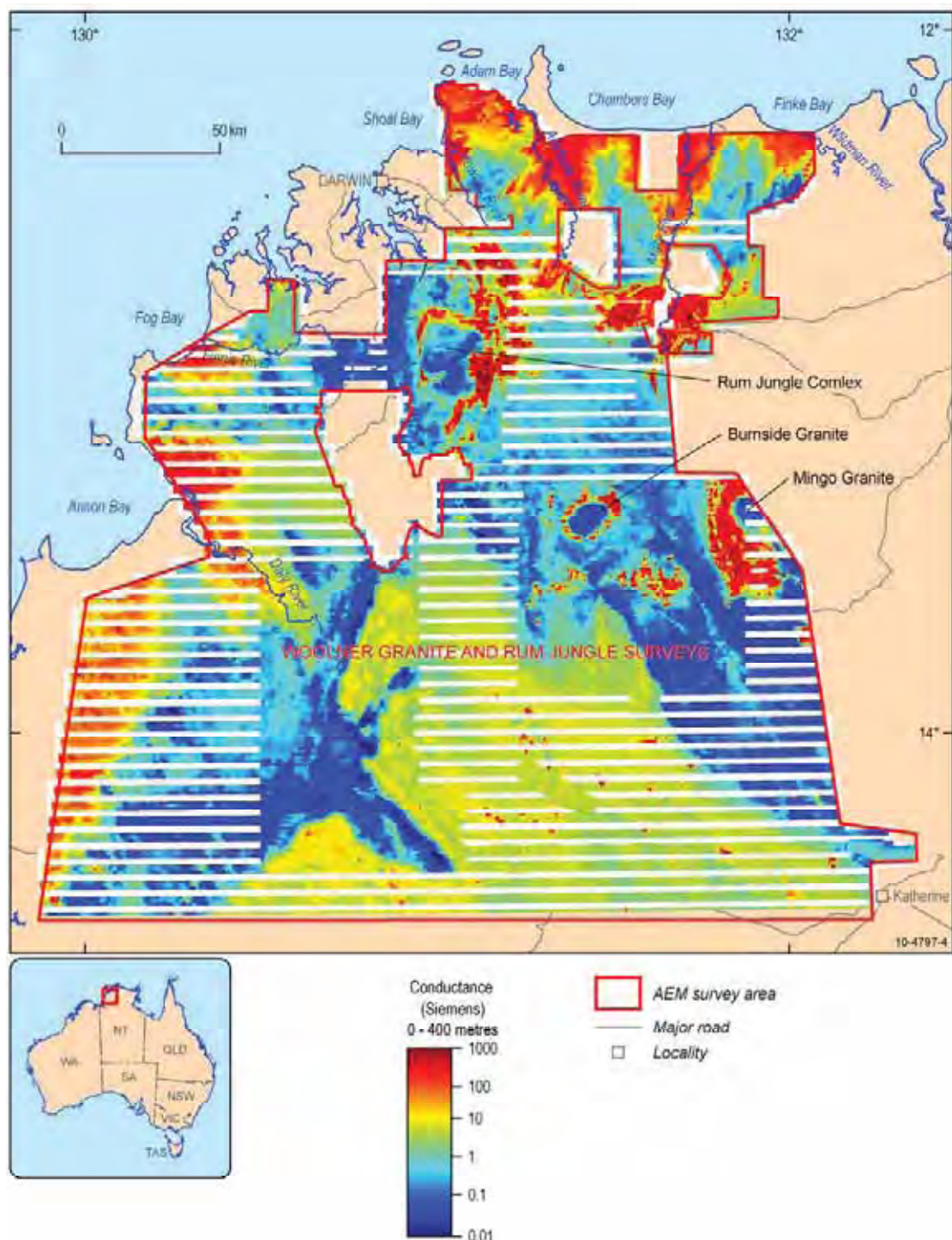


Figure 6-3: Conductance image (0-400 m) of Woolner Granite – Rum Jungle AEM survey area by TEMPEST™. Note resistive granite plutons rimmed by more conductive metasedimentary rocks.

## **6.3 GEOLOGICAL INTERPRETATION OF THE TEMPEST™ DATA IN THE WESTERN PINE CREEK REGION**

In the following sections we will first outline the major AEM conductivity signatures of different geological provinces ([Section 6.3.1](#)). Correlations of the AEM conductivity data with a number of known geological and hydrological features are presented in [Section 6.3.2](#). This is followed by the interpretations of unconformities and geological provinces within the TEMPEST™ data ([Section 6.3.2.7](#)). In general, the interpretations will start with near-surface features such as regolith and move onto deeper or older geological features or provinces. Although some anomalies will be examined in detail, in general, interpretations will be regionally focussed.

### **6.3.1 AEM signatures of geological provinces**

The regional geology of the Pine Creek AEM survey areas have been summarised in [Chapter 3](#). A generalised solid geology map of the western Pine Creek AEM survey area is presented in [Figure 6–2](#). The total calculated electrical conductance of the earth 0 to 400 m in the Woolner Granite – Rum Jungle area is shown in [Figure 6–3](#). Major AEM signatures of geological provinces in the Pine Creek region are summarised in [Table 6–4](#).

Strong conductors include carbonaceous and pyritic sediments, such as parts of the Koolpin, Whites and Cahill formations in the Pine Creek Orogen. Other sedimentary units may be weakly to moderately conductive, such as parts of the Daly River, Auvergne and Tolmer groups in the Daly Basin, Victoria Basin and Birrindudu Basin respectively. Coastal areas may be moderately to highly conductive because of saltwater ([Figure 6–3](#)). Granites and sandstones are generally resistive to very resistive.

**Table 6–4:** Major AEM signatures of geological provinces in the Pine Creek area

<b>REGION</b>	<b>AEM SIGNATURES</b>
Coastal areas	Broad, moderate conductivity anomalies. For example: Low part of Daly River on Cape Scott; Fog Bay; south and east of Shoal Bay; Adam Bay – lower part of Adelaide River; flat plains south of Adams Bay, Chambers Bay and Finke Bay
Bonaparte Basin	Broad, sub-horizontal, moderate conductors
Daly Basin	Broad, sub-horizontal, moderate conductors, with isolated discrete strong conductors
Victoria Basin	Broad, sub-horizontal, moderate conductors
McArthur Basin	Generally resistive, with sub-horizontal, weak conductors
Fitzmaurice Basin	Generally resistive, with weak to moderate conductors
Pine Creek Orogen	Linear high conductivity anomalies in a generally low conductivity background
Archean complexes	Generally resistive, with discrete weak to moderate conductors

### **6.3.2 Correlation of AEM conductivity data with geological features**

In this section AEM conductivity data are presented showing correlations with a number of selected geological and hydrological features.

Given the importance of unconformities, particularly for unconformity-related uranium mineral systems, these will be discussed in a separate section ([Section 6.3.2.7](#)). Interpretations are aimed at regional correlation of AEM data with geological features, not individual anomalies which are the focus of exploration companies.

### **6.3.2.1 Coastal areas**

Coastal areas feature moderate to high conductivities in relation to incursion of sea water including the areas of Anson Bay and Daly River, Fog Bay, Shoal Bay and Howard River, Adam Bay and Adelaide River, Chambers Bay and Mary River, and Finke Bay ([Figure 6–3](#)). The effects of saline water are also mostly restricted to the depth of the sedimentary strata. The effects of saline intrusions are visible in AEM depth and elevation slices, especially near the coast and along major river systems. These effects are discussed, and their relationship with regolith materials is highlighted in the following section.

### **6.3.2.2 Regolith and related features**

#### **6.3.2.2.1 Regolith Character and distribution**

Most of the regolith materials exposed at the surface in the Pine Creek AEM survey area are *in situ* regolith types. The dominant *in situ* material is saprolith, which is a combination of weathered and partially weathered rock more formally known as saprolite and saprock ([Figure 6–4](#)). The remainder of the exposed regolith in the survey area is either pedolith (residual materials; [Figure 6–5](#)) or a variety of transported regolith. The main transported materials are alluvial and coastal deposits ([Figure 6–6](#)).

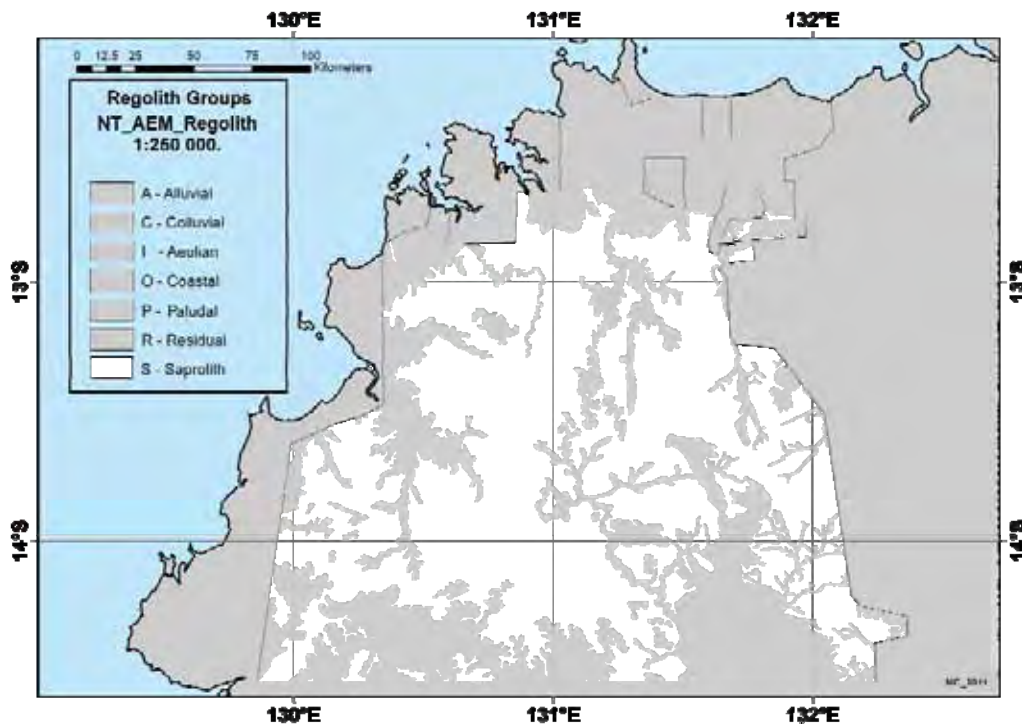


**Figure 6–4:** The distribution of saprolith throughout the Woolner–Rum Jungle AEM survey area, represented by white polygons. Non-saprolith materials are shown in grey.

#### **6.3.2.2.2 General observations**

##### **6.3.2.2.1 Transported regolith**

In the case of transported regolith, highly conductive AEM signatures immediately below the position of mapped coastal alluvial regolith ([Figure 6–6](#)), indicate sea water intrusion. This effect is present from 0–5 m depth and peaks by 20 m depth. Some sea water intrusion effects persist to about 60 m but by 100 m they are almost undetectable.

**Geological and energy implications of the Pine Creek airborne electromagnetic (AEM) survey, Northern Territory, Australia**

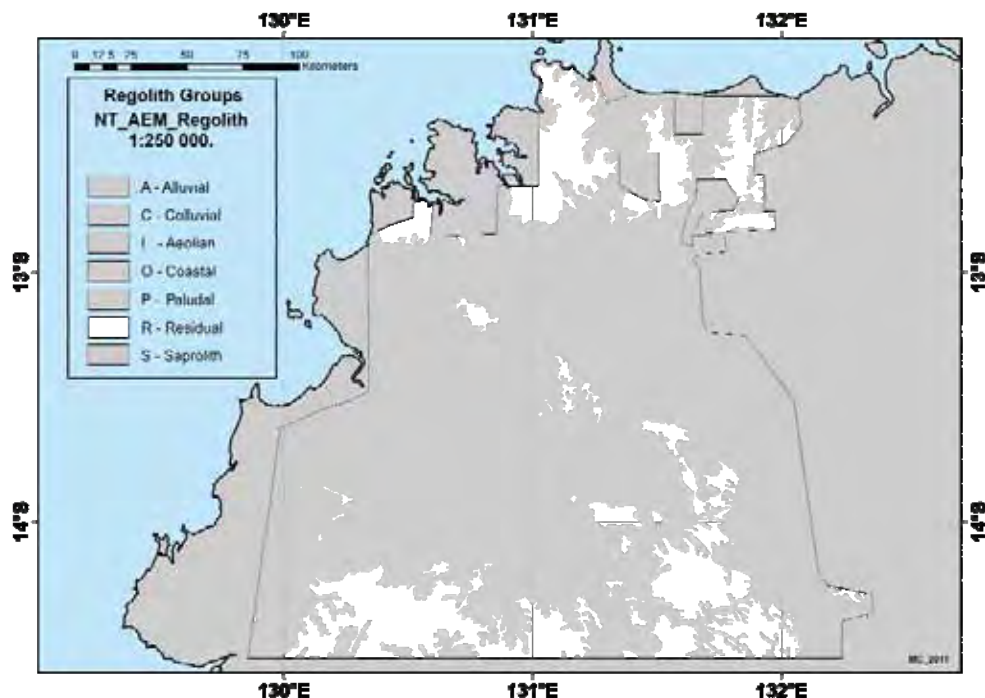


**Figure 6–5:** Regolith-landform polygons (in white) indicate the mapped distribution of residual regolith (pedolith) materials throughout the Woolner and Rum Jungle AEM survey areas. Grey areas represent non-residual materials both inside and outside the survey areas. In subsequent figures, white polygons, when made transparent, serve as windows through which the underlying AEM responses at various depths below the regolith may be examined and assessed.

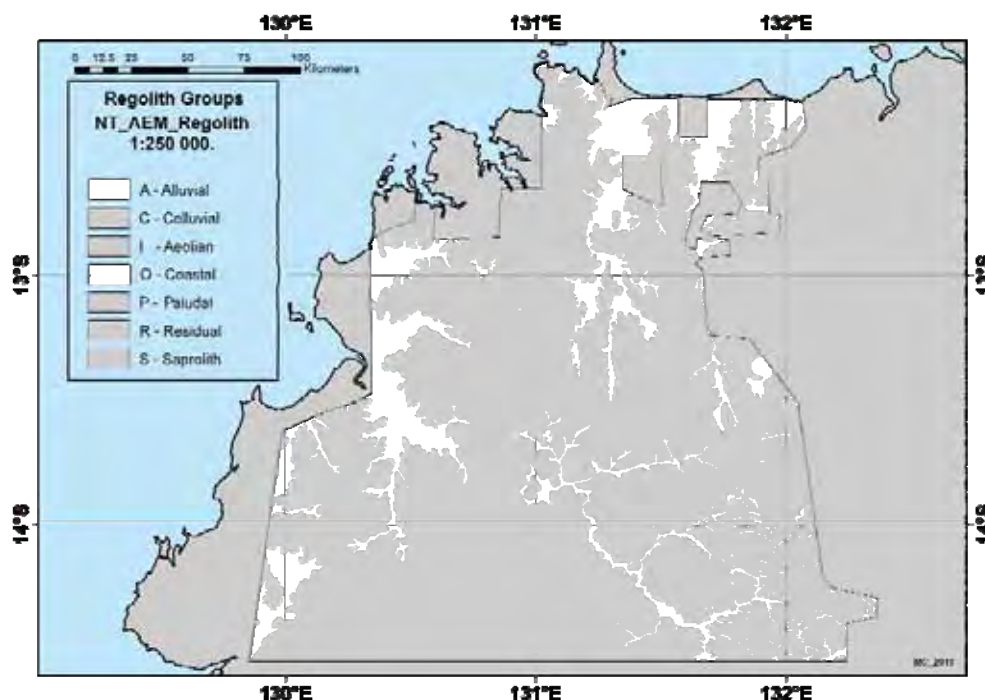


**Figure 6–6:** The distribution of alluvial and coastal regolith materials within the survey area is shown in white. All other regolith polygons are masked by grey. In subsequent figures, white polygons, when made transparent, serve as windows through which the underlying AEM responses at various depths below the regolith may be examined and assessed.

#### 6.3.2.2.2.2 Pedolith

Residual regolith materials (collectively mapped as pedolith i.e., ferricretes; “lateritic” materials, ferruginous nodules and pisoliths) mainly coincide with highly resistive AEM signatures and are especially prominent in near surface AEM depth slices. At greater depths, the more conductive effects of the deeper saprolith begin to emerge. Immediately below mapped pedolith positions, near the coast, highly conductive AEM signatures indicate that sea water intrusion becomes apparent at about 20 m depth and peaks at depths somewhere between 60 to 80 m.

#### 6.3.2.2.2.3 Saprolith

In the upper parts of the saprolith, especially close to the base of any mapped pedolith, AEM signatures show highly resistive patterns. However, as depth increases below the pedolith interface, the regolith becomes more conductive. These changes are not universal and are not the same for all regolith. They will vary according to the nature of the parent rock types, the degree and depth of weathering, and the amount of pedolith development involved. Eventually the lower unweathered part of the regolith profile is encountered. Here, deeper in the saprock part of the saprolith, the AEM signatures show that the regolith becomes progressively more resistive as it approaches the unweathered bedrock.

#### 6.3.2.2.3 Assessments of gridded data (depth slices)

##### 6.3.2.2.3.1 Transported regolith

The *alluvial and coastal* regolith materials shown in [Figure 6–6](#) are used here to provide windows through to the conductivity slices. In [Figure 6–7](#), the bluish tones (low conductance) relate to upland parts of the landscape whereas the higher conductance areas relate to lower parts of the landscape, especially the seaward fringe of the costal plain. The results indicate that highly conductive materials are present in the lower parts of the landscape and across the coastal plain. The influence of sea water is likely to be the most significant contributor to those higher conductivity responses occurring closer to the coast.

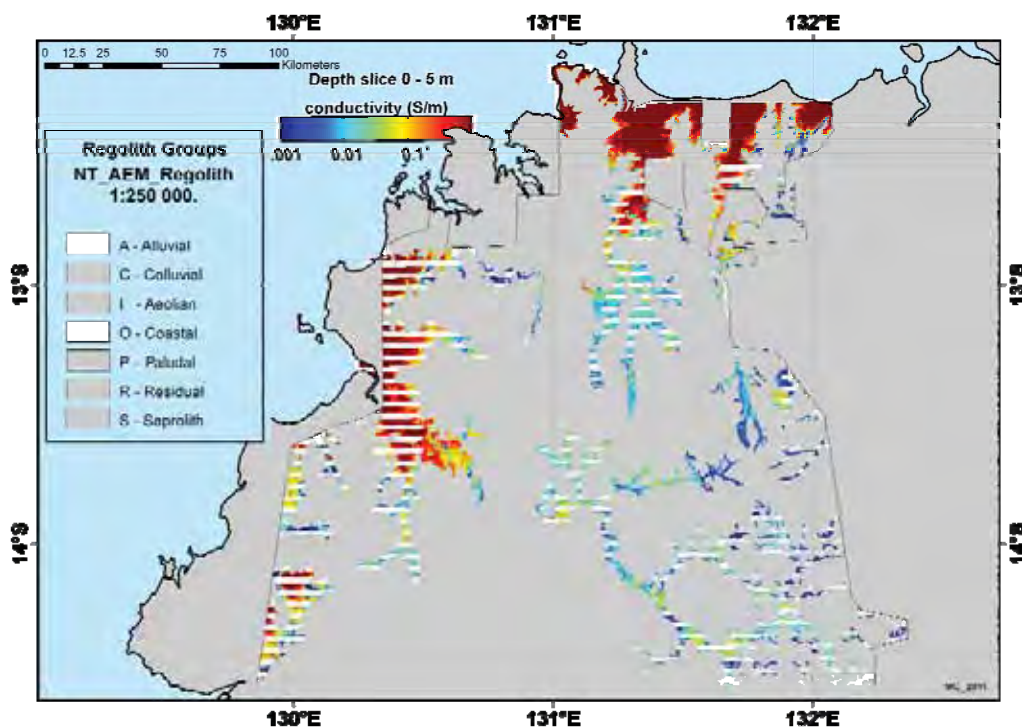


**Figure 6–7:** The GA-LEI conductivity image from 0–5 m highlighting high conductivity areas associated with the position of alluvial and coastal materials along the coastal plain, especially to the north and to the east, nearer the coastal fringes.

These highly conductive areas, highlighted in red in [Figure 6–8](#), may also be associated with saprolith that is not exposed at the surface but which may be present beneath the alluvial blanket. In the near coastal areas, it is most likely that the high conductivity responses result from the influence of saline water incursions along the coastal plains.

Areas of low conductivity probably represent the responses from less weathered materials in watersheds of the upper parts of the landscape. At greater depths ([Figure 6–8](#), [Figure 6–9](#) and [Figure 6–10](#)), the conductivity progressively declines, and is interpreted to indicate the declining influence of seawater saturation.

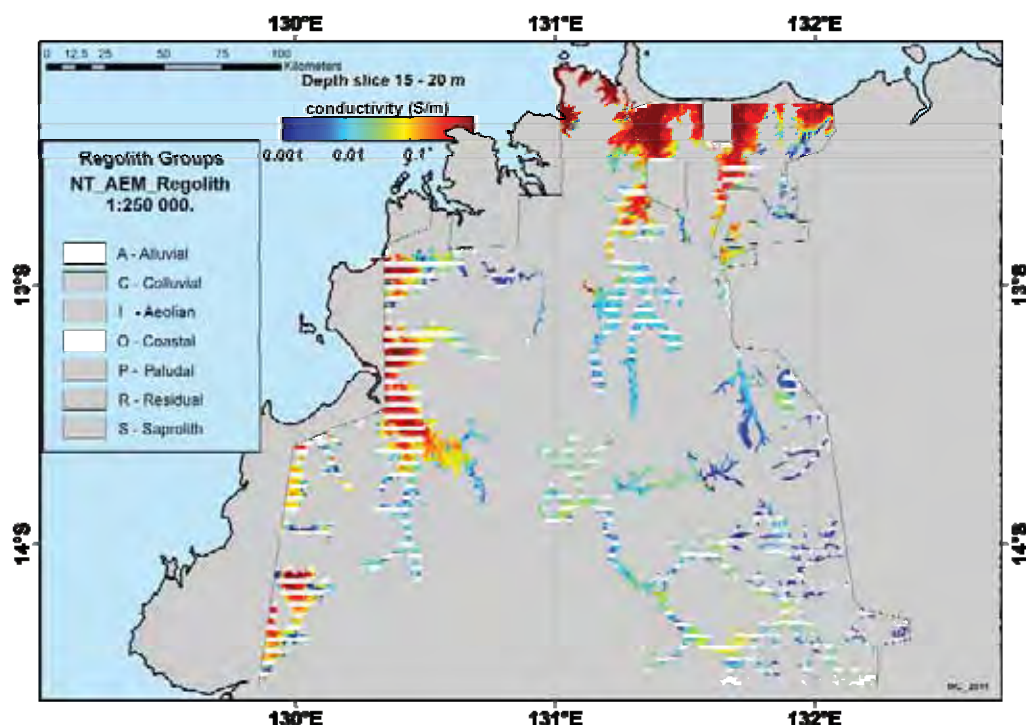


**Figure 6–8:** GA-LEI conductivity responses at the 15-20 m depth interval. These are slightly lower than those responses occurring at similar locations in the 0-5 m interval. Reduced conductivity responses are more obvious along the northern coastal plain and are present but to a lesser extent elsewhere across the survey area.

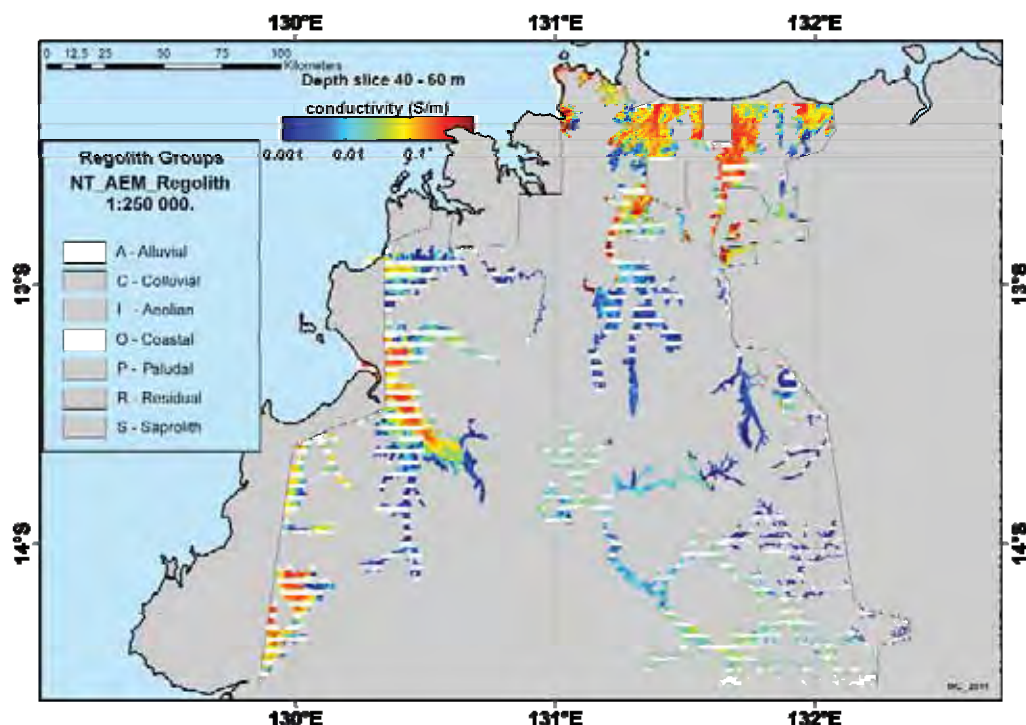


**Figure 6–9:** GA-LEI conductivity responses in the 40-60 m depth slice. This image shows the greatest decline in conductivity in areas previously most conductive at shallower intervals.

The decline in conductivity seen in the responses in [Figure 6–9](#) is likely the result of reduced pore space in the bedrock or saprolite at depth and a corresponding reduction in the influence of saline water. It is possible, although less likely, that the underlying saprolith is, alone, simply not as conductive as the near surface regolith materials even if affected by seawater. At 40-60 m depth, upland areas show a slight increase in resistivity. The simplest explanation for this change is that with increased depth, there is less weathering, pore spaces are smaller and therefore the materials become more resistive. In [Figure 6–10](#), conductivity decline is greatest near the coast suggesting at this depth sea water incursion is relatively low because it is saprock or fresh bedrock.

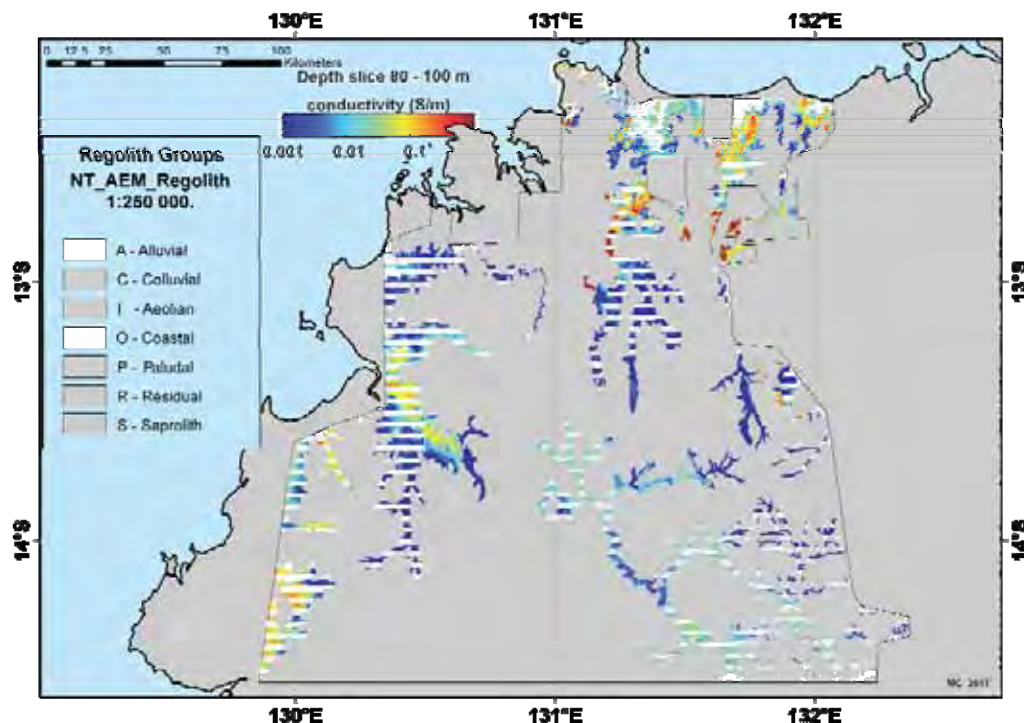


**Figure 6–10:** GA-LEI conductivity depth slice 80-100 m viewed through windows through transparent coastal and alluvial regolith polygons. Conductivity continues to decline significantly possibly due to reduced pore spaces in weathered rocks and reduced influence of seawater. No other significant anomalies are observed in this image.

#### 6.3.2.2.3.2 Pedolith

From [Figure 6–11](#) to [Figure 6–14](#), the distribution of residual regolith materials (pedolith) provides “windows” through to the corresponding parts of the GA-LEI conductivity depth slices.

Very small areas in [Figure 6–11](#) indicate moderate conductivity and are likely to represent areas of thin or eroded pedolith, especially where the areas are inland. However, near the coast, the effects may represent seawaters present in regolith in lower parts of the landscape.

Along the coast, more-conductive areas are present ([Figure 6–12](#)) and are likely due to a more conductive saprolith immediately beneath the pedolith, the presence of substantial saline water wedges extending into the coastal plains, or saline wetted or saturated saprolith. Inland, the change is less significant and may indicate an increase in conductivity due mainly to the presence of a more conductive saprolith in the higher parts of the landscape.

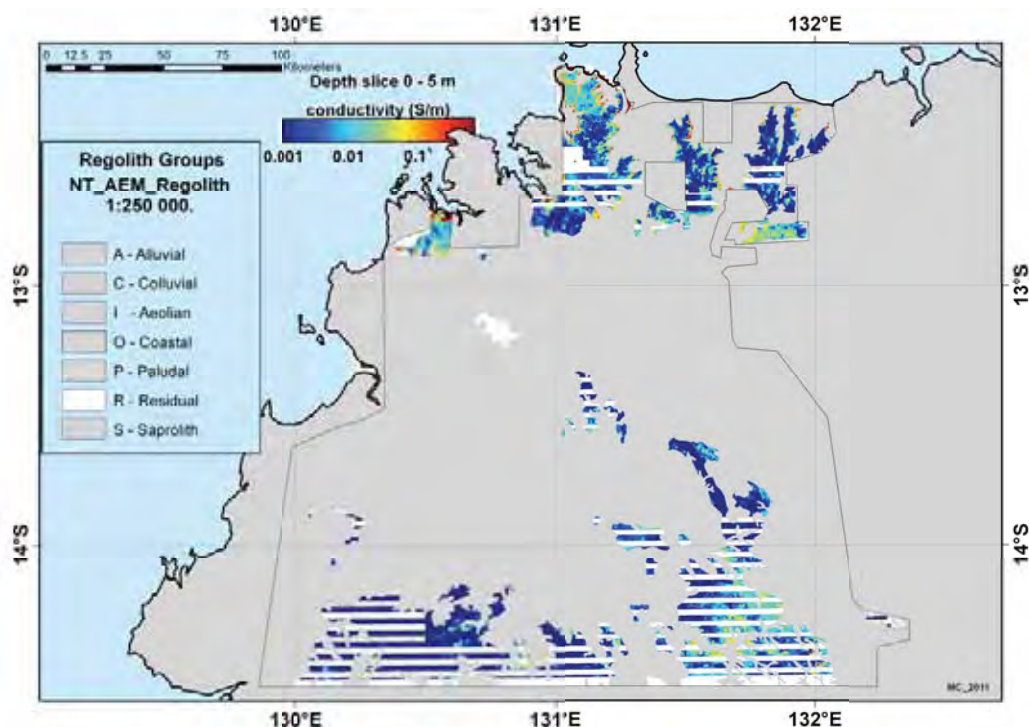


**Figure 6–11:** GA–LEI conductivity depth slice 0–5 m. The location of pedolith provides windows through to the conductivity depth slice images. The conductivity slice in this image represents the very resistive pedolith exposed at the surface and persisting at least to a depth of 5 m.

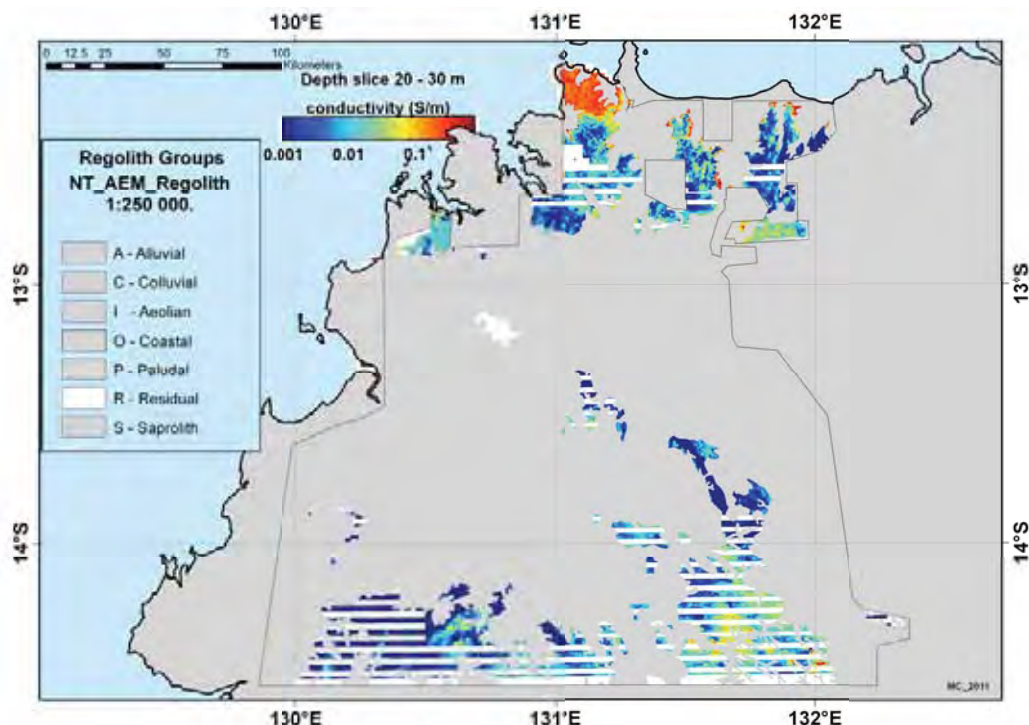


**Figure 6–12:** GA–LEI conductivity depth slice 20–30 m. Windows show that beneath the pedolith there are significant areas of moderate to highly conductive materials present within the 20–30 m depth slice.

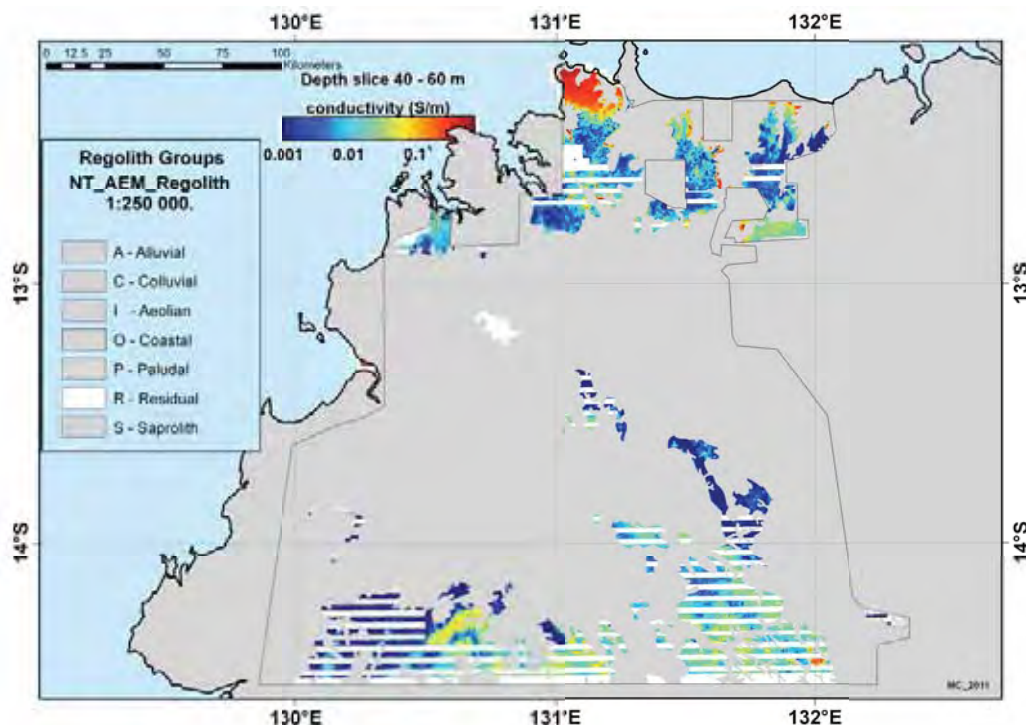


**Figure 6–13:** GA–LEI conductivity responses in the 40–60 m depth slice. Conductivity in this interval has continued to decline and is interpreted to correspond with the decline of saline saturated regolith. Elsewhere, away from the coast, there is a marked increase in non-conductive saprock.

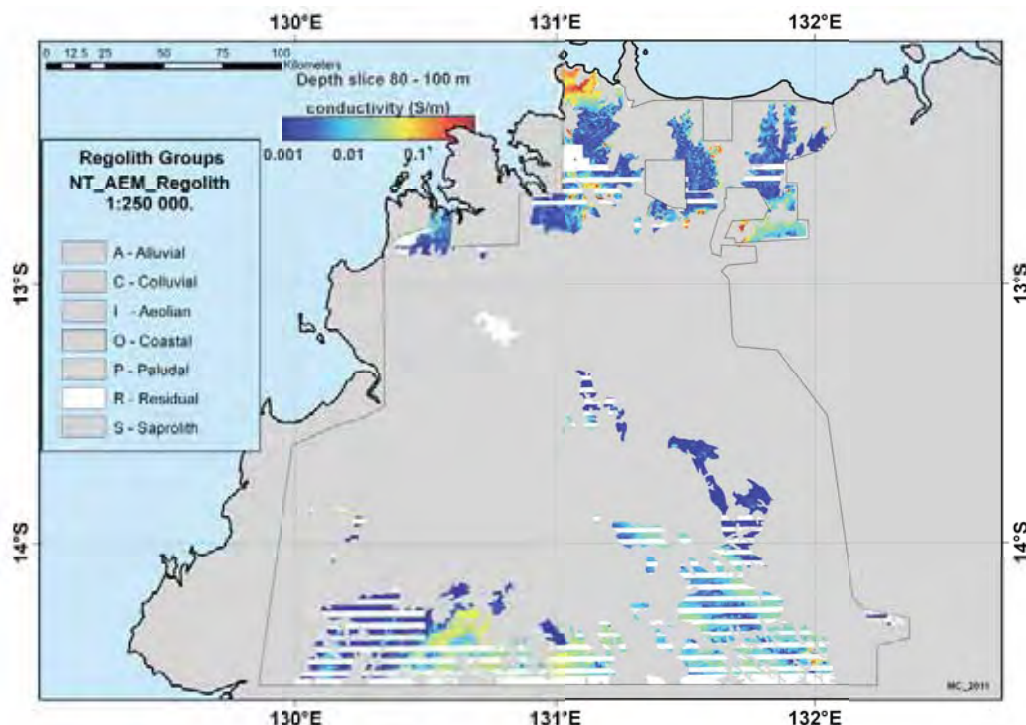


**Figure 6–14:** GA–LEI conductivity responses in the 80–100 m depth slice. At greater depths (80–100 m) below the mapped pedolith, conductivity values appear to have peaked with some parts declining significantly especially around the coast.

The effects of saline water in [Figure 6–14](#) are almost undetectable. In contrast, many areas in higher parts of the landscape have remained relatively resistive, even at these increased depths, and are interpreted as indicating less-porous saprock well below the position of the exposed pedolith.

#### 6.3.2.2.3.3 Saprolith

A further window set is based on the distribution of saprolith polygons (i.e., saprolite and saprock) to make windows through to successive conductivity depth slices. The distribution of saprolith across the Woolner-Rum Jungle survey areas is shown in [Figure 6–4](#).

The near surface responses in the higher parts of the landscape (0-5m depth interval), in [Figure 6–15](#), are mostly resistive and could be due to the saprolith (saprolite and saprock) consisting of more saprock than saprolite. Saprock is less weathered and hence would have smaller less connected pore spaces. It is more likely that in the lower parts of the landscape, the moderate conductivity responses (yellowish to greenish) are due to a dominance of saprolite (i.e., more weathered) rather than saprock in the area trending approximately NW-SE across the window centre. An area, just north of the window centre appears completely white because there are no conductivity data recorded in that area, being the Litchfield National Park.

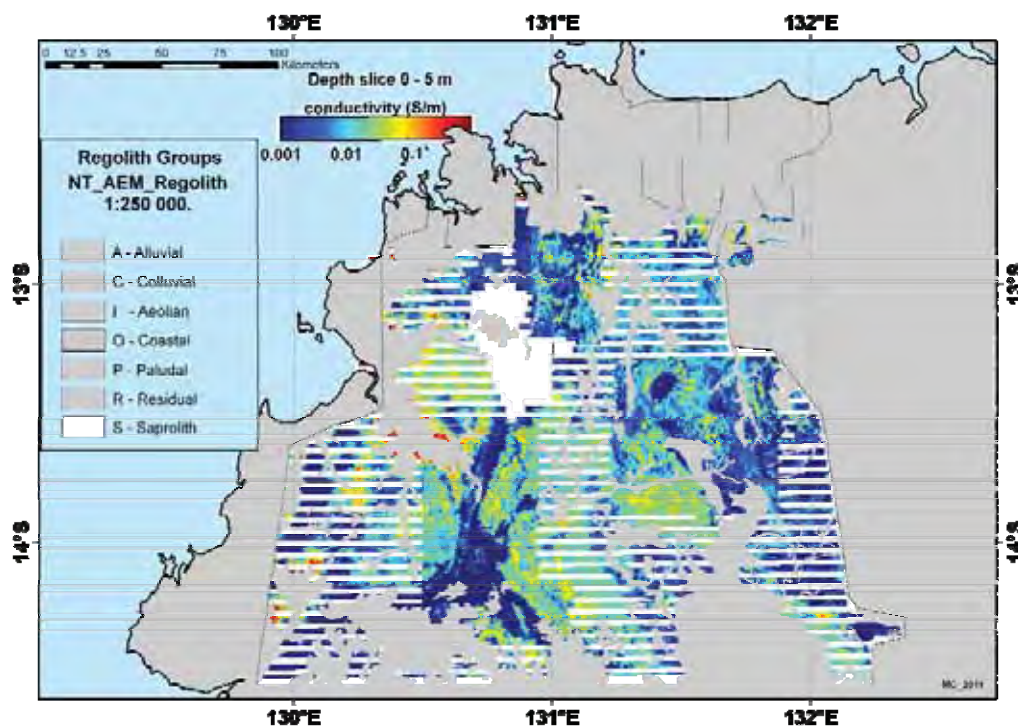


**Figure 6–15:** GA-LEI conductivity depth slice 0-5 m. The bright blue responses involve shallow saprolith and show mostly low to very low conductivity and are located in higher parts of the landscape.

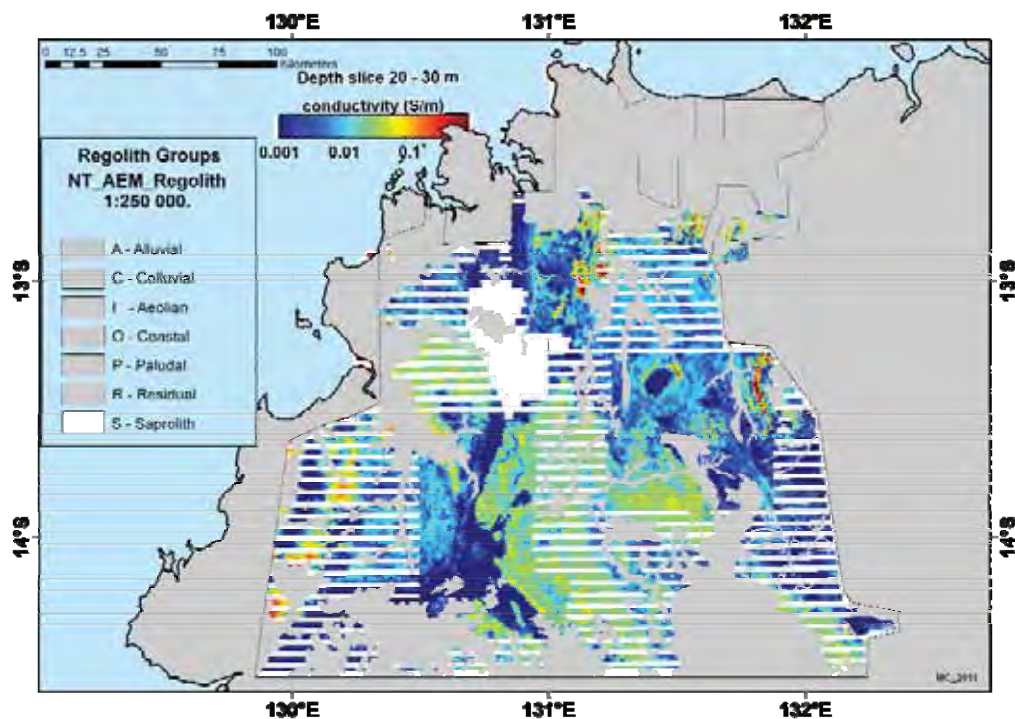


**Figure 6-16:** GA-LEI conductivity depth-slice 20-30 m. The responses show an increase in the relative proportion of moderate conductivity responses in the central NW-SE trending area which is more likely related to an increased proximity to the saprolite in the lower parts of the landscape. The relatively higher areas tend to be less weathered and are therefore likely to be more resistive.

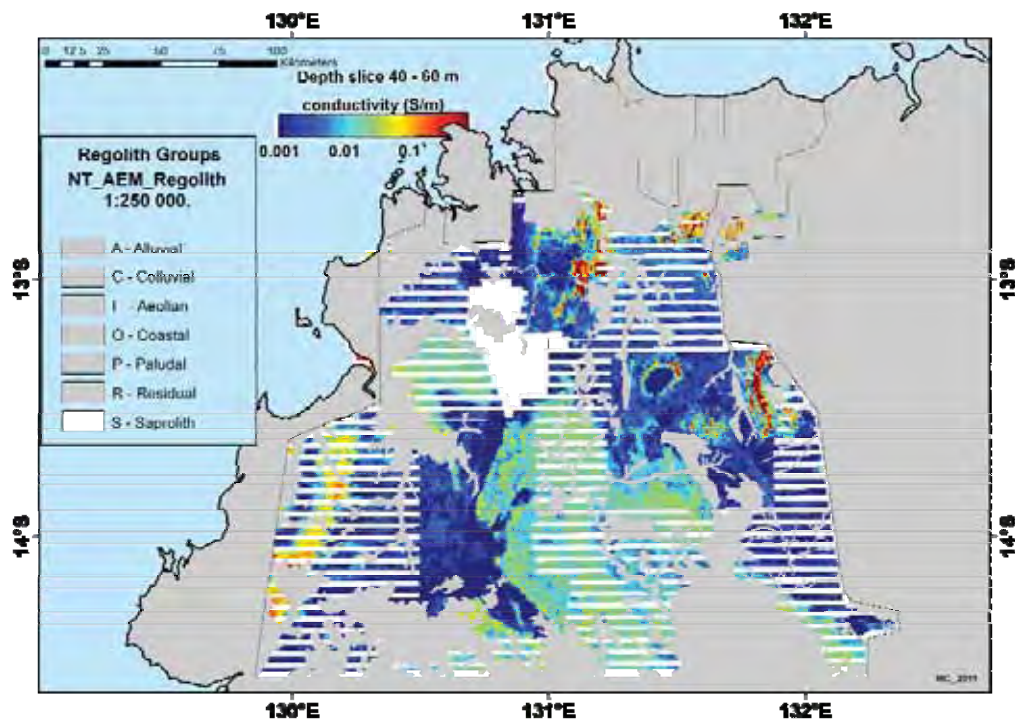


**Figure 6-17:** GA-LEI conductivity depth slice 40-60 m. Responses in the central NW-SE trending region show that conductivity may well have peaked and that signal penetration is approaching the saprock zone where the degree of weathering is expected to be less compared with that of the saprolite zone and accordingly shows a decline in conductivity.

In deeper depth slices resistive areas are becoming even more resistive (Figure 6–18) suggesting deeper penetration into saprock materials. In the local lowlands and closer to the coastal plains, the depth of signal penetration seems to again detect saline water influences (by groundwater or seawater incursion on lowlands or floodplains) either on saprock, saprolite, or at some other interface at depth and is indicated by the red–orange patterns emerging in some areas.

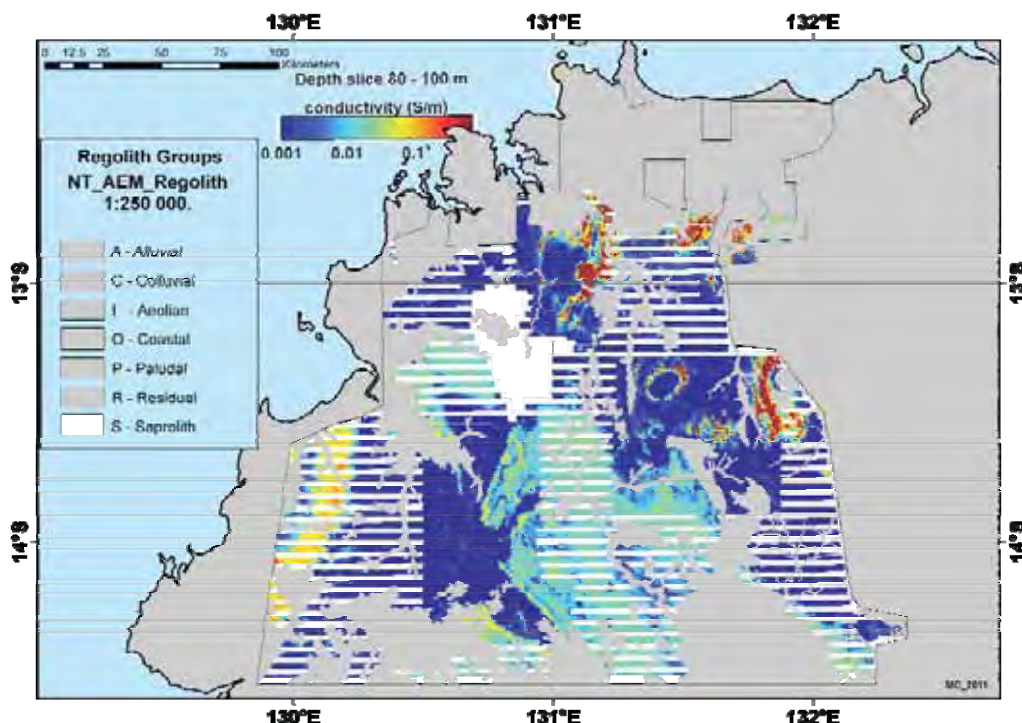


**Figure 6–18:** GA–LEI conductivity depth slice 80–100 m. The declining conductivity patterns in this windowed view appear to follow the same general trend towards the increasing influence of bedrock geology which is highlighted in the previous example, except for the new red highly conductive patches.

Some consistent correlations are revealed between the broad classes of regolith materials and in changing conductivity with depth and landscape position. Improved correlations can be gained by using reliable drillhole logs plotted onto either GA–LEI conductivity sections or EM Flow™ conductivity depth sections (CDIs).

#### 6.3.2.2.3.4 Assessments of GA–LEI conductivity sections and EM Flow™ CDI sections

During the overall assessment of the AEM survey data, GA–LEI conductivity sections and grids and EM Flow™ CDI sections and grids were used to determine the nature, extent and robustness of regolith information contained within them. Some examples provided here may help guide further regolith-related assessments. Relevant interpretations on selected lines are highlighted in the following diagrams.

The detection of weathering interfaces is of interest in regolith related assessments. The extent to which weathering interfaces are detectable will depend on the nature of the regolith materials present, and their conductivity contrast at any discontinuity present. The nature and type of any infilling materials present at the interface, the nature of any fluids present along or near the interface or the type and extent of

alteration will all influence the detectability of such an interface. The configuration, depth penetration and resolution of the AEM system used to detect these features are also critical factors.

Two block diagrams presented in [Figure 6–19](#) and [Figure 6–20](#) illustrate the area surrounding line 12460 from the Kombolgie Survey. The related CDI sections highlight the interpreted weathering interface at depth over underlying granite. [Figure 6–19](#) contains an extract of the regolith-landform map and [Figure 6–20](#) an extract of the surface geology map of the same area. Together, these block diagrams assist in relating the interface detected to those units exposed at the surface.

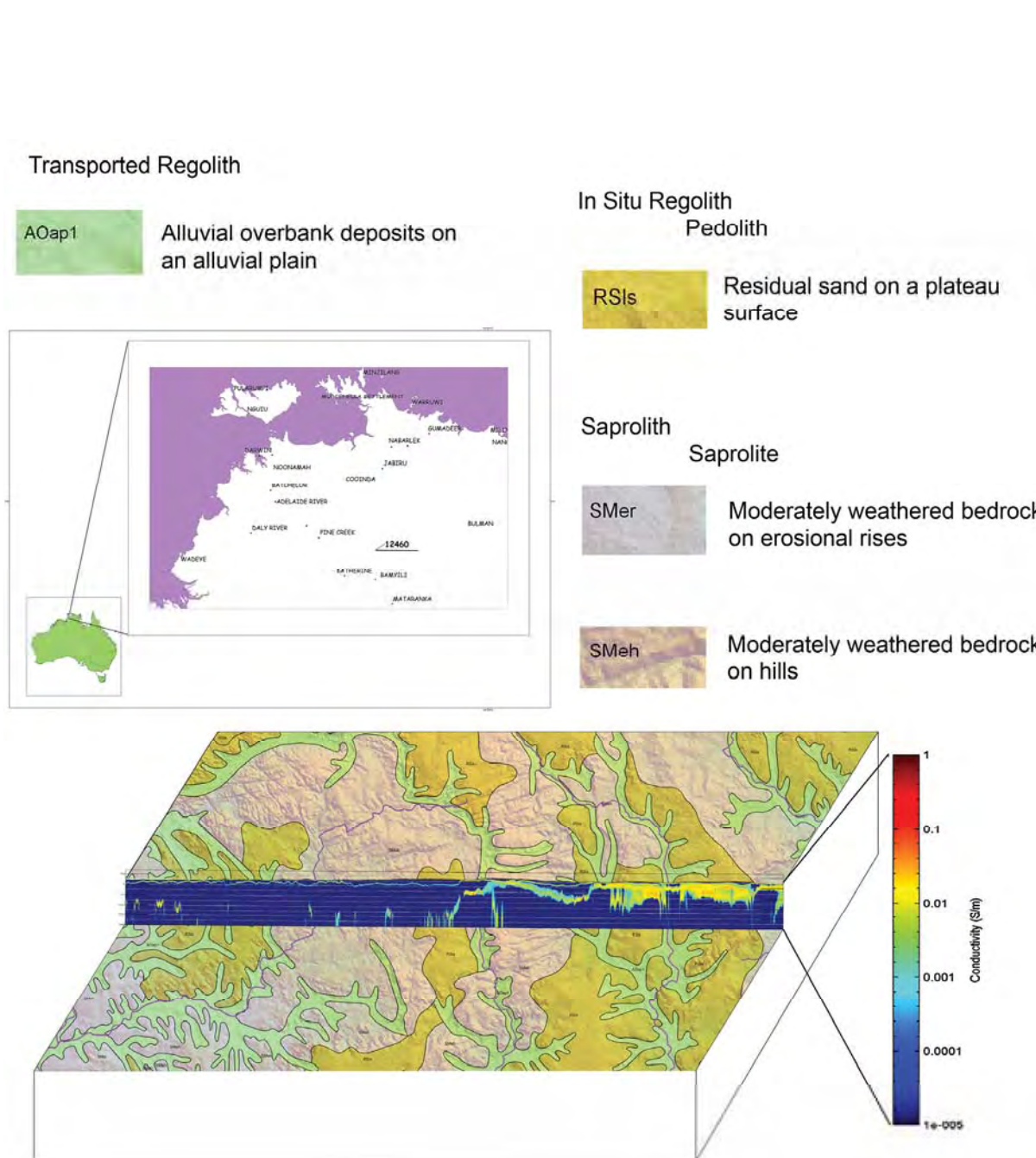


**Figure 6-19:** Block diagram indicating an AEM CDI section generated along line 12460 and related 1: 250 000 scale surface regolith landform units superimposed (with 30% transparency) onto an extract from the 9 second SRTM DEM. The southern half of the block diagram has been artificially lowered to the base of the CDI section to enable easier visual correlation with the conductivity features.

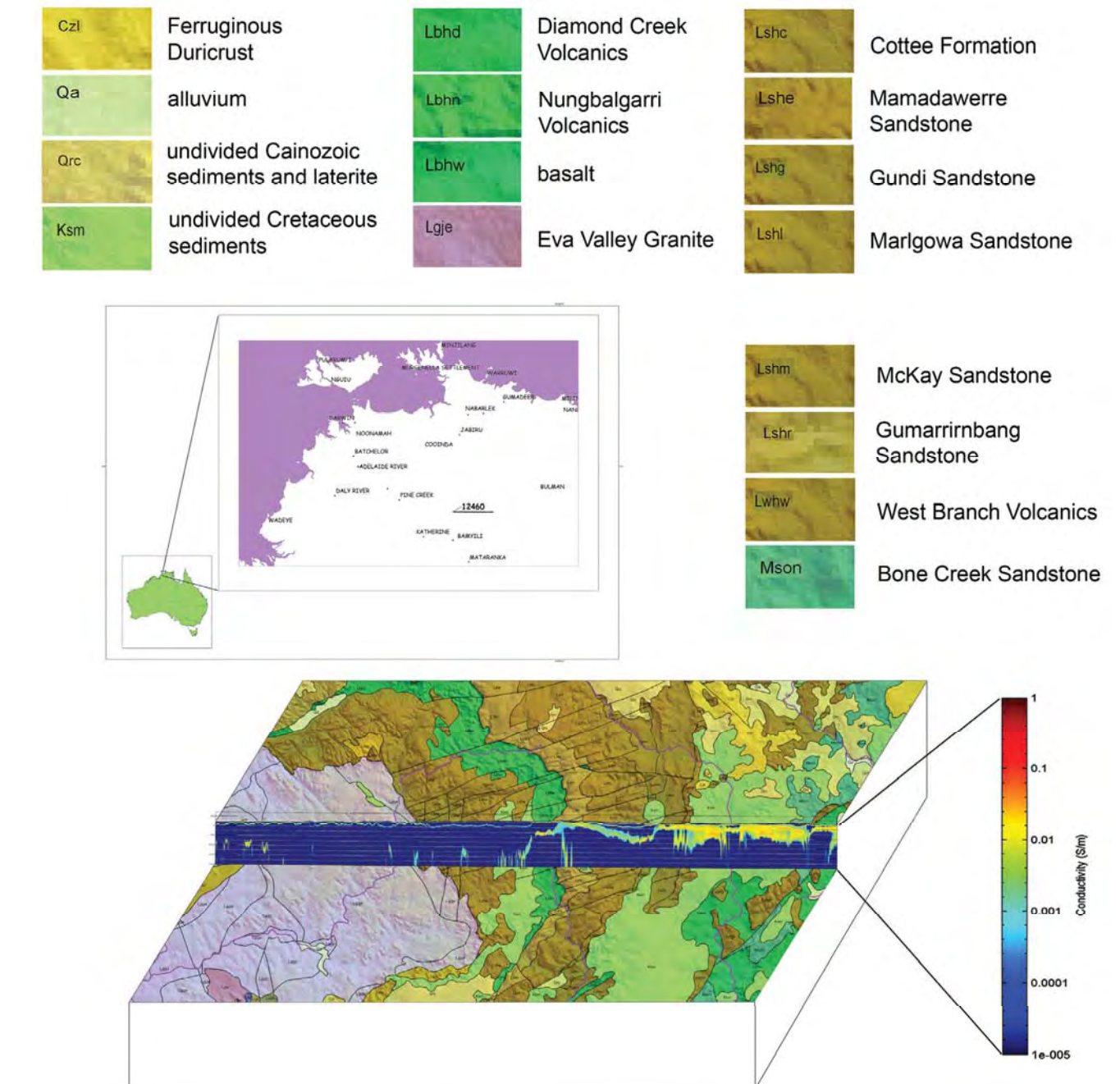


**Figure 6-20:** Block diagram illustrating an AEM CDI section generated along line 12460 and related 1:1 million scale surficial geology units superimposed (with 30% transparency) onto an extract from the 9 second SRTM DEM. The southern half of the block diagram has been artificially lowered to the base of the CDI section to enable easier visual correlation with the conductivity features.

#### 6.3.2.2.3.5 Palaeochannel environments – possible indicators and AEM evidence

Palaeochannel environments are likely present in the Pine Creek AEM area and their location would be relevant to uranium exploration. There are a few geomorphic indicators documented by Magee (2009) confirming the existence of palaeochannels elsewhere across the Northern Territory. Whether or not these environments, and others yet to be discovered, have acted as sites for precipitation of uranium is yet to be demonstrated.

The Pine Creek AEM survey was conducted in two parts and the different survey technologies used have been described earlier in this report (see [Chapter 5](#)). With these survey limitations in mind, a range of remotely sensed images was examined for any surface indicators of palaeochannels (described overleaf), regardless of their age. In addition, the available conductivity depth, elevations slices and CDI conductivity sections were also examined for possible older subsurface expressions.

#### 6.3.2.2.3.6 Image assessments

The following images of the Woolner-Rum Jungle Survey areas were used to help assess the likely presence of palaeochannel environments:

1. A MRVBF\* image (constructed for the entire Pine Creek Survey area);
2. A ternary radiometrics image;
3. An SRTM 9 second DEM;
4. A shaded, false coloured 9 second DEM;
5. Various AEM-LEI depth and elevation slices; and
6. Various AEM CDI conductivity sections.

\*Multi-Resolution Valley Bottom Flatness Index (MRVBF). Gallant and Dowling called it “MRVBF”. The MRVBF images were constructed from the 9 second DEM of Australia using Gallant and Dowling’s algorithm ([Figure 6–21](#)). A MRVBF image was also derived from the 3 sec DEM data ([Figure 6–22](#)).

These images were used in conjunction with geologic, regolith and drainage data to help provide additional information relevant to the assessment.

#### 6.3.2.2.3.7 Geomorphic and geological indicators and AEM data

In assessing the presence of palaeochannel environments in the Pine Creek AEM survey area, there are a few approaches available. One approach is to examine the geomorphic environments across the region for evidence of former drainage patterns and alluvial fan systems or for geomorphic indicators suggesting drainage tracts that may have an antiquity greater than their present appearance suggests. Patterns thereby identified may be visible also in radiometric imagery and perhaps even in other custom processed satellite imagery. Another option is to examine night-time thermal infra red imagery for evidence of buried palaeochannels. At a more detailed level, waterbore yield records and their associated drill-hole logs may indicate the presence of palaeochannels. Stratigraphic, petroleum and mineral exploration drill logs may also contain information of value in a preliminary and even a more detailed assessment.

The results of image assessments for evidence of older drainage networks which could indicate that there may also be even older developed palaeovalley and palaeodrainage systems near or just below the surface are presented in a series of figures in this section.

Some geomorphic features are present in the coloured, 9 second SRTM DEM near Pine Creek and Emerald Springs in the Rum Jungle survey area ([Figure 6–33](#)). These erosion features suggest that drainage to the SW, particularly across the Daley Basin, and further west, is old and superimposed

([Figure 6–23](#) and [Figure 6–24](#)). Whether or not these drainage features are strictly superimposed or antecedent remains unresolved. However, for this drainage style to have formed, it has to have been in existence for some considerable time. Earlier, but possibly now buried, former drainage courses may be present, especially in the mid reaches of the network. These mid-reach areas are of some interest in the search for buried palaeochannel environments containing uranium deposits.

Further west, near Peppimenarti and Pulmpar ([Figure 6–24](#)), the headwater drainage remnants still visible on the older upland region are associated with much shallower regolith compared with the lowland mid-reach drainage tracts and, consequently, may be of lesser interest for palaeochannel uranium deposits.

Radiometric images have not yielded information useful in defining palaeochannel-hosted uranium deposits. Drainage revealed in these images is primarily surface-related, indicating currently active or at least more recently active channels that do not dissect significant near surface uranium deposits. Some parts of old meander loops may be visible but do not indicate deeply buried palaeochannels.

Night-time thermal infra red imagery assessments did not form part of this work but could provide additional useful information. Examples of more recent palaeochannels are documented in Magee, (2009) but their primary value is in providing additional water resources.

Drill hole logs and water borehole records were examined but because of its large volume and large amounts not being in readily useable formats, these data required more extensive examination and re-processing than could be undertaken during this assessment.

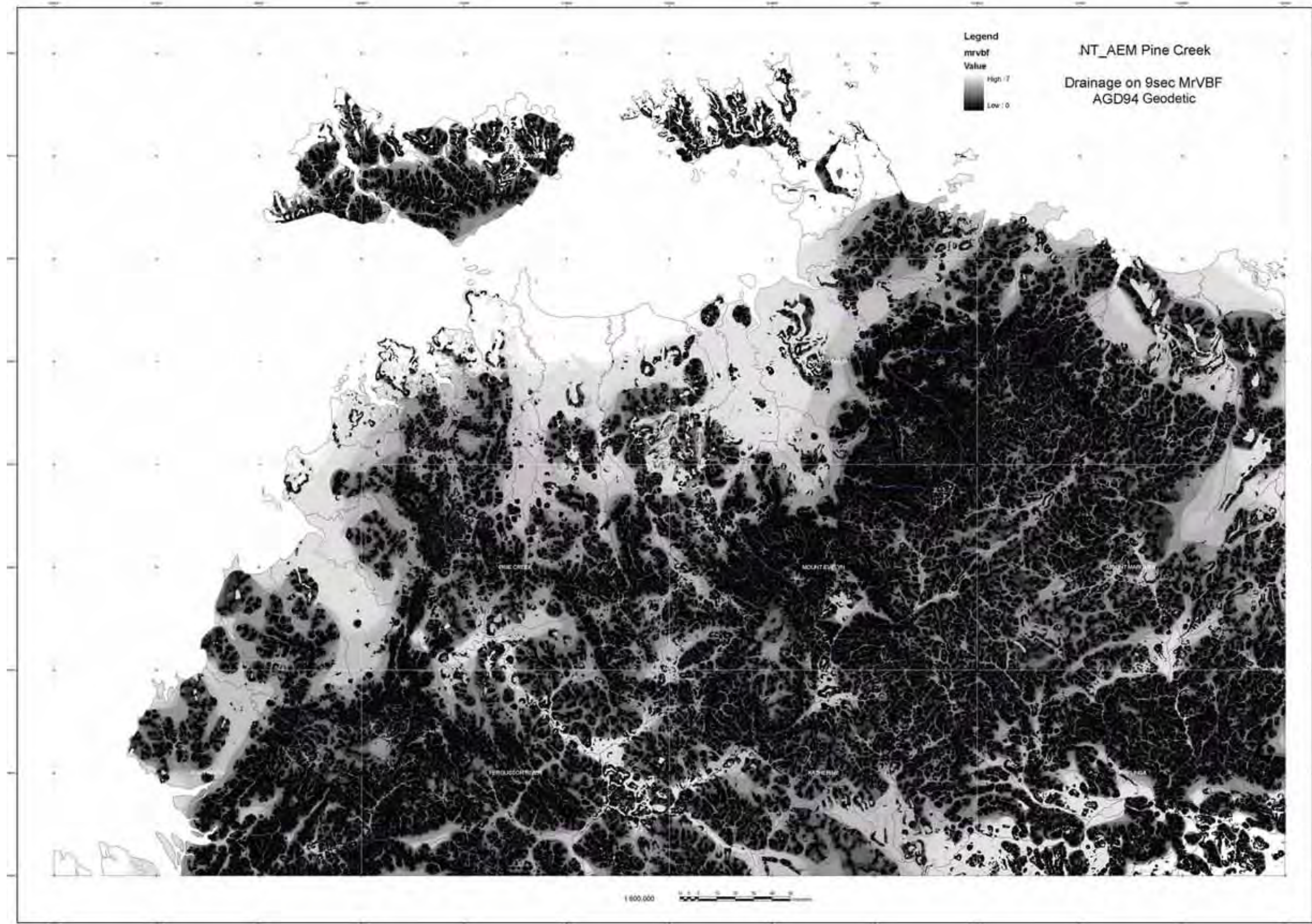
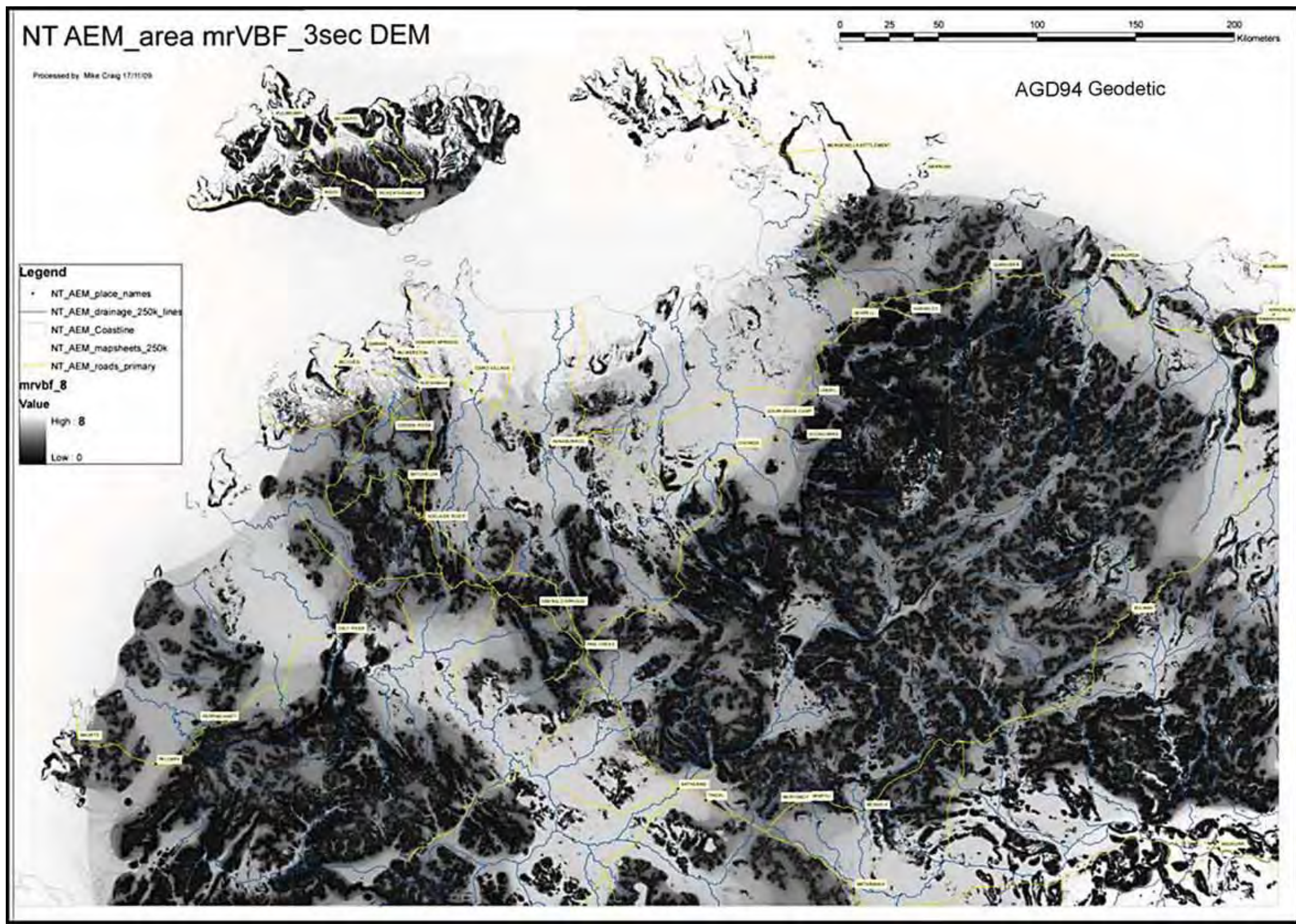
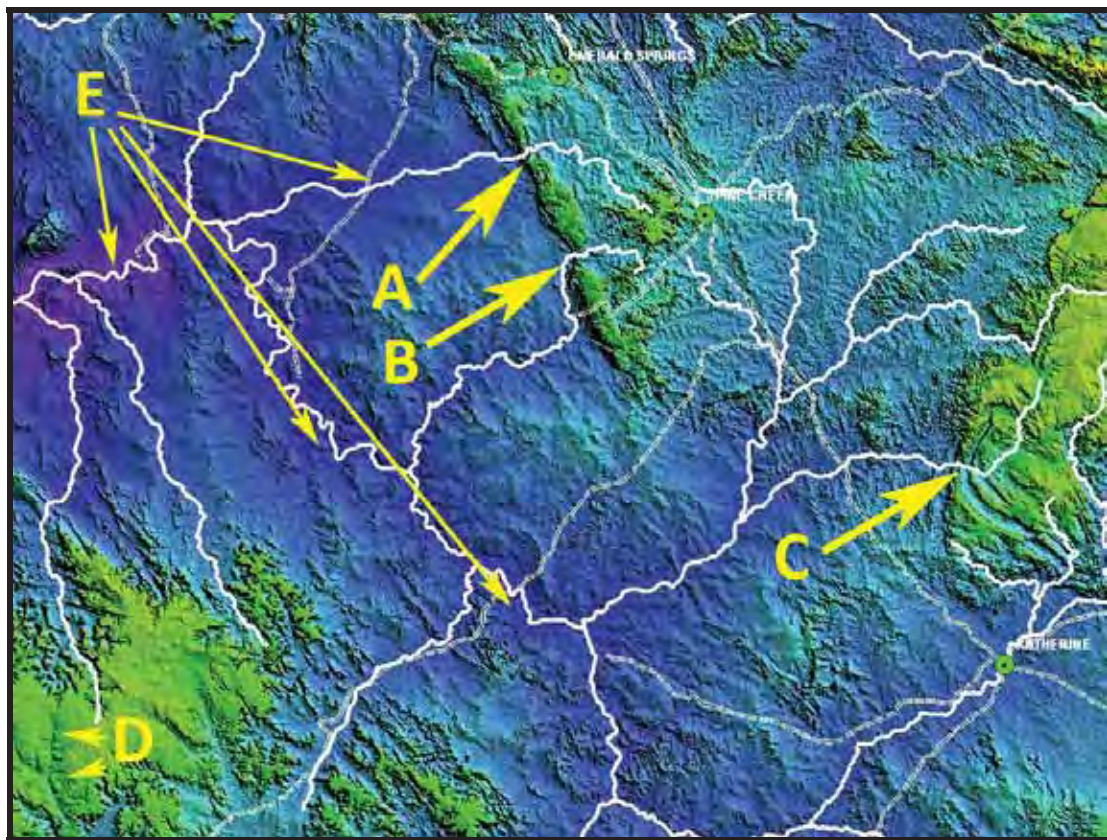


Figure 6–21: A MRVBF image derived from the 9 second DEM of Australia showing current drainage (digitised from 1:250 000 scale topographic mapping) in blue. White to light grey areas indicate the high variability of valley floor lowlands across the region. The darker areas indicate the higher elevation uplands, ridges and tablelands.



**Figure 6–22:** A MRVBF image derived from the 3 second DEM of Australia showing current drainage (digitised from 1:250 000 scale topographic mapping) in blue. White to light grey areas indicate simplified, broader valley-floor lowland expanses and major plains including extensive coastal plains. The darker areas indicate major higher-elevation uplands, ridges and tablelands (for example, the highly dissected Kombolgie plateau to the NE and in contrast, to the SW the relatively lower expanse of the Daley Basin here shown as a NW-SE trend grey trough). Roads are in yellow. Major town names are indicated.



**Figure 6–23:** A 9 second colour-shaded SRTM DEM (extracted from an SRTM DEM image prepared by R. Clifton, NTGS) showing current drainage lines in white connecting over the mid north-western end of the Daly Basin (mostly shown in shades of blue). The faint dashed lines represent major access roads in the area. Town names are shown in white text.

In [Figure 6–23](#), upland ridges and tablelands are shown in a brassy yellow and lower relief areas in shades of blue. Arrowed areas A, B and C indicate signs of drainage superimposition (perhaps antecedence) onto underlying mostly older geological substrate. Arrowed area C shows expanses of accumulating alluvial sediments. Arrowed area D indicates the eroded remnants of higher-level drainage systems on older surfaces developed mostly on Cretaceous bedrock. Some older drainage systems now merge with currently active drainage lines mid reaches shown by arrowed areas E.

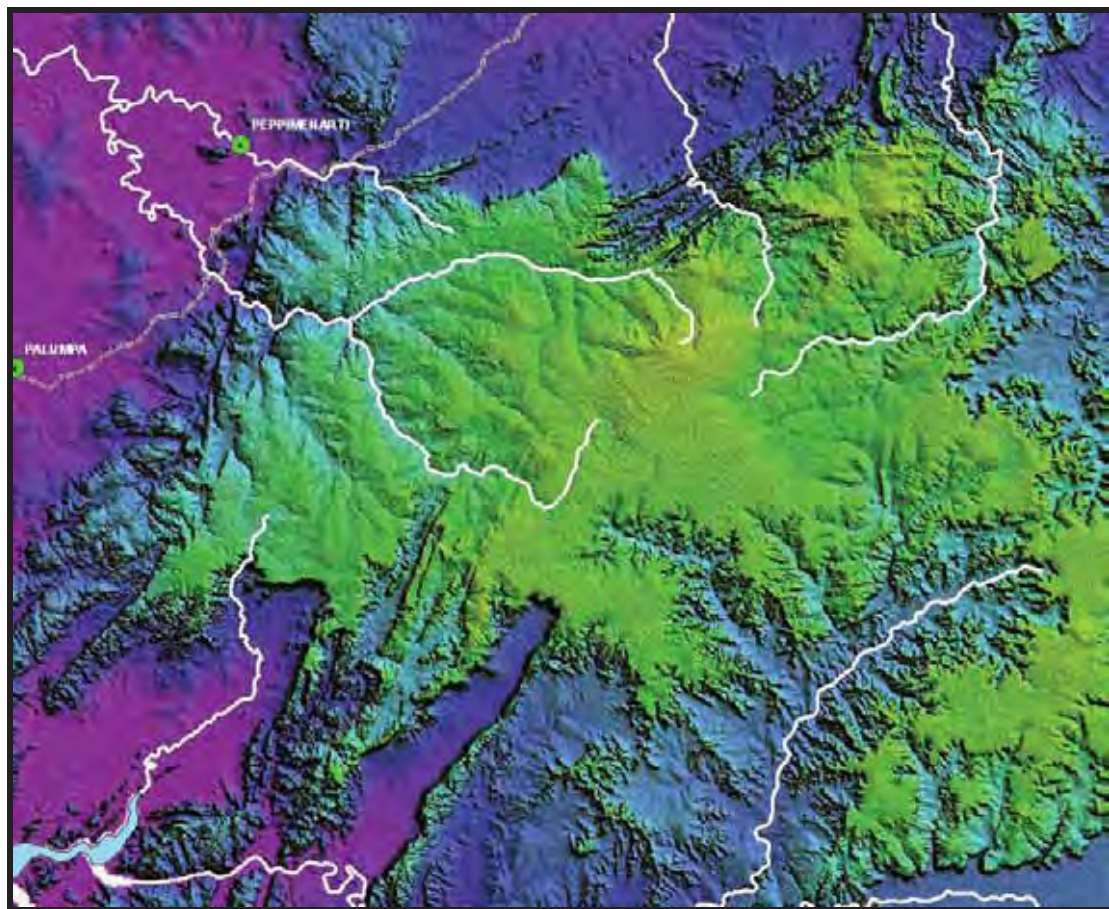


**Figure 6-24:** A 9 second colour-shaded SRTM DEM (extracted from an SRTM DEM image prepared by R. Clifton, NTGS) showing a large upland area of Cretaceous cover immediately west of the area in [Figure 6-23](#). Older, major trunk drainage patterns progressively superimposed onto underlying older bedrock structures.

These older drainage systems are also indicated in [Figure 6-24](#) and also join with currently active drainage lines on the lower, more actively eroding, tracts surrounding the retreating perimeter of the older uplands.

CDI conductivity sections generated for parts of the Pine Creek survey area ([Figure 6-25](#)) show alluvial regolith materials. Saltwater-saturated alluvial deposits are visible in some Kombolgie survey CDI conductivity sections. On the far western end of the CDI conductivity section generated for survey line 12080 ([Figure 6-26](#)), an alluvial plain corresponds with a very strong, highly conductive red response. The alluvium is visible as an initially shallow, long wedge over 10 km long, beginning near Oenpelli in the east and, thickening to approximately 50 m at the western end of the CDI section.

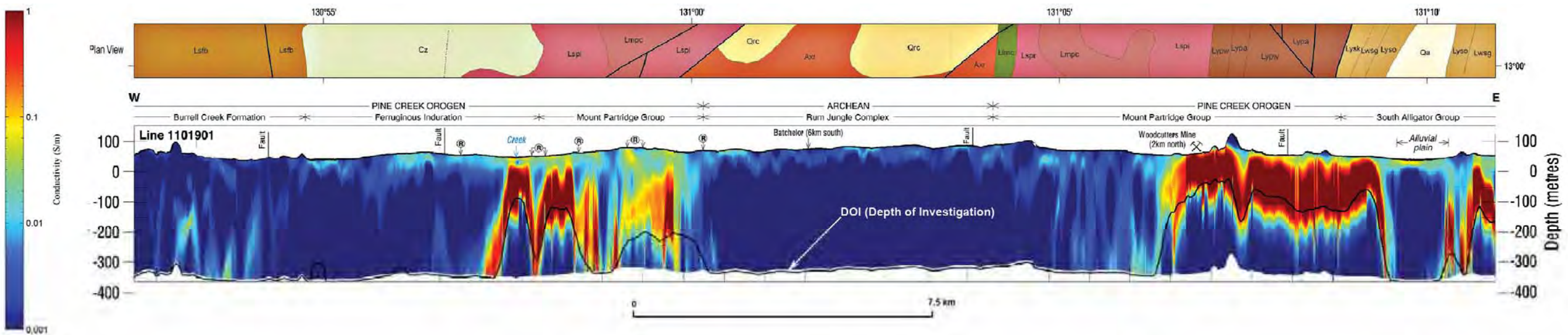


Figure 6–25: GA–LEI conductivity section of line 1101901 in the Pine Creek area. An alluvial plain marked at the far eastern end of the line corresponds to an area of moderate conductivity.



Figure 6–26: An EM Flow™ CDI section of line 12080 in the Kombolgie survey area. An alluvial plain on the western end of the line is interpreted to represent a wedge of saline water saturating alluvium, and is mapped by very high conductivities.

Pedolith is present in the survey region and usually appears in GA–LEI conductivity sections as a highly resistive upper layer. The GA–LEI conductivity section prepared for line 10280 shows pedolith consisting of ferruginous materials i.e., nodules and duricrust. The major area at the western end of the GA–LEI conductivity section is interpreted as pedolith and is associated with duricrusts developed on weathered Cretaceous sediments ([Figure 6–27](#)). Areas marked A and B in [Figure 6–27](#) are shown in greater detail in [Figure 6–28](#) and [Figure 6–29](#). Areas of pedolith indicated in [Figure 6–30](#) correlate strongly with low conductivity patterns in the areas marked A and B. They are shown in more detail in [Figure 6–31](#) and [Figure 6–32](#).

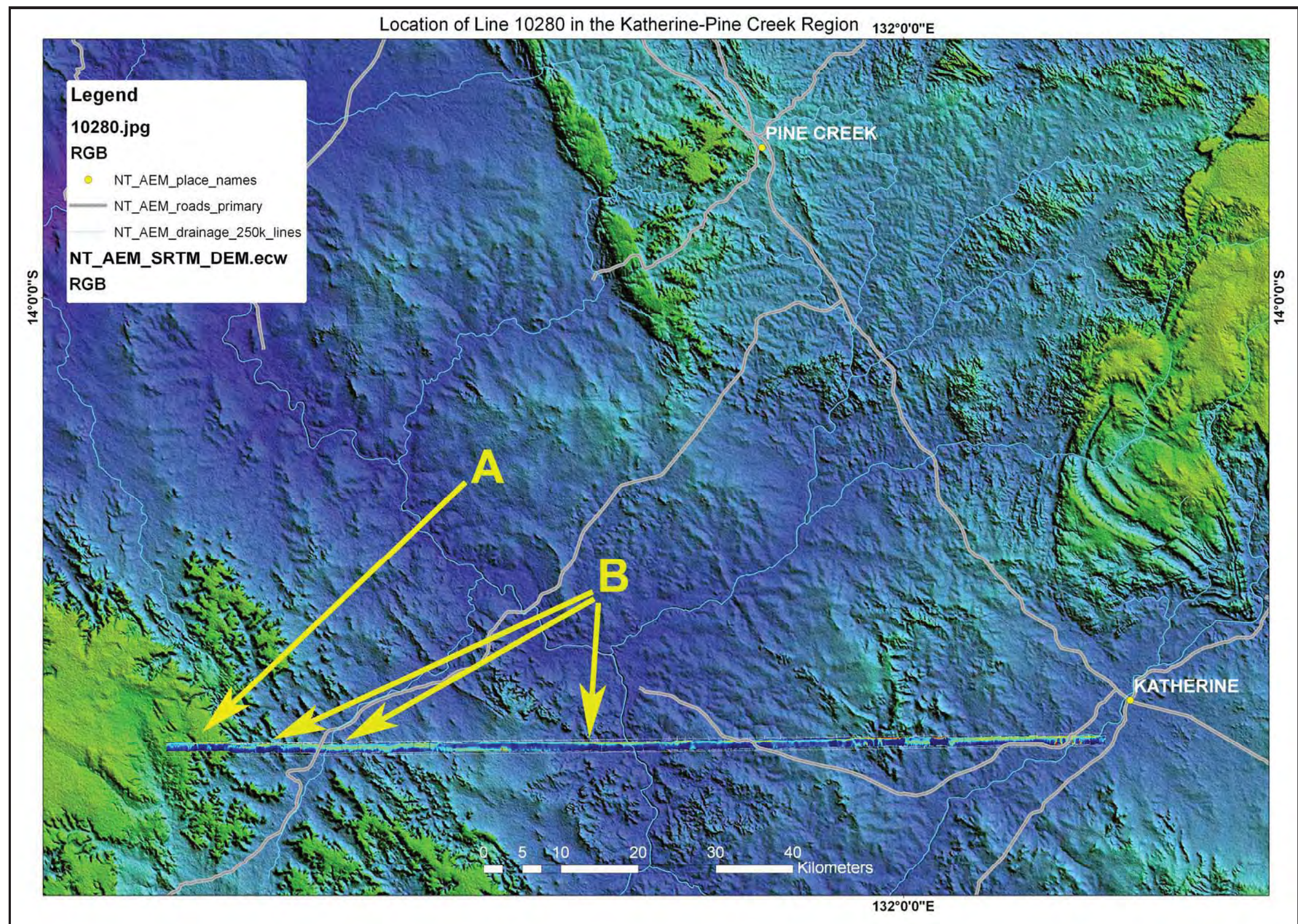
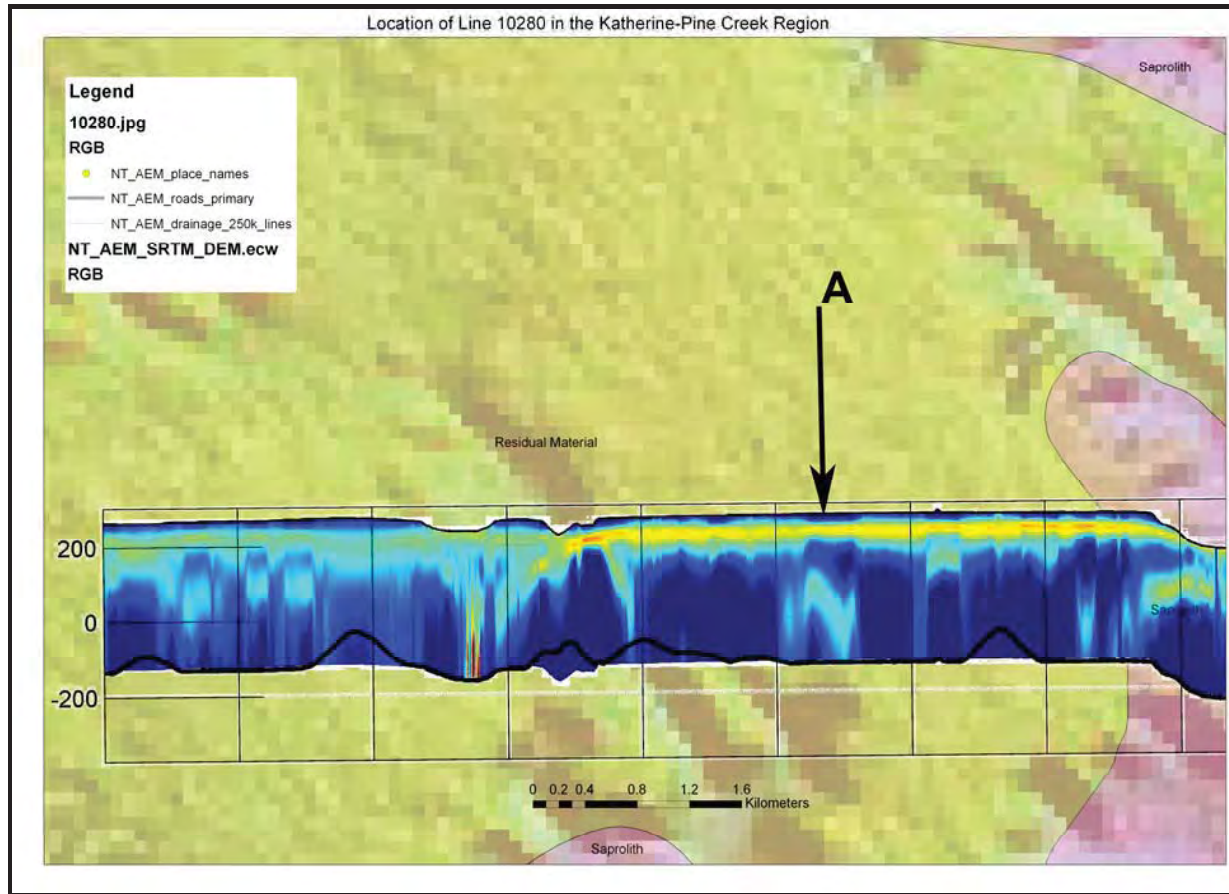
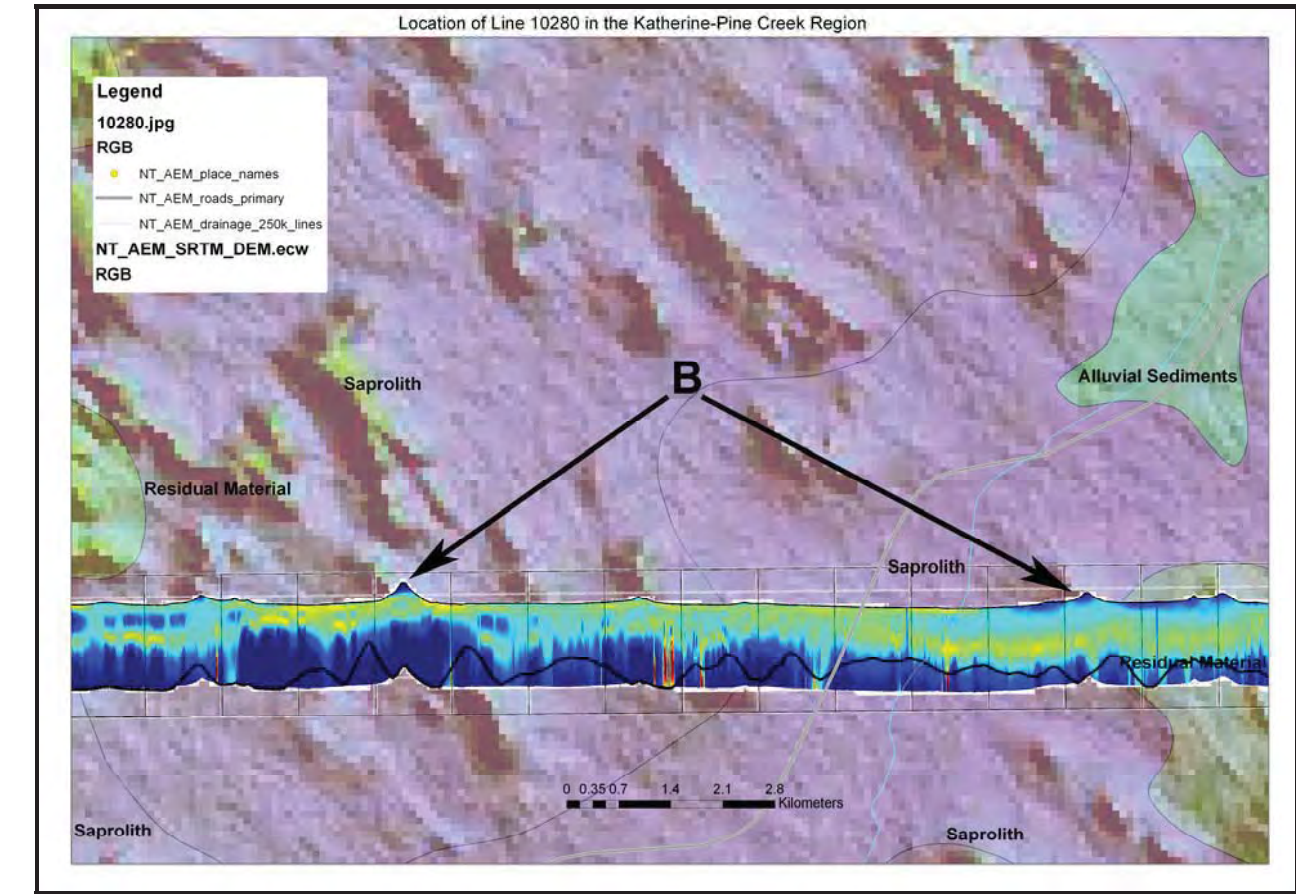


Figure 6-27: GA-LEI conductivity section of line 10280 across part of the Daly Basin overlain on a DEM image. The section shows a major area of pedolith marked A, and minor unmapped pedolith residual rises marked B.



**Figure 6–28:** Area marked A from [Figure 6–27](#) showing an upper-most resistive layer correlates with the surface expression of pedolith developed on weathered Cretaceous rocks.



**Figure 6–29:** Areas marked B from [Figure 6–27](#) showing an upper-most thin blue resistive layer correlated with the surface expression of residual rises (pedolith) also developed on weathered Cretaceous rocks.

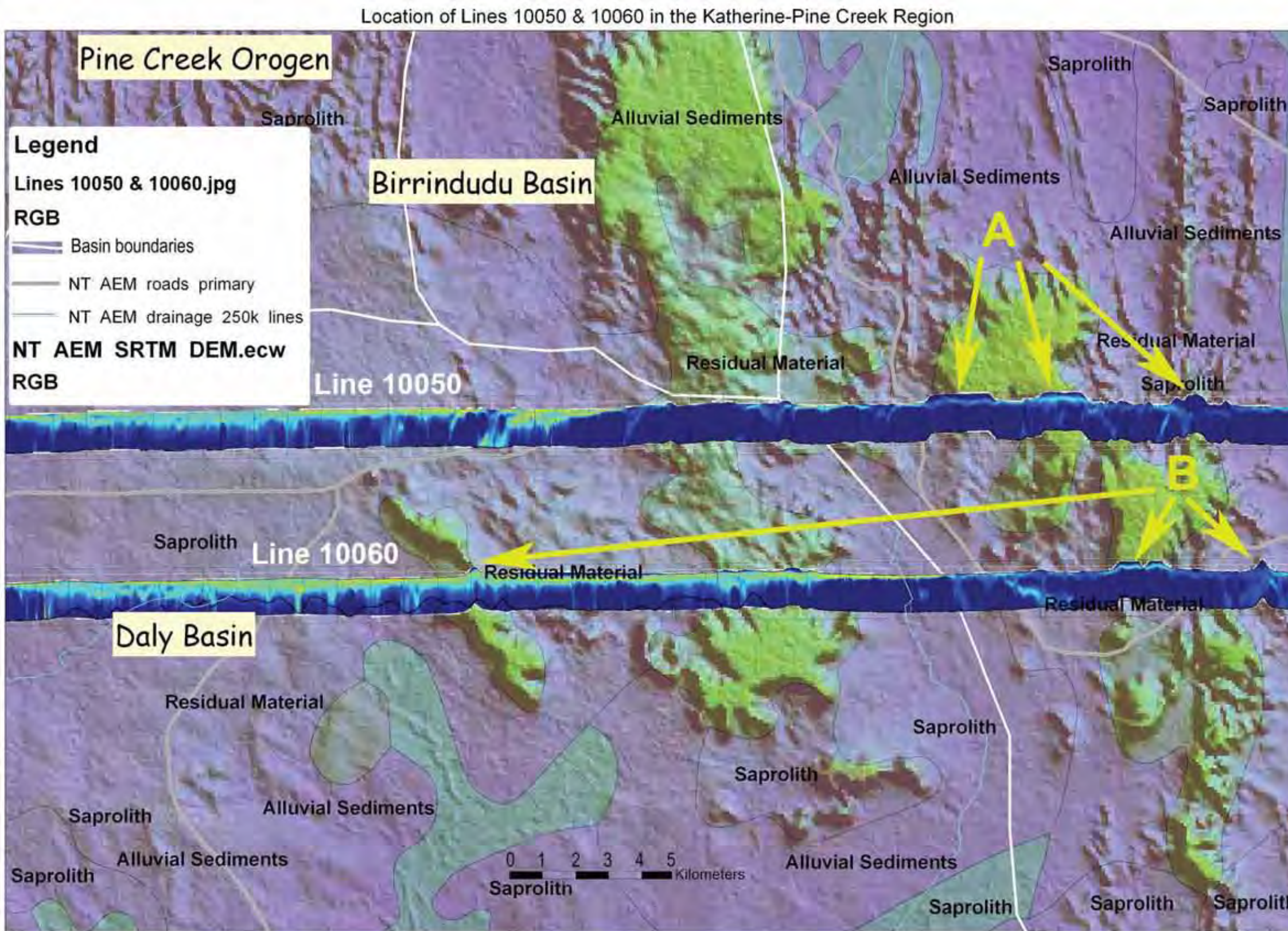
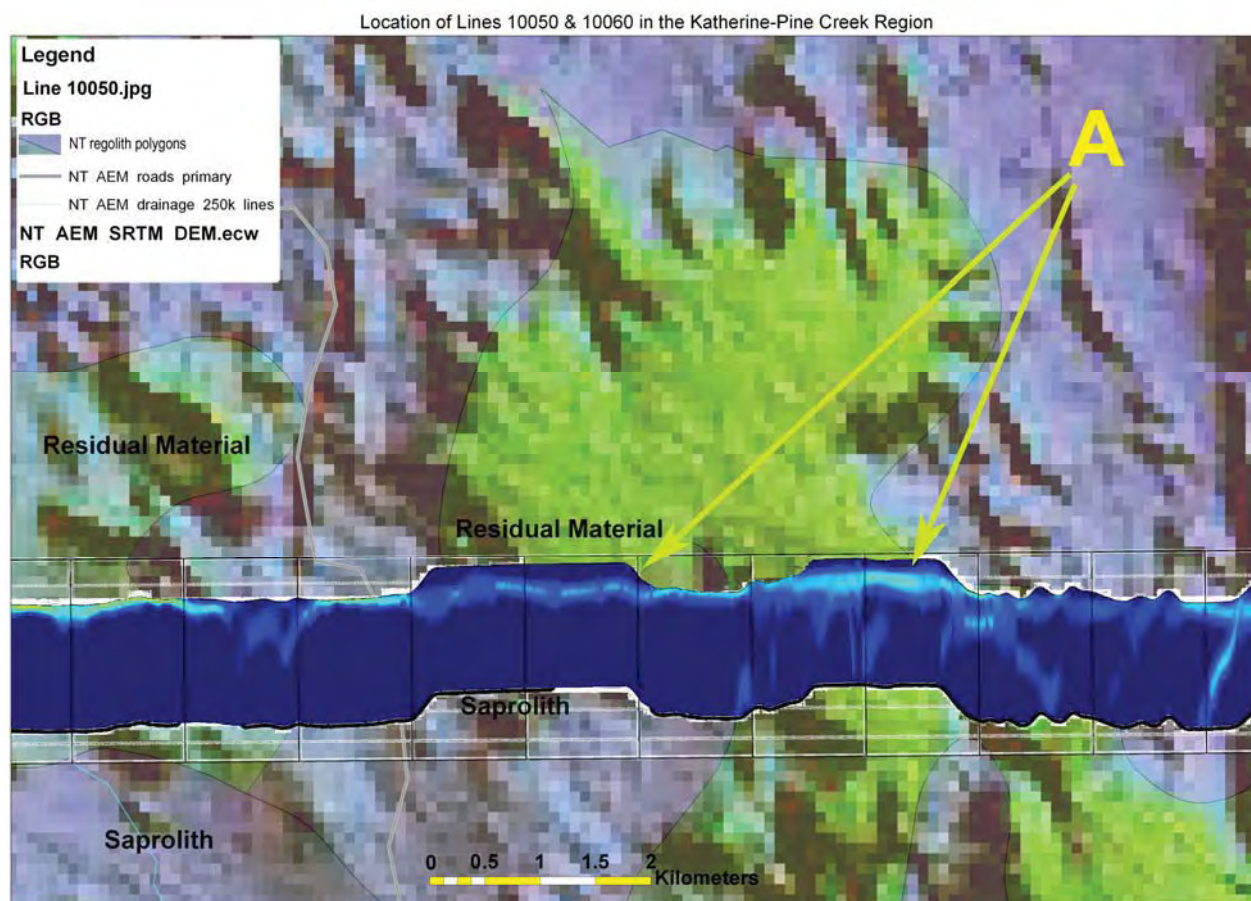
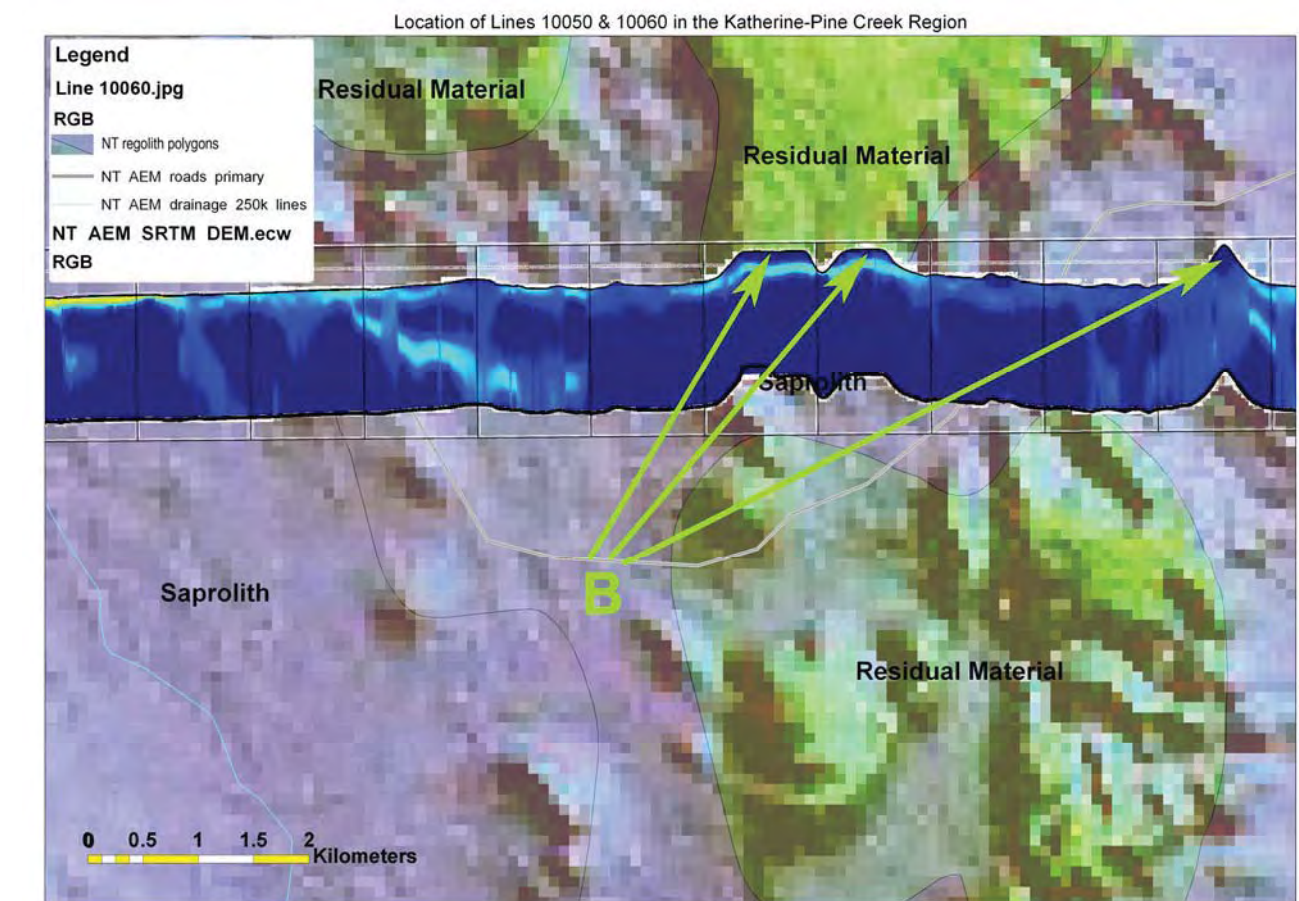


Figure 6-30: GA-LEI conductivity sections of lines 10050 & 10060 from the Rum Jungle survey displayed over a DEM image with interpreted regolith units. Pedolith is revealed at locations A and B, south of the triple junction of the Pine Creek Orogen, Birrindudu and Daly Basins regolith.



**Figure 6–31:** Areas marked A on line 10050 from [Figure 6–30](#) shows an upper-most resistive layer correlated with the surface expression of pedolith developed on weathered Cretaceous rocks.



**Figure 6–32:** Areas marked B on line 10060 from [Figure 6–30](#) shows an upper-most resistive layer correlated with the surface expression of residual rises (pedolith) developed on weathered Cretaceous rocks.

### **6.3.2.3     *Interpreted Palaeovalleys in the Pine Creek Survey area***

Palaeovalleys may be highlighted in the AEM data due to subtle differences in conductivity between the water saturated palaeovalleys and surrounding less porous areas. Variation in the salinity of water may also result in enhancement or reduction of conductivity in palaeovalleys.

Palaeovalleys are interpreted to be present at depth in the Pine Creek Survey area and in the Tolmer Group at depth within the Mt Boulder area. The palaeovalley system contains a network of lower conductivity channels ([Figure 6–33](#)). The lower conductivity in these interpreted channels may be due to the presence of relatively fresh water retained in the palaeodrainage system. Current surface drainages are clearly shown in the DEM and are mapped in detail on the Pine Creek 1:250 000 geological map (Malone, 1962).

The palaeovalleys and palaeodrainage network depicted in the AEM conductance data is similar but not identical to the current drainage system as shown on the surface geological map. The water flow directions in the palaeovalleys is interpreted to be from Bald Ridge towards Rock Candy Range, and then along the current flow direction of the Daly River. The differences in positions between the palaeovalleys and current drainage systems may reflect migration of the drainage system over time. The palaeovalleys represent possible uranium targets in this region.

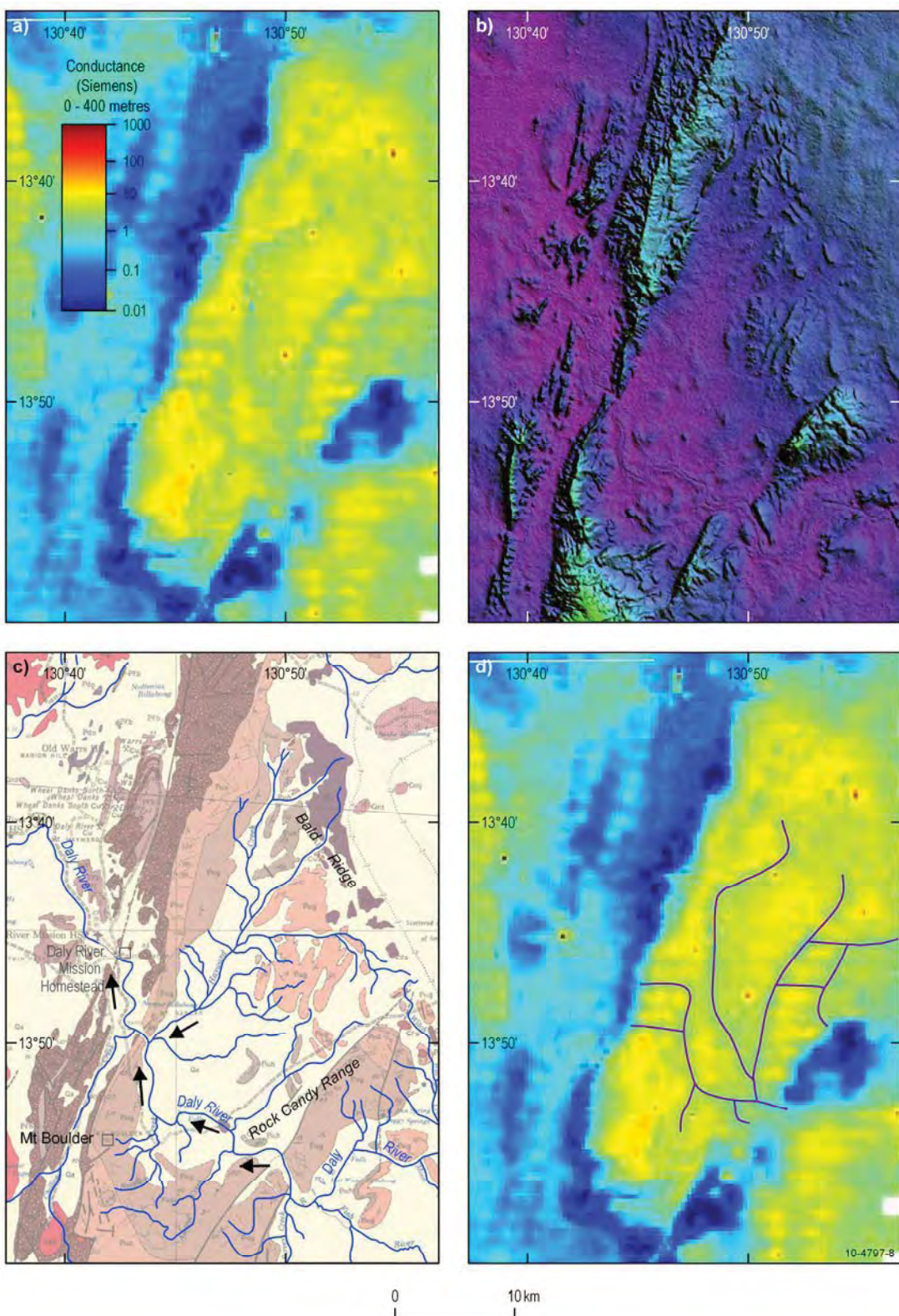


**Figure 6-33:** Current surface drainage channels and palaeochannels at depth in the Mt Boulder area  
 (a) AEM conductance image (0-400 m) from the Rum Jungle Survey  
 (b) Digital elevation model  
 (c) Current drainages mapped in the Pine Creek 1:250 000 surface geology map (Malone, 1962)  
 (d) Palaeovalleys palaeodrainage at depth interpreted from the AEM conductance image (a)

#### **6.3.2.4     *Granite plutons***

Granite generally has low conductivity, being resistive (Palacky, 1993). Pluton–pluton boundaries are generally not well depicted in the AEM conductivity data. In the Pine Creek Orogen, however, some granite plutons display their oval shapes where rimmed by more conductive surrounding metasedimentary rocks. These define the pluton boundaries, such as the Rum Jungle Complex, Burnside Granite and Minglo Granite ([Figure 6–3](#)).

#### **6.3.2.5     *Faults***

Many faults are depicted in AEM data. The presence of faults in the AEM data may be indicated by displacement of conductivity anomalies and changes in anomaly amplitude. Faults may have higher or lower conductivity than surrounding rocks of the same unit, either because of alteration along the fault or saturation by fresh or saline water.

At a number of locations, faults are depicted in AEM conductivity sections as being slightly more conductive than the host rocks, such as the fault between the Hermit Creek Metamorphics (schist) and the Moyle River Formation (sandstone) along lines 1004401 and 1004601 in the Rum Jungle survey ([Figure 6–34](#)).

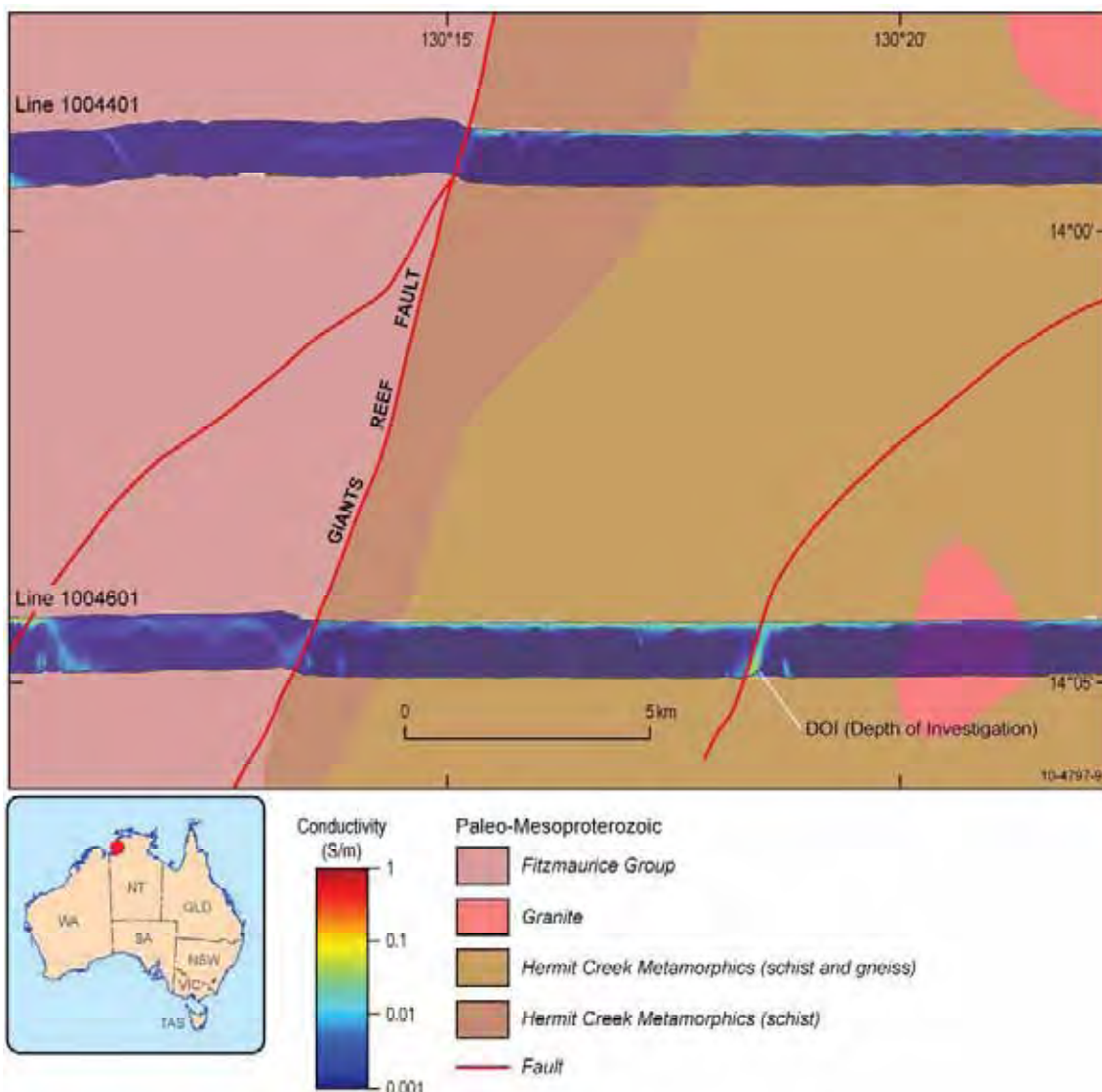


**Figure 6–34:** Faults depicted in GA–LEI conductivity sections (lines 1004401 and 1004601). Solid geology after NTGS (2005). Conductivity sections displayed at three times vertical exaggeration.

#### 6.3.2.6 Folds

Folds are common structures in the Pine Creek Orogen. Many folds are depicted in AEM conductivity sections, although the geometry of some folds as mapped in geological maps and cross sections may not be readily interpreted from the AEM conductivity sections. This is because the AEM sections may only depict the near surface part of the shallow crust, usually the top 200 to 400 metres below surface. The shapes of conductivity anomalies may not directly correspond to geological boundaries. In addition, in the cases of strong conductors, the AEM penetration depth is often shallow. However, in many cases the presence of antiform or synform may be interpreted from the AEM conductivity sections.

For example, several, approximately upright and NNW-trending, folds have been mapped in surface and solid geology in the metasediments of the South Alligator River Group south of the Mt Bundey Granite. The carbonaceous and pyritic sediments of the Koolpin Formation are very conductive. Their presence can be easily mapped from the AEM conductivity sections and can be used to detect the presence of folds and faults, such as along line 1001501 (Figure 6–35). The geometry of the conductive Koolpin Formation

is consistent with the folds mapped in geological maps in this area. More discussions will be presented in Section 6.3.2.13.

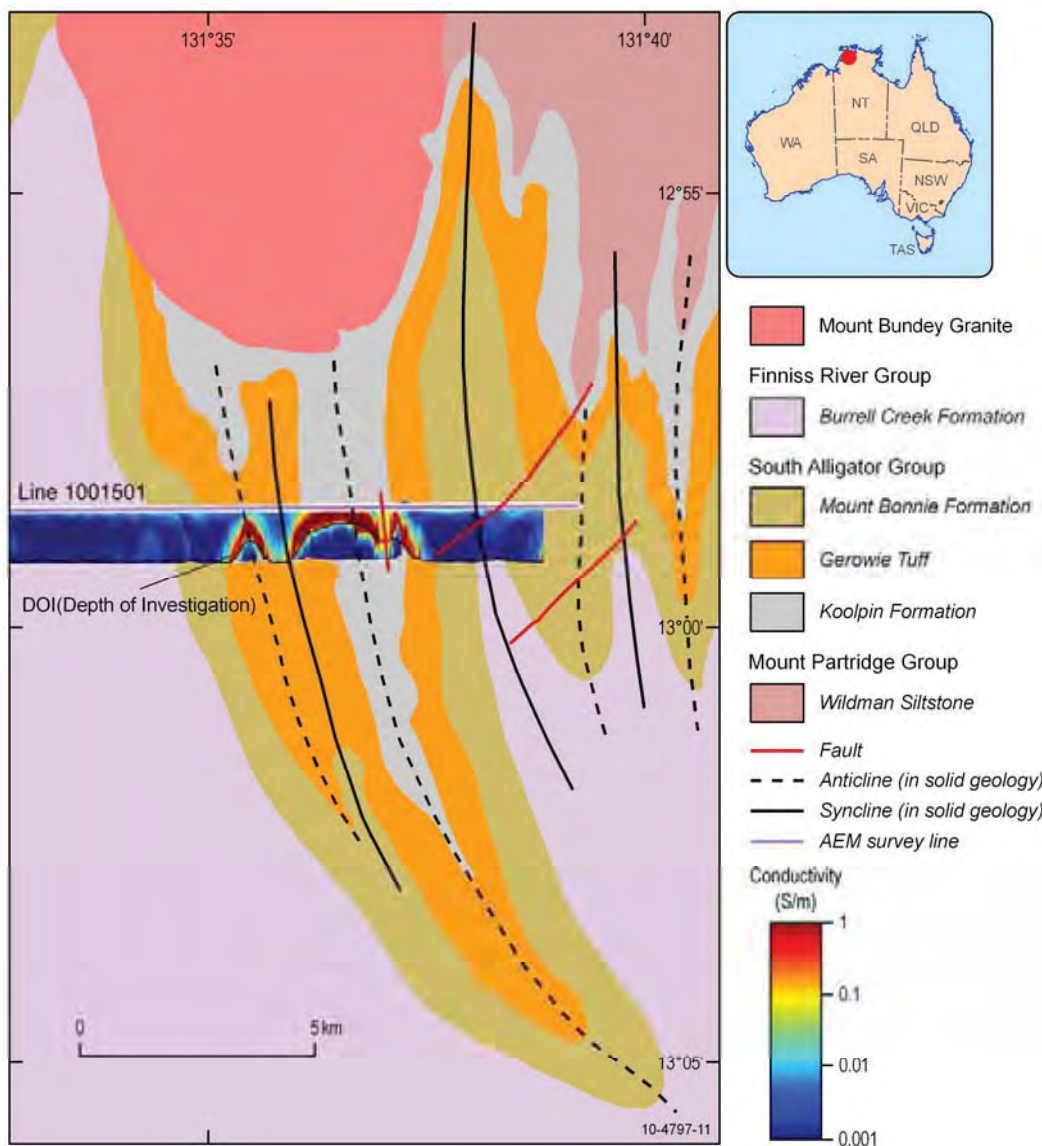


**Figure 6-35:** GA-LEI conductivity section 1001501 from the Rum Jungle Survey. Solid geology from NTGS (2005). Conductivity sections displayed at three times vertical exaggeration. Folds are defined by the strong conductor present within the South Alligator Group.

#### **6.3.2.7     *Unconformities and geological provinces in the TEMPEST™ data***

There are several geological province boundary unconformities in the Pine Creek AEM survey area, including:

- Cretaceous sediments over older rocks;
- The Bonaparte Basin over the Fitzmaurice Basin and the Pine Creek Orogen;
- The Daly Basin over the Birrindudu Basin and the Pine Creek Orogen;
- The McArthur Basin over the Pine Creek Orogen and Archean complexes: the Kombolgie–unconformity;
- The Birrindudu Basin over the Pine Creek Orogen: the Depot Creek unconformity; and,
- The Pine Creek Orogen over Archean complexes: the Pine Creek–Archean unconformity.

Some of these unconformities are well depicted in the AEM conductivity data. Within the sedimentary packages of a particular geological province there are also internal unconformities. For example, within the Pine Creek Geosyncline metasedimentary sequence, there are several unconformities between different sedimentary packages or groups as shown in [Figures 4–1](#) to [4–3](#). Within the McArthur Basin there are also unconformities between the Katherine River, Mount Rigg and Roper groups. However, not all of these unconformities are depicted in the AEM data due to a lack of contrast in conductivities of the rocks above and below the unconformity, or there is no apparent enhancement or reduction of conductivity along the unconformity.

The AEM signatures of some of the above listed geological province boundary unconformities are examined below. The AEM conductivity data may also contribute to defining the 3D architecture of sedimentary basins that have potential for unconformity-related uranium mineral systems. A 3D–model for part of the Birrindudu Basin is also presented.

#### **6.3.2.8     *Cretaceous sediments***

Cretaceous sediments are present in the Money Shoal, Bonaparte and Carpentaria basins. They comprise flat-lying strata of sandstone, siltstone and minor conglomerate. They form tablelands, mesas, buttes and isolated rounded outcrops mantling all older rock units. These sediments are remnants of a once extensive cover that may have overlain the entire Pine Creek Orogen (Ahmad *et al.* 1993; Kruse *et al.* 1994). Cretaceous sediments are expected to be much more extensive under the Cenozoic cover than the outcrops mapped in these areas.

The Cretaceous sediments on FERGUSSON RIVER were mapped as Mullaman Beds by Pontifex and Mendum (1972), comprising a 30 m thick sequence of sandstone, siltstone and porcellanite. In the Wingate Mountains area, along lines 1205201 and 1005201, there are two moderate conductors. The thin upper conductor corresponds with the Cretaceous sediments of Bonaparte Basin, while the lower conductor correlates with underlying sediments of the Auvergne Group of the Victoria Basin.

This also seems to be the case in the Carpentaria Basin, which overlies the Daly Basin on the northeast part of FERGUSSON RIVER. Here a thin weak to moderately conductive layer of the Cretaceous Mullaman Beds overlies resistive Oolloo Dolostone and conductive sediments of the Jinduckin Formation of the Daly Basin (lines 10190–10240).

#### **6.3.2.9     *Bonaparte Basin***

The AEM survey covers the east part of the Bonaparte Basin on CAPE SCOTT and PORT KEATS. Exposed geology of the Basin in this area includes undivided Cretaceous sediments and the Permian Kulshill Formation. The Kulshill Formation consists of siltstone, fine to coarse grained feldspathic and micaceous sandstone, shale, siltstone, diamictite, minor limestone and basal conglomerate.

The Bonaparte Basin sediments in the survey area dip very gently towards the sea on the west. They are moderately conductive (Figure 6–3) and include at least two conductors. In line 100461 (Figure 6–36), the lower conductor is less than 150 m thick but seems to be truncated by an east-dipping normal fault at about 500 m near the west end of the survey line. The upper conductor is probably less than 20m thick but thickened west of the fault to more than 150 m. This seems to suggest that the fault was a growth fault.

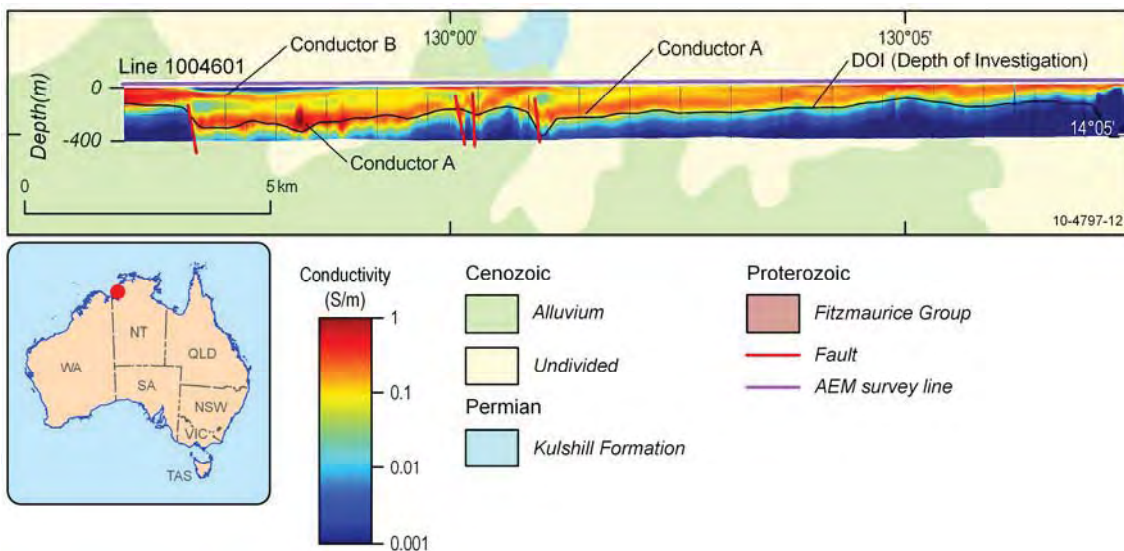


**Figure 6–36:** GA-LEI conductivity section (line 1004601) overlies the surface geology map in the Bonaparte Basin. Conductivity sections displayed at three times vertical exaggeration. Conductors A and B are interpreted to be within the Permian Kulshill Formation. Surface geology from Raymond and Retter (2010).

### 6.3.2.10 Daly Basin and Birrindudu Basin

The Cambrian – Ordovician Daly Basin overlies the Birrindudu Basin in the Adelaide River – Pine Creek area. As part of the geological interpretation of the TEMPEST™ conductivity data of the Woolner Granite – Rum Jungle AEM area, a 3D model has been constructed for parts of the area, which is discussed below.

The Daly Basin sediments are moderately conductive overall, with discrete anomalies, as depicted in the conductance image (Figure 6–3). On PINE CREEK, the Daly River Group is a 700 m thick sequence of mostly carbonate sediments. Stratigraphic units of the Group and its rock types are summarised in Table 6–5.

#### 6.3.2.10.1 Correlation with Daly Basin boundary and sedimentary units

The Daly Basin boundary is well depicted along both the east and west margins of the Basin. Moderately conductive sedimentary units of the Basin dip gently towards the centre of the Basin and are in sharp contrast of the generally resistive older basement rocks.

Along the west margin of the Daly Basin, the basal unconformity is recognizable but the sub-parallel and shallowly dipping conductors in the underlying Tolmer Group sediments may obscure the position of the basal unconformity.

In the area around the Fenton Granite, the Tindall Limestone seems to be a layer of varying thickness and is generally resistive, although parts may be weakly to moderately conductive. The Jinduckin Formation is consistently conductive and thickens towards the central part of the Basin, e.g., west of the Fenton Granite.

In the area northeast of Limestone Hill, along lines 10140 and 10150, the Jindare Formation is conductive and dips gently to the west. Overlying the Jindare Formation is a resistive layer, which is in turn overlain by a conductive layer of the Daly River Group ([Figure 6–37](#)).

The Oolloo Dolostone seems to be resistive, as depicted along lines 10140-10160 ([Figure 6–38](#)). This resistive layer becomes thinner towards the north, which may be due to the thinning of the Oolloo Dolostone towards the northern part of the Basin, regolith's contribution to conductivity or a combination of both.

**Table 6-5:** Stratigraphy of the Daly River Group on the Pine Creek 1:250 000 map sheet

	UNIT	LITHOLOGY	THICKNESS (M)
Daly River Group	Oolloo Dolostone	Ooid and stromatolitic dolostone and minor dolomitic sandstone	190
	Jinduckin Formation	Dolomitic siliciclastic siltstone, dolomitic sandstone – siltstone interbeds, dolostone and quartz sandstone	350
	Tindall Limestone	Bioclastic, mottled, oncoid and stromatolitic limestone, minor mudstone; Basal siltstone, sandstone and conglomerate	180
<hr/>			
Jindare Formation		Medium to coarse quartz sandstone, siltstone, claystone, basal conglomerate and chert	200

*After Ahmad et al. (1993)*

**Table 6-6:** Stratigraphy of the Tolmer Group

UNIT	LITHOLOGY	THICKNESS (M)
Waterbag Creek Formation	Red mudstone with thin arenite layers, abundant halite casts	150-300
Hinde Dolomite	Dolomite and minor limestone, dolomitic siltstone	120
Stray Creek Sandstone	Flaggy quartz sandstone, green siltstone and shale, dolomitic in places	180
Depot Creek Sandstone	Pink quartz sandstone, quartz pebble conglomerate lenses	300-600

*After GA's 1:1m surface geology map, Malone (1962) and Pontifex and Mendum (1972)*

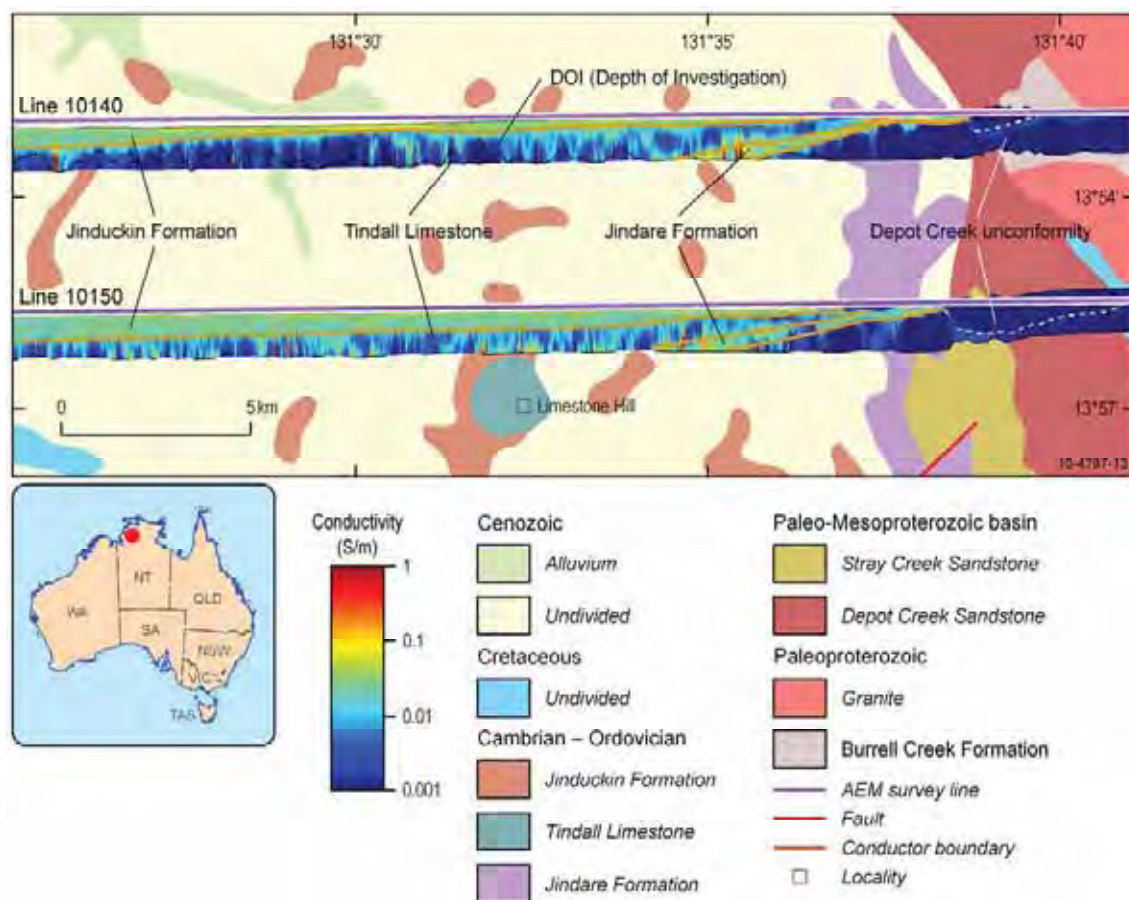


**Figure 6–37:** GA–LEI conductivity sections 10140–10150 over surface geology in the Limestone Hill area. Surface geology from Raymond and Retter (2010). AEM conductivity sections displayed at three times vertical exaggeration.

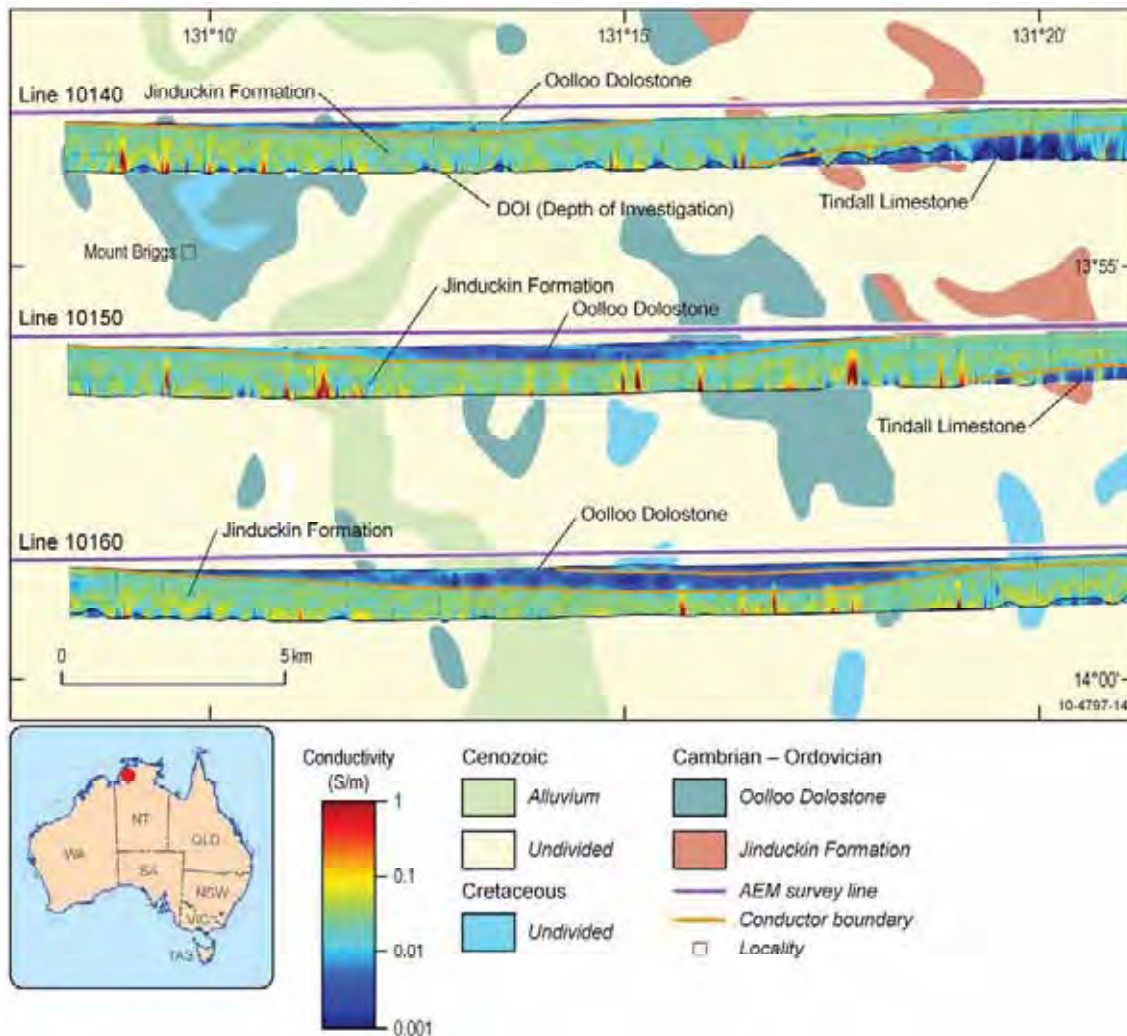


**Figure 6–38:** GA–LEI conductivity sections 10140–10160 over surface geology in the Mt Briggs area. Surface geology from Raymond and Rettter (2010). AEM conductivity sections displayed at three times vertical exaggeration.

#### 6.3.2.10.2 The Depot Creek unconformity

Remnants of the Meso- to Paleoproterozoic Birrindudu Basin cover a north-northeast trending area about 150 km wide and 700 km long from the Tanami area to the south of the Rum Jungle Complex. The northern most part of the basin is shown in [Figure 3–1](#).

On the Pine Creek and Ferguson River 1:250,000 sheets the Tolmer Group of the Birrindudu Basin is mapped in outcrops in the Rum Jungle Complex and around the northern part of the Daly Basin and is likely to be present beneath this part of the Daly Basin.

Four units of the Tolmer Group, within the Birrindudu Basin, are mapped on the Pine Creek and Ferguson River sheets, namely the Waterbag Creek Formation, Hinde Dolomite, Stray Creek Sandstone, and Depot Creek Sandstone ([Table 6–6](#)). The lower-most unit, the Depot Creek Sandstone, unconformably overlies the Pine Creek Orogen in this area. It is correlated with the Kombolgie Subgroup (or Kombolgie Sandstone).

The Depot Creek Sandstone – Pine Creek Orogen unconformity is depicted on many AEM conductivity sections along the east and west boundaries of the Birrindudu Basin, which show the unconformity dipping towards central part of the Basin. The unconformity seems to be best depicted in the following two areas:

- From Hayes Creek to the Umbravarra Leocogranite on the east margin of the Daly Basin near the southern border of the Pine Creek 1:250 000 map sheet (line 10080 to line 10180, [Figure 6–39](#)). A 3D model for the area south of Hayes Creek is shown in [Figure 6–43](#); and,
- From the Jammine Granite to Priors Knob west of the Daly Basin (line 1004401 to line 1004801).

Further north and south of these two areas, the unconformity is depicted in some AEM conductivity sections but not continuously in adjacent lines.

Strong and moderate conductors are present at or near the base of the Stray Creek Sandstone and Hinde Dolomite, and in the Waterbag Creek Formation, as seen along lines 10030 and 10041 about 18 to 23 kilometres south of Adelaide River.

West of the Daly Basin, a moderate conductor in the Stray Creek Sandstone and at least three moderate conductors can be identified within the Hinde Dolomite, for example, along line 1004001 ([Figure 6–40](#)).

**Geological and energy implications of the Pine Creek airborne electromagnetic (AEM) survey, Northern Territory, Australia**

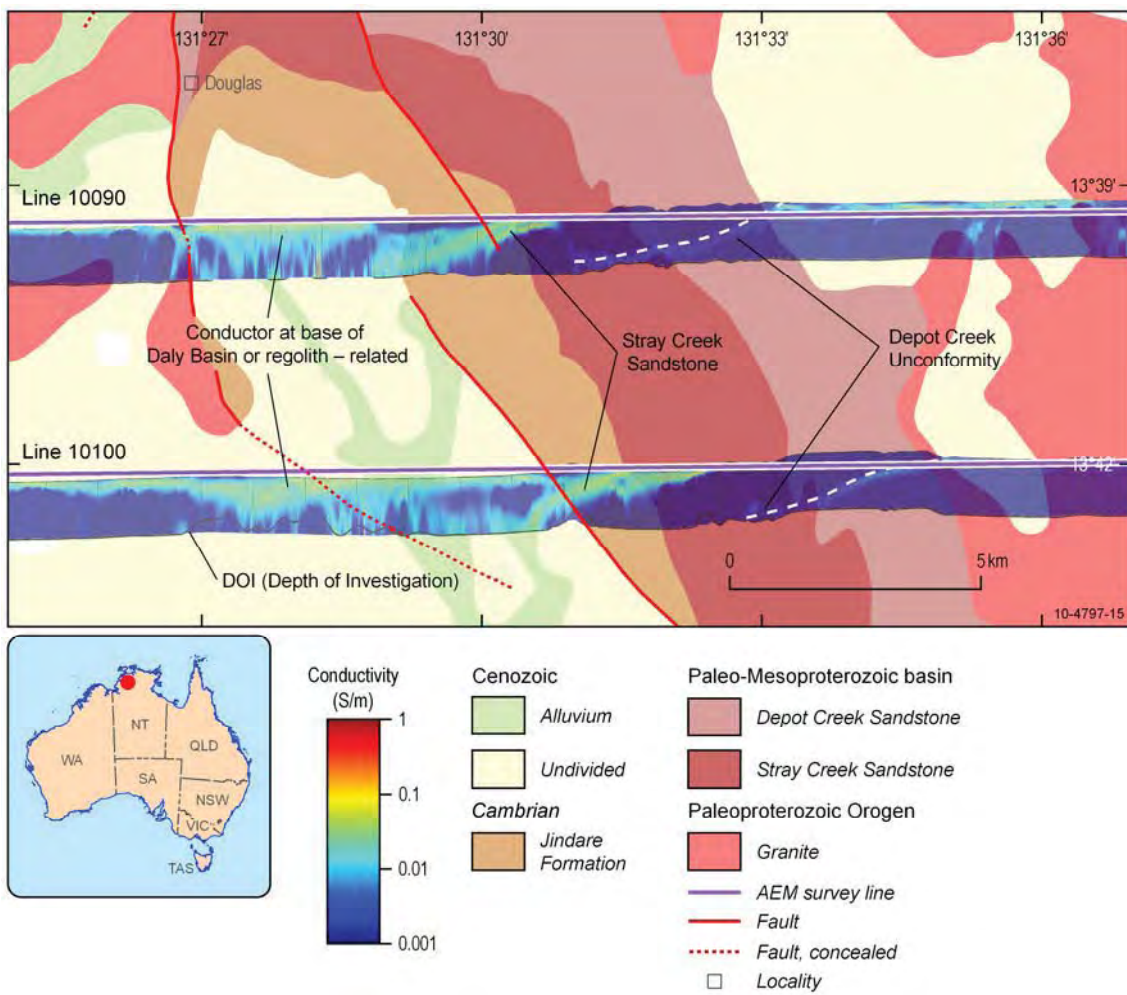


**Figure 6-39:** GA-LEI conductivity sections 10090-10100 over surface geology southeast of the Douglas township. Surface geology from Raymond and Retter (2010). Conductivity sections displayed at 40% transparency to show geology underlying, and at three times vertical exaggeration.

**Geological and energy implications of the Pine Creek airborne electromagnetic (AEM) survey, Northern Territory, Australia**

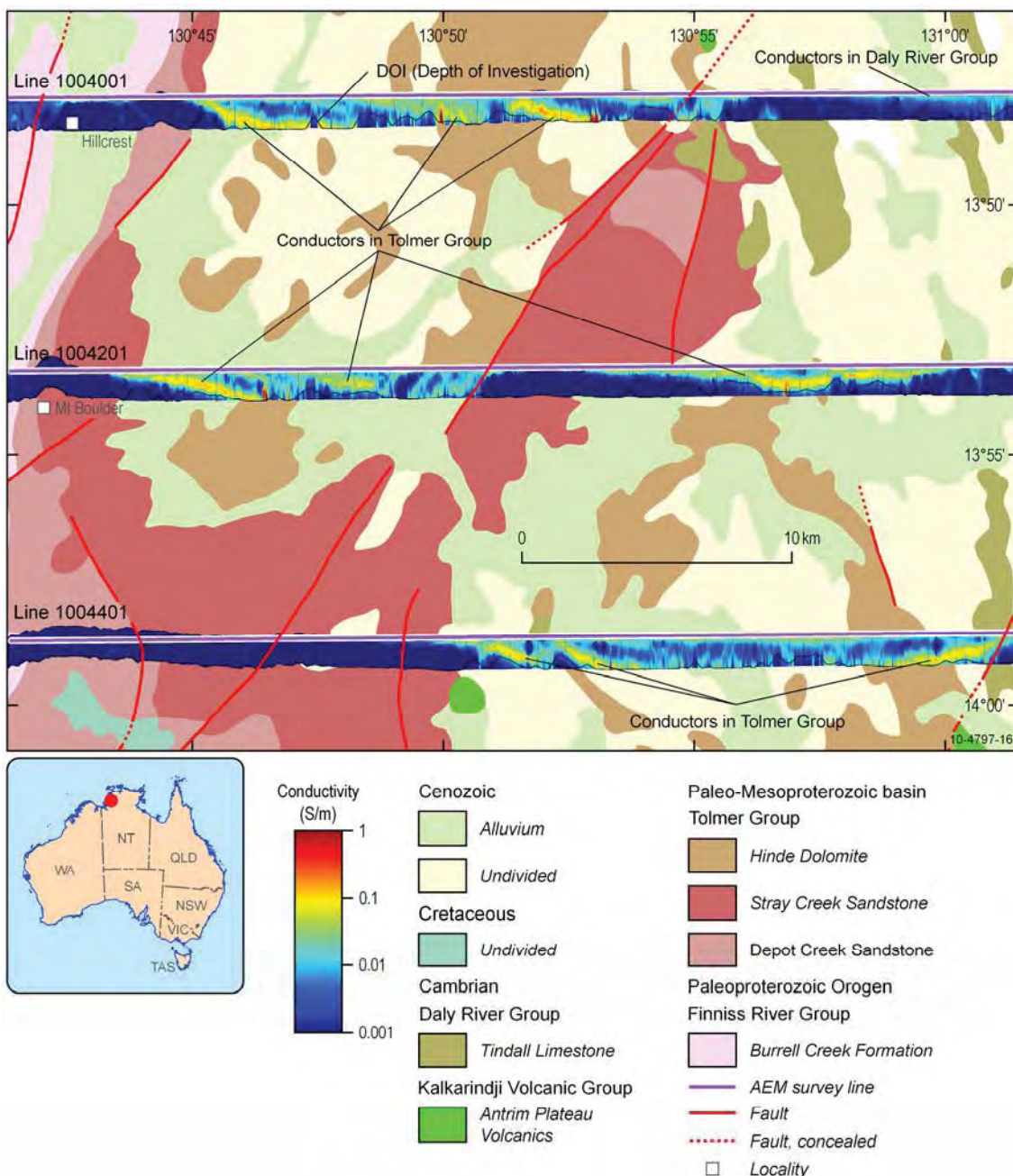


**Figure 6–40:** GA–LEI conductivity sections 1004001 – 1004401 over surface geology in the Mt Boulder area. Surface geology from Raymond and Retter (2010). AEM conductivity sections displayed at three times vertical exaggeration.

### 6.3.2.10.3 3D-modelling of the eastern Daly and Birrindudu basins

A 3D model of the northeast margins of the Daly Basin and Birrindudu Basin in the Hayes Creek area was constructed in GOCAD® 2009.1 (Paradigm™). Assessment of the GA–LEI conductivity sections revealed three key marker horizons which could be consistently identified on most GA–LEI sections in the area. Correlation of those horizons with surface geology mapping indicated that each directly correlated with a known geological contact as shown in [Figure 6–41](#). [Table 6–7](#) describes each horizon. A fourth horizon might be mappable in some parts of the region, separating the resistive Jindare Formation and conductive underlying Stray Creek Sandstone ([Figure 6–41](#)); however this was more poorly defined on many sections. Note that conductivity sections shown in this section have a different colour stretch map to those in the rest of this volume due to their display in GOCAD® and the use of different colour stretch limits to emphasise details within this localised portion of the survey area.

Using GOCAD®, the three horizons were manually digitised from east-west oriented curves identified in every flight line in the area, extending from line 10180 in the south to line 10070 in the north. The line spacings in the area vary from 5 km in the south to 1667 m in the middle and north. No extrapolation was applied when digitising the curves. They were only digitised where supported by the available GA–LEI conductivity section. The curves truncate at surface and at the deepest point to which they could be reliably traced. The curves were then linked between sections using GOCAD®’s Node Link feature ([Figure 6–42](#)), which controls how adjacent curves are connected in a surface. Node Links were used sparingly to indicate the limits of each body, and the location of particularly continuous highs or lows along each curve.

For each horizon a surface was constructed in GOCAD® by connecting interpreted curves on adjacent flight lines into surface strips which were then merged together to create a single seamless surface for each horizon. A 3D model is built for part of the Birrindudu Basin south of Hayes Creek ([Figure 6–43](#)). This 3D model graphically illustrates the relationships between the three mapped horizons with a clarity and certainty that would have not been possible without AEM. In particular, it illustrates the geometry of the shallow-dipping Depot Creek unconformity to the west and the base of the Daly Basin in this area.

**Table 6–7:** The three marker horizons used to build the 3D model of part of the Birrindudu Basin south of Hayes Creek

	CONDUCTIVITY CHARACTER	GEOLOGICAL CORRELATION
1	Second sharp conductivity contrast; separates conductive material above from resistive material below	Top of resistive Jindare Formation (sub Daly Basin), and a likely conductive basal unit of the Daly Basin
2	First sharp conductivity contrast; separates conductive material above from resistive material below	Contact between conductive Stray Creek Sandstone and resistive Depot Creek Sandstone
3	Bedding parallel conductivity anomaly between more resistive packages	Unconformity along base of Depot Creek Sandstone

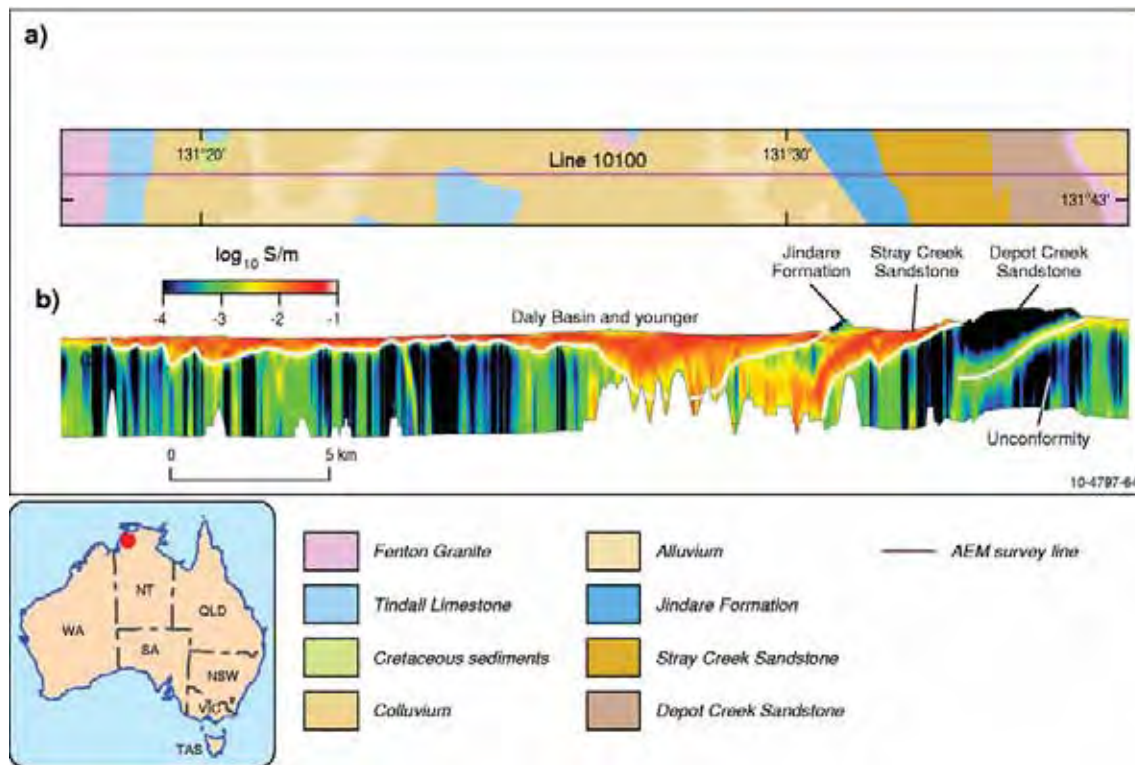


**Figure 6-41:** GA-LEI conductivity sections used in 3D modelling of the eastern Daly and Birrindudu basins.

(a): Surface geology from Raymond and Rettie (2010);  
(b): GA-LEI section 10100. The top of the section show topography and the bottom of the section is clipped by the Depth of Investigation Line (DOI). White lines on the conductivity section indicate the three horizons interpreted through out the model, as represented on this section. The depth continuation of the basal Depot Creek Sandstone unconformity is truncated where it is no longer possible to trace the conductivity anomaly, either due to AEM signal penetration limitations or potential geological truncation. Five times vertical exaggeration.

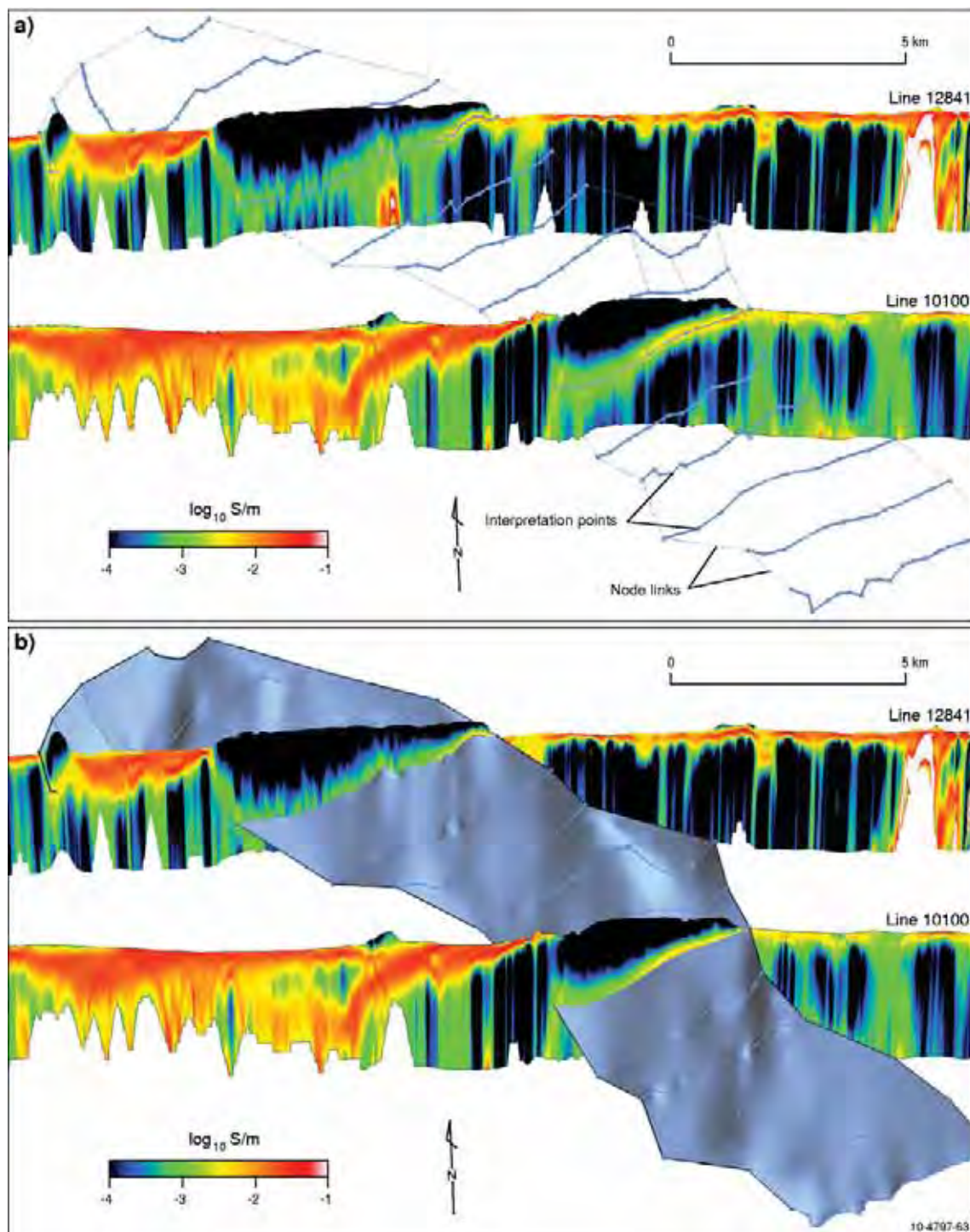


**Figure 6-42:** GOCAD® images illustrate the construction of the 3D model for the Daly and Birrindudu basins. AEM sections displayed at five times vertical exaggeration.

(a): Interpreted GOCAD® curves used to define the basal Depot Creek Sandstone unconformity in the northern portion of the model, showing lines 12841 and 10100 as examples. Node Links were used to connect adjacent curves.

(b): GOCAD® surface for the basal Depot Creek Sandstone unconformity created by merging strips of surface created between each pair of adjacent curves.

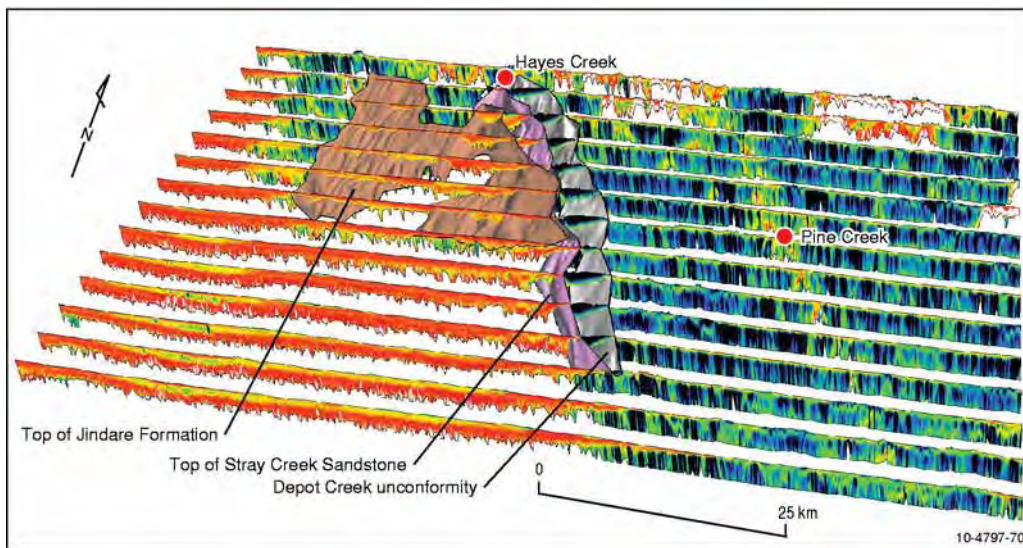


**Figure 6-43:** GA-LEI conductivity sections in 3D of the Pine Creek area and a 3D model of part of the Daly and Birrindudu basins. Five times vertical exaggerations. The conductivity sections are 600 m deep.

#### 6.3.2.11 Victoria Basin

On the Fergusson River and Port Keats 1:250000 geological map sheets, the Neoproterozoic Auvergne Group of the Victoria Basin is mapped as a package of sandstone, siltstone, dolomitic sandstone and dolomite (Table 6-7). The Rum Jungle AEM survey by TEMPEST™ covers the northern most part of the Basin, which is faulted against older Mesoproterozoic rocks in most places.

Here a number of constituents of the Auvergne Group are mapped, including (from older to younger units) the Angalarri Siltstone, the Saddle Creek Formation, the Pinkerton Sandstone, the Lloyd Creek Formation, and the Spencer Sandstone (Table 6-8). Overlying the Auvergne Group in part of this area is the Early Cambrian Antrim Plateau Volcanics of the Kalkarindji Volcanic Group, and then undivided Cretaceous sediments. The Antrim Plateau Volcanics consists of massive and vesicular basalt, minor agglomerate, and intercalated sediments.

**Table 6-8:** Stratigraphy of the Auvergne Group on the Fergusson River 1:250 000 map sheet

UNIT	LITHOLOGY	THICKNESS (M)
Shoal Reach Formation	Siltstone, minor dolomite and sandstone	60
Spencer Sandstone	Quartz sandstone, minor silty sandstone, dolomitic sandstone	60
Lloyd Creek Formation	Dolomite, algal and oolitic, sandy and silty. Also grey-green siltstone.	75
Pinkerton Sandstone	White, massive quartz sandstone, minor siltstone and shale	50
Saddle Creek Formation	Upper sandstone, siltstone, and dolomite Basal sandstone; cross-bedded,	35
Angalarri Siltstone	Siltstone, greyish green shale, silty sandstone interbeds	300
Jasper Gorge Sandstone	Massive, blocky quartz sandstone; rare siltstone interbeds	60
Stubb Formation	Siltstone and shale, minor flaggy sandstone	45

*After Pontifex and Mendum (1972)*

Overall the Victoria Basin area is moderately conductive, with patches of slightly higher or lower conductivity (see both [Figure 3-2](#) and [Figure 6-3](#)). There are at least three conductors in the Auvergne Group sediments, as depicted in the GA–LEI conductivity sections near the Victoria River Fault contact with the unexposed Paleoproterozoic Chilling Sandstone of the Finniss River Group at the north end of the Basin along lines 1005501 and 1005601 ([Figure 6-44](#)). Here the Neoproterozoic Auvergne Group sediments dip gently to the southeast. Further east the sediments are almost horizontal. [Figure 6-44](#) shows more details in the GA–LEI conductivity sections (a) compared with the EM Flow™ sections (b). This extra detail available in the GA–LEI conductivity sections emphasizes the distinct advantages of using the GA–LEI data for geological interpretations.

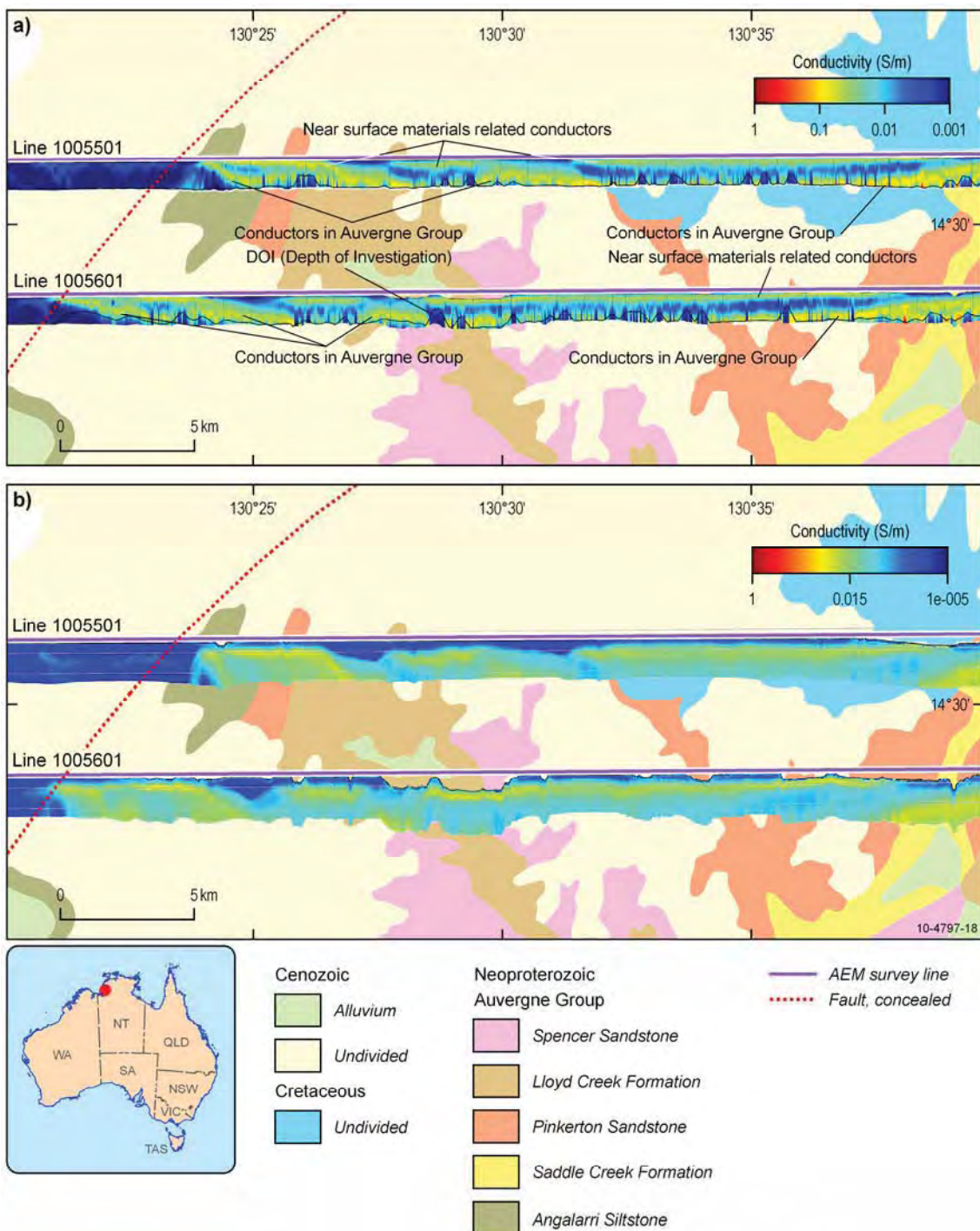


**Figure 6-44:** GA-LEI conductivity and EM Flow™ CDI sections over surface geology in the northern part of the Victoria Basin. Surface geology from Raymond and Retter (2010).

(a) GA-LEI conductivity sections displayed at three times vertical exaggeration,  
(b) EM Flow™ (Version 5.23–13) CDI sections displayed at five times vertical exaggeration.

### 6.3.2.12 Fitzmaurice Basin

In the Woolner Granite – Rum Jungle AEM survey area, the Fitzmaurice Group includes (from lower part to upper part) the Moyle River Formation, the Goobaieri Formation, the Lalngang Sandstone and the Legune Formation. The lithology and thickness are summarised in [Table 6–9](#).

The Fitzmaurice Group is faulted against the Pine Creek Orogen in most places ([Figure 6–2](#)). Overall it is resistive to very weakly conductive ([Figure 6–3](#)), but there are some discrete and weakly to moderately conductive anomalies at depth (e.g., in line 1005301). The boundaries between the Lalngang Sandstone, the Goobaieri Formation and the Moyle River Formation seem to be slightly more conductive than these units (e.g., in lines 1005201, 1005301, 1005401).

**Table 6–9:** Stratigraphy of the Fitzmaurice Group on the Port Keats 1:250 000 sheet

UNIT	LITHOLOGY	THICKNESS (M)
Legune Formation	Silica cemented quartz sandstone, siltstone	2100
Lalngang Sandstone	Sandstone	1850
Goobaieri Formation	Quartz sandstone, shale, siltstone	610
Moyle River Formation	Silica cemented quartz sandstone, minor siltstone and pebble conglomerate	1100-11 000

*After GA's 1:1000 000 Surface Geology of Australia, and Morgan (1972)*

### 6.3.2.13 Pine Creek Orogen

During the Top End Orogeny, about 1870 – 1690 Ma (Needham *et al.* 1988), the Paleoproterozoic Pine Creek Geosyncline sequence experienced regional metamorphism up to amphibolite facies and multiple deformations that produced a network of faults and tight to isoclinal folds, forming the Pine Creek Orogen, as summarised in [Chapter 3](#). The Pine Creek sequence contains strong conductors of carbonaceous and pyritic sedimentary rocks, which are potential reductants for uranium mineralisation. In this section we will examine the distribution of conductors in the Pine Creek AEM survey area.

#### 6.3.2.13.1 Strong conductors in the Central Domain

There are strongly conductive, carbonaceous and pyritic rocks in the Central Domain ([Figure 3–2](#)) of the Pine Creek Geosyncline. Examples units include the Koolpin Formation (South Alligator Group), the Whites Formation (Mount Partridge Group), and the Masson Formation (Namoona Group) ([Table 6–10](#)). Other units in the sequence may also contain conductive rocks in parts. In the Woolner Granite – Rum Jungle area in the southern part of Darwin and the northern part of Pine Creek, these strongly conductive rocks are mostly at the edge of the Burrell Creek Formation and in close proximity to granite plutons ([Figure 6–2](#), [Figure 6–3](#), [Figure 6–45](#)), including:

- The Rum Jungle complex;
- The Mt Bunday Granite;
- The Margaret and Burnside granites;
- The Prices Springs and McMinn's Bluff granites; and,
- The Minglo and Allamber Springs granites.

These strongly conductive rocks have apparently been uplifted to the current crustal level, perhaps along with the granite plutons. These granites were the sources of some inherited zircons in the Katherine River

Group (Page, R.W., unpublished data in Geoscience Australia's OZCHRON database), which means that the granites were eroded at the time of deposition of Katherine River Group.

Faults and tight to isoclinal folds are well developed in the Pine Creek Orogen. Gold mineralisation in the Orogen is structurally controlled. The conductive units and anomalies can be used to map the presence of faults and folds ([Figure 6–45](#)). In mostly resistive or weakly conductive rocks, faults may show slightly higher conductivity due to the presence of fluids, alteration and mineralisation ([Figure 6–34](#) [Figure 6–45](#)). Close examination and correlation are required to ascertain the cause. Many faults and folds are depicted in the GA–LEI conductivity sections ([Figure 6–45](#)). Close correlation and interpretation of an area south-southeast of Rum Jungle is presented in [Figure 6–46](#), which shows interpretations of several faults and folds along lines 1001902 and 1002101.

In the area between the Rum Jungle and the Water House domes, lines 1001501 and 1101901 run over resistive granites in the east to the Pine Creek Geosyncline sequence west of the Giants Reef Complex, which contains weak and strong conductors. The Pine Creek sequence here consists of the Coomalie Dolomite, the Geolsec Formation, the Whites Formation and the South Alligator Group.

In this area, the Coomalie Dolomite, the Geolsec Formation and the South Alligator Group are largely resistive. The Whites Formation consists of strong conductors in parts. There are two antiforms in the Whites Formation about 2-3 km south and southeast of Mt Burton, as defined by the folded dolerite sills. There is likely to be an N-S trending fault between the two antiforms, which is consistent with the geometry of AEM anomalies along line 1101901.

The western fold is also depicted in line 1001501. The Giants Reef Fault and several faults to the west seem to have also been depicted in the AEM data.

#### *6.3.2.13.2 Apparent shallow conductivity anomalies in GA–LEI conductivity sections*

Most strongly conductive anomalies due to carbonaceous and pyritic metasedimentary rocks in the Woolner Granite – Rum Jungle area are depicted at shallow depth, in the top 200-300 m, e.g., lines 1001401, 1001501 and 1001704 ([Figure 6–45](#) and [Figure 6–47](#)). The carbonaceous and pyritic metasedimentary rocks are present in the Koolpin Formation, the Gerowie Tuff and the Mt Bonnie Formation of the Pine Creek Orogen.

[Figure 6–47](#) shows line 1001401 over solid geology east of the Rum Jungle Complex. This presents a series of faulted and tightly to isoclinally folded, mostly N-S to NNE-trending metasedimentary sequence. Because the metasedimentary rocks mostly dip steeply (<70°), it is estimated that the carbonaceous and pyritic conductors are likely to be more than 200-300 m deep.

The apparent shallow strongly conductive anomalies, mostly in the top 200-300 m, are due to the limited penetration of AEM survey in such strongly conductive areas. In such areas, the strong conductors may be used to map the presence of faults and folds. They can not be used to map the depth of the strongly conductive rocks because the bottom of such rocks is not detected in the AEM surveys. Thus caution should be exercised in geological interpretation in areas of strongly conductive and steeply dipping sequences. Here the DOI becomes an important guide in the process.

Another noted area of apparent shallow strongly conductive anomalies is west of the Minglo Granite along lines 10020, 10030 and 10041 over the Wildman Siltstone and the Mundogie Sandstone.

**Table 6-10:** Paleoproterozoic metasedimentary rocks in the Pine Creek Orogen

	UNIT	LITHOLOGY	THICKNESS (M)
Finnis Group	Chilling Sandstone	Siliceous meta-quartzarenite	
	Burrell Creek Formation	Greywacke, shale, slate, phyllite, minor conglomerate	up to 1500
	Warrs Volcanic Member	Metamorphosed acid volcanics, tuffaceous siltstone, volcaniclastic lithic arenite	
	Mulluk-Mulluk Volcanic Member	Metamorphosed spherulitic rhyolite	
South Alligator Group	Mt Bonnie Formation	Shale, mudstone, phyllite, siltstone, greywacke, minor tuffaceous chert, tuff, banded iron formation	700
	Gerowie Tuff	Siltstone, phyllite, argillite, tuffaceous chert, tuff	400
	Koolpin Formation	Siltstone, shale, mudstone, carbonaceous mudstone, banded iron formation, dolomite, tourmalinite	500
Mount Partridge Group	Mt Dean Volcanic Member	Altered mafic volcanics	up to 20
	Acacia Gap Quartzite Member	Quartzite, commonly pyritic, sandstone, shale and phyllite	up to 300
	Whites Formation	Calcareous and carbonaceous argillite, dololutite, dolarenite, rare quartzite, calcareous para-amphibolite	up to 500
	Coomalie Dolomite	Stromatolitic magnesite and marble, metalutite, commonly graphitic, minor para-amphibolite	up to 300
	Crater Formation	Conglomerate, arkose, quartzite, sandstone, minor siltstone and shale	up to 600
	Wildman Siltstone	Siltstone, carbonaceous pyritic siltstone, phyllite, minor sandstone	up to 750
	Mundogie Sandstone	Coarse, pebbly feldspathic sandstone, conglomerate, quartzite, phyllite, carbonaceous phyllite, siltstone	500
Namoona Group	Celia Dolomite	Stromatolitic magnesite, dolomitic marble, commonly silicified at the surface	up to 300
	Beestons Formation	Quartz conglomerate, grit, arkose, quartz sandstone, minor banded iron formation	up to 300
	Masson Formation	Carbonaceous phyllite, slate, siltstone, quartzite, feldspathic quartzite, massive ironstone, marble	1000
	Hermit Creek Metamorphics	Metamorphosed mafic igneous rocks, psammitic and pelitic gneiss	

After Ahmad *et al.* (1993)

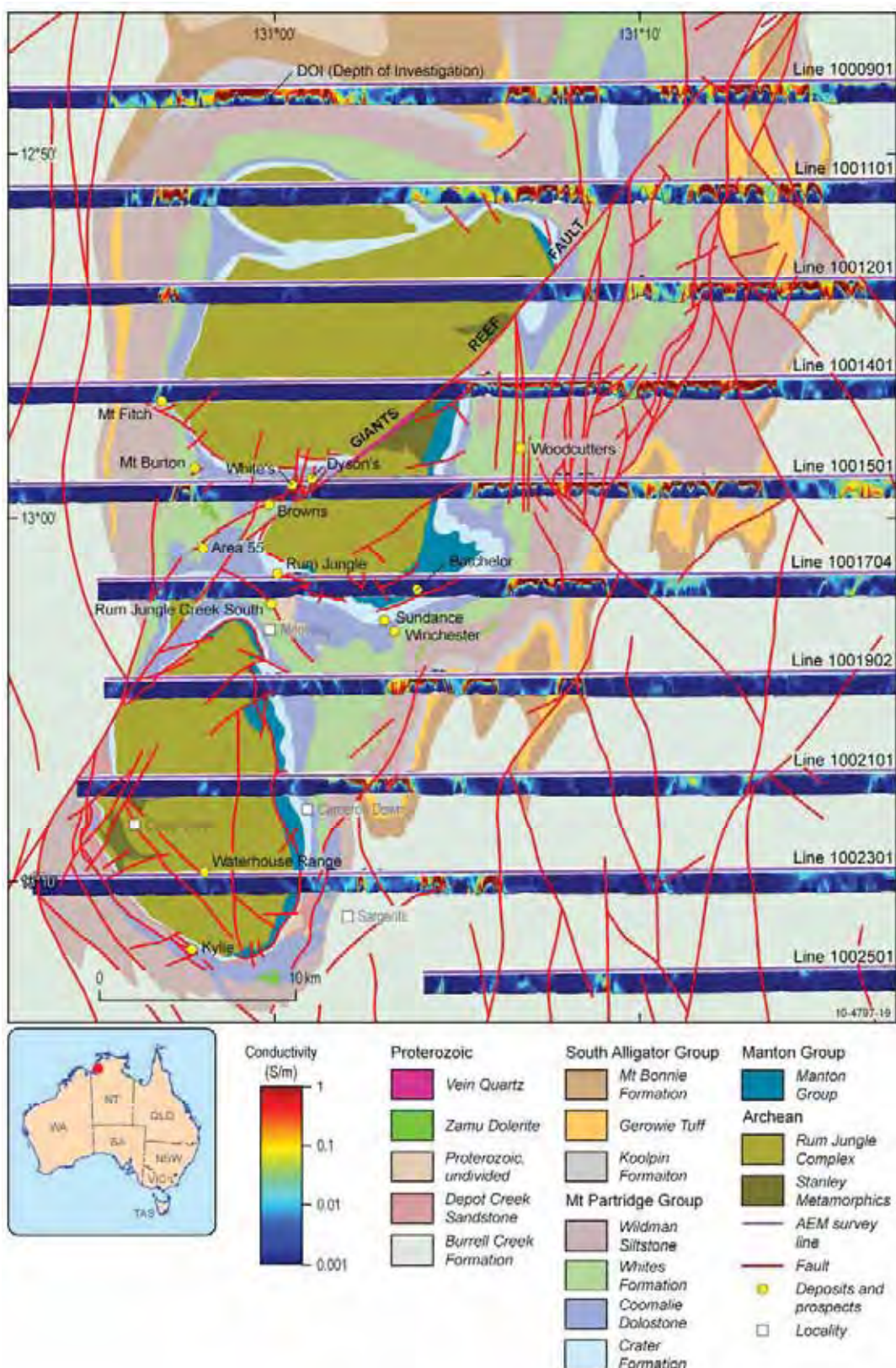


**Figure 6-45:** GA-LEI conductivity sections in the Rum Jungle area. Solid geology: after NTGS (2005). Conductivity sections displayed at three times vertical exaggeration. Strong conductors are attributed to carbonaceous and pyritic sediments within the South Alligator and Mount Partridge Groups.

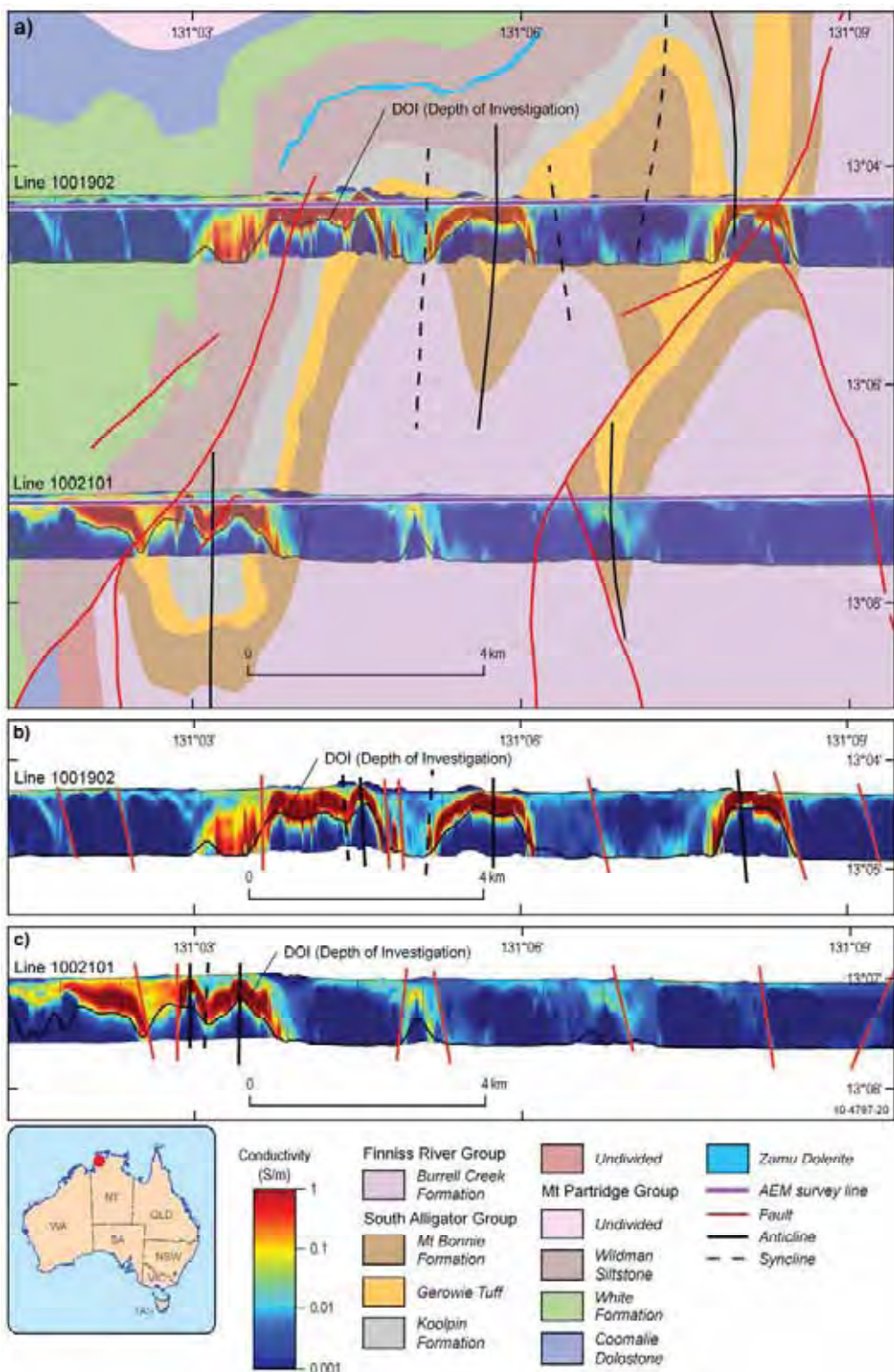


**Figure 6-46:** Interpretation of faults and folds SSE of Rum Jungle Complex. Conductivity sections displayed at three times vertical exaggeration. (a) AEM conductivity sections over solid geology (NTGS, 2005), (b) & (c) Interpretation on AEM sections. Strong conductors are attributed to carbonaceous and pyritic sediments within the South Alligator and Mount Partridge Groups.

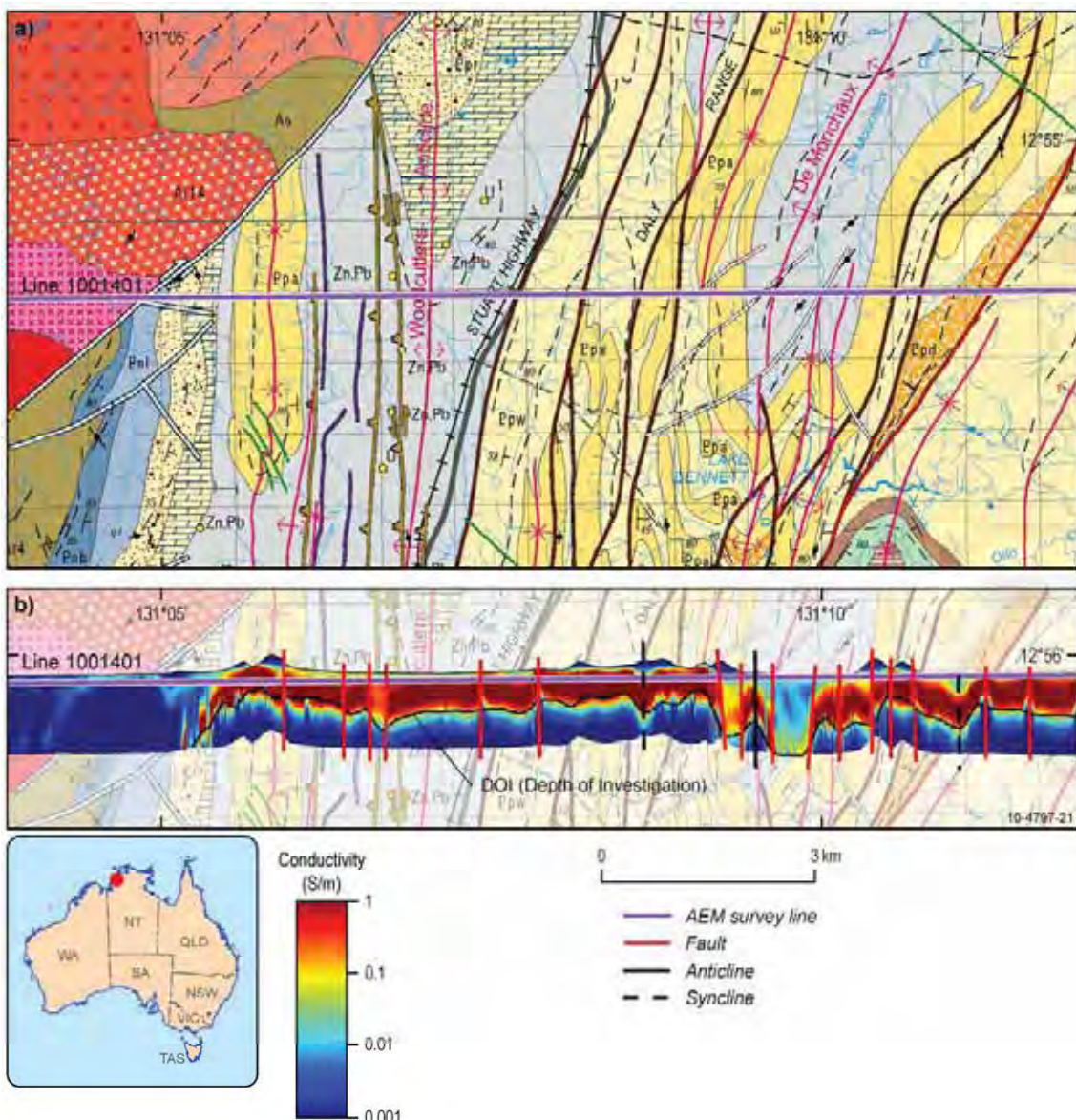


**Figure 6-47:** GA-LEI conductivity section of line 1001401 east of the Rum Jungle complex.  
(a) Solid geology with AEM survey line marked (solid geology after Lally, 2003).  
(b) Interpretation of the AEM section over semi-transparent solid geology map.

Conductivity sections displayed at three times vertical exaggeration.

#### 6.3.2.13.3 Zamu Dolerite

At or near the end of sedimentation, the continental tholeiitic suite of the Zamu Dolerite intruded the sediments mainly as sills. The Zamu Dolerite varies from quartz dolerite to granophyre. It has a composite thickness of ~1.5 km and is most abundant in the South Alligator Group (Ferguson and Needham, 1978).

In the Woolner Granite – Rum Jungle area, the Zamu Dolerite is mainly in the sediments in the areas around the Burnside Granite, between the Prices Springs Granite and the McMinn Bluff Granite, and west of the Minglo Granite. The mapped dolerite sills are in the sediments of the South Alligator Group and older units.

In general, the Zamu Dolerite has a resistive response and does not consistently correlate with AEM conductivity anomalies. However, in places there are AEM conductive anomalies over mapped dolerite:

- Lines 10041, 10050 and 10060 west of the Frances Creek Leucogranite;
- Generally resistive Mundogie Sandstone, but its carbonaceous phyllite may be very conductive; and,
- The conductive Masson Formation (carbonaceous-pyritic and dolomitic slate, phyllite and schist and carbonaceous pyritic dololutite).

In these areas the apparent AEM conductivity anomalies over the Dolerite may be due to the strong conductors below the Dolerite sills.

It is also possible that the contacts between the Zamu Dolerite and metasediments may show different and perhaps enhanced conductivities than the Dolerite and metasediments themselves due to presence of fluids and/or alteration along the contacts.

#### **6.3.2.14 Archean**

Archean rocks are mapped in four areas in the Pine Creek Orogen, namely, the Woolner Granite, the Rum Jungle Complex, the Nanambu Complex and unnamed Archean basement rocks in the Nabarlek area of Nimbuwah Domain. The two complexes are exposed, while the Woolner Granite is interpreted and confirmed from drilling.

Uranium in the Pine Creek Orogen seems to be spatially closely associated with the Archean basement rocks, which could be source rocks of uranium, and conductors in Archean metamorphic rocks may also act as reductors for uranium mineralisation.

##### **6.3.2.14.1 Rum Jungle Complex**

The Rum Jungle and Waterhouse domes in the Rum Jungle area comprise a number of phases of granitic intrusives. Overall the domes are resistive ([Figure 6–3](#)). Some weak conductivity anomalies in the complexes may be due to alteration and/or weathering, particularly alteration in structurally weak areas along fracture zones.

The rings of high conductivity anomalies around the Rum Jungle and Waterhouse domes ([Figure 6–3](#)) are due to the uplift of highly conductive carbonaceous (and pyritic) Paleoproterozoic metasediments around the Archean granite domes.

##### **6.3.2.14.2 Woolner Granite**

The Woolner Granite is not exposed at surface. It is readily interpreted from airborne magnetic data and confirmed from drilling at a depth of 50-80 metres (Pietsch 1985; Pietsch and Stuart-Smith, 1987). Below the Cenozoic sediments including alluvial sediments at surface, there are likely Cretaceous sediments overlying the granite.

A thin moderate to strongly conductive layer is present near surface, at a depth of perhaps less than 50 m ([Figure 6–3](#), [Figure 6–48](#)). The conductivity is attributed to sea water near the coast. The AEM Depth of Investigation (DOI) line in this area is very shallow, less than 20 m, indicating very poor depth penetration.

**Geological and energy implications of the Pine Creek airborne electromagnetic (AEM) survey,  
Northern Territory, Australia**

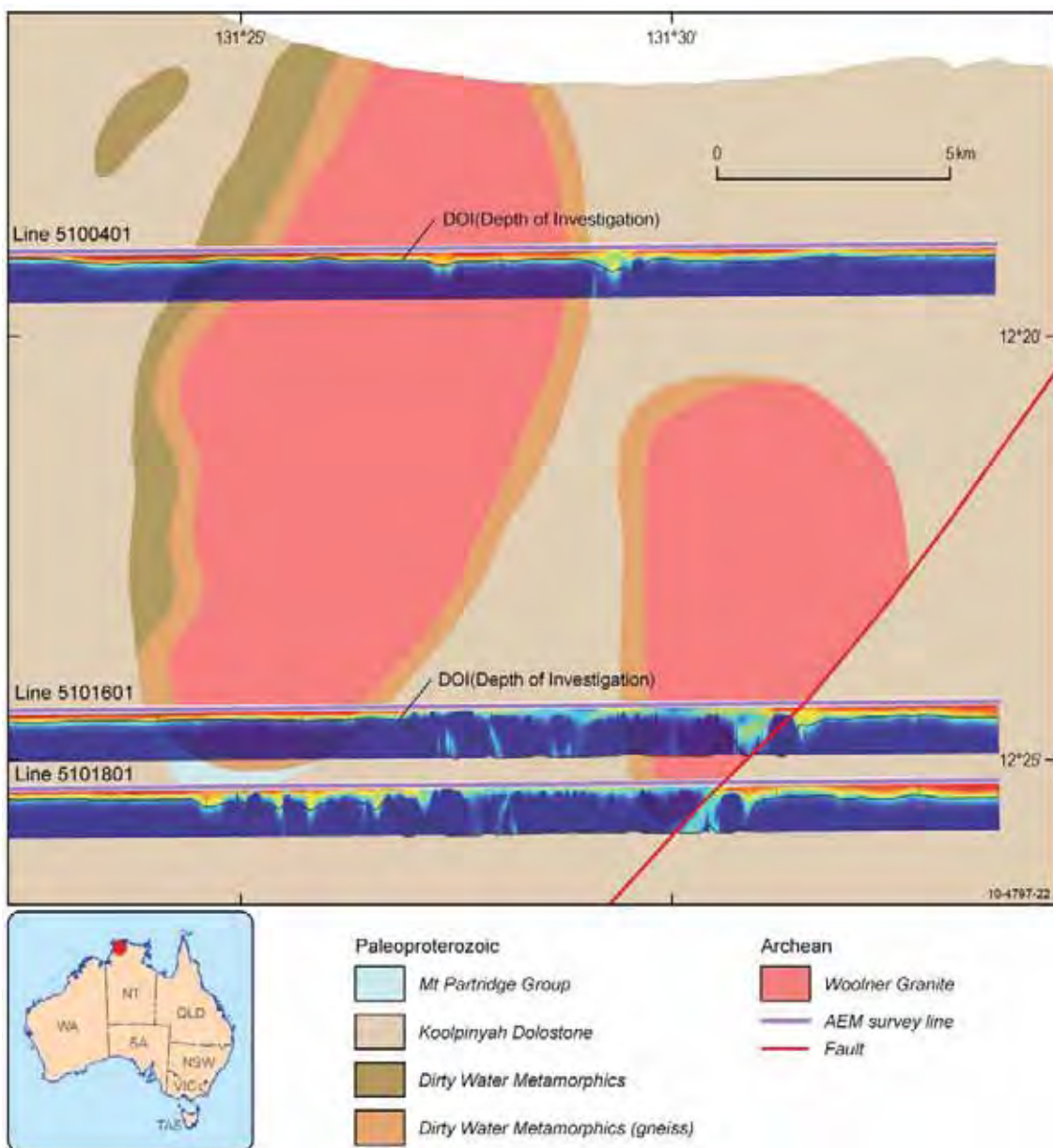


**Figure 6-48:** GA-LEI conductivity sections over solid geology in the Woolner Granite area. Solid geology after NTGS (2005). Conductivity sections displayed at three times vertical exaggeration.

**Table 6-11:** Stratigraphy of the Katherine River Group in the Pine Creek region

UNIT	LITHOLOGY AND THICKNESS	CONDUCTIVITY
West Branch Volcanics	Sandstone, conglomerate, bimodal volcanics, and porphyry (1500-2000 m)	
Gundi Sandstone	Sandstone and conglomerate (300 m)	Resistive
Diamond Creek Volcanics	Mafic lava; minor tuff and volcaniclastic sandstone (230 m)	
McCaw Formation	Mudstone, dolostone, sandstone, and conglomerate lenses (250-300 m)	Resistive
Shadforth Sandstone	Sandstone (40 m)	Resistive
Cottee Formation	Red mudstone, ferruginous sandstone and dolostone; green mudstone (200-600 m)	Resistive
Kombolgie Subgroup	McKay Sandstone	Resistive
	Marlgowa Sandstone	Resistive
	Gilruth / Henwood Creek Volcanic Members	Weakly to moderate conductive
	Gumarrirnbang Sandstone	Resistive
	Nungbalgarri Volcanics	Weakly to moderate conductive
	Mamadawerre Sandstone	Resistive

After Needham (1984; ALLIGATOR RIVER), Ferenczi and Sweet (2005; MOUNT EVELYN), and Kruse et al. (1994; KATHERINE).

## 6.4 GEOLOGICAL INTERPRETATION OF THE VTEM™ DATA IN THE EASTERN PINE CREEK REGION

### 6.4.1 Geological units and conductivity

The Kombolgie AEM survey flown using the VTEM™ system covers part of the McArthur Basin, and parts of the Central Domain and Nimbuwah Domain of the Pine Creek Orogen ([Figure 3-2](#)). Most rocks of the Kombolgie survey area are extremely resistive ([Figure 6-49](#)), thus VTEM™ was able to penetrate to a depth up to 2 km (Costelloe and Brodie, 2011), providing insights of the geology to that depth that no other geological and geophysical methods other than drilling and seismic imaging could previously achieve.

The Meso- to Paleoproterozoic McArthur Basin covers a large area from Jabiru to the Northern Territory-Queensland border. It consists of, from older to younger, the Katherine River, the Mt Rigg and the Roper groups. Unconformities separate the groups. The “Kombolgie Sandstone” or the Kombolgie Subgroup at the base of Katherine River Group ([Table 6-11](#)) is of most interest to uranium explorers because many known uranium deposits in the Jabiru area are related to the Kombolgie unconformity over the Pine Creek Orogen and Archean basement rocks.

Pre-Kombolgie Paleoproterozoic rocks in the Nimbuwah Domain include the Kakadu Group, the Cahill Formation and the Nourlangie Schist ([Table 6-12](#)). The pyritic and carbonaceous schists of the Cahill

Formation are potential AEM conductors, and also provide reductors for uranium mineralisation. Other Paleoproterozoic rocks in the Nimbuwah Domain may also be conductive to some extent.

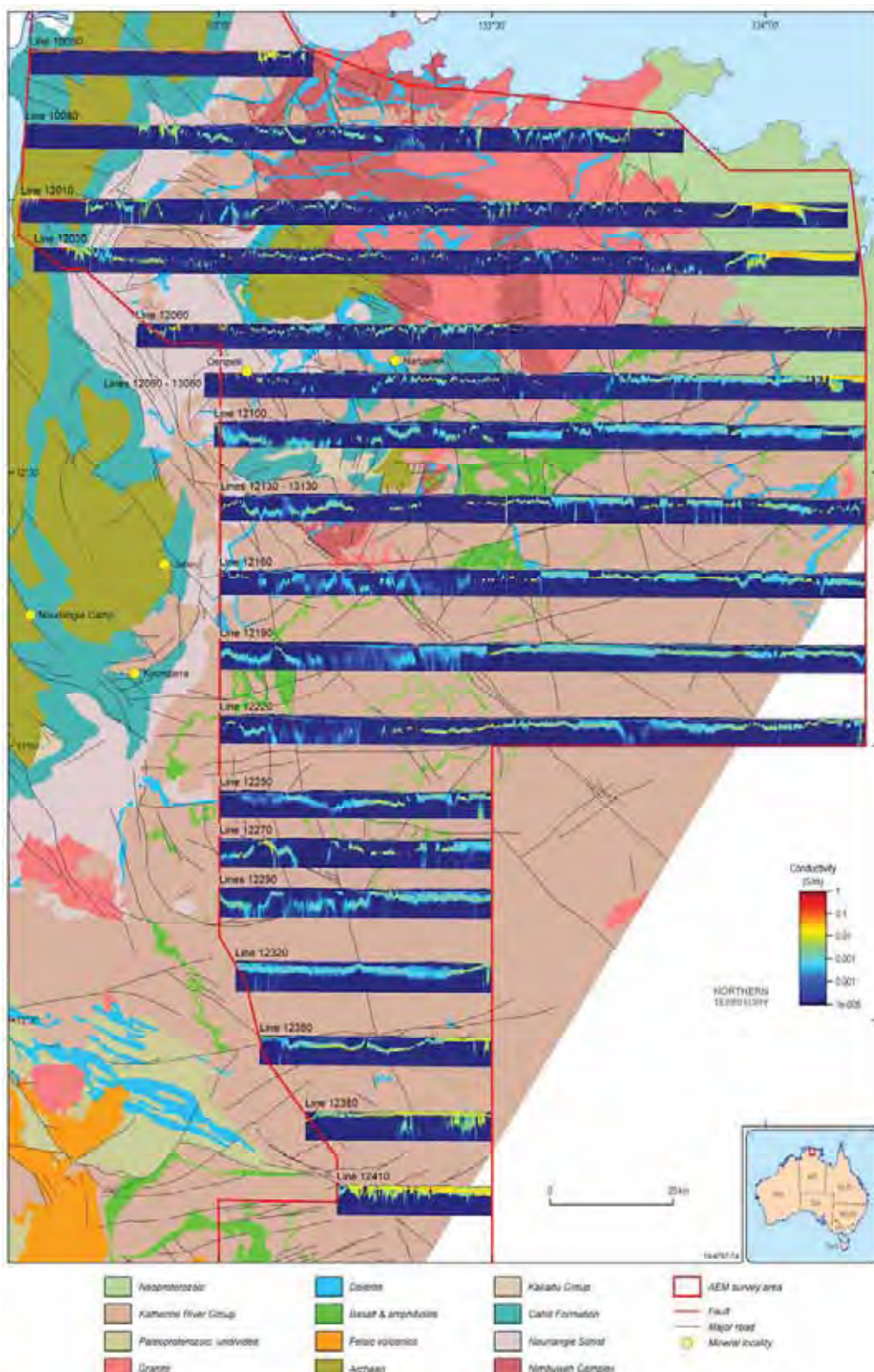


**Figure 6-49:** GA-LEI conductivity sections over solid geology in the Kombolgie area. Solid geology after NTGS (2005). Conductivity sections displayed at two and half times vertical exaggeration.

Archean basement rocks in the Nimbuwah Domain include the Nanambu Complex and recently mapped Archean Arrarra, Kukalak and Njibinjibinj gneisses in western Arnhem Land (Hollis *et al.* 2009; Hollis *et al.* 2011; Carson *et al.* 2010; **Table 6–12**). The Kombolgie AEM survey by VTEM™ covers the Cobourg Peninsula part of the Nanambu Complex.

**Table 6–12:** Stratigraphy of the pre-Kombolgie basement geological units in the Kombolgie AEM survey area

UNIT	LITHOLOGY AND THICKNESS	CONDUCTIVITY	
Nimbuwah granitic rocks (1886–1866 Ma)	Granitic rocks	Resistive	
Nourlangie Schist	Psammitic to pelitic schist with a higher proportion of mica schist than the Cahill Formation.	Resistive	
Cahill Formation	Upper member	Feldspathic quartzite, feldspar-quartz schist, feldspathic schist, garnet-mica schist, mica-quartz schist and minor conglomerate. Commonly magnetitic, chloritised in places.	
	Lower member	Feldspathic quartzite and hematitic quartz-mica schist. Commonly garnetiferous, magnetitic, and chloritised in places. Pyritic carbonaceous schist, massive crystalline carbonate, chlorite-dolomite schist, calc-silicate gneiss. Amphibole schist and amphibolite.	Pyritic, carbonaceous schist. Conductive
Kakadu Group	Kudjumardti Quartzite	Coarse orthoquartzite, muscovite quartzite, minor gneissic biotite quartzite.	Resistive
	Munmarlary Quartzite	Feldspathic quartzite, quartzite.	Resistive
	Basedow Quartzite	Gneissic meta-arkose, quartzite, interbanded biotite gneiss and schist; transitional into Nanambu Complex.	Resistive
Nanambu Complex (2470 + 47 / - 40 Ma)	Granite and granite gneiss with minor amphibolite and mica schist.	Generally resistive, amphibolite may be weakly conductive	
Arrarra Gneiss (2671 ± 3 Ma)	Quartz-feldspathic gneiss.	Resistive	
Kukalak Gneiss	Quartz-feldspathic gneiss.	Resistive	

After Needham (1984), Hollis *et al.* (2009), Worden *et al.* (2008)

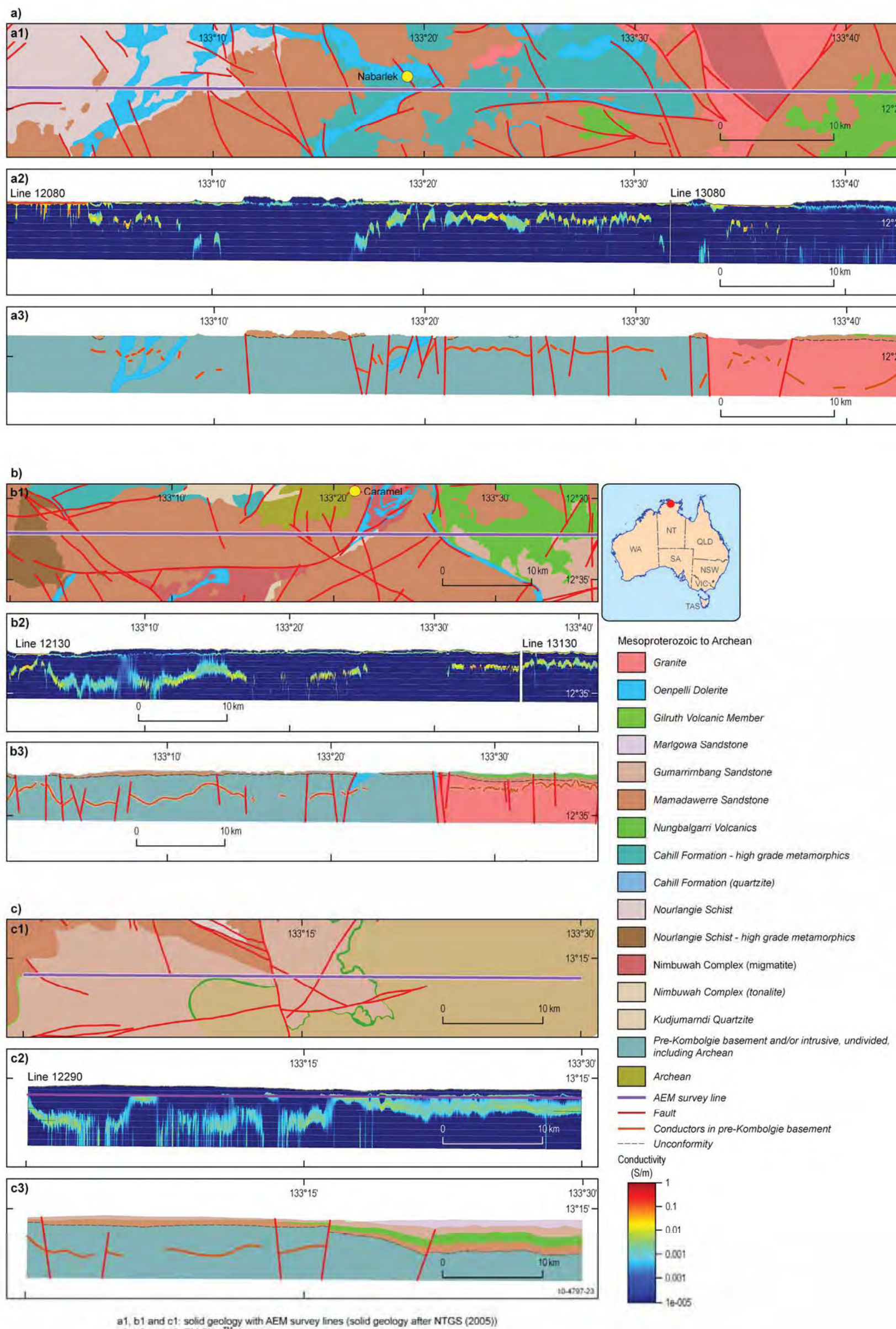
#### **6.4.2 Geological interpretations**

In the Kombolgie AEM survey area, several key geological features are well depicted in the EM Flow™ sections ([Figure 6–49](#)):

- The unconformity between the Kombolgie Subgroup and basement rocks, including the Paleoproterozoic Pine Creek Orogen and Archean basement complexes;
- The Nungbalgarri Volcanics and the Gilruth Volcanic Member of the Katherine River Group in the McArthur Basin ([Table 6–11](#)); and
- Conductors in the pre-Kombolgie basement, including carbonaceous and pyritic schists in the Cahill Formation.

Geological cross-sections are presented here along several selected AEM survey lines ([Figure 6–50](#)). The interpretations are based on the EM Flow™ (Version 5.23–13) sections, surface and solid-geology mapping by NTGS (2005), a new pre-Kombolgie Subgroup basement solid-geology interpretation (in collaboration with NTGS), and relevant drill hole data.

The EM Flow™ sections from the Kombolgie AEM survey clearly show the unconformity between the Kombolgie Subgroup and the underlying metasedimentary rocks, Archean basement and other conductors in the Katherine River Group. Importantly, the data also map conductors in pre-Kombolgie basement to a depth of up to 2 km (Minerals Alert February 2011; Costelloe and Brodie, 2011). Penetration to this depth represents a major breakthrough in AEM survey capability, achieved, in part, due to the extremely resistive rocks in the area and rigorous AEM signal processing ([Figure 6–50](#)).



a1, b1 and c1: solid geology with AEM survey lines (solid geology after NTGS (2005))  
 a2, b2 and c2: EM Flow™ sections  
 a3, b3 and c3: interpreted cross-sections

**Figure 6–50:** Geological cross-section interpretations along selected EM Flow™ sections in the Kombolgie AEM Survey. Solid geology after NTGS (2005). Conductivity sections are displayed at a vertical exaggeration of 2.5.

Line 12080 shown in (a); Line 12130 shown in (b); Line 12290 shown in (c).

### **6.4.3 Kombolgie unconformity**

The Kombolgie unconformity is mostly visible as a thin weakly to moderately conductive anomaly at a depth mostly less than 500 m in the EM Flow™ CDI sections in the northern part of the Kombolgie survey area. The unconformity is deeper in the south-eastern part of the survey area. For example, for the eastern part of the interpreted cross-section along line 12290, the Kombolgie unconformity is interpreted to be at a depth of about 1 km ([Figure 6–50](#)). This is consistent with palaeocurrent studies by Sweet *et al.* (1999) on Mount Marumba and Carson *et al.* (1999) on Milingimbi, who showed palaeocurrent directions to the south or southwest, suggesting higher ground to the north. The Mamadawerre Sandstone immediately above the Kombolgie unconformity is predominantly a fluvial sequence.

Future interpretation of the AEM conductivity data may be directed to constructing 3D–models of the Kombolgie unconformity and the units of the Katherine River Group. Such modelling should incorporate constraints from drill hole data. Such 3D modelling, in particular, the re-construction of palaeotopography and structures would assist in determining the 3D architecture of the McArthur Basin, in which the Kombolgie Subgroup was deposited. The 3D modelling of palaeotopography, including faults would assist assessment of fluid movement directions during diagenesis at late stages of Basin development and during inversion of the Basin. Such fluid movement direction assessment would be critically important for assessing the potential for uranium mineral systems in the area.

The conductivity associated with the unconformity is interpreted to be due to a combination of alteration, possibly due to the existence of a palaeoregolith, and fluids present at the unconformity surface.

### **6.4.4 Nungbalgarri Volcanics and Gilruth Volcanic Member**

Fresh unaltered mafic volcanic rocks are generally resistive. In the Kombolgie AEM survey area, however, the positions of the Nungbalgarri Volcanics and the Gilruth Volcanic Member correspond to moderate conductivity anomalies along many EM Flow™ CDI sections ([Figure 6–50](#)).

Alteration in the Nungbalgarri Volcanics and the Gilruth Volcanic Member is common (Ferenczi and Sweet, 2005). The Nungbalgarri Volcanics consist mainly of altered and weathered, massive and amygdaloidal basalt flows. Stuart-Smith *et al.* (1988) described the mineralogy of the Volcanics as mostly secondary, including hematite, chlorite, epidote, chalcedony, albite, carbonate and prehnite.

It is likely that the conductivity anomalies are due to the presence of fluid along the contacts of the mafic volcanic rocks with sedimentary rocks and/or alteration of the mafic volcanic rocks, particularly along the contacts with sedimentary rocks.

### **6.4.5 Oenpelli Dolerite**

The Oenpelli Dolerite intruded at  $1723 \pm 6$  Ma during sedimentation of the Kombolgie Subgroup (Page 1996). Alteration of the Dolerite is common and localised, although it may be extensive in the vicinity of mineralised areas (Ferenczi and Sweet, 2005; Polito *et al.* 2004). Alteration may have enhanced conductivity particularly along contacts with metasedimentary rocks. However, the Dolerite does not correspond consistently to any particularly conductivity anomaly pattern.

### **6.4.6 Sub-McArthur Basin conductors**

Many EM Flow™ CDI sections of the Kombolgie survey depict anomalies of varying conductivity at varying depth below the Kombolgie unconformity in a generally very resistive background ([Figure 6–50](#)). Their conductivity varies from weak to moderate. Pre-Kombolgie basement rocks in the Kombolgie survey area include the Nourlangie Schist, the Cahill Formation, the Kakadu Group and the Archean complexes. The conductivity anomalies in the pre-Kombolgie basement rocks may be attributed either to carbonaceous and pyritic metasediments in the Cahill Formation, metamorphosed mafic rocks in the Archean complexes, or to other undefined conductive rocks. Detailed mapping of these conductive rocks

in pre-Kombolgie basement rocks is important for defining the presence of potential reductors essential in assessing the potential of the Kombolgie unconformity-related uranium mineral systems.

Some of the pre-Kombolgie conductivity anomalies are detected at a depth down to 2 km. Detection at this depth represents a major breakthrough in AEM survey capabilities, and is partly because of the very resistive nature of rocks in the area.

#### **6.4.7 Interpretation of GA–LEI data of the Kombolgie area**

While this report was being finalised, Geoscience Australia processed the Kombolgie VTEM™ AEM data to produce conductivity estimates from the GA–LEI inversion algorithm (Lane *et al.*, 2004). The Kombolgie VTEM™ AEM Survey: Inversion Report and Data Package are available from Geoscience Australia.

[Appendix 10.8](#) details qualifying remarks relating to the Kombolgie AEM data and derived conductivity estimates. The qualifications, which are based on forward modelling and inversion analysis, highlight the need for some caution when making geological interpretations from the estimated conductivity. Selected examples are presented to demonstrate the issues in detail.

In coastal areas of the Kombolgie VTEM™ AEM survey there are moderate to strong conductors whereas in other areas, the rocks are very resistive. In conductive areas the signal-to-noise ratio is high and so the VTEM™ AEM data can be successfully fitted, by the GA–LEI algorithm. In these areas, the GA–LEI and EM Flow™ CDI conductivity sections are qualitatively similar ([Appendix 10.8.1, Figure 10–4](#)).

However, in resistive areas the signal-to-noise ratio is low and the corrections applied, by the survey contractor during the data processing, have a significant impact on the AEM responses. In these resistive areas, the GA–LEI and EM Flow™ CDI results are significantly different.

When identifying conductors and their significance in assessing the uranium potential of the region, the three are most important geological features in the Kombolgie VTEM™ survey area are:

- The Katherine River Group;
- The unconformity between the Kombolgie Subgroup over the Pine Creek Orogen (i.e., the ‘Kombolgie unconformity’); and
- The conductors at depth (a few hundred metres down to 2 km at depth) below the Kombolgie unconformity.

As discussed in the previous section, EM Flow™ CDI conductivity sections of the Kombolgie VTEM™ data show that the Katherine River Group sediments are resistive. At moderate depth, about 200 to 400 m in most places, there is a thin, weak to moderate conductor (‘the shallow conductor’), which corresponds approximately to the position of the Kombolgie unconformity. At greater depth (500 m down to 2 km), there is a thicker conductor (or several conductors) of weak to moderate conductivity (‘the deep conductor’).

For the generally resistive areas, i.e., over much of the Kombolgie survey area, the GA–LEI algorithm is able to fit the data without the need for the deep conductor (e.g., see top panel of [Appendix 10.8.2, Figure 10–6](#)) and GA–LEI results are different to the EM Flow™ results. However, in other resistive areas the deep conductor is required to fit the data and the GA–LEI and EM Flow™ CDI sections are similar at depth (e.g., [Figure 10–8](#)).

It is important to reiterate that, since inversion is a non-unique process, there is more than one conductivity-depth option to fit the data. This is illustrated in [Figure 10–6](#) and [Figure 10–10](#). It can be seen that the EM Flow™ CDI (bottom panel of [Figure 10–6](#)) has a thin conductor at ~200 to 350 m deep along all of the flight line 20390. However the GA–LEI section (middle panel) has a broader conductor from surface to ~400 m.

The right hand panel of [Figure 10–11](#) shows the situation in detail for line 20390 at Easting 312001. Here the EM Flow™ CDI conductivity model (red) shows a thin conductor at about 330 m and the GA–LEI inversion (magenta) shows a smooth broad conductor from surface to ~400 m. Forward modelling shows two other models that fit the data. They are referred to as ‘Alternate-1’ and ‘Alternate-2’ and are discussed in [Appendix 10.8.2.2](#), and shown in [Figure 10–11](#). These two models demonstrate the non-uniqueness of the modelling of AEM data.

If the correlation of the thin conductor with the Kombolgie unconformity is valid, the GA–LEI Alternate-2 model may mean the unconformity is at a shallower depth (~200 m) than predicted by the EM Flow™ model (~330 m). On the other hand, the GA–LEI Alternate-1 model may mean that the Katherine River Group is generally slightly more conductive than the pre-Kombolgie basement. All these models generated by EM Flow™ and GA–LEI inversion remain to be tested in the field, e.g., by drilling and downhole logging.

One way to resolve the non-uniqueness of this scenario would be to use downhole log information. For this particular resistive scenario inductive downhole conductivity logging tools will not be effective because they are not sensitive enough at the 0.0001 S/m (0.1 mS/m) level. Downhole resistivity logging tools are more suitable at the low conductivity end of the scale. Geoscience Australia has access to one confidential industry log through the Kombolgie Subgroup into the basement below the unconformity. This single resistivity log shows the unconformity is more conductive than the rocks above and below it. Therefore this supports the thin shallow conductor model (EM Flow™ CDI and Alternate-2) rather than the broader smoother model (GA–LEI and Alternate-1).

The interpretations in the previous sections of the Kombolgie AEM data were done on the EM Flow™ data, i.e., before the GA–LEI modelling data became available. The reader should be aware that there are alternative interpretations of the AEM data. The user of the AEM conductivity estimates by either EM Flow™ CDI or GA–LEI is reminded that one set of parameters and assumptions are used in processing the entire survey data, which does not address different geological situations satisfactorily. Exploration companies are advised to consider re-processing the data using different parameters and assumptions appropriate for regions of specific interest and different geological scenarios.

## 6.5 CONCLUSIONS

AEM provides a unique dataset that gives depth information of geological features in the shallow crust in a regional context. The Pine Creek regional AEM data are very useful in assisting mineral exploration (including uranium) in the top few hundred metres below surface. The surveys also show where more detailed airborne and ground surveys would add maximum value for exploration.

Conductivity estimates derived for the Woolner Granite – Rum Jungle area using the GA–LEI algorithm reveal several conductors in sedimentary sequences interpreted mostly within the upper 300–400 m, including:

- The Depot Creek unconformity over the Paleoproterozoic Pine Creek Orogen and Archean basement. A 3D model derived from these data shows the geometry and lateral extent of part of the Depot Creek unconformity;
- Strong conductors in carbonaceous and pyritic materials in the South Alligator River and Mt Partridge Groups;
- Moderate to weak conductors in the sedimentary sequences of the Birrindudu, Daly and Bonaparte basins;
- Moderate to strong conductors related to saline water in coastal areas; and,
- Faulted and folded conductors.

EM Flow™ CDI sections from the Kombolgie AEM survey not only clearly map the Kombolgie – unconformity and other conductors in the Katherine River Group, but also map conductors in pre-Kombolgie basement to a depth down to 2 km. Penetration to this depth represents a major breakthrough in AEM survey capability, achieved in part due to the extremely resistive rocks in the area and also advances in AEM data processing. Geological cross-section interpretations of the conductivity depth sections also incorporate available drill-hole data to improve the reliability. Caution should be exercised when interpreting AEM data, including the non-uniqueness of interpretations and the reliability depth estimates.

The implications of the AEM data for uranium and gold mineral systems in the Pine Creek region are discussed in [Chapter 7](#).

## **6.6 REFERENCES**

- Ahmad M., Wygralak A. S., Ferenczi P. A. & Bajwah Z. U. 1993, *Pine Creek SD 52-8, explanatory notes and mineral deposit data sheets*. 1:250 000 metallogenic map series. Northern Territory Geological Survey, Darwin.
- Brodie, R.C., 2011, Kombolgie VTEM<sup>TM</sup> AEM Survey: Inversion Report. Geoscience Australia, Canberra.
- Carson L. J., Haines P. W., Brakel A. T., Pietsch B. A. & Ferenczi P. A. 1999, *Milingimbi SD53-2 (2nd edition)*. 1:250 000 Geological Series – Explanatory Notes. Northern Territory Geological Survey, Darwin.
- Costelloe M. T. & Brodie R. C. 2011, Kombolgie AEM survey images to 2 km. *Preview* February 2011, 29-32.
- Ferenczi P. A. & Sweet I. P. 2005, Mount Evelyn, Northern Territory. 1:250 000 geological map series explanatory notes, SD 53-05 (2nd edition). Northern Territory Geological Survey Darwin & Alice Springs.
- Ferguson J. & Needham R. S. 1978, The Zamu Dolerite; a lower Proterozoic preorogenic continental tholeiitic suite from the Northern Territory, Australia. *Journal of the Geological Society of Australia* 25, Parts 5-6, 309-322.
- Hollis J. A., Carson C. J. & Glass L. M. 2009a, SHRIMP U-Pb zircon geochronological evidence for Neoarchean basement in western Arnhem Land, northern Australia. *Precambrian Research* 174, 364-380.
- Hutchinson D. K., Roach I. C. & Costelloe M. T. 2010, Depth of investigation grid for regional airborne electromagnetic surveys. *Preview* 145, 38-39.
- Kruse P. D., Sweet I. P., Stuart-Smith P. G., Wygralak A. S., Pieters P. E. & Crick I. H. 1994, Katherine, Northern Territory. 1:250 000 geological map series explanatory notes, SD 53-9 (second edition). Northern Territory Geological Survey, Darwin.
- Lally J. H. 2003, Rum Jungle Mineral Field integrated interpretation of geophysics and geology, Edition 1, 1:100 000 geological map special. Northern Territory Geological Survey, Darwin.
- Lane R., Brodie R. & Fitzpatrick A. 2004, A revised inversion model parameter formulation for fixed wing transmitter loop – towed bird receiver coil time-domain airborne electromagnetic data. Paper presented at ASEG 17th Geophysical Conference and Exhibition, Sydney (unpubl.).
- Lawrence M. & Stenning L. 2009, Rum Jungle Airborne Electromagnetic (AEM) Mapping Survey - Acquisition and Processing Report for Geoscience Australia. Fugro Airborne Surveys, Perth.
- Macnae J., King A., Stoltz N., Osmakoff A. & Blaha A. 1998, Fast AEM processing and inversion. *Exploration Geophysics* 29, 163-169.
- Malone E. J. 1962, *Pine Creek, N.T. (1st edition); 1:250,000 geological series explanatory notes, Sheet SD52-8*. Australia, Bureau of Mineral Resources, Geology and Geophysics, Canberra.
- Morgan C. M. 1972, Port Keats (1st edition), N.T. 1:250 000 geological series explanatory notes, Sheet SD52-11. Northern Territory Geologic Survey, Darwin.
- Needham R. S. 1983, *Alligator River, Northern Territory* (2 edition). Bureau of Mineral Resources, Geology and Geophysics, Canberra.

- Needham R. S. 1984, *Alligator River* (2nd edition). 1:250 000 Geological Series - Explanatory Notes. Bureau of Mineral Resources, Geology and Geophysics, Canberra.
- Needham R. S., Stuart-Smith P. G. & Page R. W. 1988, Tectonic evolution of the Pine Creek Inlier, Northern Territory. *Precambrian Research* 40-41, 543-564.
- NTGS 2005, *Pine Creek interpreted geology (1:500 000)*. Northern Territory Geological Survey, Darwin.
- Page R. W. 1996, Sample 88126035 (Oenpelli Dolerite). Unpublished data in Geoscience Australia's OZCHRON geochronology database. [www.ga.gov.au](http://www.ga.gov.au).
- Palacky G. J. 1993, Use of airborne electromagnetic methods for resource mapping. *Advances in Space Research* 13, 5-14.
- Pietsch B. A. 1985, Koolpinyah. 1:100 000 geological map series explanatory notes. Sheet 5173. Northern Territory Geological Survey, Darwin.
- Pietsch B. A. & Stuart-Smith P. G. 1987, *Darwin, N.T., 1:250 000 geological map series. Sheet SD52-4*. Northern Territory Geological Survey, Darwin.
- Polito P. A., Kyser T. K., Marlatt J., Alexandre P., Bajwah Z. & Drever G. 2004, Significance of Alteration Assemblages for the Origin and Evolution of the Proterozoic Nabarlek Unconformity-Related Uranium Deposit, Northern Territory, Australia. *Economic Geology* 99, 113-139.
- Pontifex I. R. & Mendum J. R. 1972, *Fergusson River, Northern Territory; 1:250,000 geological series explanatory notes, sheet SD/52-12*. Australia, Bureau Mineral Resources, Geology and Geophysics, Canberra.
- Raymond O. L. & Retter A. J. e. 2010, Surface geology of Australia 1:1,000,000 scale, 2010 edition [Digital Dataset]. Geoscience Australia, Canberra.
- Roach I. C. ed. 2010, Geological and energy implications of the Paterson Province airborne electromagnetic (AEM) survey, Western Australia Geoscience Australia Record 2010/12. Geoscience Australia, Canberra.
- Stoltz E. & Macnae J. 1998, Evaluating EM waveforms by singular-value decomposition of exponential basis function. *Geophysics* 63, 64-74.
- Stuart-Smith P. G., Needham R. S. & Bagas L. 1988, Stow Region, Northern Territory, 1:100 000 map commentary. Australia, Bureau of Mineral Resources, Geology & Geophysics, Canberra.
- Sweet I. P., Brakel A. T., Rawlings D. J., Haines P. W., Plumb K. A. & Wygralak A. S. 1999, *Mount Marumba, Northern Territory; SD 53-6 (2 edition)*. 1:250 000 Geological Map Series – Explanatory Notes. Northern Territory Geological Survey, Darwin.
- Worden K., Carson C., Scrimgeour I., Lally J. & Doyle N. 2008, A revised Palaeoproterozoic chronostratigraphy for the Pine Creek Orogen, northern Australia: Evidence from SHRIMP U-Pb zircon geochronology. *Precambrian Research* 166, 122-144.

## 7 Implications for uranium mineral systems

*S. Jaireth and S.F. Liu*

Geological interpretation of the Pine Creek AEM data was presented in [Chapter 6](#). Major mineral systems in the Pine Creek Orogen were discussed in the [Chapter 5](#). This discussion highlighted critical features of unconformity-related uranium mineral systems ([Table 4–5](#)). In this chapter we will discuss implications for uranium mineral systems in the Pine Creek region. Discussions will outline key components of relevant mineral systems, how AEM data contribute to assessment of potential of these mineral systems and recommend work that should be done in the future to facilitate further such assessments.

### 7.1 UNCONFORMITY-RELATED URANIUM MINERAL SYSTEMS

Key components of fertile unconformity-related uranium mineral systems in the Pine Creek region include (see [Table 7–1](#) for details):

- A major unconformity;
- Reduced Paleoproterozoic metasedimentary rocks below the unconformity;
- A relatively thick (> 4 to 5 km) package of Paleoproterozoic coarse-grained, dominantly fluvial sediments overlying the unconformity;
- Proximity to uranium-rich Archean granite-gneiss complex;
- Ore-localising structures; and,
- The presence of mafic and/or felsic intrusive and/or volcanics within Paleoproterozoic sedimentary package overlying the unconformity (this is a distinguishing feature of the Nimbuwah Domain which hosts world-class deposits in the Alligator Rivers Uranium Field)

The most prospective areas for unconformity-related uranium mineral systems are in the Nabarlek and Daly Basin areas which will be discussed below.

**Table 7-1:** Critical mineral system features for unconformity-related uranium deposits

ELEMENT	MAPPABLE FEATURE	USEFUL DATASETS
Setting Unconformity between Paleoproterozoic metasedimentary rocks and Paleo- to Mesoproterozoic sandstones	Katherine River and Tolmer Groups overlying or in proximity to metasedimentary rocks of the Mount Partridge, South Alligator Groups and the Welltree Metamorphics	Solid geology map showing distribution of these rocks. Solid geology map showing rocks under cover of the Katherine River and Tolmer Groups.
Basement of Archean domes/inliers flanked by Paleoproterozoic metasedimentary rocks	Rum Jungle and Nimbuwah complexes, Woolner Granite, Arrarra, Kukalak and Njibinjbini gneiss	Solid geology map (as above)
Metasediments formed in shallow marine conditions rather than turbiditic, containing units enriched in carbonaceous material	Calcareous metasediments such as the Whites, Koolpin and Cahill formations	Solid geology map (as above)
Thick (> ~ 5 km) package of Paleoproterozoic to Mesoproterozoic sediments containing sandstones formed in braided, fluvial conditions. Flat-lying at the time of mineralisation (often foreland basin). Often partially or fully eroded	Rocks of the Katherine River and Tolmer groups	Map showing pre-erosion extent of the Katherine River and Tolmer groups. AEM data showing unconformity surface and its depth. Reconstruction of basin architecture. Palaeocurrent data in sandstone
<b>SOURCE (FLUID, METAL, ENERGY)</b> <b>Fluids</b> Fluid 1: Diagenesis of sedimentary package overlying the unconformity. High salinity fluids formed from dissolution of evaporate  Fluid 2: Evolved from Fluid 1 after reacting with metasedimentary rocks below the unconformity. High salinity but higher Ca/Na ratio than Fluid 1  Fluid 3: Hydrocarbon-rich fluid formed from hydrogenation of carbonaceous material in metasediments below the unconformity	Rocks of the Katherine River and Tolmer Groups  Archean granite-gneiss complex, Metasedimentary rocks (Mount Partridge, South Alligator groups and the Welltree Metamorphics) underlying the unconformity  Metasedimentary rocks rich in carbonaceous material	Diagenetic history of Katherine River and Tolmer groups. Diagenetic history of the Tolmer Group sediments unknown. Ar/Ar dating of diagenetic clays  Mapping of alteration zones in the metasedimentary rocks. Hylogger™ data. Aeromagnetic and AEM data can pick magnetic and conductivity contrast  AEM data to map changes in the conductivity of carbonaceous units
<b>Uranium</b> Uranium-bearing detrital minerals in the sandstone such as monazite, zircon Felsic volcanics or their fragments in the sandstone package overlying the unconformity  Uraninite and or uranium-bearing minerals (monazite, zircon) in the granites and/or metasediments below the unconformity	Rocks of the Katherine River and Tolmer groups Rocks such as the West Branch Volcanics  Archean granite-gneiss complex, Metasedimentary rocks (Mount Partridge, South Alligator Groups and the Welltree Metamorphics) underlying the unconformity	Analysis of heavy mineral fraction in the Katherine River and Tolmer groups in proximity to mineralised areas and distal areas.  Uranium and thorium concentration of metasedimentary rocks below the unconformity and of the Katherine River and Tolmer Groups.
Palaeoregolith'	'Palaeoregolith' at the Granite Hill, Scinto Breccia, Ella Creek Member. Redbed alteration (?) in the basal part of the Kombolgie Subgroup and Depot Creek Sandstone	Aeromagnetic and AEM data could pick the magnetic and conductivity contrast at the unconformity indicating possible interaction with fluids
<b>Energy</b> Gravity-driven fluid-flow  Radiothermal heat produced by granitoids and Archean rocks	Pre- and post-erosional extent and shape of McArthur and Birrindudu  Archean and Paleoproterozoic felsic rocks	Architecture of basins and sub-basins in which Katherine River and Tolmer groups were deposited  Radiogenic heat generation map. Palaeogeothermal gradient
Several phases of igneous intrusives in the sandstone overlying the unconformity	Mafic dykes and sills and felsic volcanics in the Katherine River Group	Drill hole logs. Gravity to map mafic rocks. AEM can also pick them due to conductivity contrast

ELEMENT	MAPPABLE FEATURE	USEFUL DATASETS
<b>FLUID PATHWAY</b> Unconformity surface with or without palaeoregolith  Aquifers in the sandstone package overlying the unconformity  Faults and breccia zones leading up to and/or cutting the unconformity	Palaeoregolith at the Granite Hill, Scinto Breccia, Ella Creek Member. Redbed alteration (?) in the basal part of the Kombolgie Subgroup and Depot Creek Sandstone  Aquifers in the Katherine River and Tolmer groups	Maps of alteration zones. Aeromagnetic and AEM data to detect magnetic and conductive contrast  Diagenetic history of the Katherine River and Tolmer groups  Mapping faults with alteration zones. AEM data to detect magnetic and conductive contrast. Hylogger mapping of alteration zones. AEM can map faults that have channelled fluid by mapping conductivity contrast
<b>TRAP (ANY OF THE FOLLOWING)</b> <b>Structural</b> Unconformity surface Breccia zones and faults  <b>Chemical</b> Carbonaceous (graphite) rocks below the unconformity  Rocks with Fe <sup>+2</sup> -bearing silicates such as chlorite either below the unconformity or in the sandstone package above the unconformity  Reduced fluid resulting from the hydrogenation of carbonaceous material Presence of calcareous rocks (affecting pH, not fully clear)	Map of the unconformity surface at the base of Kombolgie Subgroup and Depot Creek Sandstone  Metasedimentary rocks rich in carbonaceous material (Mount Partridge, South Alligator groups and the Welltree Metamorphics). Metasedimentary rocks with chlorite (Cahill Formation, Koolpin Formation, Whites Formation, mafic volcanics in the rocks below and above the unconformity)  Rocks of the Mount Partridge, South Alligator groups	Map of pre-erosion extent of the Katherine River and Tolmer groups. Map of the unconformity surface at the base of the Kombolgie Subgroup and Depot Creek Sandstone. Map of structures (faults and fractures) and their age. AEM data can map favourable structural traps because of conductivity contrast created by graphite.  Alteration map showing distribution of chlorite and its composition AEM data can map zones of dissolution of graphite
<b>AGE</b> Proterozoic age important for world-class deposits.		
<b>TIMING</b> Mineralisation closely linked with the timing of diagenesis in the sandstone package overlying unconformity  Mineralisation linked to compression during basin inversion in the basin overlying unconformity  During extension diagenetic fluids accumulate, during inversion, the fluids move outward from the basin	Diagenetic history of the Katherine River Group is known but limited information on the diagenetic history of the Tolmer Group.  Numerous faults mapped	Diagenetic history of the Katherine River and Tolmer groups  Map of structures (faults) showing their ages and type of movement. Dating of alteration along fault zones
<b>PRESERVATION</b> Presence of sandstone above the unconformity indicates high probability of preservation of unconformity type uranium deposits Most known deposits show remnants of sandstone package overlying unconformity in close proximity	Katherine River and Tolmer groups	Map showing present day and pre-erosion extent of the Katherine River and Tolmer Group. Sediment provenance maps for these rocks  Fission track dating work to show the uplift and erosion history

**Geological and energy implications of the Pine Creek airborne electromagnetic (AEM) survey,  
Northern Territory, Australia**

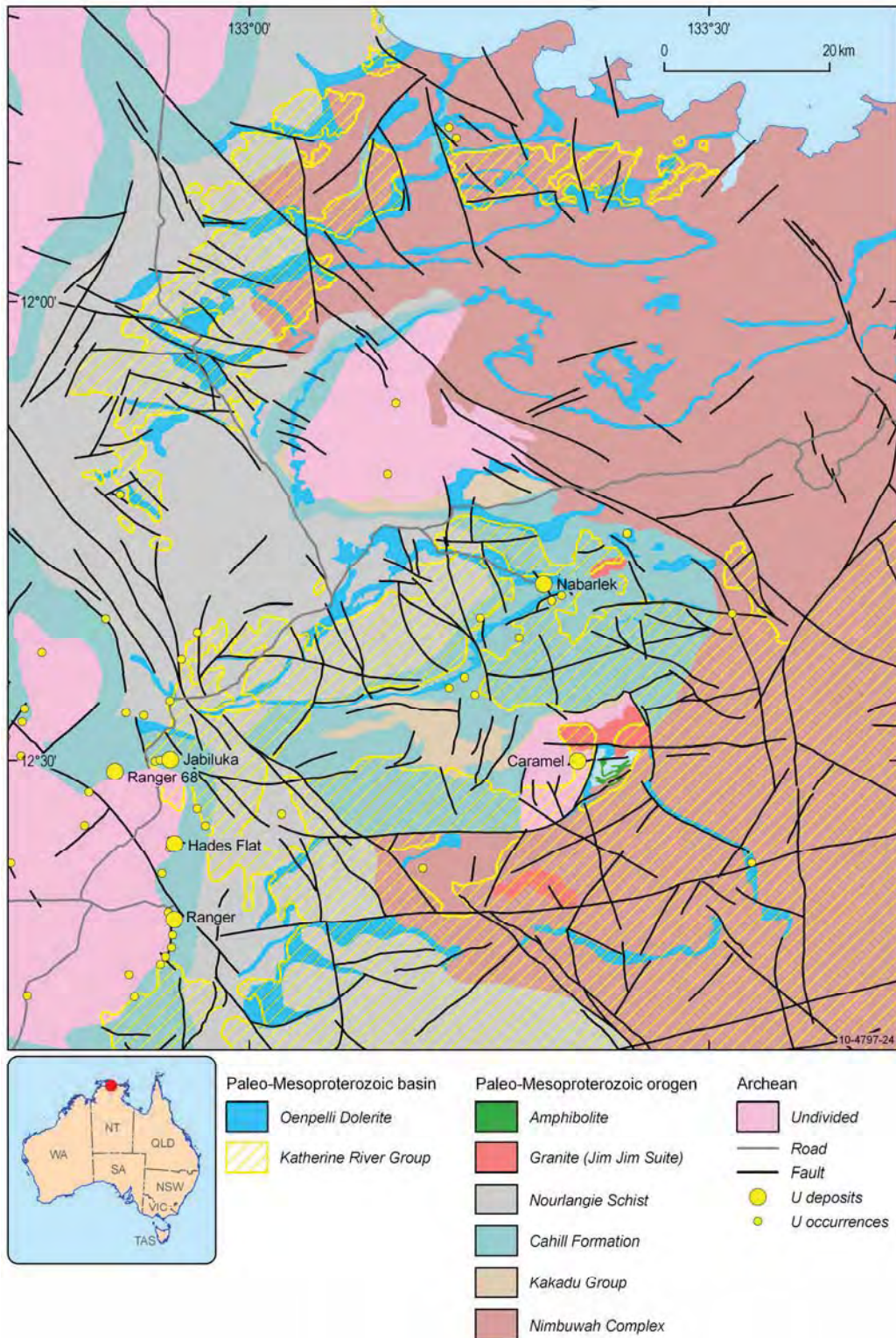


**Figure 7-1: Pre-Kombolgie solid geology map of the Nabarlek area**

**Geological and energy implications of the Pine Creek airborne electromagnetic (AEM) survey,  
Northern Territory, Australia**

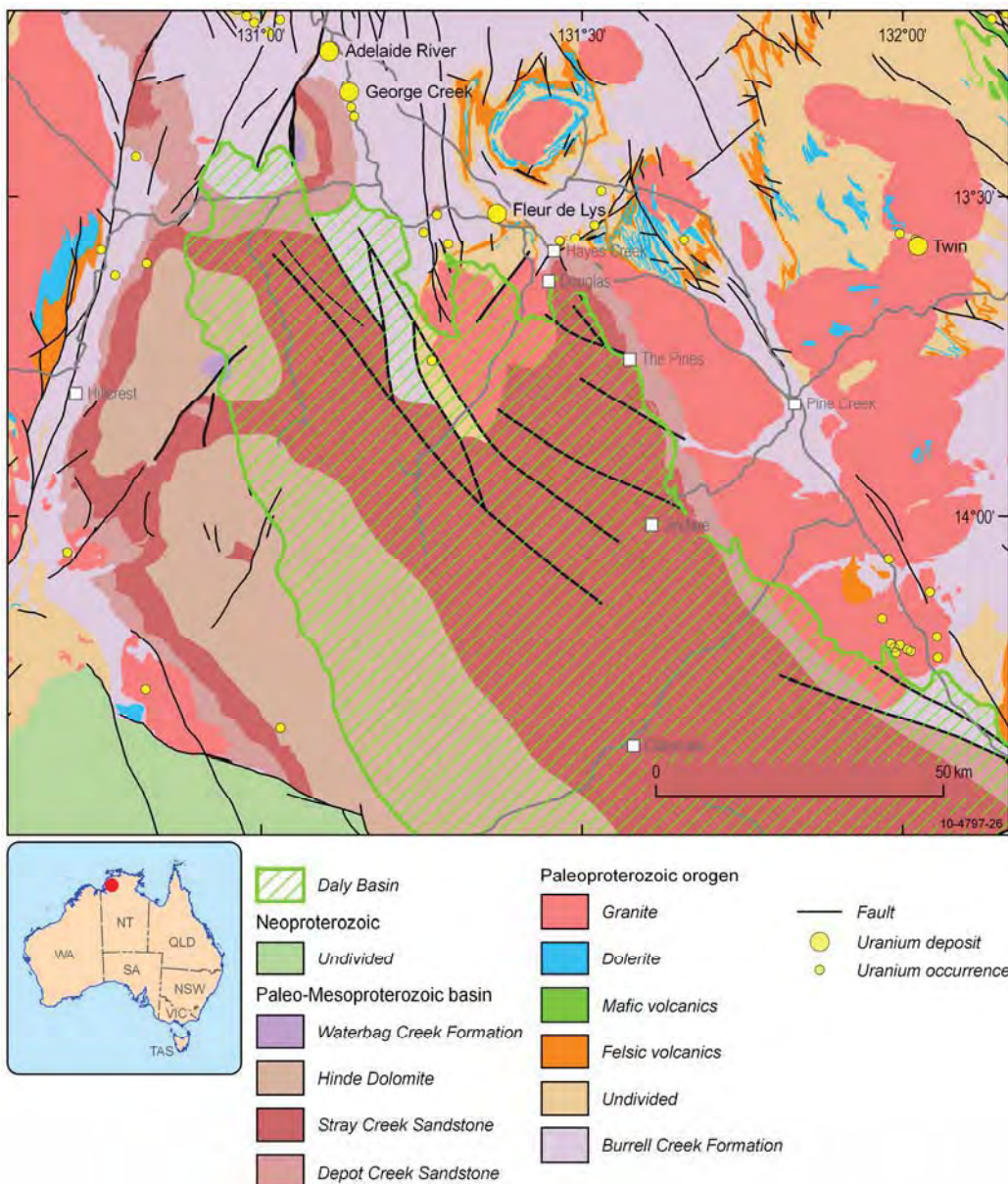


**Figure 7-2: Pre-Daly Basin solid geology map of the Pine Creek – Fergusson River area**

**Geological and energy implications of the Pine Creek airborne electromagnetic (AEM) survey,  
Northern Territory, Australia**

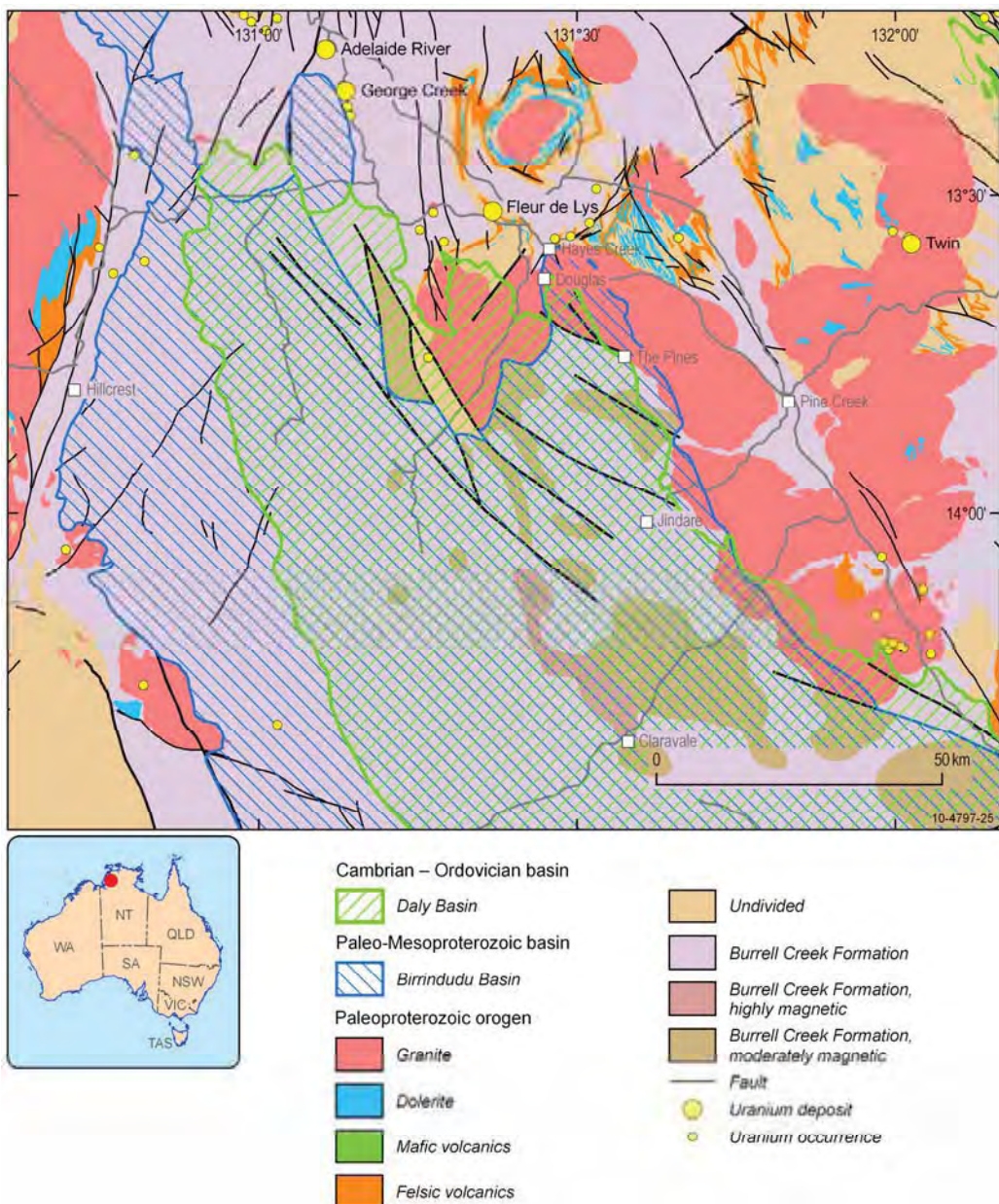


**Figure 7-3: Pre-Depot Creek solid geology map of the Pine Creek – Fergusson River area**

### **7.1.1 Nabarlek area**

More than 50% of the Nimbuwah Domain (defined in [Chapter 3](#) and shown in [Figure 3–2](#)) is covered by the rocks of the Katherine River Group and so has not been explored fully and remains prospective for both sub-unconformity deposits (Ingress-style) and Egress-style (hosted in the sandstone above the unconformity). The area is also prospective for Westmoreland-style deposits (Polito, Kyser, Rheinberger and Southgate, 2005) where mineralisation is often controlled by mafic rocks which contain silicate reductants.

Recent mapping in the area by NTGS in the Nimbuwah Domain has revealed the presence of hitherto unknown Archean rocks (Hollis et al., 2008). These areas may be more prospective for unconformity-related uranium systems ([Figure 7–1](#)). The Paleoproterozoic topography of the Nimbuwah Domain is not reliably known. Ahmad *et al.* (2006) postulate that the Archean rocks of the Nanambu Complex constituted a shelf (Nanambu Shelf) surrounded by Eastern and Central troughs to the east and west respectively, in which the Paleoproterozoic sediments were deposited. It is likely that regions with Archean rocks also formed palaeo-highs during the deposition of the Katherine River Group.

Kyser and Cuney (2008) show a cross section of the region compiled from drill hole data. Based on sequence stratigraphy and diagenetic ages of sediments in the Katherine River Group they suggest that diagenetic fluid could have flowed broadly in a south (or south-east) to north (north-west) direction, i.e., from relatively deeper parts of the McArthur Basin to relatively shallower parts. Uranium deposits such as Jabiluka, Nabarlek and Caramel could have formed when the fluids reacted with reduced metasedimentary rocks below the unconformity. The empirical observation that most known uranium deposits in the Nimbuwah Domain are located at the margins of the Archean complexes can thus be explained by the fact that the reduced metasedimentary rocks (such as Cahill Formation) were located along the margins of the palaeo-highs. It is possible that the areas with newly mapped Archean rocks in the Nimbuwah Domain ([Figure 7–1](#)) also formed palaeo-highs. The Jabiluka deposit is located on the south-western margin of such a palaeo-high (the Myra High, Polito et al., 2005). This is supported by stratigraphic mapping and palaeocurrent data (Hiatt and Kyser, 2002, cited in Polito et al., 2005). If the model proposed by Kyser and Cuney (2008) is correct, the Cahill Formation rimming newly mapped Archean rocks could be prospective for uranium deposits. Regional AEM data provide valuable information to map the distribution and geometry of the unconformity, stratigraphic units and conductors (reductants), and structures, particularly faults in the basement and cover sedimentary packages ([Chapter 6](#)). However, in order to assess the prospectivity of these two areas ([Figure 7–1](#)) and the rest of the Nimbuwah Domain it is necessary to understand:

- The 3D basin architecture of the McArthur Basin (Katherine River Group). This may be achieved from interpretation of AEM data with constraints from drill hole information;
- Reconstruct a detailed solid geology map of areas covered by Katherine River Group. The map should show distribution of key basement stratigraphic units, Cahill Formation (and the reductants within), Nourlangie Schist, Kakadu Group and Archean basement. Regional distribution of these units is mapped in the generalised pre-Kombolgie solid geology map shown in [Figure 7–1](#). Detailed mapping of these units (particularly the reductants-bearing Cahill Formation) in areas of interests would be important for exploration target selection. Such detailed basement solid geology may be compiled from drill hole data, interpretations of geophysical data and the NTGS surface geology mapping in the area;
- Map faults in the rocks below and above the unconformity. Delineate faults which could have seen fluid-flow by mapping magnetic and/or conductivity contrasts caused by fluid–rock interaction; and,
- Map areas of distal chlorite alteration (most significant in this respect is the Fe/Mg ratio of alteration chlorites) and proximal illite and/or clay alterations in the metasedimentary rocks

below the unconformity and within the Katherine River Group using hyperspectral and other techniques.

### **7.1.2 Birrindudu Basin in the Pine Creek–Fergusson area**

The Birrindudu Basin is prospective for unconformity-related uranium mineral systems because it contains a relatively thick sandstone package of the Depot Creek Sandstone, which unconformably overlies the reduced metasediments of the Finniss River and South Alligator groups.

However, unlike the McArthur Basin in the Nabarlek area, the Birrindudu Basin in the Pine Creek–Fergusson area is largely covered by the Daly River Group and younger sediments. To assist assessing the potential of unconformity-related uranium mineral systems in the Daly Basin area, two preliminary and generalised solid geology maps have been produced ([Figure 7–2](#) and [Figure 7–3](#)). The pre-Daly Basin solid geology map shows the distribution of the Tolmer Group including the Depot Creek Sandstone in the area ([Figure 7–2](#)). The pre-Depot Creek solid geology map shows the basement geology below the Depot Creek unconformity over the Pine Creek Orogen ([Figure 7–3](#)).

A 3D model has been produced for part of the eastern margin of the Birrindudu Basin ([Figures 6–41](#), [6–42](#) and [6–43](#)), that depicts the geometry of the Depot Creek unconformity, top of the Stray Creek Sandstone and top of the Jindare Formation. The 3D model shows that Depot Creek Sandstone extends and underlies Daly Basin sediments. At the margins of the basin it can be intersected at depths of less than 100 m but in the central part of the basin it is much deeper (> 500 m). The Hayes Creek Mineral Field is located close to the margin of the Daly Basin and ore-localising structures in this field appear to extend under the Daly Basin. Parts of the Daly Basin are being actively explored for unconformity-related uranium deposits associated with Depot Creek unconformity.

Factors which limit the prospectivity of this area include:

- Absence of Archean granite–gneiss complexes (more work is required to confirm this); and,
- Absence of mafic and/or felsic magmatism (similar in age to the Oenpelli Dolerite) within the Tolmer Group. The Murrenja Dolerite (< 1680 Ma) which intrudes Fitzmaurice Group is much younger in age.

In order to assess the uranium prospectivity of the area concealed beneath the Daly Basin it is essential to:

- Construct a 3D basin architecture of the Daly Basin and underlying Paleoproterozoic succession;
- Improve on the solid geology map ([Figure 7–2](#) and [Figure 7–3](#)) showing the distribution of the Finniss River, South Alligator River and Mount Partridge groups below the unconformity with the Depot Creek Sandstone, and fault architecture;
- Assess the age of deposition, diagenetic history and provenance of sediments of the Depot Creek Sandstone. This will help to estimate the pre-erosion extent of the Tolmer Group in the area;
- Evaluate the extent of Archean rocks in the region; and,
- Better understand the structural evolution of the area.

### **7.1.3 Westmoreland-style**

The Kombolgie Subgroup is interlayered with mafic units and is intruded by the Oenpelli Dolerite. Diagenetic fluids released by the Kombolgie Subgroup sediments under favourable conditions can form uranium deposits after reacting with mafic rocks (Westmoreland-style uranium deposits). Some enrichment of uranium is observed in sandstones at the contact with these units (see [chapter 4](#)). More

detailed work is required to assess the prospectivity of Westmoreland-style uranium deposits within the Kombolgie Subgroup.

#### **7.1.4 Other areas**

In addition to the above mentioned well-known unconformity-related uranium areas, the following unconformities may also be prospective for uranium deposits:

1. The unconformity between the Depot Creek Sandstone and the graphite-bearing Welltree Metamorphics (PINE CREEK);
2. The unconformity between the Fitzmaurice Group and the Welltree Metamorphics (CAPE SCOTT and FOGBAY);
3. Fitzmaurice Basin in which the Fitzmaurice Group unconformably overlies Paleoproterozoic rocks; and
4. The unconformity between Cretaceous sandstones and the underlying Paleoproterozoic rocks especially on the PINE CREEK, MOUNT EVELYN, KATHERINE and MOUNT MARUMBA sheets

### **7.2 SANDSTONE-HOSTED URANIUM MINERAL SYSTEMS**

The Pine Creek Orogen is overlain by relatively thick sandstone packages of Palaeozoic and Mesozoic ages. Some of these packages may be prospective for sandstone-hosted uranium deposits.

In the Daly Basin most units are dominated by calcareous sediments. The basal Jarong Conglomerate consists of boulder and pebble conglomerate and may be prospective for sandstone-hosted uranium deposits. In order to assess its prospectivity it is essential to understand its provenance and the distribution of possible reductants within this unit.

The Cretaceous Mullaman Beds comprise freshwater and marine sediments, some of which contain sandstones formed in lacustrine environments (Unit 1 of Skwarko, 1966). The unit is known to contain plant remains (Pontifex and Mendum, 1972). Although a significant part of the Mullaman Beds have been eroded in the inland area, the basal unit may be prospective for sandstone-hosted uranium deposits.

The AEM data show the presence of channel-like features incising the Tolmer Group ([Figure 6–33](#)). At this stage the nature of sediments infilling these channels is not clear, however this and similar channels in the Pine Creek region may be prospective for channel-related sandstone-hosted uranium deposits.

### **7.3 CONCLUSIONS**

Interpretation of AEM data in the Pine Creek region has shown that AEM can successfully map critical elements of fertile unconformity-related uranium systems such as:

- The unconformity at the base of the Katherine River and Tolmer groups;
- The thickness of the Katherine River and Tolmer groups above the unconformity;
- The metasedimentary rocks below the unconformity (especially rocks containing reductants); and,
- Faults in the metasedimentary rocks

The interpretation of AEM has demonstrated that regional-scale AEM survey in combination with drill-hole data can help to create a 3D model of McArthur River and Birrindudu basins in the Pine Creek region. This architecture can provide information on the direction of fluid flow during diagenesis of basin sediments and thereby outline areas prospective for unconformity-related uranium systems.

#### **7.4 REFERENCES**

- Ahmad, M. and Wygralak, A. S., 2006. Some aspects of metallogenesis in the Pine Creek Orogen, Northern Territory. - *Geoscience Australia Record* **2006/16**, 57-58.
- Hiatt, E. E. and Kyser, K., 2002. Sequence stratigraphy and basin analysis of the Paleoproterozoic Kombolgie Basin, Northern Territory, Australia. Abstracts with Programs - *Geological Society of America* **34**, 278.
- Hollis, J. A., Carson, C. J. and Glass, L. M., 2009. SHRIMP U-Pb zircon geochronological evidence for Neoarchean basement in western Arnhem Land, northern Australia. *Precambrian Research* **174**, 364-380.
- Kyser, K.T. and Cuney, M., 2009. Unconformity-related uranium deposits. In: Cuney M. & Kyser K. eds. Recent and not-so-recent developments in uranium deposits and implications for exploration, pp. 161-220. 39 Mineralogical Association of Canada, Quebec.
- Polito, P., Kyser, K. T., Rheinberger, G., and Southgate, P.N., 2005. A Paragenetic and Isotopic Study of the Proterozoic Westmoreland Uranium Deposits, Southern McArthur Basin, Northern Territory, Australia. *Economic Geology*; September-October; v. 100; no. 6; p. 1243-1260
- Polito, P., Kyser, K. T., Thomas, D., Marlatt, J. and Drever, G., 2005. Re-evaluation of the petrogenesis of the Proterozoic Jabiluka unconformity-related uranium deposit, Northern Territory, Australia. *Mineralium Deposita* **40**, 257-288.
- Pontifex, I. R. and Mendum, J. R., 1972. Fergusson River, Northern Territory; 1:250,000 geological series explanatory notes, sheet SD/52-12. Australia, Bureau Mineral Resources, Geology and Geophysics, Canberra.
- Skwarko, S. K., 1966. Cretaceous stratigraphy and palaeontology of the Northern Territory. Australia, *Bureau of Mineral Resources, Geology and Geophysics, Bulletin* **73**, Canberra.

## 8 Summary and Conclusions

*M.A. Craig*

### 8.1 AEM DATA ACQUISITION

The Pine Creek AEM survey delivers reliable, pre-competitive AEM data and scientific analysis of the energy resource potential of the Pine Creek region of the Northern Territory ([Figure 1–1](#)). This survey was the second regional AEM survey conducted within the Onshore Energy Security Program (OESP) by Geoscience Australia (GA). The Pine Creek AEM survey is the largest AEM survey undertaken in the Northern Territory.

The Pine Creek AEM survey area ([Figure 1–2](#)) is bounded by the approximate latitudes 11.5° S to 15° S. and approximate longitudes 129° E to 135° E. The total survey area is approximately 74 000 km<sup>2</sup>. The Pine Creek survey area is bounded by the Kakadu National Park, Litchfield National Park, Mary River National Park, Djukbinj National Park and Nitmiluk (Katherine) National Park, the coast, the area directly to the east of Darwin – which is within restricted air-space, the Mount Bundy Training Area, Tindal and Kangaroo Flats Training Area

The Pine Creek AEM survey primarily maps regional geology and images geological settings with potential for uranium mineralisation. Potential uranium systems within the Pine Creek survey area include sandstone-hosted, roll-front or palaeochannel styles; Proterozoic unconformity sedimentary-related; Westmoreland-type; and Vein-type. The data are also useful for exploration for other commodities including metals and potable water as well as for landscape evolution studies.

The region is well known for its uranium potential hosting many of Australia's uranium deposits including Jabiluka (204 000 t U<sub>3</sub>O<sub>8</sub>) and Ranger (143 000 t U<sub>3</sub>O<sub>8</sub>) (McKay and Miezitis, 2001, Beckitt, 2003; Ahmad, 1998; Lane *et al.*, 2007). Through its Geological Reference Group, GA assessed the Pine Creek area as having high prospectivity for uranium mineral systems detectable using AEM. Assessment of the potential interest in uranium is shown in [Table 1–1](#) and a priority assessment is provided in [Table 1–2](#).

In addition, the Pine Creek region hosts groundwater systems associated with fractured rock aquifers, palaeovalleys and sedimentary units of various ages. A range of users including Darwin and rural residents, indigenous communities, farmers (agriculture) as well as mining and exploration operations exploits these systems. A successful joint project (the Northern Territory Coastal Plain project) involving the National Water Commission and Geoscience Australia maps seawater intrusion within coastal plain aquifers, using airborne electromagnetic data. This hydrogeologically-focussed project utilised the Pine Creek AEM survey data in combination with additional geophysical, geological and hydrogeological datasets to assess the occurrence and potential risk of seawater intrusion into coastal aquifers in the Darwin peri-urban area as well as surface water – groundwater connectivity within the Daly Basin (English, 2007).

The traditional owners of land within the survey boundaries were identified via the National Native Title Tribunal. The principal traditional owners were recognised as members of the Northern Land Council, who have Native Title Determinations, and Native Title Claims ([Figure 1–8](#)). Communications with the Northern Land Council (NLC) commenced in November 2007 with a letter outlining the survey. Communications included letters, emails and personal meetings with traditional owners outlining the survey boundaries for the purpose of identifying the potential social and cultural impacts of the project, giving an outline of how the survey would be implemented and showing maps of the areas where the survey would be focused.

The Pine Creek AEM survey was opened to public subscription in the interests of stimulating further exploration activity in the region. The intention to fly the survey was advertised in GA's Minerals Alert, AusGEO News, email and phone calls directly to tenement holders, and through various conferences, inviting companies to fund infill flight lines. Partner companies also provided drill-hole data, land access and field support.

A total of twelve companies expressed an interest to the initial subscription request. Further negotiations with these interested parties resulted in nine companies deciding to fund infill flight lines within the survey area ([Table 1–2](#)). The companies paid the same line kilometre amount as GA when purchasing the infill lines.

A number of non-subscribers also contributed in-kind support: Northern Territory Geological Survey, Natural Resources, Environment, The Arts and Sport (NRETAS), Cameco Australia, Uranium Equities Ltd and Energy Resources of Australia Ltd provided field support as well as land access, facilitated access to boreholes and contributed lithological logs supporting the conductivity logging phase of the program.

In all, infill companies contributed \$1.14 million to the survey budget and GA, through the OESP contributed \$2.6 million for a total survey cost of \$3.74 million, a survey area of approximately 74 000 km<sup>2</sup> comprising 29 900 line km of data. Infill areas to the main survey are shown in [Figure 1–3](#). All infill companies expected to spend an amount equal or greater than their contribution to the AEM survey in follow-up exploration programs after the AEM data were delivered. This is conservatively estimated to be worth an additional \$2 million in industry exploration investment in the region.

## **8.2 ADDITIONAL DATASETS**

The Pine Creek AEM survey area includes a number of 1:2 500 000, 1:1 000 000, 1:250 000 and 1:100 000 scale and special edition geological maps. The entire area is mapped at 1:2 500 000 scale by the Northern Territory Geological Survey (NTGS) and at 1:1 000 000 by the Geoscience Australia Surface Geology of Australia (released in 2009), which was compiled from 1:250 000 maps of the area. NTGS 1:250 000 map series dates from 1987 to the most recent published in 2010. Mapping of the 1:100 000 series commenced in 1980 and is ongoing. The available map sheet names and numbers associated with the AEM survey area are provided in [Figure 2–1](#) and a comprehensive list is given in [Table 2–1](#).

There is a range of publicly available airborne geophysical data covering the Pine Creek AEM survey area including detailed and regional magnetics, radiometrics, gravity, AEM and Digital Elevation Models (DEMs). These surveys may have been commissioned by minerals exploration companies, or by State, Commonwealth or other government agencies. The Space Shuttle Radar Topographic Mission Digital Elevation Model (SRTM DEM) is also included in this compilation for completeness, although it is a satellite-borne data acquisition platform. Most public-domain data are held within the Geophysical Archive Data Delivery System (GADDS) at GA and are available for free download through the Australian Geoscience Portal (<http://www.geoscience.gov.au/>). The SRTM DEM is available for free download from the United States Geological Survey (USGS) at the National Map Seamless Server (<http://seamless.usgs.gov/>).

Borehole data were gathered from the Northern Territory Geological Survey's borehole collar database. Collar location information for those boreholes located within the AEM survey area was subsampled from the bulk data provided. A separate dataset was also compiled consisting of Open File reports relevant to the AEM survey area. From those many reports, only those Open File reports that pertained to boreholes within, or outside but proximal to, the survey boundaries were separated for further consideration.

In addition to the minerals-related borehole information held by NTGS, the Northern Territory Department of Natural Resources Arts and Environment (NRETAS) holds information for water boreholes within the Northern Territory. The NRETAS Department is responsible for a wide range of water resource information. The Pine Creek AEM Survey boundary file was provided to the Department so that waterbore collars and linked report files in the on-line database could be extracted and provided to the AEM project for subsequent examination. No filters were applied to the data extraction and this resulted in about 2,000 water bore collars being returned to the project (see [Figure 2–3](#)). Many proved to be of limited or no use to the project's requirement of boreholes suitable for AEM section or grid calibration requirements. Some however were of sufficient depth and had suitable logs, and are located near AEM CDI sections so were included in the projects GIS borehole database.

Overall, the process of gathering, locating and selecting of boreholes suitable for interpreting conductivity contrasts visible in AEM sections was not very productive, and less than 100 boreholes proved helpful for these purposes ([Figure 2–4](#)). It took considerable time and effort to assess and compile this number of useful records. Conductivity logging was undertaken by Geoscience Australia staff to provide conductivity measurements for selected areas. The locations of conductivity-logged boreholes are shown in [Figure 2–5](#).

The borehole database has been useful in showing the thickness of regolith and Cenozoic cover materials, rock types and depth to major bedrock rock groups e.g., depth to the Kombolgie subgroup and Tolmer Group sediments, and depth to Paleoproterozoic metamorphic rocks. Accurate assignment of intersections to formations, either by the logging geologist or interpreted as part of the present project, has been difficult because drilling methodologies used were dominated by percussion.

The geology and mineral resources in the Northern Territory are described in detail in a special NTGS publication (Ahmad and Munson, in prep.). Summaries of geological regions in the Northern Territory are available on the NTGS website. [Chapter 3](#) summarises the pertinent geological regions with respect to the geological interpretations of GA's AEM surveys in the Pine Creek region. It provides background information in support of the project's interpretations of AEM data and includes discussion on the implications of observations for uranium mineral systems.

The distribution of regolith and landforms of the entire NT is mapped by Craig (2006) and has been drawn on in assessments of the Pine Creek AEM Survey. The initial map compilation was at a scale of 1:250 000 but was first published as hardcopy at 1:2.5 M scale. A new regolith–landform GIS, based on the compilation scale (but generalised to 1:1 M scale) is now available from the NTGS and covers the Pine Creek AEM survey area.

An Atlas of regolith materials of the Northern Territory (Robertson, Craig & Anand, 2006) [CRC LEME Open File Report 196] compliments the 1:2.5 M scale map. It describes in detail, specimens of regolith, including weathered rocks, sands and soils and their secondary cemented products (silcrete, ferricrete, calcrete) that were collected along approximately 20 000 km of traverses. In [Chapter 3](#) and in Report 196 the regolith terminology, weathering processes, regolith modification, associated fabric changes, weathering mineral reactions and mineral stability. The regolith data extend beyond the Pine Creek AEM survey area. Therefore, in selected conductivity-depth inversion sections as well as in some depth and elevation slices, parts of the AEM imagery correlate with known regolith materials. Examples of these correlations are discussed in detail in [Chapter 6](#).

A systematic study of palaeoweathering or the possible occurrence of palaeoregolith in borehole records was outside the scope of this AEM survey. Land surfaces reported by Hays (1965, 1967 and 1968) have been used extensively to explain the observed planar features of the NT landscapes. Commonly, extensive weathering profiles (up to 60 m thick) are reportedly superimposed on the respective surfaces. Palaeoweathering is reported to occur below the Kombolgie Subgroup and

below the Cretaceous by Needham *et al.*, (1988) in widespread locations, and is also noted in some borehole records.

The palaeotopographic surface at the base of the Kombolgie Subgroup is thought to be similar to that of the undulating sand plains, which cover much of the Pine Creek Inlier today. The unconformity undulates gently with relief of ~20 m, though some scattered hills and ridges approach a height of approximately 250 m. Development of this surface appears to have involved the prior removal by erosion of some 1-2 km of crustal materials. Chemical weathering produced a saprolitic weathering profile greater than 50 m deep over a period of 40 Ma before deposition of the overlying Kombolgie Subgroup. Information about ancient weathering profiles, their distribution and subsequent erosion is pertinent to conductivity patterns and the sensible interpretation of regolith influences in the AEM survey data.

### **8.3 MINERAL DEPOSITS**

The Pine Creek Orogen (PCO) hosts world-class, unconformity-related uranium deposits. It is one of Australia's most endowed Proterozoic provinces hosting several mineral occurrences, prospects, and deposits of uranium, gold, tin-tantalum, tungsten, copper and lead-zinc deposits. Ahmad (1998) presents a brief overview of mineral deposits in the PCO. A more detailed description of deposits and mineral systems in the Rum Jungle Mineral Field is available in a review by Ahmad *et al.* (2006). Lally and Bajwah (2006), and Ahmad *et al.*, (2009) published more recent reviews of uranium and gold deposits. Frater (2005) reviewed significant pegmatite-associated tin-tantalum mineralisation in the PCO. A brief review of mineral systems in the PCO with reference to the Pine Creek Aem Survey area is presented in [Chapter 4](#).

The discussion shows that mineral systems in the (PCO) are related intricately to sedimentary, diagenetic, deformation/metamorphic and magmatic events in the PCO. Some of these events are synchronous with events occurring within or at the margins of the North Australian Craton. The geological evolution of the three domains in the PCO (see [Figure 3–2](#)) also controls differences in their metallogeny. The Nimbuwah Domain is characterised by world-class unconformity-related uranium deposits, but no significant gold, basemetal and tin-tantalum-tungsten deposits have yet been found in this domain.

The Central Domain, on the other hand, hosts a diverse set of mineral systems, which includes unconformity-related uranium, iron ore, basemetal, tin-tantalum-tungsten, and gold. The abundance of gold deposits in this domain is probably related to a combination of the following factors: presence of a thick package of turbiditic sediments; lower-greenschist facies of metamorphism, widespread felsic magmatism, and the presence to a major regional-scale structure (Pine Creek Shear zone) Johnston (1984) provides a concise summary..

The metallogeny of the Litchfield Domain is dominated by mineral systems associated with felsic magmatism (tin-tantalum pegmatite and veins). The absence of significant gold mineralisation is probably related to the granulite facies of metamorphism in the domain, as most lode gold regions are often associated with terranes exhibiting a lower grade of metamorphism (greenschist to lower amphibolite facies). (See Ahmad (1998), Ahmad *et al.*, (2006), Lally and Bajwah, (2006), and Frater, 2005).

### **8.4 AEM DATA PROCESSING**

Airborne Electromagnetic (AEM) surveys map the electrical conductivity of the subsurface over extents too large to be covered on the ground. A time-domain AEM system aircraft carries a

transmitter loop through which a time-varying current is passed inducing eddy (secondary) currents to flow in any electrically conductive subsurface material. The secondary eddy currents are recorded via the voltage that is induced in the receiver coils towed by the same aircraft. The current flow in the subsurface is related to its conductivity. An inversion of the received signal allows estimates of the conductivity to be made. The depth to which the signals can be used to map conductivity depends on the system configuration and the subsurface conductivity (Smith, 2001; Lane *et al.*, 2004b).

The Pine Creek survey areas employed two different AEM systems. The TEMPEST™ fixed wing AEM system acquired data in the Woolner Granite and Rum Jungle survey areas. GA released the TEMPEST™ survey data publicly in July and September 2009, respectively. The VTEM™ helicopter AEM system acquired data in the Kombolgie survey area. GA publicly released these data in December 2009. To assist the interpretation of the survey data a conductivity-logging program was conducted in the Pine Creek survey area. Some of the associated company data remain “in-confidence” and are not in this report.

Induction conductivity data (referred to as conductivity logs) were acquired in boreholes during April and October 2009. The data were acquired from 24 boreholes widely distributed across different geological formations. The logs guided the construction of reference models for geophysical inversions of the AEM data, and provided an independent dataset for assessing the inversion results. [Table 5–7](#) provides location coordinates and depths of the logged boreholes and [Figure 5–11](#) shows the location of the logged boreholes plotted over the conductance from 0–200 m derived from the AEM data. The conductivity logs collected in the Kombolgie survey area are “in-confidence”, and are not displayed.

In order to assess the performance of the inversion, we compare the results of the GA–LEI at selected points to the borehole conductivity logs collected in that part of the survey area. There are limitations to this technique (Reid and Vrbancich 2004, Ley-Cooper and Davis 2010) related to the footprint of the conductivity log vs. the AEM footprint.

Bore holes were sparse and in many cases not close to flight lines therefore the assessment of logs immediately adjacent to the Geoscience Australia layered earth inversion (GA–LEI) results were limited. Generally the GA–LEI results show agreement with the borehole logs in close proximity to flight lines. For a full description of the GA–LEI inversion results see Costelloe and Hutchinson (2010). For a full description of the conductivity results see Costelloe, Hutchinson and Sorensen 2010.

[Chapter 6](#) presents geological interpretations of the Pine Creek AEM data. The interpretations focus on: (1) correlation of AEM data with major geological features such as stratigraphic units and structures including faults and folds; and (2) the AEM data contributions to defining the architecture of the geological provinces in the area, particularly their boundaries (*e.g.*, unconformities). The limitations of the data and the care that should be exercised in interpretation in some cases are also discussed. The interpretation methods, datasets used, the correlation of AEM anomalies with selected geological features, and the geological interpretation of AEM data in major geological provinces are described.

The vertical AEM conductivity sections are most useful for geological interpretations because of their graphic presentation of conductivity that allows convenient correlation with geological features. For the Woolner Granite–Rum Jungle survey, flown using TEMPEST™, GA has released two sets of such sections, namely, EMFlow™ (Macnae *et al.* 1998, Stoltz *et al.* 1998) and GA–LEI (Lane *et al.* 2004) conductivity sections. However, initially only EMFlow™ conductivity sections were available for interpretation of the Kombolgie survey. During the final preparation of this report GA–LEI

conductivity sections became available for interpretation. Some analysis is included in this report (See [Section 6–4](#)).

The GA–LEI method does not rely on the primary field separation and the geometry estimates made in the standard FAS data processing of AEM data. Instead, the GA–LEI inverts the total field data (both primary and secondary) directly (see [Chapter 5](#)).

Those interpreting the two datasets need to be aware of the assumptions and models in both EM Flow™ and GA–LEI processing. For the TEMPEST™ system, the EM Flow™ processing assumes that the subsurface is resistive at depth, while the GA–LEI uses a layered earth model of 30 layers and the estimated conductivity model is constrained to be vertically smooth and to be as close as possible to a reference conductivity model.

In the process of inversion, the GA–LEI method starts with a reference conductivity value, and then inputs different conductivity values for each layer, and attempts to best fit the measured and modelled conductivity values. How well the two sets of data fit is reflected in the Percentage Data Influence (PDI, [Chapter 5](#)). A 100% value of the PDI means the inversion is totally data-driven, while 0% means the inversion is totally model-driven.

Hutchinson *et al.* (2010) introduced a concept of Depth of Investigation (DOI). The DOI is defined as the depth at which the PDI is 50%. Above the DOI, where PDI is greater than 50%, the inversion is considered relatively robust. The DOI should be regarded as indicative depth of reliable data according to the GA LEI modelling.

In a layered earth situation, such as sedimentary basins in which the sedimentary rocks are sub-horizontal, both EM Flow™ and GA–LEI modelling provide meaningful conductivity data at depth. Geological interpretations can be reliably made. In areas of folded sequences, however, particularly in areas of tightly to upright isoclinally folded sequences like the Pine Creek Orogen, both EM Flow™ and GA–LEI modelling may fail because of their assumptions using models of a horizontally layered earth.

A number of man-made features such as powerlines (Lawrence and Stenning, 2009), gas pipelines and railways, may have significant effects on AEM data because of their extremely high conductivity, or because they produce their own electromagnetic fields. This may confuse the geological interpretation of AEM data. For example, the Pine Creek Shear Zone trends north-westerly through the vicinity of Pine Creek Township. The apparent conductivity anomalies in the vicinity of the known linear Shear Zone could be interpreted to reflect enhanced conductivities along the Shear Zone. However, after closer examination, the cause of these apparent conductivity anomalies was correctly attributed to known major powerlines and a major gas pipeline.

## **8.5 AEM DATA INTERPRETATION**

The major AEM signatures of geological provinces in the Pine Creek region are summarised in [Table 6–4](#). Strong conductors include carbonaceous and pyritic sediments, such as parts of the Koolpin, Whites and Cahill formations in the Pine Creek Orogen. Other sedimentary units may be weakly to moderately conductive, such as parts of the Daly River, Auvergne and Tolmer groups in the Daly Basin, Victoria Basin and Birrindudu Basin respectively. Coastal areas may be moderately to highly conductive because of saltwater ([Figure 6–3](#)). Granites and sandstones are generally resistive to very resistive.

AEM conductivity data are presented showing correlations with a number of selected geological and hydrological features. Unconformity-related uranium mineral systems are discussed in a separate section ([Section 6.3.2.7](#)). Interpretations are aimed at regional correlation of AEM data with geological features, not individual anomalies which are the focus of exploration companies.

During the overall assessment of the AEM survey data, GA–LEI conductivity sections and grids and EMFlow™ CDI sections and grids were used to determine the nature, extent and robustness of regolith information contained within them. Some examples provided here may help guide further regolith-related assessments.

The detection of weathering interfaces is of interest in regolith related assessments. The extent to which weathering interfaces are detectable will depend on the nature of the regolith materials present, and their conductivity contrast at any discontinuity present. The nature and type of any infilling materials present at the interface, the nature of any fluids present along or near the interface or the type and extent of alteration will all influence the detectability of such an interface. The configuration, depth penetration and resolution of the AEM system used to detect these features are also critical factors.

Coastal areas feature moderate to high conductivities in relation to incursion of sea water including the areas of Anson Bay and Daly River, Fog Bay, Shoal Bay and Howard River, Adam Bay and Adelaide River, Chambers Bay and Mary River, and Finke Bay ([Figure 6–3](#)). The effects of saline water are also mostly restricted to the depth of the sedimentary strata. The effects of saline water intrusion are visible in AEM depth and elevation slices, especially near to the coast and along major river systems. These effects are discussed, and their relationship with regolith materials is highlighted.

Most of the regolith materials exposed at the surface in the Pine Creek AEM survey area are in situ regolith types. The dominant in situ material is saprolith, which is a combination of weathered and partially weathered rock more formally known as saprolite and saprock ([Figure 6–4](#)). The remainder of the exposed regolith in the survey area is either pedolith (residual materials; [Figure 6–5](#)) or a variety of transported regolith. The main transported materials are alluvial and coastal deposits ([Figure 6–6](#)). In the case of transported regolith, highly conductive AEM signatures immediately below the position of mapped coastal alluvial regolith ([Figure 6–6](#)), indicate sea water intrusion. Residual regolith materials (collectively mapped as pedolith – i.e., ferricretes; “lateritic” materials ferruginous nodules and pisoliths) mainly coincide with highly resistive AEM signatures and are especially prominent in near surface AEM depth slices. In the upper parts of the saprolith, especially close to the base of any mapped pedolith, AEM signatures show highly resistive patterns. However, as depth increases below the pedolith interface, the regolith becomes more conductive. These changes are not universal and are not the same for all regolith. They will vary according to the nature of the parent rock types, the degree and depth of weathering, and the amount of pedolith development involved. Eventually the lower unweathered part of the regolith profile is encountered. Here, deeper in the saprock part of the saprolith, the AEM signatures show that the regolith becomes progressively more resistive as it approaches the unweathered bedrock.

Palaeochannel environments are likely present in the Pine Creek AEM area and their location would be relevant to uranium exploration. There are a few geomorphic indicators documented by Magee (2009) confirming the existence of palaeochannels elsewhere across the Northern Territory. Whether or not these environments, and others yet to be discovered, have acted as sites for precipitation of uranium is yet to be demonstrated.

## **8.6 RUM JUNGLE AEM INTERPRETATION**

In the western Pine Creek Survey area, together with a range of remotely sensed images was examined for any surface indicators of palaeochannels, regardless of their age. In addition, the available conductivity depth, elevations slices and CDI conductivity sections were also examined for

possible older subsurface expressions. The results of image assessments for evidence of older drainage networks near or just below the surface are presented in a series of figures in [Chapter 6](#).

Some geomorphic features are present in the coloured, DEM image near Pine Creek and Emerald Springs in the Rum Jungle survey area ([Figure 6–33](#)). These erosion features suggest that drainage to the SW (particularly across the Daley Basin and further west) is old and superimposed ([Figure 6–23](#) and [Figure 6–24](#)). Whether or not these drainage features are strictly superimposed or antecedent remains unresolved. However, for this drainage style to have formed, it has to have been in existence for some considerable time. Earlier, but possibly now buried, drainage courses may be present, especially in the mid reaches of the network. These mid-reach areas are of some interest in the search for buried palaeochannel environments containing uranium deposits.

Further west, near Peppimenarti and Pulmpar ([Figure 6–24](#)), the headwater drainage remnants still visible on the older upland region are associated with much shallower regolith compared with the lowland mid-reach drainage tracts and, consequently, may be of lesser interest for palaeochannel uranium deposits.

Palaeovalleys are interpreted to be present at depth in the Pine Creek Survey Area and in the Tolmer Group at depth within the Mt Boulder area. The palaeovalley system contains a network of lower conductivity channels ([Figure 6–33](#)). The lower conductivity in these interpreted channels may be due to the presence of relatively fresh water retained in the palaeodrainage system. Current surface drainages are clearly shown in the DEM and are mapped in detail on the Pine Creek 1:250 000 geological map (Malone, 1962).

The palaeovalleys and palaeodrainage network depicted in the AEM conductance data is similar but not identical to the current drainage system as shown on the surface geological map. The water flow directions in the palaeovalleys is interpreted to be from Bald Ridge towards Rock Candy Range, and then along the current flow direction of the Daly River. The differences in positions between the palaeovalleys and current drainage systems may reflect migration of the drainage system over time. The palaeovalleys represent possible uranium targets in this region.

In the Pine Creek Orogen, some granite plutons display their oval shapes where rimmed by more conductive surrounding metasedimentary rocks. These define the pluton boundaries, such as the Rum Jungle Complex, Burnside Granite and Minglo Granite ([Figure 6–3](#)). Many faults are depicted in the PCO AEM data and at a number of locations, faults are depicted in AEM conductivity sections as being slightly more conductive than the host rocks, such as the fault between the Hermit Creek Metamorphics (schist) and the Moyle River Formation (sandstone) along lines 1004401 and 1004601 in the Rum Jungle survey ([Figure 6–34](#)). Folds are common structures in the Pine Creek Orogen. Many folds are depicted in AEM conductivity sections, although the geometry of some folds as mapped in geological maps and cross sections may not be readily interpreted from the AEM conductivity sections.

There are several geological province boundary unconformities in the Pine Creek AEM survey area and some of these unconformities are well depicted in the AEM conductivity data. Within the sedimentary packages of a particular geological province there are also internal unconformities. For example, within the Pine Creek Geosyncline metasedimentary sequence, there are several unconformities between different sedimentary packages or groups as shown in [Figures 4–1](#) to [4–3](#). Within the McArthur Basin there are also unconformities between the Katherine River, Mount Rigg and Roper groups. However, not all of these unconformities are detected in the AEM data due to a lack of contrast in conductivities of the rocks above and below the unconformity, or because there is no apparent enhancement or reduction of conductivity along the unconformity.

Cretaceous sediments are present in the Money Shoal, Bonaparte and Carpentaria basins and form tablelands, mesas, buttes and isolated rounded outcrops mantling all older rock units. These

sediments are expected to be much more extensive under the Cenozoic cover than the outcrops mapped in these areas. On Fergusson River they were mapped as Mullaman Beds by Pontifex and Mendum (1972), comprising a 30 m thick sequence of sandstone, siltstone and porcellanite. In the Wingate Mountains area, along lines 1205201 and 1005201, there are two moderate conductors. The thin upper conductor corresponds with the Cretaceous sediments of Bonaparte Basin, while the lower conductor correlates with underlying sediments of the Auvergne Group of the Victoria Basin. In the Carpentaria Basin, a weak to moderately conductive layer of the Cretaceous Mullaman Beds overlies resistive Oolloo Dolostone and conductive sediments of the Jinduckin Formation of the Daly Basin (lines 10190-10240).

The Cambrian – Ordovician Daly Basin overlies the Birrindudu Basin in the Adelaide River – Pine Creek area. As part of the geological interpretation of the TEMPEST™ conductivity data of the Woolner Granite – Rum Jungle AEM area, a 3D model has been constructed for parts of the area.

The Daly Basin sediments are moderately conductive overall, with discrete anomalies, as depicted in the conductance image ([Figure 6–3](#)). On Pine Creek map sheet, the Daly River Group is a 700 m thick sequence of mostly carbonate sediments. Stratigraphic units of the Group and its rock types are summarised in [Table 6–5](#). The Daly Basin boundary is well depicted along both the east and west margins of the Basin. Moderately conductive sedimentary units of the Basin dip gently towards the centre of the Basin and are in sharp contrast to the generally resistive older basement rocks. Along the west margin of the Daly Basin, the basal unconformity is recognizable but the sub-parallel and shallowly dipping conductors in the underlying Tolmer Group sediments may obscure the position of the basal unconformity.

The Depot Creek Sandstone – Pine Creek Orogen unconformity is depicted on many AEM conductivity sections along the east and west boundaries of the Birrindudu Basin, which show the unconformity dipping towards the central part of the Basin. The unconformity seems to be best depicted from Hayes Creek to the Umbrawarra Leocogranite on the east margin of the Daly Basin near the southern border of the Pine Creek 1:250 000 map sheet (line 10080 to line 10180, [Figure 6–39](#)), and from the Jammie Granite to Priors Knob west of the Daly Basin (line 1004401 to line 1004801). Strong and moderate conductors are present at or near the base of the Stray Creek Sandstone and Hinde Dolomite, and in the Waterbag Creek Formation, as seen along lines 10030 and 10041 about 18 to 23 kilometres south of Adelaide River.

A 3D model of the northeast margins of the Daly Basin and Birrindudu Basin in the Hayes Creek area was constructed in GOCAD® 2009.1 (Paradigm™). Assessment of the GA–LEI conductivity sections revealed three key marker horizons, which could be consistently identified on most GA LEI sections in the area. Correlation of those horizons with surface geology mapping indicated that each directly correlated with a known geological contact as shown in [Figure 6–41](#). This 3D model ([Figure 6–43](#)) graphically illustrates the relationships between the three mapped horizons with a clarity and certainty that would have not been possible without AEM. In particular, it maps the geometry of the shallow-dipping Depot Creek unconformity to the west, and is also the base of the Daly Basin in this area.

On the Fergusson River and Port Keats 1:250000 geological map sheets, the Neoproterozoic Auvergne Group of the Victoria Basin is mapped as a package of sandstone, siltstone, dolomitic sandstone and dolomite ([Table 6–7](#)). The Rum Jungle AEM survey covers the northern most part of the Basin, which is faulted against older Mesoproterozoic rocks in most places. Overall, the Victoria Basin area is moderately conductive, with patches of slightly higher or lower conductivity (see both [Figure 3–2](#) and [Figure 6–3](#)). There are at least three conductors in the Auvergne Group sediments, as depicted in the GA–LEI conductivity sections near the Victoria River Fault contact with the unexposed Paleoproterozoic Chilling Sandstone of the Finniss River Group at the north end of the

Basin along lines 1005501 and 1005601 ([Figure 6.44](#)). Here the Neoproterozoic Auvergne Group sediments dip gently to the southeast. Further east the sediments are almost horizontal.

In the Woolner Granite – Rum Jungle AEM survey area, the Fitzmaurice Group includes (from lower part to upper part) the Moyle River Formation, the Goobaieri Formation, the Lalngang Sandstone and the Legune Formation. The lithology and thickness are summarised in [Table 6–9](#).

The Fitzmaurice Group is faulted against the Pine Creek Orogen in most places ([Figure 6–2](#)). Overall, it is resistive to very weakly conductive ([Figure 6–3](#)), but there are some discrete and weakly to moderately conductive anomalies at depth (e.g., in line 1005301). The boundaries between the Lalngang Sandstone, the Goobaieri Formation and the Moyle River Formation seem to be slightly more conductive than these units (e.g., in lines 1005201, 1005301, 1005401).

During the Top End Orogeny, about 1870 – 1690 Ma (Needham *et al.* 1988), the Paleoproterozoic Pine Creek Geosyncline sequence experienced regional metamorphism up to amphibolite facies and multiple deformations that produced a network of faults and tight to isoclinal folds, forming the Pine Creek Orogen, as summarised in [Chapter 3](#). Faults and tight to isoclinal folds are well developed in the Pine Creek Orogen. Gold mineralisation in the Orogen is structurally controlled. The conductive units and anomalies can be used to map the presence of faults and folds ([Figure 6–45](#)). In mostly resistive or weakly conductive rocks, faults may show slightly higher conductivity due to the presence of fluids, alteration and mineralisation ([Figure 6–34](#) and [Figure 6–45](#)). Close examination and correlation are required to ascertain the cause. Many faults and folds are depicted in the GA–LEI conductivity sections ([Figure 6–45](#)). Close correlation and interpretation of an area south-southeast of Rum Jungle is presented in [Figure 6–46](#), which shows interpretations of several faults and folds along lines 1001902 and 1002101.

In the area between the Rum Jungle and the Water House domes, lines 1001501 and 1101901 run over resistive granites in the east to the Pine Creek Geosyncline sequence west of the Giants Reef Complex, which contains weak and strong conductors. The Pine Creek sequence here consists of the Coomalie Dolomite, the Geolsec Formation, the Whites Formation and the South Alligator Group.

In this area, the Coomalie Dolomite, the Geolsec Formation and the South Alligator Group are largely resistive. The Whites Formation consists of strong conductors in parts. There are two antiforms in the Whites Formation about 2-3 km south and southeast of Mt Burton, as defined by the folded dolerite sills. There is likely to be an N-S trending fault between the two antiforms, which is consistent with the geometry of AEM anomalies along line 1101901. The western fold is also depicted in line 1001501. The Giants Reef Fault and several faults to the west seem to have also been depicted in the AEM data ([Figure 6–45](#)).

The observed shallow strongly conductive anomalies associated with metasedimentary rocks in the Woolner Granite – Rum Jungle are mostly in the top 200-300 m. In such areas, the strong conductors may be used to map the presence of faults and folds. They can not be used to map the depth extent of the strongly conductive rocks because the base of such rocks is not detected in this AEM survey. Thus caution should be exercised in geological interpretation in areas of strongly conductive and steeply dipping sequences. Here the DOI (referred to earlier) becomes an important guide in the interpretation process.

In the Woolner Granite – Rum Jungle area the Zamu Dolerite, a continental tholeiitic suite, intruded the sediments as sills. The mapped dolerite sills are in the sediments of the South Alligator Group and older units. In general, the Zamu Dolerite has a resistive response and does not consistently correlate with AEM conductivity anomalies. However, in places there are AEM conductive anomalies over mapped dolerite which may be due to the strong conductors below the Dolerite sill. Alternatively, the anomalies may be due to presence of fluids and/or alteration along the contacts

between the Zamu Dolerite and metasediments which show different and perhaps enhanced conductivities.

Archean rocks are mapped in four areas in the Pine Creek Orogen, namely, the Woolner Granite, the Rum Jungle Complex, the Nanambu Complex and unnamed Archean basement rocks in the Nabarlek area of Nimbuwah Domain. Some weak conductivity anomalies in the complexes may be due to alteration and/or weathering. The rings of high conductivity anomalies around the Rum Jungle and Waterhouse domes ([Figure 6–3](#)) are due to the uplift of highly conductive carbonaceous (and pyritic) Paleoproterozoic metasediments around the Archean granite domes. The Woolner Granite is not exposed at surface, but is readily interpreted from airborne magnetic data and confirmed from drilling at a depth of 50-80 metres (Pietsch 1985; Pietsch and Stuart-Smith, 1987).

## **8.7 KOMBOLGIE AEM INTERPRETATION**

In the eastern Pine Creek region, the Kombolgie AEM survey was flown using the VTEM™ system and covers part of the McArthur Basin, and parts of the Central Domain and Nimbuwah Domain of the Pine Creek Orogen ([Figure 3–2](#)). Most rocks of the Kombolgie survey area are extremely resistive ([Figure 6–49](#)), thus VTEM™ was able to penetrate to a depth up to 2 km (Costelloe and Brodie, 2011), providing insights of the geology to that depth that no methods other than drilling and seismic imaging could previously achieve. The “Kombolgie Sandstone” or the Kombolgie Subgroup at the base of Katherine River Group ([Table 6–11](#)) is of most interest to uranium explorers because many known uranium deposits in the Jabiru area are related to the Kombolgie unconformity over the Pine Creek Orogen and Archean basement rocks. Pre-Kombolgie Paleoproterozoic rocks in the Nimbuwah Domain include the Kakadu Group, the Cahill Formation and the Nourlangie Schist ([Table 6–12](#)). The pyritic and carbonaceous schists of the Cahill Formation are potential AEM conductors, and also provide reductors for uranium mineralisation. Other Paleoproterozoic rocks in the Nimbuwah Domain may also be conductive to some extent.

The EM Flow™ sections from the Kombolgie AEM survey clearly show the unconformity between the Kombolgie Subgroup and the underlying metasedimentary rocks, Archean basement and other conductors in the Katherine River Group. Importantly, the data also map conductors in pre-Kombolgie basement to a depth of up to 2 km (Minerals Alert February 2011; Costelloe and Brodie, 2011). Penetration to this depth represents a major breakthrough in AEM survey capability.

The Kombolgie unconformity is mostly visible as a thin weakly to moderately conductive anomaly mostly shallower than 500 m in the EM Flow™ CDI sections in the northern part of the Kombolgie survey area. The unconformity is deeper in the south-eastern part of the survey area. For example, in the eastern part of the interpreted cross-section along line 12290, the Kombolgie unconformity is interpreted to be at a depth of about 1 km ([Figure 6–50](#)). This is consistent with palaeocurrent studies by Sweet *et al.* (1999) on Mount Marumba and Carson *et al.* (1999) on Milingimbi, who showed palaeocurrent directions to the south or southwest, suggesting higher ground to the north. The Mamadawerre Sandstone immediately above the Kombolgie unconformity is predominantly a fluvial sequence. The conductivity associated with the unconformity is attributed to a combination of alteration and fluids present at the unconformity surface.

Fresh unaltered mafic volcanic rocks are generally resistive. In the Kombolgie AEM survey area, however, the positions of the Nungbalgarri Volcanics and the Gilruth Volcanic Member correspond to moderate conductivity anomalies along many EM Flow™ CDI sections ([Figure 6–50](#)). It is likely that the conductivity anomalies are due to the presence of fluid along the contacts of the mafic volcanic rocks with sedimentary rocks and/or alteration of the mafic volcanic rocks, particularly along the contacts with sedimentary rocks. Of note in this area is that the Oenpelli Dolerite does not correspond consistently to any particularly conductivity anomaly pattern.

The conductivity anomalies associated with the pre-Kombolgie basement rocks may be attributed either to carbonaceous and pyritic metasediments in the Cahill Formation, metamorphosed mafic rocks in the Archean complexes, or to other undefined conductive rocks. Detailed mapping of these conductive rocks in pre-Kombolgie basement rocks is important for defining the presence of potential reductors essential in assessing the potential of the Kombolgie unconformity-related uranium mineral systems. Some of the pre-Kombolgie conductivity anomalies are detected at depths down to 2 km. Detection at this depth represents a major breakthrough in AEM survey capabilities, and is possibly because of the very resistive nature of rocks in the area.

The interpretations of the Kombolgie AEM data were done on the EM Flow™ data, i.e., before the GA–LEI modelling data became available. The reader should be aware that there are alternative interpretations of the AEM data. The user of the AEM conductivity estimates by either EM Flow™ CDI or GA–LEI is reminded that one set of parameters and assumptions are used in processing the entire survey data, which does not address different geological situations satisfactorily. Exploration companies are advised to consider re-processing the data using different parameters and assumptions appropriate for regions of specific interest and different geological scenarios.

AEM provides a unique dataset giving depth information of geological features in the shallow crust in a regional context. The Pine Creek regional AEM data are very useful in assisting mineral exploration (including uranium) in the top few hundred metres below surface. The surveys also indicate where more detailed airborne and ground surveys would add maximum value for exploration.

## **8.8 URANIUM EXPLORATION IMPACT**

Detailed geological interpretation of the Pine Creek AEM data is described in [Chapter 6](#). [Chapter 5](#) details major mineral systems in the Pine Creek Orogen and lists critical features of unconformity-related uranium mineral systems ([Table 4-5](#)). [Chapter 7](#) focuses on the implications for uranium mineral systems in the Pine Creek region. Key components include discussion about relevant mineral systems, how AEM data contribute to assessment of potential of these mineral systems and recommend work that should be done in the future to facilitate further assessments.

The key components of fertile unconformity-related uranium mineral systems in the Pine Creek region are detailed in [Table 7-1](#). They include a major unconformity, reduced Paleoproterozoic metasedimentary rocks below the unconformity, a relatively thick (> 4 to 5 km) package of Paleoproterozoic coarse-grained, dominantly fluvial sediments overlying the unconformity, proximity to uranium-rich Archean granite-gneiss complex, ore-localising structures; and, the presence of mafic and/or felsic intrusive and/or volcanics within a Paleoproterozoic sedimentary package overlying the unconformity. The latter is a distinguishing feature of the Nimbuwah Domain, which hosts world-class deposits in the Alligator Rivers Uranium Field. More than 50% of the Nimbuwah Domain (defined in [Chapter 3](#) and shown in [Figure 3-2](#)) is covered by the rocks of the Katherine River Group and so has not been explored fully and remains prospective for both (sub-unconformity) Ingress-style and Egress-style (hosted in the sandstone above the unconformity) uranium deposits. The area is also prospective for Westmoreland-style deposits (Polito, Kyser, Rheinberger and Southgate, 2005) where mineralisation is often controlled by mafic rocks which contain silicate reductants.

The Birrindudu Basin is prospective for unconformity-related uranium mineral systems because it contains a relatively thick sandstone package of the Depot Creek Sandstone, which unconformably overlies the reduced metasediments of the Finniss River and South Alligator groups. However, unlike the McArthur Basin in the Nabarlek area, in the Pine Creek–Fergusson area the Birrindudu Basin is largely covered, mostly by the River Group and younger sediments. To assist assessing the

potential of unconformity-related uranium mineral systems in the Daly Basin area, two preliminary and generalised solid geology maps have been produced ([Figure 7–2](#) and [Figure 7–3](#)). The pre-Daly Basin solid geology map shows the distribution of the Tolmer Group including the Depot Creek Sandstone in the area ([Figure 7–2](#)). The pre-Depot Creek solid geology map shows the basement geology below the Depot Creek unconformity over the Pine Creek Orogen ([Figure 7–3](#)). A 3D model has been produced for part of the eastern margin of the Birrindudu Basin ([Figures 6–41, 6–42](#) and [6–43](#)), that depicts the geometry of the Depot Creek unconformity, top of the Stray Creek Sandstone, and top of the Jindare Formation.

The Kombolgie Subgroup is interlayered with mafic units and is intruded by the Oenpelli Dolerite. Diagenetic fluids released by the Kombolgie Subgroup sediments under favourable conditions can form uranium deposits after reacting with mafic rocks (Westmoreland-style uranium deposits). Some enrichment of uranium is observed in sandstones at the contact with these units (see [chapter 5](#)). More detailed work is required to assess the prospectivity of Westmoreland-style uranium deposits within the Kombolgie Subgroup. The Pine Creek Orogen is overlain by relatively thick sandstone packages of Palaeozoic and Mesozoic ages. Some of these packages may be prospective for sandstone-hosted uranium deposits. There is also potential for sandstone-hosted and Westmoreland-type deposits associated with mafic rocks (such as Oenpelli Dolerite) within the sandstone south of Rum Jungle, and east of the Southern Area is an area that has a potential for buried Cainozoic palaeochannel-hosted uranium.

Interpretation of AEM data in the Pine Creek region has shown that AEM can successfully map critical elements of fertile unconformity-related uranium systems. Those critical elements include the unconformity at the base of the Katherine River and Tolmer groups, the thickness of the Katherine River and Tolmer groups above the unconformity, the metasedimentary rocks below the unconformity (especially rocks containing reductants), and, faults in the metasedimentary rocks. The interpretation of these data has demonstrated that a regional-scale AEM survey in combination with drill-hole data can help to create a 3D model of basin architecture. The example given in this report is the McArthur River and Birrindudu basins in the Pine Creek region. This architecture can provide information on the direction of fluid flow during diagenesis of basin sediments and thereby outline the areas prospective for unconformity-related uranium systems.

## **9 Acknowledgements**

Geoscience Australia would like to acknowledge the contributions of the following organisations groups and individuals for their support which has made possible the acquisition, processing and interpretation of the Pine Creek survey data:

- Reviewers (in alphabetical order):
  - Richard Blewett;
  - Jon Clark;
  - Pauline English;
  - Aden McKay;
  - Peter Milligan;
  - Murray Richardson;
  - Ian Roach;
  - Ned Stoltz; and,
  - K. P. Tan
- Northern Territory Geological Survey;
- Natural Resources, Environment, The Arts and Sport (NRETAS)

For field support as well as land access, access to open borehole and lithological logs supporting the conductivity logging phase of the program:

- Cameco Australia
- Uranium Equities Ltd and Energy Resources of Australia Ltd
- Subscription companies:
  - Crossland Uranium Mines Ltd.;
  - Hapsburg Exploration Pty. Ltd.;
  - The National Water Commission;
  - Rio Tinto Exploration Pty. Ltd.;
  - Rum Jungle Uranium (now Rum Jungle Resources Ltd);
  - Southern Uranium Ltd.;
  - Thundelarra Exploration and United Uranium Ltd.;
  - Uranex NL;

And,

The Northern Land Council, for granting access to traditional lands.

We would also like to acknowledge the significant contributions of Richard Lane and Professor James Macnae (RMIT) who greatly assisted with technical advice and EM Flow™ Version v5.23-13 - STEM Flow\_FULL523-13.exe which enhanced the Kombolgie dataset; The Geophysics Group, Onshore Energy and Minerals Division, Geoscience Australia; and, Camilla Sorensen for her early work in helping set up the survey and for conductivity logging, and to Alan Whitaker and Pauline English for their help and guidance during this work.

# 10 Appendices

## 10.1 INVERSION DATA

**Table 10–1:** GA–LEI inversion products for the Woolner Granite and Rum Jungle survey areas.

NAME	FORMAT	DESCRIPTION	COMMENTS
<b>linedata</b>			
master.inversion.dat master.inversion.hdr	Ascii hdr	ascii data file containing master inversion output (reference model = 0.001 S/m) associated header information in text format	1 file containing 681 lines of data 4 txt files
secondary.inversion.dat secondary.inversion.hdr	Ascii hdr	ascii data file containing inversion output used to calculate pdi (reference model = 0.01 S/m) associated header information in text format	1 file containing 678 lines of data 4 txt files
eintervals_10m.dat eintervals_10m.hdr	Ascii Hdr	ascii data file containing inversion output sliced into 10 m elevation intervals associated header information in text format	1 file containing 678 lines of data 4 txt files
<b>sections</b>			
GA_LEI_georeferenced_jpeg	.jpeg and associated .jgw	georeferenced line sections of conductivity	Linenumber.jpg Linenumber.jgw
GA_LEI_multiplots	.pdf	line sections of conductivity, compared with AEM system geometry and data misfit.	Linenumber.pdf
<b>grids</b>			
Depth Slices	.ers	conductivity grids in slices of depth below surface	15 .ers files
Elevation slices	.ers	conductivity grids in slices of elevation above sea level (10 m slices)	71 .ers files
Conductance	.ers	total conductance grids for 0-200m and 0-400m depth	2 .ers files
AEM Go Map	.ers	depth of investigation grid	1 .ers file
conductance_jpeg	.jpeg and associated .jgw	georeferenced grids conductance	2 .ers files
depth_slice_jpeg	.jpeg and associated .jgw	georeferenced grids depth slices	30 files
elevation_slice_jpeg	.jpeg and associated .jgw	georeferenced grids elevation slices	142 files
AEM_Go_Map_jpeg	.jpeg and associated .jgw	georeferenced grid AEM Go Map	1 .ers file

NAME	FORMAT	DESCRIPTION	COMMENTS
<b>report</b>			
Woolner_Granite_and Rum_Jungle_TEMPEST™ AEM_Surveys_inversion Report.pdf	.pdf	Explanatory notes	1 file
<b>shapefiles</b>			
Flight Lines Survey Boundary	.shp	Pine Creek survey shape files and associated files	19 files

## 10.2 GA–LEI INVERSION OF TEMPEST™ DATA

### 10.2.1 Introduction

The GA–LEI inversion program is capable of inverting data from most airborne time-domain AEM systems. It has the capability of inverting for layer conductivities, layer thicknesses and system geometry parameters, or some subset of these. There are options to use a multi-layer smooth-model formulation (Constable et al., 1987) or a few-layer blocky-model formulation (Sattell, 1998). For the sake of simplicity, only the aspects of the algorithm that are relevant to the inversion of TEMPEST™ data using a multi-layer smooth-model are described here.

TEMPEST™ data consist of a collection (tens of thousands to millions) of point located multi-channel samples acquired at 0.2 s (approximately 12 m) intervals along survey flight lines. The algorithm independently inverts each sample. The data inputs to the inversion of each sample are the observed total (primary plus secondary) field X-component and Z-component data. Auxiliary information input into the algorithm are the measured and assumed elements of the system geometry, the thicknesses of the layers and prior information on the unmeasured elements of the system geometry and ground conductivity. The unknowns solved for in the inversion (outputs) are the electrical conductivity of the layers and the unmeasured elements of the system geometry.

Since each sample is inverted independently, the user may elect to invert all samples or some subset of them. The inversion of each sample results in an estimate of a one dimensional (1D) conductivity structure associated with that sample. Each estimated 1D conductivity structure, although theoretically laterally constant and extending infinitely in all directions, is only supported by the data within the system footprint which is approximately a square of side length 470 m centred about the sample point (Reid and Vrbancich, 2004). So, by progressively inverting all the samples and stitching together the resultant 1D conductivity structures, a depiction of the overall laterally variable 3D conductivity structure is built up.

### 10.2.2 Formulation

Figure 10–1 shows the overall framework under which the inversion of a single airborne sample is carried out. The elements of the figure are progressively described in the following sections.

#### 10.2.2.1 Coordinate system

Since each sample is inverted separately the coordinate system is different for the inversion of each sample. A right handed xyz Cartesian coordinate system is used. The origin of the coordinate system is on the Earth’s surface directly below the centre of the transmitter loop. The x-axis is in the direction of flight of the aircraft at that sample location, the y-axis is in the direction of the left wing and the z-axis is directed vertically upwards.

#### **10.2.2.2 System geometry**

The centre of the transmitter loop is located at  $(0, 0, TX_h)$ . Roll of the transmitter loop ( $TX_r$ ) is defined as anti-clockwise rotation, about an axis through  $(0, 0, TX_h)$  and parallel to the x-axis, so that a positive roll will bring the left wing up. Pitch of the transmitter loop ( $TX_p$ ) is defined as anti-clockwise rotation, about an axis through  $(0, 0, TX_h)$  and parallel to the y-axis, so that positive pitch will bring the aircraft's nose down. Yaw of the transmitter loop ( $TX_y$ ) is defined as anti-clockwise rotation, about an axis through  $(0, 0, TX_h)$  and parallel to the z-axis, so that a positive yaw would turn the aircraft left. However since the x-axis is defined to be in the direction of flight at each sample, the transmitter loop yaw is always zero by definition. The order of operations for calculating the vector orientations is to apply the pitch, roll then yaw rotations respectively.

The position of the receiver coils relative to the transmitter loop is defined by the transmitter to receiver horizontal inline separation ( $D_x$ ), the transmitter to receiver horizontal transverse separation ( $D_y$ ), and the transmitter to receiver vertical separation ( $D_z$ ). The receiver coils are thus located at  $(D_x, D_y, RX_h = TX_h + D_z)$ . The receiver coils are always behind and below the aircraft ( $D_x < 0, D_z < 0$ ). The receiver coils' roll ( $RX_r$ ), pitch ( $RX_p$ ) and yaw ( $RX_y$ ) have the same rotational convention as for the transmitter loop except that they are rotations about the point  $(D_x, D_y, D_z)$ . The receiver coils are always assumed to be located on the y-axis ( $D_y = 0$ ) and to have zero yaw ( $RX_y = 0$ ). Although this is not in reality the case, the position and orientation is not measured and there is not enough information available to solve for these since Y-component data is not available.

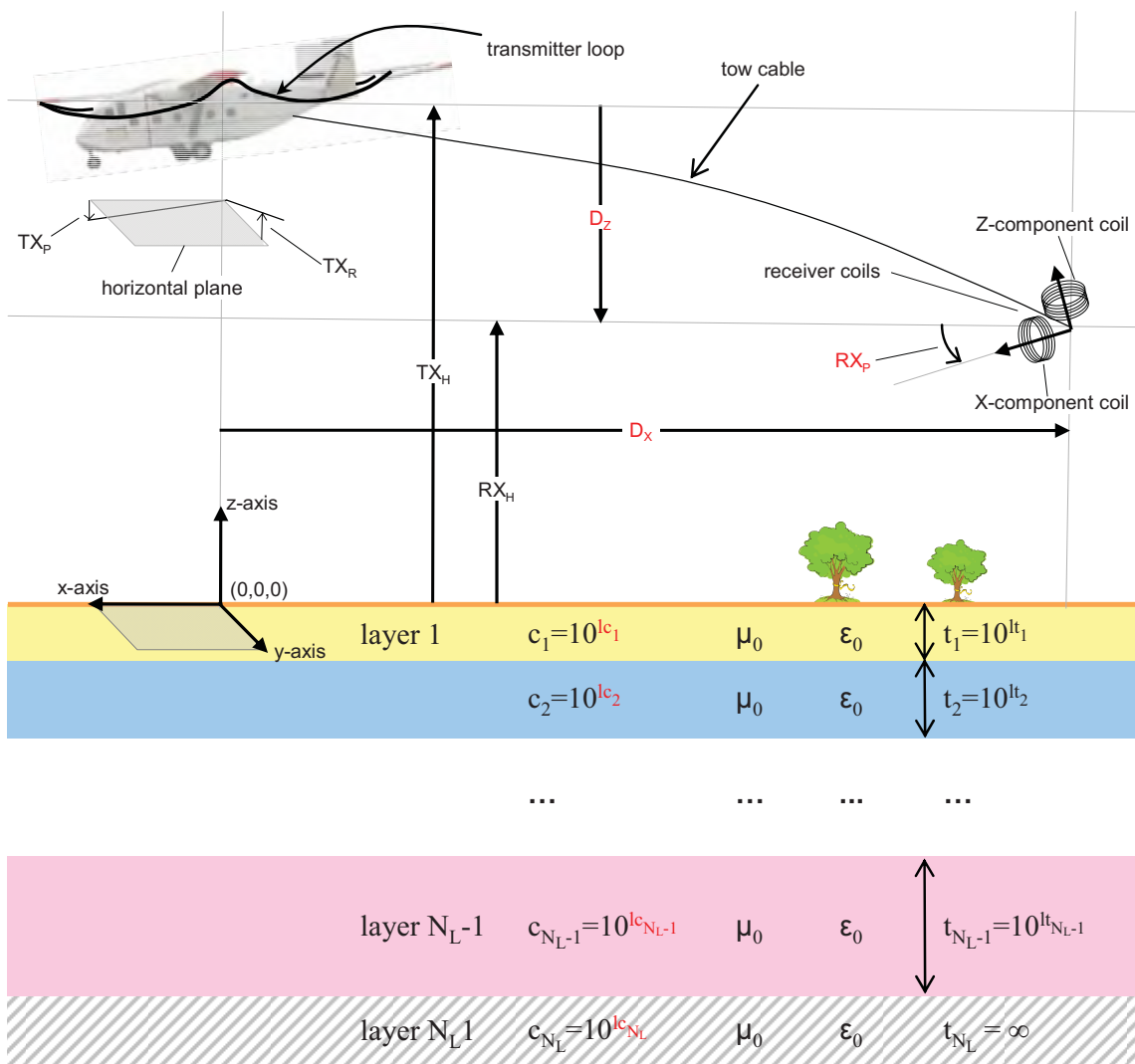


**Figure 10-1:** Schematic representation of the framework for GA–LEI inversion of TEMPEST™ AEM data. Red elements are the unknowns to be solved

Note that transmitter loop pitch data supplied by Fugro Airborne Surveys in processed TEMPEST™ data uses the convention where a positive transmitter pitch is nose up, and accordingly the supplied pitch is reversed in sign before being used in the inversion algorithm.

#### 10.2.2.3 Layered earth

The layered earth model is independent at each inverted sample location. The layered earth consists of  $N_L$  horizontal layers stacked on top of each other in layer cake fashion. The  $k^{th}$  layer has constant thickness  $t_k$  and the bottom layer is a halfspace that has infinite thickness ( $t_{N_L} = \infty$ ), extending to infinite depth. The electrical conductivity of the  $k^{th}$  layer is  $c_k$  and it is constant throughout the layer. The magnetic permeability of all layers is assumed to be equal to the magnetic permeability of free space  $\mu_0$ . The dielectric permittivity of all layers is assumed to be equal to the permittivity of free space  $\epsilon_0$ .

#### **10.2.2.4 Data**

Part of the TEMPEST™ data processing sequence involves partitioning the total (secondary plus primary) field response that is actually observed into estimates of the unknown primary and secondary field components. Then an estimate of the transmitter to receiver horizontal in-line and vertical separations  $D_x$  and  $D_z$  are made from the partitioned primary field component. The procedure uses the measured transmitter pitch ( $TX_p$ ) and roll ( $TX_r$ ) and assumes the receiver coils are flying straight, level and directly behind the aircraft ( $D_y=0$ ,  $RX_r=0$ ,  $RX_p=0$ , and  $RX_y=0$ ). It is the estimated secondary field data, the measured elements of the system geometry ( $TX_h$ ,  $TX_p$ ,  $TX_r$ , and  $TX_y$ ) and the associated estimates of the unmeasured elements of the system geometry ( $D_x$  and  $D_z$ ) that are delivered to clients. Implicit in the delivered dataset are the assumed elements of the system geometry ( $D_y=0$ ,  $RX_r=0$ ,  $RX_p=0$ , and  $RX_y=0$ ). However the estimated primary field data are not delivered to clients.

Since the GA–LEI algorithm makes its own estimate of system geometry as part of the inversion procedure it works with total field data. The input data are the total (primary plus secondary) field X-component and Z-component data. Therefore the total field data are first reconstructed. This is a simple matter of recomputing the primary field from magnetic dipole formulae (Wait, 1982) using the delivered (measured, estimated and assumed) elements of the system geometry then adding them to the delivered secondary field data. Note that the height, pitch, roll and geometry corrected data that are usually delivered as part of TEMPEST datasets are not used because the GA–LEI algorithm makes its own estimate of system geometry as part of the inversion procedure.

The reconstructed X-component and Z-component total field data for the  $k^{th}$  window are  $X_k = X^P + X_k^S$  and  $Z_k = Z^P + Z_k^S$  respectively. Here the super scripts  $P$  and  $S$  represent primary and secondary field components. Since the TEMPEST™ system has  $N_w = 15$  windows, the observed data vector of length  $N_D = 2 \times N_w = 30$  used in the inversion is,

$$\mathbf{d}^{obs} = [X_1 \ X_2 \cdots X_{N_w} \ Z_1 \ Z_2 \cdots Z_{N_w}]^T \quad (1)$$

where  $T$  represents the matrix and vector transpose operator.

Errors on the data are calculated outside of the program and input along with the data. Errors are assumed to be uncorrelated and Gaussian distributed. They are estimated as standard deviations of the Gaussian error distribution for each window and receiver component. Typically errors are calculated from the parameters of an additive plus multiplicative noise model (Green and Lane, 2003). Parameters of the noise model are determined from analysis of high altitude and repeat line data. If  $X_k^{err}$  and  $Z_k^{err}$ , represent the estimated standard deviation of the error in the  $k^{th}$  window of the X- component and Z-component data respectively then the data error vector of length  $N_D=30$  is,

$$\mathbf{d}^{err} = [X_1^{err} \ X_2^{err} \cdots X_{N_w}^{err} \ Z_1^{err} \ Z_2^{err} \cdots Z_{N_w}^{err}]^T. \quad (2)$$

#### **10.2.2.5 Model parameterisation**

The unknown model parameter vector (**m**) to be solved for in the inversion comprises earth model parameters and system geometry model parameters.

For the inversion of the TEMPEST™ dataset described here we choose to use a multi-layer smooth-model formulation (Constable *et al.*, 1987) rather than a few-layer blocky-model formulation (Sattell, 1998). Therefore we solve for the  $N_L$  conductivities of the layers but not the thicknesses. The layer thicknesses are inputs into the algorithm and are kept fixed throughout. To maintain positivity of the layer conductivities we actually invert for the base ten logarithms of the conductivities of each layer.

We solve for  $N_G=3$  system geometry parameters: the transmitter to receiver horizontal in-line separation ( $D_x$ ), the transmitter to receiver vertical separation ( $D_z$ ), and the pitch of the receiver coil assembly ( $RX_p$ ).

The unknown model parameter vector of length  $N_P=N_G+N_L$  to be solved for is the concatenated vector of log base ten layer conductivities  $\mathbf{lc} = [\log c_1 \ \log c_2 \ \dots \ \log c_{N_L}]^T$  and the geometry parameters  $\mathbf{g} = [D_x \ D_z \ RX_p]^T$ , such that,

$$\mathbf{m} = [\mathbf{lc} \ | \ \mathbf{g}] = [\log c_1 \ \log c_2 \ \dots \ \log c_{N_L} \ D_x \ D_z \ RX_p]^T \quad (3)$$

#### **10.2.2.6 Forward model and derivatives**

The forward model is the non-linear multi-valued function,

$$\mathbf{f}(\mathbf{m}) = [f_1(\mathbf{m}, \mathbf{p}) \ f_2(\mathbf{m}, \mathbf{p}) \ \dots \ f_{ND}(\mathbf{m}, \mathbf{p})], \quad (4)$$

which for a given a set of model parameters (**m**) calculates the theoretical total field data equivalent to that which would be produced for an ideal system, after the measurement and transformation by the data processing steps (Lane *et al.*, 2000). Here each  $f_k(\mathbf{m}, \mathbf{p})$  is a function, not only of the layer conductivities and system geometry parameters in the inversion model vector **m**, but also of several other fixed parameters **p** (layer thicknesses; transmitter height, pitch and roll; receiver roll and yaw, transmitter to receiver horizontal transverse separation; system waveform and window positions etc.).

The implementation of (4) is based upon the formulation of Wait (1982) in which he develops the frequency-domain expressions for the magnetic fields due to vertical and horizontal magnetic dipole sources above a horizontally layered medium. The formulation does not account for the contribution due to displacement currents. We also assume that effects of dielectric permittivity and magnetic susceptibility are negligible compared to electrical conduction, and set each layer's dielectric permittivity and magnetic permeability to that of free space ( $\epsilon_k=\epsilon_0$ ;  $\mu_k=\mu_0$ ).

The full transient (0.04 s) equivalent square current waveform, to which TEMPEST™ data are processed, was linearly sampled at 75,000 Hz (3000 samples) and transformed to the frequency domain via fast Fourier transform (FFT). Using Wait's (1982) expressions the secondary B-field was calculated for ~20 discrete frequencies between 25 Hz and 37,500 Hz (6 logarithmically equi-spaced frequencies per decade). The inphase and quadrature parts of each component were then

individually splined to obtain linearly spaced values at the same frequencies as the nodes of the FFT transformed current waveform. Complex multiplication of splined B-field with the FFT transformed current waveform, followed by inverse FFT, yielded the B field transient response.

The transient was then windowed (boxcar) into the 15 windows by averaging those samples that fell within each window. The primary field, which is constant over all 15 windows, was then computed from Wait's expressions and added to yield the total field window response in the *x-axis* and *z-axis* directions. Finally these were rotated to be aligned with the X-component receiver coil's axis and Z-component receiver coil's axis according to the receiver pitch model parameter ( $RX_p$ ) to yield  $\mathbf{f}(\mathbf{m})$ .

The inversion also requires the partial derivatives of  $\mathbf{f}(\mathbf{m})$  with respect to the model parameters (see Equation 19). These were all calculated analytically. For computation of Wait's coefficient  $R_0$ , we took advantage of the propagation matrix method (Farquharson *et al.*, 2004) because it is efficient for computation of the partial derivatives with respect to the multiple layer conductivities.

#### **10.2.2.7 Reference model**

The algorithm uses the concept of a reference model (Farquharson and Oldenburg, 1993) to incorporate prior information from downhole conductivity logs or lithologic/stratigraphic logging in order to improve inversion stability and to reduce the trade-off between parameters that are not well resolved independently. Since prior information is not available everywhere within the survey area, and the inversions are carried out in independent sample by sample fashion, it is not plausible to place hard reference model constraints on the model parameters. Instead the reference model provides a soft or probabilistic constraint only. If, from prior information, it is concluded that the likely distribution of the model parameter  $m_k$  is a Gaussian distribution with mean  $m_k^{ref}$  and standard deviation  $m_k^{unc}$ , then we would define the reference model vector as,

$$\mathbf{m}^{ref} = [lc_1^{ref} \ lc_2^{ref} \cdots lc_{N_L}^{ref} \ D_x^{ref} \ D_z^{ref} \ RX_p^{ref}]^T \quad (5)$$

and the reference model uncertainty vector as,

$$\mathbf{m}^{unc} = [lc_1^{unc} \ lc_2^{unc} \cdots lc_{N_L}^{unc} \ D_x^{unc} \ D_z^{unc} \ RX_p^{unc}]^T \quad (6)$$

The reference model mean values and uncertainties are inputs to the inversion algorithm and they may be different from sample to sample. The uncertainty values assigned to the reference model control the amount of constraint that the reference model places on the inversion results. A large uncertainty value for a particular parameter implies that the assigned reference model mean value is not well known and thus is allowed to vary a long way from the mean. On the other hand a low uncertainty implies the parameter is well known.

#### 10.2.2.8 Objective function

The inversion scheme minimises a composite objective function of the form,

$$\Phi = \Phi_d + \lambda (\alpha_c \Phi_c + \alpha_g \Phi_g + \alpha_v \Phi_v) \quad (7)$$

where  $\Phi_d$  is a data misfit term,  $\Phi_c$  is a layer conductivity reference model misfit term,  $\Phi_g$  is a system geometry reference model misfit term, and  $\Phi_v$  is a vertical roughness of conductivity term. The relative weighting of the data misfit  $\Phi_d$  and the collective model regularisation term,

$$\Phi_m = \alpha_c \Phi_c + \alpha_g \Phi_g + \alpha_v \Phi_v \quad (8)$$

is controlled by the value of regularisation factor  $\lambda$ . The three model regularisation factors  $\alpha_c$ ,  $\alpha_g$  and  $\alpha_v$  control the relative weighting within the model regularisation term  $\Phi_m$ . The algorithm requires that the  $\alpha$  values be set by the user on an application-by-application basis and they remain fixed throughout the inversion. However the  $\lambda$  is automatically determined within the algorithm by the method described in Section A3.2.4.2.

#### 10.2.2.9 Data misfit

The data misfit  $\Phi_d$  is a measure of the misfit, between the data ( $\mathbf{d}^{obs}$ ) and the forward model of the model parameters ( $\mathbf{f}(\mathbf{m})$ ), normalised by the expected error and the number of data. It is defined as,

$$\begin{aligned} \Phi_d &= \frac{1}{N_D} \sum_{k=1}^{N_D} \left( \frac{d_k^{obs} - \mathbf{f}(\mathbf{m})}{d_k^{err}} \right)^2 \\ &= [\mathbf{d}^{obs} - \mathbf{f}(\mathbf{m})]^T \mathbf{W}_d [\mathbf{d}^{obs} - \mathbf{f}(\mathbf{m})] \end{aligned} \quad (9)$$

The diagonal  $N_D \times N_D$  matrix  $\mathbf{W}_d$  is,

$$\mathbf{W}_d = \frac{1}{N_D} \begin{bmatrix} \frac{1}{(d_1^{err})^2} & & & \\ & \frac{1}{(d_2^{err})^2} & & \\ & & \ddots & \\ & & & \frac{1}{(d_{N_D}^{err})^2} \end{bmatrix} \quad (10)$$

#### **10.2.2.10      Conductivity reference model misfit**

The conductivity reference model misfit term  $\Phi_c$  is a measure of the misfit, between the logarithmic conductivity model parameters ( $\mathbf{lc}$ ) and the corresponding layer reference model values ( $\mathbf{lc}^{ref}$ ) normalised by the layer thicknesses and reference model uncertainty. It is defined as,

$$\begin{aligned}\Phi_c &= \sum_{k=1}^{N_L} \frac{t_k}{T/N_L} \left( \frac{\mathbf{lc}_k^{ref} - \mathbf{lc}_k}{\mathbf{lc}_k^{unc}} \right)^2 \\ &= [\mathbf{m}^{ref} - \mathbf{m}]^T \mathbf{W}_c [\mathbf{m}^{ref} - \mathbf{m}]\end{aligned}\quad (11)$$

where  $T = \sum_{k=1}^{N_L} t_k$ , and the diagonal  $Np \times Np$  matrix  $\mathbf{W}_c$  is,

$$\mathbf{W}_c = \frac{N_L}{T} \begin{bmatrix} \frac{t_1}{(\mathbf{lc}_1^{unc})^2} & & & & \\ & \frac{t_2}{(\mathbf{lc}_2^{unc})^2} & & & \\ & & \ddots & & \\ & & & \frac{t_{N_L-1}}{(\mathbf{lc}_{N_L-1}^{unc})^2} & \\ & & & & \frac{t_{N_L}}{(\mathbf{lc}_{N_L}^{unc})^2} \\ & & & & 0 \\ & & & & 0 \\ & & & & 0 \end{bmatrix}. \quad (12)$$

Since the bottom layer is infinitely thick, for the purposes of this term we set  $t_{N_L} = [t_{N_L-1}]^2/t_{N_L-2}$ .

#### **10.2.2.11      System geometry reference model misfit**

The system geometry reference model misfit term  $\Phi_g$  is a measure of the misfit, between the system geometry model parameters ( $\mathbf{g}$ ) and the corresponding system geometry reference model values ( $\mathbf{g}^{ref}$ ) normalised by the number of unknown system geometry parameters ( $N_G=3$ ) and their uncertainty. It is defined as,

$$\begin{aligned}\Phi_g &= \frac{1}{N_G} \sum_{k=1}^{N_G} \left( \frac{g_k^{ref} - g_k^{unc}}{g_k^{unc}} \right)^2 \\ &= [\mathbf{m}^{ref} - \mathbf{m}]^T \mathbf{W}_g [\mathbf{m}^{ref} - \mathbf{m}]\end{aligned}\quad (13)$$

The diagonal  $N_p \times N_p$  matrix  $\mathbf{W}_g$  is,

$$\mathbf{W}_g = \frac{1}{N_G} \begin{bmatrix} 0 & & & & \\ & 0 & & & \\ & & \dots & & \\ & & & 0 & \\ & & & & \frac{1}{(D_x^{unc})^2} \\ & & & & \frac{1}{(D_y^{unc})^2} \\ & & & & \frac{1}{(RX_p^{unc})^2} \end{bmatrix}. \quad (14)$$

#### 10.2.2.12 Vertical roughness of conductivity

The vertical roughness of conductivity term  $\Phi_v$  is a measure of the roughness of the conductivity profile. It sums the squared second derivative of the logarithm of the vertical conductivity profile, approximated by finite difference over adjacent layer triplets, taking into account the distance between layer centres. The result is normalised by the number of triplets ( $N_L-2$ ) and is defined as,

$$\begin{aligned}\Phi_v &= \frac{1}{N_L-2} \sum_{k=2}^{N_L-1} \left( \frac{(lc_{k-1} - lc_k)}{1/2(t_{k-1} + t_k)} - \frac{(lc_k - lc_{k+1})}{1/2(t_k + t_{k+1})} \right)^2 \\ &= \mathbf{m}^T \mathbf{L}_v^T \mathbf{L}_v \mathbf{m}\end{aligned}\quad (15)$$

where the  $N_L-2 \times N_p$  matrix  $\mathbf{L}_v$  is,

$$\mathbf{L}_v = \frac{1}{N_L - 2} \begin{bmatrix} \frac{1}{(t_1 + t_2)} \left( \frac{-1}{(t_1 + t_2)} + \frac{-1}{(t_2 + t_3)} \right) & \frac{1}{(t_2 + t_3)} \\ \frac{1}{(t_2 + t_3)} & \left( \frac{-1}{(t_2 + t_3)} + \frac{-1}{(t_3 + t_4)} \right) & \frac{1}{(t_3 + t_4)} \\ & \dots & \dots & \dots \\ & & & 0 \\ & & & 0 \\ & & & 0 \end{bmatrix} \quad (16)$$

Again for the purposes of this term we set  $t_{N_L} = [t_{N_L-1}]^2/t_{N_L-2}$ .

#### Minimisation scheme

##### 10.2.2.13 Linearisation

To minimise the objective function  $\Phi$ , a linearised gradient based iterative minimisation scheme is used. Collection of the matrix notation misfit terms, Equations 9, 11, 13, and 15 that make up  $\Phi$ , allows us to write,

$$\begin{aligned} \Phi(\mathbf{m}) = & [\mathbf{d}^{obs} - \mathbf{f}(\mathbf{m})]^T \mathbf{W}_d [\mathbf{d}^{obs} - \mathbf{f}(\mathbf{m})] \\ & + \lambda \alpha_c [\mathbf{m}^{ref} - \mathbf{m}]^T \mathbf{W}_c [\mathbf{m}^{ref} - \mathbf{m}] \\ & + \lambda \alpha_g [\mathbf{m}^{ref} - \mathbf{m}]^T \mathbf{W}_g [\mathbf{m}^{ref} - \mathbf{m}] \\ & + \lambda \alpha_v \mathbf{m}^T \mathbf{L}_v^T \mathbf{L}_v \mathbf{m} \end{aligned} \quad (17)$$

The inversion begins by setting the initial estimate of the model parameters to the reference model ( $\mathbf{m}_0 = \mathbf{m}^{ref}$ ). During the  $n^{th}$  iteration the current estimate of the model parameters  $\mathbf{m}_n$  is perturbed by the parameter change vector,

$$\Delta \mathbf{m}_n = \mathbf{m}_{n+1} - \mathbf{m}_n. \quad (18)$$

The forward model at the new set of model parameters  $\mathbf{m}_{n+1}$  is approximated by a Taylor series expansion about  $\mathbf{m}_n$ , which, after excluding high order terms reduces to,

$$\mathbf{f}(\mathbf{m}_{n+1}) \approx \mathbf{f}(\mathbf{m}_n) + \mathbf{J}_n(\mathbf{m}_{n+1} - \mathbf{m}_n) \quad (19)$$

where  $\mathbf{J}_n = \partial\mathbf{f}(\mathbf{m})/\partial\mathbf{m}$  is the Jacobian matrix whose  $i^{\text{th}}, j^{\text{th}}$  element is the partial derivative of the  $i^{\text{th}}$  datum with respect to the  $j^{\text{th}}$  model parameter evaluated at  $\mathbf{m}_n$  in model space. Making use of Equation 19 and substituting  $\mathbf{m} = \mathbf{m}_{n+1}$ , allows Equation 17 to be rewritten as,

$$\begin{aligned} \Phi(\mathbf{m}_{n+1}) = & \left[ \mathbf{d}^{obs} - \mathbf{f}(\mathbf{m}_n) - \mathbf{J}_n(\mathbf{m}_{n+1} - \mathbf{m}_n) \right]^T \mathbf{W}_d \left[ \mathbf{d}^{obs} - \mathbf{f}(\mathbf{m}_n) - \mathbf{J}_n(\mathbf{m}_{n+1} - \mathbf{m}_n) \right] \\ & + \lambda \alpha_c \left[ \mathbf{m}^{ref} - \mathbf{m}_{n+1} \right]^T \mathbf{W}_c \left[ \mathbf{m}^{ref} - \mathbf{m}_{n+1} \right] \\ & + \lambda \alpha_g \left[ \mathbf{m}^{ref} - \mathbf{m}_{n+1} \right]^T \mathbf{W}_g \left[ \mathbf{m}^{ref} - \mathbf{m}_{n+1} \right] \\ & + \lambda \alpha_v \mathbf{m}_{n+1}^T \mathbf{L}_v^T \mathbf{L}_v \mathbf{m}_{n+1} \end{aligned} \quad (20)$$

Since the value of  $\Phi$  will be minimised when  $\partial\Phi/\partial\mathbf{m}_{n+1} = 0$ , we differentiate Equation 20 with respect to  $\mathbf{m}_{n+1}$  and set the result to zero and get,

$$\begin{aligned} 0 = & -2\mathbf{J}_n^T \mathbf{W}_d \left[ \mathbf{d}^{obs} - \mathbf{f}(\mathbf{m}_n) - \mathbf{J}_n(\mathbf{m}_{n+1} - \mathbf{m}_n) \right] \\ & + \lambda \left[ -2\alpha_c \mathbf{W}_c \left[ \mathbf{m}^{ref} - \mathbf{m}_{n+1} \right] - 2\alpha_g \mathbf{W}_g \left[ \mathbf{m}^{ref} - \mathbf{m}_{n+1} \right] + 2\alpha_v \mathbf{L}_v^T \mathbf{L}_v \mathbf{m}_{n+1} \right] \end{aligned} \quad (21)$$

Collecting terms in the unknown vector  $\mathbf{m}_{n+1}$  on the left hand side yields,

$$\begin{aligned} & \left[ \mathbf{J}_n^T \mathbf{W}_d \mathbf{J}_n + \lambda (\alpha_c \mathbf{W}_c + \alpha_g \mathbf{W}_g + \alpha_v \mathbf{L}_v^T \mathbf{L}_v) \right] \mathbf{m}_{n+1} = \dots \\ & \mathbf{J}_n^T \mathbf{W}_d \left[ \mathbf{d}^{obs} - \mathbf{f}(\mathbf{m}_n) + \mathbf{J}_n \mathbf{m}_n \right] + \lambda [\alpha_c \mathbf{W}_c + \alpha_g \mathbf{W}_g] \mathbf{m}^{ref} \end{aligned} \quad (22)$$

Since Equation 22 is in the familiar form of a system of linear equations ( $\mathbf{A} \mathbf{m}_{n+1} = \mathbf{b}$ ) we are able to solve for  $\mathbf{m}_{n+1}$  using a variety of linear algebra methods. We use Cholesky decomposition.

#### 10.2.2.14 Choice of the value of $\lambda$

An initial value of  $\lambda$  is chosen such that the data and model objective functions will have approximately equal weight. This is automatically realised by computing the ratio of the data and model objective functions, from the reference model perturbed by 1%, and computing the ratio of the data and model misfits,

$$\lambda_{start} = \frac{\Phi_d(\mathbf{f}(1.01 \times \mathbf{m}_0))}{\Phi_m(1.01 \times \mathbf{m}_0)} . \quad (23)$$

Then at each iteration the inversion employs a 1D line search where, in solving for  $\mathbf{m}_{n+1}$  in Equation 22 different values of  $\lambda$  are trialled, until a value of  $\lambda_n$  is found such that,

$$\Phi_d(\mathbf{f}(\mathbf{m}_{n+1})) \approx \Phi_d^{\text{target}} = 0.7 \times \Phi_d(\mathbf{f}(\mathbf{m}_n)), \quad (24)$$

thus reducing  $\Phi_d$  to 0.7 of its previous value.

#### **10.2.2.15 Convergence criterion**

The iterations continue until the inversion terminates when one of the following conditions is encountered:

- $\Phi_d$  reaches a user defined minimum value  $\Phi_d^{\min} = 1$ ;
- $\Phi_d$  has been reduced by less than 1% in two consecutive iterations;
- $\Phi_d$  can no longer be reduced; or
- The number of iterations reaches a maximum of 100 iterations.

### **10.3 REFERENCES**

- Constable, S., Parker, R., and Constable, C., 1987. Occam's inversion; a practical algorithm for generating smooth models from electromagnetic sounding data. *Geophysics*, **52**, 289–300.
- Farquharson, C.G., and Oldenburg, D.W., 1993. Inversion of time domain electromagnetic data for a horizontally layered earth. *Geophysical Journal International*, **114**, 433–442.
- Farquharson, C. G., D. W. Oldenburg, and P. S. Routh, 2004, Simultaneous 1D inversion of loop-loop electromagnetic data for magnetic susceptibility and electrical conductivity. *Geophysics*, **68**, 1857–1869.
- Lane, R., Green, A., Golding, C., Owers, M., Pik, P., Plunkett, C., Sattel, D. and Thorn, B., 2000. An example of 3D conductivity mapping using the TEMPEST airborne electromagnetic system. *Exploration Geophysics*, **31**: 162-172.
- Reid, J.E., and Vrbancich, J., 2004. A comparison of the inductive-limit footprints of airborne electromagnetic configurations. *Geophysics*, **69**, 1229–1239
- Sattel, D., 1998, Conductivity information in three dimensions. *Exploration Geophysics*, **29**, 157–162.
- Wait, J.R., 1982, Geo-electromagnetism. Academic Press Inc.

## 10.4 CLIMATIC DATA

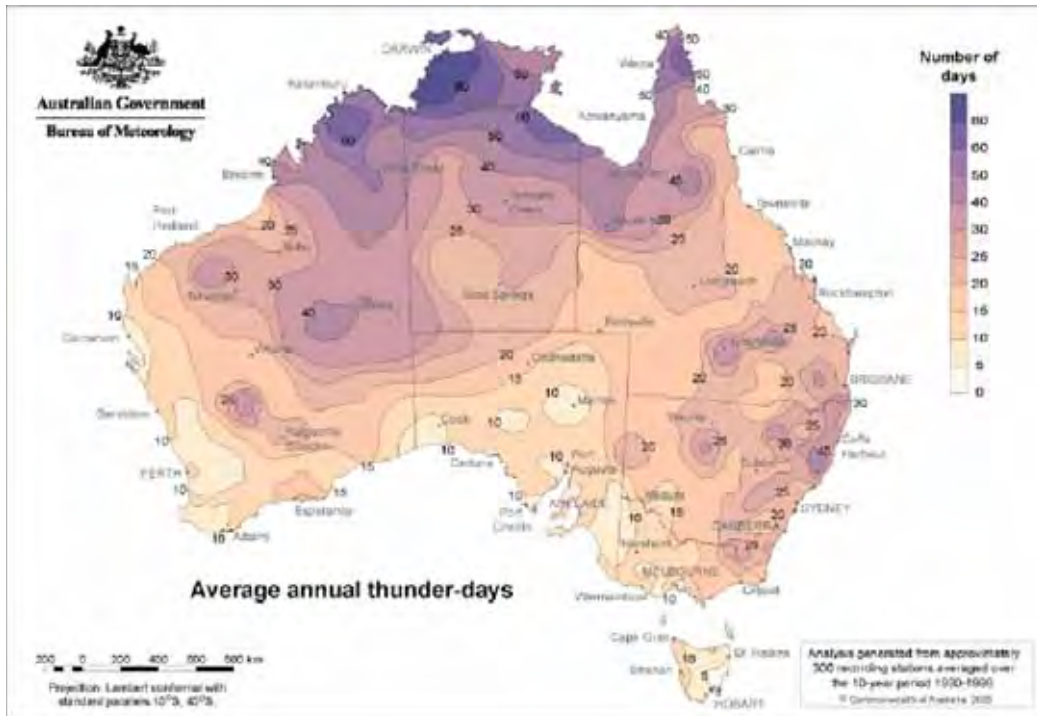


**Figure 10-2:** Average annual thunder days for Australia, From BOM (2009)

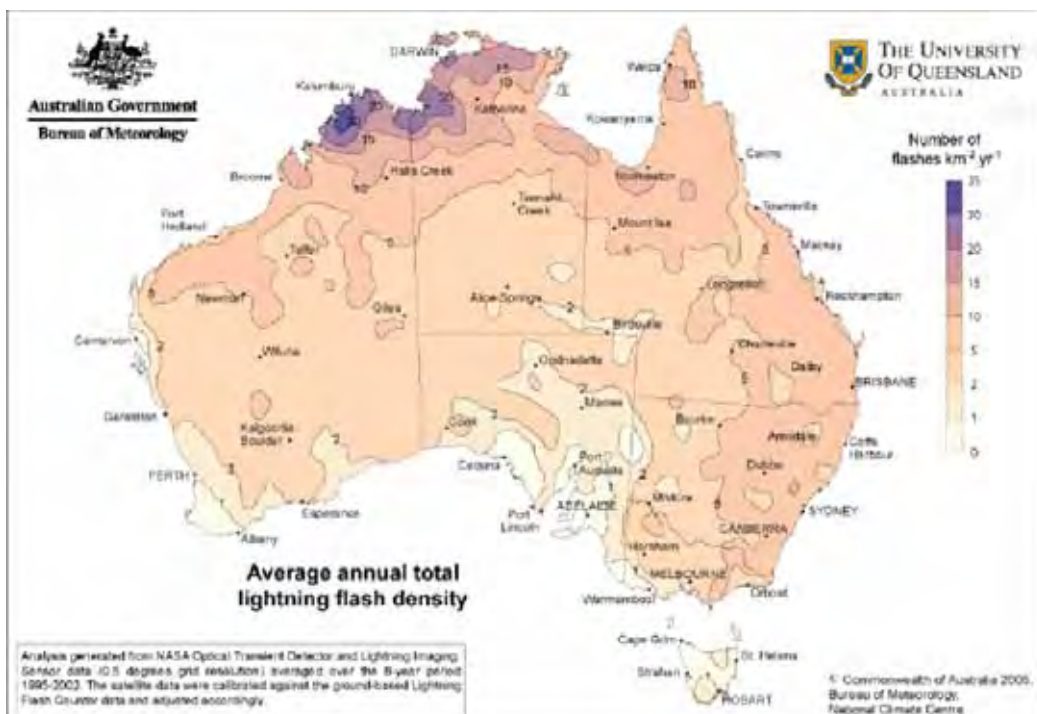


**Figure 10-3:** Average annual total lightning flash density for Australia. From BOM (2009)

## **10.5 GA-LEI INVERSION OUTPUT ASCII HEADER INFORMATION**

GA-LEI inversion output ASCII header information for Woolner Granite and Rum Jungle Survey areas

```
DEFN ST=RECD,RT=COMM;RT:A4;COMMENTS:A76
DEFN 1 ST=RECD,RT=;sequence:I7:NULL=99999
DEFN 2 ST=RECD,RT=;survey:I5:NULL=99999
DEFN 3 ST=RECD,RT=;date:I9:NULL=99999
DEFN 4 ST=RECD,RT=;flight:I3:NULL=99999,IntrepidFlightNumber
DEFN 5 ST=RECD,RT=;LINE:I8:NULL=99999,IntrepidLineNumber
DEFN 6 ST=RECD,RT=;FID:F9.2:NULL=99999,IntrepidFiducial
DEFN 7 ST=RECD,RT=;easting:F17.2:NULL=-99.000,IntrepidX
DEFN 8 ST=RECD,RT=;northing:F17.2:NULL=-99.000,IntrepidY
DEFN 9 ST=RECD,RT=;elevation:F17.2:NULL=-99.000
DEFN 10 ST=RECD,RT=;altimeter:F17.2:NULL=-99.000
DEFN 11 ST=RECD,RT=;tx_height:F17.2:NULL=-99.000
DEFN 12 ST=RECD,RT=;tx_roll:F17.2:NULL=-99.000
DEFN 13 ST=RECD,RT=;tx_pitch:F17.2:NULL=-99.000
DEFN 14 ST=RECD,RT=;tx_yaw:F17.2:NULL=-99.000
DEFN 15 ST=RECD,RT=;txrx_dx:F17.2:NULL=-99.000
DEFN 16 ST=RECD,RT=;txrx_dy:F17.2:NULL=-99.000
DEFN 17 ST=RECD,RT=;txrx_dz:F17.2:NULL=-99.000
DEFN 18 ST=RECD,RT=;rx_roll:F17.2:NULL=-99.000
DEFN 19 ST=RECD,RT=;rx_pitch:F17.2:NULL=-99.000
DEFN 20 ST=RECD,RT=;rx_yaw:F17.2:NULL=-99.000
DEFN 21 ST=RECD,RT=;nlayers:I17:NULL=-99.000
DEFN 22 ST=RECD,RT=;conductivity_01:F17.6:NULL=-99.000
DEFN 23 ST=RECD,RT=;conductivity_02:F17.6:NULL=-99.000
DEFN 24 ST=RECD,RT=;conductivity_03:F17.6:NULL=-99.000
DEFN 25 ST=RECD,RT=;conductivity_04:F17.6:NULL=-99.000
DEFN 26 ST=RECD,RT=;conductivity_05:F17.6:NULL=-99.000
DEFN 27 ST=RECD,RT=;conductivity_06:F17.6:NULL=-99.000
DEFN 28 ST=RECD,RT=;conductivity_07:F17.6:NULL=-99.000
DEFN 29 ST=RECD,RT=;conductivity_08:F17.6:NULL=-99.000
DEFN 30 ST=RECD,RT=;conductivity_09:F17.6:NULL=-99.000
DEFN 31 ST=RECD,RT=;conductivity_10:F17.9:NULL=-99.000
DEFN 32 ST=RECD,RT=;conductivity_11:F17.10:NULL=-99.000
DEFN 33 ST=RECD,RT=;conductivity_12:F17.10:NULL=-99.000
DEFN 34 ST=RECD,RT=;conductivity_13:F17.10:NULL=-99.000
DEFN 35 ST=RECD,RT=;conductivity_14:F17.10:NULL=-99.000
DEFN 36 ST=RECD,RT=;conductivity_15:F17.10:NULL=-99.000
DEFN 37 ST=RECD,RT=;conductivity_16:F17.10:NULL=-99.000
DEFN 38 ST=RECD,RT=;conductivity_17:F17.10:NULL=-99.000
DEFN 39 ST=RECD,RT=;conductivity_18:F17.10:NULL=-99.000
DEFN 40 ST=RECD,RT=;conductivity_19:F17.10:NULL=-99.000
DEFN 41 ST=RECD,RT=;conductivity_20:F17.10:NULL=-99.000
DEFN 42 ST=RECD,RT=;conductivity_21:F17.10:NULL=-99.000
DEFN 43 ST=RECD,RT=;conductivity_22:F17.10:NULL=-99.000
DEFN 44 ST=RECD,RT=;conductivity_23:F17.10:NULL=-99.000
DEFN 45 ST=RECD,RT=;conductivity_24:F17.10:NULL=-99.000
DEFN 46 ST=RECD,RT=;conductivity_25:F17.10:NULL=-99.000
DEFN 47 ST=RECD,RT=;conductivity_26:F17.10:NULL=-99.000
DEFN 48 ST=RECD,RT=;conductivity_27:F17.10:NULL=-99.000
DEFN 49 ST=RECD,RT=;conductivity_28:F17.10:NULL=-99.000
DEFN 50 ST=RECD,RT=;conductivity_29:F17.10:NULL=-99.000
DEFN 51 ST=RECD,RT=;conductivity_30:F17.10:NULL=-99.000
DEFN 52 ST=RECD,RT=;thickness_01:F17.2:NULL=-99.000
DEFN 53 ST=RECD,RT=;thickness_02:F17.1:NULL=-99.000
```

DEFN 54 ST=RECD,RT=;thickness\_03:F17.2:NULL=-99.000  
DEFN 55 ST=RECD,RT=;thickness\_04:F17.2:NULL=-99.000  
DEFN 56 ST=RECD,RT=;thickness\_05:F17.2:NULL=-99.000  
DEFN 57 ST=RECD,RT=;thickness\_06:F17.2:NULL=-99.000  
DEFN 58 ST=RECD,RT=;thickness\_07:F17.2:NULL=-99.000  
DEFN 59 ST=RECD,RT=;thickness\_08:F17.2:NULL=-99.000  
DEFN 60 ST=RECD,RT=;thickness\_09:F17.2:NULL=-99.000  
DEFN 61 ST=RECD,RT=;thickness\_10:F17.2:NULL=-99.000  
DEFN 62 ST=RECD,RT=;thickness\_11:F17.2:NULL=-99.000  
DEFN 63 ST=RECD,RT=;thickness\_12:F17.2:NULL=-99.000  
DEFN 64 ST=RECD,RT=;thickness\_13:F17.2:NULL=-99.000  
DEFN 65 ST=RECD,RT=;thickness\_14:F17.2:NULL=-99.000  
DEFN 66 ST=RECD,RT=;thickness\_15:F17.2:NULL=-99.000  
DEFN 67 ST=RECD,RT=;thickness\_16:F17.2:NULL=-99.000  
DEFN 68 ST=RECD,RT=;thickness\_17:F17.2:NULL=-99.000  
DEFN 69 ST=RECD,RT=;thickness\_18:F17.2:NULL=-99.000  
DEFN 70 ST=RECD,RT=;thickness\_19:F17.2:NULL=-99.000  
DEFN 71 ST=RECD,RT=;thickness\_20:F17.2:NULL=-99.000  
DEFN 72 ST=RECD,RT=;thickness\_21:F17.2:NULL=-99.000  
DEFN 73 ST=RECD,RT=;thickness\_22:F17.1:NULL=-99.000  
DEFN 74 ST=RECD,RT=;thickness\_23:F17.2:NULL=-99.000  
DEFN 75 ST=RECD,RT=;thickness\_24:F17.2:NULL=-99.000  
DEFN 76 ST=RECD,RT=;thickness\_25:F17.1:NULL=-99.000  
DEFN 77 ST=RECD,RT=;thickness\_26:F17.2:NULL=-99.000  
DEFN 78 ST=RECD,RT=;thickness\_27:F17.2:NULL=-99.000  
DEFN 79 ST=RECD,RT=;thickness\_28:F17.2:NULL=-99.000  
DEFN 80 ST=RECD,RT=;thickness\_29:F17.2:NULL=-99.000  
DEFN 81 ST=RECD,RT=;x\_pred\_primary:F17.6:NULL=-99.000  
DEFN 82 ST=RECD,RT=;x\_pred:15F17.6:NULL=-99.000  
DEFN 97 ST=RECD,RT=;z\_pred\_primary:F17.5:NULL=-99.000  
DEFN 98 ST=RECD,RT=;z\_pred:15F17.6:NULL=-99.000  
DEFN 113 ST=RECD,RT=;phid:F17.6:NULL=-99.000  
DEFN 114 ST=RECD,RT=;phim:F17.10:NULL=-99.000  
DEFN 115 ST=RECD,RT=;phic:F17.10:NULL=-99.000  
DEFN 116 ST=RECD,RT=;phit:F17.2:NULL=-99.000  
DEFN 117 ST=RECD,RT=;phig:F17.10:NULL=-99.000  
DEFN 118 ST=RECD,RT=;phis:F17.10:NULL=-99.000  
DEFN 119 ST=RECD,RT=;lambda:F17.10:NULL=-99.000  
DEFN 120 ST=RECD,RT=;alphac:F17.2:NULL=-99.000  
DEFN 121 ST=RECD,RT=;alphat:F17.2:NULL=-99.000  
DEFN 122 ST=RECD,RT=;alphag:F17.2:NULL=-99.000  
DEFN 123 ST=RECD,RT=;alphas:F17.2:NULL=-99.000  
DEFN 124 ST=RECD,RT=;iterations:I5:NULL=99999;END DEFN  
DEFN 1 ST=RECD,RT=PROJ; RT:A4  
DEFN 2 ST=RECD,RT=PROJ; PROJNAME:A30: COMMENT=GDA94 / MGA zone 52  
DEFN 3 ST=RECD,RT=PROJ; ELLPSNAM:A30: COMMENT=GRS 1980  
DEFN 4 ST=RECD,RT=PROJ; MAJ\_AXIS: D12.1: UNIT=m, COMMENT=6378137.000000  
DEFN 5 ST=RECD,RT=PROJ; ECCENT: D12.9: COMMENT=298.257222  
DEFN 6 ST=RECD,RT=PROJ; PRIMEMER: F10.1: UNIT=deg, COMMENT=0.000000  
DEFN 7 ST=RECD,RT=PROJ; PROJMETH: A30: COMMENT=Transverse Mercator  
DEFN 8 ST=RECD,RT=PROJ; PARAM1: D14.0: COMMENT= 0.000000  
DEFN 9 ST=RECD,RT=PROJ; PARAM2: D14.0: COMMENT= 129.000000  
DEFN 10 ST=RECD,RT=PROJ; PARAM3: D14.0: COMMENT= 0.999600  
DEFN 11 ST=RECD,RT=PROJ; PARAM4: D14.0: COMMENT= 500000.000000  
DEFN 12 ST=RECD,RT=PROJ; PARAM5: D14.0: COMMENT=10000000.000000  
DEFN 13 ST=RECD,RT=PROJ; PARAM6: D14.0:  
DEFN 14 ST=RECD,RT=PROJ; PARAM7: D14.0:  
DEFN 15 ST=RECD,RT=PROJ; END DEFN  
PROJGDA94 / MGA zone 52 GRS 1980 6378137.0000 298.257222 0.000000Transverse  
Mercator 0.000000 129.000000 0.999600 500000.00000010000000.000000  
COMMIntrepid ASEG-GDF2 Export

## **10.6 TECHNICAL SPECIFICATIONS OF MAP PROJECTIONS**

Projection Name: Map Grid of Australia, Zone 52

Units: Metres

Datum: Geocentric Datum of Australia 1994 (GDA94)

Epoch: 1994.0

Ellipsoid: GRS80

Semi-major axis (a): 6 378 137.0 metres

Inverse flattening (1/f): 298.257

Central meridian 129°00'00"

False Easting: 500 000 metres

False Northing: 10 000 000 metres

Projection Name: Map Grid of Australia, Zone 53

Units: Metres

Datum: Geocentric Datum of Australia 1994 (GDA94)

Epoch: 1994.0

Ellipsoid: GRS80

Semi-major axis (a): 6,378,137.0 metres

Inverse flattening (1/f): 298.257

Central meridian 135°00'00"

False Easting: 500 000 metres

False Northing: 10 000 000 metres

## 10.7 KOMBOLGIE EM FLOW™ SETTINGS

**Table 10–2** shows the important EM Flow™ settings that were used in the generation of the Phase 2 Kombolgie conductivity estimates. The EM Flow™ AEM system descriptor file used in the project is reproduced below in **Table 10–3**. Both the EM Flow™ parameter (.par) and descriptor file (.dsc) are available as part of the Phase 2 data release (see [Chapter 5, Section 5.4](#)).

**Table 10–2:** The EM FlowTM settings.

<b>TAU SELECTION:</b>	
No stripping	checked
Approximation type	exponential
Spurious taus	-2.50e+001
Tau selection	manual
Number of Taus	40
Early Tau	1.00e-002 ms
Late Tau	5.00e+000 ms
<b>DECONVOLUTION PARAMETERS:</b>	
Primary/Mu stripping	checked (0%)
Algorithm selection	PLS
Smoothing	0.4
Normalization condition	Tau
Error tolerance	1.0e-004
Error weighting	no weighting
<b>CDI PROCESSING PARAMETERS:</b>	
Maximum depth	2000 m
Depth resolution	10 m
Cut-off factor	1.0
Scale amplitudes to force conductor near surface	unchecked
Allow short Tau amplitude adjustment	predict checked
Conductors in air	force to surface
Use all Taus	checked from 1 to 40
Discrete conductivities	250 (0.01 to 1000 mS/m)

**Table 10-3:** The EM Flow™ descriptor file

=====

FILE FORMAT VERSION

9

SYSTEM NAME

VTEM Kombolgie Survey

VERSION

3.30

DEFINED BY

Ross Brodie and Jim Macnae

DATE DEFINED

25/11/2010

TIME SCALING

20 20 [mSec]

WAVEFORM TYPE

halfperiod

20 [mSec]

WAVEFORM NORMALIZED BY

total field

---

TxRx	TxRy	TxRz	TyRx	TyRy	TyRz	TzRx	TzRy	TzRz
0	0	0	0	0	0	0	0	30

---

++++++

+ TzRz +

++++++

---

TRANSMITTER CURRENT WAVEFORM

undefined

---

RECEIVER PRIMARY FIELD

nominal

AMPLITUDE SCALING

1 91520.20 [---]

**Geological and energy implications of the Pine Creek airborne electromagnetic (AEM) survey,  
Northern Territory, Australia**

734

TIME	CURRENT	ERROR [ ppm ]
0.0052083	-0.47057615	0
0.0156250	-0.23443657	0
0.0260417	-0.10080330	0
0.0364583	-0.04748999	0
0.0468750	-0.02851738	0
0.0572917	-0.01790537	0
0.0677083	-0.00968246	0
0.0781250	-0.00452288	0
0.0885417	-0.00215817	0
0.0989583	-0.00133725	0
0.1093750	-0.00095726	0
0.1197917	-0.00068536	0
0.1302083	-0.00046323	0
0.1406250	-0.00034269	0
0.1510417	-0.00027281	0
0.1614583	-0.00024309	0
0.1718750	-0.00020510	0
0.1822917	-0.00019131	0
0.1927083	-0.00016609	0
0.2031250	-0.00014665	0
0.2135417	-0.00013810	0
0.2239583	-0.00012789	0
0.2343750	-0.00012373	0
0.2447917	-0.00011281	0
0.2552083	-0.00010095	0
0.2656250	-0.00009918	0
0.2760417	-0.00009446	0
0.2864583	0.00000000	0
12.6510417	0.00000000	0
12.6614583	0.00015393	0
12.6718750	-0.01529238	0
12.6822917	-0.16399192	0

**Geological and energy implications of the Pine Creek airborne electromagnetic (AEM) survey,  
Northern Territory, Australia**

12.6927083	-0.51494864	0
12.7031250	-0.86330262	0
12.7135417	-1.01671477	0
12.7239583	-1.01737007	0
12.7343750	-0.98310924	0
12.7447917	-0.96917682	0
12.7552083	-0.97128189	0
12.7656250	-0.97445689	0
12.7760417	-0.97353245	0
12.7864583	-0.97061104	0
12.7968750	-0.96771548	0
12.8072917	-0.96533762	0
12.8177083	-0.96307132	0
12.8281250	-0.96076697	0
12.8385417	-0.95832785	0
12.8489583	-0.95576994	0
12.8593750	-0.95303557	0
12.8697917	-0.95023480	0
12.8802083	-0.94740386	0
12.8906250	-0.94455790	0
12.9010417	-0.94158344	0
12.9114583	-0.93846892	0
12.9218750	-0.93523391	0
12.9322917	-0.93196428	0
12.9427083	-0.92865293	0
12.9531250	-0.92524696	0
12.9635417	-0.92172376	0
12.9739583	-0.91805669	0
12.9843750	-0.91434602	0
12.9947917	-0.91057373	0
13.0052083	-0.90675322	0
13.0156250	-0.90277357	0
13.0260417	-0.89873984	0
13.0364583	-0.89454576	0

**Geological and energy implications of the Pine Creek airborne electromagnetic (AEM) survey,  
Northern Territory, Australia**

13.0468750	-0.89040727	0
13.0572917	-0.88608923	0
13.0677083	-0.88177617	0
13.0781250	-0.87721800	0
13.0885417	-0.87273224	0
13.0989583	-0.86800633	0
13.1093750	-0.86339247	0
13.1197917	-0.85873322	0
13.1302083	-0.83979988	0
13.1406250	-0.70035136	0
13.1510417	-0.37912553	0
13.1614583	-0.06243948	0
13.1718750	0.07667951	0
13.1822917	0.07792623	0
13.1927083	0.04821944	0
13.2031250	0.03721411	0
13.2135417	0.04082229	0
13.2239583	0.04533640	0
13.2343750	0.04611589	0
13.2447917	0.04512513	0
13.2552083	0.04434597	0
13.2656250	0.04418826	0
13.2760417	0.04421140	0
13.2864583	0.04418785	0
13.2968750	0.04407550	0
13.3072917	0.04397322	0
13.3177083	0.04387515	0
13.3281250	0.04380167	0
13.3385417	0.04374057	0
13.3489583	0.04366825	0
13.3593750	0.04361420	0
13.3697917	0.04353026	0
13.3802083	0.04349984	0
13.3906250	0.04342269	0

**Geological and energy implications of the Pine Creek airborne electromagnetic (AEM) survey,  
Northern Territory, Australia**

13.4010417	0.04339911	0
13.4114583	0.04331207	0
13.4218750	0.04330599	0
13.4322917	0.04320456	0
13.4427083	0.04321675	0
13.4531250	0.04309994	0
13.4635417	0.04314458	0
13.4739583	0.04299530	0
13.4843750	0.04304368	0
13.4947917	0.04311210	0
13.5052083	0.02990294	0
13.5156250	-0.10086633	0
13.5260417	-0.41318231	0
13.5364583	-0.72570750	0
13.5468750	-0.86464987	0
13.5572917	-0.86544840	0
13.5677083	-0.83186350	0
13.5781250	-0.81342018	0
13.5885417	-0.80901730	0
13.5989583	-0.80805939	0
13.6093750	-0.80565873	0
13.6197917	-0.80084742	0
13.6302083	-0.79358516	0
13.6406250	-0.78563208	0
13.6510417	-0.77920226	0
13.6614583	-0.77480040	0
13.6718750	-0.77038640	0
13.6822917	-0.76411668	0
13.6927083	-0.75639263	0
13.7031250	-0.74930380	0
13.7135417	-0.74385870	0
13.7239583	-0.73892304	0
13.7343750	-0.73276278	0
13.7447917	-0.72521901	0

**Geological and energy implications of the Pine Creek airborne electromagnetic (AEM) survey,  
Northern Territory, Australia**

13.7552083	-0.71776467	0
13.7656250	-0.71153784	0
13.7760417	-0.70599708	0
13.7864583	-0.69974206	0
13.7968750	-0.69230450	0
13.8072917	-0.68460982	0
13.8177083	-0.67776656	0
13.8281250	-0.67160491	0
13.8385417	-0.66515912	0
13.8489583	-0.65772433	0
13.8593750	-0.64990824	0
13.8697917	-0.64254104	0
13.8802083	-0.63588611	0
13.8906250	-0.62909746	0
13.9010417	-0.62167903	0
13.9114583	-0.61366364	0
13.9218750	-0.60601309	0
13.9322917	-0.59875948	0
13.9427083	-0.59171668	0
13.9531250	-0.58424352	0
13.9635417	-0.56610634	0
13.9739583	-0.46212896	0
13.9843750	-0.22995098	0
13.9947917	-0.00316802	0
14.0052083	0.09575951	0
14.0156250	0.09629064	0
14.0260417	0.07499877	0
14.0364583	0.06716492	0
14.0468750	0.06973292	0
14.0572917	0.07291385	0
14.0677083	0.07340317	0
14.0781250	0.07265738	0
14.0885417	0.07206504	0
14.0989583	0.07191280	0

**Geological and energy implications of the Pine Creek airborne electromagnetic (AEM) survey,  
Northern Territory, Australia**

14.1093750	0.07189759	0
14.1197917	0.07183135	0
14.1302083	0.07171827	0
14.1406250	0.07160208	0
14.1510417	0.07149093	0
14.1614583	0.07140823	0
14.1718750	0.07132204	0
14.1822917	0.07123033	0
14.1927083	0.07115585	0
14.2031250	0.07106335	0
14.2135417	0.07099357	0
14.2239583	0.07090838	0
14.2343750	0.07084881	0
14.2447917	0.07074866	0
14.2552083	0.07071166	0
14.2656250	0.07059901	0
14.2760417	0.07057839	0
14.2864583	0.07044881	0
14.2968750	0.07044829	0
14.3072917	0.07029857	0
14.3177083	0.07030133	0
14.3281250	0.07030669	0
14.3385417	0.06108394	0
14.3489583	-0.03071645	0
14.3593750	-0.25033555	0
14.3697917	-0.46989344	0
14.3802083	-0.56723480	0
14.3906250	-0.56694949	0
14.4010417	-0.54017066	0
14.4114583	-0.52115344	0
14.4218750	-0.51155552	0
14.4322917	-0.50682456	0
14.4427083	-0.50340123	0
14.4531250	-0.49766144	0

**Geological and energy implications of the Pine Creek airborne electromagnetic (AEM) survey,  
Northern Territory, Australia**

14.4635417	-0.48769283	0
14.4739583	-0.47603146	0
14.4843750	-0.46692338	0
14.4947917	-0.46134933	0
14.5052083	-0.45590229	0
14.5156250	-0.44735654	0
14.5260417	-0.43643614	0
14.5364583	-0.42668285	0
14.5468750	-0.41981257	0
14.5572917	-0.41385332	0
14.5677083	-0.40587756	0
14.5781250	-0.39563806	0
14.5885417	-0.38565840	0
14.5989583	-0.37783990	0
14.6093750	-0.37126396	0
14.6197917	-0.36351945	0
14.6302083	-0.35386029	0
14.6406250	-0.34387247	0
14.6510417	-0.33538747	0
14.6614583	-0.32817060	0
14.6718750	-0.32047289	0
14.6822917	-0.31123211	0
14.6927083	-0.30138002	0
14.7031250	-0.29243483	0
14.7135417	-0.28469408	0
14.7239583	-0.27687421	0
14.7343750	-0.26795912	0
14.7447917	-0.25825098	0
14.7552083	-0.24908293	0
14.7656250	-0.24084152	0
14.7760417	-0.23287717	0
14.7864583	-0.22416358	0
14.7968750	-0.21011519	0
14.8072917	-0.15786352	0

**Geological and energy implications of the Pine Creek airborne electromagnetic (AEM) survey,  
Northern Territory, Australia**

14.8177083	-0.05006782	0
14.8281250	0.05265913	0
14.8385417	0.09668059	0
14.8489583	0.09651528	0
14.8593750	0.08682616	0
14.8697917	0.08333165	0
14.8802083	0.08446722	0
14.8906250	0.08584309	0
14.9010417	0.08599596	0
14.9114583	0.08559535	0
14.9218750	0.08528046	0
14.9322917	0.08515231	0
14.9427083	0.08510756	0
14.9531250	0.08501409	0
14.9635417	0.08491643	0
14.9739583	0.08480863	0
14.9843750	0.08471405	0
14.9947917	0.08462188	0
15.0052083	0.08453674	0
15.0156250	0.08444647	0
15.0260417	0.08435974	0
15.0364583	0.08426901	0
15.0468750	0.08418878	0
15.0572917	0.08410128	0
15.0677083	0.08402409	0
15.0781250	0.08392882	0
15.0885417	0.08386549	0
15.0989583	0.08376383	0
15.1093750	0.08371098	0
15.1197917	0.08359606	0
15.1302083	0.08355006	0
15.1406250	0.08344022	0
15.1510417	0.08338507	0
15.1614583	0.08334531	0

**Geological and energy implications of the Pine Creek airborne electromagnetic (AEM) survey,  
Northern Territory, Australia**

15.1718750	0.07919121	0
15.1822917	0.03892232	0
15.1927083	-0.05613586	0
15.2031250	-0.14998484	0
15.2135417	-0.19214949	0
15.2239583	-0.19468626	0
15.2343750	-0.18611702	0
15.2447917	-0.17987760	0
15.2552083	-0.17918967	0
15.2656250	-0.18476112	0
15.2760417	-0.19305947	0
15.2864583	-0.19725359	0
15.2968750	-0.19394491	0
15.3072917	-0.18704639	0
15.3177083	-0.18298150	0
15.3281250	-0.18344417	0
15.3385417	-0.18480909	0
15.3489583	-0.18385851	0
15.3593750	-0.18200017	0
15.3697917	-0.18270275	0
15.3802083	-0.18634574	0
15.3906250	-0.18940632	0
15.4010417	-0.18870167	0
15.4114583	-0.18517423	0
15.4218750	-0.18237621	0
15.4322917	-0.18218122	0
15.4427083	-0.18313243	0
15.4531250	-0.18294904	0
15.4635417	-0.18170099	0
15.4739583	-0.18127435	0
15.4843750	-0.18267256	0
15.4947917	-0.18443691	0
15.5052083	-0.18456800	0
15.5156250	-0.18283917	0

**Geological and energy implications of the Pine Creek airborne electromagnetic (AEM) survey,  
Northern Territory, Australia**

15.5260417	-0.18103278	0
15.5364583	-0.18053141	0
15.5468750	-0.18102626	0
15.5572917	-0.18109113	0
15.5677083	-0.18037389	0
15.5781250	-0.17971065	0
15.5885417	-0.18005294	0
15.5989583	-0.18089471	0
15.6093750	-0.18118540	0
15.6197917	-0.18040971	0
15.6302083	-0.17488725	0
15.6406250	-0.13296274	0
15.6510417	-0.03631829	0
15.6614583	0.05873008	0
15.6718750	0.10029258	0
15.6822917	0.10049922	0
15.6927083	0.09148146	0
15.7031250	0.08811325	0
15.7135417	0.08913581	0
15.7239583	0.09041716	0
15.7343750	0.09058200	0
15.7447917	0.09020308	0
15.7552083	0.08990009	0
15.7656250	0.08978350	0
15.7760417	0.08971871	0
15.7864583	0.08963812	0
15.7968750	0.08953198	0
15.8072917	0.08943223	0
15.8177083	0.08933260	0
15.8281250	0.08923700	0
15.8385417	0.08914404	0
15.8489583	0.08905047	0
15.8593750	0.08896868	0
15.8697917	0.08886927	0

**Geological and energy implications of the Pine Creek airborne electromagnetic (AEM) survey,  
Northern Territory, Australia**

15.8802083	0.08879112	0
15.8906250	0.08869657	0
15.9010417	0.08861242	0
15.9114583	0.08852219	0
15.9218750	0.08844882	0
15.9322917	0.08834973	0
15.9427083	0.08828105	0
15.9531250	0.08816733	0
15.9635417	0.08811995	0
15.9739583	0.08800471	0
15.9843750	0.08794407	0
15.9947917	0.08790420	0
16.0052083	0.08378993	0
16.0156250	0.04397098	0
16.0260417	-0.04994548	0
16.0364583	-0.14251439	0
16.0468750	-0.18408168	0
16.0572917	-0.18684739	0
16.0677083	-0.17885088	0
16.0781250	-0.17298876	0
16.0885417	-0.17241242	0
16.0989583	-0.17802934	0
16.1093750	-0.18645036	0
16.1197917	-0.19072084	0
16.1302083	-0.18722683	0
16.1406250	-0.17994777	0
16.1510417	-0.17556398	0
16.1614583	-0.17604999	0
16.1718750	-0.17764867	0
16.1822917	-0.17693822	0
16.1927083	-0.17514549	0
16.2031250	-0.17587166	0
16.2135417	-0.17957693	0
16.2239583	-0.18270690	0

**Geological and energy implications of the Pine Creek airborne electromagnetic (AEM) survey,  
Northern Territory, Australia**

16.2343750	-0.18194986	0
16.2447917	-0.17822138	0
16.2552083	-0.17523220	0
16.2656250	-0.17500969	0
16.2760417	-0.17607169	0
16.2864583	-0.17604476	0
16.2968750	-0.17485371	0
16.3072917	-0.17443364	0
16.3177083	-0.17585989	0
16.3281250	-0.17768568	0
16.3385417	-0.17780762	0
16.3489583	-0.17597899	0
16.3593750	-0.17404690	0
16.3697917	-0.17351908	0
16.3802083	-0.17406555	0
16.3906250	-0.17422678	0
16.4010417	-0.17355382	0
16.4114583	-0.17289729	0
16.4218750	-0.17325975	0
16.4322917	-0.17412997	0
16.4427083	-0.17444000	0
16.4531250	-0.17362343	0
16.4635417	-0.16806485	0
16.4739583	-0.12649784	0
16.4843750	-0.03078756	0
16.4947917	0.06330553	0
16.5052083	0.10444699	0
16.5156250	0.10464223	0
16.5260417	0.09570710	0
16.5364583	0.09237128	0
16.5468750	0.09337980	0
16.5572917	0.09463942	0
16.5677083	0.09480278	0
16.5781250	0.09441561	0

**Geological and energy implications of the Pine Creek airborne electromagnetic (AEM) survey,  
Northern Territory, Australia**

16.5885417	0.09412407	0
16.5989583	0.09398841	0
16.6093750	0.09393271	0
16.6197917	0.09384096	0
16.6302083	0.09373742	0
16.6406250	0.09362749	0
16.6510417	0.09351844	0
16.6614583	0.09343221	0
16.6718750	0.09332595	0
16.6822917	0.09323830	0
16.6927083	0.09313905	0
16.7031250	0.09304943	0
16.7135417	0.09295870	0
16.7239583	0.09286370	0
16.7343750	0.09278465	0
16.7447917	0.09267187	0
16.7552083	0.09260627	0
16.7656250	0.09248858	0
16.7760417	0.09243552	0
16.7864583	0.09231683	0
16.7968750	0.09226278	0
16.8072917	0.09213516	0
16.8177083	0.09207633	0
16.8281250	0.09202562	0
16.8385417	0.08796645	0
16.8489583	0.04859210	0
16.8593750	-0.04430005	0
16.8697917	-0.13584874	0
16.8802083	-0.17706507	0
16.8906250	-0.17998704	0
16.9010417	-0.17212199	0
16.9114583	-0.16613069	0
16.9218750	-0.16543177	0
16.9322917	-0.17125801	0

**Geological and energy implications of the Pine Creek airborne electromagnetic (AEM) survey,  
Northern Territory, Australia**

16.9427083	-0.18005984	0
16.9531250	-0.18450220	0
16.9635417	-0.18078544	0
16.9739583	-0.17315148	0
16.9843750	-0.16864481	0
16.9947917	-0.16925507	0
17.0052083	-0.17100987	0
17.0156250	-0.17026975	0
17.0260417	-0.16840167	0
17.0364583	-0.16918103	0
17.0468750	-0.17309833	0
17.0572917	-0.17636922	0
17.0677083	-0.17554722	0
17.0781250	-0.17163417	0
17.0885417	-0.16853364	0
17.0989583	-0.16835903	0
17.1093750	-0.16952412	0
17.1197917	-0.16950443	0
17.1302083	-0.16826288	0
17.1406250	-0.16784768	0
17.1510417	-0.16937662	0
17.1614583	-0.17129606	0
17.1718750	-0.17141946	0
17.1822917	-0.16950213	0
17.1927083	-0.16748830	0
17.2031250	-0.16697822	0
17.2135417	-0.16757651	0
17.2239583	-0.16775701	0
17.2343750	-0.16706191	0
17.2447917	-0.16640041	0
17.2552083	-0.16679422	0
17.2656250	-0.16773070	0
17.2760417	-0.16805046	0
17.2864583	-0.16719752	0

**Geological and energy implications of the Pine Creek airborne electromagnetic (AEM) survey,  
Northern Territory, Australia**

17.2968750	-0.16162355	0
17.3072917	-0.12040367	0
17.3177083	-0.02562435	0
17.3281250	0.06750203	0
17.3385417	0.10819941	0
17.3489583	0.10837351	0
17.3593750	0.09952039	0
17.3697917	0.09622126	0
17.3802083	0.09720938	0
17.3906250	0.09845987	0
17.4010417	0.09859989	0
17.4114583	0.09823052	0
17.4218750	0.09792871	0
17.4322917	0.09779879	0
17.4427083	0.09772861	0
17.4531250	0.09763833	0
17.4635417	0.09752955	0
17.4739583	0.09741696	0
17.4843750	0.09730536	0
17.4947917	0.09721556	0
17.5052083	0.09710920	0
17.5156250	0.09700790	0
17.5260417	0.09692016	0
17.5364583	0.09682075	0
17.5468750	0.09672558	0
17.5572917	0.09662819	0
17.5677083	0.09653914	0
17.5781250	0.09643372	0
17.5885417	0.09635708	0
17.5989583	0.09624162	0
17.6093750	0.09617791	0
17.6197917	0.09605888	0
17.6302083	0.09598859	0
17.6406250	0.09587524	0

**Geological and energy implications of the Pine Creek airborne electromagnetic (AEM) survey,  
Northern Territory, Australia**

17.6510417	0.09581155	0
17.6614583	0.09575010	0
17.6718750	0.09172982	0
17.6822917	0.05274425	0
17.6927083	-0.03913533	0
17.7031250	-0.12961609	0
17.7135417	-0.17036374	0
17.7239583	-0.17338255	0
17.7343750	-0.16567400	0
17.7447917	-0.15964165	0
17.7552083	-0.15890952	0
17.7656250	-0.16493188	0
17.7760417	-0.17412446	0
17.7864583	-0.17874775	0
17.7968750	-0.17487759	0
17.8072917	-0.16689936	0
17.8177083	-0.16222098	0
17.8281250	-0.16288556	0
17.8385417	-0.16474124	0
17.8489583	-0.16400738	0
17.8593750	-0.16210313	0
17.8697917	-0.16295644	0
17.8802083	-0.16707274	0
17.8906250	-0.17048843	0
17.9010417	-0.16961572	0
17.9114583	-0.16550798	0
17.9218750	-0.16227419	0
17.9322917	-0.16212183	0
17.9427083	-0.16337226	0
17.9531250	-0.16339440	0
17.9635417	-0.16212550	0
17.9739583	-0.16173550	0
17.9843750	-0.16336480	0
17.9947917	-0.16538979	0

**Geological and energy implications of the Pine Creek airborne electromagnetic (AEM) survey,  
Northern Territory, Australia**

18.0052083	-0.16550145	0
18.0156250	-0.16347966	0
18.0260417	-0.16137202	0
18.0364583	-0.16085320	0
18.0468750	-0.16152767	0
18.0572917	-0.16175023	0
18.0677083	-0.16105506	0
18.0781250	-0.16038519	0
18.0885417	-0.16083228	0
18.0989583	-0.16184259	0
18.1093750	-0.16217253	0
18.1197917	-0.16126857	0
18.1302083	-0.15566477	0
18.1406250	-0.11479222	0
18.1510417	-0.02092244	0
18.1614583	0.07128434	0
18.1718750	0.11155969	0
18.1822917	0.11172983	0
18.1927083	0.10296040	0
18.2031250	0.09968878	0
18.2135417	0.10066732	0
18.2239583	0.10189645	0
18.2343750	0.10203611	0
18.2447917	0.10166759	0
18.2552083	0.10135328	0
18.2656250	0.10123020	0
18.2760417	0.10114637	0
18.2864583	0.10106624	0
18.2968750	0.10093938	0
18.3072917	0.10083681	0
18.3177083	0.10071237	0
18.3281250	0.10062651	0
18.3385417	0.10051957	0
18.3489583	0.10043207	0

**Geological and energy implications of the Pine Creek airborne electromagnetic (AEM) survey,  
Northern Territory, Australia**

18.3593750	0.10032912	0
18.3697917	0.10023412	0
18.3802083	0.10012993	0
18.3906250	0.10003202	0
18.4010417	0.09993949	0
18.4114583	0.09983617	0
18.4218750	0.09975437	0
18.4322917	0.09964483	0
18.4427083	0.09956162	0
18.4531250	0.09944816	0
18.4635417	0.09938002	0
18.4739583	0.09926100	0
18.4843750	0.09918522	0
18.4947917	0.09913627	0
18.5052083	0.09514849	0
18.5156250	0.05658101	0
18.5260417	-0.03433851	0
18.5364583	-0.12386535	0
18.5468750	-0.16428176	0
18.5572917	-0.16746114	0
18.5677083	-0.15997880	0
18.5781250	-0.15394270	0
18.5885417	-0.15323157	0
18.5989583	-0.15941561	0
18.6093750	-0.16891853	0
18.6197917	-0.17358478	0
18.6302083	-0.16954384	0
18.6406250	-0.16120377	0
18.6510417	-0.15643806	0
18.6614583	-0.15728658	0
18.6718750	-0.15056887	0
18.6822917	-0.06672071	0
18.6927083	0.13364120	0
18.7031250	0.33467166	0

**Geological and energy implications of the Pine Creek airborne electromagnetic (AEM) survey,  
Northern Territory, Australia**

18.7135417	0.42281627	0
18.7239583	0.42090711	0
18.7343750	0.40606389	0
18.7447917	0.41625754	0
18.7552083	0.43991800	0
18.7656250	0.45406377	0
18.7760417	0.45435864	0
18.7864583	0.45471814	0
18.7968750	0.46650845	0
18.8072917	0.48541741	0
18.8177083	0.49872040	0
18.8281250	0.50189292	0
18.8385417	0.50315067	0
18.8489583	0.51223406	0
18.8593750	0.52828333	0
18.8697917	0.54198421	0
18.8802083	0.54766200	0
18.8906250	0.54991531	0
18.9010417	0.55698841	0
18.9114583	0.57039885	0
18.9218750	0.58371872	0
18.9322917	0.59115902	0
18.9427083	0.59455226	0
18.9531250	0.60043472	0
18.9635417	0.61156889	0
18.9739583	0.62401405	0
18.9843750	0.63247578	0
18.9947917	0.63695807	0
19.0052083	0.64220829	0
19.0156250	0.65151654	0
19.0260417	0.66281353	0
19.0364583	0.67171719	0
19.0468750	0.67708707	0
19.0572917	0.68210827	0

**Geological and energy implications of the Pine Creek airborne electromagnetic (AEM) survey,  
Northern Territory, Australia**

19.0677083	0.68997510	0
19.0781250	0.70006636	0
19.0885417	0.70893480	0
19.0989583	0.71493601	0
19.1093750	0.71990010	0
19.1197917	0.72671663	0
19.1302083	0.73559931	0
19.1406250	0.74415305	0
19.1510417	0.75049462	0
19.1614583	0.75551054	0
19.1718750	0.76153820	0
19.1822917	0.76933217	0
19.1927083	0.77733651	0
19.2031250	0.78377403	0
19.2135417	0.78884517	0
19.2239583	0.79428892	0
19.2343750	0.80111995	0
19.2447917	0.80846433	0
19.2552083	0.81478597	0
19.2656250	0.81984838	0
19.2760417	0.82484328	0
19.2864583	0.83084844	0
19.2968750	0.83747269	0
19.3072917	0.84351287	0
19.3177083	0.84847676	0
19.3281250	0.85310969	0
19.3385417	0.85839593	0
19.3489583	0.86429902	0
19.3593750	0.86993101	0
19.3697917	0.87470211	0
19.3802083	0.87901065	0
19.3906250	0.88367217	0
19.4010417	0.88887698	0
19.4114583	0.89401161	0

**Geological and energy implications of the Pine Creek airborne electromagnetic (AEM) survey,  
Northern Territory, Australia**

19.4218750	0.89850782	0
19.4322917	0.90248276	0
19.4427083	0.90659982	0
19.4531250	0.91112901	0
19.4635417	0.91572370	0
19.4739583	0.91985900	0
19.4843750	0.92349821	0
19.4947917	0.92710554	0
19.5052083	0.93100321	0
19.5156250	0.93502456	0
19.5260417	0.93874027	0
19.5364583	0.94200794	0
19.5468750	0.94513876	0
19.5572917	0.94843855	0
19.5677083	0.95187982	0
19.5781250	0.95513327	0
19.5885417	0.95798914	0
19.5989583	0.96066795	0
19.6093750	0.96340364	0
19.6197917	0.96625882	0
19.6302083	0.96899912	0
19.6406250	0.97143609	0
19.6510417	0.97363122	0
19.6614583	0.97583256	0
19.6718750	0.97810510	0
19.6822917	0.98031499	0
19.6927083	0.98229216	0
19.7031250	0.98403126	0
19.7135417	0.98571110	0
19.7239583	0.98742858	0
19.7343750	0.98911458	0
19.7447917	0.99059722	0
19.7552083	0.99187493	0
19.7656250	0.99303676	0

**Geological and energy implications of the Pine Creek airborne electromagnetic (AEM) survey,  
Northern Territory, Australia**

19.7760417	0.99420006	0
19.7864583	0.99533771	0
19.7968750	0.99632618	0
19.8072917	0.99711357	0
19.8177083	0.99777258	0
19.8281250	0.99838778	0
19.8385417	0.99898345	0
19.8489583	0.99944933	0
19.8593750	0.99973982	0
19.8697917	0.99989024	0
19.8802083	0.99996026	0
19.8906250	1.00001428	0
19.9010417	0.99992728	0
19.9114583	0.99972269	0
19.9218750	0.99931818	0
19.9322917	0.99886596	0
19.9427083	0.99828944	0
19.9531250	0.99766489	0
19.9635417	0.99681559	0
19.9739583	0.99048737	0
19.9843750	0.92974555	0
19.9947917	0.74388108	0

---

RECEIVER SAMPLING

30

START	END	WEIGHT
0.05729	0.06771	1
0.06769	0.07811	1
0.07809	0.08851	1
0.08859	0.10941	1
0.10939	0.13021	1
0.13019	0.15101	1
0.15109	0.18231	1
0.18229	0.21351	1

**Geological and energy implications of the Pine Creek airborne electromagnetic (AEM) survey,  
Northern Territory, Australia**

0.21359	0.25521	1
0.25519	0.30731	1
0.30729	0.36981	1
0.36979	0.44271	1
0.44269	0.52601	1
0.52609	0.61981	1
0.61979	0.74481	1
0.74479	0.89061	1
0.89059	1.05731	1
1.05729	1.24481	1
1.24479	1.49481	1
1.49479	1.78651	1
1.78649	2.11981	1
2.11979	2.49481	1
2.49479	2.99481	1
2.99479	3.57811	1
3.57809	4.24481	1
4.24479	4.99481	1
4.99479	5.99481	1
5.99479	7.16151	1
7.16149	8.49481	1
8.49479	9.99481	1

---

TRANSMITTER GEOMETRY

moving large loop

z

12

13	0	0
11.25	6.5	0
6.5	11.25	0
0	13	0
-6.5	11.25	0
-11.25	6.5	0
-13	0	0

**Geological and energy implications of the Pine Creek airborne electromagnetic (AEM) survey,  
Northern Territory, Australia**

-11.25 -6.5 0  
-6.5 -11.25 0  
0 -13 0  
6.5 -11.25 0  
11.25 -6.5 0

XYZ POSITION:

0 0 0

---

RECEIVER GEOMETRY

moving dipole

z

0 0 1

XYZ POSITION:

0 0 0

---

DATA FORMAT

Geosoft format (1 yes, 0 no)

0

Sample file name (if available)

\nas\oemd\ae\ae\Pineck\ae\final\linedata\lines\_sample\_em\_sub5\12100.asc

Number of comment lines at the beginning of each data file

0

Number of items in each data record

268

POSITION (INDEX) OF CHANNELS IN EACH DATA RECORD

channel	????	TxRx	TxRy	TxRz	TyRx	TyRy	TyRz	TzRx	TzRy	TzRz
1	0	0	0	0	0	0	0	0	0	209
2	0	0	0	0	0	0	0	0	0	210
3	0	0	0	0	0	0	0	0	0	211
4	0	0	0	0	0	0	0	0	0	212
5	0	0	0	0	0	0	0	0	0	213
6	0	0	0	0	0	0	0	0	0	214
7	0	0	0	0	0	0	0	0	0	215
8	0	0	0	0	0	0	0	0	0	216

**Geological and energy implications of the Pine Creek airborne electromagnetic (AEM) survey,  
Northern Territory, Australia**

9	0	0	0	0	0	0	0	0	0	217
10	0	0	0	0	0	0	0	0	0	218
11	0	0	0	0	0	0	0	0	0	219
12	0	0	0	0	0	0	0	0	0	220
13	0	0	0	0	0	0	0	0	0	221
14	0	0	0	0	0	0	0	0	0	222
15	0	0	0	0	0	0	0	0	0	223
16	0	0	0	0	0	0	0	0	0	224
17	0	0	0	0	0	0	0	0	0	225
18	0	0	0	0	0	0	0	0	0	226
19	0	0	0	0	0	0	0	0	0	227
20	0	0	0	0	0	0	0	0	0	228
21	0	0	0	0	0	0	0	0	0	229
22	0	0	0	0	0	0	0	0	0	230
23	0	0	0	0	0	0	0	0	0	231
24	0	0	0	0	0	0	0	0	0	232
25	0	0	0	0	0	0	0	0	0	233
26	0	0	0	0	0	0	0	0	0	234
27	0	0	0	0	0	0	0	0	0	235
28	0	0	0	0	0	0	0	0	0	236
29	0	0	0	0	0	0	0	0	0	237
30	0	0	0	0	0	0	0	0	0	238

-----

line	4	1
FID	5	1
east	11	1
north	12	1
z_topo	19	1
altitude	26	1
Rx_pitch	0	0
Rx_roll	0	0
Rx_yaw	0	0
Tx_pitch	0	0
Tx_roll	0	0

**Geological and energy implications of the Pine Creek airborne electromagnetic (AEM) survey,  
Northern Territory, Australia**

Tx_yaw	0	0
zASL	0	2
mag	0	2
plinef	0	2

-----

## 10.8 QUALIFYING REMARKS ON KOMBOLGIE CONDUCTIVITY ESTIMATES

The purpose of this appendix is to make interpreters aware of the capabilities and uncertainties to be taken into account when interpreting the conductivity estimates generated from the Kombolgie Airborne Electromagnetic (AEM) dataset. All conductivity estimates from AEM surveys are uncertain and should be interpreted with this in mind. The uncertainty stems from the level of noise in the dataset as well as the non-uniqueness of conductivity transformations and AEM inversions.

### 10.8.1 Conductive Areas of the Kombolgie Dataset

In conductive areas of the Kombolgie dataset the AEM response (signal) is large and thus there is a high signal-to-noise ratio. In these areas the uncertainty stems mainly from the non-uniqueness, which is most pronounced below the depth of investigation.

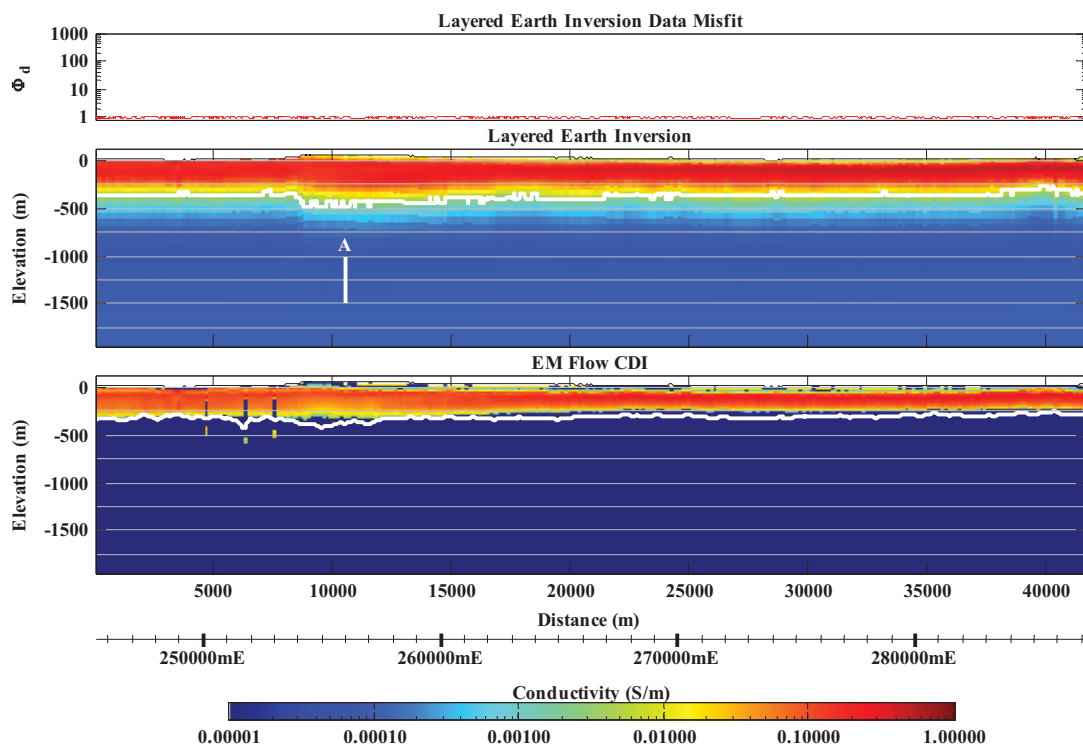


**Figure 10-4:** GA-LEI and EM Flow™ conductivity sections from a conductive part (Line 10010) of the Kombolgie survey area.

In the conductive areas the AEM data have been able to be successfully fitted, to within the ascribed noise levels, using Geoscience Australia's layered earth inversion algorithm (GA-LEI). Figure 10-4 shows an example GA-LEI and the corresponding EM Flow™ CDI conductivity section for a conductive portion (Line 10010) of the survey area. The white lines on each section are the estimated depths of investigation. Note from the top panel that the GA-LEI data misfit ( $\Phi_d$ ) is at the value of 1.0 for the entire line indicating a good data fit. In this case the GA-LEI and CDI show qualitatively similar results.

Figure 10-5 shows the details of the data and fitted model at the position 'A' marked on the conductivity sections in Figure 10-4. The left hand panel shows, in order of VTEM™ data processing steps, the filtered (blue), filtered and drift corrected (green) and final levelled (black) data transients. The forward models of the GA-LEI (magenta) and EM Flow™ CDI (red) conductivity

models are shown in the same colours on the right hand panel. Although difficult to see in this particular case, because they are small, the estimated data error ( $\pm 1$  standard deviation) bars are also shown on the final levelled data (black). The GA–LEI and EM Flow<sup>TM</sup> CDI were both generated using the final levelled data as input. The first four windows (i.e., left of the vertical black line on the left hand panel) are not used in the GA–LEI because the algorithm does not account for parasitic capacitance (Macnae and Baron-Hay, 2010) effects that have been observed in the data.

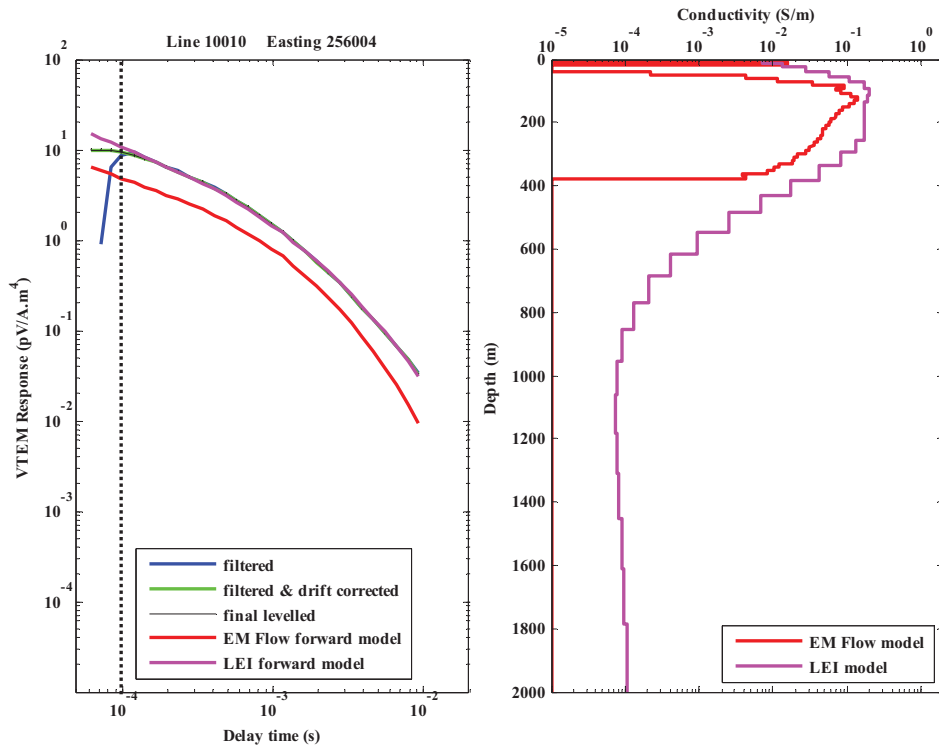


**Figure 10-5:** VTEM data (left) at the sample located at 'A' on Figure 10-4 and the corresponding GA–LEI and EM Flow<sup>TM</sup> CDI conductivity models (right).

Firstly, note that the filtered (blue) and drift corrected (green) data are mostly obscured by the final levelled data. This is because the drift and levelling corrections in this case are small compared to the amplitude of the data. The main correction is at early time (<0.1 ms delay time) where the drift correction is typically large. However over the remainder of the transient the corrections are small and the transients plot coincident with each other. This indicates that the signal-to-data correction ratio, and hence the signal-to-noise ratio is large in this conductive area.

Secondly, it can also be seen in Figure 10-5 that the GA–LEI model (magenta) has been able to fit the final levelled (black) data transient within the estimated error, except at very early time where the data are not used in the inversion. Note also in the left hand panel of Figure 10-5 that the forward model of the EM Flow<sup>TM</sup> CDI (red) does not match the final levelled data – its values are of the order of a factor 2 to 3 times smaller than the input data. Although we might have expected the match to be better, the EM Flow<sup>TM</sup> CDI algorithm is a fast approximate transformation rather than a data fitting inversion. Notwithstanding this, as noted earlier in the discussion on Figure 10-4, the GA–LEI and CDI conductivity sections are qualitatively similar.

### 10.8.2 Resistive Areas of the Kombolgie Dataset

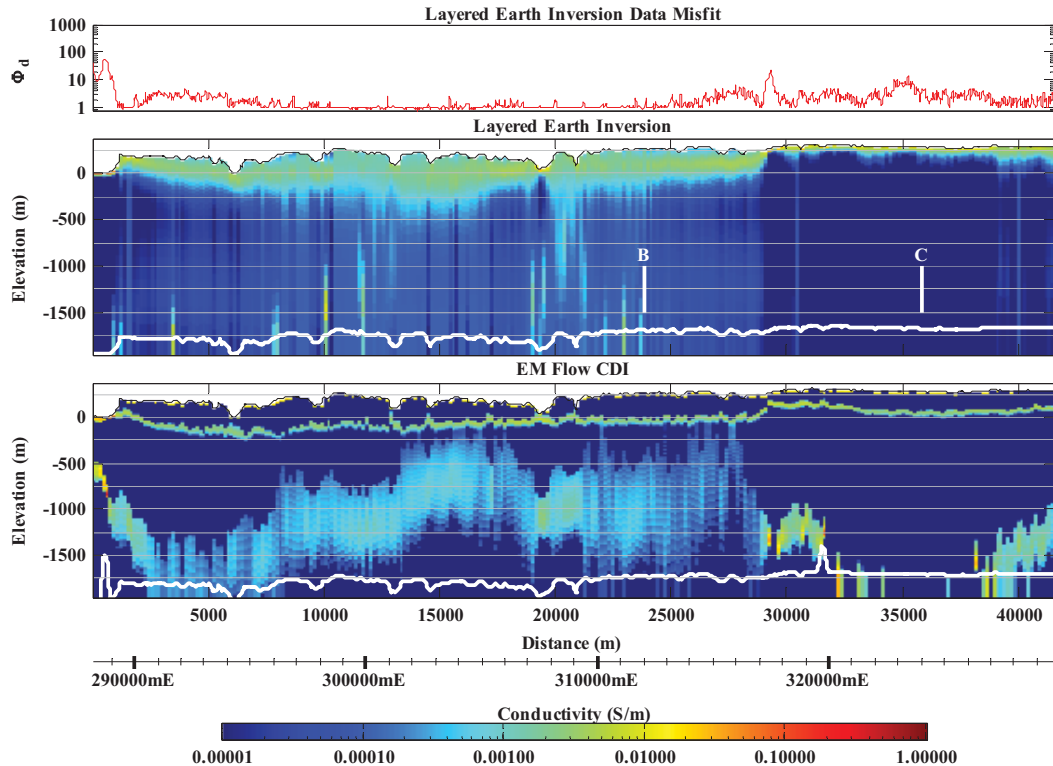


**Figure 10-6:** GA-LEI and EM Flow™ conductivity sections from a resistive part (Line 20390) of the Kombolgie survey area.

We turn our attention now to an example of a more resistive part of the survey area, Line 20390, whose GA-LEI and EM Flow™ CDI conductivity sections are shown in Figure 10-6. The two sections are quite different in this case. The GA-LEI has resolved a broad smooth (weak) conductor over the top ~250 m depth, below which it is largely lacking coherent character. On the other hand the EM Flow™ CDI shows a thin conductor at the surface and a more prominent thin conductor at ~250 m depth (i.e., approximately at the base of the smooth GA-LEI conductor). The CDI also contains the deeper (~1000 m) and thicker (~750 m) conductor that is not apparent in the GA-LEI.

The details of the data and fitted models at positions ‘B’ and ‘C’ marked on the conductivity sections in Figure 10-6 are shown in Figure 10-7 and Figure 10-9 respectively. In the left hand panel of Figure 10-7 it can be seen that the drift correction that was applied to the data at ‘B’ (i.e., the difference between the green and blue transients) is an order of magnitude larger than the final levelled data (black). This means that drift or zero-level error makes up the majority of the total measured response in this resistive area. With this in mind, it is clear that small relative errors in the drift correction estimated from high-altitude data will translate into significantly larger relative errors in the drift corrected and the final levelled data.

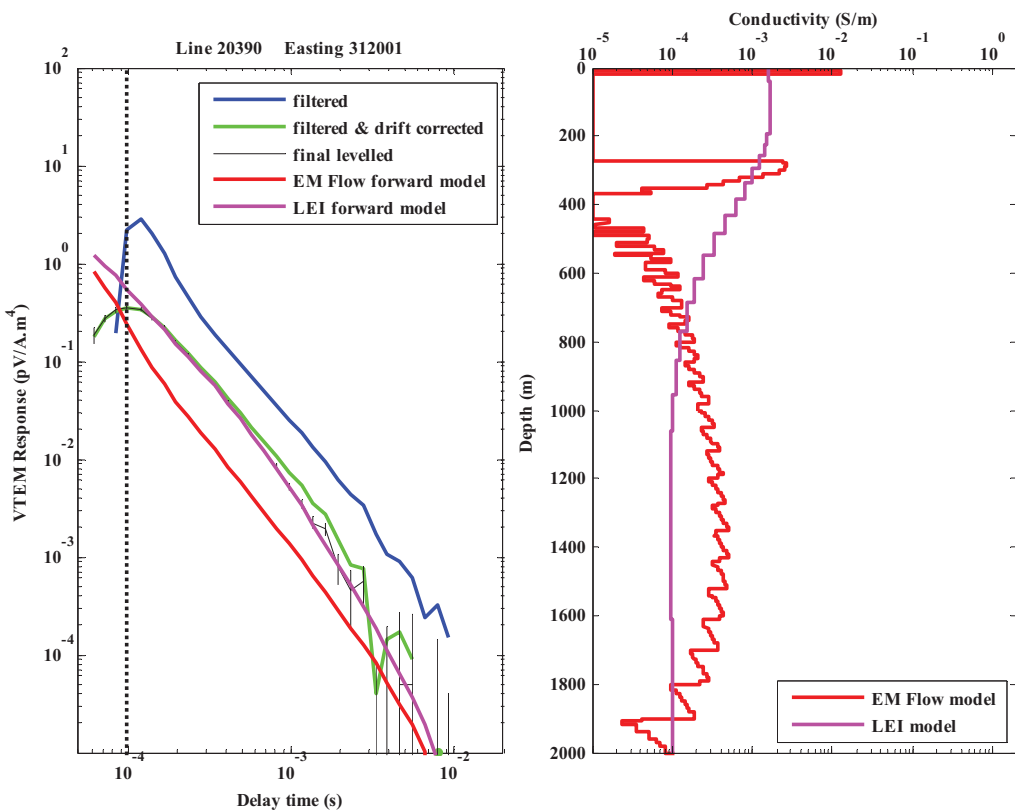
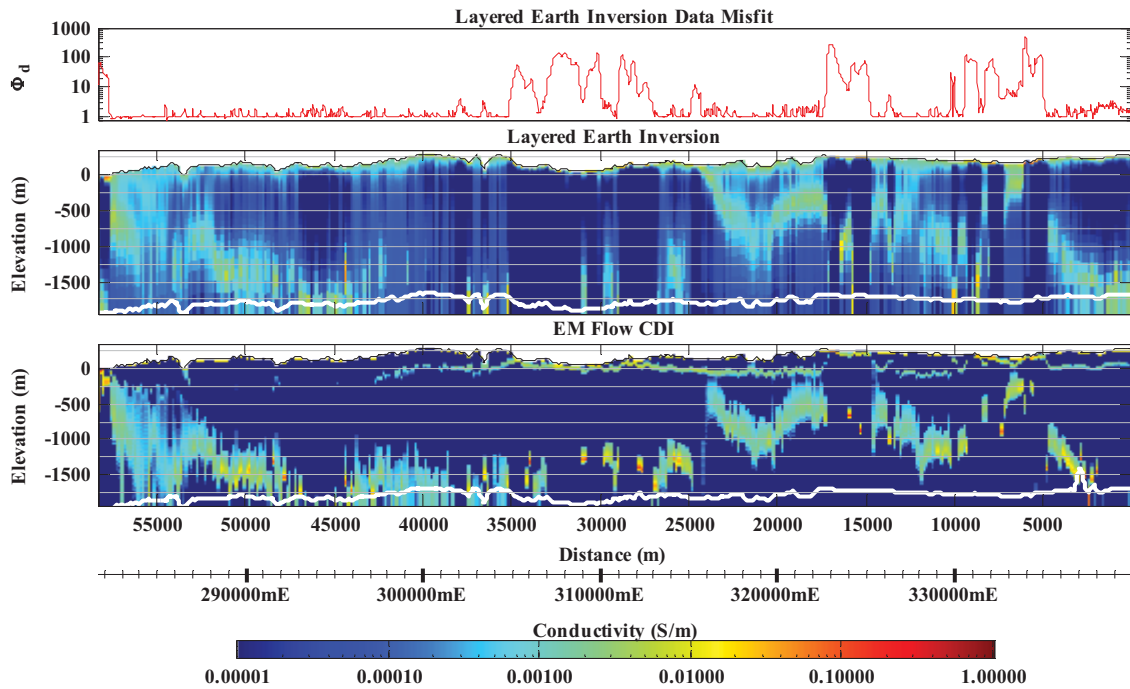


**Figure 10-7:** VTEM data (left) at the sample located at 'B' on Figure 10-6 and the corresponding GA-LEI and EM Flow<sup>TM</sup> CDI conductivity models (right).

#### 10.8.2.1 Deep conductor in resistive areas

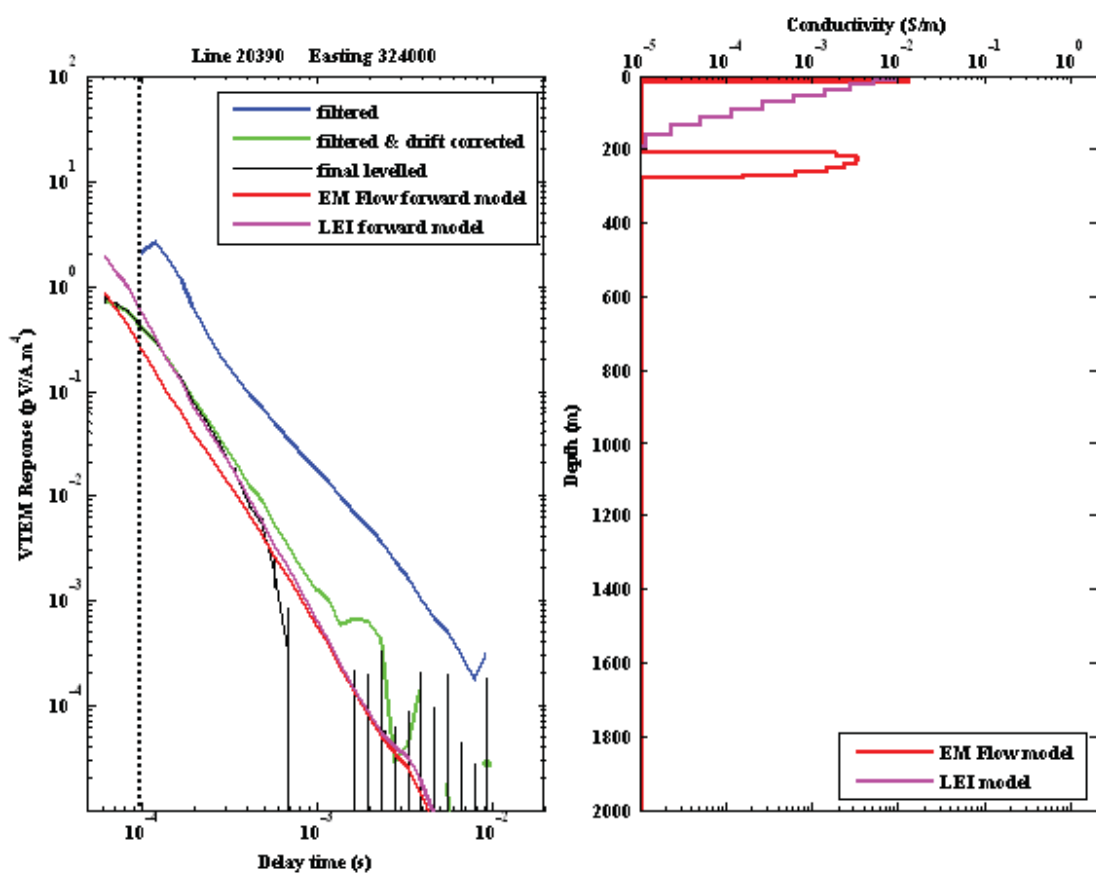
It can also be seen in Figure 10-7 that there is a good match between the final levelled data (black) and the forward model response of the GA-LEI inversion model (magenta). This is also reflected in the low data misfit (top panel) shown in Figure 10-6. Because the data were fitted satisfactorily by the GA-LEI, without the deep and thick conductor that is apparent in the corresponding EM Flow<sup>TM</sup> CDI section, we can say it was not required by the data. It is not clear to us what is causing the need for the deep conductor in the EM Flow<sup>TM</sup> CDI section. Thus Geoscience Australia advises caution when attempting to make geological interpretations of the conductivity sections.

However, on the other hand we are not suggesting that these deep conductors are simply artefacts. Geoscience Australia can also point to other flight lines where the GA-LEI does require a deeper conductor, with similar character to that in the corresponding EM Flow<sup>TM</sup> CDI section, to adequately fit the data. One such example is shown in Figure 10-8.



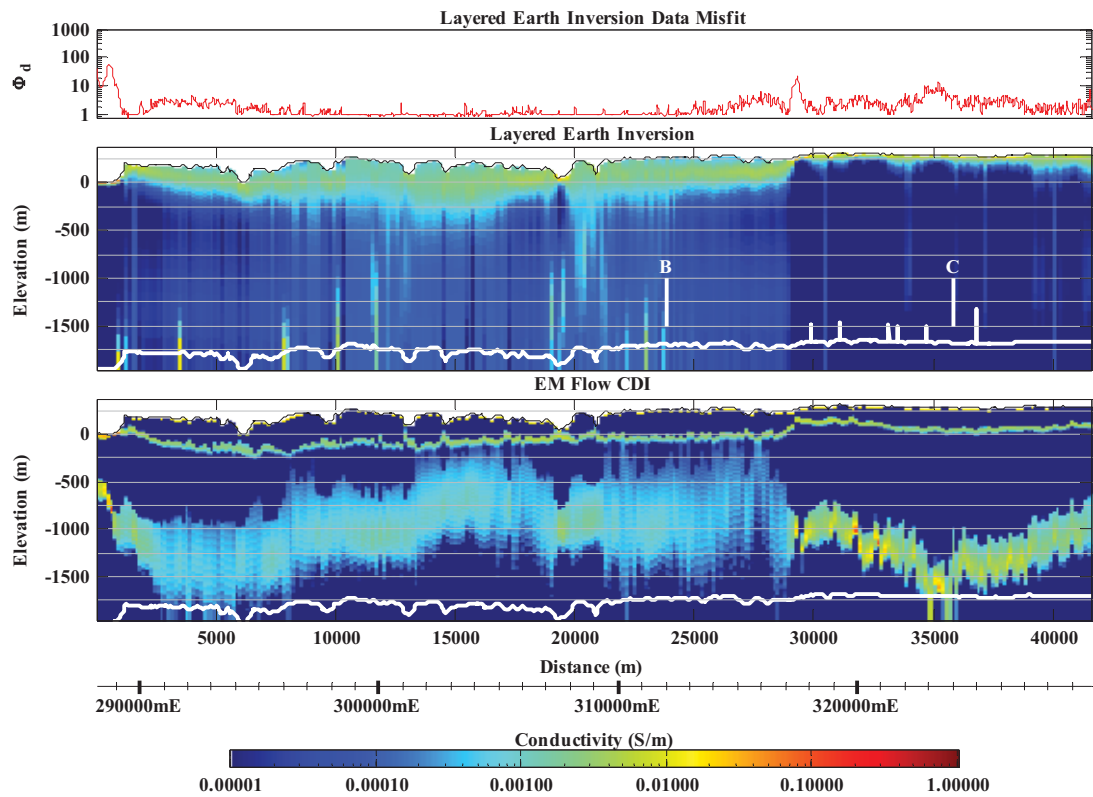
**Figure 10-8:** GA-LEI and EM Flow™ conductivity sections from a resistive part (Line 12100) of the Kombolgie survey area.

Figure 10–9 shows the details of the data and models at location ‘C’ marked on Figure 10–6, which is 12 kilometres further along the same flight line. Here the deeper conductor is absent from both the GA-LEI and the EM FlowTM CDI sections. Here the final levelled data (black) transient decays rapidly from  $\sim 0.0004$  s, after which neither the GA-LEI nor the EM FlowTM CDI can fit the data. Here a large levelling correction (i.e., the difference between the black and green transients) has been applied to the late-time data in the last step of data processing. The justification for this correction is not clear, however it has had the effect of pushing the deeper conductor off the bottom of the EM FlowTM CDI section between easting 321000 mE and 326000 mE (bottom panel of Figure 10–6).



**Figure 10-9:** VTEM data (left) at the sample located at 'C' on [Figure 10-6](#) and the corresponding GA-LEI and EM Flow<sup>TM</sup> CDI conductivity models (right).

[Figure 10-10](#) shows the same conductivity sections as in [Figure 10-6](#) (i.e., Line 20390), except in this case the GA-LEI and EM Flow<sup>TM</sup> CDI conductivity sections were generated from the drift corrected data (green transients on [Figure 10-7](#) and [Figure 10-9](#)) instead of the final levelled data (black transients on [Figure 10-7](#) and [Figure 10-9](#)). By comparing [Figure 10-6](#) with [Figure 10-10](#) in the portion of the line east of 317000 mE, it is clear that the final manually-derived levelling correction has 'broken-up' the more continuous deep conductor that would have been derived from the data prior to final levelling. This highlights the impact that subjective manually determined levelling corrections can have on the dataset, and gives reason to Geoscience Australia's advice of caution when attempting to make geological interpretations of the conductivity sections.



**Figure 10-10:** Similar to [Figure 10-6](#), except in this case conductivity sections were generated from the drift corrected data (i.e., green transients on [Figure 10-7](#)) instead of the final levelled data (black transients).

#### 10.8.2.2 Shallow conductor in resistive areas

We now turn our attention back to the shallow (<250 m) portion of the conductivity sections for Line 20390 ([Figure 10-6](#) and [Figure 10-10](#)). Here the GA–LEI resolved a smooth broad conductor and the EM Flow™ CDI resolved a thin conductor at the surface and a more prominent thin conductor at ~250 m depth (i.e., approximately at the base of the smooth GA–LEI conductor).

The information shown in [Figure 10-11](#) demonstrates the degree of ambiguity in the resolved models in the shallow zone. In similar fashion to [Figure 10-7](#), it shows the details of the data and the GA–LEI and EM Flow™ CDI models at location ‘B’ marked on [Figure 10-6](#) and [Figure 10-10](#). However, it also includes two additional models, denoted alternate-1 and alternate-2, that fit the data just as well as the GA–LEI. Again it can be seen that a layered-earth forward model of the EM Flow™ CDI (red transient) does not match the final levelled data (black transient). However, the model alternate-2 (blue) does fit the data reasonably well.

This suggests that a thin-layer model, similar in geological character to that shown on the upper ~250 m of the EM Flow™ CDI conductivity sections, is plausible. However, in this case, the layered-earth modelling suggests that it is likely to be somewhat (~130 m) shallower. Notwithstanding this, the broader and smoother GA–LEI and the alternate-1 models are also just as likely.

This appendix has highlighted the implications of the low signal levels in resistive areas, the impact of levelling corrections, and non-uniqueness of the resulting conductivity models. Given these

qualifications, we recommend caution in the interpretation of the results and advocate the consideration of alternate models.

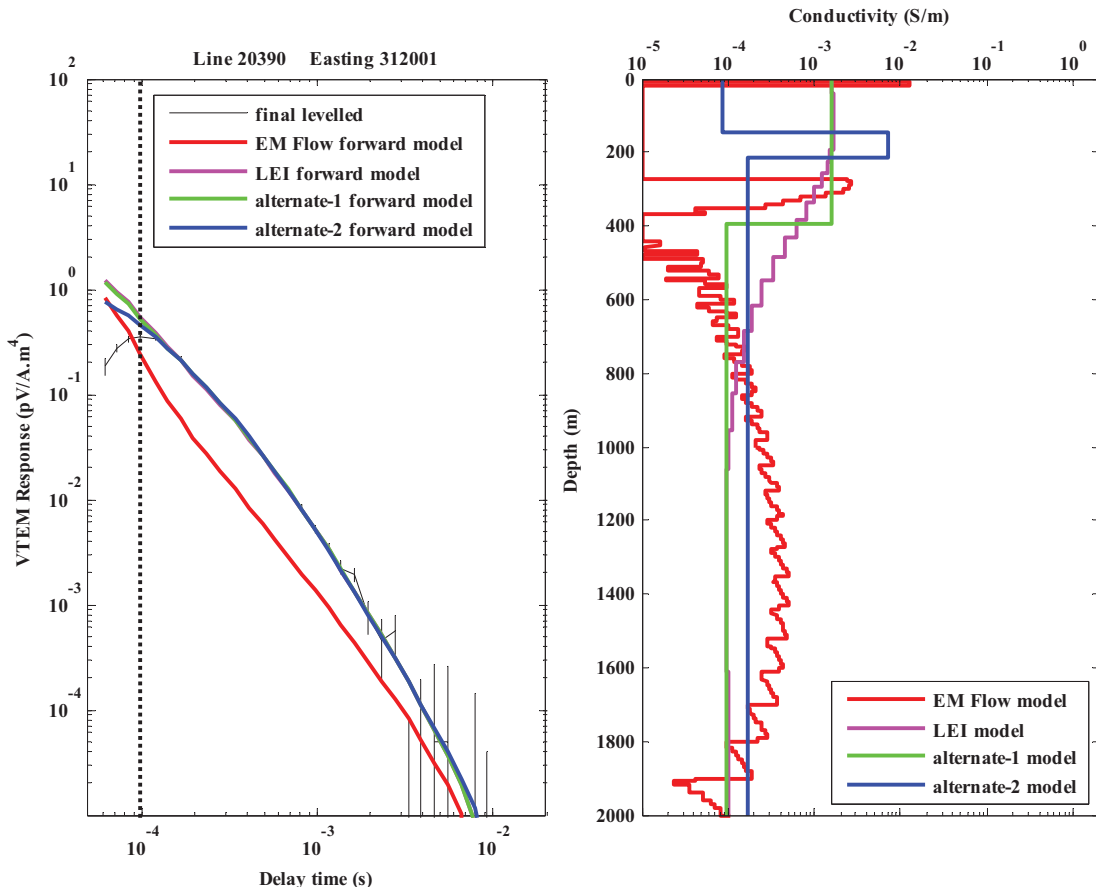


**Figure 10-11:** VTEM data (left) at the sample located at 'B' on [Figure 10-6](#) and the corresponding GA-LEI and EM Flow<sup>TM</sup> CDI conductivity models, and two alternative models that also fit the data (right).

## 10.9 REFERENCES

Macnae, J. and Baron-Hay, S., 2010, Reprocessing strategy to obtain quantitative early time data from historic VTEM surveys: ASEG Extended Abstracts 2010.

## **10.10 REGOLITH AND LANDFORM: THEIR CLASSES, PATTERNS, MAP SYMBOLS AND MEANINGS.**

The RTMAP regolith and landforms hierarchical nomenclature and their meaning and map symbols are listed in the following two tables:

**Table 10–4:** Regolith classes, unit codes, descriptions and map symbols.

CLASS (RTMAP UNIT DATABASE CODE)	PATTERN (RTMAP UNIT DATABASE CODE)	(RTMAP UNIT DATABASE CODE)	DESCRIPTION	MAP SYMBOL
<b>Terrestrial Sediments</b>		SDT00		T
	<b>Alluvial</b>	SDA00		A
		SDA10	Channel deposits	AC
		SDA20	Overbank deposits	AO
	<b>Aeolian</b>	SDE00		I
		SDE01	Aeolian sand	IS
		SDE02	Loess	IL
		SDE03	Pana	IP
	<b>Colluvial</b>	SDC00		C
		SDC05	Sheet flow deposits	CH
		SDC06	Colluvial fan deposits	CF
		SDC07	Scree	CS
		SDC08	Landslide deposit	CL
		SDC09	Mudflow deposit	CM
		SCD10	Creep deposit	CC
		SDC06	fanglomerate	CG
	<b>Evaporite</b>	EVA00		E
		EVA01	Halite	EH
		EVA02	Gypsum	EG
		EVA03	Calcrete	EC
	<b>Lacustrine</b>	SDL00		L
	<b>Glacial</b>	SDG00		G
	<b>Volcanic</b>	VOL00		V
		VOL02	Tephra	VT
		VOL03	Lava Flow	VF

CLASS (RTMAP UNIT DATABASE CODE)	PATTERN (RTMAP UNIT DATABASE CODE)	(RTmap Unit database code)	Description	Map Symbol
	<b>Fill</b>	SDF00		F
	<b>Coastal</b>	SDS00		O
		SDS01	Beach sediments	OB
		SDS02	Esturine sediments	OE
		SDS03	Coral	OC
		SDS04	Marine sediments	OM
	<b>Paludal</b>	SP00		P
		SP01	Peat	
	<b>Residual material</b>	WIR20		R
		WIR21	Lag	RL
		WIR22	Residual sand	RS
		WIR23	Residual clay	RC
		WIR*	Bauxite	RX
		WIR24	Soil on Bedrock	RB
		WIR*	Ferruginous residuum	RF
	<b>Saprolith</b>	WIR*		S
		WIR*	Saprolite	SP
		WIR15	Completely weathered bedrock	SC
		WIR14	Very weathered bedrock	SV
		WIR13	Highly weathered bedrock	SH
		WIR12	Moderately weathered bedrock	SM
		WIR11	Saprock	SS
	<b>Unweathered Bedrock</b>	BU00		BU
		UOS00	Sand	US
		UOC00	Clay	UC
		UOM00	Weathered material	UW
<b>Water Bodies</b>				WT

**Table 10–5:** Landform classes, unit codes, descriptions and map symbols.

CLASS (RTMAP UNIT DATABASE CODE)	PATTERN (RTMAP UNIT DATABASE CODE)	(RTMAP UNIT DATABASE CODE)	DESCRIPTION	MAP SYMBOL
<b>AL00</b>			<b>alluvial landforms</b>	<b>a</b>
	AL10		alluvial plain	ap
	AL11		flood plain	af
		AL12	anastomotic plain	aa
		AL13	bar plain	ab
		AL14	covered plain	ac
		AL15	meander plain	am
		AL16	floodout	ao
		AL17	stream channel	ar
	AL20		alluvial terrace	at
	AL30		stagnant alluvial plain	as
	AL40		terraced land	al
	AL50		alluvial swamp	aw
<b>CO00</b>			<b>coastal lands</b>	<b>c</b>
	CO01		beach ridge	cb
	CO02		chenier plain	cc
	CO03		coral reef	cr
	CO04		marine plain	cm
	CO05		tidal flat	ct
	CO06		coastal dunes	cd
	CO07		coastal plain	cp
	CO08		beach	cc
<b>DE00</b>	<b>DE00</b>		<b>delta</b>	<b>d</b>
<b>DU00</b>	<b>DU00</b>		<b>aeolian landforms</b>	<b>u</b>
	DU10		aeolian dunes	ud
		DU11	longitudinal dunefield	ul
		DU12	transverse dunefield	ut
		DU13	irregular dunefield	ui
		DU14	source bordering dune	ub
		DU15	lunette	uu

**Geological and energy implications of the Pine Creek airborne electromagnetic (AEM) survey,  
Northern Territory, Australia**

CLASS (RTMAP UNIT DATABASE CODE)	PATTERN (RTMAP UNIT DATABASE CODE)	(RTMAP UNIT DATABASE CODE)	DESCRIPTION	MAP SYMBOL
		DU20	aeolian sheet	us
		DU21	climbing sheet	uc
<b>ER00</b>	<b>ER00</b>		<b>erosional landforms</b>	<b>e</b>
	ER10		erosional plain	ep
	ER11		pediment	ei
	ER12		pediplain	ea
	ER13		peneplain	en
	ER14		etchplain	ee
	ER20		rises	er
	ER21		residual rise	eu
	ER30		low hills	el
	ER31		residual low hill	es
	ER40		hills	eh
	ER50		mountains	em
	ER60		escarpment	ec
	ER70		badlands	eb
	ER80		drainage depression	ed
<b>FA00</b>	<b>FA00</b>		<b>fan</b>	<b>f</b>
	FA01		alluvial fan	fa
	FA02		colluvial fan	fc
	FA03		sheet-flood fan	fs
<b>GL00</b>	<b>GL00</b>		<b>glacial features</b>	<b>g</b>
	GL10		depositional glacial features	gd
	GL20		erosional glacial features	ge
<b>KA00</b>	<b>KA00</b>		<b>karst</b>	<b>k</b>
<b>MA00</b>	<b>MA00</b>		<b>made land</b>	<b>m</b>
<b>ME00</b>	<b>ME00</b>		<b>meteor crater</b>	<b>t</b>
<b>PL00</b>	<b>PL00</b>		<b>plain</b>	<b>p</b>
	PL01		depositional plain	pd
	PL02		lacustrine plain	pl
	PL03		playa plain	pp
	PL04		sand plain	ps

**Geological and energy implications of the Pine Creek airborne electromagnetic (AEM) survey,  
Northern Territory, Australia**

<b>CLASS (RTMAP UNIT DATABASE CODE)</b>	<b>PATTERN (RTMAP UNIT DATABASE CODE)</b>	<b>(RTMAP UNIT DATABASE CODE)</b>	<b>DESCRIPTION</b>	<b>MAP SYMBOL</b>
	PT00		plateau	
	PT01		plateau edge	le
	PT02		plateau surface	ls
<b>VO00</b>	<b>VO00</b>		<b>Volcano</b>	<b>v</b>
	VO01		caldera	vc
	VO02		cone (volcanic)	vv
	VO03		lava plain	vl
	VO04		ash plain	va
	VO05		lava flow	vf
	VO06		lava plateau	vp